AN EXPLORATORY STUDY OF PARAMETER SENSITIVITY, REPRESENTATION OF RESULTS AND EXTENSIONS OF PSHA: CASE STUDY – UNITED ARAB EMIRATES

A thesis submitted to the Imperial College London

for the degree of Doctor of Philosophy

By

Guillermo Aldama Bustos

Department of Civil and Environmental Engineering

Imperial College London

London, SW7 2AZ

March 2009

ABSTRACT

Despite the wide use of probabilistic seismic hazard analysis (PSHA) for the evaluation of seismic hazard, some degree of confusion and misunderstanding exists regarding how the hazard calculations should be performed as well as how the hazard results should be interpreted.

In this thesis, different aspects of PSHA that are commonly misunderstood, as well as some new developments, are investigated. To this end, a comprehensive case study PSHA for three cities in the United Arab Emirates is carried out. Previous publications present contradictory interpretations of the earthquake threat in this country, creating confusion regarding appropriate seismic design levels. The results of this PSHA confirm low hazard levels in most of the country (UBC97, Zone 0) that increase as one moves northwards (UBC97, Zone 1).

Using the case study as a point of reference, the mechanics and implications of performing hazard disaggregation when using multiple ground-motion prediction equations (GMPEs) within a logic-tree framework are investigated. Logic-tree approaches receive significant attention as different ways of representing hazard results from logic trees are discussed as well as issues associated with the identification of hazard-dominating scenarios and how these may influence the definition of scenario spectra for the selection of ground-motion records for seismic design.

The sensitivity of the hazard results to key parameters in PSHA such as: the minimum magnitude deemed to be of engineering significance; the activity parameters of seismic sources; the use of alternative GMPEs and the standard deviations associated with these models; and the allocation of weights to logic-tree branches is investigated. Furthermore, recently proposed alternatives to the specification of a minimum magnitude as the criteria for identifying non-damaging earthquakes are studied.

Finally, correlations between the hazard results obtained in terms of spectral accelerations and hazard results in terms of peak ground velocity and spectral intensity are explored.

ACKNOWLEDGMENTS

I want to express my most sincere gratitude to Professor Julian Bommer for giving me the opportunity of doing my PhD under his supervision and for proposing such an interesting topic of research. I am in debt with him for his thorough and patient supervision throughout the development of this thesis and for his teachings on Engineering Seismology. My gratitude also to Dr. Clark Fenton for his supervision during the first stage of my research helping me on the setting up of the seismic source zonation for the case study presented in this thesis. My highest gratitude to Dr. Peter Stafford; without his patient and thorough teaching, and his assistance with proofreading, this thesis would not have reached its current state. I owe to him most of my understanding on the mechanics of probabilistic seismic hazard assessment (PSHA). I am certainly in debt with him for all his support.

I would also like to thank Dr. Mario Ordaz from the National Autonomous University of Mexico for providing the software, Crisis2003, to perform the hazard calculations and for a series of improvements that he made to the program attending some of the necessities of this research. These improvements are now part of a new version of the software, Crisis2007.

Special thanks to Dr. Fleur Strasser for her friendship and for many productive discussions on different issues related to this thesis. Special thanks to my friends: John Alarcón, Elizabeth O'Nions, Francisco Cortez and Giovanny Alvarado who have become my family in England.

Finally, I want to thank to my brothers, Gustavo and Gabriel, for encouraging me to undertake this project. Doubtless, without all their support it would not have been possible to complete this task. Many thanks brothers.

INDEX

LIST OF FIGURES

LIST OF TABLES

Chapter 1.

INTRODUCTION

Of all natural hazards, earthquakes are those which historically have caused the most extensive impact and disruption in terms of damage to infrastructure, human-casualties and economic losses (Oliveira *et al.*, 2006). In order to limit this impact, engineers have to design structures and facilities to withstand certain levels of ground shaking due to the occurrence of future earthquakes without suffering extensive damage. The specification of the parameters that characterize the ground motions that must be designed against is one of the most difficult and most important problems in engineering seismology (Kramer, 1996). In order to specify appropriate levels of these parameters, the seismic-hazard analyst has to face not only the natural random variability of earthquake processes but he/she must also rely on subjective decisions based on incomplete or uncertain information, as well as inadequate understanding of the underlying earthquake process (this lack of information and understanding both leading to epistemic uncertainty). Probabilistic seismic hazard analysis (PSHA), performed within a logic tree framework, provides an approach via which both random variability and epistemic uncertainty, can be identified, quantified and combined in a rational manner in order to provide a comprehensive picture of the seismic hazard (Kramer, 1996).

Since the printing, in the mid-to-late 1960's, of the pioneering publications of Esteva (1967) and Cornell (1968), PSHA has become the most widely used method for assessing seismic hazard. It is not only used to provide the inputs for the seismic-resistant design of structures but is also fundamentally linked to risk assessment and seismic risk mitigation, among other applications. Important developments to the original proposal of

Cornell (1968) have been implemented since its publication. Among the most important contributions to the original approach are the explicit incorporation of the aleatory variability of the ground motion (Cornell, 1971), the introduction of logic trees to PSHA (Kuljarni *et al.*, 1984), the representation of the hazard results via disaggregation (Bazzurro & Cornell, 1999; Kramer, 1996; McGuire, 1995) and, most recently, the computation of the joint hazard of multiple ground-motion parameters, better known as vector-valued PSHA (Bazzurro & Cornell, 2002). Although logic trees were originally introduced as a tool for dealing with epistemic uncertainties in seismic hazard analyses (not necessarily "probabilistic" seismic hazard analyses), the approach has become an integral part of PSHA and is nowadays the standard approach.

Despite the wide use of PSHA for the evaluation of seismic hazard, some degree of confusion and misunderstanding remains concerning the details of how the hazard calculations in a PSHA framework should be performed and how the hazard results should be interpreted (e.g., Abrahamson, 2006; Bommer, 2006; Bommer & Abrahamson, 2006). The reason for this, at least partially, has been that many of the developments of this discipline have only been published in work that is not widely accessible (i.e., conference proceedings, client reports, etc.).

Among the most common misunderstandings associated with PSHA are: the appropriate treatment of aleatory variability, a misunderstanding that commonly leads to the underestimation of the seismic hazard (Bommer & Abrahamson, 2006), and the clear differentiation between aleatory variability and epistemic uncertainties (Bommer & Scherbaum, 2008; Bommer *et al.*, 2005). In addition to this, there is no consensus as to how the results of a PSHA study, carried out within a logic tree framework, should be treated, interpreted and finally used for seismic-resistant design, risk assessment or any other decision making process regarding seismic

hazard (c.f., Abrahamson & Bommer, 2005; Bommer & Scherbaum, 2008; McGuire *et al.*, 2005; Musson, 2005).

Another issue of common concern when performing PSHA is the sensitivity of the hazard results to key parameters such as the minimum earthquake magnitude that is deemed to be of engineering significance (m_{min}), and the earthquake recurrence parameters (β and υ_{min}) and the maximum magnitude (m_{max}) describing the seismic activity of the different seismic sources. Also of interest is the implication of incorporating multiple ground-motion prediction equations (GMPEs) in the hazard analysis through the use of a logic tree, and the influence on the hazard results of the weights assigned to the alternative branches of the logic tree (Sabetta *et al.*, 2005; Scherbaum *et al.*, 2005).

Another topic that has recently piqued interest among researchers has been the correlations between the most commonly used ground-motion parameters for the assessment of the seismic hazard [i.e., peak ground acceleration (PGA) and 5%-damping spectral accelerations (SA)] and other ground-motion parameters that are also of interest to engineers. Parameters such as peak ground velocity (PGV) and spectral intensities (SI), despite being good predictors of the damage potential of a ground motion and of the dynamic behaviour of structures, are usually inferred from hazard results in terms of SA using fairly crude "rules of thumb". This is done instead of directly evaluating the seismic hazard in terms of these parameters from the outset. A typical example of this practice is the scaling of PGV from SA at 1.0 s, as embodied in the HAZUS programme of the Federal Emergency Management Agency of the United States (FEMA, 2003).

The aim of this thesis is to explore and discuss many of the issues previously mentioned by making use of a case study as a point of reference. Where possible, resolutions to these outstanding issues are put forward. In addition to this, new developments of the hazard-assessment process, such

as the use of the cumulative absolute velocity (CAV) as an alternative to m_{min} for distinguishing among earthquake scenarios that should or should not be included in the integration process (Hardy *et al.*, 2006), are explored. To treat this variety of topics, the thesis has been divided into seven chapters; a brief outline of each chapter is presented in what follows.

In Chapter 2 an overview is presented of the main elements of PSHA and the related logic-tree framework. The main goal of this section is to provide the reader with a broad overview of the basic elements of earthquake catalogues, seismicity models, ground-motion prediction, hazard calculations and logic trees.

In Chapter 3 a comprehensive PSHA study for three cities of the United Arab Emirates (UAE) is presented. This case study is conducted with two key objectives: (1) to assess the seismic hazard in three of the most important cities of the UAE; and, (2) to establish a point of reference for conducting subsequent analyses. This study includes a critical review of previous publications on the assessment of the seismic hazard in the UAE and its surroundings.

In Chapter 4 the mechanics and implications of performing disaggregation when using multiple ground-motion prediction equations (GMPEs) within a logic-tree framework are investigated. Different representations of the hazard results are also discussed, i.e., mean vs. median hazard curve; and hazard vs. ground-motion domain. Additionally, the implications of using multiple GMPEs on the identification of hazard-dominating scenarios are discussed in conjunction with how one would specify scenario spectra for seismic design based upon time-history analyses.

In Chapter 5 sensitivity analyses are carried out for the case study presented in Chapter 3. This is done in order to gain an appreciation of the influence of key parameters in the PSHA. In the first section of this chapter

the impact on the seismic hazard of considering an active fault running along the west coast of the UAE, as mapped by Johnson (1998), is addressed. Other variables considered in the sensitivity analyses of this chapter are the m_{min} value, the β values and m_{max} values of the seismic sources with the highest contributions to the hazard, the use of multiple GMPEs, the standard deviation associated with the predictions of these GMPEs, and, finally, the weights assigned to the logic-tree branches. Chapter 5 also studies a recent approach, proposed by Hardy *et al.* (2006), for using CAV instead of m_{min} as an alternative way to identify scenarios of engineering significance. This approach is applied to the case study of Chapter 3 and the implications on the hazard results of using this methodology are discussed. In addition to this, the use of Arias intensity (I_a) as an alternative to the use of CAV, as a parameter to discriminate between damaging and non-damaging scenarios is studied. To this end, an equation for predicting I_a is derived and used within the framework proposed by Hardy *et al.* (2006).

Chapter 6 presents an exploration of the relationships between the hazard results for SA(T), at different response periods and for different damping levels, and the expected values of PGV and SI obtained from hazard analyses performed in terms of these parameters. In order to do this, a new ground-motion prediction equation for SI is derived. Based on the findings of this chapter, recommendations for inferring values of SI and PGV from hazard results conducted in terms of SA(T) are presented.

Finally, in Chapter 7 a summary of the main findings of the research carried out in Chapters 3 to 6 is presented, along with the conclusions and recommendations for future research in light of these conclusions.

Chapter 2.

OVERVIEW OF PSHA

In this chapter, an overview is presented of the main elements of probabilistic seismic hazard analysis (PSHA) and the related logic tree framework. The fundamental components of earthquake catalogues, seismicity models, ground-motion models, hazard calculations and logic trees are described and commented upon.

PSHA provides a framework in which uncertainties regarding earthquake magnitude, location and rate of occurrence of future earthquakes can be identified and quantified in a rational manner to provide a transparent and comprehensive panorama of the seismic hazard (Kramer, 1996).

In the mid 1960's, the joint efforts of Allin Cornell and Luis Esteva led to the foundation of modern PSHA. The two pioneering publications in this field were Esteva (1967) and Cornell (1968), with the latter being the most well known and cited work. McGuire (2008) has recently presented a succinct and candid historical outline of the early history of PSHA.

Regardless of the approach used to estimate seismic hazards due to possible future earthquakes, the basic elements of the PSHA are the same. The first element is a seismicity model, which is constructed with due consideration of the seismotectonic environment of the region under study and consist of the earthquake catalogue and the earthquake occurrence models that represents the seismic activity rated of the identified seismic sources. This seismicity model defines the spatial and temporal locations and magnitudes of possible future earthquakes.

The second element is a model for predicting the expected ground motion at a specific site due to each earthquake scenario. This prediction

can be for any ground-motion parameter of interest (e.g. peak ground acceleration [PGA], spectral accelerations [SA], and peak ground velocity [PGV]). This model is usually a relatively simple empirical equation, which is commonly known as attenuation equation but preferably called as ground-motion prediction equation. Consistently ground-motion prediction equations define ground-motion measures as functions of source-to-site distance and earthquake magnitude. However, nowadays most of the equations also take account of the site conditions and the faulting mechanism. Other phenomena that affect ground motions such as directivity and hanging wall effects are rarely considered in ground-motion prediction equations.

Based on these two elements (the seismicity and the ground-motion models), it is possible to estimate the probability that a threshold ground-motion level will be exceeded in a period of time at a particular location due to future earthquakes. This ground-motion level can be with respect to any ground-motion parameter of interest. For example we can assess the probability that PGA will exceed 0.5 g within a period of 50 years. If the probability of exceedance for a given ground-motion parameter is estimated at multiple ground-motion levels, a seismic hazard curve can be built up. This seismic hazard curve shows the annual frequency that a ground motion exceeds a given value.

Disaggregation is one of the most important elements of PSHA. It shows how different scenarios of magnitude (M), distance (R) and some times epsilon (ε) contribute to the seismic hazard at a specific site for a given ground-motion parameter and at any given exceedance probability. Where epsilon represents the number of standard deviations that the target ground motion is from the median ground motion predicted by a given attenuation equation.

The importance of representing the hazard results in a disaggregated format lies on that, based on them, decisions can be taken regarding the selection of scenario-based ground-motion records and response spectra scenarios for structural seismic design and risk assessment. Additionally, disaggregated results allow one to identify the most hazardous seismic source in order to incorporate secondary parameters for seismic design such as near-to-source effects and duration of the ground motion.

Conventional PSHA for a specific site provides hazard curves for a single ground-motion parameter. The most common of these are PGA and SA. However, for predicting potential damage to structures caused by earthquakes, the estimation of a single ground-motion parameter could be insufficient and the joint probability of two or more of them could be regarded as being a more useful indicator. A good example of this is liquefaction, where both intensity and duration of the ground-motion shaking are critical. For the computation of the joint hazard of multiple ground-motion parameters, Bazzurro & Cornell (2002) present a vector-valued probabilistic seismic hazard analysis (VPSHA).

In what follows, each of these elements of PSHA are described in more detail.

2.1. Earthquake catalogues and seismicity

Earthquake catalogues are the starting point for a seismic hazard assessment (SHA). These, consist of estimates of past earthquake origins, described by three spatial and one time co-ordinate, and the magnitudes of events that have occurred in or near the region of interest. The quality, consistency and homogeneity of this data are directly reflected in the accuracy of the results of a SHA. Earthquake catalogues, along with a good understanding of the geology and seismotectonic environment are the

fundamental bases for constructing the seismicity model, which is the first element needed to carry out a seismic hazard assessment.

The determination of the earthquake location has improved steadily with time as problems with instrumentation, timing, earth modelling and station distribution have been addressed.

The first global seismic network was set up in 1898 by the Englishman, John Milne, with about 30 widely dispersed monitoring stations. Among the earliest institutions to undertake global earthquake location was the Bureau Central International de Seismologie at Strasbourg, which remained a major source of global earthquake location data until 1963.

In 1922 the International Seismological Summary (ISS) was created and produced the most comprehensive global earthquake catalogue for the time period between 1918 and 1963 (Stoneley, 1970). In 1964 the ISS was restructured as the International Seismological Centre (ISC), with an increasing number of stations becoming available and a more carefully monitored computer location program. Consequently, 1964 is considered a watershed moment in the reliability of global earthquake location, although much uncertainty remained in depth estimation for events around this time.

At about the same time as the creation of the ISS, the U.S. government formed the U.S. Coast and Geological Survey (USCGS), which started the production of the Preliminary Determination of Epicenters (PDE) in 1928. Currently, this work is carried out by the National Earthquake Information Center (NEIC) as part of the U.S. Geological Survey (USGS).

A major breakthrough came in the early 1960's, with the setting up, under the auspices of the U.S., of a World Wide Standard Seismograph Network (WWSSN) of over 100 stations with identical instruments for both short and long periods.

Another significant improvement in earthquake catalogues was achieved by Robert Engdahl, Rob van der Hilst and Raymond Buland in 1998 (Engdahl *et al.*, 1998), who relocated the best constrained events reported by the ISC and NEIC occurring in the period from 1964 to 1995, using an improved global travel time model (Kennet *et al.*, 1995). Their catalogue is considered as a major refinement of the ISC and NEIC earthquake origin data, particularly with respect to determination of depths.

2.1.1. Historic and instrumental records

It is generally considered that the instrumental seismicity era began around 1900. Prior to this date the study of earthquakes was based only on the collection of contemporary reports of earthquakes and earthquake effects reported in newspapers, paintings, diaries, church records, diplomatic notes, etc.

Many publications, such as those by Ambraseys and collaborators (Ambraseys & Adams, 2001; Ambraseys & Melville, 1982; Ambraseys *et al.*, 1994), Berberian (Berberian, 1973; Berberian, 1994), Suleiman *et al.* (2004), Albini *et al.* (2004) and Musson (2004), cover historical seismicity (before 1900) for many regions around the World, as well as re-evaluate earthquake locations and magnitudes for more than the first half of the twentieth century. These are based mainly on macroseismic information, which, when well constrained, may be more reliable than instrumental data for that period.

The key to compiling catalogues of historical seismicity is to interpret reports of felt and damaging effects and transform them into macroseismic intensities. Empirical relationships based on modern data can then be used to estimate earthquake magnitudes and locations from the observed intensity distribution of the event.

A helpful aid when compiling historic catalogues, particularly for earthquake scenarios with long recurrence intervals, are studies of paleoseismology, which involves the geologic study of the past behaviour of active faults. This process involves digging a trench across, or along-side, the fault in order to identify and date organic matter trapped in the sediments that have been disrupted by past earthquakes. Results of these studies give constraints on the timing of large historic earthquakes, the amount of offset, and hence the slip rate.

These studies are particularly useful for assessing the seismic activity of faults that behave in a characteristic manner and can provide the basis for estimating the probability of the next earthquake (McCalpin, 1996). The recurrence intervals of these events are usually longer than the length of the instrumental, and often the historical, part of the catalogue, and these events would therefore not be recognised if analyses only considered activity in recent times. Unfortunately, these studies are not evenly spread around the world, but concentrated mainly in California, other parts of the United States and Japan.

Earthquake catalogues covering most of last century are easily obtainable for any part of the world from a number of national, regional and international agencies such as the previously mentioned ISC and NEIC. Other agencies with broad coverage are the International Institute of Earthquake Engineering and Seismology (IIEES) and the European-Mediterranean Seismological Centre (EMSC).

These agencies produce routine earthquake locations, which at present carry errors of at least 10 to 15 km in the epicentral location and even larger errors in the focal depth. In addition, reported earthquakes before 1960 could carry errors greater than 100 km in the epicentral location (Berberian, 1979).

A careful assessment of the reliability of these catalogues for the region of interest is always recommended before their use in a seismic hazard analysis. Improved instrumental earthquake catalogues such as Engdahl *et al.* (1998) and macroseismic based catalogues (e.g. Ambraseys & Melville, 1982; Ambraseys *et al.*, 1994; Berberian, 1994) must be used to complete missing data or identify mislocations and thus increase the reliability of the earthquake database used in the hazard analysis.

Finally, the earthquake catalogue must include all the paleoseismic, historical and instrumental data available. Although events with no magnitude reported but with a reliable location cannot be used in the hazard analysis, it is always a good idea to consider them as part of a main catalogue as they could help developing a better understanding of the seismicity in the region of interest.

2.1.2. Foreshocks and aftershocks

When performing a PSHA based on the original approach of Cornell (1968), one of the main assumptions is that all the earthquakes in the catalogue are independent events in time, and in space within each of the identified seismic sources. In other words, the occurrence of the events in an earthquake catalogue is expected to follow a Poissonian distribution.

Aftershocks clearly break this assumption as they are dependent on the occurrence of the main shock. For this reason, clusters of dependent events must be identified and removed from the catalogue and only main events must be included.

Aftershock sequences are generally well characterised and algorithms such as those proposed by Gardner & Knopoff (1974), Reasenberg (1985) and Knopoff (2000) are commonly used to identify them. These algorithms assume that any earthquake that occurs within a specific area surrounding a prior earthquake is an aftershock and should, therefore, be considered

statistically dependent upon the prior event. For cluster identification, these algorithms make use of space-time windows around and following each event, whether it belongs to a cluster or not.

On the other hand, foreshocks are difficult to identify and usually for PSHA purposes no attempt is made to identify them. However, if, during the identification of aftershocks, “the main event” is considered as that with the highest magnitude in the cluster and not merely the first to occur, then technically those events prior the main event could be considered as foreshocks.

The occurrence of events in catalogues covering large areas, declustered in this way can be reasonable considered as Poissonian in nature (Gardner & Knopoff, 1974; Knopoff, 1964).

2.1.3. Catalogue completeness

An important issue that must be addressed, before any statistical analysis can be carried out, is to assess the completeness of the data in the earthquake catalogue. The incompleteness of data when performing statistics analysis is an important issue and cannot be disregarded as the quality of any statistical analysis is strongly affected by the quality of the data on which it is based.

An earthquake catalogue is a clear example of data-set affected by incompleteness in both location and time due to the lack of data, mainly in the historical and early-instrumental eras. However, differences of incompleteness as function of space are generally ignored.

Catalogues are incomplete for different threshold magnitudes at different time periods. A threshold magnitude is defined as the magnitude above which it is considered that all events are reported. Below this magnitude a fraction of events are regarded as having been missed.

The incompleteness of a catalogue is dependent on various factors, including the historical and socio-economical context, demographic variations, level of macroseismic intensity reported and in recent times the development of seismic networks in the region. The threshold magnitude changes (generally decreases) with time; in recent times these changes are strongly associated with upgrades to the network of seismic recording instruments in the region, and to a lesser degree to the improvement of location algorithms. Factors such as the historical and socio-economical context and demographic variations have a stronger influence on the completeness of the historical part of the catalogue; regions that have been highly populated historically, such as China, have a well documented historical record of earthquake occurrence, while in scarcely populated regions, such as the south-eastern part of the Arabian Peninsula, quantifying rates of earthquake occurrence from historical information is a difficult, if not impossible, task.

Many works regarding the estimation of the threshold magnitudes at different time periods in an earthquake catalogue have appeared in the literature (e.g., Rotondi & Garavaglia, 2002; Stepp, 1972; Woessner & Wiemer, 2005). Some of these proposed methods are essentially based on the principle that the period covered by an earthquake catalogue can be considered as unchanged in terms of tectonic regime, or kinematic context if we compare it with the length of geological phases (Gutenberg & Richter, 1944).

Once the different periods of completeness for different threshold magnitudes have been estimated, the data can then be used in the estimation of the earthquake occurrence rate for the seismic model.

2.2. Seismicity models

The key to a good analysis is to make credible estimates and express uncertainties about the source properties and effects of future earthquakes (McGuire, 2004).

For deterministic seismic hazard analysis (DSHA) the seismicity model only has to identify seismic sources and the associated maximum-magnitude event that could occur within each source. Often in DSHA the shortest source-to-site distance is used for the analysis; however in some occasions the analyst defines a "credible" source-to-site distance. For instance, when the fault is located beneath or too close to the site under study the analyst could chose to not consider the shorter distance for considering it too conservative and to define a more "realistic" source-to-site distance.

For a PSHA the seismicity model is far more complicated. It needs to define and characterise all the earthquake sources as in DSHA but with the difference that the probability distribution of potential future earthquake needs to be characterised as well. In most PSHA, if not in all, the location of the future earthquake is considered to be equally likely to occur anywhere within the seismic source. In DSHA, the largest earthquake is hypothesised to occur at the worst location for the site.

It is important to highlight the fact that future seismicity may not demonstrate uniformity of occurrence within source, not over the short term and might not over the long term. In other words, these assumptions only represent the present understanding of regional seismicity (McGuire, 2004).

When sufficient information exists to justify nonuniform spatial distribution of the seismicity within a given source, then two area sources could be used to represent earthquake occurrence. Well studied faults, such as San Andreas Fault, are often divided into segments in which rupture recurrence are preferentially restricted in each segment separately, although multiple segments may rupture in large earthquakes.

Additionally, PSHA needs to define the temporal distribution of earthquake occurrence for different magnitudes, for each seismic source. This temporal distribution of the seismicity is generally represented by recurrence relationships such as that proposed by Gutenberg & Richter (1944) that considers an exponential recurrence model, which has been found to be consistent with the recurrence statistics for large areas. Youngs & Coppersmith (1985) propose a characteristic recurrence model that may better represent the seismic activity in areas like subduction zones or major faults in continental regions. In these areas, largest events occur quasi-periodically with little or no earthquakes expected with magnitudes in the interval immediately below of the size of the characteristic earthquake; earthquakes with smallest and medium size magnitudes are expected to follow the general form of the Gutenberg & Richter relationship. In Figure 2.1 are presented examples of magnitude- frequency plots showing characteristic earthquake behaviour.

In most seismic hazard analyses, if not in all, a doubly-bounded version of the Gutenberg & Richter (1944) model is used (Cornell & Vanmarcke, 1969) instead of the untruncated version. The magnitude distribution is truncated at an upper-bound value m_{max}, which is the maximum expected magnitude that the seismic source is considered capable of producing, and at a lower bound, m_{min}, which is chosen in the basis of the minimum magnitude that might cause damage to engineered structures.

These two earthquake recurrence models, the doubly-bounded Gutenberg & Richter (1944) and Youngs & Coppersmith (1985), are the most commonly used in current engineering practice and there is a lot of evidence to support both models. However, there are many other models that may be used to represent seismic activity with a strong statistical fit to data; Utsu (1999) describe many of these earthquake recurrence models.

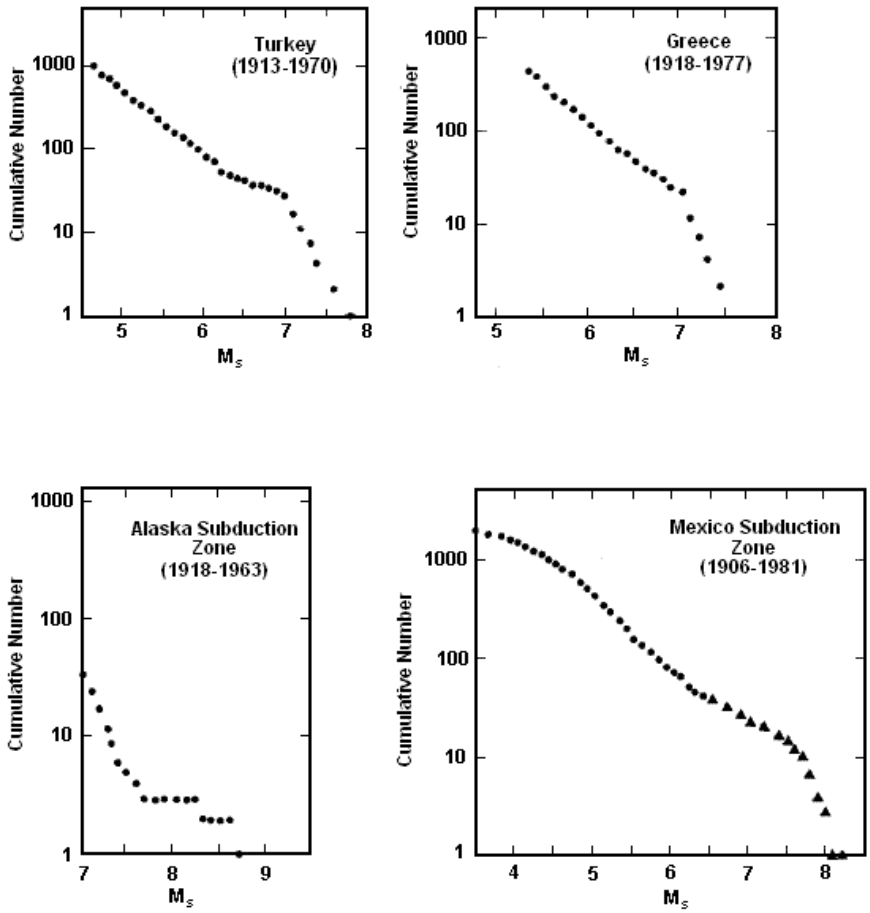

Figure 2.1. Frequency-magnitude plots for seismic sources showing seismicity with "nonlinear" or "characteristic earthquake" recurrence behaviour (Youngs & Coppersmith, 1985).

In addition to these models that consider the occurrence of events to be independent of time, time-dependent earthquake recurrence models have been developed to estimate the conditional probability of occurrence of an event given that previous events either have or have not occurred in the seismic source. These models are discussed in more detail later in this chapter.

2.2.1. Seismic source definition

The first step when constructing a seismicity model is to define all the seismic sources that may be important for the seismic hazard at the site in consideration. The geometries of seismic sources depend on the tectonic framework of the region and past seismicity. These are usually modelled as

three general types: areal sources, fault sources, and point sources (Figure 2.2).

When seismicity is clearly concentrated in small well defined areas, for example those associated with volcanic activity, seismic sources may be characterized as point sources.

Fault sources are usually individual faults or regions of faulting with clear surface evidence, or when no surface evidence is found faults can be inferred through past earthquake activity, seismicity patterns, tectonic interpretations of crustal stress and strain or any other indirect evidence.

Fault sources can be considered as two-dimensional sources, with a strike and dip, following the mapped geometry of the fault (Figure 2.2b). In some cases, for simplicity, faults can be modelled as a linear source where this line can be the projection of the fault on the surface or a line along a seismogenic depth (Figure 2.2a).

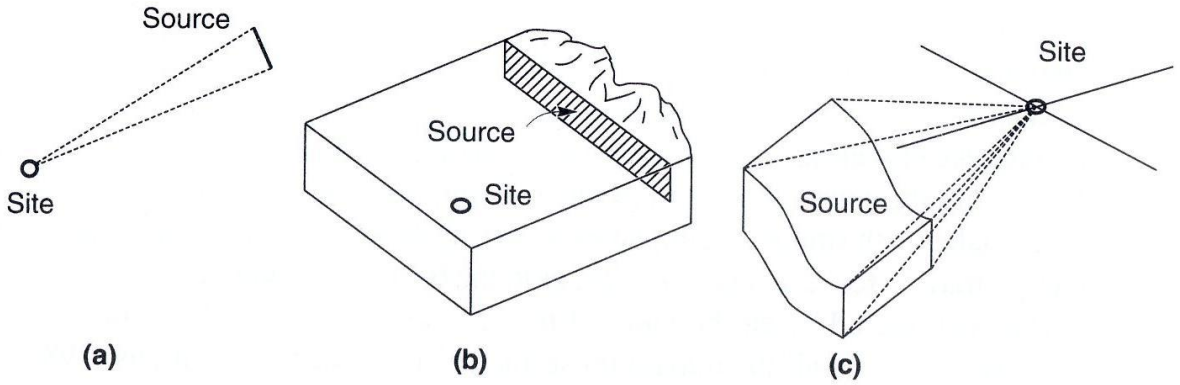

Figure 2.2. Typical seismic source geometries considered in seismic hazard assessment. (a) A single fault can be modelled as a line source, alternatively a short fault relatively far from the site or seismicity clearly concentrated in a small area can be modelled as a point; (b) a fault can be modelled as a 2D plane source; (c) a 3D source for regions where focal depth can be constrained within a given range (Kramer, 1996).

Area sources are defined as zones or regions within which future events are expected but geologic or tectonic structures are poorly defined or where faulting is so extensive that it makes it impossible to attribute seismic activity to individual faults. Frequently the geometry is defined based only on

historical and instrumental seismicity, however information from regional crustal geology, tectonic style of crustal deformation, local geology (including observed and inferred intrusive bodies), states of crustal stress, rates of crustal strain among others must be considered.

Areal sources are generally modelled as horizontal planes with a fixed depth or as a three-dimensional source when enough data to constrain the variation with depth is available (Figure 2.2c); however, the variation with depth is normally not included in the models.

In general, the aim of defining seismic sources is to identify regions with similar seismic activity; thus, if multiple neighbouring faults present similar seismic activity they might be better modelled as a single area source rather than multiple individual fault sources. On the other hand, if two segments of the same fault present clear differences in their seismic activity, two seismic sources should be modelled.

2.2.2. Exponential recurrence model

The original form of the exponential earthquake recurrence model, known as the Gutenberg-Richter model, is typically expressed by the equation:

$$Log_{10}N(m) = a - bm, \qquad 2.1$$

where N is the number of earthquakes of magnitude m or greater per unit of time, a is the Log_{10} of the number of events of $m \geq 0$, and b defines the relative frequency of occurrence between events of different magnitudes.

This relationship was first expressed in terms of intensities by Ishimoto & Iida (1939) before Gutenberg & Richter (1944) expressed this in terms of magnitudes, and used it to characterise Californian seismicity. Gutenberg & Richter (1944) found b values close to 1.0 over a reasonable range of magnitudes for Californian seismicity. Since then, this relationship

has been applied in many other regions of the world and only minor deviations from a *b* value of 1.0 have been observed.

Generally, *a* and *b* are obtained by maximum likelihood regression on a dataset of seismicity from the seismic source of interest; this dataset is part of the earthquake catalogue compiled for the PSHA and usually contains both historical and instrumental seismicity. For PSHA purposes the earthquake catalogue must be clear of foreshocks and aftershocks and the completeness assessed for reasons expressed previously in this chapter.

For seismic hazard analysis, Equation 2.1 is usually expressed in the equivalent form:

$$N(m) = \nu_o e^{-\beta m}, \qquad 2.2$$

where $\upsilon_o = 10^a$ is the number of events per unit of time with $m \geq 0$, and $\beta = b*Ln(10) \approx 2.3b$.

Often, the range of magnitudes considered in the hazard analysis is doubly-bounded (Cornell & Vanmarcke, 1969). At the lowest magnitude it is bounded to a minimum threshold magnitude, m_{min}, which is considered as the appropriate minimum magnitude to use for buildings of good design and construction (e.g., McCann & Reed, 1989). In the highest magnitudes the distribution is truncated at an upper-bound value m_{max}, which is usually the magnitude of the maximum "possible" or "credible" earthquake that can be produced by that seismic source.

If Equation 2.2 is modified to incorporate minimum and maximum threshold magnitudes, then the number of earthquakes, *N(m)*, with magnitude $\geq m$ per unit of time is expressed as:

$$N(m) = \nu_{m_{\min}} \left[1 - k + ke^{-\beta(m-m_{\min})}\right], \qquad m_{\min} \leq m \leq m_{\max} \qquad 2.3$$

where

$$k = \left[1 - e^{-\beta(m_{\max} - m_{\min})}\right]^{-1}. \qquad 2.4$$

Usually, historical and instrumental seismicity is used to estimate $\nu_{m_{min}}$ and β; many methods for doing so have been published and include those of Cosentino *et al.* (1977), Dong *et al.* (1984), Kijko & Graham (1998; 1999) and Weichert (1980). The last of these, probably being the most used and widely accepted due to its ability to consider earthquake catalogues with different levels of completeness over different periods of time.

On the other hand, m_{max} can be estimated through statistical analysis when enough data is available in the earthquake catalogue (e.g. Kijko, 2004; Pisarenko *et al.*, 1996). Otherwise, this estimation can be done based on geological features (length of the fault or tectonic structures), geophysical data, slip rate, analogies to similar tectonic regimes or in the worst case scenario the maximum observed magnitude might be increased by an amount based on "expert" opinion.

2.2.3. Characteristic recurrence model

Although in most cases the exponential model adequately describes recurrence statistics of events in large areas, in some areas such as subduction zones and major faults, the extrapolation of the recurrence frequency inferred from smaller-magnitude events tends to underestimate the occurrence of large-characteristic events (Figure 2.1). In such situations a characteristic earthquake recurrence model is usually employed.

Paleoseismic evidence has shown that in very well defined geological structures, individual faults and fault segments tends to move by approximately the same distance in each earthquake. This suggests that these faults tend to repeatedly generate essentially the "same size earthquakes"; usually within one-half of a magnitude unit (Youngs & Coppersmith, 1985).

The characteristic model, originally proposed by Schwartz & Coppersmith (1984), presents the same distribution for small and moderate magnitude events as the exponential model, but based on geological data they suggest a variation in the slope of the recurrence curve to *b'* at some *m'* magnitude.

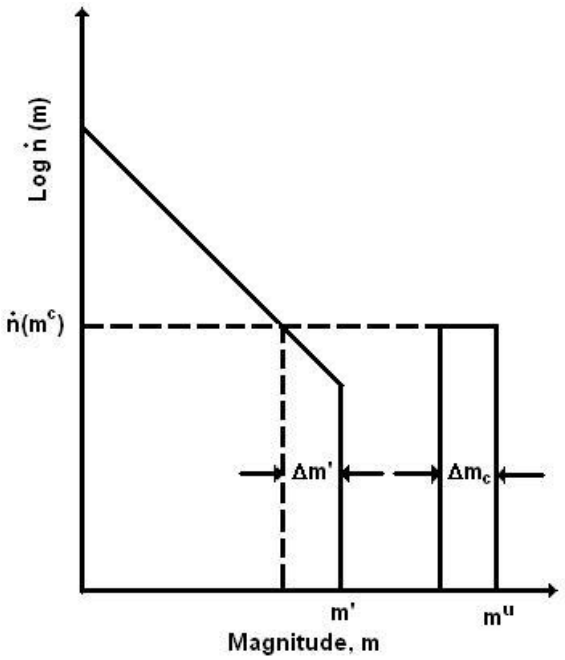

Figure 2.3. Generalized frequency magnitude density function for the characteristic earthquake model (Youngs & Coppersmith, 1985).

Afterwards, Youngs & Coppersmith (1985) developed a generalized magnitude-frequency density function that combines an exponential distribution at lower magnitudes up to magnitude level *m'*, and above this value lies the characteristic component with a uniform distribution about the characteristic event. The model proposed by Youngs & Coppersmith (1985) is shown in Figure 2.3.

Other models for characteristic earthquakes have been presented by Wesnousky *et al.* (1984) and Wu *et al.* (1995).

2.2.4. Time-dependent recurrence models

During an earthquake the average stress along the fault changes, dropping an amount $\Delta\sigma$ below the average stress condition prior to the event occurring. After the earthquake has occurred, elastic energy starts building up in the surroundings of the fault due to the interaction of the tectonic plates. In this way, the average stress along the fault increases with time and deformation can be observed on both sides of the fault. When the resistance of the fault is exceeded it ruptures, relaxing the stress in the fault and the cycle re-starts. This theory is called "elastic rebound"; it was originally proposed by H.F. Reid (1910) and has been widely accepted.

This process does not agree with time-independent models (e.g., exponential model or characteristic model), which are based on memoryless Poissonian behaviour. Time-dependent models (e.g., Cramer *et al.*, 2000; Petersen *et al.*, 2007; Shimazaki & Nakata, 1980) have been developed to encompass some of the physics behind the earthquake cycle, permitting the statistical "renewal" of the recurrent process.

Time-dependent models require the specification of more parameters than Poisson models. This constrains their application to well defined faults where parameters such as the mean slip rate, mean displacement, mean recurrence interval, stressing rate and the time since the last event, among others must be clearly defined, being the last of these the most important parameter to define.

Cornell & Winterstein (1988) examined a range of time- and magnitude-dependent earthquake recurrence models and compare their influence upon hazard results against the traditional Poisson model. They conclude that the Poisson model is adequate in most cases with the notable exception being when the hazard is controlled by a single feature for which the elapsed time since the last significant event exceeds the average time

between such events and the fault exhibits strongly regular, characteristic time behaviour.

2.3. Ground-motion prediction

The next basic element in both PSHA and DSHA is the ground-motion model for predicting the expected ground motion at a specific site due to future earthquakes. These models are function of parameters such as magnitude of the earthquake, distance from the source to the site, geological conditions at the site and mechanism of rupture of the fault, among the most common.

Multiple definitions for each of these parameters are used in the literature. To measure earthquake magnitude many scales are used in ground-motion models, the most common are: M_s, m_b, M_L and M_w, with the latter being the preferred magnitude scale as it is directly related to the seismic moment of the earthquake (Hanks & Kanamori, 1979). For this reason the majority of the most recent ground-motion equations use this magnitude scale.

Many definitions are also commonly used for the source-to-site distance. The most common definitions for this variable are: the closest horizontal distance to the surface projection of the rupture (r_{jb}); the closest distance to the rupture surface (r_{rup}); the closest distance to the seismogenic part of the rupture surface (r_{seis}); and the hypocentral distance (r_{hypo}). These different distance definitions are schematically shown in Figure 2.4 for vertical and dipping faults.

For site classification as well, several schemes are found in literature. Commonly site classification is a broad and qualitative description of the surface geology. However, some equations, mainly those recently derived as part of the NGA (Next Generation of Attenuation) project in the U.S., use a more quantitative description base on the shear-wave velocity corresponding

to the uppermost 30m of the soil deposit (V_{s30}). Nevertheless the use of V_{s30} for describing site conditions goes back to Boore *et al.* (1993).

The influence of the style of faulting on the nature of the strong motion is not included in all ground-motion equations, but among those that do include this factor agree that reverse faulting produces the strongest ground motions.

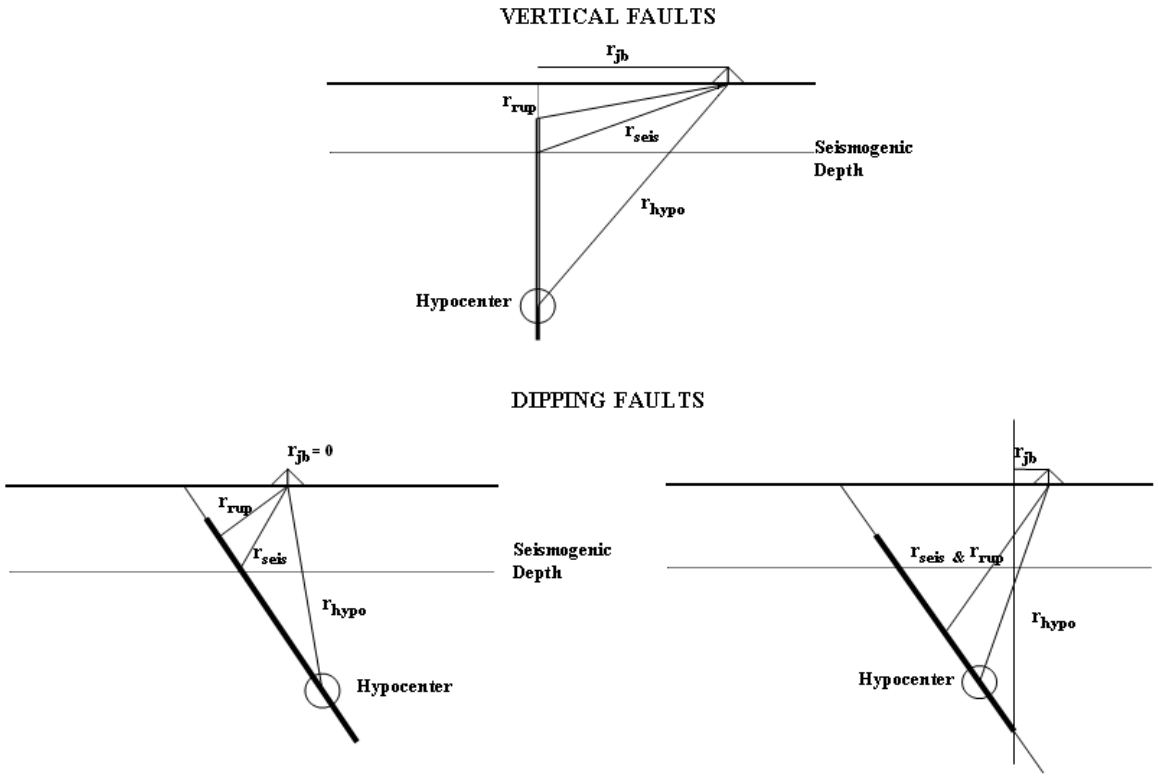

Figure 2.4. Source-to-site distance definitions used in ground-motion models (Abrahamson & Shedlock, 1997).

Since the pioneering publication of the ground-motion model of Esteva & Rosenblueth (1964), a large number of models for predicting ground-motion parameters of engineering interest have been developed. A comprehensive summary of ground-motion prediction equations for predicting peak ground acceleration (PGA) and spectral amplitudes (SA) is presented in two publications of Douglas (2004; 2006).

Most ground-motion equations are based on statistical analysis of recorded ground motions which are updated as new information becomes available. These types of equations are better known as empirical ground-motion equations. On the other hand, when not enough data is available to derive empirical equations, stochastic methods can be applied to derive ground-motion models, although it is more common to use empirical ground-motion equations from some other region.

Based on the seismotectonic environment, ground-motion models can usually be classified into one of three categories: shallow crustal earthquakes in active tectonic regions, shallow earthquakes in stable continental regions and subduction zone earthquakes (Abrahamson & Shedlock, 1997).

Regardless the methodology applied to derive a particular ground-motion equation, there is always a variance term which represents the uncertainty associated with the predicted ground motion. This variance term represents the scatter in the data used in the regression analysis; however, the most common measure of this scatter is the standard deviation, which is defined as the square root of the variance. The variance in a ground-motion equation not necessarily represents the lack of fit of a particular equation to real data; it rather represents the distribution of the ground motion observed in the field given a particular set of predictor variables such as magnitude, distance and site condition.

In both PSHA and DSHA, variability in ground-motion prediction has a very relevant position as it defines how likely a ground-motion level is to be reached given a particular earthquake scenario. Usually the variability in ground-motion predictions, along with the occurrence of earthquakes within a seismic source, are the only aleatory variabilities that are modelled in PSHA. In DSHA this variability is considered through a rather arbitrary decision on the number of standard deviations that should be added to the

expected value of ground motion. In any case, the proper treatment of ground-motion variability plays an important role in seismic hazard analysis (Bommer & Abrahamson, 2006).

2.3.1. Ground-motion parameters

There are a considerable number of quantitative parameters that can be calculated from ground-motion records. Each of these parameters provides a piece of information that represents a particular characteristic of the ground motion record. Most of these parameters measure one of the following characteristics of the ground motion: absolute amplitude of the ground motion, duration of the shaking or frequency content of the motion. There are also energy-based parameters which are based on a combination of these characteristics (Bommer, 2005).

Of these parameters, only a few of them are routinely used for seismic design proposes. Peak ground acceleration (PGA) and maximum spectral acceleration for different response periods [SA(T)], at 5% damping, are by far the most commonly used ground-motion parameters, followed probably by the peak ground velocity (PGV). Parameters such as Arias intensity (I_a) and cumulative absolute velocity (CAV) have been found to be a good estimator of potential damage, not only for structures but for landslides and liquefaction (Kramer & Mitchell, 2006; O'Hara & Jacobson, 1991).

PGA is simply the largest absolute peak acceleration recorded at a site during a particular event. Up until 2006 around 207 equations had been derived to predict PGA (Douglas, 2004, 2006). However, while PGA is the most commonly used parameter to characterise strong ground motion it is not particularly well related to potential damage to engineering structures, landslides or liquefaction; it is merely useful for analysis of short period ($T \leq 0.3$ s) structures (Douglas, 2003b).

Peak ground velocity (PGV) and peak ground displacement (PGD) are obtained in the same way as PGA but using associated velocity and displacement time histories, respectively. However, since ground-motion recordings tend to be acceleration time-histories, a numerical integration is required to obtain the corresponding velocity and displacement time-histories and from them read PGV and PGD, respectively. Special care must be taken when obtaining velocity and displacement time-histories from accelerograms as both, especially the latter, are sensitive to the filtering processes applied to the accelerograms (Boore & Bommer, 2005). Of these two parameters, PGD is rarely used, while PGV, although not widely used, has shown some reliable correlation with structural damage due to earthquake shaking (Akkar & Özen, 2005).

SA(T) is the maximum spectral acceleration of a damped linear oscillator subjected to a seismic excitation. A damping value of 5% of critical is the most commonly used, however a few equations have been derived for other levels of damping. In most of the cases the predicted SA is not the maximum absolute spectral acceleration but the maximum absolute pseudo-acceleration (PSA) since it is derived from spectral displacements. Response spectral ordinates have proved to be useful ground-motion parameters for the seismic design of structures, since these can be modelled approximately as an equivalent linear oscillator. Up until 2006 about 128 equations had been derived to predict SA or PSA (Douglas, 2004, 2006).

Many definitions of strong-motion duration can be found in literature; a good summary is presented by Bommer & Martinez-Pereira (1999). Although equations have been derived to predict some of the duration definitions, their use is still low regardless of it has been proved the importance of duration for potential damage assessment. Particularly, studies employing damage measures assessing cumulative energy or displacement usually find a correlation between strong-motion duration and

structural damage (Hancock & Bommer, 2006). In soil dynamics is recognized a clear correlation between the number of cycles, and hence durantion, and the increase of pore water pressure, leading this to potential liquefaction (Kramer, 1996). Duration definitions differ so widely that comparison among equations for different definitions is not possible.

The most widely used energy-based parameters are Arias intensity (I_a) and cumulative absolute velocity (CAV). Damage to normal structures is essentially related to the amount of energy transmitted to the structure due to ground shaking. All the energy that is not dissipated through elastic damping is absorbed through cracking and inelastic deformations. For this reason, energy-based parameters have an important role as indicators of damage to structures due to strong ground motion.

I_a relates to the cumulative energy per unit weight absorbed by an infinite set of single degree of freedom oscillators uniformly distributed in frequencies, along a given direction, at the end of the ground motion. The definition of I_a was originally proposed by Arias (1970). The most common representation of I_a for the undamped case is:

$$I_a = \frac{\pi}{2g}\int_0^{t_o} a(t)^2\, dt, \qquad 2.5$$

where t_o is the total duration of the earthquake, $a(t)$ is the acceleration time history in g units and g is the accelerations of gravity.

I_a is the basis for some duration definitions that consider the interval between the times at which two percentages of the total I_a are reached. Most commonly these measures are for the interval between 5% and 75%, or alternatively between 5% and 95% of the total I_a (Figure 2.5).

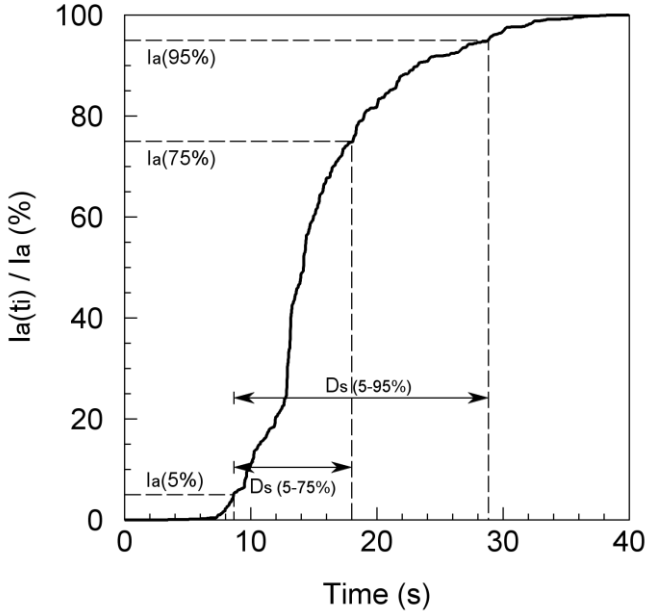

Figure 2.5. Husid plot normalized to the total I_a of the record. D_s are the significant duration for the intervals 5-75% and 5-95% of the total I_a.

Probably the most interesting application of this parameter is the construction of the Husid plot. This plot shows the build-up of I_a with time and has the advantage of showing not only the amount of energy released by the ground shaking, but also the rate at which this energy is transmitted to the structure. Figure 2.5 shows an example of the Husid plot and the estimation of the significant duration.

Another common parameter is CAV. It is defined as the integral of the absolute value of a ground motion acceleration recording. In other words, it is the sum of the absolute peak-to-valley velocity changes (Reed *et al.*, 1988). O'Hara & Jacobson (1991) modified the original definition of CAV to consider only 1-second time windows having amplitudes of at least 0.025 g. This with the aim of considering only strong ground shaking rather than small amplitudes that can continue for a long time after the strong shaking (coda waves). This definition of CAV is given by:

$$CAV = \sum_{i=1}^{N} H\left(pga_i - 0.025\right) \int_{t=t_i}^{t_{i+1}} \left|a(t)\right| dt \qquad 2.6$$

where N is the number of 1-second time windows, pga_i is the peak ground acceleration, in g, during the time window i, t_i is the start of the time window i and $H(x)$ is the Heaviside function (unity for x > 0 and 0 otherwise).

The good correlations that have been found between CAV and structural damage (e.g., Cabañas *et al.*, 1997) has lead to it being considered within PSHA as an alternative to using some minimum earthquake magnitude to distinguish between damaging and non-damaging earthquakes (Hardy *et al.*, 2006).

2.3.2. Empirical ground-motion equations

The large and continually increasing number of ground motion records that are available allows engineering seismologists to derive, for any ground-motion parameter of interest, a robust estimate of the correlation between these parameters and an associated set of independent variables. These independent variables characterize ground motion records in terms of magnitude, source-to-site distance, some description of the site conditions at the recording site and some classification of the style-of-faulting, as well as possible other variables.

An empirical ground-motion equation is a rather simple relationship between a set of these independent variables and the median value of the parameter of interest. These equations also provide a measurement of the variability about the predicted median value; this variability is quantified by the standard deviation associated with the prediction of the ground motion and in some equations it is function of magnitude, site conditions or ground motion amplitude.

Empirical ground-motion equations typically have the following form:

$$log(Y) = \mu(M, R, \theta) + \varepsilon\sigma \qquad 2.7$$

where Y is the ground motion amplitude, $\mu(M, R, \theta)$ represents a generic function in terms of the magnitude of the earthquake, source-to-site distance and other conditions such as the influence of the surficial geology and the style-of-faulting, ε is a random variable taking on a specific value for each observation and σ is the standard deviation.

Typically it is assumed that ground motions are lognormally distributed, so the mean value of *Log(Y)* would correspond to the median and not to the mean value of *Y*. Note that the base of the logarithm is not important.

Although the independent variables used in most of the ground-motion equations are the same, such as magnitude, source-to-site distance, and site conditions; as commented previously, there are many definitions or different classifications for each of these variables. For example, there are at least nine different definitions for earthquake magnitude and eight definitions for distance from source to site (Douglas, 2006). Likewise, many definitions of the horizontal component of motion of the predicted variable can be founded in literature (Beyer & Bommer, 2006). These differences in the definitions of the predictor and independent variables can lead to important incompatibilities when using or comparing the results of multiple equations; adjustments need to be made to ensure that the predictions are consistent. Procedures to handle these incompatibilities are addressed in section 2.5.2.

For most ground-motion measures, values of the ground motion will decrease with increasing distance and decreasing magnitude. The earliest ground-motion equations predicted values based only on these two parameters. The most recent equations also depend heavily on magnitude and distance, but since the first equations many different functional forms

have been proposed in an attempt to best capture the variation of ground-motions with respect to these variables.

In addition to the scaling of the predicted ground-motions with magnitude, distance, site conditions and style-of-faulting, there are other factors that may affect the ground motion but that are seldom included in ground-motion equations. Examples of these are hanging-wall or footwall effects (Abrahamson & Somerville, 1996), directivity (Abrahamson, 2000a; Somerville *et al.*, 1997), basin effects (Choi *et al.*, 2005) and topographic modifiers (Toshinawa *et al.*, 2004). When these effects are not implicitly included in the ground-motion equation they are commonly applied as correction factors to the base models. In fact, the effect of topographic modification has not been incorporated into any ground-motion equation so far.

2.3.3. Directivity

Directivity is a physical phenomenon of a fault rupturing in which earthquake ground motion in the direction of rupture propagation is more severe than in other directions from the earthquake source. This phenomenon is observed specially for low frequencies (<0.5 Hz) (Somerville, 2000) and is not commonly included using explanatory variables in ground-motion models.

Variations in amplitude and duration depend on the location of the site with respect to the fault rupture and the direction of the rupture propagation. When the rupture propagates towards the site (forward directivity), at a velocity that is often close to the shear wave velocity (~ 80%), the seismic energy from the rupture can arrive in a single large concentrated pulse of motion. This concentration of energy produces larger ground-motion amplitudes and shorter duration than for the average directivity conditions. Two conditions are required to observe forward directivity effects: (1) the

rupture front propagates towards the site, and (2) the direction of the propagation of the rupture is aligned with the site. These conditions are easily met in strike-slip faulting, where the fault slip direction is orientated horizontally in the direction along the strike of the fault, and rupture propagated horizontally along the strike either unilaterally or bilaterally. When the rupture propagates away from the site the opposite effect is observed (backward directivity); long duration motions having low amplitudes at long periods (Somerville *et al.*, 1997). An example of directivity for the Landers 1992 earthquake is shown in Figure 2.6.

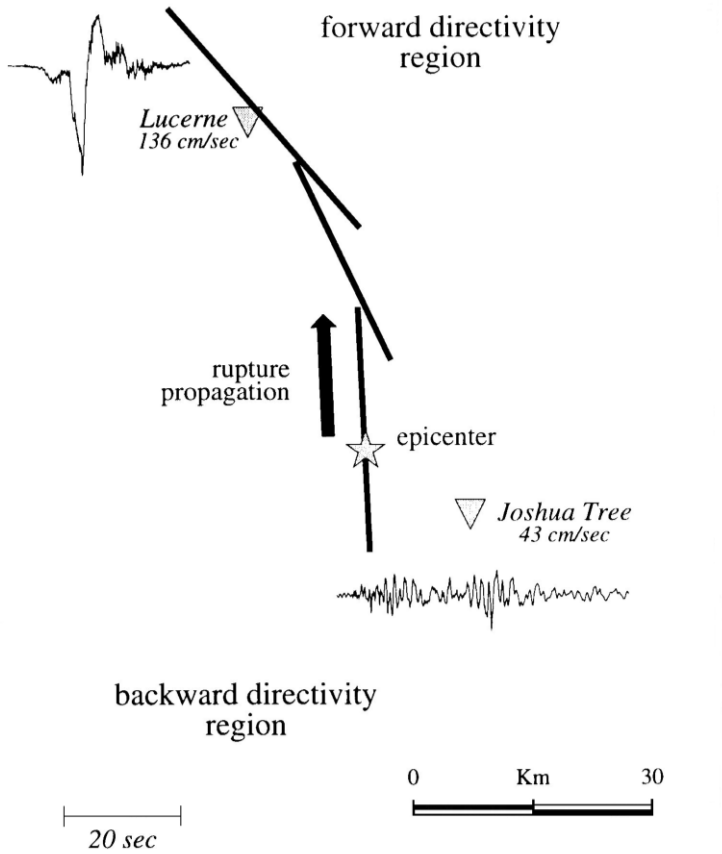

Figure 2.6. Example of directivity effects for the Landers earthquake of the 28th of June of 1992 (Somerville *et al.*, 1997).

Important spatial variation on the ground motion due to directivity effects have been observed in the earthquakes of Landers, California, of 28th of June of 1992 (Bernard & Herrero, 1994; Somerville *et al.*, 1997), Kobe,

Japan of the 16th of January of 1995 (Pitarka *et al.*, 1998), and Bojnurd, Iran of the 4th of February of 1997 (Hollingsworth *et al.*, 2007) among others.

Modifications to ground-motion equations have been developed to account for directivity effects on strong motion amplitudes and duration. Somerville *et al.* (1997) present one of the most known models to incorporate directivity effects in ground-motion prediction equations. Improvements to this model have been presented by Abrahamson (2000a) and more recently by Rowshandel (2006) in order to avoid some practical difficulties of the original model. Spudich & Chiou (2008) have introduced a new models based on a physically-based directivity predictor to be applied to the NGA prediction equations.

Alternative to these factors, empirical relationships for the estimation of PGV and period of the velocity pulse (T_v), considering forward-directivity effects, have been derived (e.g. Bray & Rodriguez-Marek, 2004).

2.4. PSHA calculations

A PSHA for a specific site consists of estimating the annual rate that a ground-motion threshold will be exceeded at a particular location due to future earthquakes. This ground-motion threshold is arbitrarily specified and can be with respect to any ground-motion parameter of interest.

A thorough understanding of PSHA requires knowledge of the basic concepts of probability theory. These concepts are applied through the entire process of the PSHA; first, during the estimation of earthquake-recurrence rates and the spatial distribution of future events and subsequently when, given a magnitude-distance scenario, the probability of the ground-motion threshold being exceeded at the site needs to be estimated.

2.4.1. Fundamentals of Probability for PSHA

Seismic hazard assessment has to grapple with the inherent variability in the location and magnitude of future earthquakes as well as the ground motion induced at a specific site due to the occurrence of an earthquake.

Probability theory deals with the analysis of random phenomena. The central objects of probability theory are random variables, stochastic process and events. In a stochastic process or random process, as opposed to a deterministic process, the outcomes of the process are indeterminate random variables that can be described by probability distributions. In probability theory, stochastic processes are often described, in a general sense, as a series of experiments.

In statistics, the set of all possible outcomes of an experiment is called sample space (Ω), and each element of the sample space is called sample point. Generally, sample spaces are classified as finite, discrete and continuous, according to the number of elements (points) which they contain. A sample space is said to be finite if it has a countable number of elements; it is said to be discrete if it has a countable infinity of elements, for instance, the whole set of natural numbers; finally, if the elements of the sample space represent a continuum, for instance, all the point on a line, the sample space is said to be continuous.

Probabilities are always associated with the occurrence or the non-occurrence of events. Thus, an event is defined as an individual outcome or as a set of outcomes of an experiment. In other words, an event is a subset of the sample space.

Under the frequentist's interpretation of probability, for a finite sample space the probability of an event A, $P(A)$, is defined as the relation between the size of the event A (number of sample points in the subset) and the size of the sample space. This probability is represented by a real number in the range from 0 to 1 (Miller & Freund, 1977).

Again, using the frequentist's interpretation of probability, the probability $P(A)$ is defined in such a way that it satisfies the Kolmogorov axioms. These axioms are:

First axiom. The probability of an event is a non-negative real number.

$$P(A) \geq 0 \quad \forall A \subseteq \Omega \tag{2.8}$$

where Ω is the sample space.

Second axiom. The probability that a certain event in the sample space will occur is 1.

$$P(\Omega) = 1 \tag{2.9}$$

This axiom is commonly neglected in some erroneous probability calculations; if it is not possible to precisely define the whole sample space, then the probability of any subset cannot be defined either.

Third axiom. Any countable sequence of pairwise disjoint events (independent) events A_1, A_2…A_i satisfies:

$$P(A_1 \cup A_2 \cup \ldots) = \sum_i P(A_i) \tag{2.10}$$

These axioms can be used to develop the rules and theorems that comprise the mathematical theory of probability. An important concept in probability theory, which is widely used in PSHA, is the probability of the "complement" of an event. The complement of an event *A* is the event "*not-A*", where *not-A* consists of all sample points in the sample space that does not belong to *A*; its probability is given by $1 - P(A)$.

Two other concepts in probability theory that are also widely used within PSHA are the definitions of the probabilities of independent and mutually exclusive events.

Two events are independent if the occurrence of one event has no bearing on the occurrence of the other event. That is, that the occurrence of

one event makes it neither more nor less probable that the other occurs. Now, if *A* and *B* are independent events of the same sample space their joint probability, this is, the probability of both occurring on a single trial (or experiment), is defined as: $P(A \cap B) = P(A)P(B)$.

If *A* and *B* are not statistically independent the conditional probability of *A* given that *B* had occurred is defined by $P(A \mid B) = P(A \cap B)/P(B)$.

Two events are said to be mutually exclusive (or disjoint) if they share no common sample points. This can be expressed as $A \cap B = \phi$ where ϕ is the null set or empty space. If *A* and *B* are events mutually exclusive then the probability of either occurring is: $P(A \cup B) = P(A) + P(B)$. Now, if the events are not mutually exclusive the probability of either occurring is: $P(A) + P(B) - P(A \cap B)$ (Easton & McColl, 2008).

Any probabilistic calculation must satisfy the Kolmogorov axioms to be valid. In PSHA, and within a logic-tree framework, to fulfil these requirements is not an easy task. For instance, one of the main assumptions in PSHA is that earthquakes in a catalogue are independent events; an assumption that oppose Elastic Rebound Theory (Reid, 1910). Nevertheless, it has been shown that, if only main shocks are considered in the earthquake catalogue, the distribution of their magnitudes is sufficiently close to the Poissonian distribution to treat them as independent events (Knopoff, 1964).

It is as well difficult to assert that all possible future earthquake scenarios are included in a particular PSHA study (collectively exhaustive). However, this does no necessarily invalidate the probabilistic framework underlying PSHA and logic trees, since under the most favourable conditions the weights assigned to the branches of the logic tree can at best be treated as nominal probabilities (Bommer & Scherbaum, 2008).

Another fundamental concept is the probability distribution. Probability distributions describe the probabilities associated with a random

event. The distribution must cover all possible values of the event, while the total probabilities must sum exactly to 1. These distributions can be either discrete distributions, where there are a countable number of discrete outcomes with positive probabilities, or continuous distributions, which describe probabilities of events with values over a continuous range.

Probably the most important distribution in Probability theory, and widely used in PSHA, is the normal or Gaussian distribution, which is defined as:

$$f\left(x \mid \mu, \sigma^2\right) = \frac{1}{\sigma\sqrt{2\pi}} e^{\frac{-1}{2}\left(\frac{x-\mu}{\sigma}\right)^2}, \quad -\infty < x < \infty \qquad 2.11$$

where μ and σ are its mean and standard deviation.

The so-called standard normal distribution is recovered from Equation 2.11 by setting μ = 0 and σ^2 = 1. An arbitrary normal distribution can be converted to a standard normal distribution by scaling and shifting the variable x to $Z = (x-\mu)/\sigma$.

It is important to note that, for continuous distributions, a value of $f(x)$ does not give the probability that the corresponding random variable takes on the value x; in the continuous case probabilities are given by integrals and not by the values of $f(x)$. Thus, the probability that a random variable will take on a value between a and b is given by:

$$P(a < x < b) = F(b) - F(a), \qquad 2.12$$

where $F(x)$ is the probability that a random variable, with a given probability distribution, takes on a value less than or equal to x. $F(x)$ is usually referred as the cumulative distribution function of the random variable (Miller & Freund, 1977). For the case of the standard normal distribution, the cumulative distribution function, represented as $\Phi(z)$, is given by:

$$\Phi(z) = \frac{1}{\sqrt{2\pi}} \int_{-\infty}^{z} e^{\frac{-t^2}{2}} dt \qquad 2.13$$

A controversial topic that commonly arises in PSHA is subjective probability. A subjective probability describes an individual's personal judgement about how likely an event is of occurring. It is not based on any precise computation but is often a reasonable assessment of an expert in the topic. It is frequently referred as "expert opinion". A person's subjective probability of an event describes his/her degree of belief in the event (Easton & McColl, 2008).

In seismic hazard assessment the analyst is often required to use expert opinion when the available information is not good enough to perform a rigorous probabilistic assessment. This is not an exclusive characteristic of PSHA; expert opinion is also widely use in DSHA. Although in DSHA expert opinion usually does not provide a distribution of probabilities over a range of possible outcomes but rather determines a single outcome at which a probability equal to 1 is assigned.

2.4.2. Hazard estimation

The main output of a PSHA is a seismic hazard curve, which describes the annual frequency of exceedance of different values of a selected ground-motion parameter. The basis of the modern PSHA framework was laid out by Esteva (1967) and Cornell (1968). These original efforts were later modified to explicitly incorporate the aleatory variability of the ground-motion (Cornell, 1971).

The basic concept of the computations required to obtain this curve is fairly simple. First a target ground-motion level, *z*, of a ground motion parameter, *Z*, is selected. Subsequently, the probability of exceeding this target value (*z*) is calculated for one of the magnitude-distance scenarios considered in the seismicity model and then multiplied by the probability that that particular scenario would occur. Finally, this probability is

multiplied by the total rate of earthquakes that occur with magnitudes above some minimum magnitude of interest, for the seismic source corresponding to the magnitude-distance scenario. This process is repeated for all possible magnitude-distance scenarios in the seismicity model and the associated rates of each scenario are summed up. When this process is performed for different ground-motion levels a seismic hazard curve can be built up (c.f., McGuire, 2004; Oliveira *et al.*, 2006).

Thus, the average rate of exceedance of a given ground-motion level is given by:

$$\gamma(Z>z)=\sum_{i=1}^{N_{sources}}\nu_i\int_{m_{\min}}^{m_{\max}}\int_{r=0}^{\infty}\int_{\varepsilon=-\infty}^{\infty}f_{mi}(M)\,f_{ri}(r)\,f_{\varepsilon}(\varepsilon)\,P(Z>z\mid M,r,\varepsilon)\,dMdrd\varepsilon \quad 2.14$$

where $P(Z>z\mid M,r,\varepsilon)$ is obtained from the ground-motion model, $f_{mi}(M)$, $f_{ri}(r)$ and $f_{\varepsilon}(\varepsilon)$ are the probability density functions for magnitude and distance, respectively, ε is the number of standard deviations in the ground-motion model required to reach the target ground motion given a particular magnitude and distance, and ν_i is the earthquake occurrence rate of events with magnitudes equal to or greater than m_{min} for source i. Note that this formulation is strictly relevant when dimensionless ruptures are considered only.

Events with magnitude below m_{min} are regarded as not capable of producing ground motions that could cause damage to engineered structures. The value of m_{min} used for the integration process may, and normally will, differ from the minimum magnitude used to estimate the recurrence parameters during the seismicity analysis (see section 2.2).

All of the variables represented in the form of probability distributions in the integrals of Equation 2.14 are random variables. That is, they represent aleatory variability that, in principle, cannot be reduced through the acquisition of additional data or improved theories. The seismic hazard

analysis integrates over these variabilities and the shape of the seismic hazard curve (i.e., annual frequencies of exceedance for fixed ground-motion levels) reflects them.

An important discussion is still going on whether the integration process should be truncated at a given value of ε, or ground-motion level, or not (Bommer *et al.*, 2004). However, no empirical basis have been found to support any attempt to truncate the hazard integration at a given threshold (Strasser *et al.*, 2008).

2.4.3. Treatment of site response

The geological and geotechnical conditions underlying a site can exert a strong influence on the resulting ground motions at surface level. In some cases these conditions have a very important contribution to the amplification of ground-motion to the point that they can completely dominate the hazard (Bommer, 2005). A typical example of site effects is the response of the lacustrine clays of the valley of Mexico City that, on the 19th of September 1985, were excited by an earthquake that nucleated on the pacific coast of Mexico, 400 km from Mexico City, and caused great destruction due to site effects.

Site conditions are commonly included in PSHA through the use of ground-motion prediction equations that take into consideration (in a very crude way) the surficial geological conditions at the site. Most of these equations use a broad and qualitative classification of the soil condition, in the best case, site conditions are represented by the average shear-wave velocity over the upper 30m of the soil deposit (see section 2.3). This method is the most simple to apply and probably the most common when the site conditions are not expected to be a critical factor in the ground motion at surface level or when the PSHA is developed for an area or region. For instance, when constructing seismic hazard maps.

An alternative approach to incorporating site conditions into PSHA is by first performing the hazard analysis for some reference site condition, for example “rock” site conditions, and then transforming these results into those for a specific site condition.

One approach for performing these transformations is to multiply the ground-motion amplitudes for rock conditions by an amplification function obtained from a site-specific site-response analysis. There are numerous techniques available in the literature to perform site response analysis in order to obtain the amplification function for a specific site. Thus, the spectral amplitude at the surface (soil conditions) is given by:

$$Sa_s(T) = AF(T)Sa_r(T), \qquad 2.15$$

where $AF(T)$ is the frequency dependent amplification function at a period T and $Sa_s(T)$ and $Sa_r(T)$ are the spectral amplitudes for soil and rock conditions, respectively.

The amplification function obtained from a site response analysis should present median values of amplification as well as the variability associated with the median amplifications. Nevertheless, it is current practice to ignore the variability of the amplification function and only use the median value in estimating the surface (soil) spectral amplitudes. However, uncertainties in the soil response should be explicitly considered in the analysis.

There are a limited number of techniques available in the literature for handling this problem. McGuire *et al.* (2002) proposed that for a rock UHS at any return period, the soil amplitudes corresponding to that UHS can be estimated as:

$$a^{s}{}_{rp} = a_{rp}\,\overline{AF}_{rp}\exp\left[\frac{0.5K_H\sigma^2{}_{\delta}}{(1-K_{AF})^2}\right] \qquad 2.16$$

where a^s_{rp} is the amplitude of the ground-motion on soil (at a given period, T) for return period *rp*, a_{rp} is the corresponding rock amplitude, $\overline{AF}_{rp}$ is the mean soil amplification factor (soil amplitude/rock amplitude) for rock motions with amplitude a_{rp}, K_H is the (negative) log-log slope of the rock hazard curve, K_{AF} is the (negative) log-log slope of the soil amplification versus rock amplitude, and σ_δ is the logarithmic standard deviation of the soil amplification function.

Alternatively, Bazzurro & Cornell (2004) propose two different approaches for performing a fully probabilistic analysis. These approaches are referred to as the convolution method and the soil-specific attenuation equation method.

The convolution method estimates the hazard curves for the specific site condition by convolving the hazard curve for rock conditions, obtained from a PSHA or by hazard maps, with the probability distribution function of the amplification function. The hazard curve for the surface is then obtained from:

$$G_Z(z) = \sum_{allx_j} P\left[Y \geq \frac{Z}{X} \mid x_j \right] p_X\left(x_j\right) \qquad 2.17$$

where $G_Z(z)$ is the hazard curve for ground motions at the surface, $Z = S_a^s(T)$ and $X = S_a^r(T)$ are the spectral amplitudes (at a given period) at the surface and on rock, respectively, Y is the amplification function $AF(T)$, and $p_X\left(x_j\right)$ represents the probability that the rock-input level is equal to x_j.

The soil-specific attenuation method consists in producing an attenuation equation for a particular soil condition or site of interest. This approach requires a considerable number of time-history accelerations to be driven through a model of the soil profile, making it in this way, tedious and complicated to implement.

The median value of the surface spectral acceleration using this approach is given by the expression:

$$\ln S_a^s(f) \approx c_0 + (c_1+1)\ln \tilde{S}_a^r(f) + (c_1+1)\varepsilon_{\ln S_a^r(f)}\sigma_{\ln S_a^r(f)} + \varepsilon_{\ln AF(f)}\sigma_{\ln AF(f)} \quad 2.18$$

Where c_0 and c_1 are coefficients of the linear regression in logarithmic space of $AF(f)$ on $S_a^r(f)$, $\ln \tilde{S}_a^r(f)$ is the median of $\ln S_a^r(f)$, $\varepsilon_{\ln AF(f)}$ is a standard normal variable, and $\sigma_{\ln AF(f)}$ represents the standard error of estimation.

The number of approaches to incorporate site response into seismic hazard analysis has increased in the last decades, and many other techniques to those here presented are available in literature.

2.4.4. Representation of seismic hazard

The results of PSHA can be expressed in many different ways. The most common is through seismic hazard curves. As an alternative to the typical representation of the seismic hazard curves, annual frequency of exceedance vs. ground-motion level, the hazard curves also can be represented in terms of return period or as function of the probability of exceedance within a fixed period of time (Figure 2.7).

A hazard curve provides a convenient way to determine the design level of a particular ground-motion parameter for different return periods or probabilities of exceedance. Hazard curves suggests that the hazard at a particular site is a smoothly varying function with the time of exposure, hence the longer a project is exposed at the site, the greater will be the level of the expected ground motion. This is correct in so far as it becomes more likely that stronger levels of ground motion will occur at the site over long rather than short periods of exposure. However, the real hazard at a site during a real time of exposure is not a smoothly varying function but a step function. The real hazard of shaking at the site will be due to a finite number of real earthquakes, each with a particular recurrence interval and each producing particular levels of shaking at the site. In this sense, a hazard

curve is not very informative regarding ground motions that may be expected to occur at the site; it only represents ground motions with specified return periods according to the seismicity models and the ground-motion attenuation in the region (Bommer, 2005).

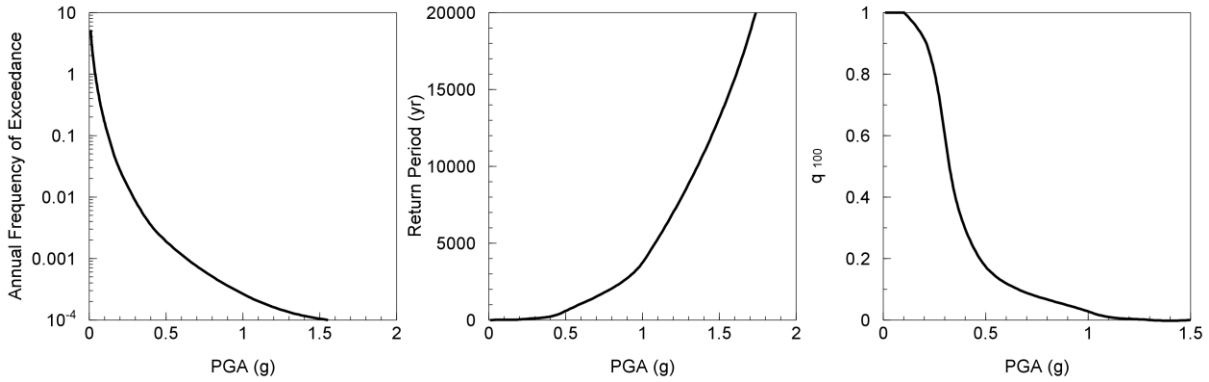

Figure 2.7. Alternative representations of seismic hazard curves for a specific site. From left to right the seismic hazard curve is expressed as function of the annual frequency of exceedance, as function of return period and as function of the probability of exceedance within a fixed period of time, for example 100 years, (q_{100}).

Another way to represent seismic hazard is through seismic hazard maps or seismic zonation maps. Seismic hazard maps show the variation in seismic hazard over a particular region. These types of map are constructed by carrying out hazard assessments at a large number of locations within the region under study, for example at the nodes of a grid covering the whole region. The seismic hazard at any other point in the region is obtained through interpolation and thus contours of equal ground motion values are drawn for a given return period. Seismic hazard maps must be constructed for a single ground-motion parameter and for a preselected return period or probability of exceedance. Most maps that have been developed have been for PGA at a return period of 475 years. Although the use of other return periods is not uncommon, the mapping of other ground-motion parameters rather than PGA is still not a common practice.

Seismic zonation maps are a simplified version of the seismic hazard maps and their objective is to define broad areas within which seismic

hazard can be assumed to be uniform. These types of map are particularly useful for seismic building codes and land-use regulations.

Nowadays most areas of the world are covered by regional or national seismic hazard maps. In 1992 the Global Seismic Hazard Assessment Project (GSHAP) was launched within the framework of the United Nations International Decade for Natural Disaster Reduction (UN/IDNDR). The aim of this project was to create a worldwide seismic hazard map and four regional maps through a compilation of independent studies developed for many regions around the world. All maps were created for PGA values corresponding to a 10% probability of exceedance in 50 years (Giardini, 1999).

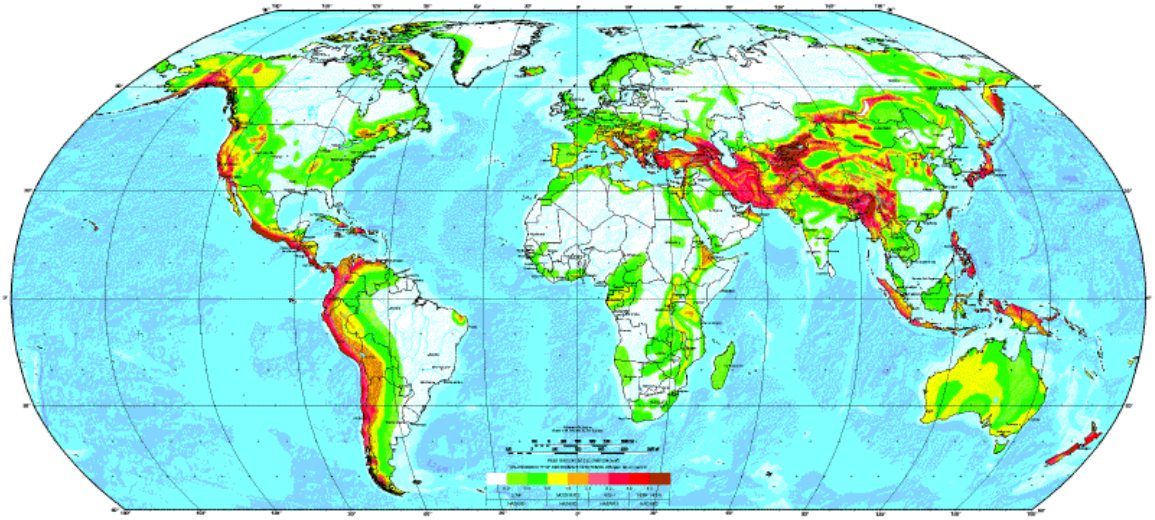

Figure 2.8. The GSHAP global seismic hazard map. Developed for PGA with a 10% chance of exceedance in 50 years, corresponding to a return period of 475 years (Giardini *et al.*, 1999).

An additional manner to represent seismic hazard, which is widely used in seismic design, is the response spectrum. There are two different approaches to obtaining a response spectrum as an output of a PSHA. The most computationally efficient approach, and that which is often used in seismic design codes is to calculate seismic hazard in terms of PGA and then

to anchor a standard spectral shape, which is defined according to geological site conditions, to this reference PGA. Approximations to uniform hazard spectra (UHS) obtained in this way have significant limitations as they does not take into account the variation in the shape of the spectrum with magnitude and distance (Ambraseys *et al.*, 1996). Additionally, the only ordinate at which the return period is actually known is at zero period (PGA), at any other response period it is unknown (McGuire, 1977). Hence, a response spectrum obtained in this way does not guarantee that the hazard will be uniform all over the spectrum.

An improvement to this approach is to obtain a uniform hazard spectrum by performing the hazard assessment multiple times and obtaining PGA and the spectral amplitudes (SA) corresponding to each response period for the desired return period. Design spectra obtained in this way are legitimately called uniform hazard spectra since the hazard level is genuinely uniform across the entire range of periods. Figure 2.9 shows the process to construct a UHS from the seismic hazard curves for different response periods.

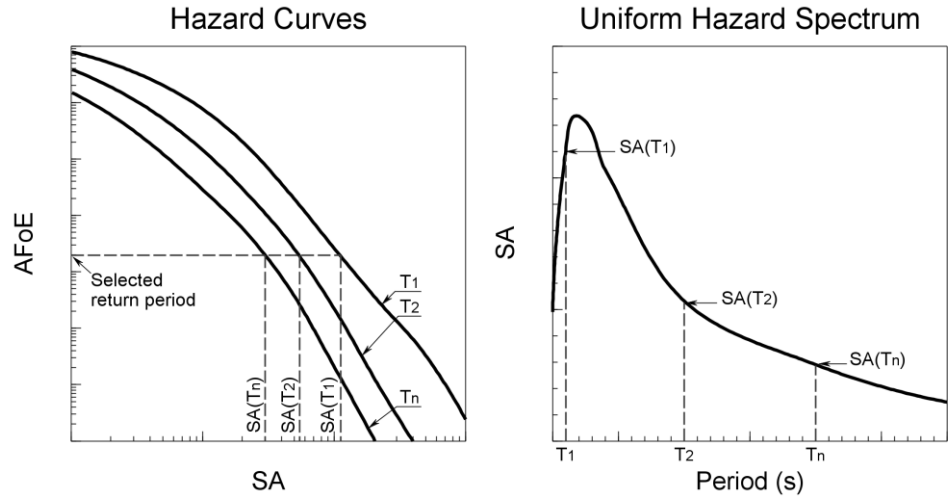

Figure 2.9. Process of constructing a uniform hazard spectrum from seismic hazard curves for different response periods.

A very useful way to represent seismic hazard is through plots showing the contribution to the hazard at the site for couples of magnitude and distance values. These plots are the disaggregated representation of the results of a seismic hazard analysis. Due to the importance of disaggregation in PSHA it is treated independently in the following section.

2.4.5. Disaggregation

As described in section 2.4.2, a seismic hazard curve is calculated as the integration (aggregation) of the hazard from all magnitude-distance scenarios considered possible of occurring in the future; as defined by the seismicity model. In this manner, the rate of exceedance represented by the hazard curve is not associated with any particular earthquake magnitude or source-to-site distance (Kramer, 1996).

However, it is useful to know how different magnitude-distance, and some times epsilon (ε), scenarios contribute to the total hazard for a specified ground-motion level. Where, epsilon is the number of standard deviations that the target ground motion is from the median ground motion as predicted by a GMPE.

The process of obtaining the rates of exceedance expressed in the hazard curve into rates of exceedance in terms of magnitude-distance scenarios is called disaggregation. Some authors prefer to use the word deaggregation, but this is just a matter of semantics. In computational terms, this process simply involves the reordering of terms in Equation 2.14. Thus, the rate of exceedance of a given ground-motion level for a particular magnitude-distance scenario is given by:

$$\gamma\left(Z > z \mid m_j, r_k\right) = \sum_{i=1}^{N_{sources}} \nu_i P\left(M = m_j\right) P\left(R = r_k\right) \int_{\varepsilon=-\infty}^{\infty} f_\varepsilon\left(\varepsilon\right) P\left(Z > z \mid m_j, r_k, \varepsilon\right) d\varepsilon \quad 2.19$$

where $P\left(M = m_j\right)$ and $P\left(R = r_k\right)$ are the probabilities of an event occurring in the i^{th} seismic source with magnitude M at a distance from the site R,

respectively, and $P\left(Z > z \mid m_j, r_k, \varepsilon\right)$ is obtained from the ground motion model.

Disaggregated results are usually presented in terms of magnitude-distance scenarios, but other representations such as contributions by seismic source, can be useful as well. Bazzurro & Cornell (1999) present a comprehensive review of the seismic hazard disaggregation procedures available in the literature at that time. They also examine how different assumptions made during the disaggregation process, and issues regarding the particular binning scheme that is used, affect the results.

Disaggregated representations of seismic hazard are useful for having a clear definition of the specific earthquake scenarios that contribute most to the hazard at a given site. Furthermore, secondary parameters for design, such as duration of the strong motion, can be derived and accelerations time-histories can be selected based on the dominant magnitude-distance scenarios. Ground-motion parameters or acceleration time-histories, real, synthetic or artificial, obtained in this way are in some sense compatible with a specific probability of occurrence.

2.5. Logic trees

Logic trees were originally introduced as a tool for treating epistemic uncertainties when performing SHA by Kulkarni *et al.* (1984). Nowadays, logic trees are widely used for seismic hazard analysis and have become a standard feature of PSHA (Bommer *et al.*, 2005).

As discussed in section 2.4.2, PSHA incorporates aleatory variability directly into the calculations of the annual frequencies of exceedance. On the other hand, epistemic uncertainties are treated through a logic tree, where each node represents an element of epistemic uncertainty and the branches extending from each node are the different discrete options that reflect the uncertainty through alternative possibilities. It is of common practice to

place nodes representing assumptions, models or parameters that do not depend on others on the left, while those nodes which are dependent of others are placed to the right. This is done in order to have the sections of the logic tree in the order of execution; however, it is irrelevant to set the logic tree from right to left or from top to bottom or vice versa, what matters is to keep the logical sequence of the different steps throughout all branches of the logic tree.

One of the requirements of logic-tree branches is that they, in theory, must be mutually exclusive and collectively exhaustive (Bommer & Scherbaum, 2008). For each branch added to the logic tree a cost in terms of additional calculations is paid and the total number of calculations can rapidly become very large. Hence, it is advisable to avoid the use of branches representing options with very small difference (Bommer *et al.*, 2005).

To satisfy the conditions of mutual exclusivity and collective exhaustiveness in the branches is in principle impossible. However, this does not necessarily invalidate the underlying probabilistic framework but that under the most favourable conditions the weights assigned to each of the logic-tree branches can be treated as approximate probabilities (Bommer & Scherbaum, 2008).

Once the logic tree has been set up, weights representing the confidence of the analyst (subjective probabilities) on each branch are assigned. For example, if two different ground-motion attenuation equations are used and the analyst has twice the confidence that equation 1 will better model the seismic attenuation in the region he or she could assign a confidence of 10 to equation 2 and 20 to equation 1. For practicality these weights are usually assigned in such a way that the sum of them, at each node, is equal to one.

In order to illustrate the setting up of a logic tree, a schematic logic tree is shown in Figure 2.10. This logic tree addresses three different

epistemic uncertainties which are commonly faced in practice: earthquake rupture model, slip rate estimation and ground-motion prediction equation. In this example, the first of these uncertainties has two nodes; the first of them considering two alternatives, a non-segmented and a segmented rupture of the fault, sub-dividing the latter in two possible scenarios.

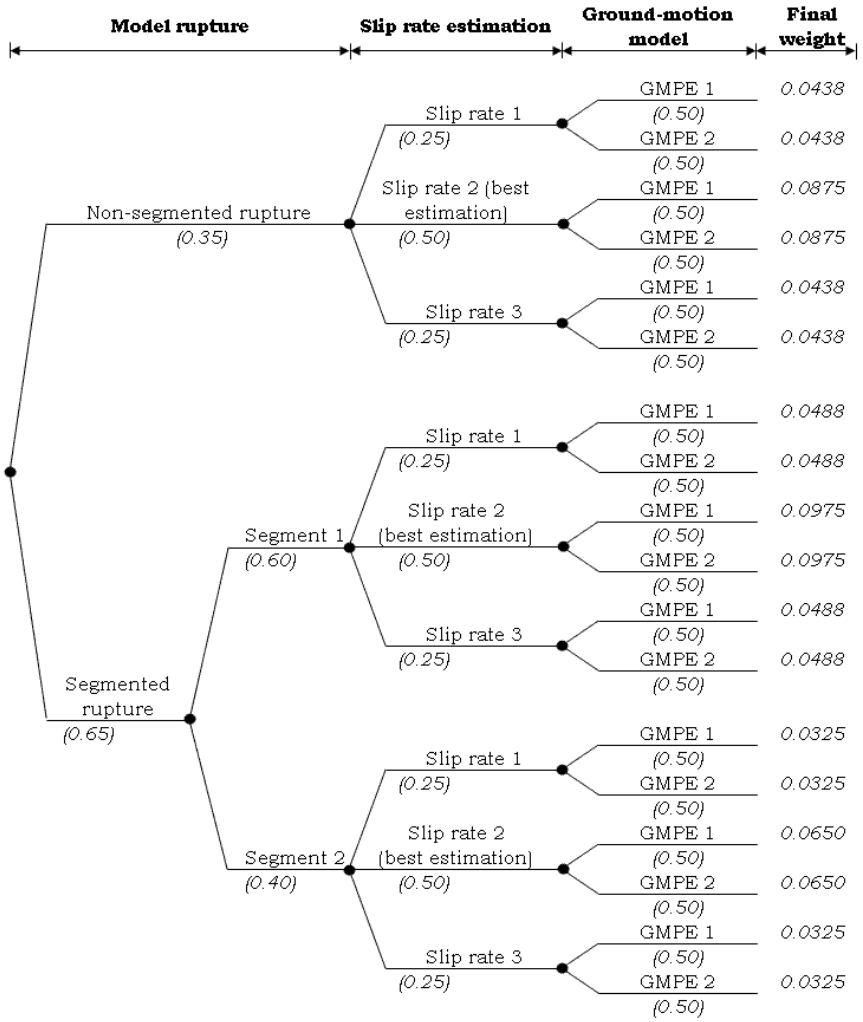

Figure 2.10. Schematic logic tree for a hypothetical case with four levels of epistemic uncertainties, two for the rupture model, one for slip rate and one for the ground-motion model. Black dots are the nodes of the logic tree representing epistemic uncertainties and each branch growing from them represents the different discrete options for that uncertainty. Italic numbers in brackets are the assigned weights representing the analyst's degree-of-belief in that option. Italic numbers in the right hand side are the final weights for each tip of the logic tree.

It is a common pitfall when setting up branches for different rupture models to consider only one node with different branches, one branch for the

non-segmented rupture model and additional branch for each different segmentation model. This violates the principle of mutual exclusivity since the occurrence of a non-segmented rupture would imply that all the segments of the fault would rupture at the same time (Abrahamson, 2000b).

The second of the uncertainties, slip ratio estimation, presents a common situation where the weights are centered on a best estimate. This is the case, for instance, for slip rates, where commonly a set of estimated values is reported but some tendency to a central value can be observed. In this case the analyst may give a higher weight to the central value and lower weights to the upper and lower values of the set of slip rates reported.

Finally, the third uncertainty in this example, ground-motion model, is the most common source of uncertainty that the analyst has to face and the one that incorporates the highest levels of epistemic uncertainty in PSHA (see Figure 2.11). Regarding ground-motion models in logic trees, it is common to find uniform weights on branches for different ground-motion models representing equal levels of confidence of the analyst on the different options. However, as it was previously discussed, if the weights assigned to each branch are considered as being subjective probabilities then uniform weights would represent an equi-probability distribution. However, if it is the analyst's belief that one of the equations represents the seismic attenuation in the region better than the other(s) a higher weight must be assigned to it.

Frequently, great attention is given to the weights assigned to the logic-tree branches regarding different GMPEs; however, once there are more than a few branches the hazard is almost insensitive to the weighting process. Of greater impact is the selection of the GMPEs themselves rather than the relative weights assigned to the models (Sabetta *et al.*, 2005; Scherbaum *et al.*, 2005).

The use of a logic tree to assess epistemic uncertainties has many benefits and is technically easy to implement. The most important benefit of

using logic trees is that they help to organise one's thinking where alternative models or interpretations might apply.

However, many dangers can arise from the misuse of logic trees. One of them is the trivialization of the weighting of the branches that could obscure the effort that has been done on the assessment of the value assigned to a particular branch. Additionally, careful considerations must be made to ensure compatibility among the models employed at each of the different branches; for example when using alternative ground-motion models with different distance definitions (Bommer *et al.*, 2005).

In the view of how PSHA is employed in current engineering practice, different interpretations of the logic-tree outputs have been proposed in recent years (c.f., Abrahamson & Bommer, 2005; McGuire *et al.*, 2005; Musson, 2005). An overview of these proposals is presented in section 2.5.3.

2.5.1. Epistemic uncertainties

Although philosophers of science as a whole have not found a satisfying definition for the different types of uncertainties and the best approach to assess them, contemporary practice on PSHA divides uncertainties in two groups: aleatory variability and epistemic uncertainty. Aleatory variability, also known as random variability, is that related to the occurrence of an uncertain event in repeated trials or experimental sampling of the outcome. In other words, it is the uncertainty that arise because the system under study can potentially behave in many different ways (natural randomness). Aleatory variability, in principle, cannot be reduced through the increase of knowledge (Bommer & Scherbaum, 2008).

Epistemic uncertainty, on the other hand, is that related to the belief or confidence in the outcome of an uncertain event, given the state of knowledge at the time it is assessed. In other words, it is the uncertainty related to the lack of knowledge regarding a specific event (Helton &

Oberkampf, 2004; Vick, 2002). Epistemic uncertainty is expected to decrease with time as the amount of relevant data increases and a better understanding of the uncertain event is acquired.

As was previously mentioned, in a logic-tree framework, epistemic uncertainties are represented by the nodes and branches of the tree, and the weight assigned to each branch represents the analyst's degree of believe or conviction in the outcome. The degree-of-belief allows the analyst to incorporate the full range of understanding that he or she possess in ways that correspond to how he or she actually thinks. The treatment of this degree-of-belief that the analyst has for each of the considered possibilities, typically described as "weights", as subjective probabilities is merely a pragmatic matter. The justification for this lies in the purposes of probability, which is to communicate uncertainty to others, and to communicate uncertainties associated with events that have not been or cannot be evaluated directly it is required to quantify these uncertainties in numerical form (Vick, 2002).

One of the problems that underlies this approach is that the knowledge and/or opinion of a single analyst will almost certainly not be sufficiently refined to characterize all the epistemic uncertainties (Helton & Oberkampf, 2004). Given this, identification of the epistemic uncertainties to be considered in the logic-tree framework must be the result of a multidisciplinary work with the aim of identifying the uncertainties with the most influence on the seismic hazard and to correctly assess the weight that should be assigned to each branch.

As Helton & Oberkampf (2004) comment on an old cartoon showing two geologist fighting in front of a rock outcrop, where the caption says "*One rock, two geologist, three opinions*", different experts could have, and in fact will have, different opinions about the same event, giving with this different set of assumptions that may be appropriate to consider as an epistemic

uncertainty into the logic tree. In order to cover all possible outcomes of an epistemic uncertainty the opinions of all different experts must be considered and weighted in the process of setting up the logic tree.

The selection of the ground-motion prediction equation is the source of epistemic uncertainty that exerts the greater influence on the results of PSHA (Toro, 2006). In Figure 2.11 it is clearly shown how the prediction of the median ground motion is the main contributor to the total uncertainty in PSHA.

The most important issue regarding uncertainty in PSHA is to make sure all sources of uncertainty, whether they are defined as aleatory or epistemic, are included and are clearly traceable through the hazard estimation process.

It is important to properly differentiate between aleatory and epistemic uncertainties as aleatory variability is integrated into the hazard curves directly and contributes to the shape of the curves, while epistemic uncertainties lead to alternative hazard curves. Therefore, the distribution corresponding to the full suite of hazard curves captures both aleatory and epistemic uncertainties. However, the differentiation between aleatory and epistemic uncertainties may not always be free of ambiguity (Bommer & Scherbaum, 2008).

An extreme hypothesis regarding epistemic uncertainty is the Laplacian view that the world is completely deterministic; under this hypothesis all uncertainty is epistemic. Even under this assumption it is pragmatically convenient to treat the world as if some uncertainties are not due to limited knowledge but are actually random when enough information is available to determine a probability distribution (McGuire *et al.*, 2005). In any case, probability might still be a good representation of epistemic uncertainty under the understanding that we may not be able to determine the probabilities perfectly.

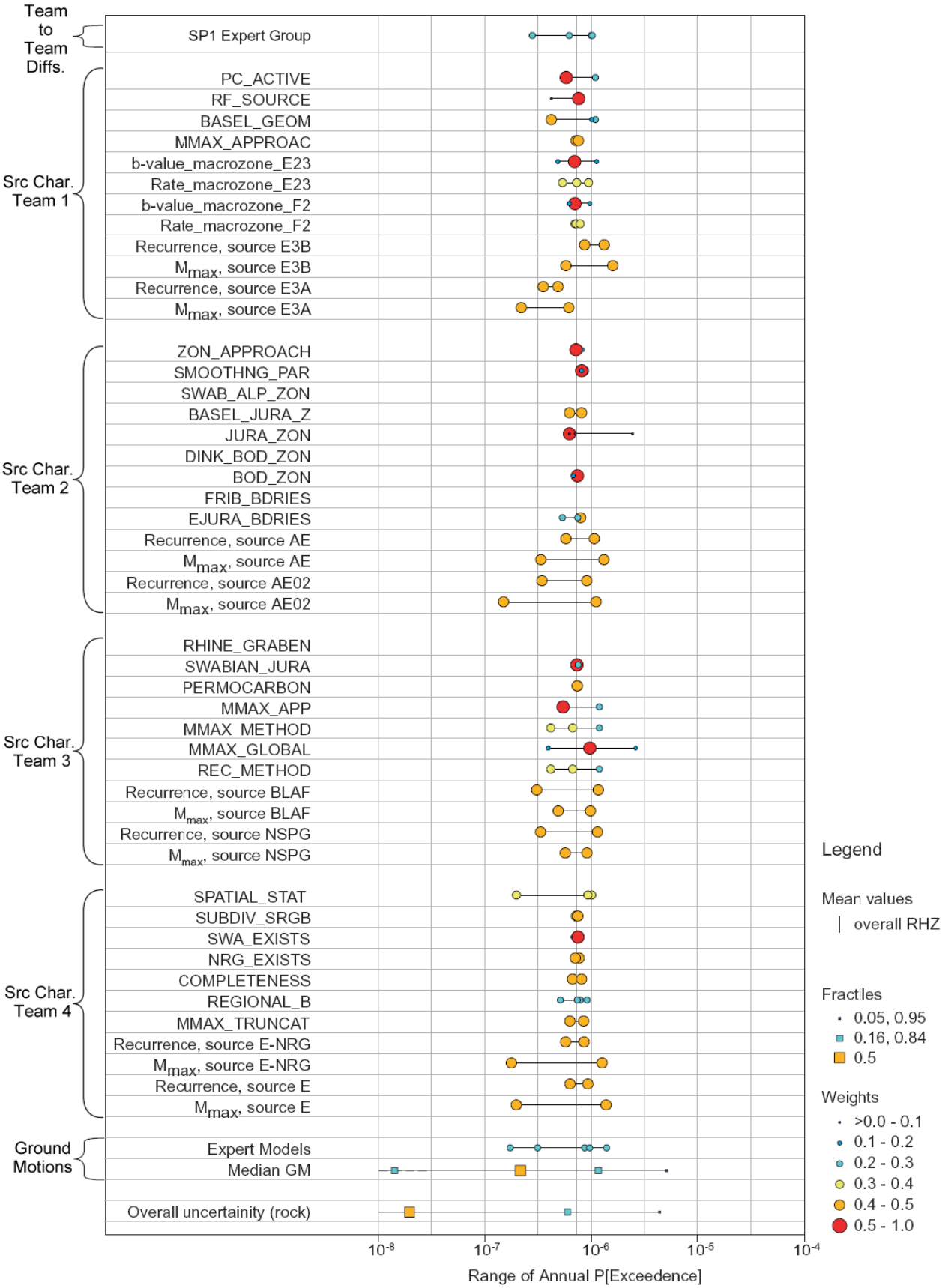

Figure 2.11. Sensitivity analysis of PSHA results from the PEGASOS project comparing relative contributions to the variation in hazard estimates from uncertainty in the seismicity models, as presented by four different source characterisation teams, and uncertainty in the ground-motion models (Toro, 2006).

2.5.2. Compatibility of ground-motion prediction equations

Commonly, logic trees require the combination of ground-motion models which are rarely uniform in terms of definitions of the independent variables such as distance and magnitude scale, and the predictive variable (e.g., horizontal component of motion). A wide variety of independent and predictive variable definitions can be found in literature (e.g., Douglas, 2003b, 2004).

With the aim of making the different ground-motion models assigned to each branch of the logic tree compatible, adjustments need to be made. Failure to make such conversions can result in an appreciable misrepresentation of the epistemic uncertainty (Bommer *et al.*, 2005; Sabetta *et al.*, 2005). However, as result of these adjustments a large penalty due to propagation of uncertainty can be paid, with values of standard deviation in the ground-motion models potentially becoming so large that they cannot be used for practical purposes (Scherbaum *et al.*, 2006).

Most of the conversions required to address the incompatibility of the parameters are themselves empirical correlations carrying an associated aleatory variability (and epistemic uncertainty) that must be carried across into the aleatory variability of the GMPEs. To carry this variability into the $\sigma[\log(Y)]$ of the ground-motion prediction equation the following expression should be used (Bommer *et al.*, 2005):

$$\sigma^2_{Total} = \sqrt{\sigma^2_{\log(Y)} + \left(\frac{\partial \log(Y)}{\partial X}\right)^2 \sigma^2_x}\,, \qquad 2.20$$

where X is the independent variable to be adjusted with an associated measure of aleatory variability σ_x, and Y is the predictive variable of the ground-motion equation.

The independent and predictive parameters in the GMPEs that must be checked to ensure compatibility are: magnitude scale, distance, site

condition (or alternatively V_{s30}), style-of-faulting, horizontal component of motion and potentially others.

The compatibility with respect to magnitude scale must not only be between the GMPEs but also between the ground-motion models and the magnitude used for the seismicity model. A large number of empirical relationships to convert from one magnitude scale to another are available (e.g., Ambraseys & Bommer, 1990; Ambraseys & Free, 1997; Karnik, 1973; Scordilis, 2006). Some of these equations have been derived for specific regions and these should be preferred when the hazard analysis is performed for that region (e.g. Ambraseys & Free, 1997).

The distance definition is probably the most important incompatibility between GMPEs (Bommer *et al.*, 2005). Scherbaum *et al.* (2004b) present relations to convert the most popular metric distance definitions to the Joyner-Boore distance (r_{jb}). These relations are magnitude and distance dependent with an associated aleatory variability. This is an important issue as it will cause an increase on variability of the "modified" ground-motion model and cause the aleatory variability to become both magnitude and distance dependent, even if they were not in the original model. For these reasons, conversions using the Scherbaum *et al.*, (2004b) relationships should be avoided, and in fact they would not be necessary is PSHA is done properly. It is important noting that, as these conversions are magnitude dependent, it is necessary to keep in mind that the order in which the conversions are made matters. Any required magnitude conversion must be applied before applying the distance conversion.

The use of different distance definitions more than a real problem of compatibility is a shortage on the most software used to perform PSHA. Software such as SEISRISK (Bender & Perkins, 1987) and EZ-FRISK (McGuire, 1997) implicitly consider for the hazard analysis the epicentral distance (r_{epi}) regardless of the ground-motion prediction equation that is

assigned to each of the seismic sources. This situation can be solved with the use of software such as CRISIS2007 (Ordaz *et al.*, 2007) that calculates the appropriate distance, for the most commonly used distance definitions, depending on the ground-motion model used for the analysis. In this way, the correction for distance definition is unnecessary.

It is also worth noting that, if different distance definitions are used in the hazard analysis, for disaggregation proposes only a single distance definition must be considered. This would imply either, two distance definitions are calculated by the software during the analysis, one required by the GMPE and other to present the disaggregated results, or corrections must be applied to the disaggregated results of neighbouring branches to make them compatible.

One of the independent variables that GMPEs invariably include is site conditions. In most of the equations this factor is present as an explanatory variable for fixed site conditions, which generally are: rock, stiff soil and soft soil and in some occasions, hard rock. Only a few GMPEs explicitly include the shear-wave velocity in the uppermost 30m (V_{s30}) as an independent variable (see section 2.3.2).

In most of the cases, only a wide range of V_{s30} is known for a given site condition, hence to make conversions to a fixed V_{s30} value could be complicated. Bommer *et al.* (2005) suggest two different approaches to make conversions to a pre-defined V_{s30} value. The first is using factors derived from ground-motion models that predict PGA or spectral ordinates as function of V_{s30} values and which can be used therefore to infer ratios between sites of different V_{s30}. The second consists of performing a proper site-response analysis using generic rock models with V_{s30} as a single parameter or using real shear-wave velocity profiles. For practical proposes, GMPEs with site-condition definitions corresponding to similar range of V_{s30} values are considered to be compatibles.

One of the most common explanatory variables included in ground-motion models, after magnitude, distance and site conditions, is the style-of-faulting. Bommer *et al.* (2003) present a methodology to adjust for style-of-faulting ground-motion predictions made with equations that do not consider this as an explanatory variable. This methodology take into account the three basic faulting mechanisms, normal, reverse and strike-slip.

Since adjusting a GMPE for style-of-faulting implies the inclusion of an additional predictive variable, in a strict sense, a reduction in the aleatory variability would be expected. However, this reduction is likely to be too small to make the adjustment of $\sigma[\log(Y)]$ necessary (Bommer *et al.*, 2005).

The most common predictor variables in GMPEs are: the horizontal peaks of acceleration and velocity, and the peak horizontal response spectral ordinates. However, there are many alternative definitions for the horizontal component of motion based on different treatments of the two horizontal traces from an accelerogram.

since there are many ways to treat the two horizontal components of motion from an accelerogram, there are also many definitions of these components.

Beyer & Bommer (2006) present relationships between the median values and aleatory variabilities for different horizontal-component definitions and the geometric mean of the two horizontal components. Most of the horizontal component definitions considered in Beyer & Bommer's (2006) work present correlations on the median values with the geometric mean equal to one. Only the larger PGA (larger component), MaxD (maximum spectral ordinate) and Env_{xy} (Envelope of x and y spectra) presented ratios greater than one. These conversions, as for the previous ones, lead to an increase of the aleatory variability of the "modified" ground-motion equation.

2.5.3. Mean vs. Median, G-M vs. Hazard

The outcome of PSHA performed through a logic-tree framework is a set of seismic hazard curves that the engineer has to consider in order to come up with a ground-motion value to be employed in seismic design. Here, the question that arises is which of the curves should be used?

In current engineering practice, and for design purposes, a single hazard curve is obtained as the weighted mean of the set of hazard curves in the rate domain (for fixed values of ground motion) and from this, according to the pre-selected return period, read the value of ground motion to be used for seismic design. The decision of which return period to use is based on what level of seismic safety is required. Most of the seismic design codes worldwide use the value of 475 years (10% chance of exceedance in 50 years).

An alternative proposal to obtain a single hazard curve from the set of curves resulting from a PSHA performed within a logic-tree framework is to consider the hazard curve corresponding to a particular fractile instead of the weighted mean. Abrahamson & Bommer (2005) have suggested using the 85^{th} fractile for critical projects and values as low as the median for non critical projects. Abrahamson & Bommer (2005) assert that when choosing a hazard curve in this way, the fractile would reflect the degree of confidence that the safety level implied by the selected return period will be achieved in the light of the uncertainty in the estimation of the hazard.

This position has been argued by McGuire *et al.* (2005) and Musson (2005) who defend that, for seismic design proposes, only the weighted mean and not any fractile must be used as it is the only statistical estimator that represents the “expected value”. These authors state that the median or any other fractile should be used only to represent the scatter of the set of hazard curves due to epistemic uncertainty.

Regardless of which summary statistic is used to obtain a single curve, two different perspectives could apply. One can either obtain the weighted mean value of the annual rate of exceedance (or any desired fractile) for fixed values of a ground motion or of ground motions for fixed values of exceedance probability (Bommer & Scherbaum, 2008). As mentioned above, the common practice is to obtain the weighted-mean hazard curve for fixed values of ground motion, since hazard curves are calculated in this way (see section 2.4.2); otherwise, to obtain the hazard curve for fixed values of exceedance probability interpolation will be required.

Any of these approaches could be applied depending on which is one's interest. The first approach would apply when the interest is to know the expected exceedance rate of a fixed value of ground motion. On the other hand, if one wants to know the expected value of ground motion for a fixed exceedance rate (return period), the second approach would apply.

In current practice, first a value of exceedance probability is selected and from it a value of ground motion is read from the hazard curve. Hence, it could be argued that the logical choice would be to use the weighted-mean hazard curve for fixed values of return period (Bommer & Scherbaum, 2008).

All these different approaches can lead to significantly different hazard curves. These differences do not have serious implications at the return periods generally considered for typical engineering projects (500 to 2500 years), but when ground-motion levels at very long return periods are required the differences become important (Abrahamson & Bommer, 2005; Bommer & Scherbaum, 2008). Considering all this, decisions must be taken to select the hazard curve that better represents the hazard according to the requirements of the project.

Chapter 3.

CASE STUDY, PSHA FOR THE UNITED ARAB EMIRATES

In this chapter a probabilistic seismic hazard assessment (PSHA) performed for three cities in the United Arab Emirates is presented as a case study. This study was carried out with two key objectives; (1) to assess the seismic hazard in three of the most important cities of the UAE and (2) to establish a point of reference for conducting further sensitivity analyses.

Historically the seismicity in the northeast of the Arabian Peninsula and particularly in the United Arab Emirates (UAE) has been relatively low, with very few historic reports of earthquakes having been felt in the region (Ambraseys & Melville, 1982; Ambraseys *et al.*, 1994). This might be, at least partly, due to the low population of the region. However, even at present, detection and location of small events in this region is not particularly reliable due to the lack of a national seismic network operating in the UAE. Nonetheless, the first seismic network was expected to be in operation during the first half of 2006 (UAEInteract.com, 2005).

There are similar issues associated with limited data regarding the geology and tectonics in both the UAE and the Oman Mountains. The scarcity of information on faults, including length, slip rate and faulting mechanism generates large uncertainties on the characterisation of seismic sources. This situation makes problematic the seismic hazard assessment of the region.

Contemporary seismic hazard maps are now available for most of the world as a result of compendia such as that of McGuire (1993) and the Global Seismic Hazard Assessment Project, GSHAP (Giardini, 1999). Most of these maps express seismic hazard in terms of the level of peak ground acceleration (PGA) corresponding to a return period of 475 years (10%

probability of exceedance in 50 years, assuming a Poisson distribution of ground motion values).

A few studies have been carried out in order to estimate the seismic hazard in the UAE and its surroundings (e.g. Abdalla & Al-Homoud, 2004; Al-Haddad *et al.*, 1994; Musson *et al.*, 2006; Peiris *et al.*, 2006; Sigbjornsson & Elnashai, 2006; Wyss & Al-Homoud, 2004). This region is also covered by regional hazard maps as the GSHAP (Giardini *et al.*, 1999) and regional seismic codes as the Uniform Building Code (UBC, 1997).

Some of these studies indicate sufficiently low seismic hazard to allow earthquake-resistant design considerations to be ignored for normal structures in most of the UAE territory (e.g., Al-Haddad *et al.*, 1994; Musson *et al.*, 2006; Peiris *et al.*, 2006; UBC, 1997). The exception is the northern tip of the country, where Musson *et al.* (2006) report seismic hazard levels high enough to warrant consideration of earthquake-resistant design practices. To this area Musson *et al.* (2006) assign the zones 1 and 2A of the UBC97 seismic zonation map (see section 3.3.7).

On the other hand, the GSHAP map (Giardini *et al.*, 1999) and published papers, such as Abdalla & Al-Homoud (2004) and Sigbjornsson & Elnashai (2006) recommend the use of much higher seismic design loads. Although even the higher values of seismic hazard are not particularly severe, the cost implications are significant. This is particularly important if it is considered the high construction rate prevalent in the UAE.

It is important to mention that most of these publications contain some inconsistencies in their adopted seismic hazard analysis procedure. Many of them presenting seismic source zonations that are incompatible with the regional seismotectonic framework. An exhaustive discussion of these shortcomings is presented in section 3.3.

Inconsistencies between existing seismic hazard studies, the lack of well-established seismic code requirements for structural design, and a very

high construction rate in the UAE (mainly in Dubai which is probably the city with the highest construction rate in the world) has led to some local governments to establish stringent requirements for seismic design. For instance, the Dubai Municipality recommends the use of zone 2A of the UBC (1997) as design criteria for five-storey buildings or higher. This takes designers to use a PGA value of 0.15 g when considering rock-site conditions.

In order to understand the reasons for these observed inconsistencies, a probabilistic seismic hazard analysis (PSHA) has been carried out for three locations in the UAE. The selected locations are the cities of Abu Dhabi, Dubai and Ra's Al Khaymah (see Figure 3.1). The main outcomes of this study are seismic hazard curves, uniform hazard spectra (UHS) and disaggregated results for return periods of 500, 1000, 2500, 5000 and 10,000 years for PGA and structural response periods up to 3.0 s for rock-site conditions.

Figure 3.1. Map of the UAE. The three locations considered in this study are indicated as stars.

The most relevant seismotectonic data for the region was used in order to develop a detailed model characterizing the region's seismic sources. However, some studies regarding the geology and tectonics of the regions could not be considered for the model although their existence is acknowledged (e.g. Musson *et al.*, 2006). Although such studies are rigourous, their commercial nature precludes open access to the data and incorporation of the findings herein.

For this study the latest seismotectonic data for the region was used in order to develop a detailed model characterizing the region's seismic sources. A full treatment of epistemic uncertainty was made through the use of a logic tree in order to implicitly address the inherent uncertainties in the source characterization process.

3.1. Seismotectonic setting

As first step on the development of the PSHA presented in this chapter and at the light of the divergent seismic source zonations adopted by researchers in previous hazard analyses within the UAE; a comprehensive description of the seismotectonic and geologic setting of the UAE and surrounding areas is presented in this section.

3.1.1. Regional tectonics

The Arabian Plate is bounded to the west by the spreading boundary of the Red Sea and the Dead Sea transform faults, and to the south by the spreading ridge of the Gulf of Aden; these structures separate the Arabian Plate from the African Plate. To the east, the Owen Fracture Zone, a major right-lateral strike-slip boundary, marks the contact between the Indian and Arabian Plates (Johnson, 1998; Vita-Finzi, 2001). To the north, the Arabian Plate is bounded by the Makran subduction zone and the Arabia-Eurasia collision zone, which extends from the Makran through the Zagros fold-and-

thrust belt in Iran and up to Turkey in the Northwest (Jackson & McKenzie, 1984). Figure 3.2 diagrammatically portrays this tectonic setting of the Arabian Peninsula.

The Arabian Plate is moving N13°E at a rate of about 22 ± 2 mm/yr relative to Eurasia (Vernant *et al.*, 2004). This convergence involves intracontinental shortening through Iran with the exception of its southern margin, east of about 58°E, where the Oman Sea subducts northward beneath the Makran (Bayer *et al.*, 2006; Farhoudi & Karig, 1977). Figure 3.3 shows the kinematic setting and current deformation rates for the Arabia-Eurasia collision zone.

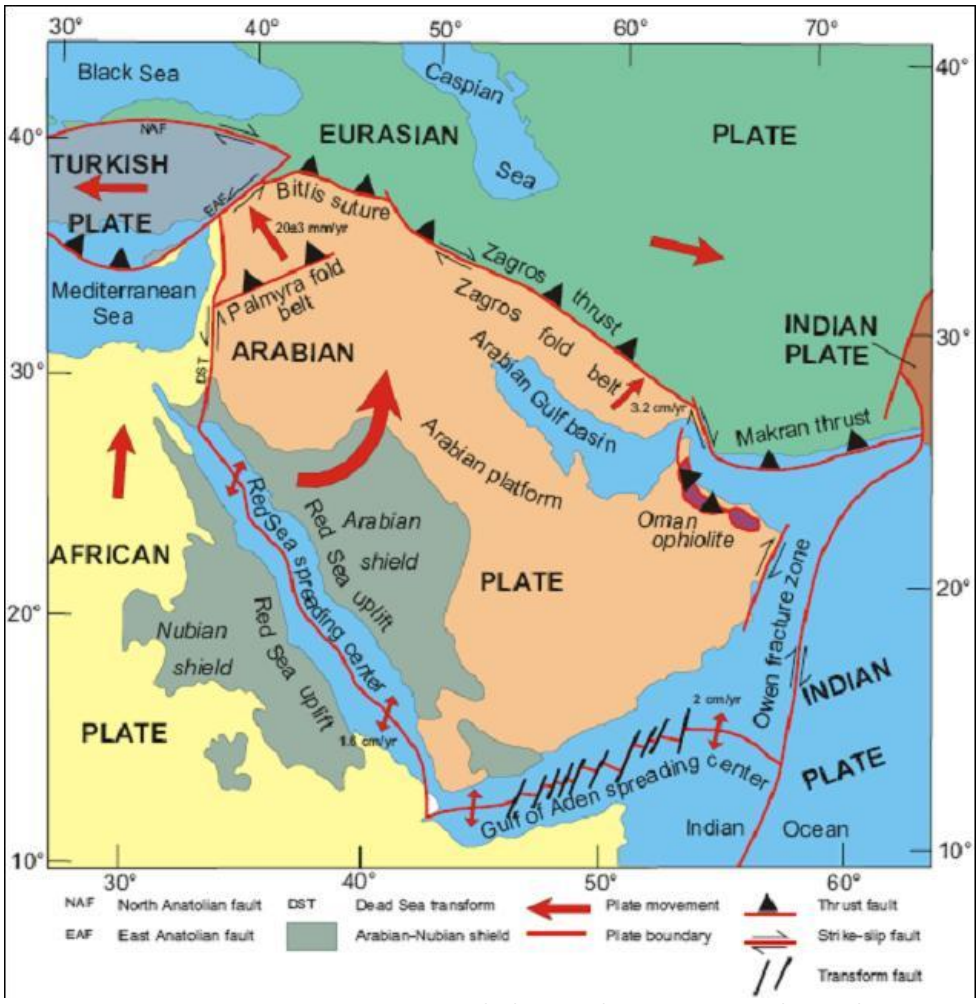

Figure 3.2. Cenozoic tectonic setting of the Arabian Peninsula (Johnson, 1998).

The two main tectonic zones that have the greatest potential to influence the seismic hazard in the UAE, in addition to any local activity, are the Makran subduction zone and the Zagros collision zone. The tectonic map of Saudi Arabia (Figure 3.2) shows some tectonic and geological structures in northern Oman (Johnson, 1998) that could also potentially contribute to the seismic hazard in the UAE. Unfortunately, the scarcity of geological information within the UAE and in the northeastern region of the Arabian Peninsula hinders the evaluation of local seismic activity and the definition of seismic sources within this region.

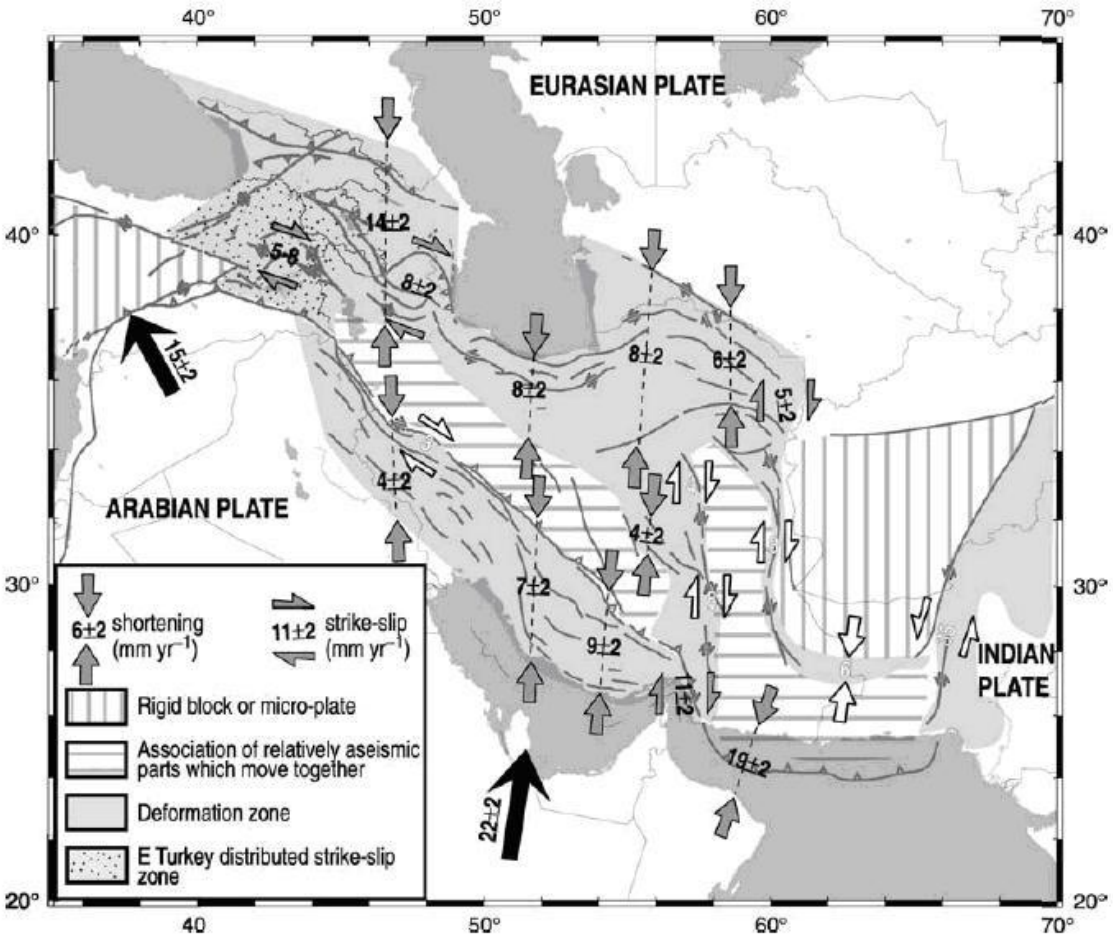

Figure 3.3. Present-day kinematics in Iran by Vernant *et al.* (2004).

In contrast, several complete maps of the geological features in southern Iran are available (Hessami *et al.*, 2003), along with many

publications regarding the tectonics and geology of well-defined structures in the region (e.g., Berberian, 1995; Berberian & Yeats, 1999; Regard *et al.*, 2005; Walker & Jackson, 2002; Walker *et al.*, 2004). Such sources enable a better, or at least a higher resolution, characterization of the seismic sources in southern Iran. A geological map with the major active faults in southern Iran is presented in Figure 3.4.

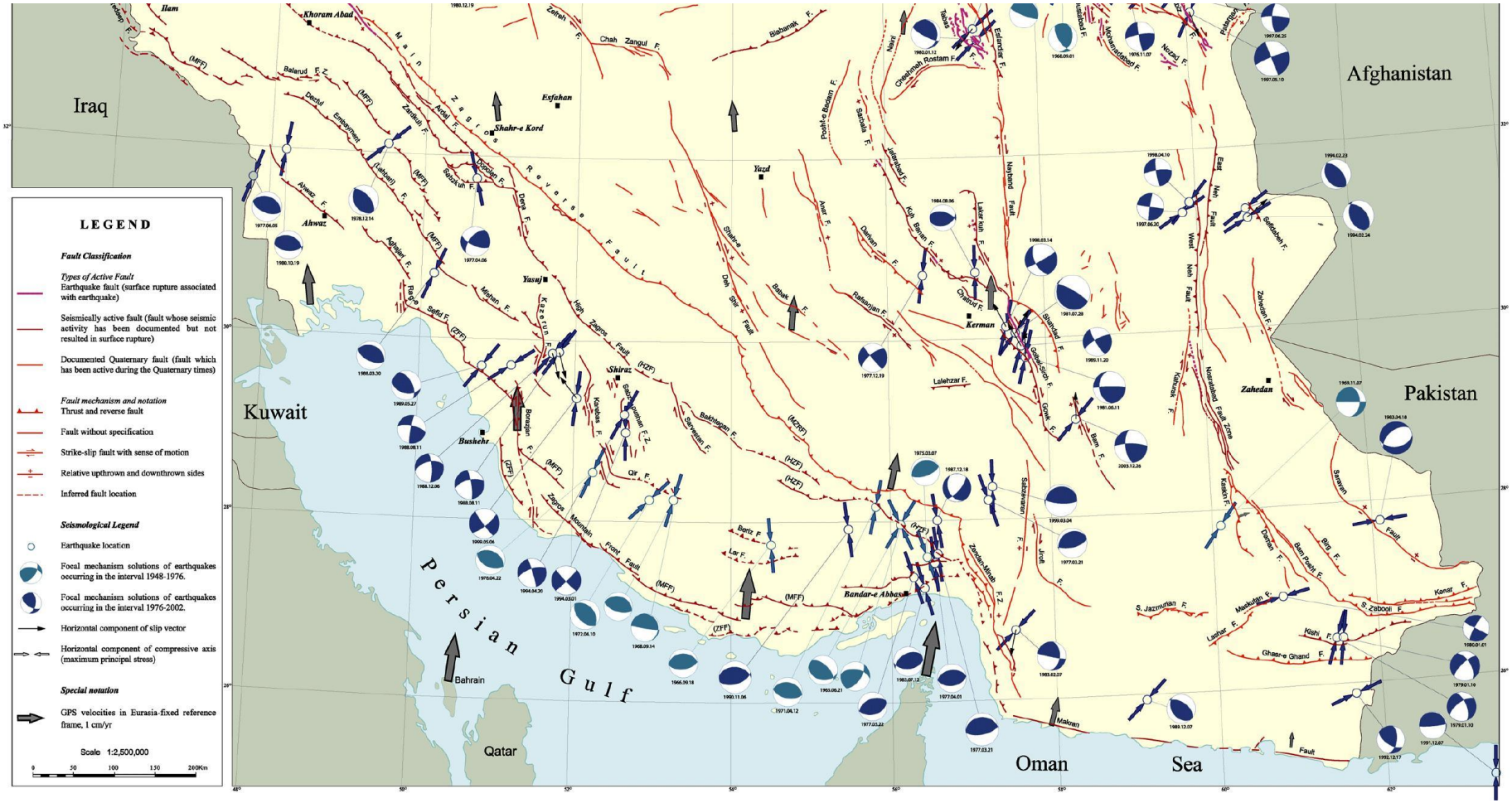

Figure 3.4. Major active faults in southern Iran (after Hessami *et al.*, 2003).

3.1.2. Zagros Collision Zone.

The active Zagros fold and thrust belt is located along the northeastern margin of the Arabian Plate and is part of the Alpine-Himalayan mountain chain. This belt extends for more than 1500 km in a NW-SE direction from eastern Turkey to the Minab-Zendan-Palami fault system in southern Iran. Deformation commenced during the Pliocene and the region is currently undergoing about 10 mm/yr shortening in its southeastern section and 5 mm/yr in its northwestern part as a result of the collision between the Arabian and central Iranian plates (Allen *et al.*, 2004; Berberian, 1995; Jackson & McKenzie, 1984; Vernant *et al.*, 2004).

Due to the presence of several ductile sedimentary layers in the Zagros, decoupling of the Phanerozoic cover from the Precambrian metamorphic basement has occurred along the Lower Cambrian Hormoz Salt ("lower Hormoz detachment zone") and above the Eocene-Oligocene Asmari Limestone, along the Miocene Gachsaran Evaporites ("upper Gachsaran detachment zone") (Berberian, 1995). As a result, large-magnitude earthquakes fail to rupture the near-surface deposits in the Zagros. Instead, the 6-15 km thick Phanerozoic sedimentary cover is folded, producing active anticlinal uplift and synclinal subsidence (Berberian, 1995).

Most of the seismicity in the folded belt appears to occur on high angle reverse faults (40°-50°) in the basement with consistent motion at azimuths of north to northeast (30°-40°) (Berberian, 1995), and with strikes approximately parallel to the SE to ESE trend of the regional fold axes. Teleseismic body-wave modelling demonstrates that most of the larger earthquakes to have occurred in this region nucleated at depths of 10-20 km, below the sedimentary layers (Jackson & Fitch, 1981b; Jackson & McKenzie, 1984).

There is no evidence for subcrustal seismicity in the Zagros (Jackson & McKenzie, 1984). Furthermore, no evidence of intermediate-depth earthquakes (depths from 30 to 100 km) and brittle deformation in the upper mantle, associated with lithospheric delamination has been found in the Zagros (Berberian, 1995).

Morphotectonic units of the Zagros

Berberian (1995) divides the Zagros belt into five morphotectonic units that step down towards the southeast in five prominent levels with different degrees of thrusting, folding, erosion and sedimentation: (1) the High Zagros Thrust Belt; (2) the Simple Fold Belt; (3) the Zagros Foredeep; (4) the Zagros Coastal Plain; and (5) the Persian Gulf-Mesopotamian lowland.

These units are separated by “deep-seated and discontinuous master thrust faults” (see Figure 3.4 and Figure 3.5). These faults are: (1) the Main Zagros Reverse Fault (MZRF; the Zagros suture) which continues along its northwestern side as the Main Recent Fault (MRF; exposed at the surface); (2) the High Zagros Front Fault (HZF; partially exposed at the surface); (3) the Zagros Mountain Front Fault (MFF); (4) the Dezful Embayment Fault (DEF) (this fault is only shown in Figure 3.4 and not in Figure 3.5 as it is farther west of the cross section location); (5) the Zagros Foredeep Fault (ZFF); and (6) the Zagros-Arabia boundary (southern limit of the Zagros active fold-thrust belt) (Berberian, 1995). The MRF and the DEF are located beyond the northern limits of the area considered in the present study, and therefore excluded from further discussion.

Due to topographic and morphotectonic features the master blind thrust 2 through 5 can be identified at surface. Segments of these boundary faults have partially reached the surface and usually the Hormoz Salt has intruded along parts of them. This indicates that the faults are deep seated, cutting at least the entire Phanerozoic section of the sedimentary cover.

A simplified transverse cross section of the Zagros active fold-thrust mountain belt, illustrating the major morphotectonic units is presented in Figure 3.5. In this cross section Berberian (1995) incorporates results of topographic, morpho-seismo-tectonic, seismologic, stratigraphic, tectonic and gravity data.

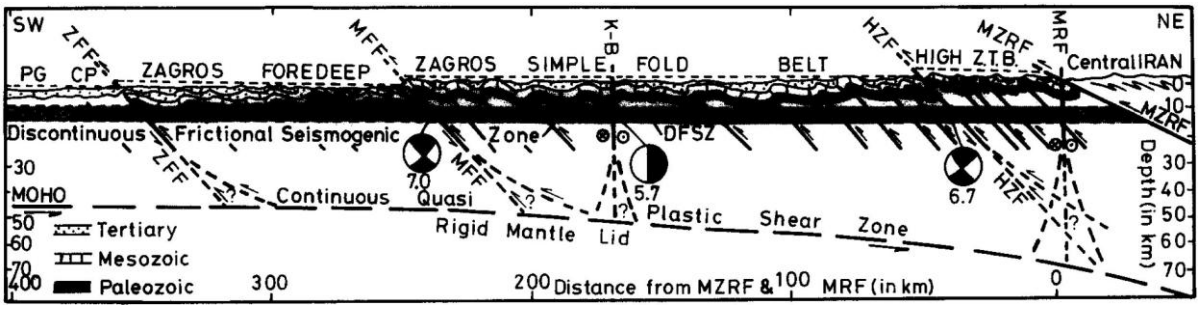

Figure 3.5. Simplified transverse cross section of the Zagros active fold-thrust mountain belt illustrating major morphotectonic units (Berberian, 1995).

Despite a greater length and continuity of the master blind thrusts in the Zagros (see Figure 3.4), the fault segments are rarely continuous for more than 110 km, and the segments are separated by structural gaps at depth. These have presumably controlled the extent of rupture and the magnitude of the earthquakes known to have occurred at depth (Berberian, 1995).

The Main Zagros Reverse Fault (MZRF: the Zagros suture).

The MZRF represents a fundamental change in sedimentary history, paleogeographic structure, morphology and seismicity. It marks the suture between the two colliding plates of the central Iran active continental margin, to the northeast, and the Afro-Arabian passive continental margin (the Zagros fold-thrust belt) to the southwest. It has a NW-SE strike from western Iran to the area of Bandar Abbas, where it changes to a N-S trending structure (Minab fault) and marks the boundary between the Zagros belt, to the west, and the Makran accretionary flysh and the active subduction zone, to the east (Berberian, 1995).

The MZRF is an old geological feature that has existed since at least the lower Palaeozoic and controlled the deposition of sediments in the Mesozoic and Cenozoic Zagros basin (Jackson & McKenzie, 1984). The most recent sense of motion on this structure is of reverse/thrust faulting. However, there is no surface evidence of recent thrusting or meizoseismal areas of large earthquakes on the MZRF (Berberian, 1995; Jackson & McKenzie, 1984).

The High Zagros thrust belt.

The High Zagros is a narrow thrust belt with a maximum width of 80 km, and with a NW-SE trend between the MZRF to the northeast and the High Zagros Fault (HZF) to the southwest. The belt is strongly dissected by numerous reverse faults and is upthrusted to the southwest along different segments of the HZF. The High Zagros is characterized by extensively deformed overthrust anticlines and longitudinal reverse faults. The belt was affected by the Late Cretaceous (subduction) and the Pliocene (continent-continent) collisional orogenies (Berberian, 1995).

The High Zagros Fault.

The High Zagros Fault separates the thrust belt of the High Zagros, to the northeast, from the Simple Fold Belt to the southwest. Geological studies based on evidence from the present position of the Paleozoic rocks (Hubert, 1977) demonstrates that the vertical displacement along the HZF is more than 6 km (Berberian, 1995).

In the Khurgu area, north of Bandar Abbas (the southeastern Zagros), the HZF reaches the Mountain Front Fault (MFF) and it follows the 1000-1500 m altitude contours at the surface. To the northwest, it diverts from the MFF and becomes parallel to the Zagros suture (MZRF). Presumably, the southeastern segments of the HZF are responsible for several earthquakes that have occurred in the region (see Figure 3.4). The northern and

northeastern nodal planes of the fault plane solutions for these events are consistent with the strikes and dips of segments of the HZF. However, very few of these fault-plane solutions have been constrained by SH waves (Berberian, 1995), thus making it difficult to unambiguously associate those events with specific fault structures.

The Simple Fold Belt

The simple fold belt is limited to the northeast by the High Zagros Fault and to the southwest by the Mountain Front Fault. It has an average width of about 250 km in the southeast, 120 km in the northwest, and a length of roughly 1375 km. The belt is only 50 to 60 km wide in the Bakhtiari Mountains.

The Simple Fold Belt contains very large, elongated hogback or box-shaped anticlines, penetrated by salt plugs from the Hormoz Salt. Structures are trending NW-SE in Lorestan and Fars, E-W in Lorestan, and ENE-WSW in the northern Bandar Abbas area (Berberian, 1995).

Most of the seismicity in the folded belt appears to occur on high-angle reverse faults in the basement, with strikes approximately parallel to the SE-to-ESE trend of the regional fold axes. Teleseismic body-wave modelling demonstrates that most of the larger earthquakes nucleate at depths of 10 to 20 km, below the sedimentary cover (Jackson & McKenzie, 1984).

The Mountain Front Fault

The MFF, which delineates the Zagros Simple Fold Belt from the Eocene-Oligocene Asmari limestone outcrops to the south and southwest, is a segmented master blind thrust fault with important structural, topographic, geomorphic and seismotectonic characteristics. The MFF consists of discontinuous, complex thrust segments of 15 to 115 km length, with a total length of more than 1350 km. The fault segments at depth, together with their contiguous asymmetric folds at the surface, are separated

by structural gaps and steps in the observed topographic and morphotectonic features (Berberian, 1995). Because the maximum observed frontal asymmetric surface folds, which conceal contiguous segments of the MFF, are less than 115 km long, it is unlikely that they are capable of generating “great” earthquakes (Berberian, 1995).

The longitudinal MFF is right-laterally displaced by at least 140 km due to the Kazerun-Borazjan active transverse fault, also known as Kazerun Line, which runs for about 250 km. This displacement is accompanied by about 500 m of vertical displacement at the surface expression of the MFF (Baker *et al.*, 1993; Berberian, 1995). Fault-plane solutions of earthquakes along the MFF yield nearly pure thrust faulting with nodal planes striking parallel to the trend of the regional geological structures and the MFF.

The Zagros Foredeep and the Dezful Embayment.

The Zagros Foredeep Fault (ZFF), marking the northeastern edge of the alluvium-covered Coastal Plain of the Persian Gulf, bounds the Zagros Foredeep to the southwest. To the northeast, the Zagros Foredeep is bounded by the MFF. The formation of the Zagros Foredeep was associated with motion along the MFF and uplift of the Simple Fold Belt. The anticlines associated with the Zagros Foredeep are still growing, and the evidence from continuous unconformities in the Pliocene freshwater sediments and recent folded gravels show they have been active since just prior to the beginning of the Pliocene (Berberian, 1995; Falcon, 1961; Lees & Falcon, 1952).

There are two regional saddles in the Zagros Foredeep, namely the “Dezful” (in Iran) and the “Karkuk” (in Iraq) embayments. The Dezful embayment appears to be a discrete structural unit, with boundaries defined by the Dezful Embayment Fault to the north, the Kazerun Line to the east, segments of the MFF to the southwest and the ZFF to the southwest.

The Zagros Foredeep Fault (ZFF).

The ZFF separates the Zagros Foredeep, to the north and northeast, from the Zagros Coastal plain, in the south and southwest. It forms the northeastern edge of the alluvium-covered Coastal Plain of the Persian Gulf and is principally a reverse-slip system. In a similar manner as the MFF, the ZFF is a discontinuous line and is roughly parallel to the MFF. It is displaced for about 150 km right-laterally by the Kazerun Line (Berberian, 1995).

The Zagros Coastal Plain.

The Zagros Coastal Plain is a narrow feature bounded to the north by the Zagros Foredeep Fault. To the south it is bounded by the Persian Gulf and the Zagros-Arabia boundary, which is the southern edge of the significantly thrusted Zagros folds. The Coastal Plain slopes very gently to the south at a rate of 1 m per 5 km (Berberian, 1995).

The Persian Gulf-Mesopotamian lowland.

This morphotectonic unit lies south and southwest of the Zagros Coastal Plain, and is partly covered by the Persian Gulf. The Persian Gulf is a shallow epicontinental sea with a tectonic origin that covers the Arabian shelf platform with water depths of less than 100 m. Some small offshore islands in the Persian Gulf are Hormoz salt plugs. The larger islands near the Iranian coast are gentle anticlines (Berberian, 1995; Kassler, 1973; Ross *et al.*, 1986).

The Kazerun-Borazjan active strike-slip fault.

Also known as the Kazerun Line, this fault is located along a line marking the projected continuation of the Qatar peninsula into Iran. It crosses the Zagros with a north-south trend bending, dragging and offsetting the fold axes along Zagros in a right-lateral sense. Cumulative right-lateral displacement of 140 to 150 km of the Zagros Mountain Front and the Zagros

Foredeep faults can be measured, respectively (Baker *et al.*, 1993; Berberian, 1995).

The Kazerun line consists of two right-stepping segments separated by a gap, the Kazerun (to the north) and Borazjan (to the south) faults. The Kazerun segment is a nearly N-S trending fault situated 15 km west of Kazerun, with a surface length of about 125 km. The Borazjan segment, with a length of about 180 km, is located south of the Kazerun segment with a right-stepping gap. The Borazjan fault scarp is clearly visible from the area north of Borazjan to Ahram and Khormuj (Berberian, 1995).

Berberian (1995) estimates an average slip rate of 14.5 mm/yr for the Kazerun and Borazjan faults. However, more recent studies (Vernant *et al.*, 2004) based on GPS measurements consider this value to be overestimated due to the lack of large differential motion between different sites in the southern Zagros margin. Although Vernant *et al.* (2004) do not attempt to estimate the slip rate for the Kazerun Line, considering the shortening rates that they give for the central Zagros (7±2 mm/yr) and northwest Zagros (4±2 mm/yr), a slip rate of between 1 and 7 mm/yr seems to be more realistic.

Baker *et al.* (1993) conclude that the Kazerun Line represents the surface expression of a buried right-lateral strike-slip fault with a north-south strike. This buried faulting affects the metamorphic basement and is not confined to within the sedimentary cover. High-angle reverse faulting earthquakes also occur near the Kazerun Line. Using the dip angles associated with focal mechanisms reported by Baker *et al.* (1993) for different events, an approximate dip of 73°E has been estimated for the Kazerun Line.

3.1.3. Makran Zone.

Makran Subduction Zone.

The Makran region, bounding southern Pakistan and southeastern Iran, is a 1000-km section of the Eurasia-Arabian plate boundary where northward subduction of oceanic crust has occurred continuously since the Early Cretaceous (Byrne & Sykes, 1992). The Makran subduction zone has no recognized bathymetric trench, though most other features typical of subduction zones can be identified (Figure 3.6).

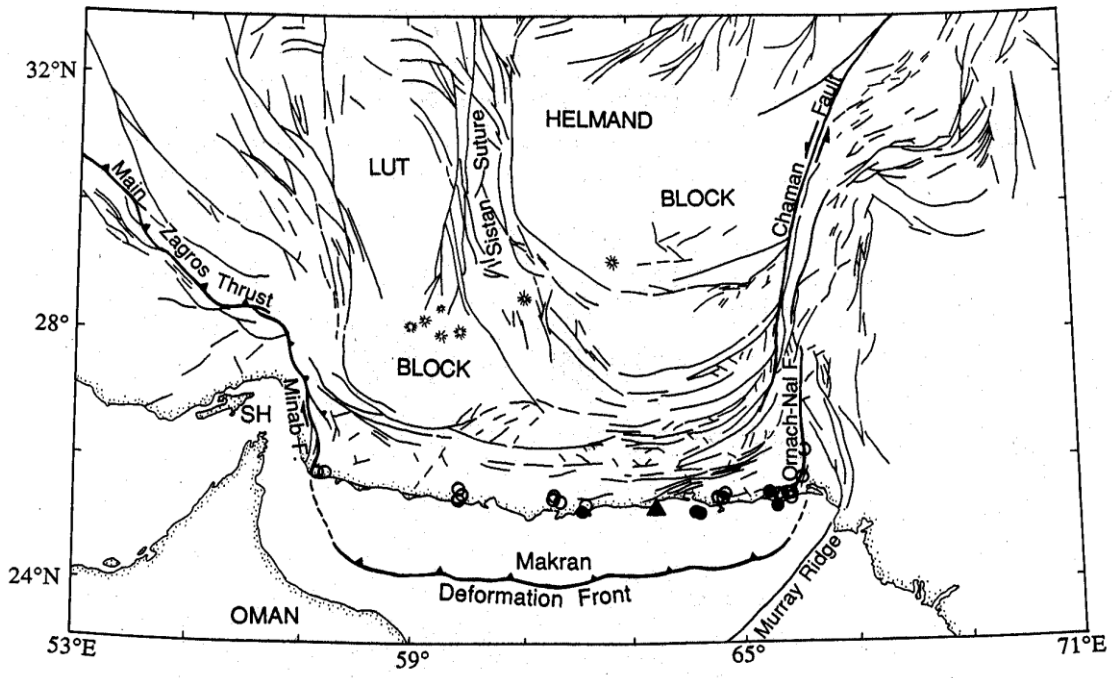

Figure 3.6. Faults and major tectonic features of Makran subduction zone (Byrne *et al.*, 1992). The epicentre of the 1945 earthquake is shown as solid triangle. Mud volcanoes are shown by open circles; those activated by 1945 event are shown as solid circles. Concentric radiating spokes show calc-alkaline volcanoes.

The biggest event recorded in this region is the 1945 earthquake with surface-wave magnitude (M_s) of 8.0 (Quittmeyer & Jacob, 1979). The distribution of intensities and the long-term aftershock activity suggest that the length of the rupture zone was between 100 and 200 km, and that it extended to the east of the epicentre (Byrne & Sykes, 1992; Quittmeyer, 1979).

Using teleseismic activity, Quittmeyer (1979) and Jacob & Quittmeyer (1979) define a shallow dipping seismic zone that extends to depths of about

80 km just south of the volcanic arc (Figure 3.7). They locate the trench about 150 km south of the Makran coast (approximately at a latitude of 24°N).

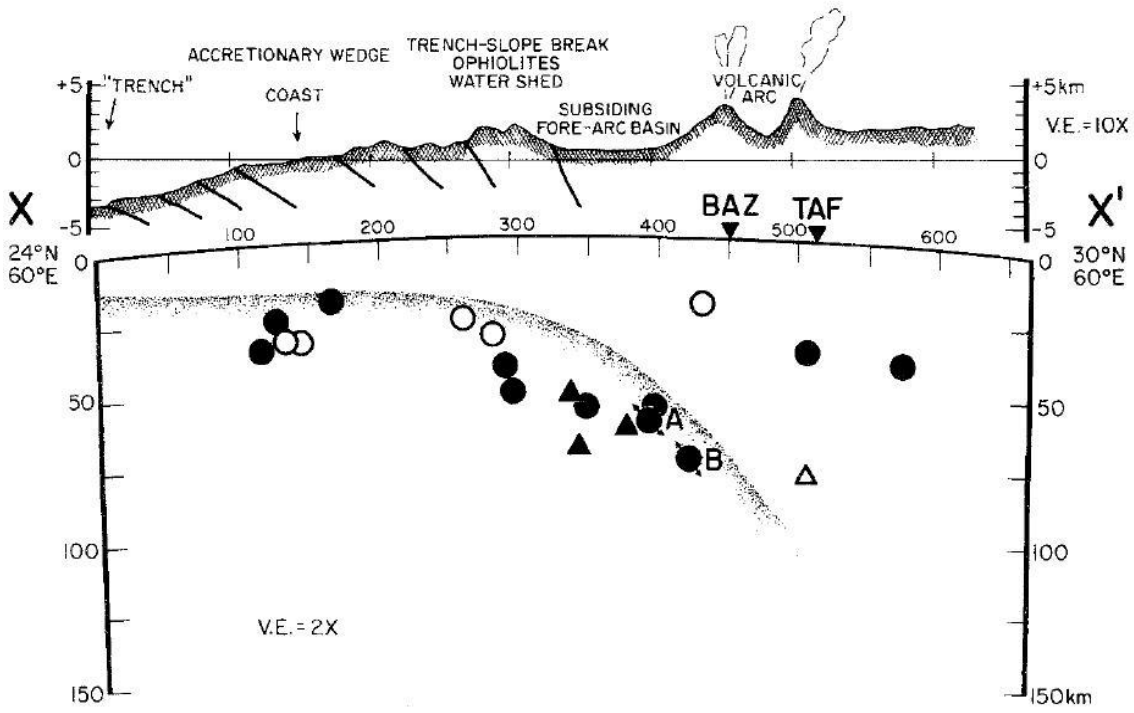

Figure 3.7. Cross section through the western Makran region showing earthquake hypocentres, the inferred dipping Benioff zone, topography and some surface tectonic features. This section is along longitude 60°E, between latitudes 24° and 30°N. Circles represent events up to 200 km to the east of the section line, triangles up to 200 km to the west. Filled symbols represent events for which Quittmeyer (1979) constrained the depth by at least one reported depth phase. Open symbols represent events for which Quittmeyer (1979) determined the depth by minimizing the residuals of first P arrivals only. The arrows at the two hypocentres labelled A and B show plunges of the T axes for these two events, taking into account the 2X vertical exaggeration (Quittmeyer, 1979).

The absence of seismicity and the presence of unconsolidated and semi-consolidated sediments with low seismic velocities and high pore fluid pressures lead Byrne & Sykes (1992) to suggest that the toe of the plate boundary at eastern Makran is aseismic. This aseismic area covers from the deformation front ("trench" in Figure 3.7) to the seismic front, a distance of about 70 km northward the trench. The absence of seismicity in the western Makran does not allow a robust determination of the seismogenic potential

of this zone to be made, but a similar situation as in the eastern Makran might be expected.

A cross section through the Makran subduction zone using the EHB earthquake catalogue (Engdahl *et al.*, 1998), updated to include data until 2004 (Engdahl, personal communication, 2006) is presented in Figure 3.8. In this figure is possible to observe an aseismic area at the toe of the subducting plate, between the trench and a distance of about 70 km towards the north; just as Byrne *et al.* (1992) state.

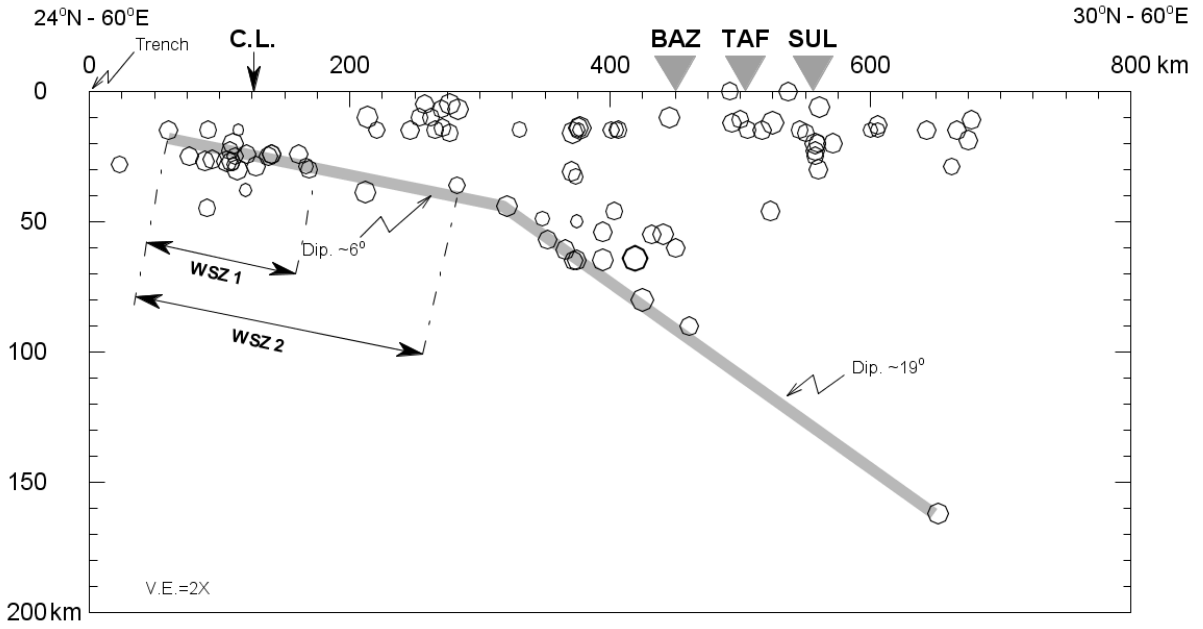

Figure 3.8. Cross section through Makran subduction zone along longitude 62°E, between latitudes 24°N and 30°N and covering events from longitudes 58°E to 66°E, using the EHB catalogue updated to 2004. Triangles represent the Bazman (BAZ) and Taftan (TAF) volcanoes in the Lut Block and the Sultan (SUL) volcano in the Helmand Block. C.L. is the coast line. The thick grey line is the inferred upper boundary of the oceanic lithosphere of the Arabian Plate. The inclination shown is taking into account the 2X vertical exaggeration. WSZ1 and WSZ2 are the likely widths for the seismogenic zone (See Figure 3.38).

From the end of the aseismic zone and up to a distance of about 110 km (~180 km northwards of the trench) an important concentration of events is observed. These events clearly delineate the subducting plate with a dip of about 6° (WSZ1, Figure 3.8). This dip becomes steeper, with a dipping angle of about 19°, at latitude of approximately 26.5°N.

Based only on this information, it could be asserted that the seismogenic zone of Makran is what is shown in Figure 3.8 as WSZ1. However, studies regarding the maximum depth of the seismogenic zone in other subduction zones around the world (Tichelaar & Ruff, 1993), have found that on average the seismogenic zone finishes at around 40 km depth from the surface. This would suggest that for Makran the seismogenic zone could extends up to about 285 km northwards of the trench (WSZ2 in Figure 3.8).

Quittmeyer (1979) references Page *et al.* (1978) regarding a series of uplifted marine terraces, found at various locations along the coast, resulting from coseismic uplift similar to that which exposed a terrace at Ormara in 1945. The number of terraces appears to increase from one at Jask (western edge of the subduction zone) to nine in eastern Iran and an unknown number at Ormara in Pakistan. Even though some of the coseismic uplift will be cancelled by subsidence during the interseismic period, it seems to be a net uplift associated with some earthquake cycles along the entire coast. Thus, while not historically documented for the entire coast, large earthquakes probably have affected the Makran coast, from Jask (in the western end of Makran) to the 1945 rupture zone, a number of times in the past (Quittmeyer, 1979).

The Makran subduction zone is unusual in several respects: the eastern and western halves of the Makran exhibit very different patterns of seismicity, having historical records with and without great events respectively. Segmentation is further suggested by the offsets in the volcanic arc and by the large-scale two-block structure of the overriding plate (see Figure 3.6). The boundary between the segments seems to occur near 61°E, coincident with the Sistan suture zone (Byrne & Sykes, 1992).

On the other hand, many geologic and tectonic parameters show no segmentation along the Makran subduction zone. The margin remains nearly

straight for its entire 1000 km length. Present marine geophysical data show no significant offsets anywhere offshore along the region. The age of the subducting plates lies between approximately 70 and 100 Ma along the entire arc (Byrne & Sykes, 1992; Quittmeyer, 1979).

Vernant *et al.* (2004) estimate a minimum possible subduction rate for the Makran of 19.5±2 mm/yr, and as a maximum, the velocity of the Arabian margin of the Gulf of Oman relative to Eurasia, which is 27±2 mm/yr.

Minab-Zendan Fault System (MZF).

The boundaries of the Makran subduction zone are quite complex tectonic areas. The western boundary forms a transition zone between the Zagros continental collision and the Makran oceanic subduction and is marked by the MZF. The MZF itself consists of two main fault systems with right-lateral displacements. The first system consists of three sub-parallel faults (Minab, Zendan and Palami), whose mean trend is N20°W with a very low seismic moment release. The second includes two major north-trending faults, the Sabzevaran and Jiroff faults and a secondary fault, the Kahnuj fault (Regard *et al.*, 2005). See Figure 3.4 and Figure 3.6.

The Minab-Zendan fault system could have two major roles on a lithospheric scale: (1) to accommodate the plate convergence obliquity and (2) to transform the Zagros collision process into the Makran subduction. Regard *et al.* (2004) show that this transfer is accommodated by combined reverse and right-lateral faulting, distributed over a wide domain.

Regard *et al.* (2005) estimate the Minab-Zendan fault slip rate as 5.6±2.3 or 7.4±2.7 mm/yr in a direction trending about N12°W while the Jirof-Sabzevaran fault slips at 5.7±1.7 mm/yr in a direction N9±12°E. Vernant *et al.* (2004) estimate that if no large rotation occurs in this region the slip rate for the Minab-Zendan fault system is 11±2 mm/yr.

There is only one moderate magnitude earthquake recorded in this zone (5.9 M_w, 2nd July 1983, 26.87N-57.57E). The focal mechanism reported in the Harvard CMT database gives evidence for a right-lateral component of slip on a N05°E-trending focal plane and a dip of 42°E, which is consistent with the kinematics of the fault system.

The Minab fault is visible at the surface for approximately 50 km and runs parallel to the coast of the Hormoz strait. It consists of discontinuous and non-linear segments of 25°-45° east-dipping thrust faults.

The Zendan fault represents the main lithological boundary between the Zagros and the Makran. It is roughly 250 km long, running from the MZT in the north to the Gulf of Oman in the south. It is highly segmented and arranged in "en echelon" segments along the northernmost 50 km. These are, on average, about 20 km in length with a maximum length of 35 km (Regard *et al.*, 2004)

The Palami fault is nearly parallel and is similar to the Zendan fault. It is a high-angle west-dipping fault, whose trace throughout its length is underlined by east-facing scarps and associated Quaternary fans. It is less segmented than the Zendan fault having segments with average lengths of about 25 km and maximum length of 41 km (Regard *et al.*, 2004).

The Sabzevaran fault is 60 km long and runs along the western front of the Zamin Band-Bargah valley. The trace of this fault is particularly well expressed and is associated with numerous morphological features. These features and the linear characteristics of the fault trace suggest a nearly vertical fault plane (i.e., dipping about 80°W) and that strike-slip faulting has dominated its recent activity. It is characterized by fault segments whose lengths vary from roughly 26 to 32 km.

The Jiroff fault is about 75 km long and represents the boundary between a mountainous zone to the west and the Jaz Murian depression to the east. At its southern end it splits into several segments bifurcating into

southeastern and east-trending directions. This fault is highly segmented, with lengths ranging from 10 to 40 km (Regard *et al.*, 2004).

Nayband-Gowk Fault.

The Nayband-Gowk fault represents the western boundary of the Lut Block (see Figure 3.6). It is a right-lateral strike-slip fault zone and extends for more than 400 km. No large-magnitude historical earthquakes have occurred within most of this faulting zone, with the exception of that in its southern half, where two earthquakes have occurred close together in space and time. On 11th June 1981, the Gowk fault ruptured with an M_s 6.7 event. Then, less than 2 months later, on 28th July the M_s 7.1 Sirch earthquake occurred.

Walker & Jackson (2002) estimate a 2.5 mm/yr slip rate along the entire fault system. While Vernant *et al.* (2004) report a rough estimation of 7 mm/yr along the southern part of the fault and 3 mm/yr in the northern part. However, Vernant *et al.* (2004) emphasize that these rates suffer from large uncertainties.

East and West Neh, and Kahurak Fault systems.

The fault system formed by the West Neh and East Neh faults constitutes the eastern boundary of the Lut Block (see Figure 3.6). It is formed by straight, strike-slip faults, 10 to 20 km apart from each other. Although segmented, the West and East Neh faults both have a total length of approximately 200 km (Walker *et al.*, 2004; Walker & Jackson, 2004). They are not know to have produced large historical earthquakes along 360 km of the fault system, raising the possibility that these long faults could produce earthquakes with magnitudes greater than 8.0 M_w in the future (Berberian & Yeats, 1999).

The lateral displacement along the Neh-Zahedan fault system has been estimated by Walker & Jackson (2002) to be 15 mm/yr. This value was

obtained under the assumption that the faults are 5 Ma old, and that the present-day shear across eastern Iran is 20 to 25 mm/yr based on global plate motions. However, Vernant *et al.* (2004) estimate a slip rate of 9 mm/yr based on GPS measurements which report only 15 mm/yr of shear in eastern Iran.

3.1.4. Oman Mountains and Dibba Line.

The Oman Mountains, also known as the Hajar Mountains, are located along the NE margin of the Arabian Plate, in northern Oman. They reach over 3 km in height at Jabal Shams and display many juvenile topographical features, such as straight mountain fronts and deep, steep-walled canyons that probably reflect active tectonism in mountain uplift (Kusky *et al.*, 2005). A simplified geological map showing the Hajar mountains and major structures of the area is presented by Kusky *et al.* (2005) is shown in Figure 3.9.

The present height and ruggedness of the Hajar Mountains area is a product of Cretaceous ophiolite obduction, Tertiary extension, and rejuvenated uplift and erosion. Kusky *et al.* (2005) propose that this process has initiated at the end of the Oligocene and continues to these days. Clear evidence for recent uplift of the Hajar Mountains come from the Quriyat and Tiwi areas, where a set of WNW-striking faults comprise a major group of linked faults occurring with *c.* 50 km spacing. Another set striking NNE also shows *c.* 50 km spacing between fault arrays, and is intersected by a third, NE-striking fault set that shows less well developed 50 to 100 km spacing between arrays (Kusky *et al.*, 2005).

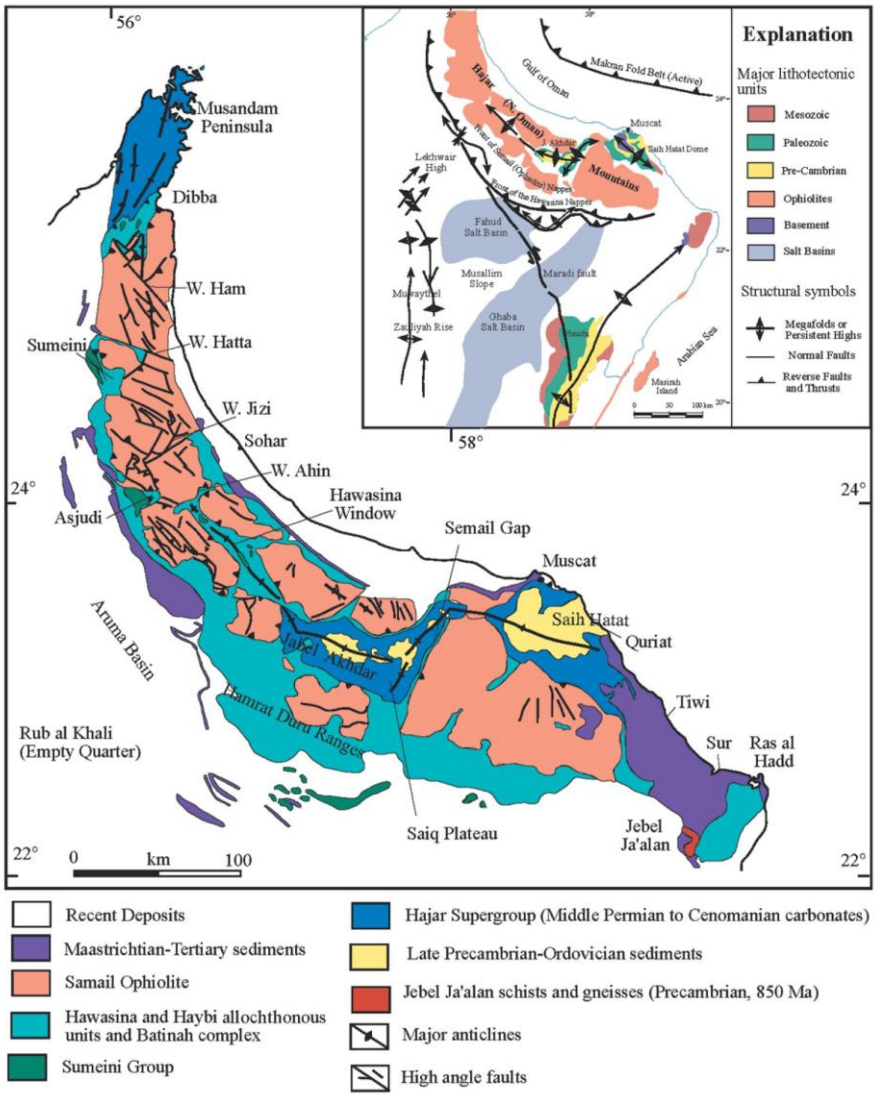

Figure 3.9. Simplified geological map of northern Oman showing the Hajar Mountains and major structures (Kusky *et al.*, 2005).

All of these faults cut the Tertiary limestones and several cut Quaternary marine terraces. The terraces occur at five main levels oriented WNW, parallel to the coast. The observation that these terraces are elevated well above the highest Pliocene-Quaternary eustatic sea-level highs shows that the region has experienced considerable Pliocene-Quaternary uplift that exceeds 100 m.

There is also historical evidence of earthquake activity in the region, in Wadi Dayqah in the eastern Hajar, local villagers speak of a time of several generations ago when the ground shook, destroying buildings in the village

(Kusky *et al.*, 2005). This anecdotal evidence may be used to infer a rough estimate of an intensity VII event (MMI scale; high damage to weak structures).

Faults on the Dayqah fracture-intensification zone were mapped by Kusky *et al.* (2005) across the entire area for more than 50 km. In the field they appear to consist of at least three parallel zones, each a few meters wide, separated by tens to hundreds of meters and characterized by a denser fracture network than in surrounding areas.

Unfortunately, little research has been conducted in northern Oman on neotectonics. The British Geological Survey recently carried out a detailed geological survey of the northern part of the UAE helping to cover the lack of available geological information in the region (Ellison & Styles, 2006). As a result of this project previously known structures were better identified; among these structures are the Dibba Line, the Wadi Shimal and the Wadi Ham faults that lie within the Dibba-Masafi-Fujairah area of the northern UAE.

The Dibba Line is almost parallel to the Zendan-Minab fault system, separating the Makran and Zagros fold belt, suggesting that this has manifestations in both the upper and lower plates (Kusky *et al.*, 2005). It has a NE-SW strike and right-lateral strike-slip motion (Kusky *et al.*, 2005; Lippard *et al.*, 1982; Rodgers *et al.*, 2006; Styles *et al.*, 2006).

On 11 March 2002, a small (~5 M_w) earthquake struck the northeastern UAE, provoking concern among the population. It had a normal mechanism with a slight right-lateral strike-slip component which is consistent with the large-scale tectonics of the region. The normal component suggest relaxation of obducted crust of the Semail ophiolite, while the right-lateral strike-slip component is consistent with shear across the Oman Line (Rodgers *et al.*, 2006).

3.2. Seismicity

With the aim of characterizing the seismic activity rates of the identified seismic sources, an earthquake catalogue was compiled using several data sources. In this section the process of compiling the earthquake dataset, the identification of foreshocks and aftershocks, and the completeness analysis of the cleaned up earthquake catalogue are presented.

3.2.1. Earthquake Catalogue (Historical and Instrumental seismicity).

The earthquake catalogue for the present study was compiled using information from:

- the United States Geological Survey *On-line bulletin* (USGS, 2003), which includes information from the National Ocean and Atmospheric Administration (NOAA) and the Preliminary Determination of Epicentres (PDE) provided by the National Earthquake Information Center (NEIC);
- the International Seismological Centre *On-line bulletin* (ISC, 2003);
- two regional catalogues compiled by Ambraseys and co-workers (Ambraseys & Melville, 1982; Ambraseys *et al.*, 1994);
- the EHB catalogue (Engdahl *et al.*, 1998) updated to consider events up to 2004 (Engdahl, personal communication, 2006);
- the *Earthquake Data Bank* of the International Institute of Earthquake Engineering and Seismology (IIEES, 2003) and
- the first earthquake catalogue of Iran by Berberian (1994).

The catalogue was compiled for a region considered to lie within 47°E to 66°E and 21°N to 31°N, including all events with magnitude 4 and above, reported on any magnitude scale. For events prior to 1900, even those events without reported magnitude were considered with the aim of comparing locations and dates from different sources.

The catalogue covers the period from 3000 BC up to the 1st of October of 2003. It was cut at the 1st of October of 2003 since at the time of compilation of all data sources, the ISC *On-line bulletin* (2003) only reported events prior to this date as being definitive data.

A careful search through each of the source catalogues was done in order to eliminate duplicate events and compare times, locations and magnitudes reported for each of the events. The criteria applied to determinate which records from different sources were actually the same event was as follows: for events prior to 1900, events reported in the same year and when available events within the same month and day; for events after 1900, events reported with the same date, and when time was available events with a difference not bigger than 1 min were considered as the same event. No restrictions on distance between reported locations were applied since one of the goals when comparing different catalogues is to find tendencies on error locations as well as mislocated events.

Particular effort was made to gather additional information regarding events with magnitude of 6.5 and greater (on any reported scale) from more detailed studies that can be found in the literature, either for particular events or regions (e.g., Ambraseys & Bilham, 2003a, b; Baker *et al.*, 1993; Berberian, 1973; Berberian, 1995; Berberian *et al.*, 2001; Berberian & Yeats, 1999; Jackson & Fitch, 1981b; Jackson & McKenzie, 1984; Maggi *et al.*, 2000; Maggi *et al.*, 2002; Melville, 1978; Quittmeyer, 1979; Talebian & Jackson, 2004; Walker *et al.*, 2005).

A preliminary earthquake dataset was compiled showing the different locations, dates and magnitudes (including all the magnitude scales reported) for all events for all of the data sources.

In order to establish a criterion to clean up the preliminary earthquake dataset and compile a final catalogue, including only the most reliable information for each event from the different data sources, a subset of the

preliminary earthquake catalogue was selected. This subset includes only events with reported magnitude greater than 6.5 (in any magnitude scale) and is presented in Appendix A. The preliminary dataset was then divided into three periods: events occurring prior to 1900 (historical), events occurring between 1900 and 1963 (early instrumental) and events occurring from 1964 to 2003 (modern instrumental).

The first period includes only events with macroseismic information. The second period is a mix of macroseismic and instrumental data, with the latter not being of particularly high quality. For the third period, after 1964, the quantity and quality of instrumental data increases with specific studies regarding some of the most important events being available, as well as catalogues with reassessed locations and depths being produced.

After a careful review of each event of this subset the following comments and conclusion can be made for each of the periods.

Historical Seismicity (Period prior to 1900)

The main source of information for this period were Ambraseys & Melville (1982), Ambraseys *et al.* (1994) and the first catalogue of Iran by Berberian (1994).

Great uncertainties in location are reported for this period by the different sources. The macroseismic epicentre was considered to be the most reliable for this period. If the macroseismic epicentre was not reported then, and only then, any instrumental epicentre was allowed to govern the final location of the events. For all of the events, the differences in reported locations are not significant considering the typical range of location uncertainty for this period, with the exception of two events, one occurring in 815 and the other in 1483. Nevertheless, in both cases Berberian (1994) reports that these locations result from *"not enough reliable macroseismic data"*.

The most common magnitude scale reported for this period is M_s (estimated from felt reports). Additionally, Berberian (1994) reports estimates of M_w magnitudes for some events. For all events for which the three sources report an M_s magnitude the values are the same, with the exception of the 1440 earthquake for which Ambraseys & Melville (1982) report a magnitude of M_s 7.1 and Berberian (1994) report a magnitude of M_s 6.9. However, Berberian, in a later publication (Berberian, 1995) reports the same earthquake as having a magnitude of M_s 7.1.

On the basis of such findings, for the final catalogue, the location and M_s magnitude reported by Ambraseys & Melville (1982) and Ambraseys *et al.* (1994) were selected in addition to the M_w magnitudes reported by Berberian (1994).

Berberian (1994), in his final catalogue, report some events that are no reported by any other source as having a magnitude greater than or equal to a particular magnitude value. These events were retained in the final catalogue by assigning a magnitude equal to the lower boundary of the interval (e.g., an event reported as $M_s \geq 5.5$ was included as and event of M_s 5.5).

Instrumental Seismicity – First Part (Period from 1900 to 1963).

The main data sources for this period were Ambraseys & Melville (1982), Ambraseys *et al.* (1994), the ISC *On-line bulletin* (2003), the USGS – NOAA- *On-line bulletin* (2003) and the *Earthquake Data Bank* of the IIEES (2003). Additional information was retrieved from the preliminary map of epicentres and focal depths (Berberian, 1973) and Quittmeyer (1979) who re-evaluated the location of all the earthquakes in the Makran zone prior to 1965.

Ambraseys & Melville (1982) report location and M_s and m_b magnitudes for all events from this period but do not report depth. The ISC

On-line bulletin (2003) reports location, M_s magnitude and depth for events prior to the 3rd October 1947. It is important to highlight the fact that the ISC does not report any earthquake for the period from 3rd October 1947 to 19th January 1964 in its *On-line bulletin* (ISC, 2003). In order to cover this gap, additional information was retrieved from the on-line *Earthquake Data Bank* of the IIEES (2003). IIEES (2003) cites the International Seismological Summary (ISS) as reference for the information during this period.

Considering that epicentral locations of large earthquakes in Iran have errors greater than 30 km for events prior to 1963 (Berberian, 1979), it can assert that the locations reported by Ambraseys & Melville (1982) and Ambraseys *et al.* (1994) show a good correlation with those of Quittmeyer (1979) in the Makran region and with Berberian (1973) in the Zagros zone. The ISC *on-line bulletin* (2003) locations tend to have larger discrepancies than the sources cited above, but are more closely correlated with the USGS–NOAA (2003) locations.

An important mislocation was found in the USGS–NOAA (2003) location of the 1949 event of magnitude 6.5 M_s. While Ambraseys *et al.* (1994) report this event in southern Iran, near to the Zagros-Makran transition zone, the USGS–NOAA (2003) reports it about 500 km further south, in Oman (Figure 3.10). Additional studies by Berberian (1973) and the IIEES (2003) confirm the location reported by Ambraseys *et al.* (1994) for this event.

For this period, M_s continues to be the most common magnitude scale reported, followed by m_b. A clear tendency of the USGS-NOAA (2003) to report magnitude values equal to or larger than the ISC *On-line bulletin* (2003) or the *Earthquake Data Bank* of the IIEES (2003) was observed. On the other hand, magnitudes reported in both Ambraseys & Melville (1982) and Ambraseys *et al.* (1994) tend to be smaller than those reported in the ISC *On-line bulletin* (2003). These differences can be very significant and at

times reach values of 0.9 magnitude units. Unfortunately, for some of the events the only additional information retrieved was from the preliminary map of epicentres and focal depths (Berberian, 1973), in which only ranges of magnitude are reported.

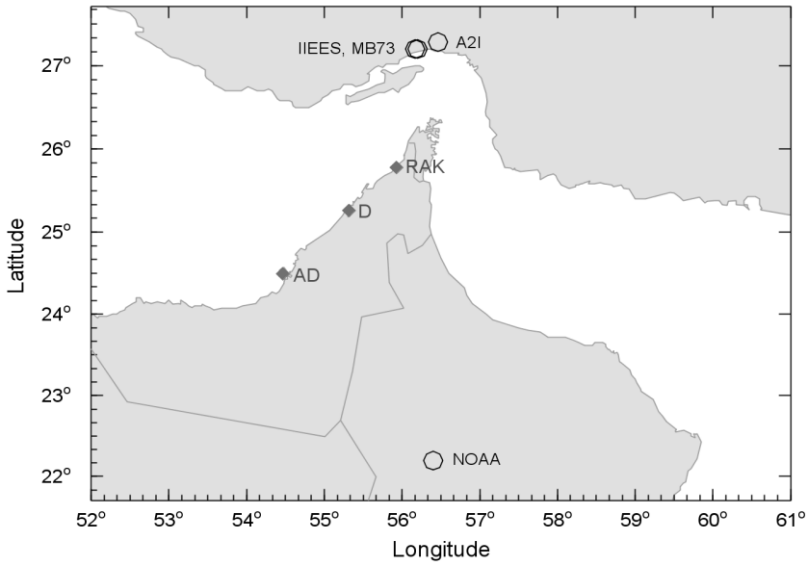

Figure 3.10. Location from different agencies for the 1949 event of magnitude 6.5 M_s, southern Iran. Open circles are the locations reported by the agencies. AD - Abu Dhabi; D - Dubai; RAK - Ra's Al Khaymah; A2I - Ambraseys *et al.* (1994); MB73 - Berberian (1973); IIEES - Earthquake data bank on-line of the IIEES (2003); NOAA – USGS-NOAA (2003).

Regarding focal depth, the ISC *On-line bulletin* (2003) is the only source that systematically reports focal depths. For all events, the depth reported by the ISC *On-line bulletin* (2003) is consistent with that reported by other sources (e.g., Berberian, 1973; Quittmeyer, 1979).

On the basis of the above considerations, the criteria for cleaning up the preliminary earthquake dataset for this period was to consider the Ambraseys catalogues (Ambraseys & Melville, 1982; Ambraseys *et al.*, 1994) as being the most reliable source for location and magnitude, followed by the ISC *On-line bulletin* (2003) and the Quittmeyer (1979) publication. For depths, the values reported by the ISC *On-line bulletin* (2003) were considered as the most reliable, followed by Quittmeyer (1979).

The information retrieved from the *Earthquake Data Bank* of the IIEES (2003) was included only in the case when it was the only source of information for a particular event, which only occurred for events with magnitudes smaller than 6.0 M_s. Data from USGS-NOAA O*n-line bulletin* (2003) was not included at all (as it was already covered by the other data sources).

Instrumental Seismicity – Second Part (Period from 1964 to October 2003)

For this period, additional publications with relocated epicentres, improved depths and focal mechanisms were retrieved (Berberian *et al.*, 2001; Engdahl *et al.*, 1998; Jackson & Fitch, 1981b; Jackson & McKenzie, 1984; Maggi *et al.*, 2000; Talebian & Jackson, 2004). One of the most valuable publications for events occurring during this period is the EHB catalogue (Engdahl *et al.*, 1998) updated to include events up to 2004 (Engdahl, personal communication, 2006). Engdahl *et al.* (1998) perform a global teleseismic earthquake relocation of all the events reported by the USGS and the ISC with magnitudes of $M_w > 5.5$, as well as including many events of smaller magnitude that are well constrained by teleseismic phase arrival times.

After 1964 the location reported by the different agencies began to have errors less than 30 km (Berberian, 1979). For the region of Iran, the epicentres of large magnitude events are generally accurate to within 10 to 20 km and are often better than this (Jackson & McKenzie, 1984). Considering this, locations reported by the ISC *On-line bulletin* (2003), USGS-PDE (2003) and Engdahl *et al.* (1998) have a good correlation.

During this period, it became common to report earthquake size using many other scales. The most commonly reported scales are M_s, m_b and M_w, with m_b being reported for almost all events in several references. Other

scales of magnitude such as duration magnitude (M_D), local magnitude (M_L) and coda magnitude (M_C) are sporadically reported.

Only the ISC *On-line bulletin* (2003) and the EHB catalogue (Engdahl *et al.*, 1998) report magnitudes for all events, the latter being the only catalogue that reports magnitude values in terms of M_s, m_b and M_w scales for almost all events. As for the earlier periods, the values of magnitude reported by the USGS *On-line bulletin* (2003), PDE and NOAA catalogues, tend to be systematically higher than those from other sources.

Ignoring the magnitudes reported by the USGS *On-line bulletin* (2003), the differences between the values reported by the other agencies for magnitudes M_s, m_b and M_w do not exceed 0.2, 0.2 and 0.4 magnitude units respectively. The magnitudes reported by Engdahl *et al.* (1998) are consistent with those reported by the ISC *On-line bulletin* (2003). Additional references retrieved for this period report slightly different values of magnitude but do not show any consistent trends of higher or lower estimates.

For this period, depth continues to be the most difficult earthquake parameter to constrain; the uncertainty associated with the focal depth is still large, as can be appreciated through consideration of the estimates reported by the different data agencies. In general, re-calculated depths from the EHB catalogue (Engdahl *et al.*, 1998) are similar to, and often within the error bounds of those re-calculated by Talebian & Jackson (2004), Jackson & Fitch (1981a) and Baker *et al.* (1993).

The criteria to clean up the preliminary earthquake dataset for this period was to consider, for the earliest events in this period, the locations and M_s magnitudes reported by Ambraseys & Melville (1982) and Ambraseys *et al.* (1994), and to complement these records with depth, m_b and M_w values reported by the EHB catalogue (Engdahl *et al.*, 1998). For events not reported by Ambraseys & Melville (1982) or Ambraseys *et al.* (1994) the EHB catalogue (Engdahl *et al.*, 1998) was considered as the most reliable source

of information. For the smaller events, not covered by the EHB catalogue the information retrieved from the ISC *On-line bulletin* (2003) was considered, replacing the depth values with those reported by Jackson & Fitch (1981a) wherever possible. The information from the USGS *On-line bulletin* (2003), PDE and NOAA catalogues, as well as the *Earthquake Data Bank* of the IIEES (2003) were not used for this period.

Based on these criteria a final catalogue with location, time, depth and magnitude for all reported events, covering the time span from 658 to 2003 was compiled. The catalogue is homogeneous for M_s magnitude; when necessary the equations presented by Ambraseys & Bommer (1990) and Ambraseys & Free (1997) were used to transform m_b and M_w values to M_s, respectively. All the earthquakes with magnitude $M_s < 4.0$ were not included in the final catalogue. The final catalogue is presented in Appendix B and is plotted in Figure 3.11.

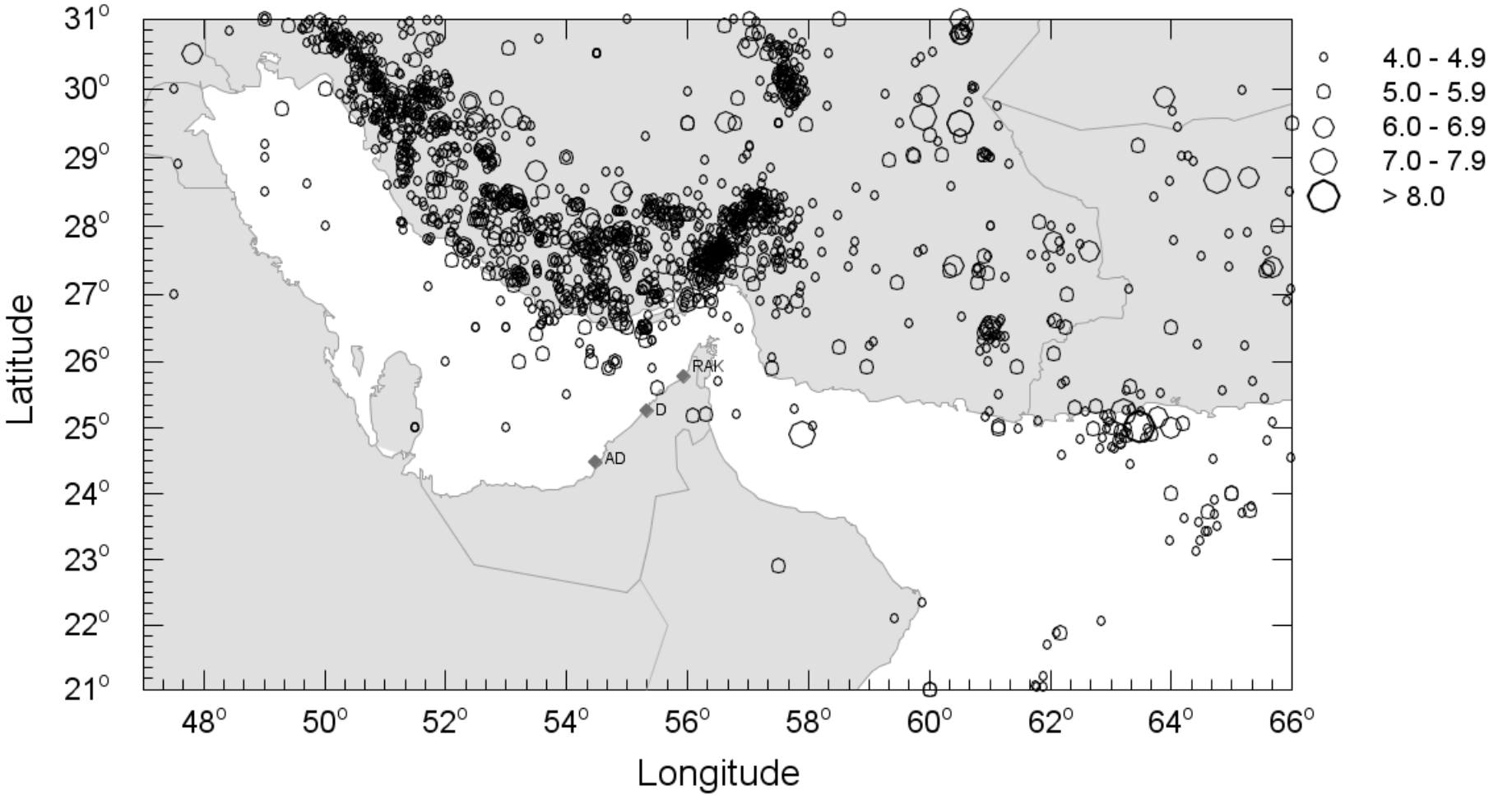

Figure 3.11. Earthquake catalogue for the UAE including main shocks, foreshocks and aftershocks, for M_s magnitude. Diamonds show the cities of Abu Dhabi (AD), Dubai (D) and Ra's Al Khaymah (RAK).

3.2.2. Foreshocks and Aftershocks.

Since PSHA is commonly based on the assumption that seismicity follows a Poissonian process (i.e., all events are assumed to be independent in both space and time), it is necessary to decluster the catalogue by removing all dependent events, namely foreshocks and aftershocks. If only mainshocks are considered, then the Poissonian assumption is generally found to satisfactorily model the seismicity patterns of large areas (e.g., Gardner & Knopoff, 1974; Knopoff, 1964), in which case the use of models for hazard analysis that assume a Poisson model is justified.

To decluster earthquake catalogues, algorithms such as those by Gardner & Knopoff (1974), Knopoff (2000) and Reasenberg (1985) are generally used. Within these models algorithms for defining magnitude-dependent time and space windows are proposed and then used to identify foreshocks and aftershocks. In this study, these three algorithms were explored, with some modifications being made to the latter two, and the results compared.

The algorithm proposed by Knopoff (2000) only defines temporal and spatial windows for events with magnitudes between 4.2 and 6.0. For magnitudes greater than 6.0, Knopoff (2000) proposes a more elaborate procedure which requires individual inspection of each event; an approach that becomes very time-consuming and difficult to implement in a systematic manner.

The values for spatio-temporal windows given for M 4.2 (which represent the lower bound of applicability for this algorithm) were assumed to apply for all events with magnitudes less than this value. For events with magnitude greater than M 6.0 an extrapolation was performed, for both spatial and temporal windows, mimicking the tendency of the values presented by Gardner & Knopoff (1974) (Figure 3.12).

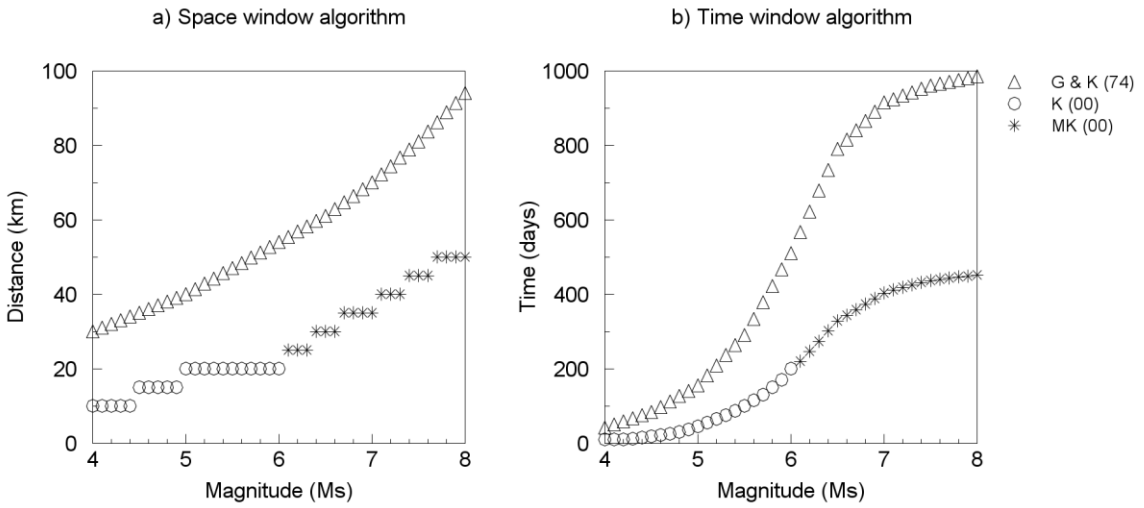

Figure 3.12. Spatio-temporal window algorithms for aftershock identification. G & K (74) - Gardner & Knopoff (1974); K (00) - Knopoff (2000); MK (00) - modifications to the algorithm of Knopoff (2000).

From the full algorithm proposed by Reasenberg (1985), only the temporal window algorithm was used. The temporal windows thus obtained were combined with the space window values given by Knopoff (2000) and the modifications of this latter model for the extrapolation to magnitudes greater than 6.0 as shown in Figure 3.12a.

To identify all of the clusters in the catalogue a procedure similar to those presented by Reasenberg (1985) and Musson (2000) was applied as described below.

The earthquake catalogue is arranged in chronological order and all the events are considered as “independent”. The earthquake with the largest magnitude in the catalogue is automatically considered to be a “main shock”. On the basis of the properties of this event, the subsequent events are then considered and checked to see if they fall within the space-time windows of the algorithm selected to perform the cleaning up of the catalogue. If an event falls within the space/time window it is marked as an aftershock. Events thus identified are regarded as belonging to a cluster and the clusters grow by rules of association. Once no more aftershocks are identified as

being associated with the main event the process re-starts with the next largest independent event in the catalogue.

When an independent event (one not yet associated with a cluster) is associated with a previous clustered event, it becomes a member of the existing cluster. When two events belonging to different clusters are associated, the respective clusters are redefined as one cluster. The largest event in a cluster is considered as the mainshock. If two events of equal size occur, the first is considered the mainshock. In this way it is possible to discriminate between foreshocks and aftershocks. Through this process, all of the events in the catalogue are eventually identified as a "mainshock", an "aftershock" or a "foreshock".

The summary of the number of clusters, mainshocks, foreshocks and aftershocks is shown in Table 3.1. As it can be observed, the algorithm that less events identify as foreshock or aftershocks is modified Reasenberg (1985) with 1290 mainshocks out of a total of 1956 included in the final catalogue. It is followed closely by modified Knopoff (2000) with 1172 mainshocks; Gardner & Knopoff (1974) being the one that removes the larger number of events, with only 947 mainshocks.

Table 3.1. Summary of clusters, main shocks, foreshocks and aftershocks after cleaning up the final catalogue using different algorithms.

Algorithm	Clusters	Mainshocks	Foreshocks and Aftershocks	Percentage of fore- and aftershocks	Total
Modified Reasenberg (1985)	118	1290	666	34.05%	1956
Modified Knopoff (2000)	133	1172	784	40.08%	1956
Gardner & Knopoff (1974)	181	947	1009	51.58%	1956

Despite Reasenberg (1985) being the less restrictive algorithm, in terms of number of foreshocks and aftershock identified, for the purposes of seismic hazard analysis it is the most conservative, as it leads to a larger number of events included in the catalogue, and hence to higher earthquake

occurrence rates. Therefore, for the subsequent analyses the final catalogue, cleaned of foreshocks and aftershocks through the modified Reasenberg (1985) algorithm will be used. The cleaned-up catalogue for M_s is shown in Figure 3.13.

During the declustering process using the three different methods, it was observed that the size of identified clusters is much more sensitive to the size of the temporal window rather than to the size of the spatial window. This was observed in particular when using the Reasenberg (1985) algorithm. Therefore, replacing the spatial criteria proposed by Reasenberg (1985) by another spatial window as described above would probably not have a strong influence on the number and size of the clusters.

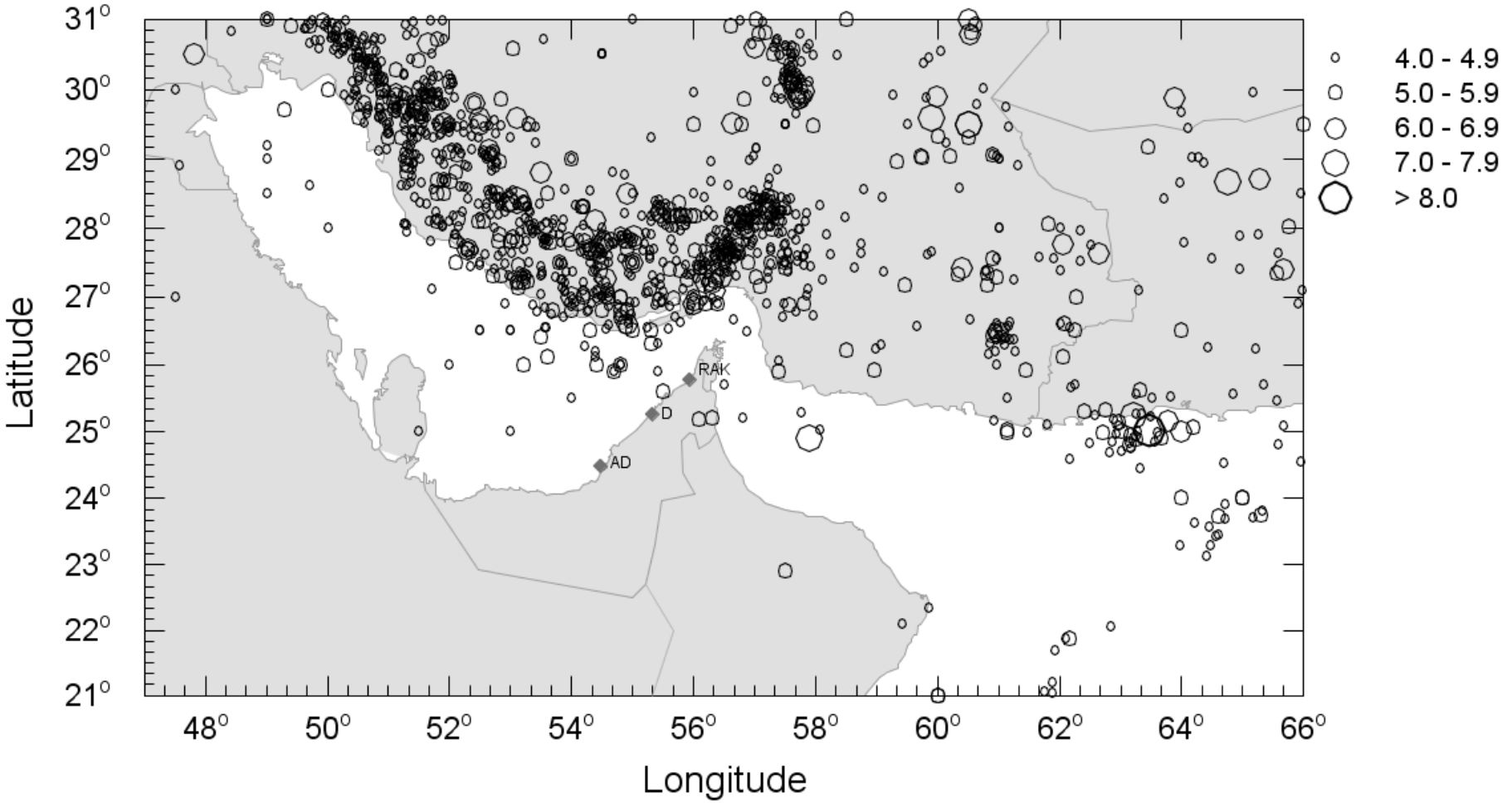

Figure 3.13. Earthquake catalogue of mainshocks for the UAE, for M_s magnitude. Diamonds show the cities of Abu Dhabi (AD), Dubai (D) and Ra's Al Khaymah (RAK).

3.2.3. Completeness Analysis.

As with any seismicity catalogue, the catalogue considered within the present study is incomplete for different magnitude thresholds over different time periods. The catalogue is expected to be complete for earthquakes with M_s 4.0 and above only for the most recent years. As we move back in time through the catalogue, events become more likely to be missing and the threshold magnitude of completeness increases. The points in time where the levels of completeness changes tend to be associated with upgrades to the network of seismic recording instruments in the region.

If we compare the period of time covered in a seismic catalogue with the length of geological processes, it is reasonable to assume that the physical processes responsible for generating earthquakes remain basically unchanged in terms of, for instance, tectonic regime, or kinematic context. Based on the principle that earthquake activity is a relatively stationary process (Gutenberg & Richter, 1944) it is possible to estimate the completeness periods of a catalogue for different magnitudes through a procedure similar to that used by the software Wizmap II (Musson, 2001) and originally proposed by Stepp (1972).

The process may be described as follows. One first defines a parameter that is equal to the number of earthquakes per year exceeding a given magnitude. One then, calculates this parameter for the last five years followed by the last ten years, then the last fifteen years and so on. The resulting values plotted against time results in figures such as those shown in Figure 3.14.

The result will be a graph that will typically show a relatively large variation for the most recent years, where the mean is unstable and is considerably affected by single events. Going back in time the mean should become stable and the graph flattens. When the part of the catalogue that is

not complete for the magnitude under consideration is reached, the mean occurrence rate starts to decline steadily. The break point where that final decline starts shows the date after which the catalogue is complete for that magnitude. Sometimes the break point can be difficult to identify and some judgement is required. In particular when larger events are considered one must keep in mind the recurrence intervals of these events.

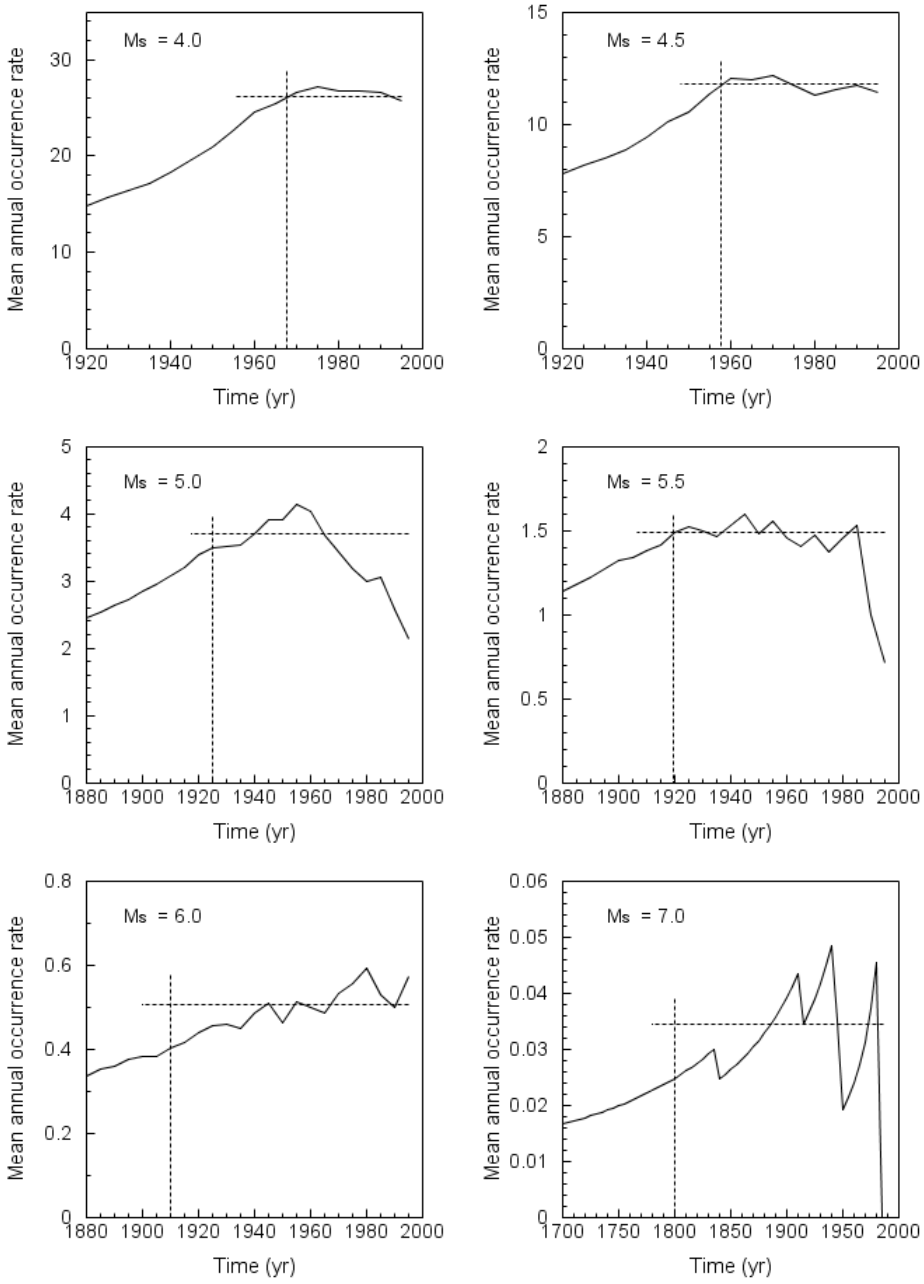

Figure 3.14. Estimation of the year of completeness for magnitudes 4.0, 4.5, 5.0, 5.5, 6.0 and 7.0. Horizontal dashed lines indicate the mean annual occurrence rate estimated and vertical dashed lines show the identify year of completeness for the specified magnitude.

Table 3.2. Years of completeness for different magnitudes.

Magnitude (M_S)	Year of Completeness	Magnitude (M_S)	Year of Completeness
4.0	1967	5.6	1911
4.1	1967	5.7	1911
4.2	1965	5.8	1910
4.3	1965	5.9	1910
4.4	1957	6.0	1910
4.5	1957	6.1	1910
4.6	1952	6.2	1903
4.7	1950	6.3	1903
4.8	1945	6.4	1900
4.9	1945	6.5	1900
5.0	1925	6.6	1892
5.1	1925	6.7	1892
5.2	1925	6.8	1890
5.3	1925	6.9	1890
5.4	1920	7.0	1800
5.5	1920	---	---

Using this procedure the completeness of the catalogue for increments of magnitude $\Delta = 0.1$ was calculated. The mean annual occurrence rate versus time for magnitudes 4.0, 4.5, 5.0, 5.5, 6.0 and 7.0 are shown in Figure 3.14, and a summary of the years of completeness for different threshold magnitudes is presented in Table 3.2.

3.2.4. Seismic activity in the surroundings of Dubai, UAE.

The city of Dubai is one of the cities with the highest rates of construction in the world and the issue of what is the most appropriated level of seismic hazard for the region has consequently become very important. The lack of historical records as well as the national seismic network in the UAE having only very recently being created and still under development (Al Khatibi *et al.*, 2007) makes it difficult to estimate the earthquake recurrence rates of the local seismicity.

In a recent study of the ISC *On-line bulletin* (2006) an apparent increase in the seismic activity in the surroundings of the city of Dubai was

detected. The search was performed for a radius of 150 km from Dubai and for events occurring between January 1900 and December 2006; the date of the on-line search was February 2007.

From Figure 3.15, can be observed that for the period from 1924 (date of the first registered event in this catalogue) to the end of 1999 only 49 events have been recorded, 17 of them without a reported magnitude. Of these 49 events, only three are inland, within the Arabian Peninsula (events 39, 42 and 46; see Figure 3.15 and Table 3.3) and four near the shore (events 7, 8, 16, 33).

Meanwhile, from 2000 to 2006 (Figure 3.16) 18 events were recorded of which six are inland, within the Arabian Peninsula (events 51, 52, 53, 57, 64 and 66) and two are near the shore (events 65 and 67). A particularly noteworthy event is event 65, which is reported as occurring on 16th August 2006 with a magnitude 4.9 m_b just 32 km from the city of Abu Dhabi.

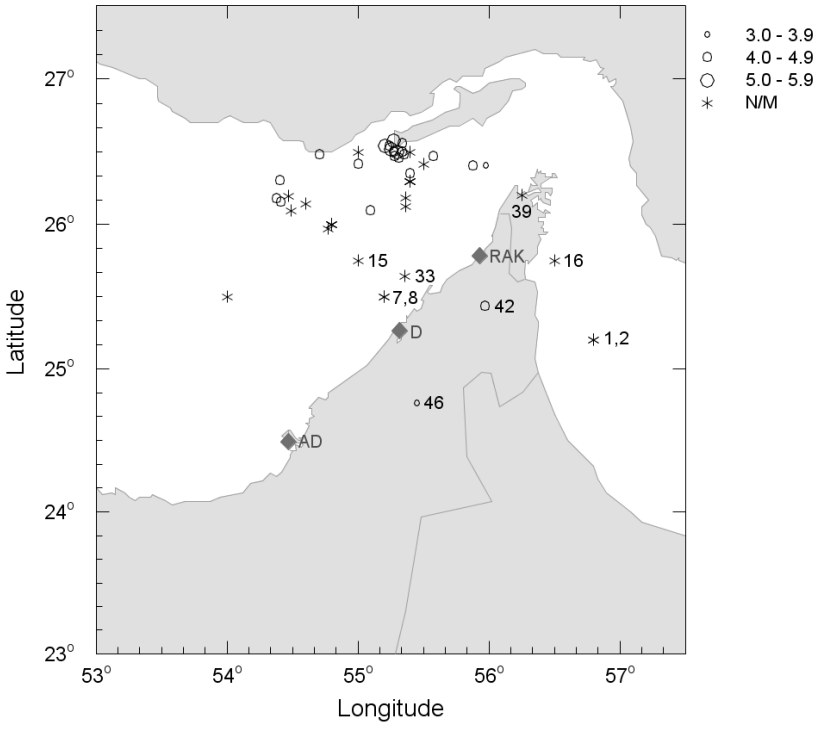

Figure 3.15. Events reported by the ISC *On-line bulletin* (2006) from 1900 to 1999, within a radius of 150 km from Dubai. N/M - No magnitude reported. RAK - Ra's Al Khaymah; D - Dubai; AD - Abu Dhabi. Numbers indicate the number of the event in Table 3.3.

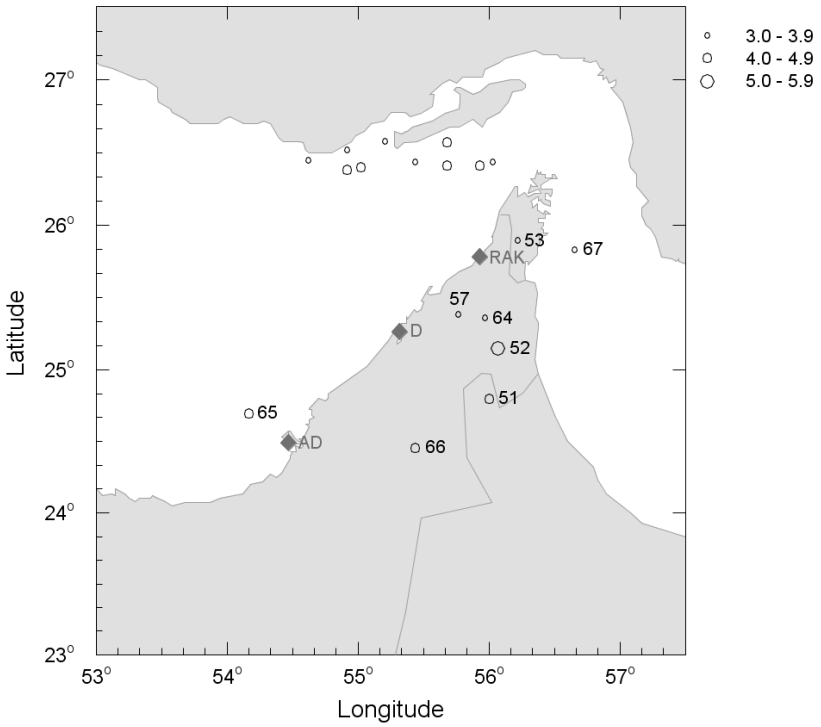

Figure 3.16. Events reported by the ISC *On-line bulletin* (2006) between 2000 and 2006, within a radius of 150 km from Dubai. RAK - Ra's Al Khaymah; D - Dubai; AD - Abu Dhabi. Numbers indicate the number of the event in Table 3.3.

It is important to highlight that the ISC state (at the date of the search) that all of the events occurring on or after the 1st of November of 2004 have not been reviewed by the ISC and that 15 of the 18 observed events for the 2000-2006 period occur after this date. Therefore, the locations corresponding to these events should be considered as being preliminary.

Table 3.3 details all of the events retrieved from the ISC *On-line bulletin* (2006) and Figure 3.17 shows the frequency distribution of the events vs. time for 5-year bins. In this figure a clear increase in the activity in the 2001-2006 period can be observed. A similar increase can be observed for the 1966-1971 period, but in this case, 10 of the 11 events are a cluster of foreshocks and aftershocks that occurred over a period of 3 days (events 19 to 28 on Table 3.3).

Table 3.3. Earthquakes reported by the ISC On-line bulletin (2006) from 1900 to 2006 within a radius of 150 km from Dubai.

Event number	Year	Month	Day	Hour	Minute	Seconds	Latitude	Longitude	Depth	Magnitude			Agency
										M_s	m_b	M_L	
1	1924	12	11	23	1	0	25.2	56.8	--	--	--	--	uk ISS
2	1928	9	20	14	59	0	25.2	56.8	--	--	--	--	uk ISS
3	1931	5	5	11	40	7	26	54.8	--	--	--	--	uk ISS
4	1931	5	5	14	10	45	26	54.8	--	--	--	--	uk ISS
5	1931	5	7	0	45	40	26	54.8	--	--	--	--	uk ISS
6	1934	2	16	7	59	53	26	54.8	--	--	--	--	uk ISS
7	1935	7	2	15	24	53	25.5	55.2	--	--	--	--	uk ISS
8	1936	6	17	8	40	52	25.5	55.2	--	--	--	--	uk ISS
9	1945	1	11	2	3	2	26.3	55.4	--	--	--	--	uk ISS
10	1945	1	15	17	21	21	26.3	55.4	--	--	--	--	uk ISS
11	1947	5	4	0	49	55	26.3	55.4	--	--	--	--	uk ISS
12	1947	5	4	22	34	2	26.3	55.4	--	--	--	--	uk ISS
13	1950	2	2	22	45	13	25.5	54	--	--	--	--	uk ISS
14	1957	10	2	13	9	7	26.5	55	--	--	--	--	uk MOS
15	1960	1	2	14	41	35	25.75	55	--	--	--	--	uk BCIS
16	1963	5	20	10	19	0	25.75	56.5	--	--	--	--	uk BCIS
17	1963	10	31	9	56	57	26.5	55.4	--	--	--	--	uk BCIS
18	1966	7	8	3	51	4	26.48	54.71	38	--	4.4	--	uk ISC
19	1967	1	29	3	53	59	26.5	55.27	36	--	4.9	--	uk ISC
20	1967	1	29	7	5	58	26.48	55.35	38	--	4.7	--	uk ISC
21	1967	1	29	7	12	6	26.56	55.34	33	--	4.8	--	uk ISC
22	1967	1	29	7	13	10	26.47	55.28	33	--	4.8	--	uk ISC
23	1967	1	29	7	13	38	26.5	55.3	0	--	5.3	--	uk ISC
24	1967	1	29	7	56	40	26.54	55.21	34	--	5.1	--	uk ISC
25	1967	1	29	13	20	27	26.5	55.34	4	--	4.5	--	uk ISC
26	1967	1	31	19	0	24	26.52	55.25	13	--	5.1	--	uk ISC
27	1967	1	31	20	6	38	26.46	55.31	26	--	4.8	--	uk ISC
28	1967	2	1	1	7	20	26.58	55.27	22	--	5	--	uk ISC
29	1970	10	27	20	11	8	26.54	55.24	45	--	4.6	--	uk ISC
30	1971	6	28	21	33	20	26.4159	55.5005	149.4	--	--	--	uk ISC
31	1972	5	3	11	58	6	26.1953	54.4691	23.5	--	--	--	uk ISC
32	1975	6	20	9	16	44	26.1774	54.3782	41.6	--	4.6	--	uk ISC
33	1975	12	24	22	55	27	25.6453	55.359	33	--	--	--	uk ISC
34	1976	3	7	21	37	58	25.9695	54.772	33	--	--	--	uk ISC
35	1976	3	16	17	28	23	26.1272	55.3626	33	--	--	--	uk ISC
36	1976	3	20	18	24	34	26.1857	55.3671	0	--	--	--	uk ISC
37	1976	3	24	21	14	22	26.0965	54.4906	0	--	--	--	uk ISC
38	1976	4	10	23	28	8	26.147	54.5987	33	--	--	--	uk ISC
39	1977	9	4	22	14	28	26.2009	56.2529	33	--	--	--	uk ISC
40	1979	11	25	1	7	10	26.3037	54.4041	51.9	3.7	4.6	--	uk ISC
41	1981	5	23	14	28	46	26.4059	55.8766	33	--	4.3	--	uk ISC
42	1984	4	12	11	19	10	25.4349	55.9727	33	--	4.2	--	uk ISC
43	1984	9	6	22	21	4	26.1542	54.4127	27.1	4.8	4.9	--	uk ISC
44	1993	11	16	1	32	30	26.4156	55.0027	46.5	--	4.1	--	uk ISC
45	1994	9	17	8	57	53	26.4682	55.5777	30.1	4	4.7	--	uk ISC
46	1996	4	20	20	39	39	24.76	55.45	0	--	3.8	--	uk EIDC
47	1997	10	28	1	4	46	26.0966	55.0959	33	--	4.1	--	uk ISC
48	1998	1	15	4	0	53	26.3502	55.398	45.2	3.4	4	--	uk ISC
49	1999	12	28	13	0	33	26.404	55.978	33	--	3.8	--	ISC
50	2000	9	10	21	27	54	26.38	54.92	34	--	--	4.2	KISR
51*	2002	1	9	14	2	28	24.797	56.003	10	--	4.3	--	ISC
52*	2002	3	11	20	6	37	25.148	56.068	10	4.1	5.1	--	ISC
53*	2005	1	4	16	59	11	25.895	56.22	14.2	--	--	3.2	THR
54	2005	5	13	0	27	50	26.4	55.02	26.2	--	4.1	3.9	se NEIC
55	2005	6	12	0	18	53	26.578	55.206	32.9	--	--	3.5	THR
56	2005	7	23	17	57	7	26.515	54.919	14.1	--	--	3.4	THR
57*	2005	7	28	15	59	8	25.385	55.769	14.1	--	--	3.8	THR
58	2005	11	22	15	13	26	26.445	54.62	14.1	--	--	3.1	THR
59	2005	11	27	18	48	34	26.436	56.029	14.1	--	--	3.5	THR
60	2005	11	28	5	39	59	26.4328	55.4386	0	3.7	3.9	--	uk IDC
61	2006	3	25	11	57	26	26.409	55.681	33	--	4	--	MOS
62	2006	4	28	0	52	39	26.573	55.683	10	--	4.2	--	MOS
63	2006	6	3	13	14	19	26.41	55.93	34	--	4	3.8	se NEIC
64*	2006	7	16	7	32	14	25.36	55.967	33	--	3.6	--	NAO
65*	2006	8	16	8	1	33	24.695	54.17	33	--	4.9	--	NAO
66*	2006	9	10	8	57	20	24.45	55.435	33	--	4.2	--	NAO
67*	2006	9	27	9	41	54	25.829	56.657	33	--	3.8	--	NAO

Note:

-- - No value reported.

* - Events discussed in the text

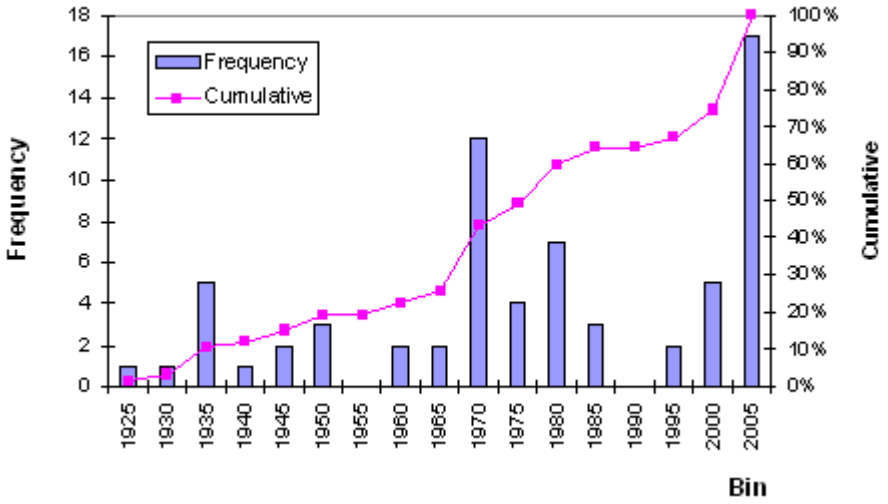

Figure 3.17. Frequency distribution of earthquakes reported by the ISC On-line bulletin (2006) with respect to time.

This apparent increase in the seismicity could be, due to three reasons:

- The seismicity in the region has genuinely increased;
- Some of the events reported in the ISC *On-line bulletin* (2006) for the 2000-2006 period, mainly those after November 2004, are mislocated events; or
- Many events in the past were lost and a more sensitive or dense seismic network in the region is detecting more accurately small magnitude earthquakes.

The consequences of considering any of these three scenarios as the reason for the apparent increase of the seismic activity in the surroundings of Dubai would impact in very different ways any attempt of evaluating seismic hazard in the region.

3.2.4.1. Reappraisal of source parameters for 2000-2006 events.

With the aim of confirming the true occurrence of events after January 2000 inland within the Arabian Peninsula (events 51 to 53, 57 and 64 to 67) other on-line catalogues from different agencies were consulted. Additionally,

a search through recent literature and on-line news in the UAE was performed in order to retrieve felt reports of these events.

The sources consulted were the United States Geological Survey *On-line bulletin* (USGS, 2006), the *Earthquake data bank* of the International Institute of Earthquake Engineering and Seismology (IIEES, 2006) and the *Earthquake data bank* of the European-Mediterranean Seismological Centre (EMSC, 2006). The search criteria used were the following: hypocentral location between 23° to 28° latitude and 52° to 58° longitude and date of occurrence between 1st January 2000 and 31st December 2006. This was done with the aim of identifying probable mislocations of the events reported by the ISC *On-line bulletin* (2006) into the Arabian Peninsula.

The seismicity retrieved from the USGS *On-line bulletin* (2006), the *Earthquake data bank* of the IIEES (2006) and the EMSC (2006) is shown in Figure 3.18, Figure 3.19 and Figure 3.20 respectively. Table 3.4 and Table 3.5 show the events with epicentral location within the Arabian peninsula or close to the shore reported by the USGS *On-line bulletin* (2006) and the *Earthquake data* bank of the IIEES (2006) respectively. The *earthquake data bank* of the EMSC (2006) only reports events after September 2004 none of which is within or near the shore of the Arabian Peninsula.

The information gathered for the inland and near-the-shore events, marked by asterisks in Table 3.3, is presented and analysed on what follows.

Event 51: 9th January 2002

This event reported as having a magnitude of m_b 4.3 and located about 86 km southeast of Dubai, is also reported by the USGS (2006) with similar location and same magnitude, but not reported by the other agencies. Rodgers *et al.* (2006) refers to this event as a foreshock of the 11th March 2002 earthquake (Event 52). Hypocentre and magnitude were computed by the ISC.

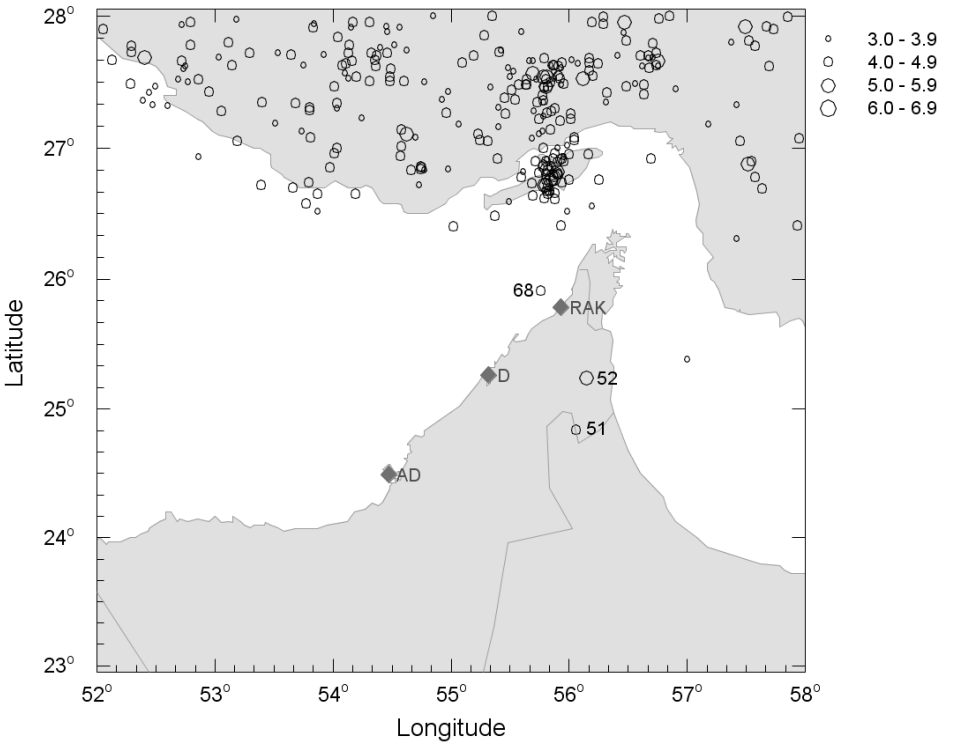

Figure 3.18. Events reported by the USGS *On-line bulletin* (2006) between 2000 and 2006. RAK - Ra's Al Khaymah; D - Dubai; AD - Abu Dhabi. Numbers indicate the number of the event in Table 3.4.

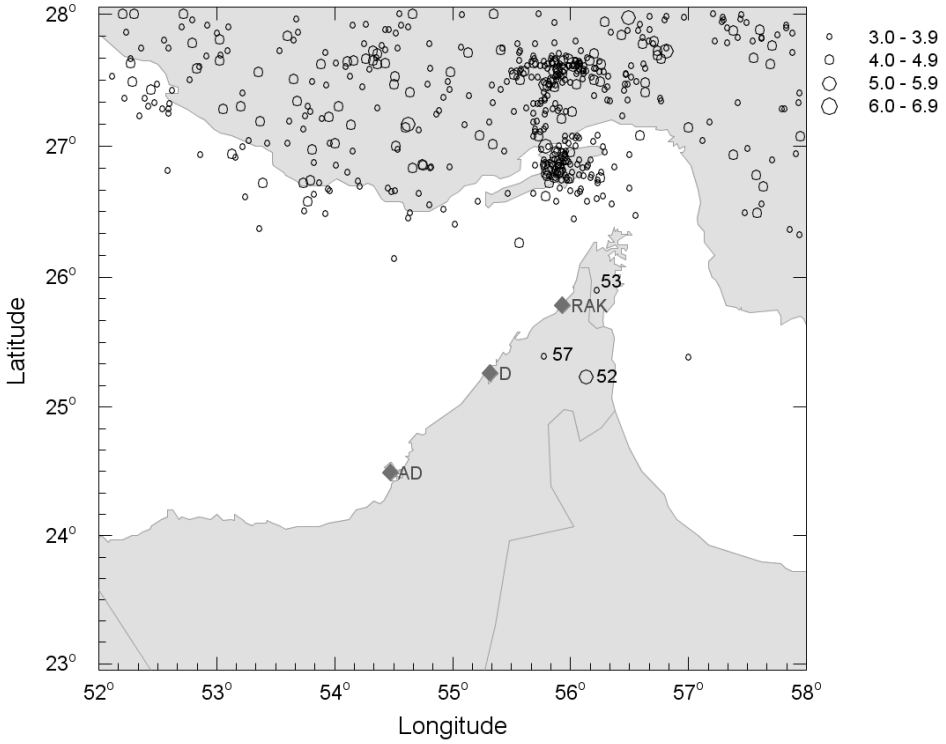

Figure 3.19. Events reported by the *Earthquake data bank* of the IIEES (2006) between 2000 and 2006. RAK - Ra's Al Khaymah; D - Dubai; AD - Abu Dhabi. Numbers indicate the number of the event in Table 3.5.

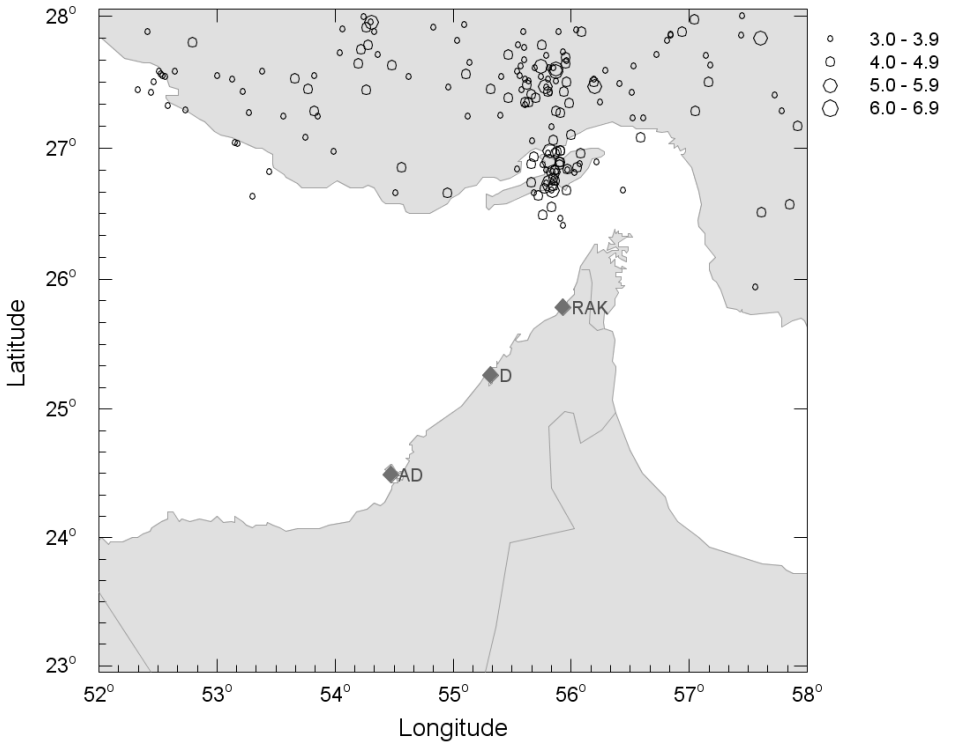

Figure 3.20. Events reported by the EMSC (2006) between September 2004 and 2006. The EMSC (2006) does not report events in the region before September 2004. RAK - Ra's Al Khaymah; D - Dubai; AD - Abu Dhabi.

Table 3.4. Earthquakes reported by the USGS *On-line bulletin* (2006) inland the Arabian Peninsula or near the shore, between 2000 and 2006.

Event number	Year	Month	Day	Hour	Minute	Seconds	Latitude	Longitude	Depth	Magnitude			Agency
										Ms	mb	ML	
51	2002	1	9	14	2	27.92	24.84	56.06	10	--	4.3	--	USGS
52	2002	3	11	20	6	37.18	25.24	56.15	10	--	5	--	USGS
68	2005	12	1	21	58	26.93	25.91	55.76	10	--	4	--	USGS

Table 3.5. Earthquakes reported by the *Earthquake data bank* of the IIEES (2006) inland the Arabian Peninsula or near the shore, between 2000 and 2006.

Event number	Year	Month	Day	Hour	Minute	Seconds	Latitude	Longitude	Depth	Magnitude			Agency
										Ms	mb	ML	
52	2002	3	11	20	6	37	25.23	56.13	10	--	5.1	--	NEIC
53	2005	1	4	16	59	11	25.90	56.22	14	--	--	3.2	IIEES
57	2005	7	28	15	59	8	25.39	55.77	14	--	--	3.8	IIEES

Event 52: 11th March 2002

This event is reported as having a magnitude of m_b 5.1 and located about 76 km southeast from Dubai, about 72 km from Ra's Al Khaymah and a few kilometres northward of event 51. Masafi is the nearest city to the epicentre, located at a distance of about 20 km away. This event is also

reported by the USGS (2006), the EMSC (2006) and the IIEES (2006) with similar location and magnitude. Hypocentre and magnitude were computed by the ISC.

This event and aftershocks were widely felt in all cities of the east coast of the UAE as well as in cities as far away as Dubai and Ra's Al Khaymah (Kazmi, 2002; Shaghouri, 2002). Many smaller events accompanied the largest event over a period of several months, the most significant being a foreshock (m_b 4.3) on the 9th of January 2002 (Rodgers *et al.*, 2006). Damage was greatest near the town of Masafi where cracks appeared in a good number of buildings and major damage occurred in old buildings of the Fujairah Masafi area; some photos of damage to building can be seen at the web page of the American University of Sharjah (http://www.aus.edu/engr/quakelab/Photo_masfai_Eq.php, latest access on October 2007). No structural damage to buildings and lifeline systems was reported (Al-Homoud, 2003; Rodgers *et al.*, 2006). A report (in Arabic) of this event and the associated damage by Othman (2002) is mentioned by Rodgers *et al.* (2006), but could not be retrieved by the author for the present study. However, it is already clear that this event is a legitimate event.

Event 53: 4th January 2005

Reported with a magnitude of M_L 3.2 and located about 32 km northeast from Ra's Al Khaymah. This event is also reported by the IIEES (2006) with the same location and magnitude. It is important to highlight that the source parameters of this event have not been computed by the ISC and the agency that reported this event to the ISC is the IIEES, Tehran, Iran (THR). The USGS (2006) and the EMSC (2006) do not report this event. No felt reports were found in the news from the UAE.

Event 57: 28th July 2005

Reported with a magnitude of M_L 3.8 and located about 47 km northeast of Dubai. This event is also reported by the IIEES (2006) with the same location and magnitude. Again, it is important to highlight that the magnitude and location of this event have not been computed by the ISC and that the agency that reported this event to the ISC is the IIEES, Tehran, Iran (THR). The USGS (2006) and the EMSC (2006) do not report this event. No felt reports have been found in the news.

Event 64: 16th July 2006

Reported with a magnitude of m_b 3.6 and located about 66 km northeast of Dubai and 47 km southwest from Ra's Al Khaymah. A similar event, occurring the same day but at a different time (exactly twelve hours difference) with magnitude 3.2 M (scale unspecified) is reported by the EMSC (2006), in southern Iran, 290 km northward of the location reported by ISC (2006). None of the other agencies reports this event or any other nearby for this date. No felt reports of an earthquake in the UAE were found for this date. This event has not been computed by the ISC and the agency that reported this event is NTNF/NORSAR, Kjeller, Norway (NAO).

Event 65: 16th August 2006

Reported with a magnitude of m_b 4.9 and located about 132 km south-west of Dubai and only 32 km from Abu Dhabi. No other agency reports this event or any other in the surrounding area for the same date. No felt report of an earthquake, either in Abu Dhabi or in Dubai, was found for this date. This event has not been computed by the ISC and the agency that reported this event is NTNF/NORSAR, Kjeller, Norway (NAO).

Event 66: 10th September 2006

Reported with a magnitude of m_b 4.2 and located about 90 km southeast of Dubai and 108 km eastward of Abu Dhabi. The same event is

reported by the USGS (2006), the EMSC (2006) and the IIEES (2006) in southern Iran about 380 km northwest from the location reported by the ISC (2006) and with magnitudes 4.8 m_b, 4.7 m_b, 4.8 M_L respectively. No felt report of an earthquake, either in Abu Dhabi or in Dubai, was found for this date. This event has not been computed by the ISC and the agency that reported this event is NTNF/NORSAR, Kjeller, Norway (NAO). The location of this event is therefore likely to be inaccurate and most likely is the same as the event on southern Iran.

Event 67: 27th September 2006

Reported with a magnitude of m_b 3.8 and located about 150 km northeast of Dubai and 73 km east of Ra's Al Khaymah. The same event is reported by the USGS (2006), the EMSC (2006) and the IIEES (2006) in southern Iran about 430 km north-west from the location reported by the ISC (2006) and with magnitudes 3.6 m_b, 3.7 M (scale not specified), 3.5 M_L respectively. No felt report of an earthquake in the UAE was found for this date. This event has not been computed by the ISC and the agency that reported this event is NTNF/NORSAR, Kjeller, Norway (NAO). Again, this event is likely to be mislocated.

3.2.4.2. Discussion.

For events 51 and 52 it was possible to confirm the magnitude and location from the USGS (2006). It was also possible to retrieve reports in the news of these events being felt in cities as far away as Dubai (~76 km) (Kazmi, 2002; Shaghouri, 2002), as well as in published papers regarding the focal mechanism and depth (Rodgers *et al.*, 2006) of the event. It is therefore safe to conclude that this event is legitimate.

Events 53 and 57 are only reported by the IIEES (2006) and the information shown in the ISC *On-line bulletin* (2006) has not been reviewed by the ISC. Due to the low magnitude of these events, the absence of felt

reports in the news does not exclude with any certainty the possibility that these events were genuinely within the Arabian Peninsula. Additionally, their location close to the Hajar Mountains in Oman supports the possibility that these events have genuinely occurred within the Arabian Peninsula but that they are probably mislocated and should be positioned further towards the mountains.

For event 64 a similar event was located in the *Earthquake data bank* of the EMSC (2006) but with a difference in the origin time. On the basis of such limited data it is difficult to assert that both events are the same. For event 65, no report of a similar event from any other agency that could confirm either the ISC location or that the event is mislocated.

For events 66 and 67, reports of the same event but with different locations to those reported by the ISC (2006) were found in the USGS (2006), the IIEES (2006) and the EMSC (2006) catalogues showing errors up to 400 km in the ISC location. This evidence would suggest that these events occurred in southern Iran (Zagros fold belt), rather than within the Arabian Peninsula.

3.2.4.3. Conclusions to the section.

With the information available so far it is not possible to assert that the seismic activity in the UAE and its surroundings has genuinely increased. Only events 51 and 52 are sufficiently well supported and documented to be considered as events that have genuinely occurred within the Arabian Peninsula (as reported by ISC *On-line bulletin* (2006)).

Sufficient evidence was found to strongly support a mislocation of events 66 and 67. This suggests a tendency of the agency NTNF/NORSAR, Kjeller, Norway (NAO) to mislocate small events in the Zagros towards the southeast, with errors of up to 400 km. Based on this, we may conjecture,

within limited confidence, that events 64 and 65 may also have been significantly mislocated.

For events 53 and 57, it will be necessary to wait for the final report of the ISC (2006) to decide whether or not they have genuinely occurred within the Arabian Peninsula.

It is clear that the lack of a fully operational seismic network in the UAE makes it difficult to accurately locate small events, many of which could currently being occurring without being detected. It is important to mention that given the current level of coverage, the recent installation of the first seismic network on the UAE (UAEInteract.com, 2005) might contribute to an increase on the number of small events reported in the region, along with better location of such events.

In conclusion, the apparent increase in seismicity is therefore most likely to not be real but result of mislocated events. Nevertheless, this assertion must be confirmed once the final reports of these events become available. Based on this, the seismic catalogue compiled in this section may be used with confidence for deriving the earthquake recurrence parameters for the identified sources.

3.3. Review of previous hazard studies

In this section, published works on the assessment of the seismic hazard in the UAE and its surroundings are critically reviewed. Observations regarding the methodology and assumptions that underlie the results of these works are made in each case.

3.3.1. Uniform Building Code (UBC97)

The 1997 version of the Uniform Building Code (UBC, 1997) provides a seismic zonation map for the USA dividing the country into six zones, from 0 (no seismic design required) up to 4 for sites near active seismic sources,

with zone 2 being subdivided into two zones 2a and 2b. For each of these zones a seismic zone factor is provided, which corresponds to the peak ground acceleration (PGA) for rock-site conditions and for a 10% probability of exceedance in 50 years. These seismic zone factors are shown in Table 3.6.

Table 3.6. Uniform Building Code 1997 seismic zone factors. For zone 0 no seismic design is required.

Zone	0	1	2A	2B	3	4
z(g)	---	0.075	0.15	0.20	0.30	0.40

The UBC97 also presents seismic zonation factors for many cities around the world corresponding to locations of US embassies and consulates. Some cities in the UAE and in surrounding countries are included in this section of the UBC97. The relevant cities and their associated zone factors are presented in Table 3.7.

Table 3.7. UBC97 seismic zone factors for cities in the Arabian Peninsula.

Country	City	Seismic Zonation
Bahrain		
	Manama	0
Kuwait		
	Kuwait	1
Oman		
	Muscat	2A
Qatar		
	Doha	0
Saudi Arabia		
	Al Batin	1
	Dharan	1
	Jiddah	2A
	Khamis Mushayt	1
	Riyadh	0
UAE		
	Abu Dhabi	0
	Dubai	0

The UBC97 assigns a zonation of 0 to the cities of Abu Dhabi and Dubai. It is interesting to notice that Manama (Bahrain) and Doha (Qatar) are also classified as zone 0, whereas Dharan (Saudi Arabia) and Kuwait (Kuwait) are classified as zone 1. Muscat (Oman) is classified as zone 2A, which might reflect the influence of earthquakes in the Makran subduction zone in southern Iran rather than local activity.

3.3.2. Global Seismic Hazard Assessment Project (GSHAP)

The GSHAP was launched in 1992 by the International Lithosphere Program (ILP) with the support of the International Council of Scientific Unions (ICSU), and was endorsed as a demonstration program in the framework of the United Nations International Decade for Natural Disaster Reduction (UN/IDNDR). The GSHAP project terminated in 1999. As result of this project, a worldwide seismic hazard map and four regional maps were created through a compilation of independent studies conducted for various parts of the globe.

All maps were created for PGA values corresponding to a 10% probability of exceedance in 50 years. The Arabian Peninsula is included in the map for Europe, Africa and the Middle East (Grünthal *et al.*, 1999). One of the few areas not covered by individual studies in GSHAP is the northeast of the Arabian Peninsula, which includes the northern part of Oman, UAE, Bahrain and Qatar, as well as Kuwait and Iraq (Figure 3.21). For these areas *"the hazard was mapped by simulating the attenuated effect of the seismic activity in the Dead Sea fault area (Near East) and in the Zagros province of Iran"* (Grünthal *et al.*, 1999).

As result of this approach, a high level of activity is reported in the north-eastern part of the UAE with PGA values reaching 0.4 g, which would correspond to the seismic zone 4 of the UBC97. The PGA values assigned by the GSHAP project are shown in Table 3.8, along with what would be the

corresponding UBC97 seismic zonation for the three sites under study. These values seem to be unreliably high; by just spreading the seismic activity in Zagros southwards they over-estimate the seismicity in the UAE. For this reason it would not be recommendable the use of these results for seismic design.

Table 3.8. PGA values assigned by GSHAP for the sites under study with the UBC97 seismic zones corresponding to those values of PGA and the actual seismic zones assigned by the UBC97.

City	PGA (g) (GSHAP)	UBC97 (GSHAP)	UBC97
Ra's Al Khaymah	0.40	4	---
Dubai	0.32	3	0
Abu Dhabi	0.24	2B	0

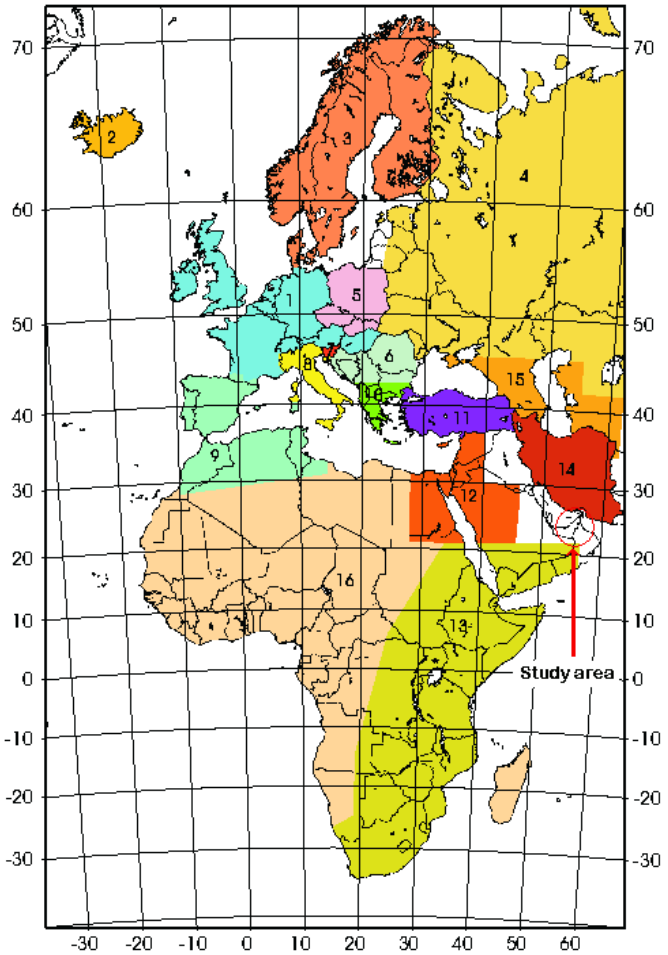

Figure 3.21. Areal coverage of hazard maps compiled and integrated to produce the GSHAP-regional map for the Europe-Africa-Middle East region (Grünthal *et al.*, 1999). Region 14 corresponds to the seismic hazard assessment of Iran by Tavakoli & Ghafory-Ashtiany (1999) and it is from this study that the seismicity in the UAE was extrapolated.

3.3.3. Al-Haddad *et al.* (1994)

Al-Haddad *et al.* (1994) present preliminary seismic design criteria for the Kingdom of Saudi Arabia. One of the outcomes of this study is an iso-acceleration map for 10% probability of exceedance in 50 years for the entire Arabian Peninsula for rock site conditions. They also present a seismic zonation map using the seismic zonation criteria applied by the UBC97.

The authors divide the Arabian Peninsula into 14 seismic sources (Figure 3.22). The closest zones to the sites of interest in the current study, and those with the greatest contribution to seismic activity in the UAE territory are numbered 10 and 11. These zones correspond to the Zagros fold-thrust belt province of Iran. This source zonation is almost entirely seismicity based and does not have a clear correlation with the geologic or tectonic environment of the region. Zone 10 covers the seismicity in the northwestern Zagros region but terminates at latitude of 28.7° N without any specific geological or tectonic reason. A similar situation occurs with zone 11, where the authors incorporate seismicity from two different tectonic regimes, the southeastern Zagros collision zone and the Makran subduction zone.

Additionally, the Makran subduction zone is not considered as being an independent seismic zone, despite the fact that this region is probably the second-most influential seismic region in the eastern part of the Arabian Peninsula after the Zagros.

An important weakness of this study is the use of only one ground-motion prediction equation for all seismic sources without consideration of the different tectonic processes in the region.

The ground-motion prediction relation selected was originally developed by Campbell (1985) for the western USA. The coefficients of the equation were adapted by Thenhaus (1987) for the western region of the Kingdom of Saudi Arabia. This equation is therefore most suited to shallow

crustal earthquakes and applying this equation to events occurring in the Zagros region is most likely not appropriate.

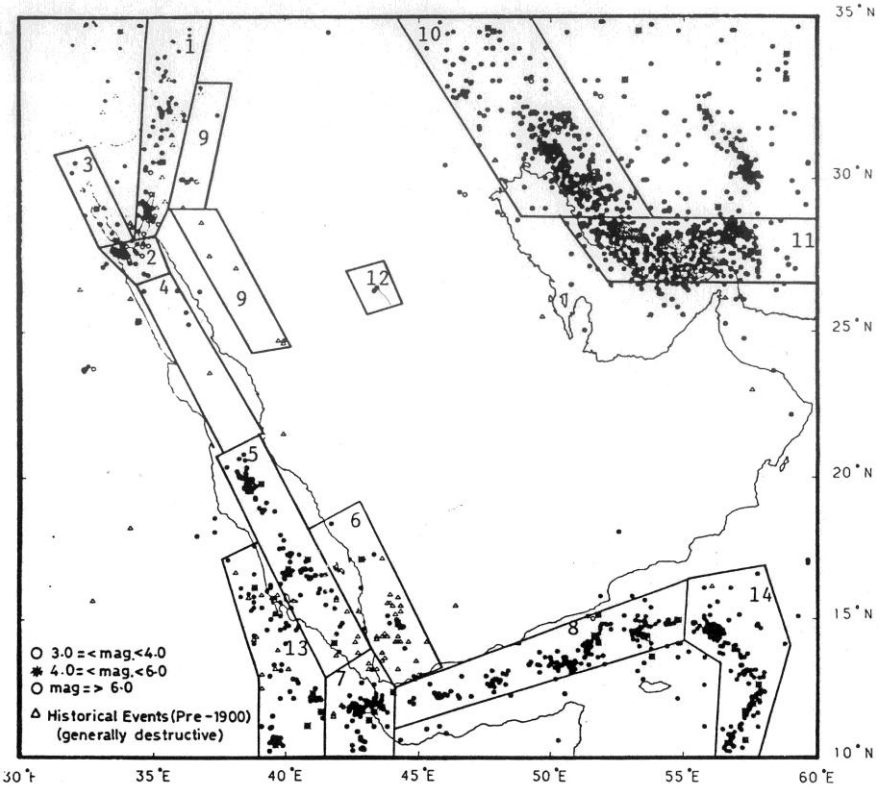

Figure 3.22. Seismic source regionalization map of the Arabian Peninsula and surrounding regions, Al-Haddad *et al.* (1994).

It is also important noting that no details are provided regarding which horizontal-component definition was used for the derivation of the ground-motion prediction equation. This is important as several different conventions may be adopted when deriving prediction equations for 'horizontal acceleration' from the two as-recorded horizontal components of an accelerogram (Douglas, 2003a). The different approaches may result in values that differ by almost 20% from one definition to another (Beyer & Bommer, 2006). Neither information is provided regarding the distance metric definition or faulting mechanism used in the ground-motion models.

From the zonation map shown in Figure 3.22 and the modified GMPE, the highest PGA level for the UAE is on the northernmost tip of the territory,

which is associated with a value close to 0.1 g for the 475-year return period. For most of the country, including the cities of Abu Dhabi, Dubai and Ra's Al Khaymah, the mapped 475-year ground motion level is below 0.05 g (Figure 3.23). Such PGA levels correspond to Zone 0 according to the UBC97.

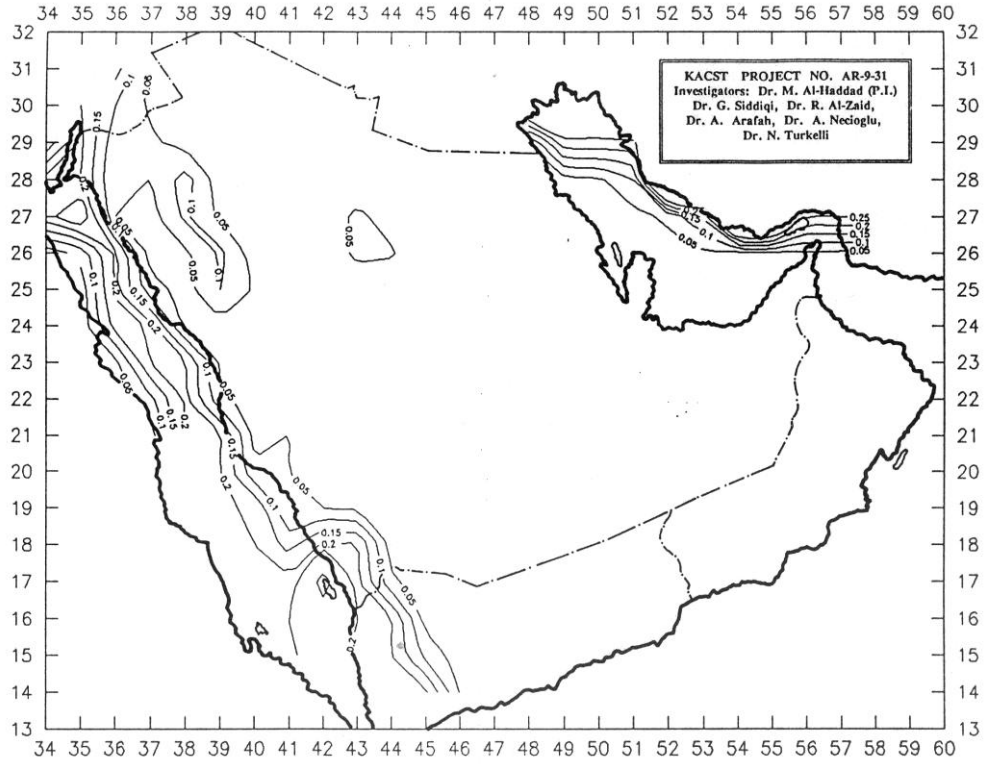

Figure 3.23. Iso-acceleration map for 10% probability of exceedance in 50 years, Al-Haddad *et al.* (1994).

3.3.4. Abdalla & Al-Homoud (2004)

Abdalla & Al-Homoud (2004) present a PSHA for the UAE and its surroundings, producing maps for PGA with return periods of 475, 950 and 1900 years for rock-site conditions. They also present a seismic zonation map for the 475-year return period using similar criteria for defining the boundaries of the seismic zones as the UBC97.

The seismic source zonation defined for this study does not correlate well with the regional seismotectonic environment. Abdalla & Al-Homoud

(2004) assert, when discussing the absence of seismic source zones in the northeast of the Arabian Peninsula in the hazard study by Al-Haddad *et al.* (1994), that "*…there is no clearly defined tectonic structure in that area and no significant earthquake activity. It would be very difficult to define a seismic source zone to capture the very limited earthquake* [data] *in that area*". However, they then proceed to define source zones that include this area.

Without any apparent rational basis, they define two source zones (Region III and VII, Figure 3.24) covering onshore areas within the UAE, and assign them maximum magnitudes of M_w 6.0 and M_w 7.5 respectively. For both sources, they combine areas with completely different tectonic characteristics. Region III, which is supposed to be representative of the northern UAE, as drawn, incorporates parts of the Arabian stable craton (in the south), the Zagros compression zone (in the north) and the Zagros-Makran transition zone (Minab-Zendan fault system) (in the east).

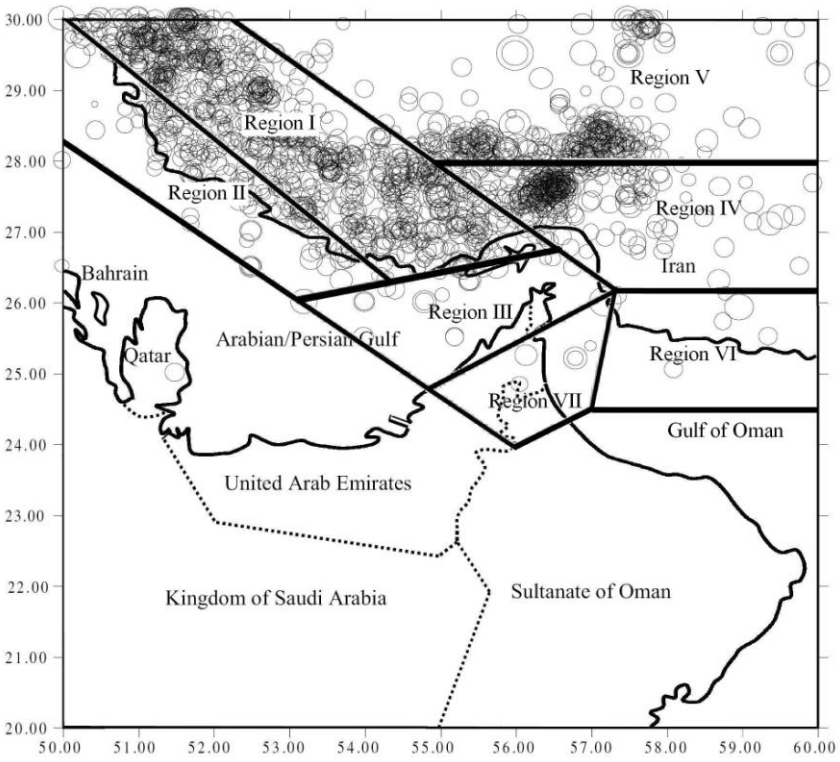

Figure 3.24. Seismicity of the UAE and its surroundings with seismic source regions superimposed (After Abdalla & Al-Homoud, 2004). Circles show the location of the events and its size represents the magnitude.

Similarly, Region VII incorporates parts of the Arabian stable craton, the Zagros-Makran transition zone and the High Mountains of Oman. This, combined with a probable mislocation of an M_w 7.0 event (upper-right corner of Region VII), leads to the assumption that an earthquake of M_w 7.5 could occur inland of the UAE (within the stable craton). Situation that might be possible but it would be associated with very low occurrence rates - ~0.004 events/year per 10^6 km^2 - (c.f. Fenton *et al.*, 2006; Johnson *et al.*, 1994). It was not possible to find an M_s 7.0 event (or similar) within this region in any of the catalogues consulted for the current study (i.e. Ambraseys & Melville, 1982; Ambraseys *et al.*, 1994; Berberian, 1994; IIEES, 2003; ISC, 2003; USGS, 2003). The nearest event of similar magnitude is the 1483 earthquake (M_s 7.7) located on the trench of the Makran subduction zone.

Regarding the ground-motion prediction equation used, Abdalla & Al-Homoud (2004) base their calculations on a single equation derived for Iran (Zaré, 2002). The reference cited by Abdalla & Al-Homoud (2004) for this equation was not able to be recovered as part of the present study, but the same model and coefficients for the Zagros zone are reported in another paper by Zaré *et al.* (1999). The equation was derived from Iranian strong-motion data and predicts PGA as function of moment magnitude, M_w, and hypocentral distance, r_{hypo}. Zaré *et al.* (1999) use both components as the horizontal-component definition. It is important to note that the Zaré (2002) relationship has a standard deviation in log(PGA) units of 0.334, which is among the highest values encountered in recent predictive equations (Douglas, 2003a).

In their 475-year return period hazard map, PGA reach values up to 0.18 g at the northernmost tip of the UAE and are above 0.10 g for much of the national territory (Figure 3.25). As drawn, this leads to values of about 0.16 g, 0.15 g and 0.10 g for the cities of Ra's Al Khaymah, Dubai and Abu

Dhabi respectively. These PGA values correspond to seismic zonations according to the UBC97 of 2A for the three locations.

Given the large variability associated with the ground-motion prediction equation and the poor correlation of the seismic zonation with the seismotectonic features of the region, the PGA values reported by Abdalla & Al-Homoud (2004) should be considered as being highly conservative.

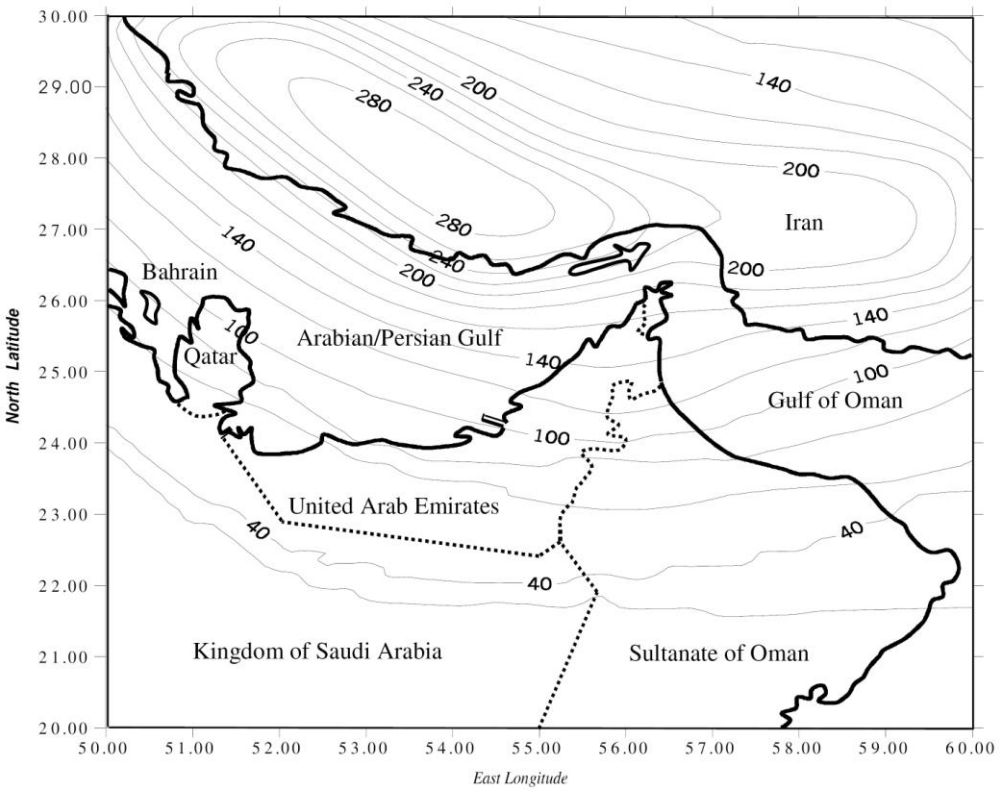

Figure 3.25. PGA (cm/s²) with a 10% of probability of being exceedance in a 50 year time span (Abdalla & Al-Homoud, 2004).

3.3.5. Peiris *et al.* (2006)

Peiris *et al.* (2006) present a regional seismic hazard assessment undertaken for the Arabian Gulf Region, including regional tectonic features from the Zagros, Makran, Dead Sea, Red Sea, Gulf of Aden, Owen Fracture Zone and the Stable Continental Arabian Plate.

The seismic hazard is presented in the form of PGA and UHS for 475- and 2475-year return periods (10% and 2% probability of exceedance in 50

years respectively) for rock-site conditions. They present this for selected cities in the region, among them the cities of Dubai and Abu Dhabi.

The seismic source zonation (Figure 3.26) presented by Peiris *et al.* (2006) is generally consistent with the zonation for Saudi Arabia presented by Al-Haddad *et al.* (1994) for the western parts of the peninsula. For the Zagros and Makran regions, it is consistent with the zonation developed by Tavakoli & Ghafory-Ashtiany (1999) for Iran. This hybrid source zonation is broadly consistent with the seismotectonic environment of the region.

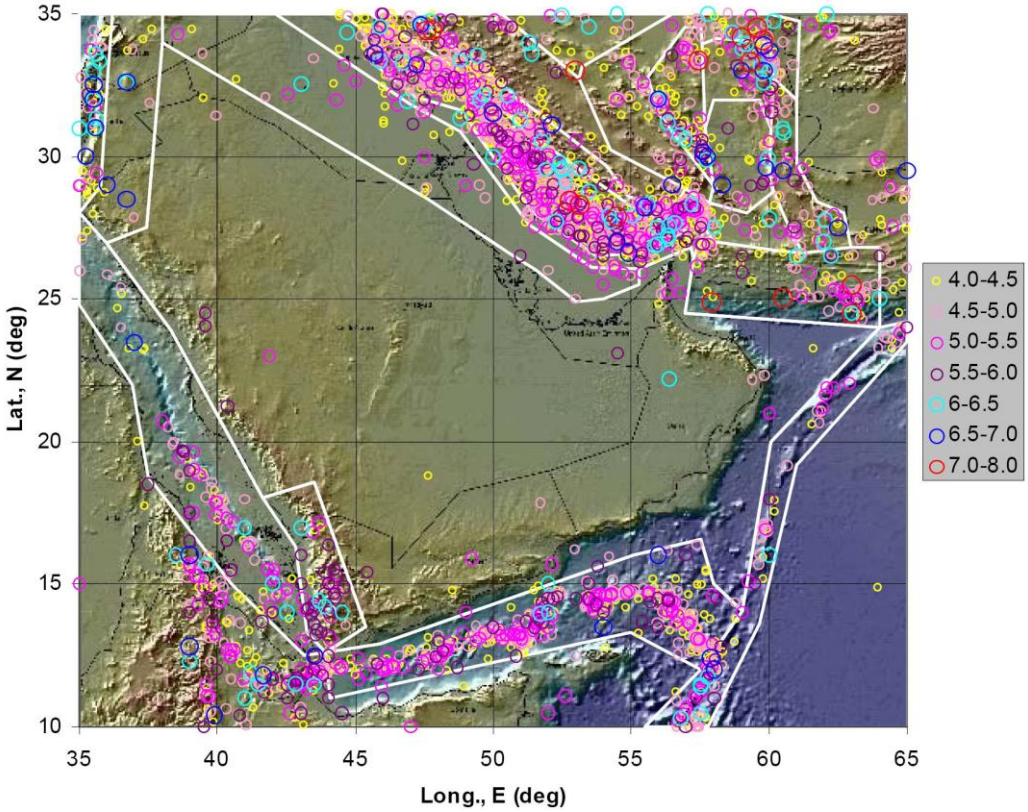

Figure 3.26. Seismic source model (Peiris *et al.*, 2006).

Peiris *et al.* (2006) make the first attempt at assessing seismic activity in the Arabian stable craton. However, they do not explain how the earthquake recurrence parameters (*a* and *b* values of the Gutenberg-Richter distribution) were calculated for this region given the scarcity of the data available. This methodological omission is important due to the fact that, for

PGA, the hazard is mainly dominated by local activity from the stable craton as shown by the plot of the disaggregated hazard for Dubai (Figure 3.27).

In general, the *b*-values used to define the earthquake recurrence seem to be rather high for this region. For instance, if we compare those used by Peiris *et al.* (2006) with the values presented by Tavakoli & Ghafory-Ashtiany (1999) for the Zagros region (who assign *b*-values of 0.69, 0.68 and 0.81 for zones 11, 12 and 13 respectively; Figure 3.26), Peiris *et al.* (2006) assign significantly higher values to these same zones, i.e. *b*-value of 1.15.

Given that *b*-values for a region are typically quite stable, such significant differences between the values adopted by these two studies are of some concern.

It is also important to highlight the fact that the seismic activity of two different tectonic regions; the Arabian stable craton and the Makran subduction zone, are allocated the same *b*-value in the study of Peiris *et al.* (2006).

Concerning ground-motion prediction equations, Peiris *et al.* (2006) selected the ground-motion equations of Ambraseys *et al.* (1996) and Sadigh *et al.* (1997) for shallow-crustal earthquakes for sources in Iran and Makran. The equations of Dahle *et al.* (1990) and Atkinson & Boore (1997) for events in the Arabian Plate and the equations of Spudich *et al.* (1999) for the extensional tectonic regions in the Red Sea and the Indian Ocean.

However, they misuse the first two equations when applying these to estimate ground motions from events in the Makran subduction zone. Additionally, Peiris *et al.* (2006) do not explain who they address the issue of using equations with different horizontal component definitions. For instance, Ambraseys *et al.* (1996) use larger horizontal component, while Sadigh *et al.* (1997) and Spudich *et al.* (1999) use geometric mean. Similar situation occur with the distance metric definitions (e.g., Ambraseys *et al.*

(1996) consider r_{jb} for events $M_s > 6$ and r_{epi} for events $M_s < 6$; Sadigh *et al.* (1997) use r_{rup} and Spudich *et al.* (1999) r_{jb}).

Other issue of compatibility between the different ground-motion equations is the use of different site-condition definitions used in the models. The authors do not explain how they considered in the calculation the fact that Dahle *et al.* (1990) and Atkinson & Boore (1997) models were derived for very hard rock conditions, while the remaining equations were derived for rock or soil conditions.

As a result of this study, Peiris *et al.* (2006) obtain, for a 475-year return period, PGA values of 0.06 g and 0.05 g for the cities of Dubai and Abu Dhabi respectively. These levels of PGA correspond to Zone 1 according to the UBC97 seismic zonation criteria.

For these two cities they also give values for spectral acceleration, with 5% damping of critical, for response periods of 0.2 s and 1.0 s at 475-year and 2475-year return periods (Table 3.9). Additionally, they present the 5%-damped UHS for the city of Dubai at the same return periods (Figure 3.28) and plots of the disaggregated hazard for PGA and 1.0 s at 475-year return period (Figure 3.27).

Table 3.9. PGA and SA for the cities of Dubai and Abu Dhabi at 475-year and 2475-year return periods, from Peiris *et al.* (2006).

Ground-motion parameter	Abu Dhabi		Dubai	
	475-year	2475-year	475-year	2475-year
PGA (g)	0.05	0.1	0.06	0.12
0.2 s SA (g)	0.081	0.145	0.107	0.186
1.0 s SA (g)	0.038	0.074	0.053	0.102

The disaggregation plots show, as Peiris *et al.* (2006) assert, that PGA is governed by near-to-source small-magnitude events (local activity) and that SA at 1.0 s is governed by more distant events with larger magnitudes. Worth to notice that Peiris *et al.* (2006) are well outside of the range of applicability of the ground-motion prediction equations used for their study,

for both distance and magnitude. In Figure 3.27 they present disaggregated results for a maximum magnitude of M_w 9.25 and distances up to 500 km, while, for example, Spudich *et al.* (1999) model was developed for a maximum magnitude M_w = 7.2 and distances up to 100 km. It is also important to mention that extrapolating beyond the strict limits of applicability of the ground-motion models is inevitable when assessing the seismic hazard of the UAE. The present work is also affected by this limitation on the ground-motion models and could only be avoided through the use of detailed seismological models that are not currently available for this region.

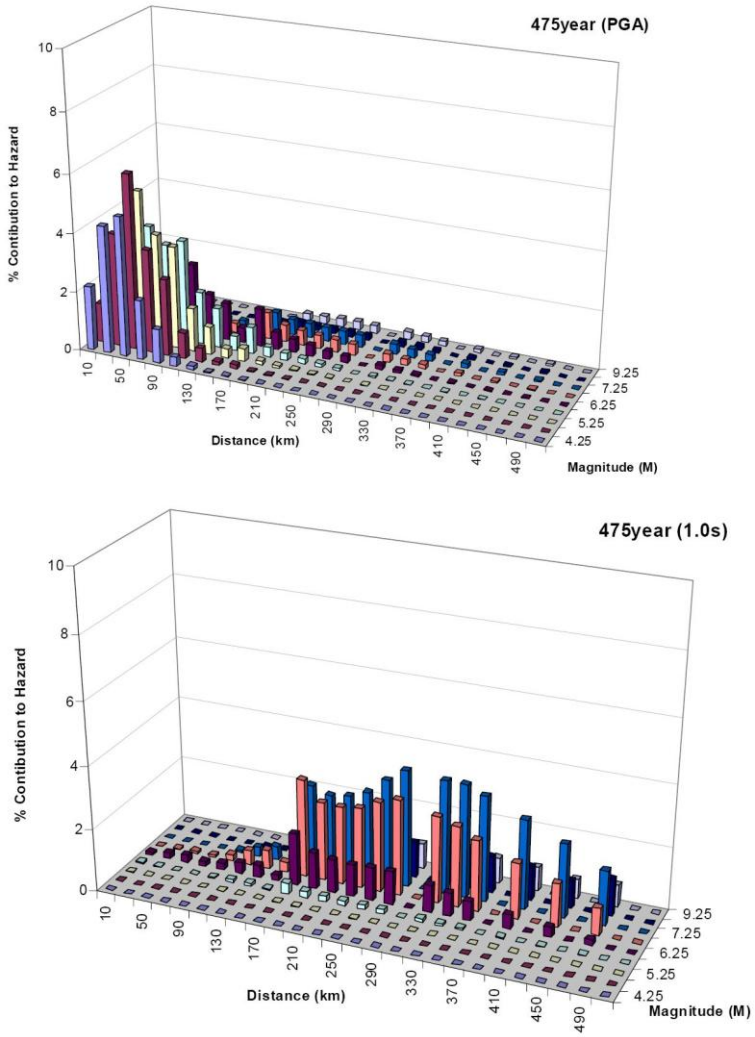

Figure 3.27. Disaggregation of seismic hazard in Dubai for PGA and 1.0 s at 475-year return period (Peiris *et al.*, 2006).

Other issue to highlight is that they do not state what metric distance definition was used to plot the disaggregated results. This is important since as it was previously mentioned, the equations used for the hazard analysis consider different distance definitions. This issue could strongly affect the distribution of the magnitude-distance scenarios.

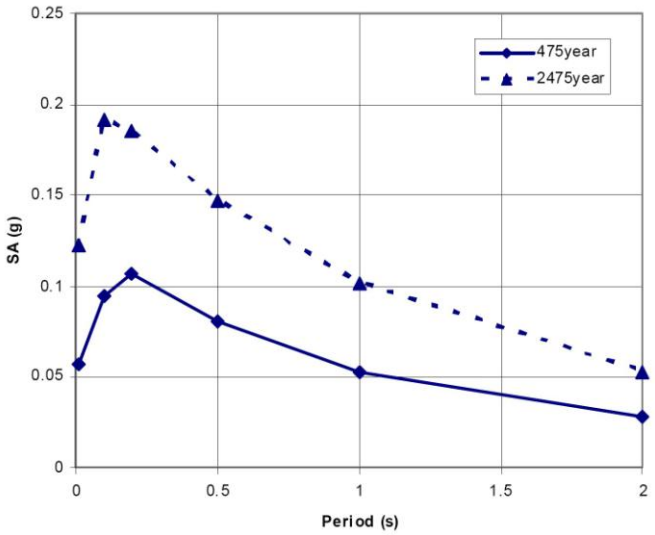

Figure 3.28. Bedrock UHS for Dubai (5% damping) for 475-year and 2475-year return periods (Peiris *et al.*, 2006).

3.3.6. Sigbjornsson & Elnashai (2006)

Sigbjornsson & Elnashai (2006) present a seismic hazard analysis for Dubai, UAE. They present PGA values and UHS for 974-year and 2475-year return periods (5% and 2% probability of exceedance in 50 years, respectively). The site condition for which the PGA values and UHS were calculated is not stated. Additionally, they present synthetic earthquake ground-motion accelerograms for conducting dynamic time-history analyses.

The hazard analysis presented by Sigbjornsson & Elnashai (2006) has some important features that warrant comment. They compile their catalogue based on previous work (Ambraseys & Melville, 1982; Ambraseys *et al.*, 1994; GSHAP, 1999) for the period from 189 BC to 1996. For the period from 1994 to 2004 they include information from the National

Earthquake Information Center (NEIC, 2006) for events with epicentres less than 1000 km from Dubai.

They do not present a seismic zonation map or even tabulate the earthquake recurrence parameters adopted for their analysis, but apparently base their source zonation on the work of Tavakoli & Ghafory-Ashtiany (1999). They extend this model adding the Dibba fault and a fault along the west coast of the UAE. The latter is a seismic source also considered by Wyss & Al-Homoud (2004) and present in the tectonic map of Saudi Arabia and adjacent areas by Johnson (1998).

To the knowledge of the author, there are no well-founded bases for asserting the existence of a fault running along the west coast of the UAE. Even if the existence of this fault were irrefutable, the complete lack of any reported event in the vicinity of this fault would make it very difficult to consider this structure as being an active fault. A sensitivity analysis considering this source as an active source is presented in section 5.1.

For ground-motion prediction, Sigbjornsson & Elnashai (2006) select the equations of Ambraseys *et al.* (1996) and Simpson (1996) for all sources without accounting for the varying tectonic regime of the sources. As in the studies previously discussed, the applicability of such equations to the Makran subduction zone is easily refuted. Sigbjornsson & Elnashai (2006) also consider predictions of peak ground displacements (PGD) and for this purpose they adopt the model proposed by Ambraseys & Srbulov (1994).

Although the authors correctly assert that "*the data for this region seems to be too limited for derivation of a site-specific equation*" they then go on and derive coefficients to extend the range of the Ambraseys *et al.* (1996) model up to response periods of 4 s. Worth to comment that extending the period range is unlikely to be appropriated as discussed by Akkar & Bommer (2006).

Although the horizontal component definition used in the discussed study is not explicitly mentioned, it is assumed to be the large horizontal component as it is the horizontal definition used by both Ambraseys *et al.* (1996) and Simpson (1996). Regarding the metric distance definition both ground-motion models use the same definition, r_{jb} for events > 6.0 M_s and r_{epi} otherwise.

Sigbjornsson & Elnashai (2006) present a hazard curve for PGA and the 5%-damped UHS for 974-year and 2475-year return periods (Figure 3.29). Although the values obtained by Sigbjornsson & Elnashai (2006) are lower than those reported by GSHAP (Grünthal *et al.*, 1999), they are still significantly higher than the values presented by Adballa & Al-Homoud (2004) which should be regarded as highly conservative.

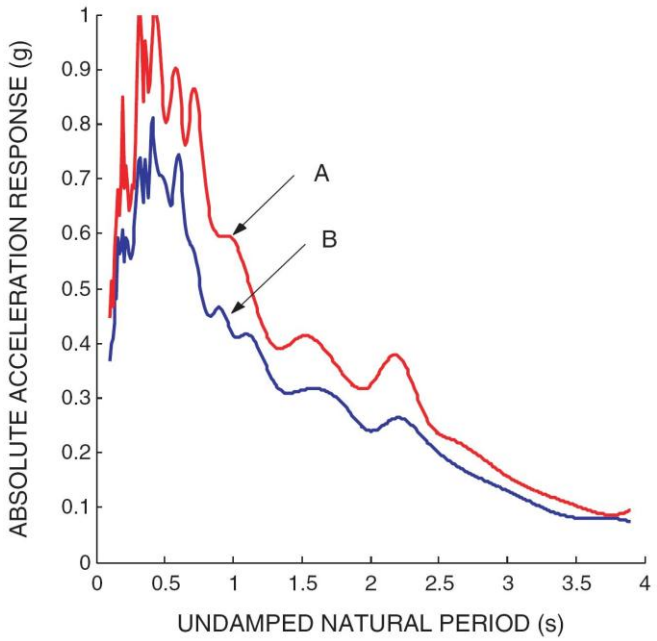

Figure 3.29. Uniform hazard spectrum for Dubai, showing the horizontal acceleration response for 5% probability of being exceeded (B curve) and 2% probability of being exceeded (A curve) in 50 years. Damping ratio is 5% of critical (Sigbjornsson & Elnashai, 2006).

Finally, they correctly assert that, "*large distant events contribute most to the long-period part of the uniform hazard spectrum, while the short -period part is mainly affected by moderate-size events with short source distances.*"

However, they attempt to demonstrate this by comparing response spectra obtained from two arbitrarily chosen earthquake scenarios, an M_w 7.0 event at 100 km and an M_w 6.0 event at 20 km. They do this instead of disaggregating the results of the hazard analysis and using this to define the magnitude-distance scenarios corresponding to the relevant parts of the UHS.

Their demonstration using an M_w 7.0 event at 100 km and an M_w 6.0 event at 20 km is entirely decoupled from the seismic source model and is therefore uninformative.

3.3.7. Musson *et al.* (2006)

In 2002 the government of the UAE contracted the British Geological Survey (BGS) to undertake a detailed geological mapping of the mountainous north-eastern region of the country. As part of this project geohazard maps, including seismic hazard maps, were developed for the entire country.

The complete project is reported in 5 volumes, with volume 4 corresponding to the seismic hazard analysis (Musson *et al.*, 2006). They present hazard maps for PGA (for bed rock site conditions) at 475-year, 1000-year and 10,000-year return periods and Intensity maps (EMS-98) for 1000-year and 10,000-year return periods. They also present seismic hazard curves for PGA and uniform hazard spectra (UHS), up to 2 s, for the 7 capitals of the emirates at return periods of 475 years, 1000 years and 10,000 years. One of the main outcomes of this report is a summary seismic hazard map showing PGA values for firm rock for a 475-year return period and the corresponding seismic zonation according to the UBC97 zonation criteria.

Musson *et al.* (2006) present an earthquake catalogue for events of surface wave magnitude > 3.0 (Figure 3.30). The basis for this catalogue is the BGS World Seismicity Database (WSD) and is complemented with data

from other publications related to both the historical and the instrumental part of the catalogue (e.g., Ambraseys, 2001; Ambraseys & Melville, 1982). However, for the subsequent seismic analysis they only consider events with magnitude greater than 4.0 M_S. It worth mentioning that in their earthquake catalogue, Musson *et al.* (2006) present newly found historical events and relocations. However the seismicity analysis presented herein was completed prior to the author being made aware of this fact. The present work does not benefit from these recent findings, but the additional events would act to supplement the robust catalogue of Ambraseys & Melville (1982). The impact of omitting these events on the hazard results is thought to be very small, albeit most likely in an unconservative manner.

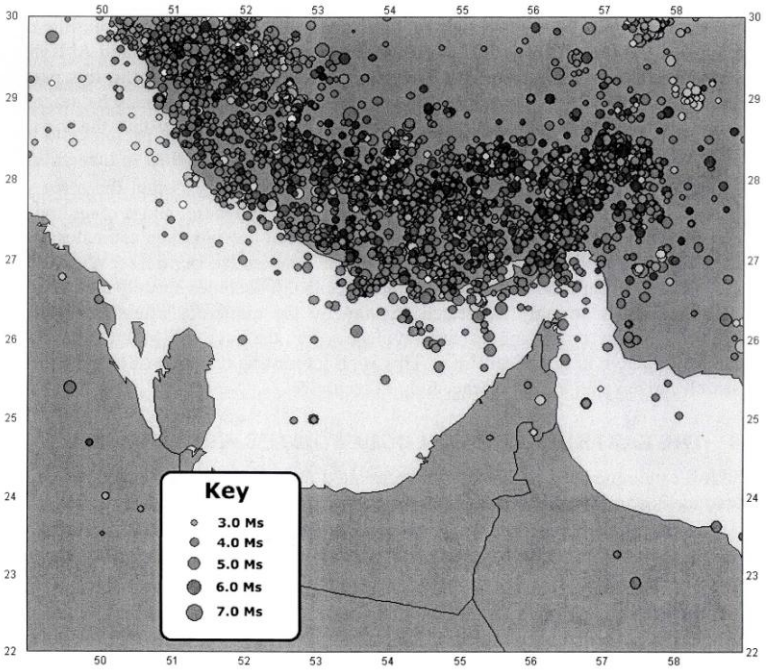

Figure 3.30. Earthquake catalogue for the study area (Musson *et al.*, 2006).

For the seismic source zonation Musson *et al.* (2006) divide the region into 19 seismic sources which are broadly consistent with the seismotectonic environment of the region (Figure 3.31).

In terms of ground-motion prediction equations, Musson *et al.* (2006) use the model of Ambraseys (1995) for PGA, the model of Ambraseys *et al.*

(1996) for SA and a modified version of the Gaull *et al.* (1990) model for intensity that was originally developed for use in western Australia. No prediction equations specifically developed for subduction earthquakes are used and the Makran subduction zone is treated as a region that generates shallow earthquakes.

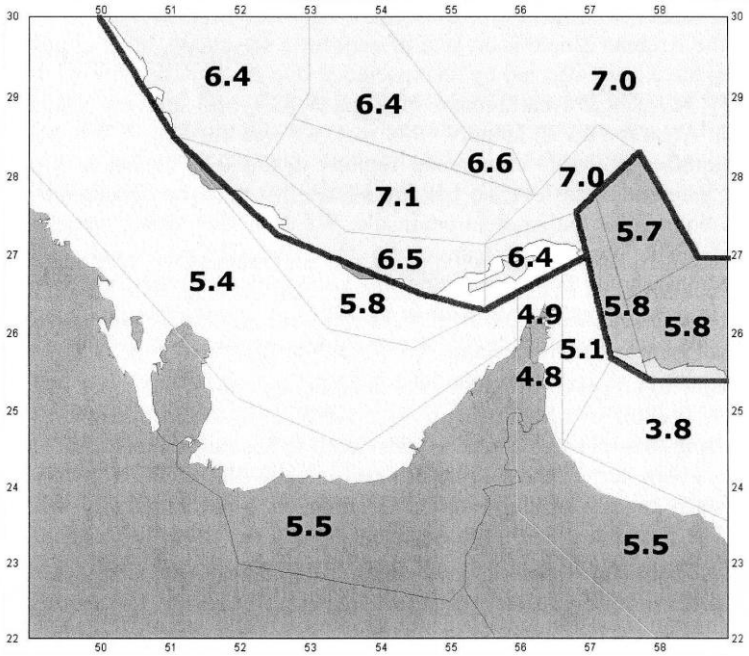

Figure 3.31. Seismic source zonation and maximum magnitudes for each source (Musson *et al.*, 2006).

Additionally, no account is made for prediction equations for stable continental regions, for PGA and SA. Instead, prediction equations for active regions are used to predict ground-motions from events occurring in the stable Arabian plate. This latter point is particularly interesting given that they acknowledge this regime through the use of the Gaull *et al.* (1990) model.

Although the horizontal component definition and the metric distance definitions are not directly stated in the discussed work, both ground-motion equations, Ambraseys (1995) and Ambraseys *et al.* (1996), use the larger horizontal component, r_{jb} distance for events > 6.0 M_s and r_{epi} otherwise. The distance definition for the Gaull *et al.* (1990) model is r_{hypo}.

An interesting issue in this project is the discussion on the differences in the seismic activity between the eastern and western halves of the Makran subduction zone. Musson *et al.* (2006) consider the possibility, without reaching a conclusion, that at the western half of this zone either subduction occurs aseismically, or the plate boundary is locked and at some point will rupture causing a great earthquake.

Despite such considerations, they decide to discount the possibility that the 1483 Hormuz earthquake was in fact a large subduction front event on the western Makran and thus consider the western region of the Makran as aseismic and with a maximum observed magnitude of 3.8 M_s. As result of this hypothesis, they relocate the 1483 Hormuz event supposed to have occurred in the straits of Hormuz, to a position 250 km north-east of the original position reported by Ambraseys & Melville (1982). Nevertheless, they assign to this source a maximum magnitude for the hazard analysis of 7.0 M_s.

Musson *et al.* (2006) attempt to support this decision by conducting a sensitivity analysis on the PGA, 0.2 s and 1.0 s SA values corresponding to a return period of 475 years for both cases of including or ignoring seismic activity in the western Makran. Their results show that differences in ground-motion levels between these two cases are small enough to enable the possibility of a large earthquake occurring in this region to be neglected. However, it is necessary to take into consideration the fact that the strongest influence of large events with long recurrence intervals occurring at the west half of the Makran subduction zone would be seen in the UHS at long response periods and at longer return periods.

Since the objective of the Musson *et al.* (2006) study is to produce a seismic hazard map of the UAE, they do not present disaggregated results to accompany the hazard analysis. These disaggregated results would help to better understand which of the seismic sources as well as magnitude-

distance scenarios contribute most to the seismic hazard at various response and return periods, and which are relatively unimportant. However, disaggregation is site-specific by definition and is not particularly amenable to regional hazard analyses. The contribution of west Makran and the impact of Musson *et al.* (2006) assumption regarding the activity in this region would be better understood within this context.

In general terms Musson *et al.* (2006) conclude that the seismic hazard in the UAE is low and that the hazard increases from south to north towards the Musandam peninsula (see Figure 3.32). Regarding the locations of interest for the present study, they use the scheme of UBC97 to classify the cities of Abu Dhabi and Dubai as zone 0 and the city of Ra's Al Khaymah as zone 1, with PGA values of 0.035 g, 0.050 g and 0.080 g, respectively (Figure 3.32).

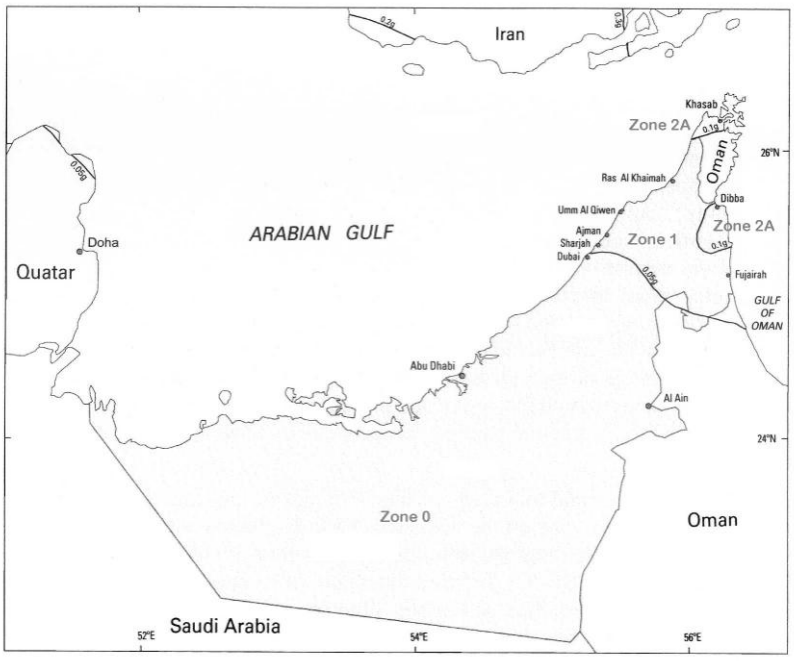

Figure 3.32. Summary seismic zonation map showing peak ground-motion acceleration contours (firm bedrock) with 10% probability of exceedance in 50 years and Unified Building Code (1997) seismic zones 0, 1, and 2A (Musson *et al.*, 2006).

3.3.8. Malkawi *et al.* (2007)

The most recent study, to the knowledge of the author, regarding seismic hazard assessment in the UAE is that by Malkawi *et al.* (2007). This study presents seismic hazard maps for different return periods for the whole country. Additionally, seismic hazard curves and uniform response spectra are presented for 15 major cities in the Emirates. The hazard results are presented for rock-site conditions.

Malkawi *et al.* (2007) consider for their analysis two alternative seismic sources. In both cases they treat all earthquakes in the Makran, Zagros and Stable craton regions as a single source. Source I is defined as window traced from 15.7N, 46.1E to 31.6N, 67.3E. This region covers basically all southern Iran (Zagros and Makran), northern Oman, the Persian Gulf and the UAE. Source II is defined as an area that includes "*all seismic events that can effectively influence any site within the UAE boundaries and induce significant ground motion*" (Malkawi *et al.*, 2007). To spatially define this area they took an area traced by 1000 km from the boundaries of the UAE.

They compiled the earthquake catalogue for m_b magnitude. For converting from M_s and M_L to m_b, Malkawi *et al.* (2007) derived two relationships based on their earthquake catalogue. Enormous differences can be observed from a quick comparison of the results of these equations with well known published relationships (i.e. Ambraseys & Free, 1997; Griscom & Arabasz, 1979; Scordilis, 2006).

They use a single equation for predicting PGA, the eastern North America equation of Atkinson & Boore (1997). This equation was derived for PGA on very hard rock sites. Response spectra are then constructed by finding pairs of magnitude and distance, corresponding to different return periods, and applying the Joyner & Boore (1988) equation.

As result of this, they report PGA values of 0.09, 0.15 and 0.21 g for the cities of Abu Dhabi, Dubai and Ra's Al Khaymah respectively, for a return period of 475 years.

In general terms, Malkawi *et al.* (2007) show a serious lack of understanding regarding the tectonic environment of the region. In combination with a considerable number of shortcomings regarding the fundamentals of PSHA, this makes the findings of this study highly questionable.

Thus far, all the existing published studies of seismic hazard in the UAE have not answered in a clear and conclusive way what is the real level of the seismic hazard in the region. Instead, they present an incomplete and contradictory image. These studies fail on defining how the different seismic sources contribute to the hazard and which the dominating magnitude-distance scenarios are for different return and response periods.

As it is stated at the beginning of this chapter, some of the main cities of the UAE have a very high construction rate, as is the case of Dubai and Abu Dhabi; being the first, one of the cities with the highest construction rate in the world. Therefore, there is scope and justification for a new, stringent and transparent seismic hazard analysis; being this the main goal of the study presented in this chapter.

3.4. Source zonation

Based on the geology, tectonics and seismicity of the region presented in section 3.1, twenty distinct seismic sources were identified. A list of the seismic sources showing source name and number is presented in Table 3.10. In the Zagros region these seismic sources match with the morphotectonic units defined by Berberian (1995); zones 1 to 7.

Table 3.10. List of seismic sources.

Source number	Source name	Source number	Source name
1	High Zagros thrust belt	11	Makran Intraplate
2	Simple Fold belt	12	Makran background
3	Dezful Embayment	13	Sabzevaran-Jorift fault
4	Zagros Foredeep	14	Minab-Zendan fault
5	Persian Gulf (I, II & III)	15	Stable craton (I, II & III)
6	Kazerum fault	16	Owen fracture zone
7	Borazjan fault	17	Oman mountains
8	Aliabad zone	18	Makran interplate
9	Nek south fault	19	Makran Inter east
10	Gowk fault zone	20	Makran Inter west

Within the Arabian Peninsula two seismic sources were defined, the Stable craton and the Oman Mountains (zones 15 and 17). Despite the scarce information regarding geology and seismicity in this region, a special effort was made in defining these seismic sources due to their potential influence on the hazard for the sites under consideration.

In the Makran region and in eastern Iran, seven seismic sources were defined (zones 11 to 14 and 18 to 20) taking into consideration the most important geological features and the seismicity associated with them. For the subduction zone, two seismic sources were defined: Makran Interplate and Makran Intraplate. The boundary between these two zones was taken as the point where the subducting plate changes its slope (see Figure 3.7 and Figure 3.8).

Although it could be argued that defining the seismic sources primarily on the basis of the morphotectonic units of the region may not be the optimal approach given the inhomogenous nature of the occurrence of past events within some of the seismic sources, the seismic source zonation presented herein is considered adequate. This is valid mainly in light of the purpose of the sensitivity analysis presented in subsequent chapters.

Most of the sources were modelled as areal sources with the exception of sources 6, 7, 11, 13, 14, 18, 19 and 20 which were modelled as sloping plane sources that have the average dips and strikes of the main faults. In Figure 3.33 sources 6, 7, 13 and 14 are shown as dash-dotted lines indicating the strike of the main faults. The surrounding area, denoted by dotted lines, indicates the area of influence of these faults or fault systems. In other words, all the seismicity that is observed to occur within these areas is considered as being related to these main faults and is associated with these sources accordingly.

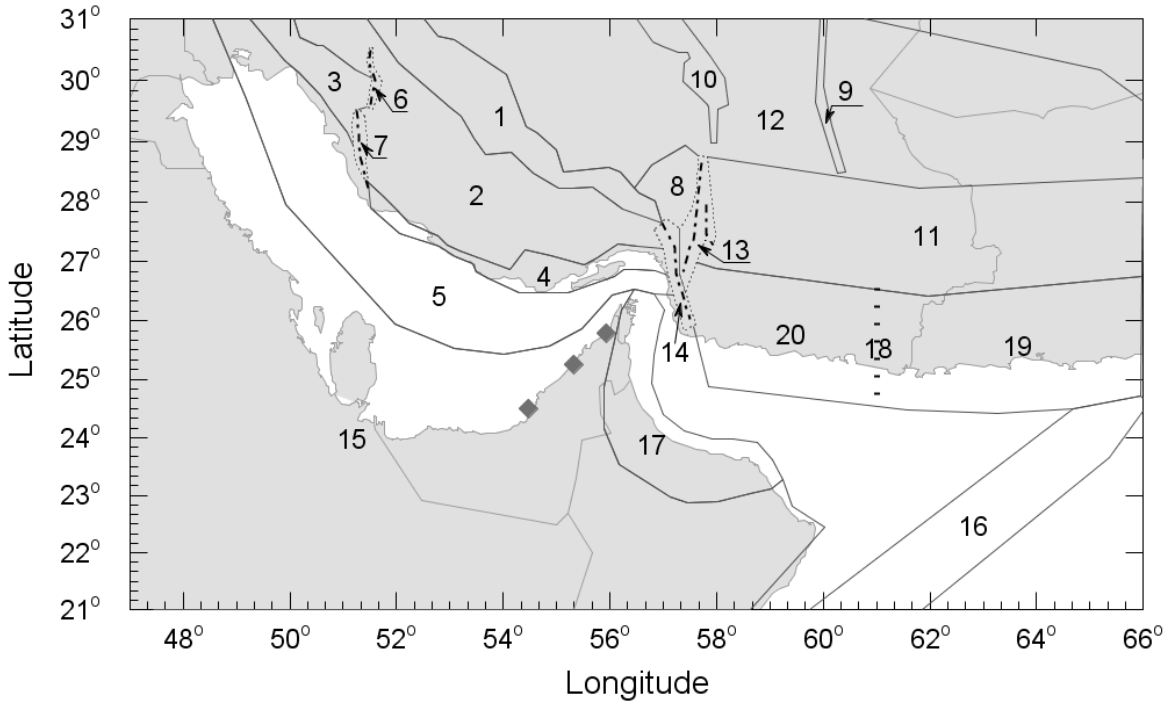

Figure 3.33. Seismic source zonation option I. Sources 6, 7, 13 and 14 are modelled as 2D planes according to the average dip and strike of the main faults. Dotted lines surrounding these faults show the area for which seismicity is associated with the fault sources. Dash-dotted lines show the location of the faults. The large-dotted line is the division between eastern and western Makran. Diamonds show the cities of Abu Dhabi, Dubai and Ra's Al Khaymah. Numbers correspond to the seismic source zones presented in Table 3.10.

Due to epistemic uncertainty regarding boundary locations between seismic sources, as well as the complicated tectonics associated with the Makran subduction zone, it was necessary to consider three alternative

seismic source zonations (Figure 3.33 to Figure 3.35). The results arising from these alternatives were combined through the use of a logic tree.

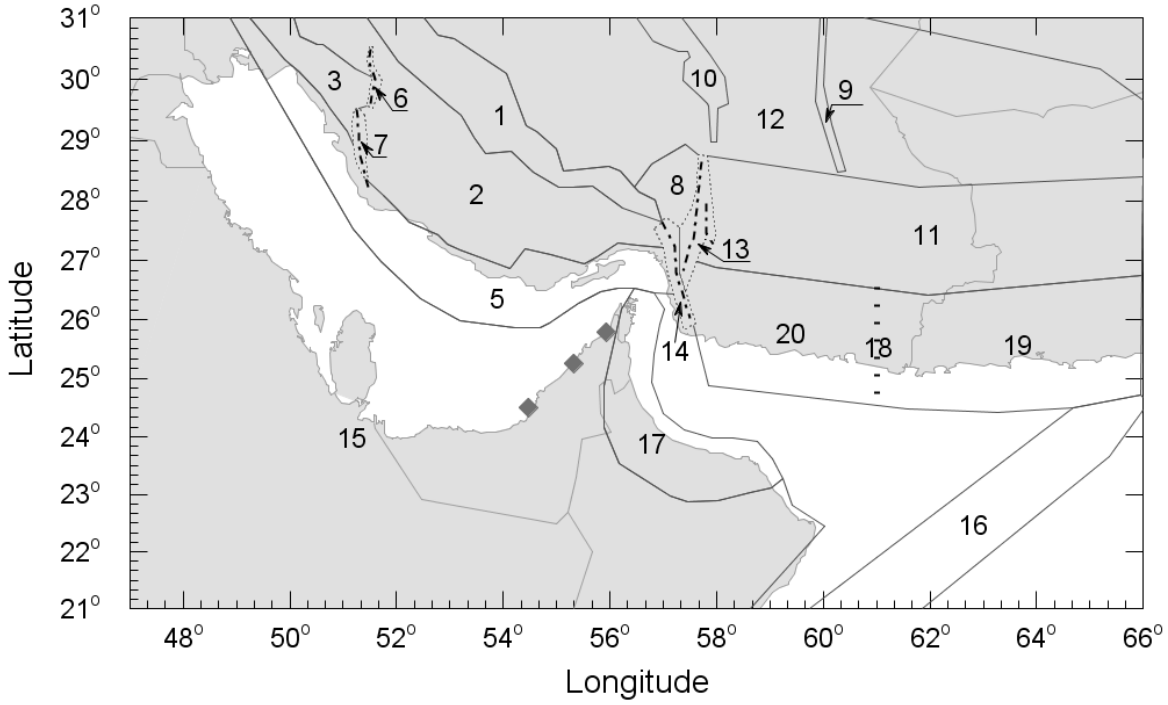

Figure 3.34. Seismic source zonation option II. For this option the boundary between sources 5 and 15 has moved northwards of the boundary between these sources in option I (Figure 3.33), and the seismicity of source 4 (option I, Figure 3.33) has merged with the seismicity of source 5.

These three seismic source zonations consider two alternative locations for the boundary between the Arabian stable craton (zone 15) and the Zagros fold belt (zone 5); see seismic source zonation option II and III (Figure 3.34 and Figure 3.35). These alternatives also address whether or not the Zagros Foredeep region (zone 4) should be considered as an independent seismic source but include its seismicity into the Persian Gulf source (zone 5); see seismic source zonation option I and III (Figure 3.33 and Figure 3.35).

A similar situation occurs in the Makran Interplate zone, where the apparent difference in earthquake activity between the eastern and western regions, as well as the unlikely but possible rupture along the whole subduction zone leads to splitting the Makran Interplate seismic source

(zone 18) into two sources, Makran Interplate East (zone 19) and Makran Interplate West (zone 20).

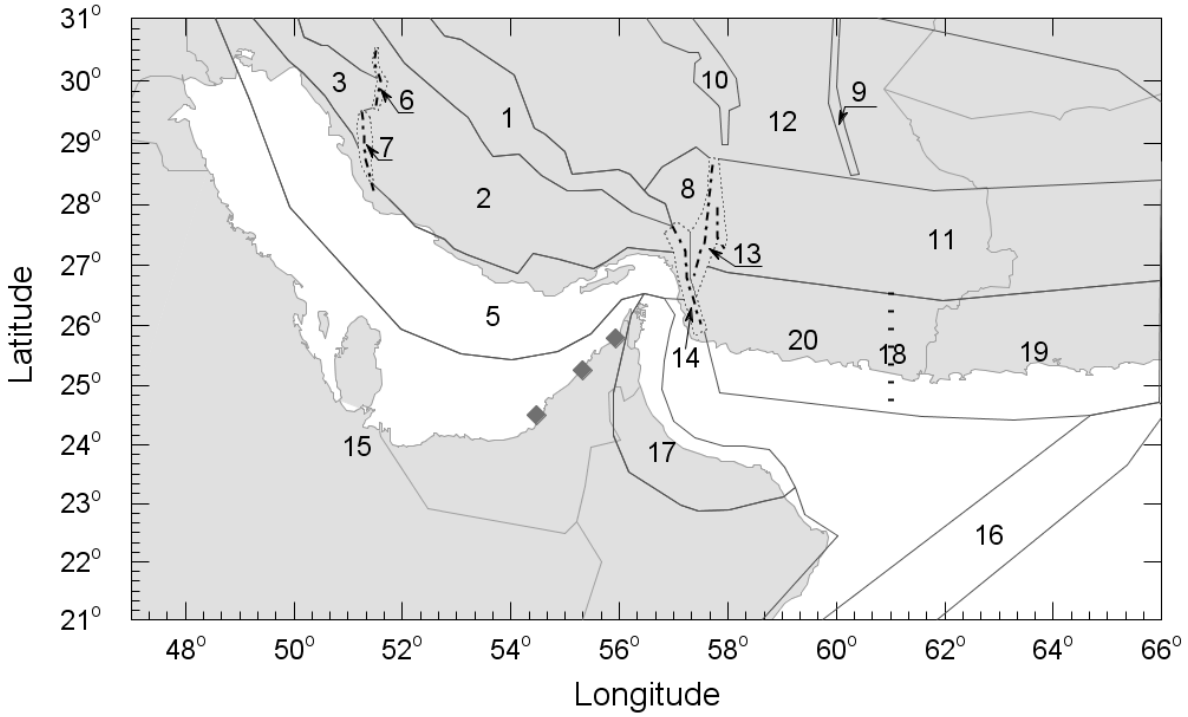

Figure 3.35. Seismic source zonation option III. For this option the boundary between sources 5 and 15 has the same location as in option I (Figure 3.33), however the seismicity of source 4 (option I, Figure 3.33) has merged with the seismicity of source 5 (as in option II, Figure 3.34).

These genuine uncertainties may have a significant impact upon hazard estimates for locations within the UAE. At this point one must entertain alternative possibilities. The most common approach for handing such alternatives is to use a logic-tree. This is what is used herein but is explained in detail later in the text.

Figure 3.36 show the three options for the seismic source zonation with the seismicity superimposed. Dotted lines are the different options for the boundaries of sources 4, 5 and 15, and the division between east and west Makran.

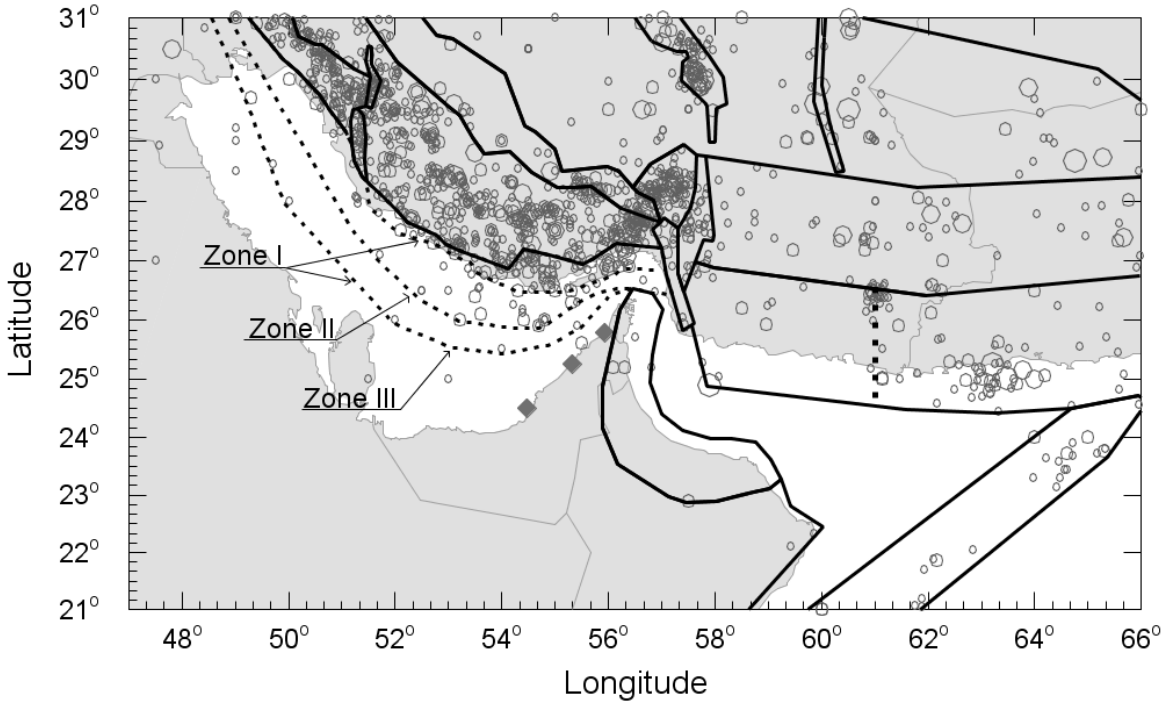

Figure 3.36. Seismic source zonation with seismicity superimposed. Dotted lines show different boundaries for zones 4, 5 and 1 5.

3.4.1. Earthquake occurrence parameters and maximum magnitudes.

For the estimation of the earthquake occurrence parameters two different magnitude-frequency distributions were considered depending on the seismicity observed in each of the seismic sources as well as tectonic/mechanistic considerations. For most of the sources an exponential magnitude distribution (Cornell & Vanmarcke, 1969; Gutenberg & Richter, 1944; Richter, 1958) truncated at lower and upper magnitude limits was considered, except for sources 18, 19 and 20, for which a characteristic distribution (Schwartz & Coppersmith, 1984; Youngs & Coppersmith, 1985) was considered. An overview of the exponential and characteristic recurrence models is presented in section 2.2.

Due to the varying completeness levels of the seismicity catalogue it is not appropriated to adopt a straightforward estimation of the occurrence parameters (β and υ_{min}) through common regression approaches. For this reason, methods such as that described by Weichert (1980) must be applied.

Alternative methods for solving this issue are also addressed by Cosentino *et al.* (1977), Kijko & Sellevoll (1989; 1990), Dong *et al.* (1984) among others.

The earthquake occurrence parameters, β, υ_{min} and their associated standard deviations, for exponential distributions, were estimated applying the methodology proposed by Weichert (1980) that considers different periods of completeness for different threshold magnitudes.

For the seismic sources for which the characteristic earthquake model was applied, the occurrence rate of the characteristic earthquake was calculated based on the seismic moment estimated from geological slip rate and fault geometry as suggested by Youngs & Coppersmith (1985). The fault geometry was inferred from mapped faults and in some cases the seismicity associated with the fault was used in addition to the mapped length.

The Oman Mountains zone is a particular case, where geological features and the estimated slip rate for the region were used to estimate the seismic moment and based on it determine β and υ_{min} (Youngs & Coppersmith, 1985).

For the Arabian stable craton, different values of β were used based on two publications. The first of these is Fenton *et al.* (2006) who propose a β value of 1.84 as a world average for seismicity in stable cratonic cores and an annual long-term rate of 0.004 per 10^6 km^2 for events of magnitude ≥ 6 M_w. A second publication, this by Johnson *et al.* (1994), reports a β value of 2.26 as the average of all the stable continental regions and an annual occurrence rate of ~0.004 per 10^6 km^2 for events 6 M_w and greater. For this case the υ_{min} values were calculated by fixing the β values within Weichert's (1980b) procedure and fitting the curves to the Arabian stable craton seismicity.

For estimation of the maximum magnitude (m_{max}) the relations proposed by Wells & Coppersmith (1994) were used when consistent data

regarding fault type and total length of the faults were able to be retrieved. When this was not possible, the maximum magnitude was estimated using the statistical procedure proposed by Kijko (2004). In any remaining case the common, yet subjective, practice of adding 0.5 units to the maximum observed magnitude was applied (see Table 3.11).

Due to the characteristics of the software used for the hazard analysis (Ordaz *et al.*, 2007), to be able to consider seismic sources with a characteristic magnitude distribution (sources 18, 19 and 20) it was necessary to consider for each one of them two seismic sources with exactly the same spatial location. One seismic source having an exponential distribution and the other a purely characteristic distribution, in such a way that the sum of the occurrence rates from both models corresponds to the target occurrence rate of the desired characteristic earthquake distribution of Youngs & Coppersmith (1985). A schematic representation of this process is presented in Figure 3.37.

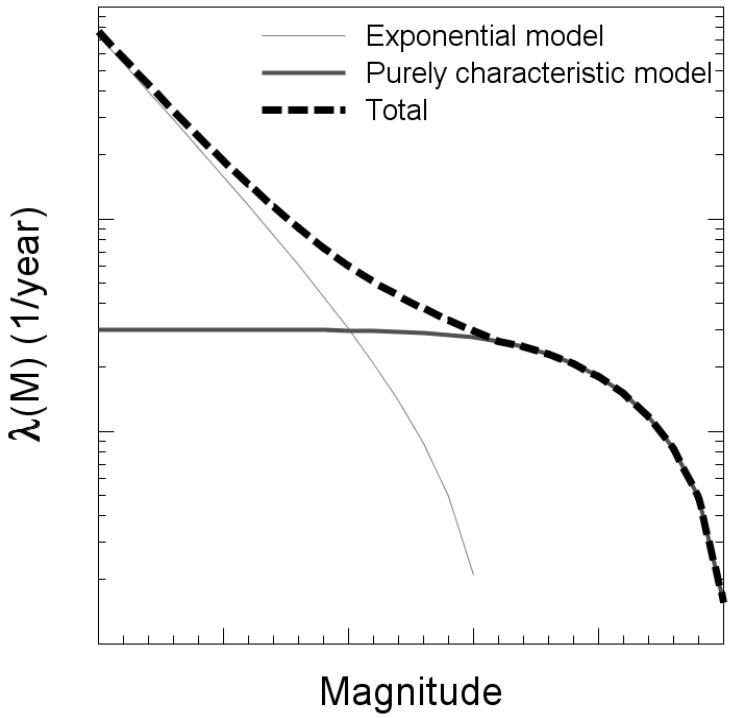

Figure 3.37. Shapes of the occurrence rates for exponential and purely characteristic models as well as the addition of both curves.

Table 3.11. Summary of the earthquake recurrence parameters. m_{max} - maximum magnitude; $m_{max(obs)}$ - maximum observed magnitude; m_{min} - minimum magnitude considered for the analysis; m_{ch} - expected value of the characteristic earthquake; N of events - number of events in the region or seismic source; a and b are the constants in the Gutenberg-Richter equation; $\beta = b\ \mathrm{Ln}(10)$; v_{min} - number of earthquakes per year with magnitude greater than m_{min}; σ() - standard deviation associated with the estimation of the parameter between brackets.

Exponential Seismicity

Zone / Region	m_{max}	σ (M_{max})	$m_{max(Obs)}$	m_{min}	Number of events	β	σ (β)	b	σ (b)	v_{min}	σ (v_{min})	a
All Catalogue			**8.0**	**4.0**	**1290**	**1.66**	**0.037**	**0.72**	**0.016**	**24.10**	**0.019**	**4.26**
Zagros	**7.2**	**0.12**	**7.1**	**4.0**	**840**	**1.86**	**0.055**	**0.81**	**0.024**	**17.24**	**0.021**	**4.47**
High Zagros	6.8	0.20	6.6	4.0	55	1.52	0.203	0.66	0.088	1.07	0.019	2.67
Simple Fold	7.3	0.17	7.1	4.0	466	1.91	0.075	0.83	0.033	9.66	0.021	4.31
Dezful Embayment	5.8	0.14	5.7	4.0	122	1.77	0.186	0.77	0.081	2.56	0.021	3.51
Zagros Foredeep	6.9	0.14	6.8	4.0	83	1.40	0.157	0.61	0.068	1.56	0.019	2.63
Persian Gulf I	6.1	0.23	5.9	4.0	52	1.78	0.261	0.77	0.113	1.08	0.021	3.14
Persian Gulf II	6.9	0.12	6.8	4.0	129	1.57	0.133	0.68	0.058	2.52	0.020	3.14
Persian Gulf III	6.9	0.12	6.8	4.0	135	1.59	0.130	0.69	0.057	2.65	0.020	3.18
Kazerum Fault	6.8*	0.23*	6.0	4.0	24	1.45	0.301	0.63	0.131	0.46	0.019	2.18
Borazjan Fault	6.9*	0.23*	5.5	4.0	27	2.10	0.348	0.91	0.151	0.58	0.021	3.41
Makran	**8.2**	**0.24**	**8.0**	**4.0**	**401**	**1.76**	**0.070**	**0.76**	**0.031**	**8.02**	**0.070**	**3.96**
Aliabad zone	6.6	0.16	6.4	4.0	90	1.95	0.187	0.85	0.081	1.89	0.021	3.66
Nek south fault	8.0*; 8.0~	0.28*	7.0	4.0	7	0.99	0.363	0.43	0.158	0.11	0.016	0.77
Gow fault zone	8.1*; 8.0~	0.28*	7.0	4.0	62	1.76	0.179	0.77	0.078	1.24	0.000	3.16
Makran Interplate	LT	0.00	8.0	4.0	85	1.83	0.162	0.79	0.070	1.64	0.020	3.40
Makran Interplate East	LT	0.00	8.0	4.0	62	1.74	0.182	0.76	0.079	1.18	0.020	3.10
Makran Interplate West	LT	0.00	7.7	4.0	22	2.06	0.358	0.89	0.155	0.44	0.021	3.22
Makran Intraplate	6.8	0.24	6.6	4.0	54	1.63	0.212	0.71	0.092	1.07	0.020	2.87
Makran Background	7.5	0.50	7.0	4.0	87	1.66	0.149	0.72	0.065	1.71	0.020	3.11
Jorift-Sabzevaran fault	6.7*	0.28*	5.7	4.0	21	2.42	0.448	1.05	0.195	0.47	0.022	3.87
Minab-Zendan fault	6.5*	0.28*	5.8	4.0	11	1.25	0.455	0.54	0.198	0.20	0.018	1.49
Stable craton I & III	7.0**	0.50	6.5	4.0	13	LT	LT	LT	LT	LT	LT	LT
Stable craton II	7.0**	0.50	6.5	4.0	19	LT	LT	LT	LT	LT	LT	LT
Owen fracture zone	6.0	0.20	5.8	4.0	26	1.57	0.364	0.68	0.158	0.52	0.020	2.47
Oman Mountains	LT	LT	5.1	4.0	5	1.00	LT	0.43	LT	LT	LT	LT

Characteristic seismicity

Zone / Region	Option	m_n	$m_{ch\text{-}min}$	m_{ch}	σ (m_{ch})	Occurrence Interval (yr)
Makran Interplate	WSZ 1	8.5*	7.8	8.2	0.25*	203
	WSZ 2	8.6*	7.9	8.3	0.25*	428
Makran Interplate East	WSZ 1	8.3*	7.5	8.0	0.25*	139
	WSZ 2	8.5*	7.8	8.2	0.25*	422
Makran Interplate West	WSZ 1	8.2*	7.4	7.8	0.25*	121
	WSZ 2	8.4*	7.6	8.0	0.25*	356

Notes:

~ Proposed by Berberian & Yeats (1999)

* Calculated using Wells & Coppersmith's (1994) relationships.

** Maximum magnitude observed plus 0.5.

LT - See logic tree

WSZ 1 and WSZ 2 are the two likely widths considered for the seismogenic zone in Makran Interplate.

All magnitudes are in M_s scale. When not specified, m_{max} was calculated using the procedure proposed by Kijko (2004).

Bold numbers are the regional earthquake recurrence parameters for the whole catalogue, Zagros and Makran regions.

In this case, the expected magnitude of the characteristic earthquake (m_{ch}) was estimated as 0.5 units below the maximum magnitude (m_u) calculated using Wells & Coppersmith's (1994) empirical relationships. The maximum magnitude ($m_{ch\text{-}min}$) for the exponential part was fixed at 1.0 unit below the maximum magnitude with a standard deviation of zero.

The parameters considered for all the sources and for both models (exponential and purely characteristic) are shown in Table 3.11. Uncertainties regarding the estimation of the maximum magnitude and recurrence rates of characteristic earthquakes for Makran, as well as the occurrence parameter for the Stable craton and Oman mountains, were addressed through the use of a logic tree as will be explained in detail later in the text.

3.5. Ground-motion prediction equations

The selection of the most suitable ground-motion prediction equations (GMPEs) for a particular region has been shown to be one of the main sources of epistemic uncertainty in PSHA. This is of particular concern in regions of low seismicity such as the UAE, where there are not ground-motion recordings available to develop indigenous ground-motion models or to assess the applicability of foreign ground-motion models (c.f., Scherbaum *et al.*, 2004a).

There are not GMPEs specific to the UAE and consequently it has been necessary to adopt foreign ground-motion models. In general terms the criteria for selecting ground-motion models for specific regions as suggested by Cotton *et al.* (2006) was applied. A total of seven well-known ground-motion prediction equations were considered for the hazard analysis in order to address the epistemic uncertainty associated with not knowing what is the optimal model for this region; if one currently exist.

Abrahamson & Silva (1997), Akkar & Bommer (2007b), Ambraseys *et al.* (2005) and Boore & Atkinson (2006) were selected for modelling ground motions from shallow earthquakes in active regions. Since Ambraseys *et al.* (2005) and Akkar & Bommer (2007b) are derived from datasets including Iranian strong-motion records and since all the equations allow specification of style-of-faulting in addition to magnitude, distance and site conditions, it is believed that they are likely to be applicable.

Atkinson & Boore (2006), which was developed for the stable continental region (SCR) of eastern North America, was used to predict ground motions in the Arabian stable craton. However, since the region is close to actively deforming margins, the assumption of the UAE being an SCR cannot be proven, so the previous four equations for active shallow crustal regimes are adopted in addition.

Atkinson & Boore (2003) and Youngs *et al.* (1997) were selected as two alternative models for estimating ground motions from events occurring in Makran subduction zone. Both are well-known equations derived from datasets including ground-motion records from several subduction zones. A summary of the main characteristics of these ground-motion models is given in what follows.

Abrahamson & Silva (1997) present a ground-motion model to predict PGA and SA for 5% damping. This equation was derived for shallow crustal earthquake in active regions with magnitudes, M_w > 4.5. They use two generic site categories, rock (V_{s30} >600 m/s) and deep soil and account (albeit simply) for nonlinear site response. For the style of faulting, they consider three options: reverse, reverse/oblique and others (strike-slip and normal). The distance definition used is r_{rup} and the horizontal component definition is the geometric mean.

Akkar & Bommer (2007b) present an equation for the prediction of displacement response ordinates for damping ratios of 2, 5, 10, 20 and 30 %

of critical, for response periods up to 4.0 s and also for PGA, using the strong-motion databank from Europe and the Middle East. The equation was derived for moment magnitudes between 5.0 and 7.6 and for distances up to 100 km. They include into the equation style-of-faulting and site class as explanatory dummy variables. The distance definition is the Joyner & Boore distance (r_{jb}) and the horizontal component definition is the geometric mean.

Ambraseys *et al.* (2005) estimate PGA and SA for damping ratio of 5% and for response periods between 0.05 s and 2.5 s. The equation was derived for shallow crustal earthquakes with magnitudes M_w > 5.0 and distance to the surface projection of the fault (r_{jb}) up to 100 km using data from Europe and the Middle East. They consider faulting mechanism and local site conditions as explanatory variables in the equation; they consider V_{s30} >760 m/s for rock site condition. This equation was derived for the prediction of the larger horizontal component of ground motions.

Boore & Atkinson (2006) present an empirically-based equation for shallow earthquakes, predicting PGA, PGV and PSA for response periods up to 3 s. They use the average horizontal component definition and the distance metric is r_{jb}. They include style-of-faulting as an explanatory variable in the equation and consider site amplification based on the average shear-wave velocity of the upper 30 m (V_{s30}). For rock site conditions they consider a V_{s30} value of 760 m/s.

Atkinson & Boore (2006) developed a stochastic ground-motion prediction equation for hard-rock and soil sites in eastern North America (ENA). The equation was developed for response spectra with a 5% damping ratio, PGA and PGV for hard-rock sites (V_{s30} > 2 km/s) as function of moment magnitude and closest distance to the fault rupture. However, relations are also presented for a reference site condition with V_{s30} = 760 m/s (rock) and non linear amplification factors are presented that enable conversion from this reference site condition to softer site conditions. In the

present study the relations presented for the reference site condition (rock) were used to ensure consistency with other equations. The simulated ground-motion database used to derive this equation includes ground motions of events with magnitudes from 3.5 to 8.0 and distances to the site up to 1000 km.

Atkinson & Boore (2003) present a ground-motion relationship for earthquakes that occur in subduction zones. The equation was developed for PGA and pseudo-spectral accelerations (PSA) with a damping ratio of 5% of critical and for response periods up to 3.0 s. They use databases from the Cascadia subduction zone, Japan (Kyoshin-Net data), Mexico (Guerrero data) and Central America (El Salvador). The equation was derived for moment magnitudes between 5.0 to 8.0 and 8.5 for Intra-Slab and Interface events respectively, for distances up to 550 km and for rock site conditions (V_{s30} > 760 m/s). Furthermore, they include dummy site class variables into the equation for different site conditions. The distance definition used is the closest distance to fault source (r_{rup}); additionally, they include the focal depth as a variable in the equation. The horizontal component definition is the random horizontal component. The maximum depth they consider is 100 km, and they recommend fixing the focal depth to 100 km for deeper events.

Youngs *et al.* (1997) present an equation for predicting PGA and 5% damped SA for subduction zone interface and intra-slab earthquakes of M_w 5 or greater, distances between 10 and 500 km and rock site conditions. They use the M_w magnitude scale and the r_{rup} distance definition. In addition to r_{rup}, focal depth is included as an explanatory variable in their equation. The horizontal component definition used in this equation is the geometric mean. The range of magnitudes used to derive this equation goes from M_w 5.0 to M_w 8.2. A summary of the main characteristics of these equations is presented in Table 3.12.

Table 3.12. Summary of the characteristics of the selected ground-motion prediction equations.

Equation	Magnitude scale	M_{min}***	M_{max}***	Site conditions*	Distance definition	D_{max}** (km)	Horizontal component definition	Faulting mechanism	Tectonic environment
Abrahamson & Silva (1997)	M_w	4.4	7.4	Rock (V_s >600 m/s)	r_{rup}	220	Geometric mean	Reverse/Reverse-Oblique/Others	Active regions, shallow earthquakes
Akkar & Bommer (2007)	M_w	5.0	7.6	Rock (V_s >750 m/s)	r_{jb}	100	Geometric mean	Normal/Reverse	Active regions, shallow earthquakes
Ambraseys *et al.* (2005)	M_w	5.0	7.6	Rock (V_s >750 m/s)	r_{jb}	100	Larger horizontal component	Normal/Thrust/Odd	Active regions, shallow earthquakes
Atkinson & Boore (2003)	M_w	5.0	8.3	Rock (V_s >760 m/s)	r_{rup}	550	Random horizontal component	Interface/In-Slab	Active regions, subduction zones
Atkinson & Boore (2006)	M_w	3.5	8.0	Rock (V_s = 760 m/s)	r_{rup}	1000	Unspecified	Unspecified	Stable continental regions
Boore & Atkinson (2006)	M_w	4.2	7.9	Rock (V_s = 760 m/s)	r_{jb}	300	GMRotDpp; GMRotIpp	Unspecified/Strike-slip/Normal/Reverse	Active regions, shallow earthquakes
Youngs *et al.* (1997)	M_w	5.0	8.2	Rock (V_s >760 m/s)	r_{rup}	500	Geometric mean	Interface/In-Slab	Active regions, subduction zones

Notes:
* - Site condition considered for this study. Other site conditions are reported by the modellers.
** - Maximum distance source-to-site distance in data set.
*** - Maximum and minimum magnitudes in data set.

All these ground-motion models were incorporated and weighted within a logic tree framework which is described in detail in section 3.6. The compatibility of the equations with respect to magnitude scale, distance metric, horizontal component, site condition and faulting mechanism must be taken into account in order to implement these models within a logic-tree framework (Bommer *et al.*, 2005).

All of the equations use the moment magnitude scale (M_w); however, since the earthquake catalogue compiled here is homogeneous only for M_s magnitude, the Ambraseys & Free (1997) equations were used to adjust the ground-motion prediction equations from M_w to M_s.

Despite the fact that different distance metrics are required, given that the software used to perform the hazard analysis –Crisis2007- (Ordaz *et al.*, 2007) allows the use of different distance definitions for different equations, compatibility is not an issue and hence conversions are not need. In other words, Crisis2007 calculates the appropriate distance according to the distance definition required by the prediction equation that is being used. The program also calculates the focal depth, making it possible to use

equations such as those of Atkinson & Boore (2003) and Youngs *et al.* (1997) were the focal depth is a variable in the equation.

Most of the equations use compatible horizontal component definitions, with exception of Ambraseys *et al.* (2005) who use the larger horizontal component. In this case the correction factors suggested by Beyer & Bommer (2006) were applied.

In all cases relations for rock site conditions considering V_{s30} values of about 760 m/s are presented; corresponding to the boundary between NEHRP-A and NEHRP-B site classifications (BSSC - Building Seismic Safety Council, 1994). The only exception to this being the model of Abrahamson & Silva (1997) who consider a lower boundary (V_{s30} > 600 m/s) for rock sites. However, as it is stated as a range (all sites with V_{s30} > 600 m/s) and the difference is relatively small, it can considered compatible and hence corrections for site conditions were not made.

All equations consider faulting mechanisms; therefore no adjustments or corrections were needed for this component of the models.

3.6. The logic tree formulation

All of the epistemic uncertainties associated with the seismogenic sources and the selection of ground-motion prediction equations were captured within a logic tree framework. Under such a framework; whenever some uncertainties arise, the considered options are presented and subjective weights are allocated to the branches that reflect our relative confidence in each of the alternative options (c.f., Bommer *et al.*, 2005; McGuire, 2004; Scherbaum *et al.*, 2005).

For five of the individual seismogenic sources, it was necessary to make use of the logic tree to address the epistemic uncertainty associated with the spatial definition of the source zones. The first of these

uncertainties is with respect to the location of the boundary between two seismic sources, the Arabian stable craton and the Persian Gulf. Due to the lack of detailed geological information in the Persian Gulf, the boundary was established on the basis of recorded seismic activity in the region alone.

Two different locations were considered for this boundary (see Figure 3.34 and Figure 3.35). The northern boundary covers most of the events observed in the Persian Gulf that could be associated with the Zagros fold belt. This boundary location leaves just a few events that are not associated with this source, all of which have magnitudes below M_s 5.0 and which are covered by the southern boundary (see Figure 3.36). These events could belong to the northern margin of the stable craton or could even be slightly mislocated events given that all of them were recorded prior to 1960.

A second uncertainty is with respect to the possibility of whether the Zagros Foredeep region (zone 4 in Figure 3.33) is an independent seismic source in its own right or not. Given the geological and seismicity similarities with the Persian Gulf region, both regions could be modelled as a single seismic source (see Figure 3.35).

These two uncertainties, together, shape the first part of the logic tree with three branches, on for each of the seismic source zonations presented in section 3.4. These options are presented in the logic tree (Figure 3.38) as SSZ I, SSZ II and SSZ III and were weighted 0.6, 0.25 and 0.15 respectively. The weights were assigned according to the confidence on which of the three options will better represent what is truly happening in the region.

Other of the epistemic uncertainties is associated with the seismic activity rates of the Stable craton. The lack of historical and instrumental events reported in the region in combination with the seismic quiescence characteristical of the stable regions makes difficult to assess the activity rates only using the seismicity data available. As explained in section 3.4.1 two different sets of occurrence rate parameters were considered, based on

the same number of publications (Fenton *et al.*, 2006; Johnson *et al.*, 1994). The weights were assigned 0.6 for the β value proposed by Fenton *et al.* (2006) and 0.4 for the β value proposed by Johnson *et al.* (1994). A higher weight was assigned to Fenton *et al.* (2006) since they use a more recent catalogue for the estimation of the seismicity rate.

One of the most difficult seismic sources to characterise was the source zone corresponding to the Oman Mountains. The small number of seismic events that have been recorded in this region and the scarcity of geological information lead to the consideration of three nodes in the logic tree: the first regarding maximum magnitudes, the second regarding the uplift rate in the Oman Mountains, and the third and final one regarding the average dip of the faults in the region. All of these factors were considered in order to estimate the average slip rate of the faults in the region. For all of the three nodes in the logic tree, a maximum, a minimum, and a most-likely value were estimated based on geological features. A higher weight was assigned to the most-likely value (0.4) and equal weights to the maximum and minimum values (0.3). Since the uncertainty on which is the right value is big the difference between the extreme values and the most likely is only 0.1.

The last of the epistemic uncertainties regarding seismogenic sources is related to the Makran subduction zone. The different seismicity patterns on the east and west halves as well as the offset in the volcanic arc suggest a segmentation in two parts of the subduction zone with a boundary coincident with the Sistan structure (~61°E) (Byrne & Sykes, 1992). However, many geologic and tectonic features, like a practically straight margin along its 1000 km length and the absence of significant offsets anywhere offshore suggest no segmentation along the Makran.

Additionally, not enough information regarding the width of the seismogenic zone for the Makran could be retrieved. Here two different

widths were considered (see Figure 3.7 and Figure 3.8) based on instrumental seismicity as well as on information from other subduction zones (Tichelaar & Ruff, 1993). More details regarding these issues were presented in section 3.1.3.

Given this uncertainty, for the Makran Interplate seismic source it was necessary to set up a two-level logic tree. The first level considers the rupture model, for which two options were considered: (i) complete rupture of the subducting slab as a single unit with uniform seismicity, and (ii) a segmented rupture (east and west halves) for which the subducting slab is divided along the 61°E meridian. The option (i) is considered as very unlikely to occur but still possible, for this reason only a 0.05 weight was assigned to it, and 0.95 to the option (ii). The two options for the segmented rupture (east and west halves) were equally weighted as both are considered the same likely to rupture. Finally, among the two possible widths considered for the seismogenic zone, option 1 (WSZ 1) was weighted higher (0.6) as this option is supported by seismic evidence (see section 3.1.3, Figure 3.8).

Generally speaking, the epistemic uncertainty associated with the modelling of ground motions has a bigger influence on the results of a hazard analysis than the other sources of epistemic uncertainty associated with the seismicity model (Bommer *et al.*, 2005). This component of epistemic uncertainty is particularly important, and this uncertainty increases, when sources within different seismotectonic regimes are involved in the analysis as is the case in this work. In particular for this study, seismic sources in stable continental regions and in active regions with both shallow and subduction-zone earthquakes are involved.

Three different levels in the logic tree were included regarding which prediction equation to use. The first of them is regarding the prediction equation to be used for the Arabian stable craton; here two options are considered: (i) to use a prediction equation specifically derived for use in SCR

and that is compatible with the rest of equations used in the analysis (Atkinson & Boore, 2006), and (ii) to use an empirical prediction equation derived for shallow earthquakes in active regions for the reasons previously stated. The second level of the logic tree considers which prediction equation to use for modelling shallow earthquakes in active regions; here four different equations (four branches) are proposed (i.e., Abrahamson & Silva, 1997; Akkar & Bommer, 2007b; Ambraseys *et al.*, 2005; Boore & Atkinson, 2006). The third and last level of the logic tree for the ground-motion models considers which prediction equation to use for modelling earthquakes occurring in subduction zones. For this last level two different equations were proposed (i.e., Atkinson & Boore, 2003; Youngs *et al.*, 1997).

For the first level of the logic tree regarding GMPEs, the largest weight (0.55) is assigned to the model for stable regions [option (i)], and a smaller weight (0.45) is assigned to the models for shallow earthquakes in active regions [option (ii)]. On the second level, all models are assigned the same weight, showing an equal level of confidence in all models as not reasons were found to give a higher weight to any of them. On the third and last level of the logic tree regarding GMPEs, the model of Atkinson & Boore (2003) was given a higher weight (0.65) since it is derived from a larger and more recent dataset.

The logic tree for all of the different epistemic uncertainties considered in the analysis and the weights assigned to each of the branches is shown in Figure 3.38. This tree also shows the different parameters corresponding to each of the branches. Due to all the epistemic uncertainties incorporated in the logic tree a total of 15552 branches were set up, representing each one of them an alternative seismic scenario.

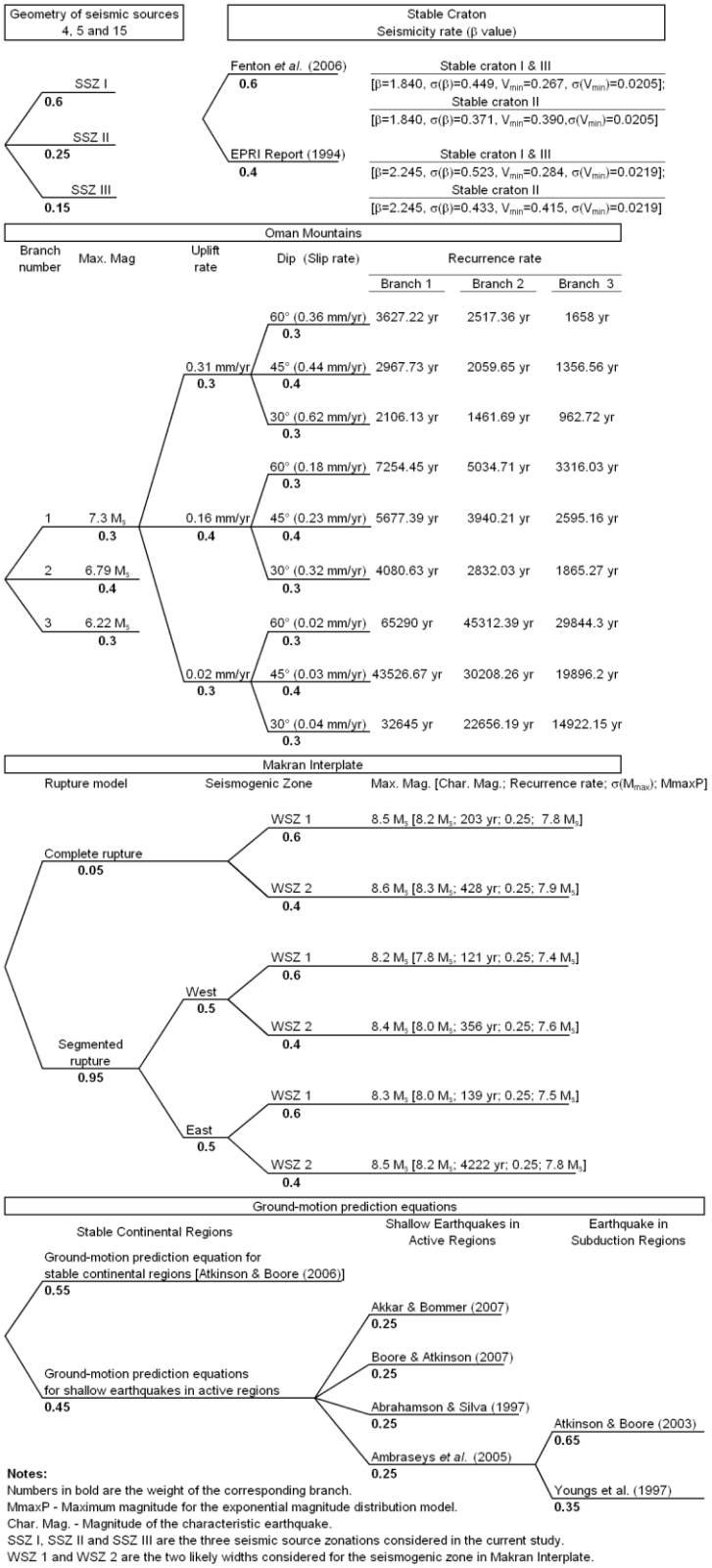

Figure 3.38. Logic tree for the five epistemic uncertainties considered in the hazard analysis. (1) the boundary between seismic sources 5 and 15, and the consideration of source 4 as an independent source or not; (2) alternative occurrence rate parameters for the stable craton; (3) estimation of the maximum magnitude, uplift rate and average dip of the faults in the Oman Mountains; (4) rupture model for Makran; and, (5) optimal ground motion model for the different seismotectonic environments. In each branch the different parameters considered in the analysis are shown together with the weight assigned to the branch.

3.7. Hazard analysis

The hazard analysis was carried out using the freely distributed software Crisis2007 (Ordaz *et al.*, 2007) which computes seismic hazard based on the original Esteva-Cornell approach (Cornell, 1968; Esteva, 1967) modified to explicitly include the aleatory variability in the ground-motion.

As explained earlier, earthquake occurrence was modelled either as a Poissonian process or as a Purely Characteristic earthquake process, depending of the seismic characteristics of the seismic source (see section 3.4.1).

For the Poisson model the parameters required by Crisis2007 are: the minimum magnitude to be use in the integration process (m_{min}), the exceedance rate for events of magnitude m_{min} or greater (υ_{min}), the b-value of the exponential model, the maximum magnitude for the source (m_{max}) and the standard deviations associated of the latter two.

The standard deviation of β and m_{max} were obtained from the statistical analysis of the seismicity; in some cases m_{max} and $\sigma(m_{max})$ were obtained from correlations with the geometry of the faults using Wells & Coppersmith (1994); see Table 3.11. In both cases a Gaussian probability distribution was assumed. However, for m_{max} the distribution is truncated by upper and lower levels in order to avoid the possibility of considering very low magnitudes as the maximum expected magnitude or computing unrealistically high magnitudes. Although, in both cases (very low or high values of m_{max}), if the distribution were unbounded the probabilities assigned to these scenarios would be very small. In all cases, the upper and lower boundaries were set equal to $m_{max} \pm 2\sigma(m_{max})$.

For the Purely Characteristic model Crisis2007 requires: the minimum possible magnitude of the characteristic earthquake ($m_{ch\text{-}min}$); the median value of the time between characteristic earthquakes, which correspond to the inverse of the annual recurrence rate for $m_{ch\text{-}min}$; the maximum

magnitude of the characteristic earthquake to be used in the integration process (m_u); and the expected value of the characteristic earthquake (m_{ch}) and its standard deviation associated ($\sigma(m_{ch})$). This is, that the probability density function for the characteristic earthquake used in the integration will be double-truncated, being $m_{ch\text{-}min}$ the lower level and m_u the upper level. For purposes of the current study m_u was considered equal to the maximum magnitude expected for the seismic source, m_{ch} equal to 0.5 moment-magnitude units below m_u and $m_{ch\text{-}min}$ equal to 1.0 moment-magnitude units below m_u (all the set or values for the different sources and different options are presented in Figure 3.38).

Within the options for the characteristic model, Crisis2007 allows to define the expected magnitude of the characteristic earthquake as function of the time elapsed since the last occurrence of a characteristic earthquake. However this option was excluded of the analysis here presented and hence this time-dependent model will not be discussed further.

Other characteristic of Crisis2007 is that it allows the truncation of the hazard integration at a given value of epsilon (number of standard deviations) or ground-motion level. For proposes of this study the hazard integration was performed without truncation (Bommer *et al.*, 2004).

Both β and m_{max} are variables fully dependent on the seismic moment related to the seismic source, therefore considering the aleatory variability associated with the estimation of these variables in the integration process could be arguable as this would imply that β and m_{max} are independent variables. However, the inclusion in the hazard calculations of the variability on the estimation of these parameters was done in order to carry out further sensitivity analysis.

As previously mentioned, most of the seismic sources were modelled as areas with a constant depth corresponding to the average depth of earthquakes in each seismic source. Only the Makran subduction-zone

sources (sources 11 and 18 to 20), the Kazerum-Borazjan fault, the Minab-Zendan fault and the Sabzevaran-Jorift fault were modelled as sloping fault planes where the slope corresponds to the average dip of the fault or the fault system.

As result of all the epistemic uncertainties addressed through the logic-tree framework, a total of 15552 hazard curves (one for each branch on the logic tree) and its corresponding disaggregated results were generated for PGA and spectral accelerations ranging from 0.001 to 1.0 g.

Because it is common practice, and in order to be able to compare the results of this study with similar studies, the suite of hazard curves from the logic tree were summarised by taking the weighted mean of the rates of occurrence corresponding to each considered level of ground-motion. The epistemic uncertainty was estimated as the variance among branches. In a similar manner to the hazard curves, the weighted mean of the disaggregated results was calculated in order to summarise the relative contributions made by the various magnitude-distance scenarios (Bazzurro & Cornell, 1999).

Other representations of the outcomes of the logic tree such as the median or the weighted mean of the levels of ground motion are presented in Chapter 4 (c.f., Abrahamson & Bommer, 2005; McGuire *et al.*, 2005; Musson, 2005).

The outcomes of this analysis are presented and analysed in the following section.

3.8. Results

In this section all the results of the probabilistic seismic hazard analysis are presented and discussed. Furthermore, the uniform hazard spectra and PGA values for different return periods obtained in this study are compared to those presented by the publications discussed earlier in

section 3.3. Finally the conclusions to the PSHA developed in this chapter are presented.

The seismic hazard curves for the cities of Abu Dhabi, Dubai and Ra's Al Khaymah for PGA and SA at 0.1, 0.2, 0.4, 1.0, 2.0 and 3.0 s response periods are presented in Figure 3.39.

The uniform hazard spectra (UHS) for the three sites for return periods of 500, 1000, 2500, 5000 and 10,000 years are shown in Figure 3.40 and Figure 3.41. The variation of the UHS with return period at each site can be observed in Figure 3.40, while the variation of the UHS with location (of the different sites) for a given return period is observed in Figure 3.41.

Disaggregation plots with respect to magnitude-distance scenarios for the city of Abu Dhabi showing the variation of the contribution for PGA and SA for response periods of 0.2, 1.0 and 3.0 s and for different return periods are shown from Figure 3.42 to Figure 3.45. The same plots are shown from Figure 3.46 to Figure 3.48, but re-arranged to show the variation of the contributions with respect to the response period for a fixed return period. In a similar manner the disaggregated results for the city of Dubai are presented from Figure 3.49 to Figure 3.55 and from Figure 3.56 to Figure 3.62 for the city of Ra's Al Khaymah.

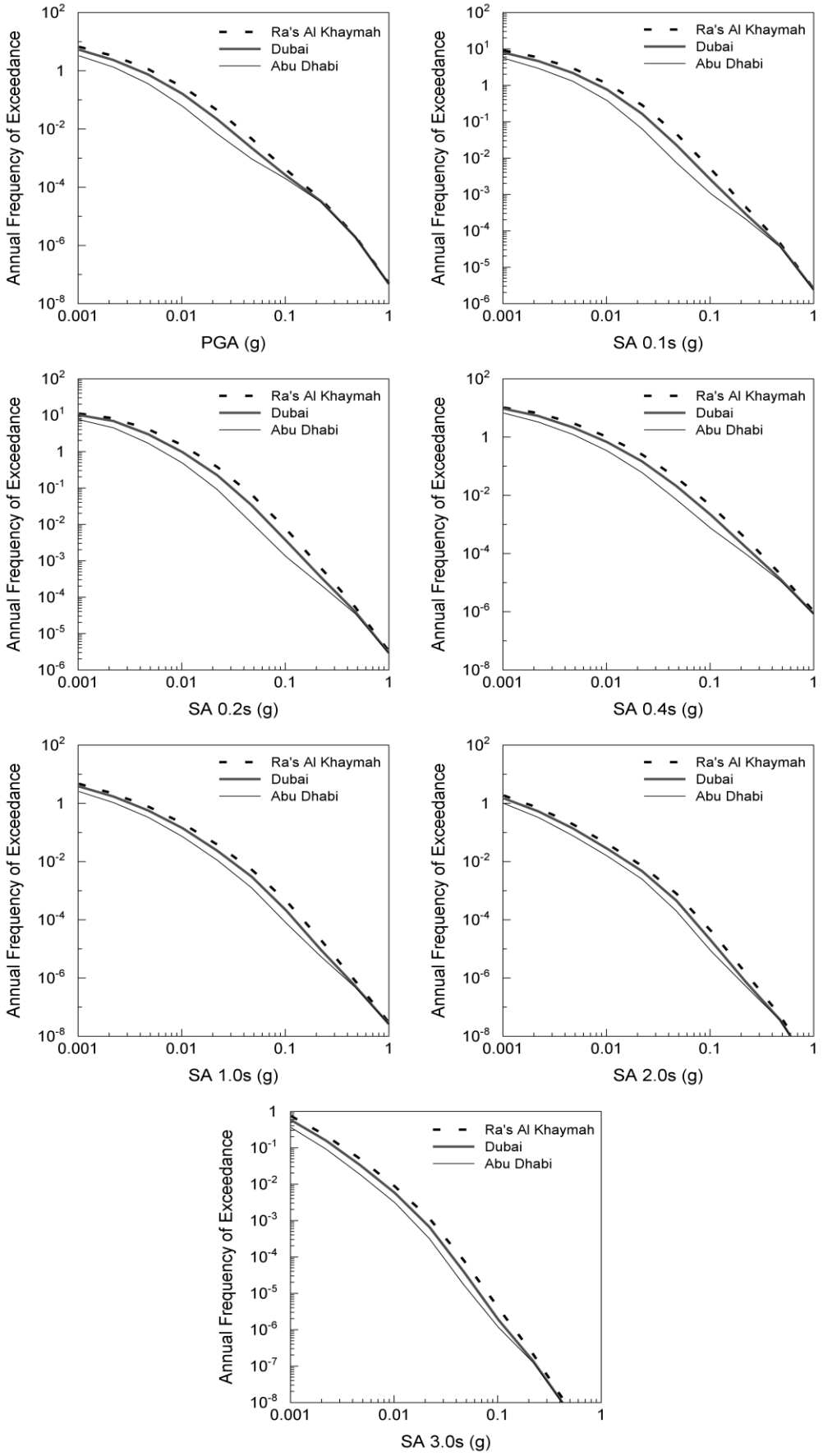

Figure 3.39. Hazard curves for PGA and SA for response periods of 0.1, 0.2, 0.4, 1.0, 2.0 and 3.0 s, for the three sites.

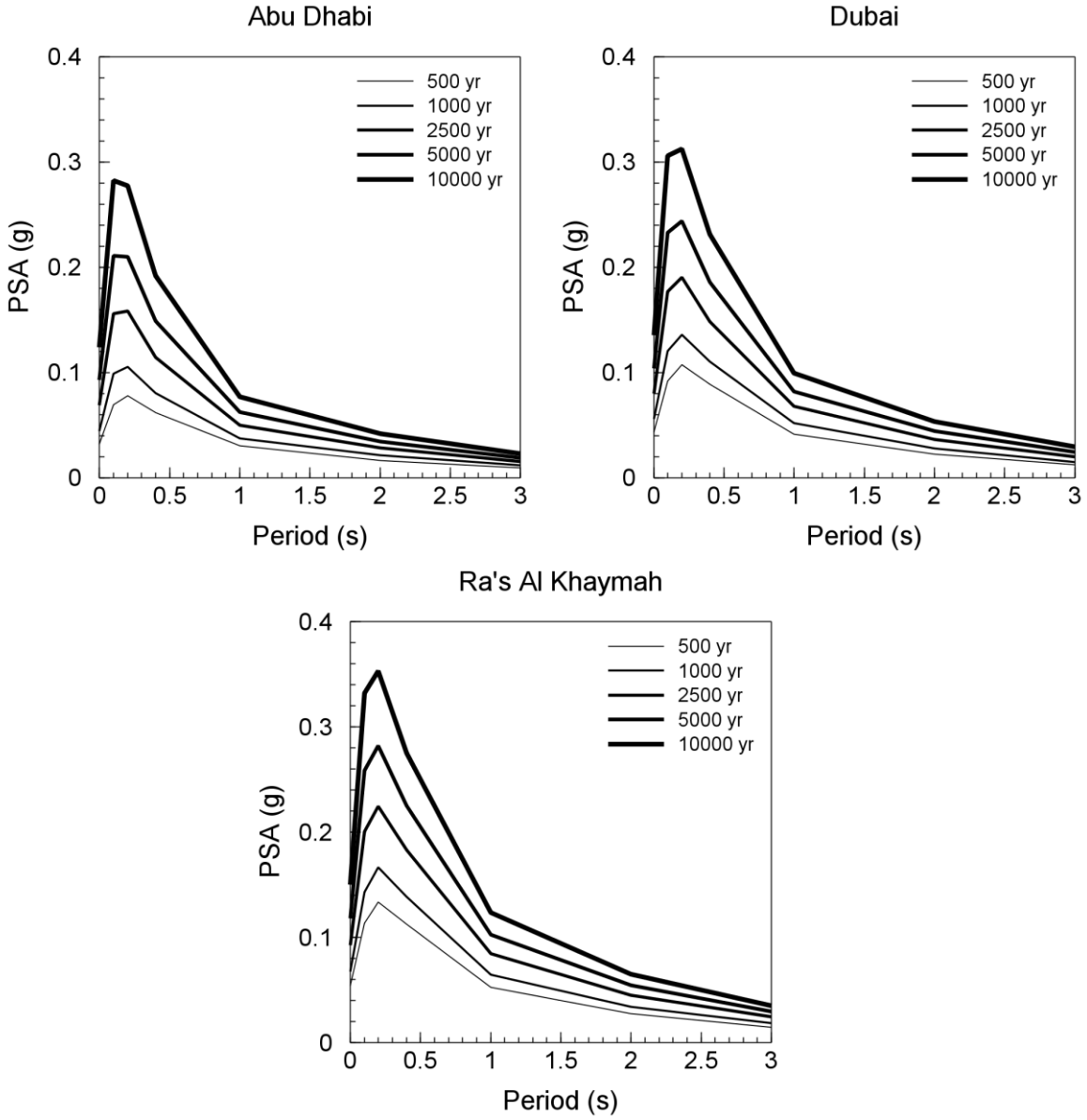

Figure 3.40. Uniform hazard spectra for the three cities at different return periods.

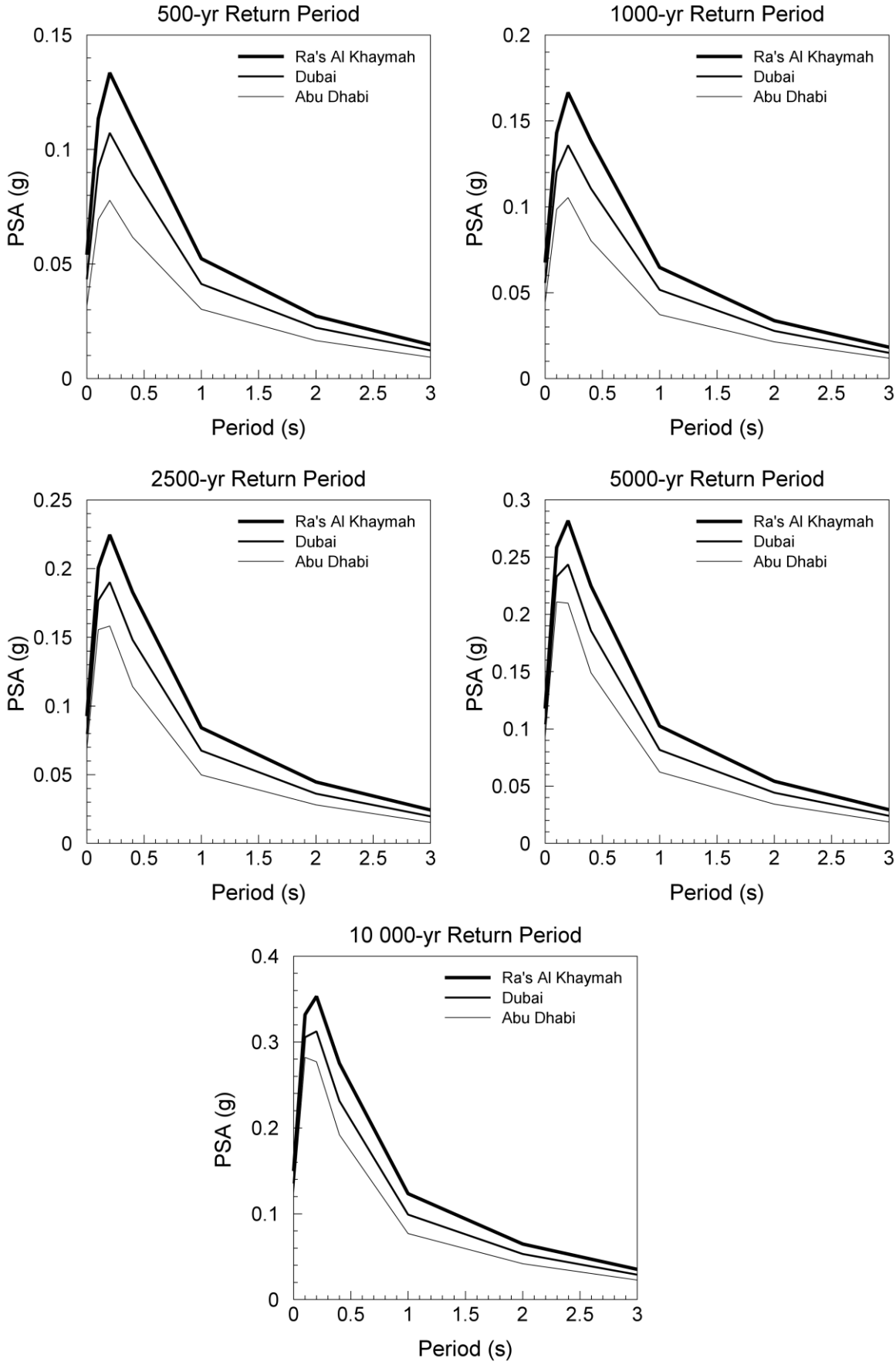

Figure 3.41. Uniform hazard spectra at different return periods for the three cities.

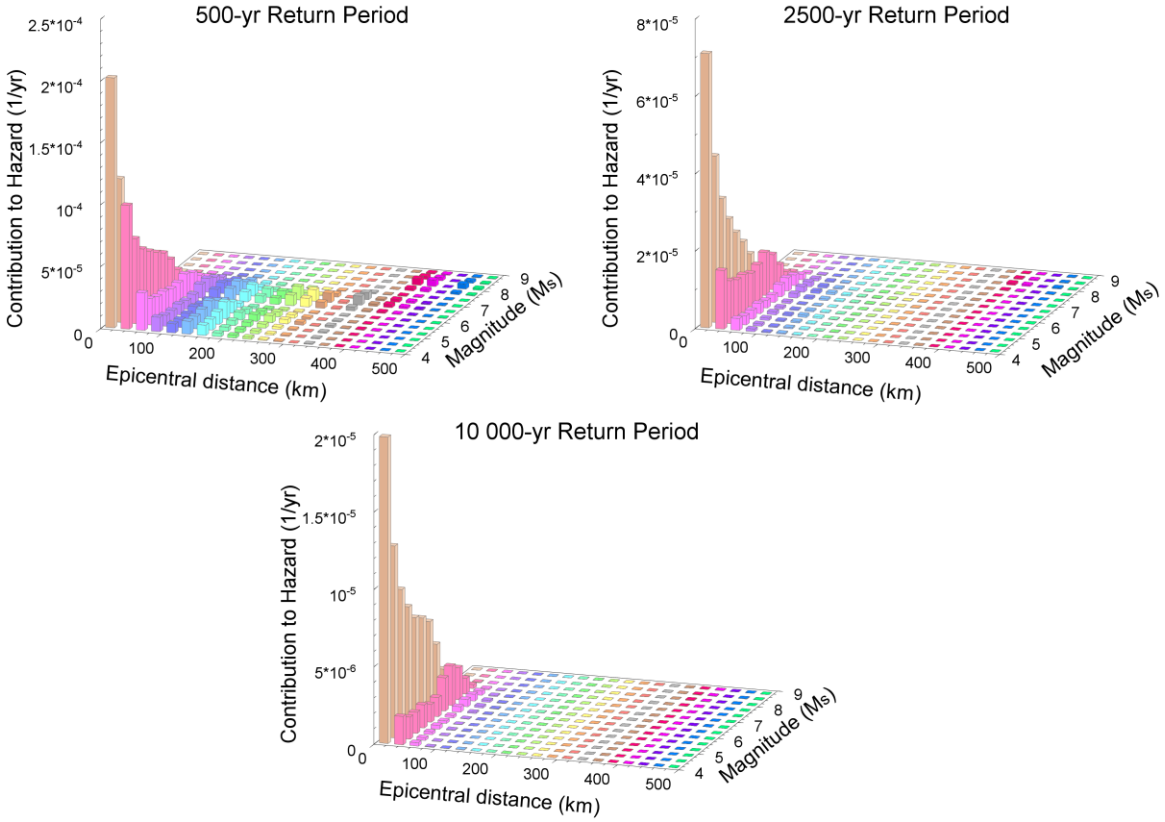

Figure 3.42. Disaggregation for the city of Abu Dhabi at PGA and for 500, 2500 and 10,000 yr return period.

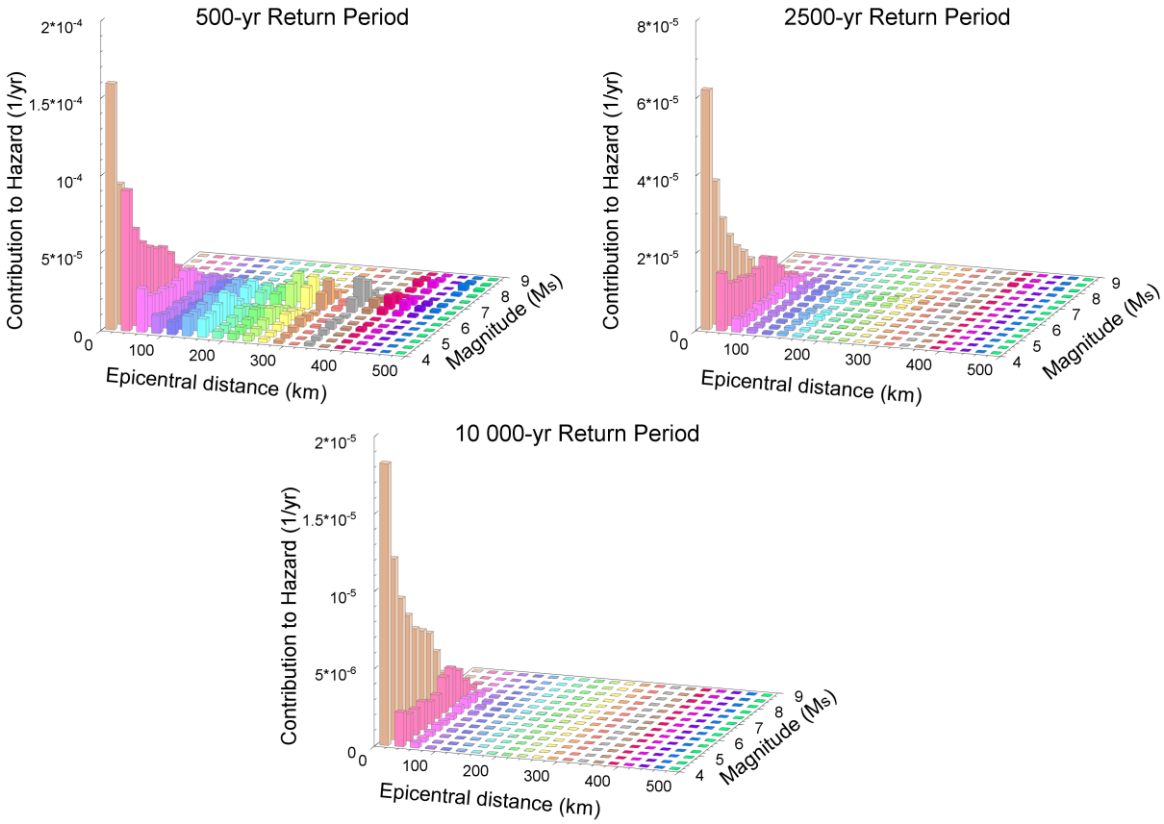

Figure 3.43. Disaggregation for the city of Abu Dhabi at 0.2 s response period and for 500, 2500 and 10,000 yr return periods.

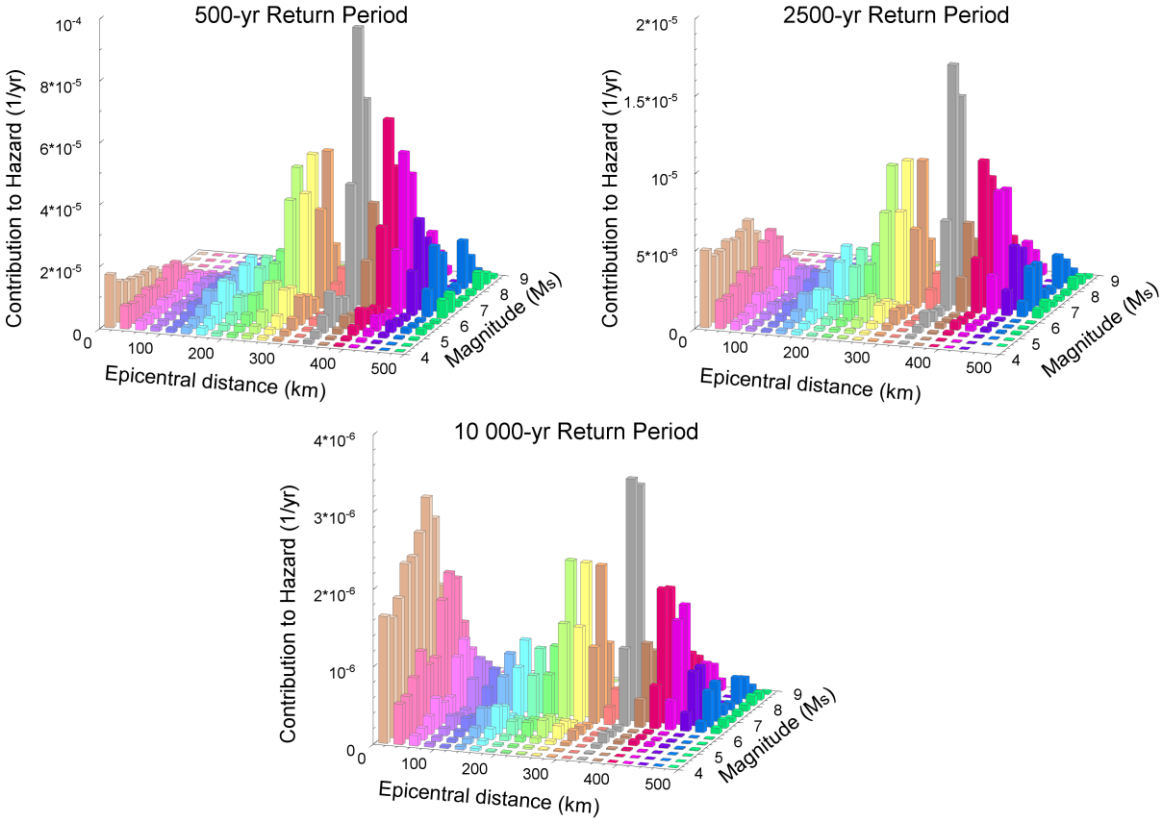

Figure 3.44. Disaggregation for the city of Abu Dhabi at 1.0 s response period and for 500, 2500 and 10,000 yr return periods.

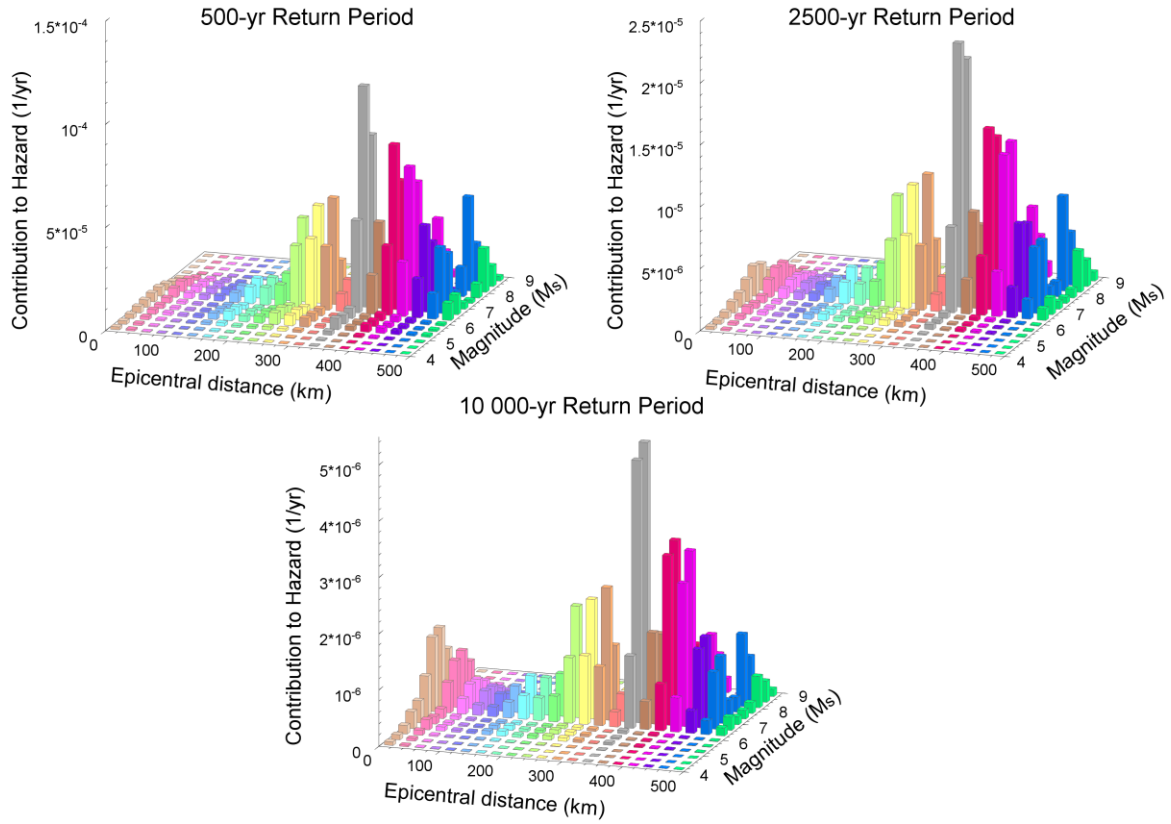

Figure 3.45. Disaggregation for the city of Abu Dhabi at 3.0 s response period and for 500, 2500 and 10,000 yr return period.

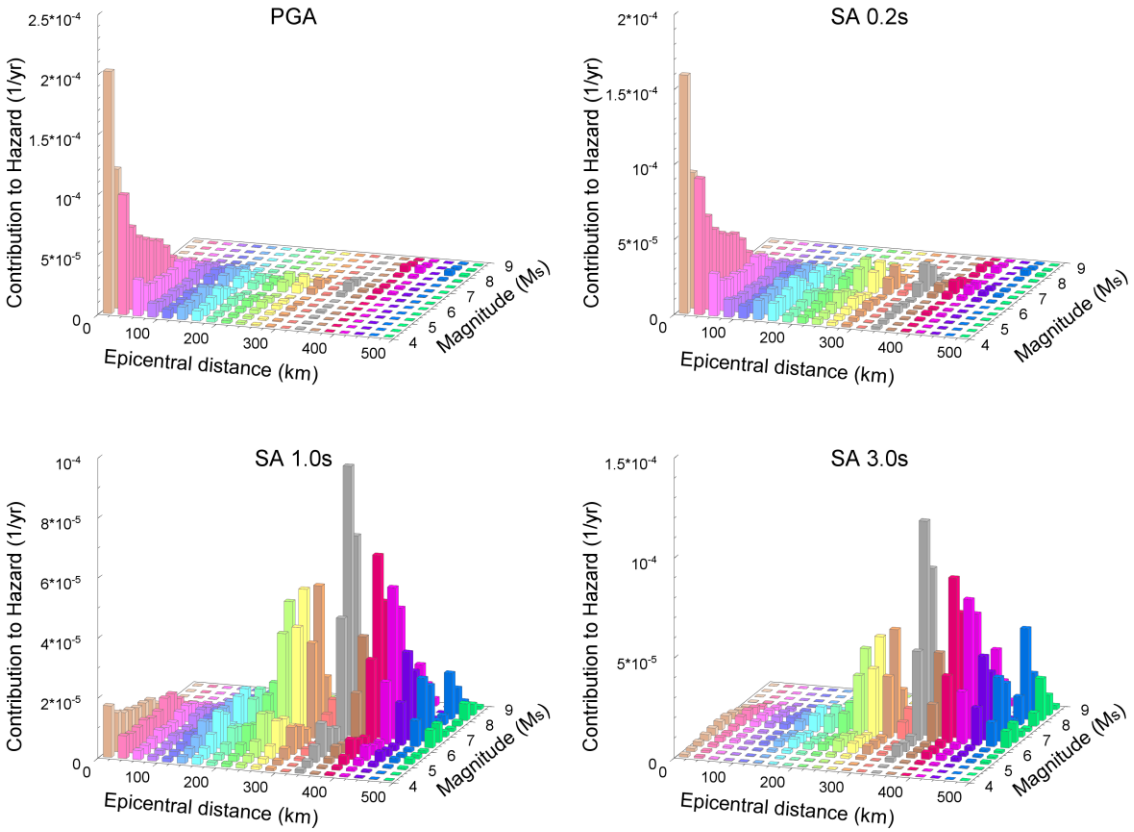

Figure 3.46. Disaggregation for the city of Abu Dhabi at 500 yr return period for PGA and SA at 0.2, 1.0 and 3.0 s.

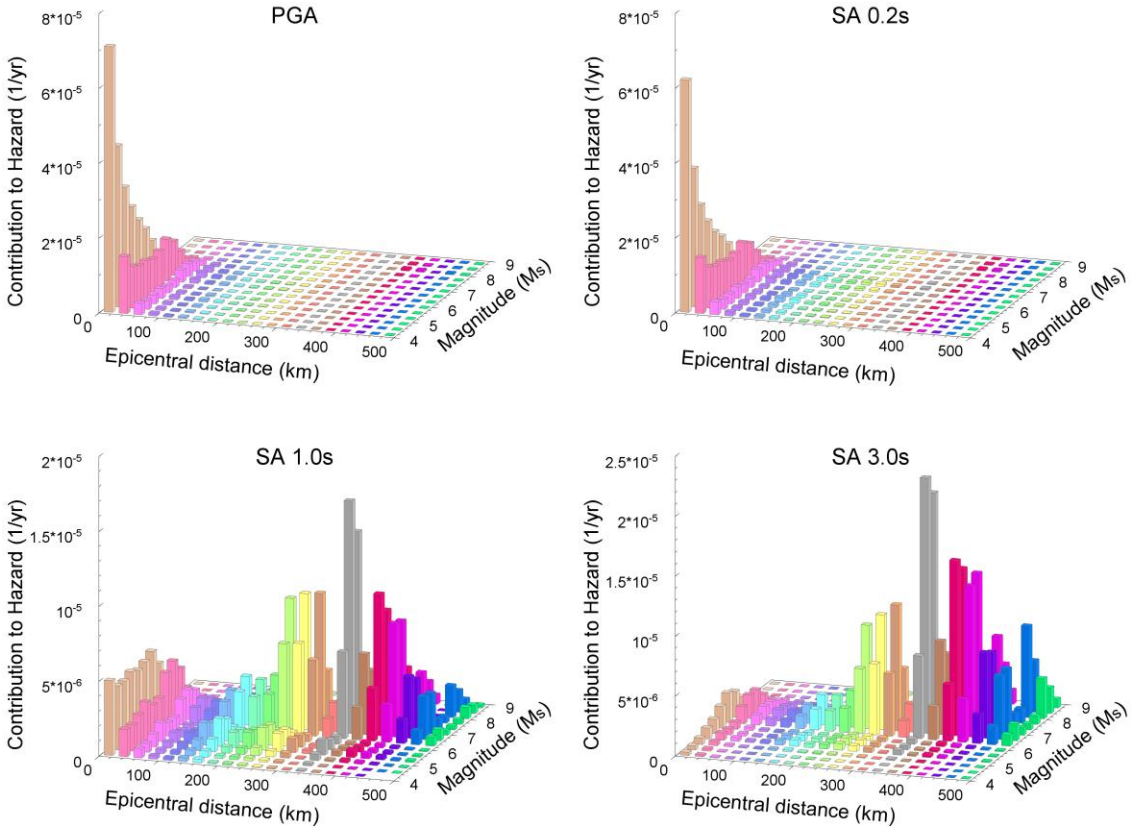

Figure 3.47. Disaggregation for the city of Abu Dhabi at 2500 yr return period for PGA and SA at 0.2, 1.0 and 3.0 s.

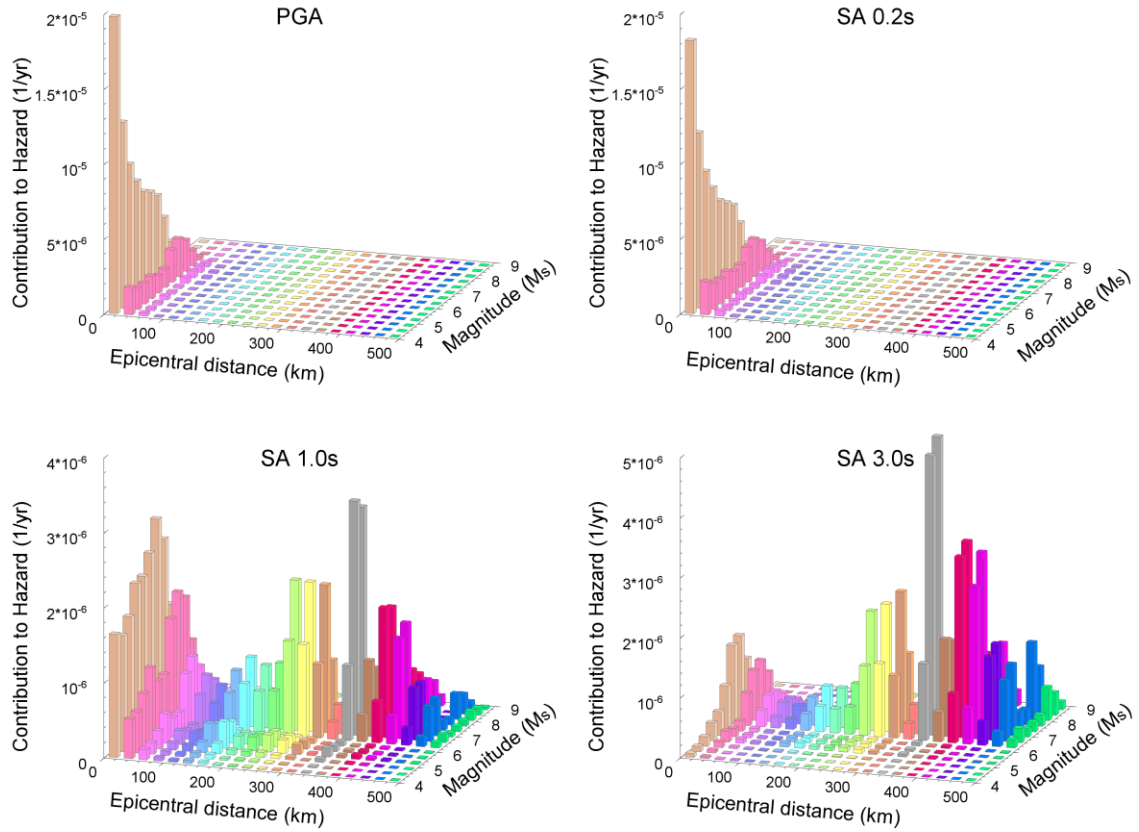

Figure 3.48. Disaggregation for the city of Abu Dhabi at 10,000 yr return period for PGA and SA at 0.2, 1.0 and 3.0 s.

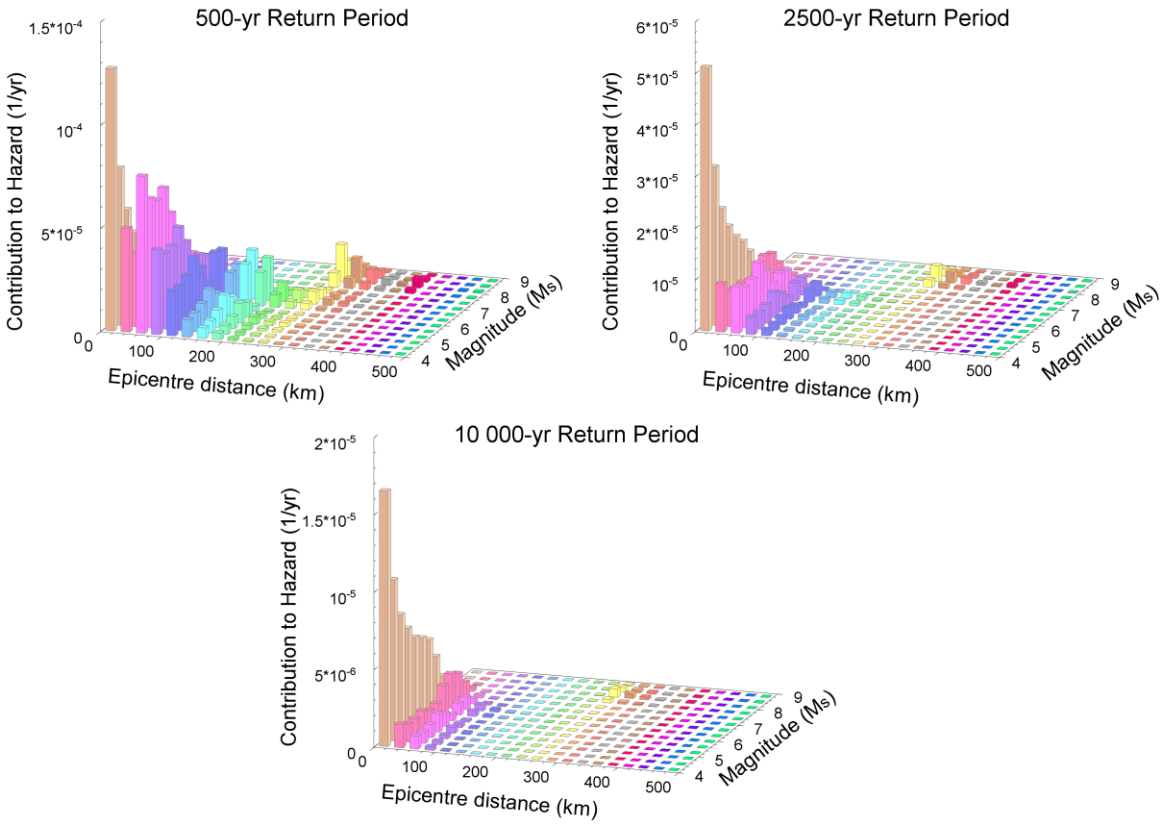

Figure 3.49. Disaggregation for the city of Dubai at PGA and for 500, 2500 and 10,000 yr return period.

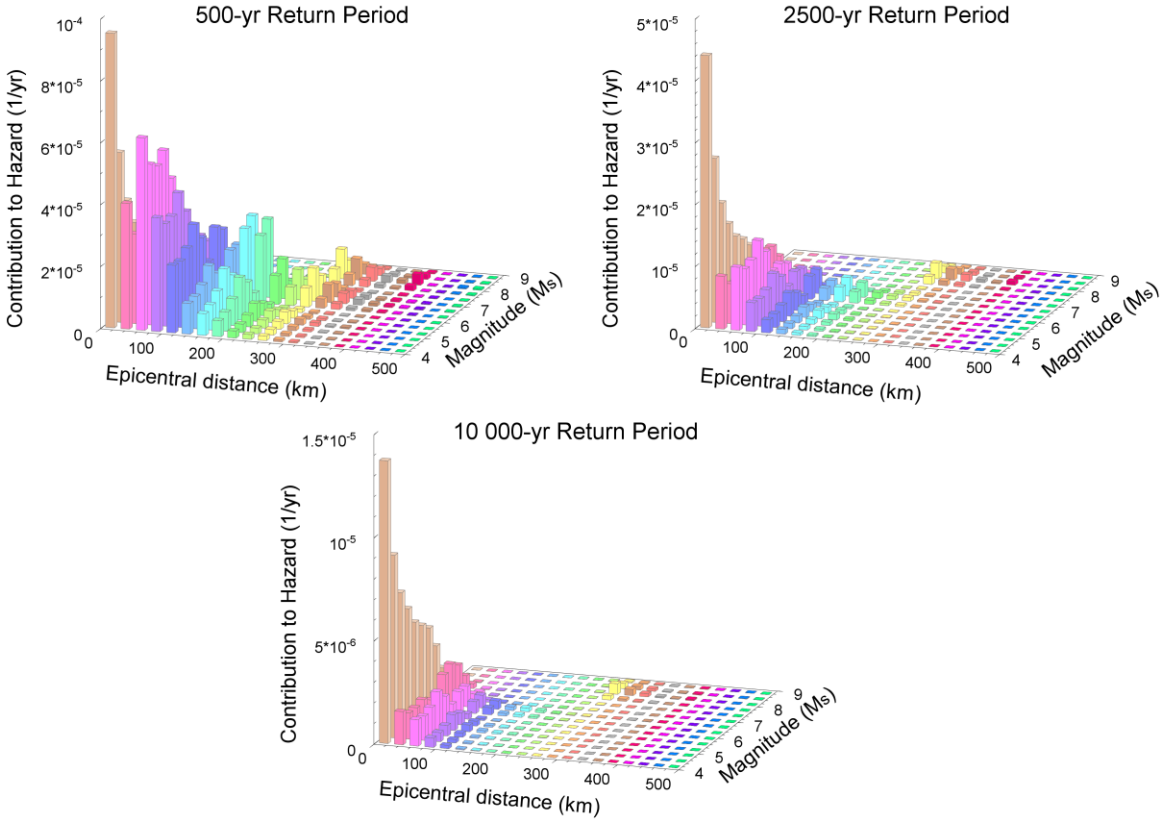

Figure 3.50. Disaggregation for the city of Dubai at 0.2 s response period and for 500, 2500 and 10,000 yr return period.

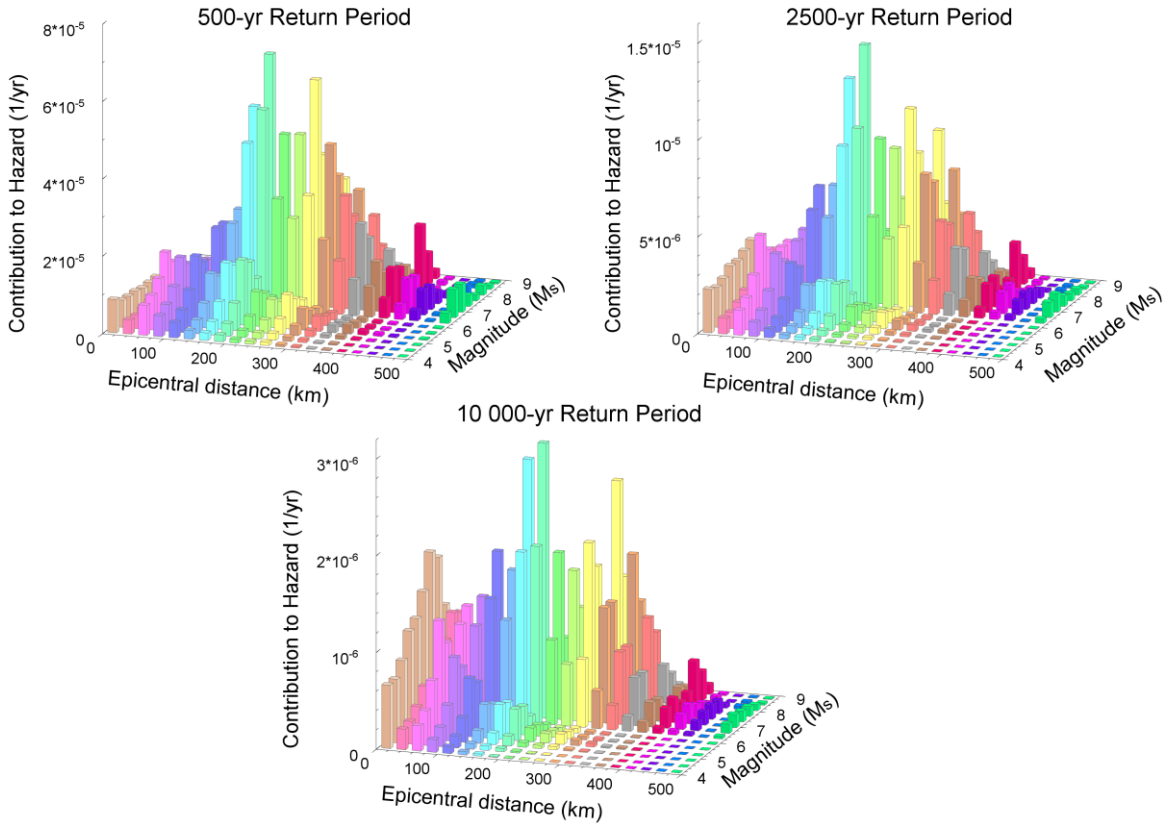

Figure 3.51. Disaggregation for the city of Dubai at 1.0 s response period and for 500, 2500 and 10,000 yr return period.

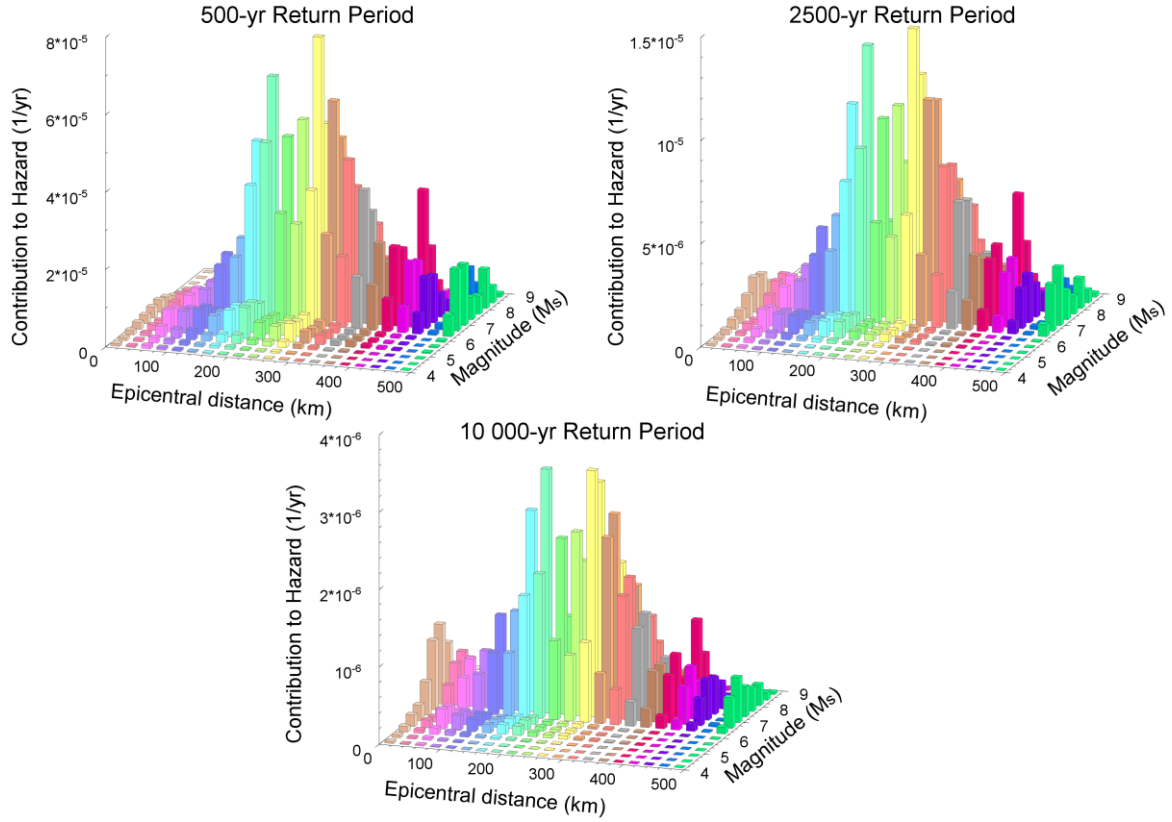

Figure 3.52. Disaggregation for the city of Dubai at 3.0 s response period and for 500, 2500 and 10,000 yr return period.

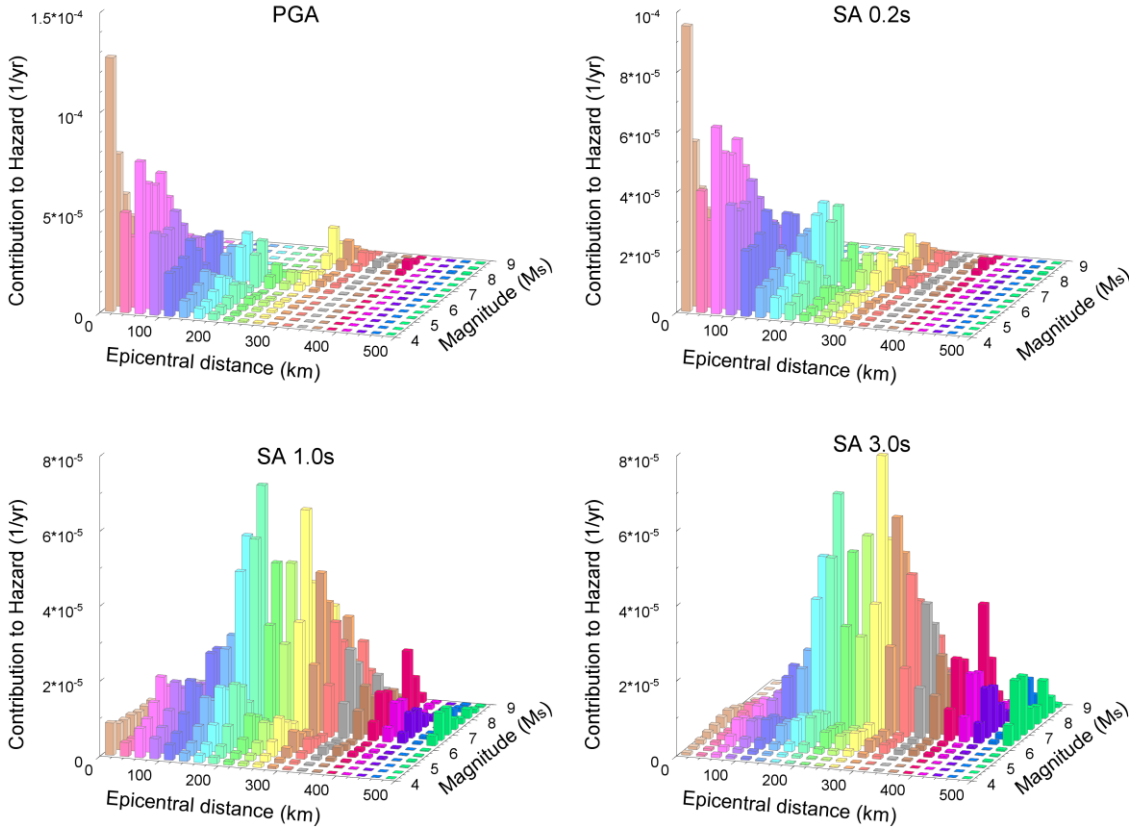

Figure 3.53. Disaggregation for the city of Dubai at 500 yr return period for PGA and SA at 0.2, 1.0 and 3.0 s.

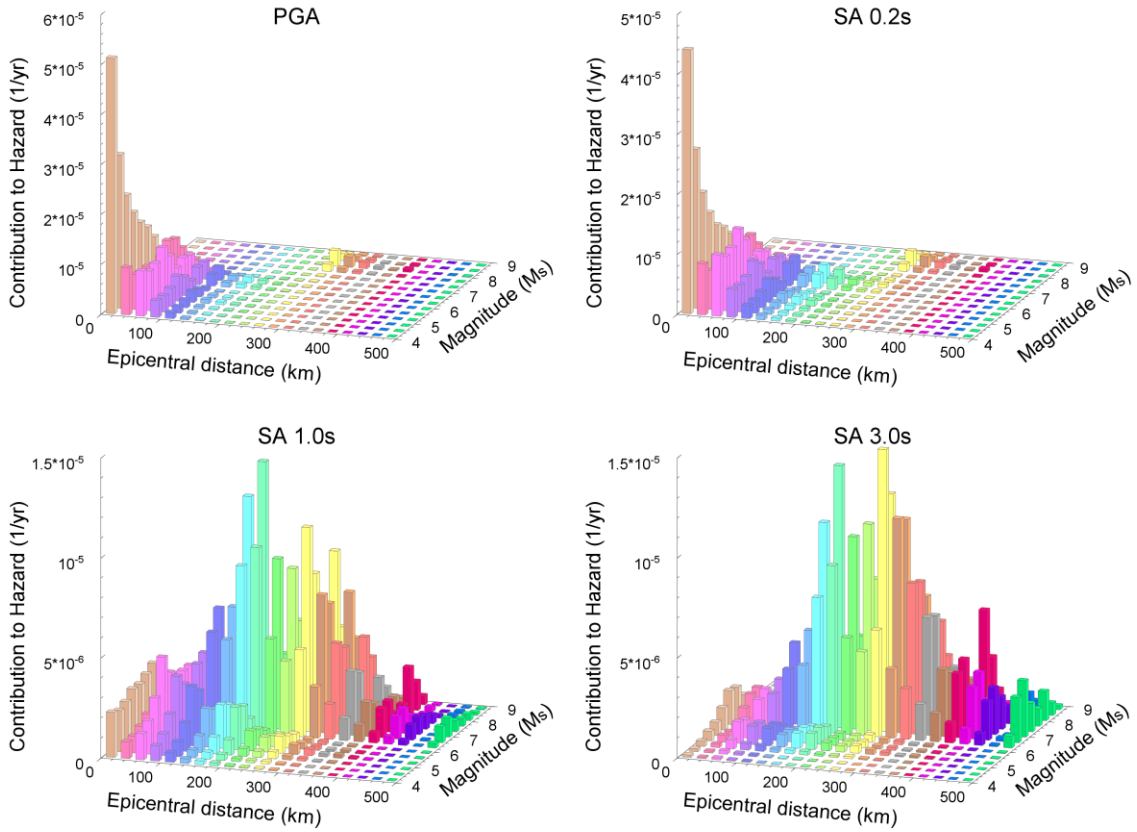

Figure 3.54. Disaggregation for the city of Dubai at 2500 yr return period for PGA and SA at 0.2, 1.0 and 3.0 s.

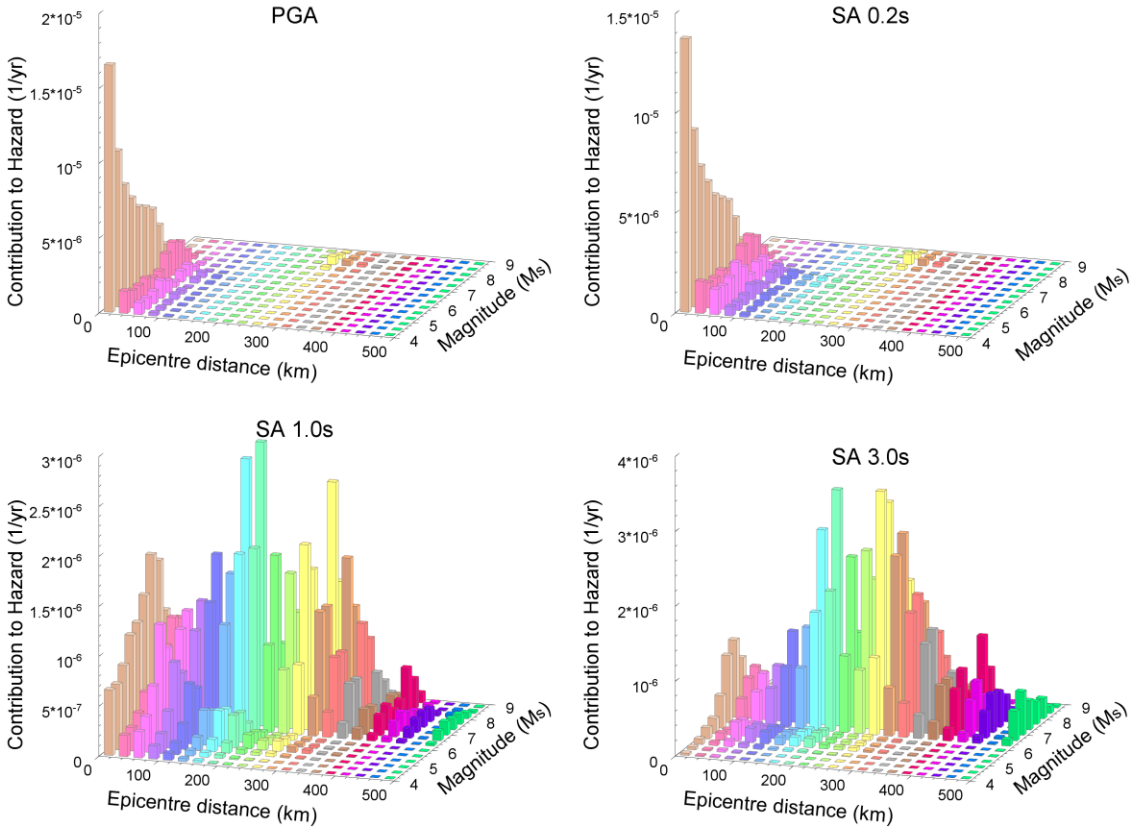

Figure 3.55. Disaggregation for the city of Dubai at 10,000 yr return period for PGA and SA at 0.2, 1.0 and 3.0 s.

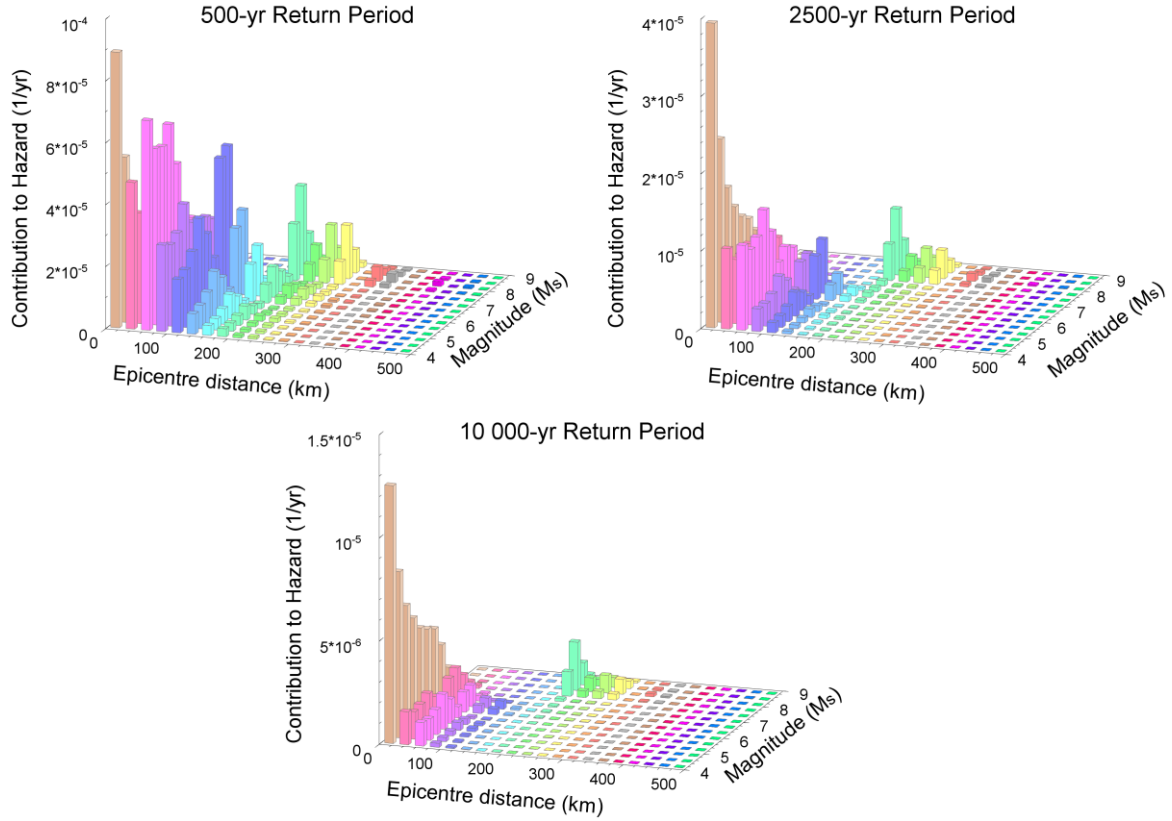

Figure 3.56. Disaggregation for the city of Ra's Al Khaymah at PGA and for 500, 2500 and 10,000 yr return period.

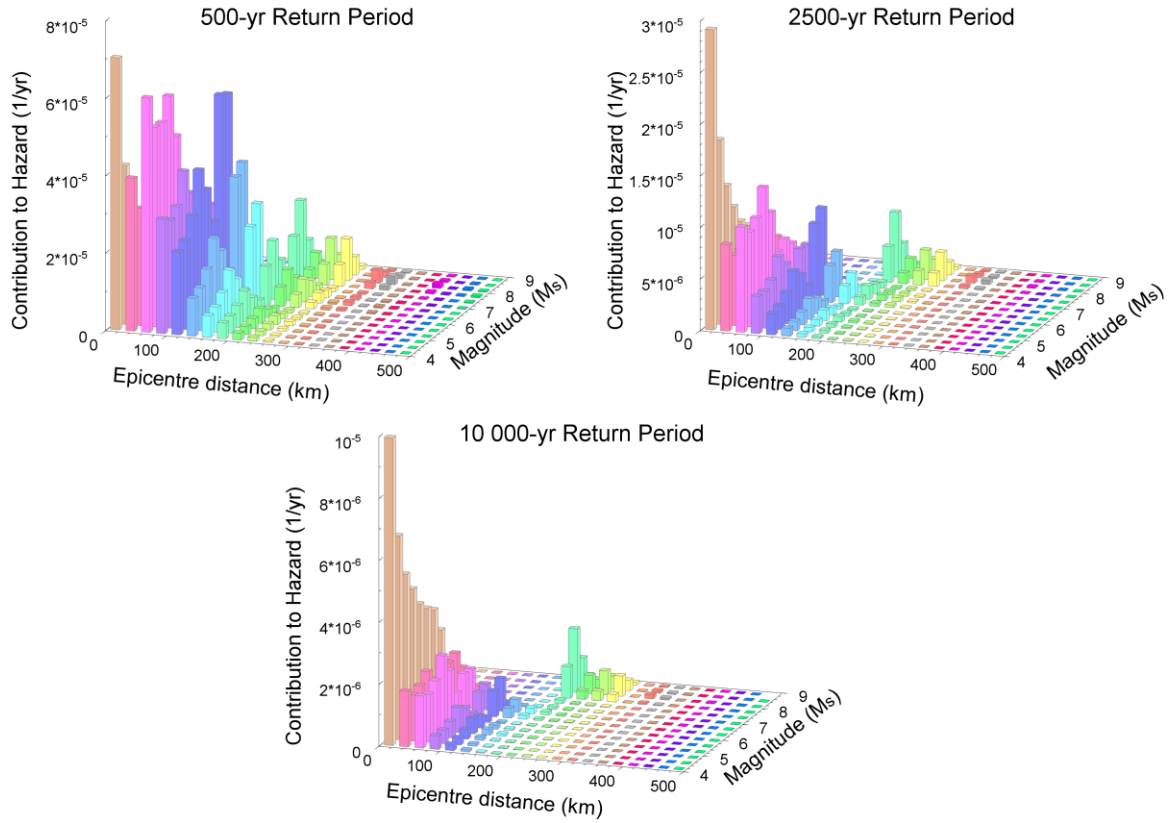

Figure 3.57. Disaggregation for the city of Ra's Al Khaymah at 0.2 s response period and for 500, 2500 and 10,000 yr return period.

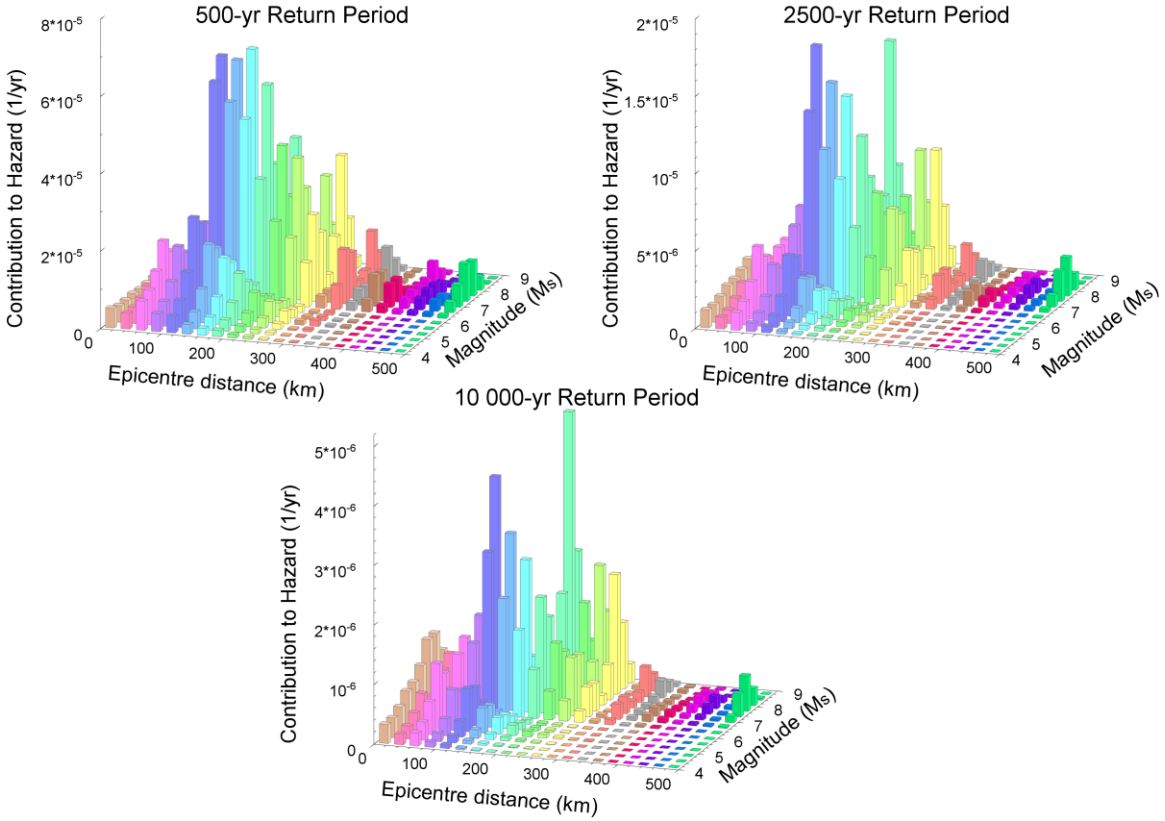

Figure 3.58. Disaggregation for the city of Ra's Al Khaymah at 1.0 s response period and for 500, 2500 and 10,000 yr return period.

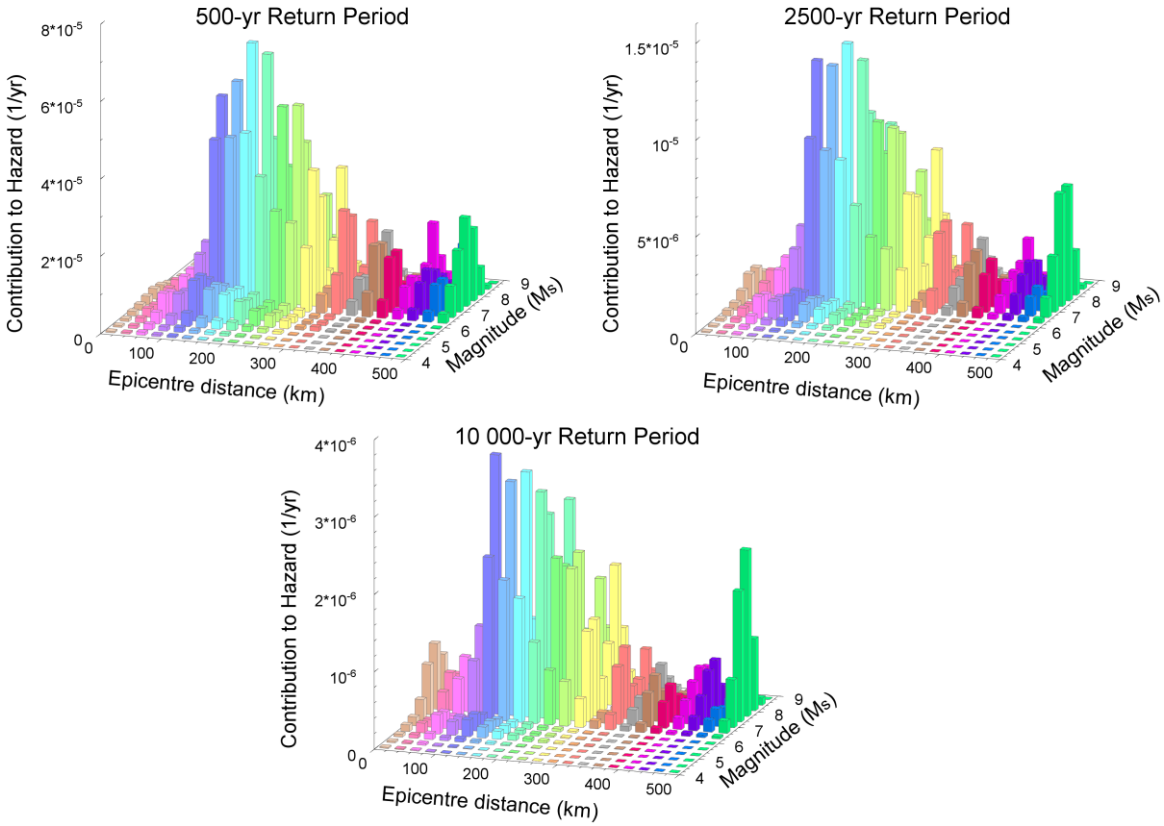

Figure 3.59. Disaggregation for the city of Ra's Al Khaymah at 3.0 s response period and for 500, 2500 and 10 00 yr return period.

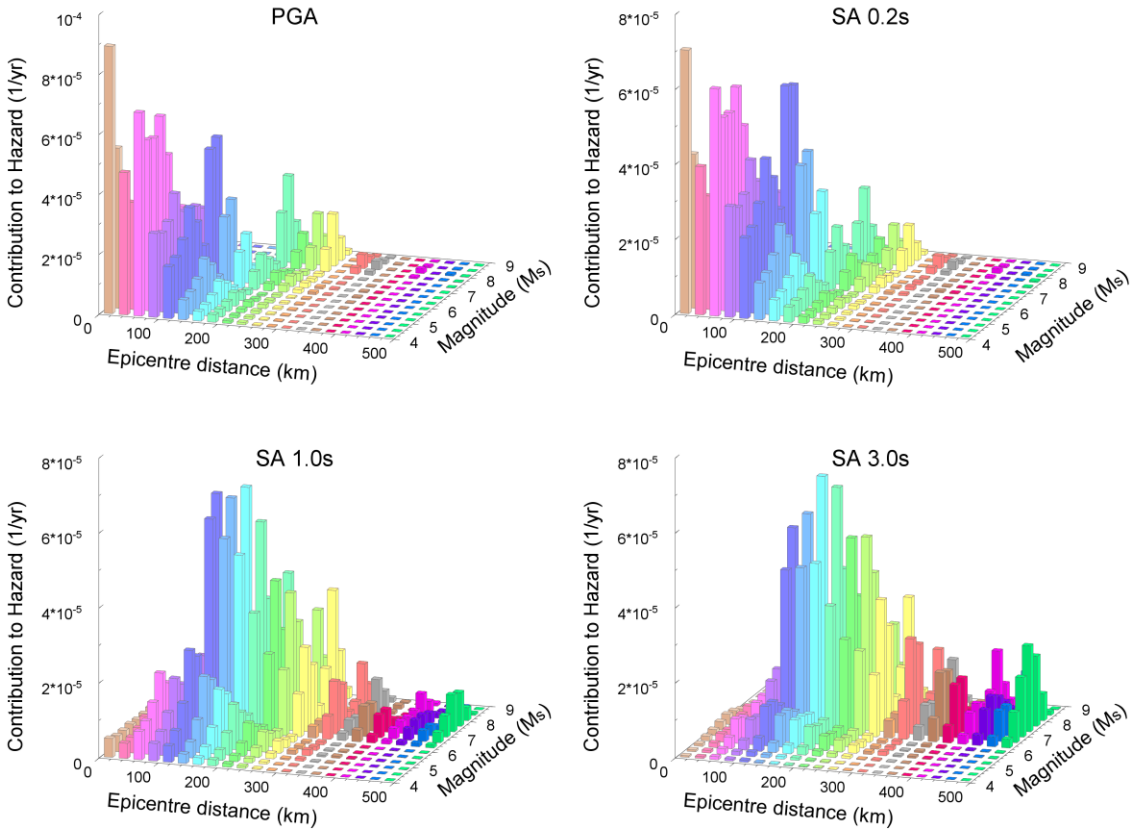

Figure 3.60. Disaggregation for the city of Ra's Al Khaymah at 500 yr return period for PGA and SA at 0.2, 1.0 and 3.0 s.

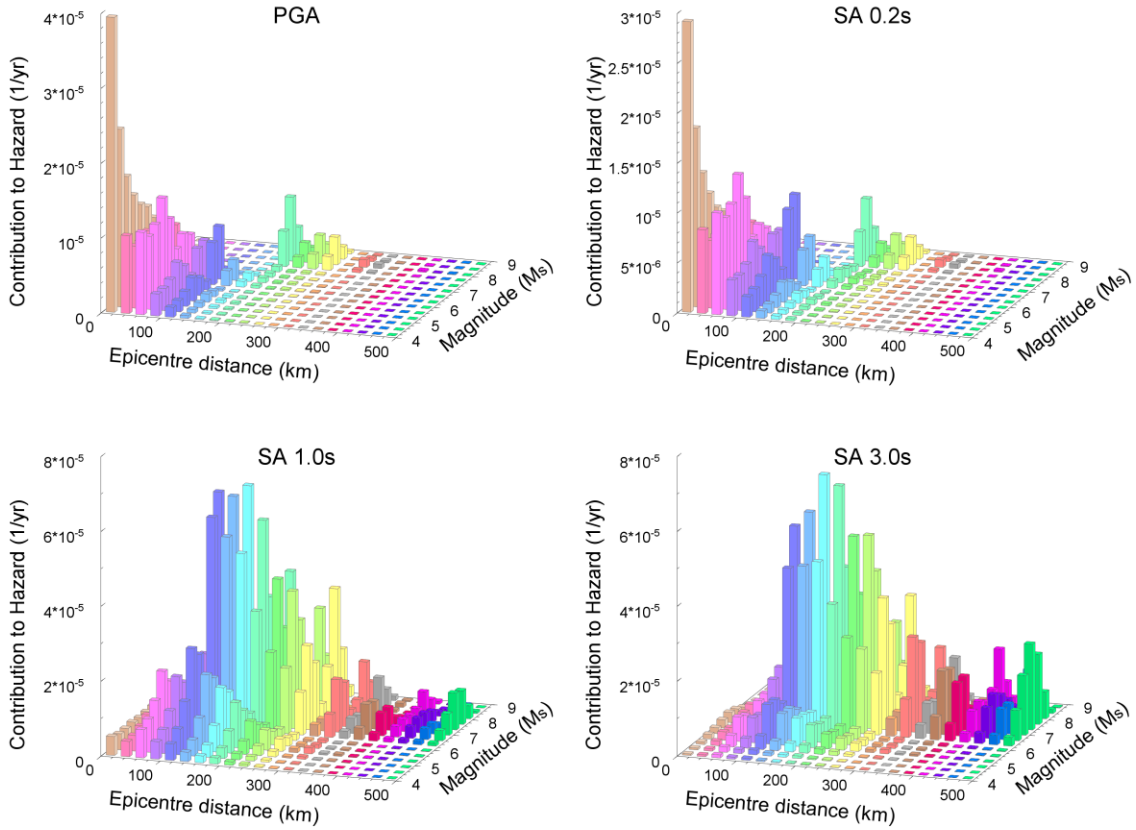

Figure 3.61. Disaggregation for the city of Ra's Al Khaymah at 2500 yr return period for PGA and SA at 0.2, 1.0 and 3.0 s response period.

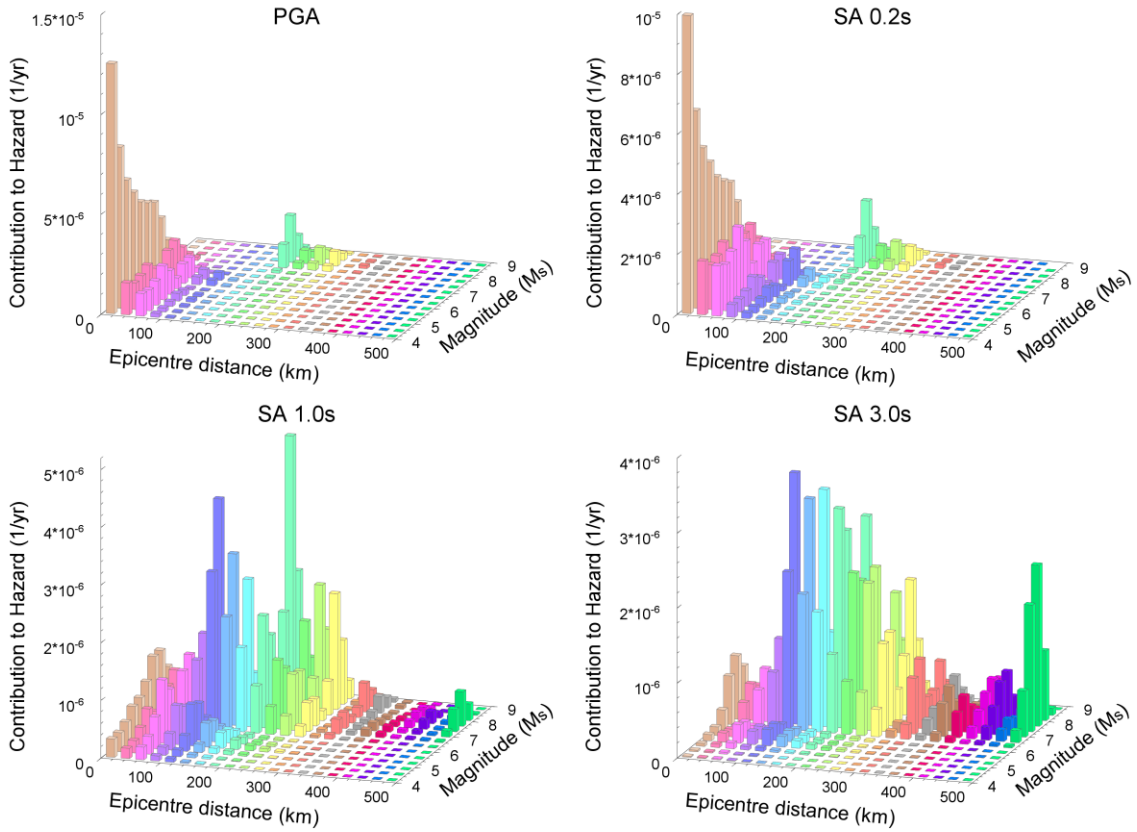

Figure 3.62. Disaggregation for the city of Ra's Al Khaymah at 10,000 yr return period for PGA and SA at 0.2, 1.0 and 3.0 s response period.

The contributions to the hazard from each of the seismic sources for PGA and the different response periods are shown in Figure 3.63, Figure 3.64 and Figure 3.65 for the cities of Abu Dhabi, Dubai and Ra's Al Khaymah respectively.

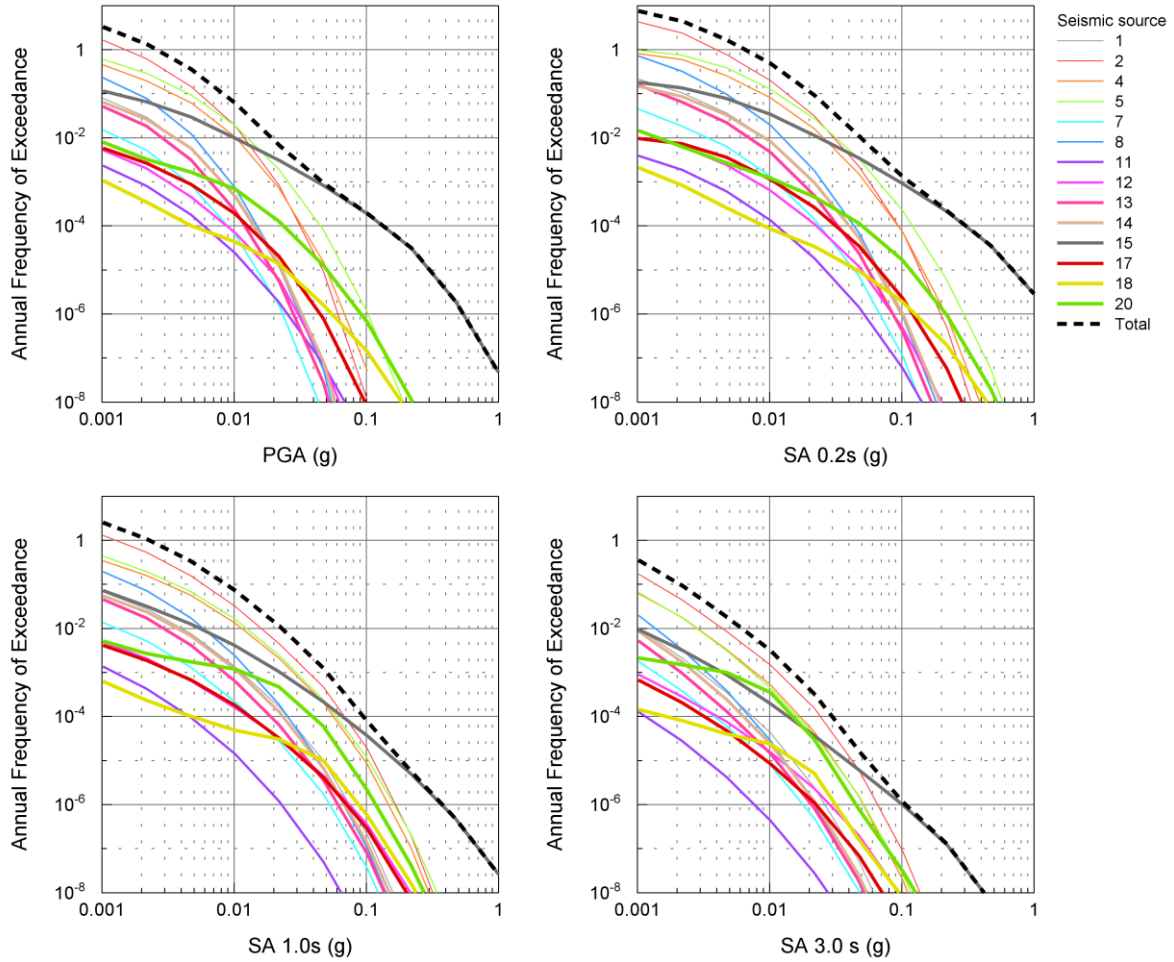

Figure 3.63. Contribution to the hazard from each of the seismic sources for the city of Abu Dhabi. See Table 3.10 for source number. Dashed line is the mean hazard curve.

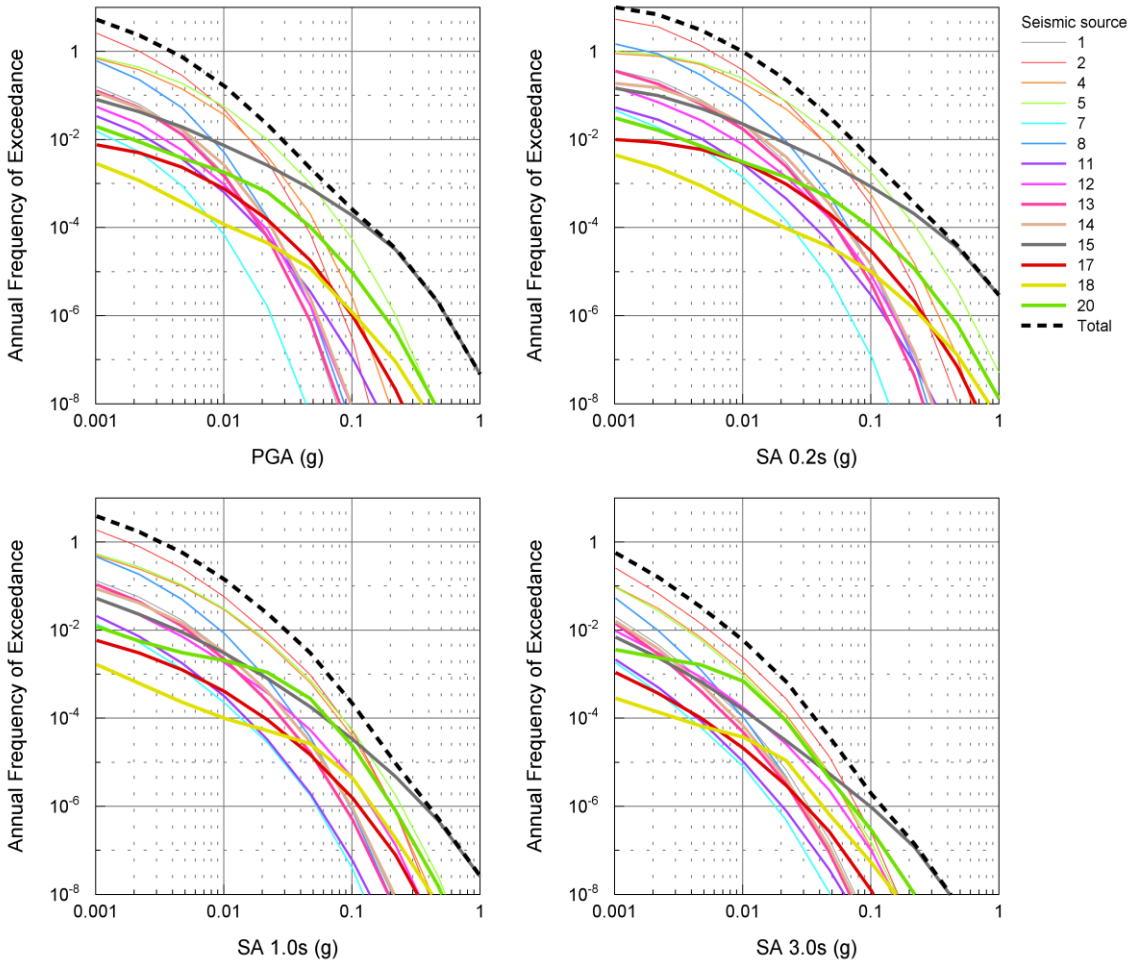

Figure 3.64. Contribution to the hazard from each of the seismic sources for the city of Dubai. See Table 3.10 for source number. Dashed line is the mean hazard curve.

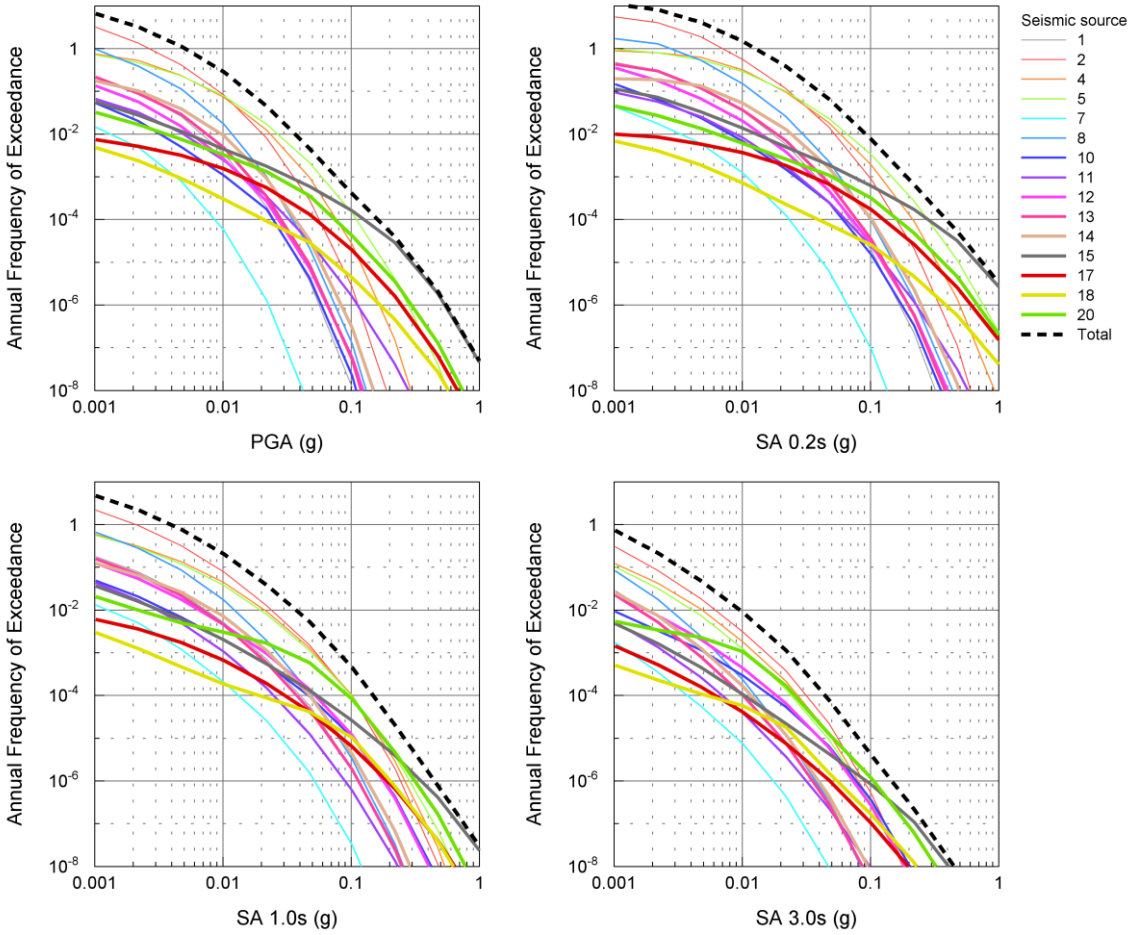

Figure 3.65. Contribution to the hazard from each of the seismic sources for the city of Ra's Al Khaymah. See Table 3.10 for source number. Dashed line is the mean hazard curve.

3.8.1. Discussion

As expected, the three sites under consideration have low to very low levels of seismic hazard. The highest hazard is observed for the city of Ra's Al Khaymah and decreases towards the south, with the lowest hazard being determined for the city of Abu Dhabi.

PGA values of 0.031 g, 0.043 g and 0.054 g, for the 500-year return period, were obtained for the cities of Abu Dhabi, Dubai and Ra's Al Khaymah respectively. Based on these results the cities of Abu Dhabi and Dubai should be classified as zone 0 while the city of Ra's Al Khaymah should be classified as zone 1, according to the UBC97 seismic zonation scheme.

It is worth noting that the hazard curves for the three sites tend to coincide at very long return periods (very low probabilities of exceedance) when the seismic hazard is completely dominated by the stable craton seismic source. This can be appreciated in Figure 3.39 and from Figure 3.63 to Figure 3.65. Given that all three sources are located within the stable craton the hazard should be the same for this scenario.

In all cases, the PSA at 3.0 s for the different return periods tends to similar values for the three sites (see Figure 3.40). The biggest differences between the UHS for the three sites occur between response periods of 0.3 s and 0.5 s. A similar situation is observed when comparing hazard spectra with same return period for different sites (see Figure 3.41). In general, for the three sites and at all return periods the uniform hazard spectra maintains the same shape, implying that similar sources are dominating different periods for all the sites.

Despite the low seismicity of the region, it is interesting to note how the contribution to the seismic hazard according to different magnitude-distance scenarios and from different seismic sources changes at different return periods and different response periods for the three sites. The disaggregated results for the three sites are discussed on what follows.

Contributions to the seismic hazard for the city of Abu Dhabi.

For the city of Abu Dhabi, the contribution to the seismic hazard for PGA for the 500-year, 2500-year and 10,000-year return periods comes mainly from events of low to medium magnitudes ($4.0<M_s<6.5$) occurring at close distances from the site ($r_{epi}<50$ km) as can be seen in Figure 3.42. The distribution of the contribution by magnitude-distance scenario for PGA, only changes slightly with return period; only for the 500-year return period can a minor contribution from events of $M_s<6.0$ and distances up to ~200

km be appreciated (Figure 3.42 and Figure 3.46). These contributions are not significant at longer return periods.

The seismic source that dominates the hazard for PGA at this city is the stable craton. As can be seen at Figure 3.63, it is only for return periods less than 100 years that the stable craton is not the main contributor to the hazard. The Persian Gulf is the seismic source that contributes second-most to the hazard. The seismic sources Zagros Foredeep and the Simple Fold belt have some minor contribution at the 500-year return period, but these contributions disappear at higher return periods.

A similar pattern in terms of the contribution to the hazard can be observed for SA at 0.2-s response period. However, for a return period of 500 years a slightly larger contribution from events at magnitude between M_s 6.0 and M_s 7.0 occurring at distances between 100 km and 350 km can be appreciated (Figure 3.43 and Figure 3.47). For this response period the stable craton still dominates the hazard for return periods greater than 100 years (Figure 3.63) followed by the Persian Gulf with only a modest contribution. An increase in the contribution to the hazard from the Simple Fold belt and the Zagros Foredeep can be noticed as well as one moves to longer return periods.

At 1.0-s response period, a clear change in the contribution by magnitude-distance scenario can be noticed. At the 500-year return period the main contribution comes from events between M_s 6.0 and M_s 7.2 and distances between 220 km and 460 km. Only a small contribution comes from events with magnitudes M_s < 6.5 and distance r_{epi} < 100 km. Here, a clear variation of the contribution by magnitude-distance scenario with return period can be appreciated. For the 2500-year return period a similar contribution by magnitude-distance scenario to that of the 500-year return period is observed, but with an increase in the contribution to the hazard from earthquakes with M_s < 6.5 and r_{epi} < 100 km. The contribution of these

events keeps increasing with the return period and at the 10,000-year return period the contribution is as important as those events that dominate the hazard at 500 years. A modest contribution from events with M_s ~8.2 and distances of 380 km< r_{epi} <480 km can be appreciated as well for all the return periods (Figure 3.44).

The seismic hazard at the 1.0-s response period is mostly dominated by the Simple Fold belt, followed closely by the Persian Gulf and the Zagros Foredeep. All three of these seismic sources are the most likely to generate the events that dominate the hazard (6.0< M_s <7.2 and 220 km r_{epi}< 460 km). The stable craton has a small contribution at 500-year return period, but this contribution increases with return period to the point that it becomes the main contributor at the 10,000-year return period. The Makran West seismic source has a modest contribution to the hazard, which despite being modest remains basically unchanged for the 500-year, 2500-year and 10,000-year return periods. It seems logical to assume that the Makran West source generates those events of magnitudes 6.0< M_s< 7.8 and 220 km< r_{epi}< 460 km that can be seen in Figure 3.44 for the 10,000-year return period.

At the 3.0-s response period the magnitude-distance scenario that dominates the hazard is similar to those for 1.0-s response period (6.0< M_s< 7.2 and 380 km< r_{epi}< 480 km). The main contributor to this magnitude-distance scenario is primarily the Simple Fold belt followed by the Zagros Foredeep and the Persian Gulf seismic sources. For this response period, events of 8.0< M_s< 8.2 at distances 380 km< r_{epi}< 480 km have a larger contribution than at the 1.0-s response period and basically do not change with return period (Figure 3.45). The Stable craton has less of a contribution than at the 1.0-s response period, but it still has some important contribution at the longest return periods (Figure 3.63).

Contributions to the hazard for the city of Dubai.

For the city of Dubai, the seismic hazard for PGA is mainly dominated for small to moderate magnitude events (M_s< 6.5) with distances of r_{epi}< 200 km. As the return period increases the r_{epi} of the events dominating the hazard decreases; becoming r_{epi}< 75 km for the 2500-year return period and r_{epi}< 50 km for the 10,000-year return period. For a return period of 500 years the hazard is dominated by the Persian Gulf and the Stable craton. As the return period increases the Stable craton becomes the main contributor to the hazard and the Persian Gulf losses its influence (Figure 3.64). A very modest contribution from the Makran West source can be seen at the 2500-year and 10,000-year return periods (Figure 3.49 and Figure 3.54).

For the 0.2-s response period similar contributions to the hazard as for PGA can be appreciated. However, there is an increase in the contribution from events at larger distances, mainly at the 500-year return period, where some contribution from events with distances up to r_{epi} = 300 km can be appreciated.

The Persian Gulf is still the major contributor to the hazard at the 500-year return period, followed by the Stable craton (Figure 3.64). Also, a modest contribution from the Zagros Foredeep and the Simple Fold belt can be appreciated at this return period. For the 2500-year return period, in a similar manner as for PGA, the Stable craton becomes the dominating source, basically being the only contributor to the hazard for return periods up to and beyond 10,000 years.

In a similar manner to the city of Abu Dhabi, in Dubai at the 1.0-s response period the distribution of the contribution to the hazard by magnitude-distance scenario changes radically from that at 0.2-s response period. Here, three different magnitude-distance scenarios can be observed: (i) events of M_s< 7.0 and r_{epi} < 200 km, (ii) events of 6.5< M_s< 7.5 and 260 km< r_{epi}< 400 km, and (iii) events of 7.5< M_s< 8.4 and 260 km< r_{epi}< 420 km.

These three scenarios can be clearly identified across the different return periods. The events corresponding to (ii) (above) represent the dominating scenario at 500-year, 2500-year and 10,000-year return periods. The events corresponding to (i) (above) have a modest contribution at the 500-year return period, but increase with return period until they become almost as important a contributor to the hazard as the events in (ii) at the 10,000-year return period. The events corresponding to the scenario in (iii) have an increasing contribution with return period but always have a relatively modest contribution to the overall hazard.

The seismic sources that dominate the hazard for the 1.0-s response period are the Simple Fold belt, the Persian Gulf and Zagros Foredeep (Figure 3.64). These seismic sources, due to their distances from the city of Dubai and the maximum magnitudes assigned to them, seem to be principally responsible for the events within magnitude-distance scenario (ii). Following the same reasoning, the events from magnitude-distance scenario (i) would be generated by the Stable craton, which increases relative its contribution to the hazard as the return period increase (see Figure 3.64). Similarly, the Makran West source would be primarily responsible for the events corresponding to scenario (iii).

At the 3.0-s response period the same three magnitude-distance scenarios identified for the 2.0-s response period are present. This is, scenario (ii) dominates the hazard at the 500-year, 2500-year and 10,000-year return periods. Here the influence of the Simple Fold belt becomes more important and the relative contributions from the Zagros Foredeep and the Persian Gulf reduce. The magnitude-distance scenario (i) loses most of its contribution as the Stable craton is no longer a main contributor to the hazard. The scenario (iii) remains basically unchanged, with a modest contribution.

Contributions to the hazard for the city of Ra's Al Khaymah.

For the city of Ra's Al Khaymah, the contribution by magnitude-distance scenario for PGA is basically divided between two scenarios; one with magnitudes $M_s < 6.5$ and distances $r_{epi} < 150$ km, and a second, with a smaller contribution, from events with magnitudes $7.5 < M_s < 8.4$ and distances 180 km $< r_{epi} <$ 280 km (Figure 3.56). Both scenarios are present at 500-year, 2500-year and 10,000-year return periods. In all cases the first scenario is that which always dominates the hazard. The second scenario has a modest contribution at the 500-year and decreases with increasing return period to the point that its contribution is almost nil at the 10,000-year return period.

The seismic source that contributes the most to the hazard at the 500-year return period is the Persian Gulf, followed by the Stable craton, which are the seismic sources most likely to generate the events of the first magnitude-distance scenario ($M_s < 6.5$ and $r_{epi} < 150$ km). The contribution of the Persian Gulf source decreases with increasing return period, with the Stable craton becoming the dominating source at return periods of 2500 and 10,000 years (Figure 3.65).

The Zagros Foredeep and Makran West sources also provide an important contribution to the hazard but at relatively lower level. Both of them can be related to the events of the second magnitude-distance scenario, principally the Makran West source, given the magnitude of the events ($7.5 < M_s < 8.4$).

At the 0.2-s response period the distribution of the contributions by magnitude-distance scenarios remain basically the same as for PGA. However, just as for the cities of Abu Dhabi and Dubai, at the 0.2-s response period an increase in the contribution from events at larger distances than those for PGA is observed.

For the 500-year return period, the Persian Gulf dominates the hazard, followed by the Stable craton and Zagros Foredeep sources. In addition a most modest contribution is observed from the Makran West source. For the 2500-year and 10,000-year return periods the Stable craton becomes the main contributor to the hazard but the Persian Gulf source still provides an important contribution.

At the 1.0-s response period, four main magnitude-distance scenarios can be identified: (i) events of $M_s < 6.0$ and $r_{epi} < 250$ km; (ii) events with $6.0 < M_s < 7.2$ and $100 \text{ km} < r_{epi} < 280$ km; (iii) events with $7.6 < M_s < 8.4$ and $180 \text{ km} < r_{epi} < 280$ km; and, with a relatively lower contribution, (iv) events with $6.0 < M_s < 8.0$ and $r_{epi} > 300$ km (Figure 3.58).

At this response period the magnitude-distance scenario that dominates the hazard for the return periods of 500, 2500 and 10,000 years is the scenario (ii). The scenario (i) has a relatively modest contribution to the hazard which slightly increases with return period. The scenario (iii) has a stronger contribution than scenario (i) and at the 10,000-year return period dominates the hazard together with events in scenario (ii). Events in scenario (iv) have a much smaller contribution and this contribution decreases with increasing return period becoming almost nil at the 10,000-year return period.

The seismic sources that contribute the most to the hazard at 1.0-s response period are the Simple Fold belt, Zagros Foredeep, Persian Gulf and Makran West; each of these contribute almost equally to the hazard at the 500-year, 2500-year and 10,000-year return periods (Figure 3.65). The Stable craton generally has a smaller contribution that increases with increasing return period, only becoming of importance at very long return periods (see Figure 3.65).

At the 3.0-s response period the four dominating scenarios described for the response period of 1.0 s remain. Scenario (ii) is still the dominating

scenario at the 500-year and 2500-year return periods (Figure 3.59). At the 10,000-year return period, scenarios (ii) and (iii) both equally dominate the hazard. Scenario (i) decreases its contribution in comparison with that for the 1.0-s response period. Scenario (iv) still retains some contribution at the 500-year and 2500-year return periods; however, an important increase can be observed at the 10,000-year return period. This is probably due to some contribution from the Makran Intraplate seismic source that has a small but still important contribution to the hazard at the 10,000-year return period (see Figure 3.65).

3.8.2. Comparison with previous studies

In general terms, the PGA values for the 500-year return period calculated in this study lie within the same range as the values proposed by Al-Haddad *et al.* (1994), Peiris *et al.* (2006) and Musson *et al.* (2006). This place the cities of Abu Dhabi and Dubai as zone 0 and the city of Ra's Al Khaymah as zone 1 according to the UBC97 seismic-zone classification.

The UHS for the city of Dubai presented by Peiris *et al.* (2006), for 475-year and 2475-year return periods, and the UHS obtained in the current study are compared in Figure 3.66.

In Figure 3.67 the UHS presented by Musson *et al.* (2006) for the cities of Abu Dhabi, Dubai and Ra's Al Khaymah for return periods of 475 years, 1000 years and 10,000 years are compared with the corresponding UHS calculated in this study.

In both cases (i.e., Musson *et al.*, 2006; Peiris *et al.*, 2006) they present UHS for 475-year return period and these are compared with the UHS for the 500-year return period of the current study. However, not significant difference is expected between 475-year and 500-year return periods.

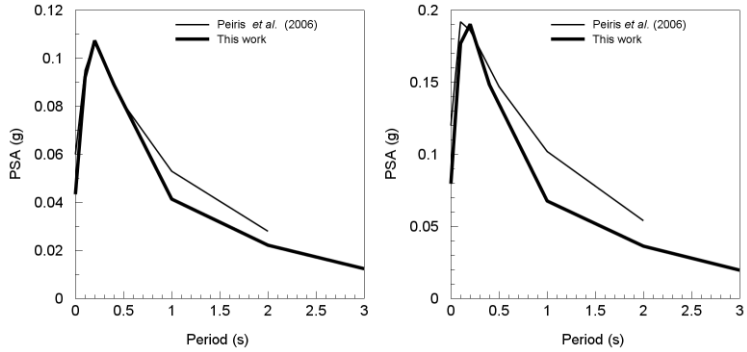

Figure 3.66. Comparison of the uniform hazard spectra for the city of Dubai from this work and that of Peiris *et al.* (2006). The UHS for this work were calculated for 500-year and 2500-year return periods, while those of Peiris *et al.* (2006) were calculated for 475-year and 2475-year return periods.

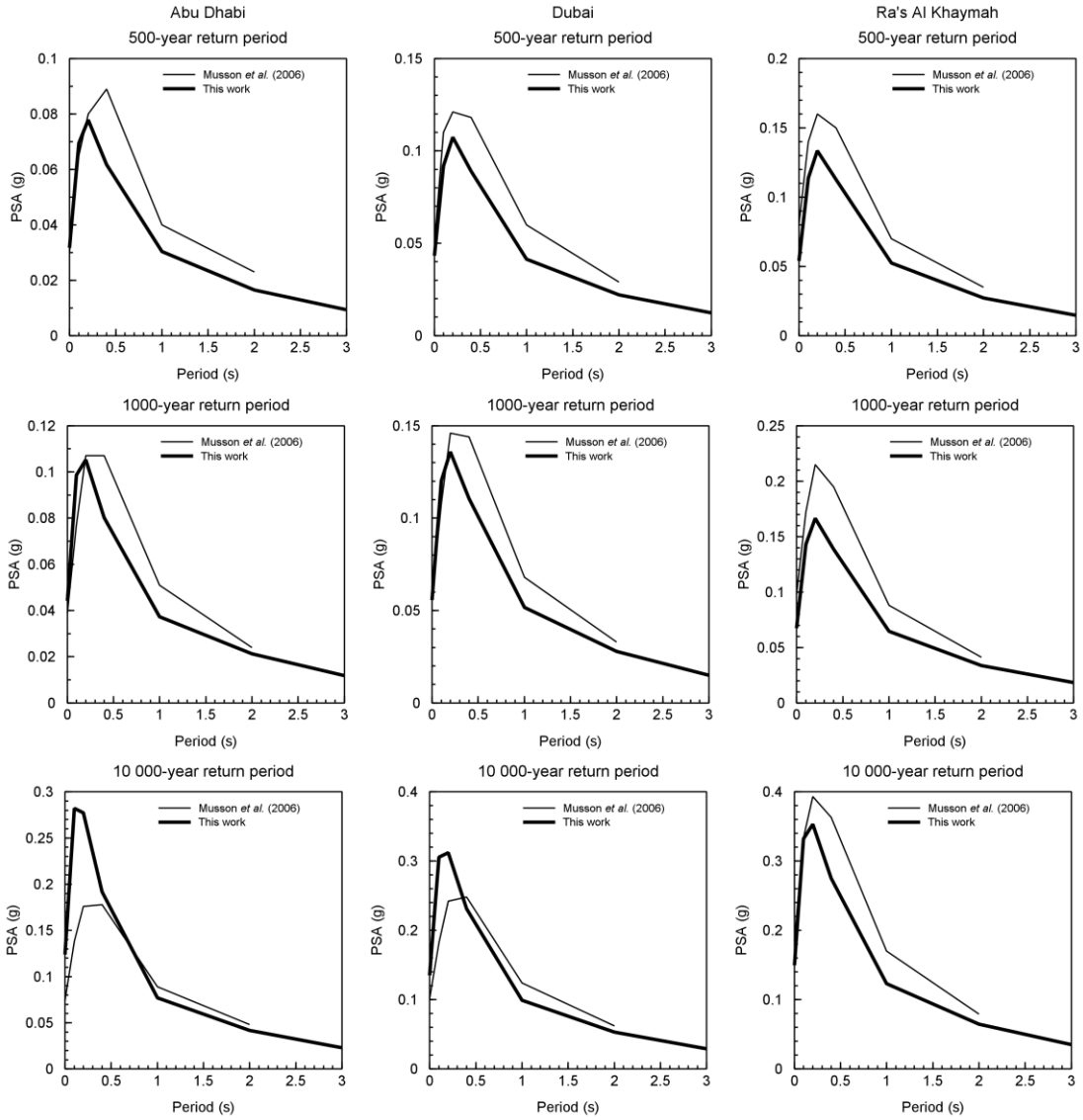

Figure 3.67. Comparison of the uniform hazard spectra from this work and that of Musson *et al.* (2006). The UHS for this work were calculated for 500-year return period, while those by Musson *et al.* (2006) were calculated for 475-year return period. PGA and spectral amplitudes for Musson *et al.* (2006) were read at 0.1, 0.2, 0.4, 1.0 and 2.0 s from figures 6.10, 6.12 and 6.13 and Table 8.1 of the referenced publication.

On the other hand, the PGA values presented by the GSHAP project (Grünthal *et al.*, 1999), Abdalla & Al-Homoud (2004) and Sigbjornsson & Elnashai (2006) clearly overestimate the seismic hazard in the region. In Figure 3.68 the UHS for the city of Dubai presented by Sigbjornsson & Elnashai (2006), for 974-year and 2475-year return periods, and the response spectrum obtained in the current study, for 1000-year and 2500-year return periods, are compared.

The UHS presented in Figure 3.67 and Figure 3.68 as Musson *et al.* (2006) and Sigbjornsson & Elnashai (2006) were constructed using only PGA and the spectral amplitudes at the response periods of 0.1, 0.2, 0.4, 1.0, 2.0 and 3.0 s, making them look smoother than those presented in the original publications.

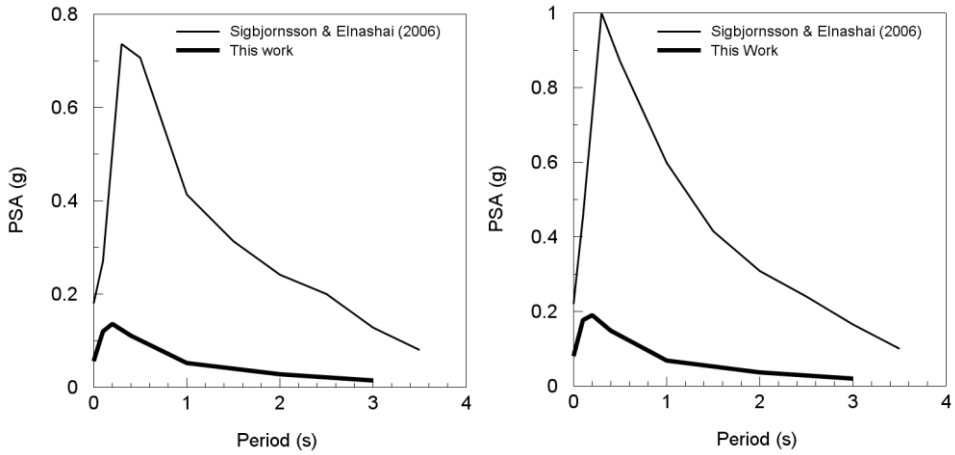

Figure 3.68. Comparison of the uniform hazard spectra from this work with that of Sigbjornsson & Elnashai (2006) for the city Dubai. The UHS for this work were calculated for 1000-year and 2500-year return periods, while those by Sigbjornsson & Elnashai (2006) were calculated for return periods of 974 years and 2475 years.

Additionally, in Figure 3.69 the 500-year UHS for the three sites are compared with the UBC97 UHS for Zone 1 and rock site conditions. In all the cases the UBC97 UHS are significantly larger than those obtained during this study.

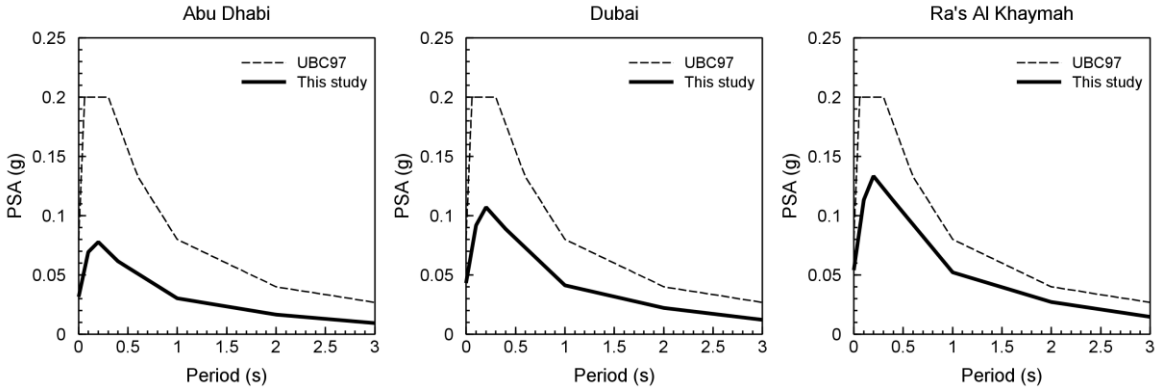

Figure 3.69. Comparison of the uniform hazard spectra for 500-year return period from this study with the UBC97 response spectra for Zone 1 and for rock site conditions (760 m/s < Vs < 1500 m/s).

Since most of the published hazard analysis report PGA values and SA for the city of Dubai but not for Abu Dhabi and Ra's Al Khaymah, in Table 3.13 a comparative summary of the results, for the city of Dubai and at 475-year and 2475-year return periods is presented.

Table 3.13. Comparison of the results of different published hazard analysis for the City of Dubai, UAE.

Source	Ground-Motion Parameter (g)	475 yr Return Period	2475 yr Return Period	Comments
UBC97	PGA	<0.075	--	Classified as zone 0
GSHAP (Grünthal *et al.*, 1999)	PGA	0.320	--	Read off GSHAP map for Europe, Africa and Middle East.
Al-Haddad *et al.*, 1994	PGA	<0.050	--	Read off Figure 4 of the cited paper.
Abdalla & Al-Homoud, 2004	PGA	0.150	--	Read off Figure 4 of the cited paper.
Peiris *et al.*, 2006	PGA	0.060	0.120	From Table 2 of the cited paper
	0.2 s SA	0.107	0.186	From Table 3 of the cited paper
	1.0 s SA	0.053	0.102	From Table 3 of the cited paper
	2.0 s SA	0.028	0.054	Read off Figure 6 of the cited paper.
Sigbjornsson & Elnashai, 2006	PGA	0.160	0.220	From Table 2 of the cited paper
	0.1 s SA	--	0.451	Read off Figure 11 of the cited paper.
	1.0 s SA	--	0.597	Read off Figure 11 of the cited paper.
	2.0 s SA	--	0.307	Read off Figure 11 of the cited paper.
	3.0 s SA	--	0.164	Read off Figure 11 of the cited paper.
Musson *et al.*, 2006	PGA	0.050	--	From Table 8.1 of the cited publication
	0.1 s SA	0.110	--	Read off Figure 6.10 of the cited publication
	0.2 s SA	0.121	--	From Table 8.1 of the cited publication
	0.4 s SA	0.118	--	Read off Figure 6.10 of the cited publication
	1.0 s SA	0.060	--	From Table 8.1 of the cited publication
	2.0 s SA	0.029	--	Read off Figure 6.10 of the cited publication
This work	PGA	0.043	0.080	PGA and PSA were calculated for 500-year and 2500-year return periods
	0.1 s SA	0.092	0.177	
	0.2 s SA	0.107	0.190	
	0.4 s SA	0.089	0.148	
	1.0 s SA	0.041	0.068	
	2.0 s SA	0.022	0.036	
	3.0 s SA	0.012	0.020	

3.8.3. Conclusions

On the basis of the comprehensive PSHA described in this chapter the seismicity in the region can be regarded as being low to very low. The hazard is higher at the northern tip of the UAE and decreases towards the south. Of the three considered cities in this study, Abu Dhabi and Dubai can be classified as zone 0, while Ra's Al Khaymah is classified as zone 1 according to the UBC97 classification scheme.

Current seismic design requirements in the UAE (e.g., the municipality of Dubai) seems to overestimate the hazard in the region when recommending the use of zone 2A from the UBC (1997) as the design criteria for buildings of five or more storeys. Even for the northern-most city, Ra's Al Khaymah, the zone 2A design criteria seems to be highly conservative as can be appreciated from comparing the UHS of this study with the response spectra from UBC97 for zone 1 and rock site conditions (Figure 3.69).

Some of the previous studies, such as GSHAP (Grünthal *et al.*, 1999), Abdalla & Al-Homoud (2004) and Sigbjornsson & Elnashai (2006) clearly overestimate the hazard in the region. The hazard estimation in the GSHAP project for the UAE territory is fundamentally lacking of any sound scientific basis, and the latter two studies are based on seismic source zonations that seem not to be consistent with the regional seismotectonic environment, in addition to the inappropriate use of ground-motion prediction equations. Both of these flaws may be leading to exaggerated estimates of the expected values of PGA and SA for any given return period.

On the other hand, studies such as those of Peiris *et al.* (2006) and Musson *et al.* (2006) present more realistic approaches and are generally in very good agreement with the results presented in this study.

In general terms, the seismic hazard in the region for PGA and short response periods is dominated by events of medium to low magnitudes, usually $M_s < 6.0$, and short distances, $r_{epi} < 75$ km, both for short and long

return periods. The Stable craton and the Persian Gulf seismic sources dominate the hazard at these response periods and PGA. With a lesser degree some contribution also comes from the Simple Fold belt and the Zagros Foredeep sources. The contribution of the latter two sources becomes more important at Ra's Al Khaymah, where some contribution also comes from the Makran West source at this location.

For the response periods above 1.0 s the seismic hazard is primarily dominated by events with magnitudes between M_s 6.0 and M_s 7.5 and distances between 200 km and 350 km. However, important contributions can also be observed from events with magnitudes of M_s< 6.0 at short distances and events with M_s ~8.0 at longer distances. The seismic sources that contribute the most at these periods are the Simple Fold belt, Zagros Foredeep and Persian Gulf for all three sites; and the Makran West source for the city of Ra's Al Khaymah. This latter source also provides a small contribution to Dubai. The Stable craton has an important contribution at long return periods for the cities of Abu Dhabi and Dubai, but its contribution to the hazard at Ra's Al Khaymah is less important.

It is important to highlight that the PGA and SA presented here are for rock conditions, and that site effects must be considered where these may be appropriate or influential. Since in many cases (as in the city of Dubai) new buildings are being located on land reclaimed from the sea or on man-made islands, site effects, such as liquefaction, may be particularly important.

It is recommended that a re-evaluation of the degree of epistemic uncertainty be carried out once new geologic and tectonic information, as well as more recorded seismicity, becomes available for the Arabian Peninsula, and in particular for the UAE and the Hajar Mountains.

Chapter 4.

DISAGGREGATION AND REPRESENTATION OF RESULTS

In this chapter the mechanics and implications of performing disaggregation when using different ground-motion prediction equations (GMPEs) within a logic-tree framework are investigated. Additionally, different representations of the hazard results, such as the mean and median hazard curves are discussed along with issues associated with the identification of hazard-dominating scenarios and, specifically, how these influence the specification of scenario spectra for seismic design and record selection for dynamic structural analysis.

4.1. Implications of using multiple GMPEs in disaggregation

The main advantage of PSHA over alternative approaches for estimation of the seismic hazard at a specific site is that PSHA integrates over all possible earthquake scenarios and across the entire possible range of ground motions that those scenarios are likely to produce. This integration is done in order to calculate the probability of exceedance of a given ground-motion level at the specified site.

This characteristic of PSHA allows the presentation of the hazard results in a disaggregated format. Disaggregated results are generally presented in terms of the contribution to the hazard by earthquake scenarios of magnitude (M), source-to-site distance (R), and epsilon (ε). Where epsilon represents the number of standard deviations that the target ground motion is above the median ground motion predicted by a given attenuation equation. Alternative representations of the disaggregated results, such as

the contributions to the hazard from each seismic source, can be useful as well.

The main purpose of the disaggregation is to have a clear panorama of how the different seismic sources and M-R-ε scenarios contribute to the seismic hazard at a given site. Based on this panorama, decisions on the selection of scenario-based ground-motion records and response spectra scenarios can be taken, which in some way are compatible with a specific probability of exceedance. Additionally, the identification of the most hazardous seismic source may allow the incorporation of secondary parameters for seismic design, such as the propagation path, near-source effects and the duration of the ground motion.

The earthquake scenario, in terms of M, R and ε, that contributes the most to the seismic hazard is commonly called the hazard-dominating scenario. This hazard-dominating earthquake scenario is usually defined by the modal values of M, R and ε (M*, R*, ε*) of the disaggregated results. Strictly speaking, the modal values are the most likely set of M-R-ε that may induce a ground-motion level that will equal or exceed the target ground motion (Bazzurro & Cornell, 1999). These modal values (M*, R* and ε*) are expected to vary not only for different ground-motion parameters (e.g, spectral accelerations at different response periods) but also for different ground-motion levels, and hence return periods.

In order to address the epistemic uncertainty associated with not knowing which ground-motion model is the optimal for a given region, the use of multiple GMPEs in PSHA has become a standard practice. As has been previously mentioned (section 2.5), the use of multiple GMPEs within a logic-tree framework requires, in some occasions, the transformation of the inputs and outputs of the equations involved into common metrics to guarantee compatibility (Bommer *et al.*, 2005). Nevertheless, although the compatibility of the inputs and outputs of the alternative GMPEs guarantee

the coherence of the results, there are still some issues of concern which result from the use of multiple GMPEs in PSHA.

One of the issues when multiple ground-motion equations are used in a PSHA is the distance definition used to display the disaggregated results. Some software, such as that used in this work to perform the hazard analysis in the case study, Crisis 2007 (Ordaz *et al.*, 2007), allows the user to select the distance metric to be used for displaying the disaggregated results by M, R. In practice it is not uncommon to find software in which the distance definition of the disaggregated results is not clearly stated. In some instances the resulting distance is a mix of the different distance definitions used for each GMPEs considered in the analysis, making these results difficult to interpret.

The use of different distance definitions in the disaggregated results might lead, to some extent, to different distributions of the contributions to the hazard from the different bins of M, R and ε. These differences can be significant mainly at short distances, where the differences between alternative distance definitions are largest; with these differences increasing with increasing magnitude (Scherbaum *et al.*, 2004b).

Unless it is a specific requirement of the project, there is no apparent reason why one distance definition should be preferred over the others for the representation of the disaggregated results (by M-R-ε). Nevertheless, it would be recommendable to select the most common distance definition among the ground-motion equations used in the analysis, in order to reduce the number of conversions from one distance definition to another when using the R value of the dominant scenario in subsequent analyses.

Keeping in mind the distance definition used to represent the disaggregated results, in most cases, it will be possible to identify the seismic source to which the dominant earthquake-scenario corresponds. Nevertheless, the contributions to the hazard from each seismic source can

be a helpful tool when there is ambiguity regarding the identification of the seismic source controlling the dominant scenario.

Bazzurro & Cornell (1999) propose to display the disaggregated results not in terms of R, but in terms of latitude and longitude, in addition to M and ε. This representation of the disaggregated results seems to be quite promising as it allows one to directly display the contributions to the hazard from each seismic source on a map. This representation makes it much easier to associate the dominant earthquake-scenario to a specific seismic source. However, even under this scheme, a distance metric must be chosen to display the hazard results.

The selection of the distance definition when displaying the disaggregated results in terms of latitude and longitude has a higher impact than when these are displayed in terms of M-R-ε. Since in PSHA, earthquakes are generally assumed to have hypocentres that are equally likely to occur anywhere within a seismic source, when distance definitions such as r_{epi} and r_{hypo} are used, the contribution to the hazard is expected to be smoothly spread along the surface projection of the fault. In contrast, when distance definitions such as r_{jb} and r_{rup} are used to display the disaggregated results, a concentration of the seismic hazard should be observed at the closest distance from the source to the site. This is due to larger events tending to rupture larger portions of the seismic source, making the closest location from the surficial projection of the source to the site the most likely point, within the seismic source, to contribute to the hazard.

Given this, r_{jb} and r_{rup} seem to be the most suitable distance definitions when the disaggregated results are displayed in terms of latitude and longitude, as they would identify the most “hazardous” location on a map. However, some differences in the disaggregated results, displayed in terms of latitude and longitude, should be expected from using either r_{jb} or

r_{rup} when sources of uniform seismicity are considered in the surroundings or beneath of the site under study. Furthermore, the majority of the most recent ground-motion equations use either r_{jb} or r_{rup} as an explanatory variable (c.f., Douglas, 2006).

When the analyst incorporates alternative GMPEs into the logic tree to perform the hazard analysis (one per branch), the disaggregated results at the end tips of the logic tree might differ in terms of the contribution to the hazard by each M-R-ε scenario. However, these contributions in the disaggregated results for the different GMPEs are not expected to present significantly different panoramas, for the same ground-motion levels.

For example, in Figure 4.1 the disaggregated results from two branches of the logic tree in the case study are presented. These results are presented for the city of Dubai for spectral amplitudes at 0.2 s response period and a target ground motion of 0.21 g; this value corresponds to the target ground motion of the mean hazard curve at the 2500-year return period.

On the left-hand-side is shown the disaggregation for the branch where the GMPE of Akkar & Bommer (2007b) was used to model ground-motion attenuation for shallow earthquakes in the Zagros region and the Stable craton. On the right-hand-side is shown the disaggregation for the branch where Boore & Atkinson (2007) was used to model ground-motion attenuation for the above mentioned regions. In both cases, ground-motion attenuation for the Makran was modelled using the GMPE of Atkinson & Boore (2003). For these combinations of GMPEs the influence on the seismic hazard of the seismicity in Makran is null at this level of ground motion (i.e., 0.21 g); therefore it is a good example of the difference of using different GMPEs in alternative branches of the logic tree (one GMPE per branch). In both cases the dominant earthquake scenario is M_w = 5.1 and r_{epi} = 12.5 km.

Note that the magnitude units in Figure 4.1 are in M_s scale, the relationship of Ambraseys & Free (1997) was used to transform from M_s to M_w.

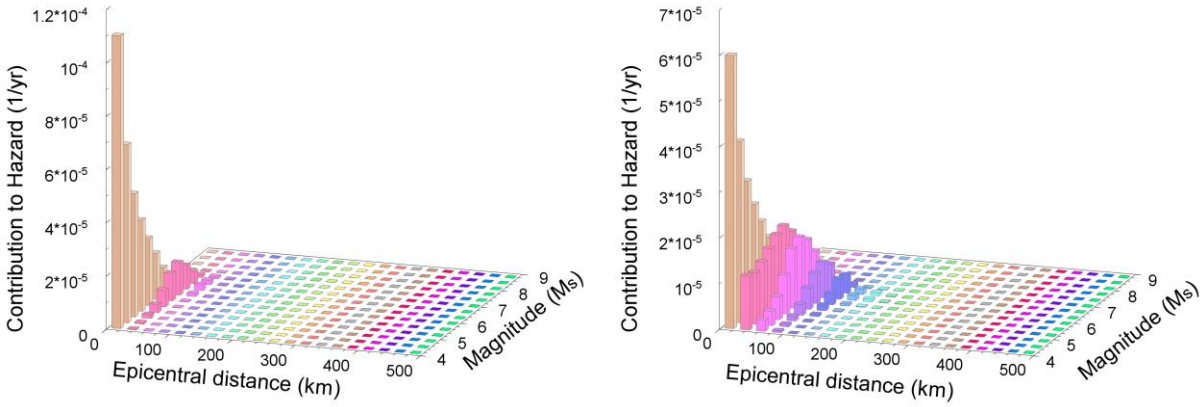

Figure 4.1. Disaggregated results for the city of Dubai for SA at 0.2 s and a target ground motion of 0.21 g, using the GMPEs of Akkar & Bommer (2007) –left– and Boore & Atkinson (2007) –right– for shallow earthquakes in the Zagros region and the Stable craton, and in both cases Atkinson & Boore (2003) was use for the Makran subduction zone.

The interpretation of the disaggregated results becomes more complicated when two or more ground-motion equations are used simultaneously in a single branch of the logic tree. This is the case, for instance, when two different tectonic environments such as shallow earthquakes in active regions and earthquakes in subduction zones are likely to produce ground-motion levels of importance at the specified site. In this case, the analyst will wish to use equations specifically derived for each tectonic environment.

When multiple equations are simultaneously used in alternative branches of the logic tree, not only the contributions by M-R-ε might change among branches, but also the relative contributions to the hazard from each of the seismic sources is likely to change. In this case, the distributions of the contributions by M-R-ε for the same ground-motion level might be significantly different. These considerations have direct consequences for the

identification of the hazard-dominating earthquake scenario that represents the seismic hazard.

An example of this situation is shown in Figure 4.2, where the disaggregated results are presented once more for the city of Dubai for SA at 0.2 s and a target ground motion of 0.21 g. In this case, on the right-hand-side, we display, the disaggregation for the branch where the GMPE of Akkar & Bommer (2007b) was used to model ground-motion attenuation for the Zagros region, Atkinson & Boore (2006) for the Stable craton and Youngs *et al.* (1997) for the Makran subduction zone. Note that the disaggregated results on the left-hand-side of the Figures 4.1 and 4.2 correspond to the same set of GMPEs.

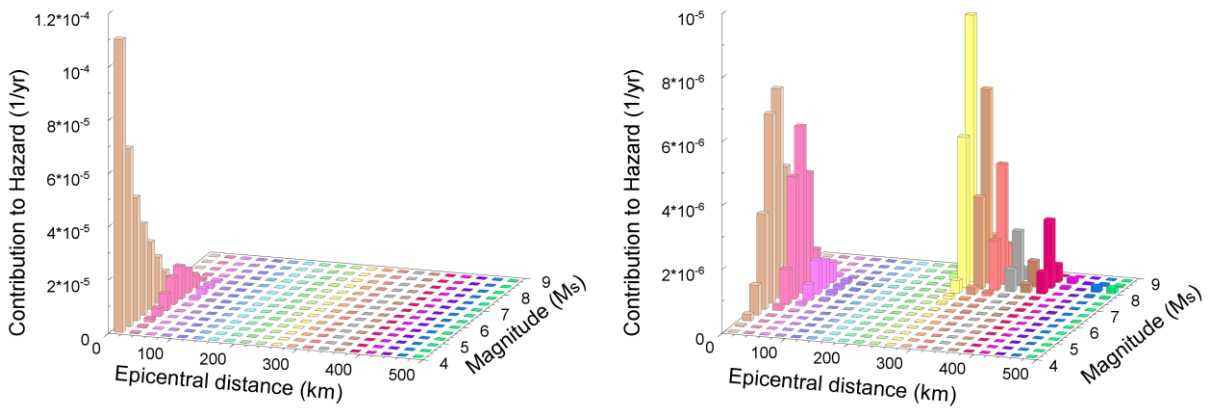

Figure 4.2. Disaggregated results for the city of Dubai for SA at 0.2 s and a target ground motion of 0.21 g, using the GMPEs of Akkar & Bommer (2007) for the Zagros region and the Stable craton and Atkinson & Boore (2003) for Makran –left– and Boore & Atkinson (2007) for the stable craton, Akkar & Bommer (2007) for the Zagros region and Youngs *et al.* (1997) for Makran –right–.

As can be seen, both sets of equations present completely different panoramas for the contributions by M-R-ε, and hence radically different dominant earthquake scenarios. The dominant scenario goes from M_w = 5.1 and r_{epi} = 12.5 km (left-hand-side of Figure 4.2) to M_w = 8.4 and r_{epi} = 262.5 km (right-hand-side of Figure 4.2).

It is worth noting that the return periods corresponding to each of the disaggregated results presented in Figure 4.1 and Figure 4.2 are different. The results shown on the left-hand side in Figure 4.1 and Figure 4.2 correspond to a return period of ~2700 years, while the results on the right-hand-side in Figure 4.1 correspond to a return period of ~2300 years, and those on the right-hand-side in Figure 4.2 correspond to a return period of ~12000 years.

One of the main questions that the hazard analyst faces when using multiple GMPEs in PSHA is how to merge the suite of hazard curves and their corresponding disaggregated results from the end tips of the logic tree into a single hazard curve; then, how to obtain from that final hazard curve, and its corresponding disaggregation, a single (or small set of) earthquake scenario(s) that represents the seismic hazard at the site at a given return period.

To this end, different statistical estimators such as the weighted mean or the median (or any other fractile) can be used, depending on the interest of the analyst. Additionally, these estimators can be applied either in the exceedance-frequency (hazard) domain (the most widely used approach in current practice) or the ground-motion domain (Bommer *et al.*, 2005). In any case, the analyst must be aware of the implications in the final hazard curves and the disaggregated results of the selection of any of these methods. In the following sections the implications of using either the weighted mean or the median in the hazard domain or ground-motion domain are discussed.

When only one ground-motion equation is used in the hazard analysis, the estimation of the expected ground motion based on the dominant earthquake scenario (M*, R*, ε*) is rather simple, as the same equation considered for the hazard analysis can be used. Given that traditional hazard analyses are performed to estimate the probability of exceeding a

target ground motion, the ground motion predicted by the attenuation equation for the dominant scenario will generally need to be adjusted to match the target ground motion. This adjustment is performed by modifying in a heuristic manner the value of ε in the ground-motion equation to be equal to the predicted value to the target ground motion (McGuire, 1995).

McGuire (1995) proposes disaggregating the hazard results in such a way that the contributions to the hazard equal but do not exceed the target ground motion. In this case the value predicted by GMPE will equal the target ground motion, within the precision associated with a certain M, R and ε bin size, for the triplet of M*-R*-ε*. This procedure will be discussed later in this chapter.

The estimation of the expected ground motion based on the dominant earthquake scenario becomes more complex when different tectonic regimes are involved in the analysis and two or more ground-motion equations need to be used simultaneously in a PSHA (multiple GMPEs in a single branch). In such a case, the selection of which equation to use for predicting the ground motion using M*-R*-ε* might not be a straightforward decision.

In the simplest case, the dominant earthquake scenario will clearly correspond to one of the tectonic regimes. This might be possible if the ranges of distances and/or magnitudes from each of the regimes are clearly different. If we use, as an example, any of the disaggregated results presented in Figure 4.1, it is clear that the dominant seismic source is the Stable craton as it is the only seismic source within 25 km from Dubai. Therefore, the equation assigned to that source can be used to estimate the expected ground motion. When it is not possible to make such a distinction, the relative contribution to the hazard by seismic source could be helpful, showing which seismic source is contributing the most to the hazard at the specified target ground-motion.

In more complex situations, when it is not obvious which sources, and hence tectonic regimes, are dominating the hazard, the disaggregation of the hazard curves for each of the seismic sources might be necessary in order to show which seismic source is contributing the most in terms of M, R and ε.

For the case when multiple GMPEs are used in alternative branches of the logic tree, the combined hazard curve and its corresponding disaggregated results are the weighted mean (or any other appropriate statistical estimator used in the calculation of the combined curve) of the contributions of each of the M, R and ε bins from each of the branches. The combination of the disaggregated results in this way represents the epistemic uncertainty incorporated into the hazard analysis, which in part is due to the selection of the most appropriated GMPE for the region. Given this, the final values of M*, R* and ε* do not correspond to any particular GMPE, and hence any attempt to estimate the expected ground motion for the dominant scenario using only one of the GMPEs does not have any theoretical foundation.

As has been discussed earlier in this section, the use of multiple GMPEs in alternative branches of the logic tree has direct implications on the seismic-hazard panorama presented by the disaggregated results and for the interpretation of such results. The use of multiple GMPEs in PSHA has implications not only for the disaggregated results but also for the representation of the final hazard results, the identification of the hazard-dominating scenarios and for the specification of scenario spectra and selection of ground-motion records for seismic design. These topics are discussed in the following sections.

4.2. Mean vs. Median Hazard

The question regarding how to best represent the suite of hazard curves resulting from the different branches of a logic-tree is still open to discussion (Abrahamson & Bommer, 2005; McGuire *et al.*, 2005; Musson, 2005). An overview and discussion on this topic is presented in section 2.5.3.

In this section a comparison is presented among the weighted mean, the weighted mean ±1σ, the median and the 85th and 15th fractiles of the suite of hazard curves from the logic tree of the case study. All of these statistical estimators were calculated for fixed values of ground motion. In other words, these are the weighted mean and fractiles of the exceedance probabilities (hazard) given some ground-motion level. These calculations were performed in this way and not in terms of ground-motion levels given some annual rate of exceedance in order to follow common practice. However, in the following section a discussion of the estimation of the mean hazard curve of the ground-motion levels is presented. In what follows the term "mean" should be taken to mean "weighted mean" for brevity.

The standard deviation associated with the mean hazard curve was calculated as the standard deviation of the logarithm of the exceedance probabilities as the hazard values appear to be approximately lognormal distributed. This standard deviation corresponds only to the epistemic uncertainty. In other words, these values of standard deviation represent the scatter, in the hazard domain, of the hazard curves at the end tips of the logic tree (epistemic uncertainty) for any particular ground-motion level.

Additionally, the disaggregated results for PGA and SA at 0.2, 1.0 and 3.0 s response period were obtained for both, the mean and median hazard curves. The disaggregated results are presented in two forms: (1) by magnitude-distance scenarios and (2) by seismic source contributions.

Since the aim of this analysis is only to evaluate different representations of the hazard results obtained from a PSHA performed within a logic-tree framework, only the results for the city of Dubai are presented. However, the same behaviour was observed between the mean and median hazard curves for the cities of Abu Dhabi and Ra's Al Khaymah.

The mean and median hazard curves for the city of Dubai for PGA and spectral amplitudes (SA) at response periods of 0.2, 1.0 and 3.0 s are presented in Figure 4.3.

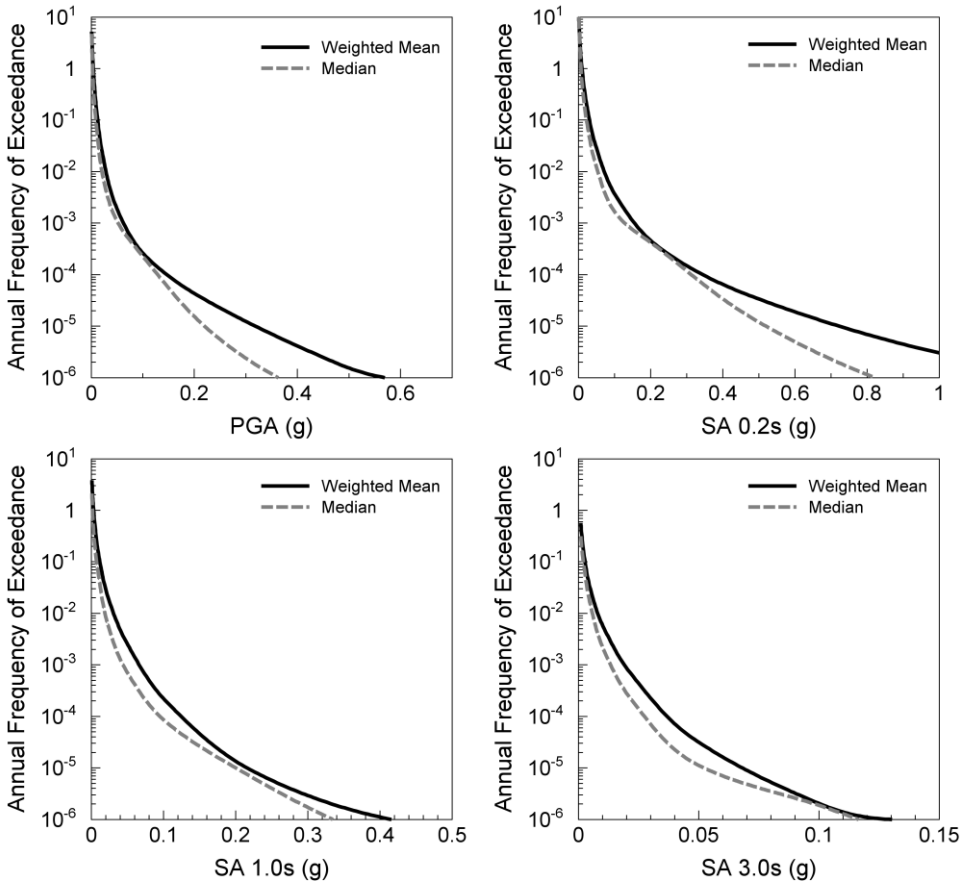

Figure 4.3. Weighted mean and median hazard curves of the city of Dubai for PGA and SA at 0.2, 1.0 and 3.0 s response periods.

As expected, the exceedance probabilities for the median hazard curves are lower than for the mean hazard curve (Abrahamson & Bommer, 2005) although not in any systematic way. For PGA and the response period of 0.2 s, the differences between both hazard curves increase as the

exceedance frequencies decrease. However, for 1.0 and 3.0 s response periods a more unstable behaviour of the median curve can be observed.

In Figure 4.4 all of the hazard curves from each branch of the logic tree (15552 in total) are shown, in addition to the mean, mean ± 1σ, and the 15th, 50th (median) and 85th fractile hazard curves. From inspection of Figure 4.4, it can be appreciated that the mean curve is more stable across the exceedance probabilities than the median curve, which tends to have abrupt changes in the slope when different groups of hazard curve cross each other. However, as was commented in section 2.5.3, it can be observed that the median hazard curve and the 15th and 85th percentiles are a better statistical representation of the scatter in the suite hazard curves.

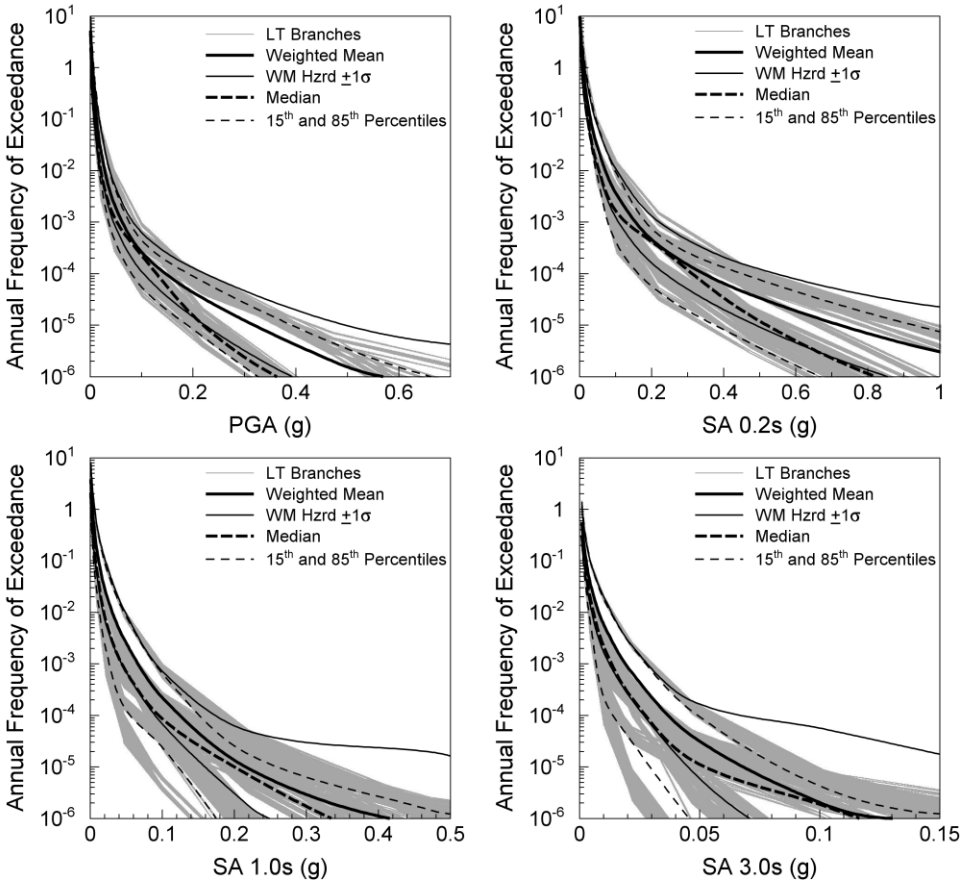

Figure 4.4. Weighted mean, weighted mean ±1σ and the 15th, 50th (median) and 85th percentiles hazard curves for the city of Dubai for PGA and SA at 0.2, 1.0 and 3.0 s response periods. LT Branches are hazard curves for each of the 15552 branches of the logic tree.

The mean and mean ± 1σ hazard curves fail to adequately represent the scatter in the hazard curves, particularly at the longest return periods. As can be seen in Figure 4.4, the mean +1σ curve has a good agreement with the 85th percentile curve at the shorter return periods (below 1000 years). However, at longer return periods, the mean +1σ curve lies clearly above the suite of hazard curves from the logic tree. For the case of the mean -1σ curve, this tends to follow the trend of the median curve rather than the 15th fractile curve. All of this clearly reflects the non-lognormal distribution of the set of hazard curves produced by a PSHA performed within a logic-tree framework.

Comparisons of the disaggregated results in terms of magnitude (M) and distance (R) scenarios between the mean and the median hazard curves are presented in Figure 4.5 to Figure 4.7. These results are presented for the city of Dubai for PGA and SA at response periods of 0.2, 1.0 and 3.0 seconds and for 500, 2500 and 10,000-year return periods. On the left-hand-side the disaggregated results corresponding to the mean hazard curve are presented, while on the right-hand-side the disaggregated results for the median hazard curve are presented.

As can be seen, radically different M-R scenarios correspond to the mean and median hazard curves. The most radical differences in the disaggregated results are for the response periods of 1.0 and 3.0 seconds and become more radical as the return period increases. Whence, choosing either the mean or the median hazard curve not only leads to different levels of ground motion for a given return period, but it also leads to different dominant earthquake scenarios. This has significant implications for the selection of ground-motion records and the scenario spectra to be considered for seismic design. These implications are discussed later in section 4.5.

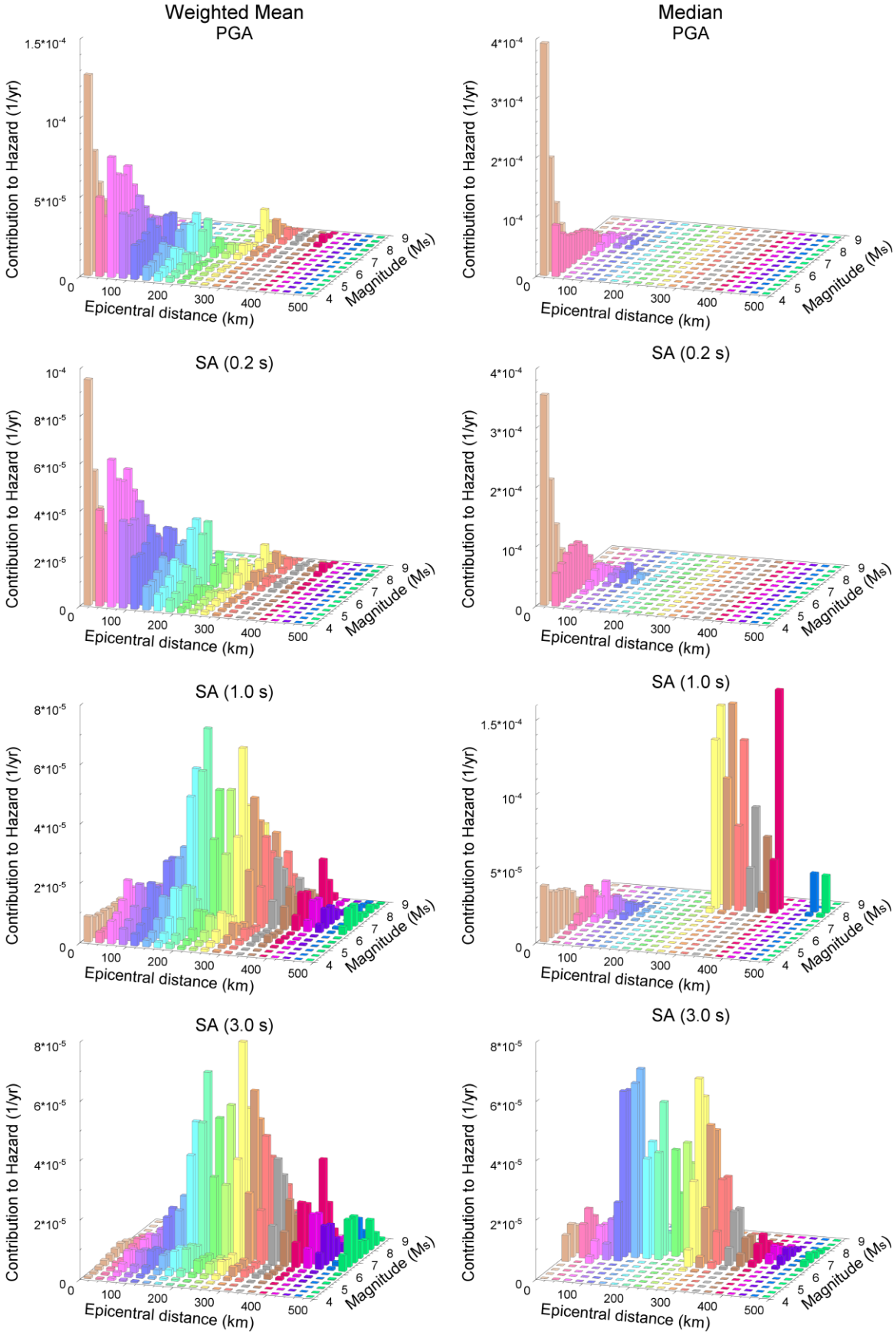

Figure 4.5. Disaggregated results, for the mean (left column) and median (right column) hazard curves, for the city of Dubai at 500-yr return period for PGA and SA at 0.2, 1.0 and 3.0 s response periods.

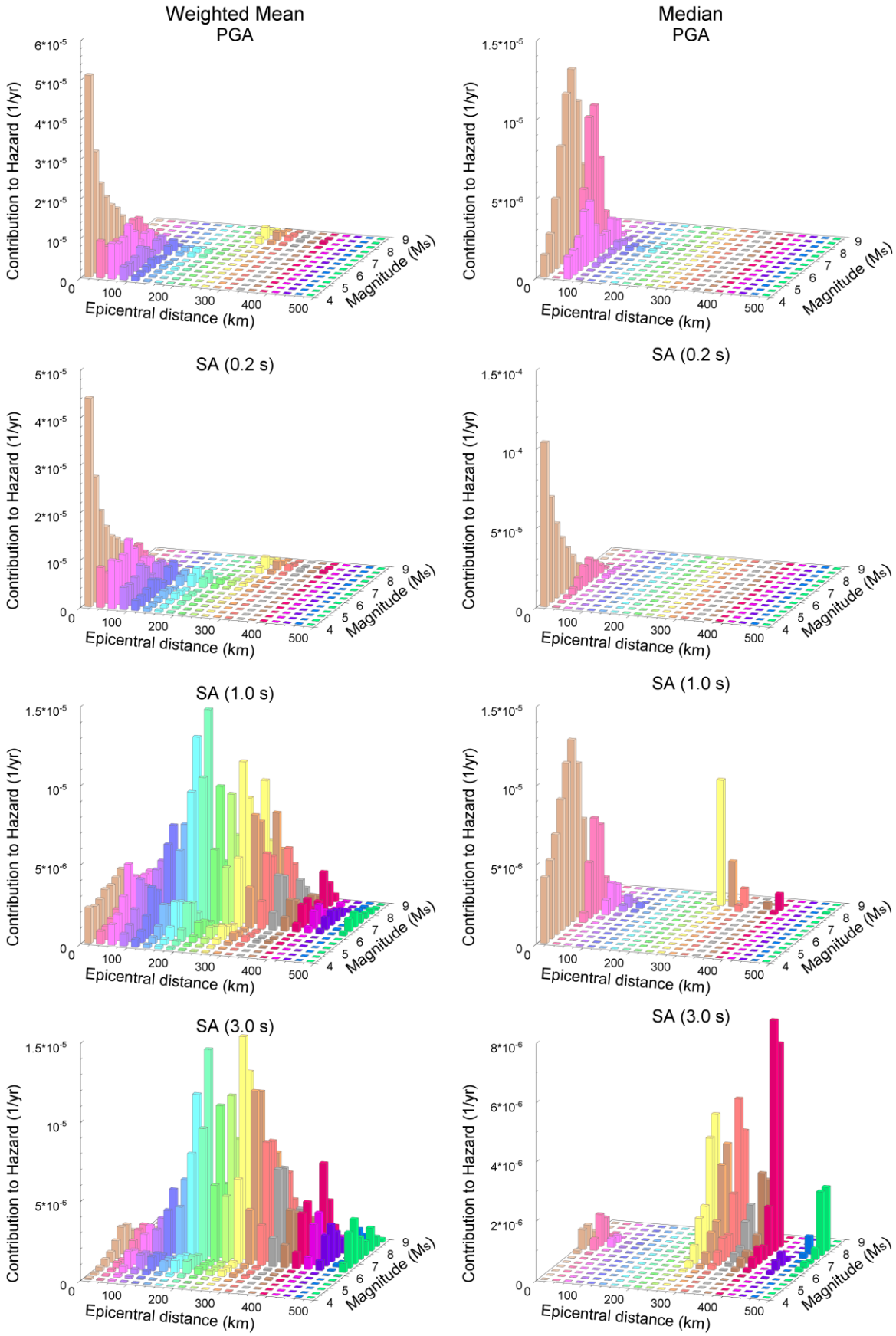

Figure 4.6. Disaggregated results, for the mean (left column) and median (right column) hazard curves, for the city of Dubai at 2500-yr return period for PGA and SA at 0.2, 1.0 and 3.0 s response periods.

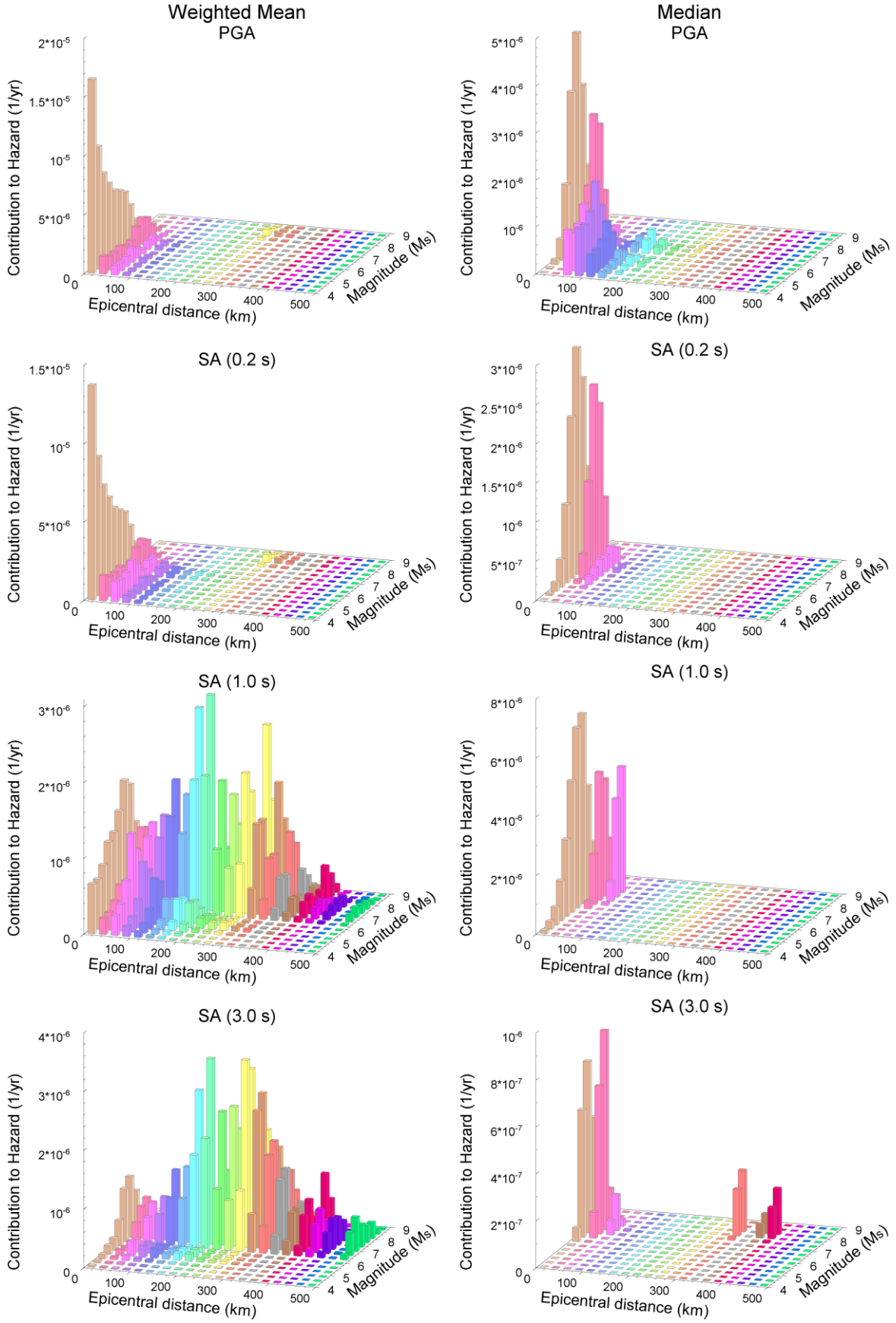

Figure 4.7. Disaggregated results, for the mean (left column) and median (right column) hazard curves, for the city of Dubai at 10,000-yr return period for PGA and SA at 0.2, 1.0 and 3.0 s response periods.

Disaggregated results represented in terms of the contribution to the hazard from each seismic source, for the mean and the median hazard curves, are shown in Figure 3.64 (same as in Chapter 3) and Figure 4.8, respectively.

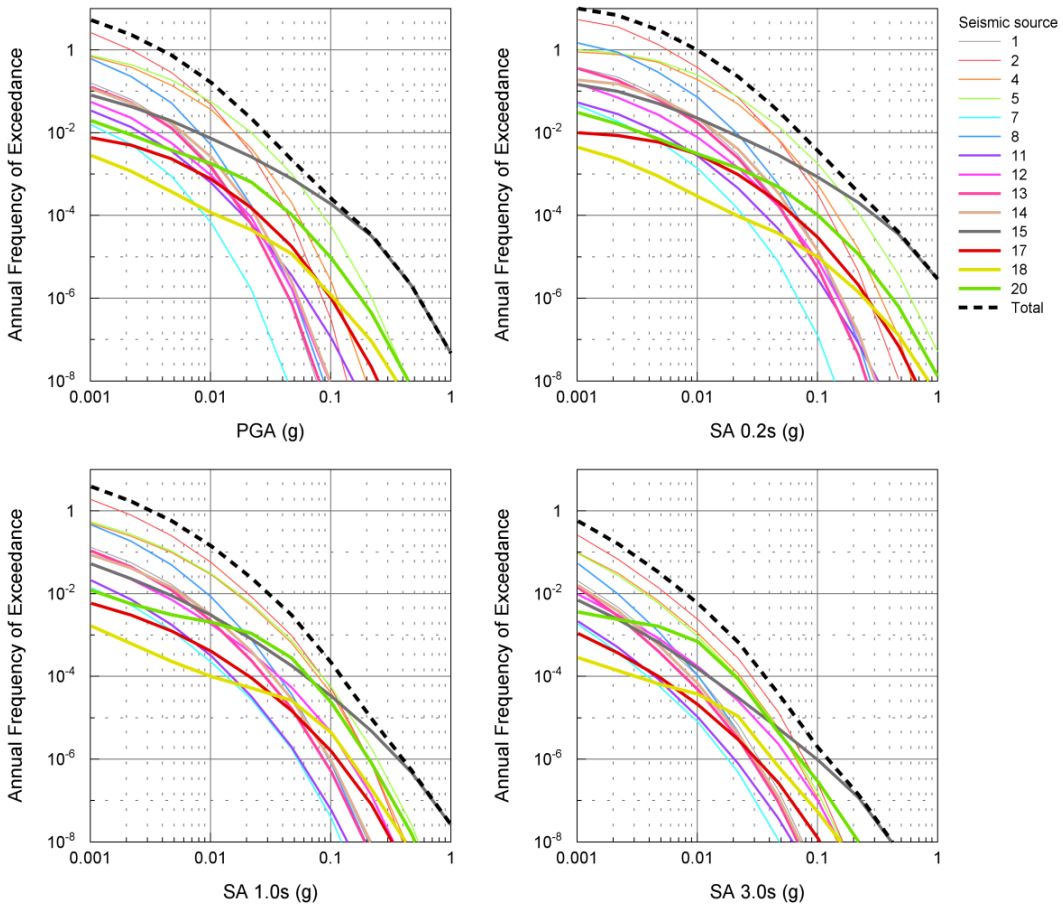

Figure 3.64. Contribution to the hazard from each of the seismic sources for the city of Dubai. See Table 3.7 for seismic source number identification. The heavy dashed line is the mean hazard curve.

While in Figure 3.64 the probability of exceedance for the different seismic sources smoothly decreases with increasing ground-motion, in Figure 4.8 the probability of exceedance for the different seismic sources have a very erratic behaviour. For the case of the median hazard curve (Figure 4.8), in some instances the probability of exceedance apparently increases as the ground-motion level increases, which is physically impossible given that the ordinate represents a cumulative rate of

exceedance and must be monotonically decreasing with increasing ground motion.

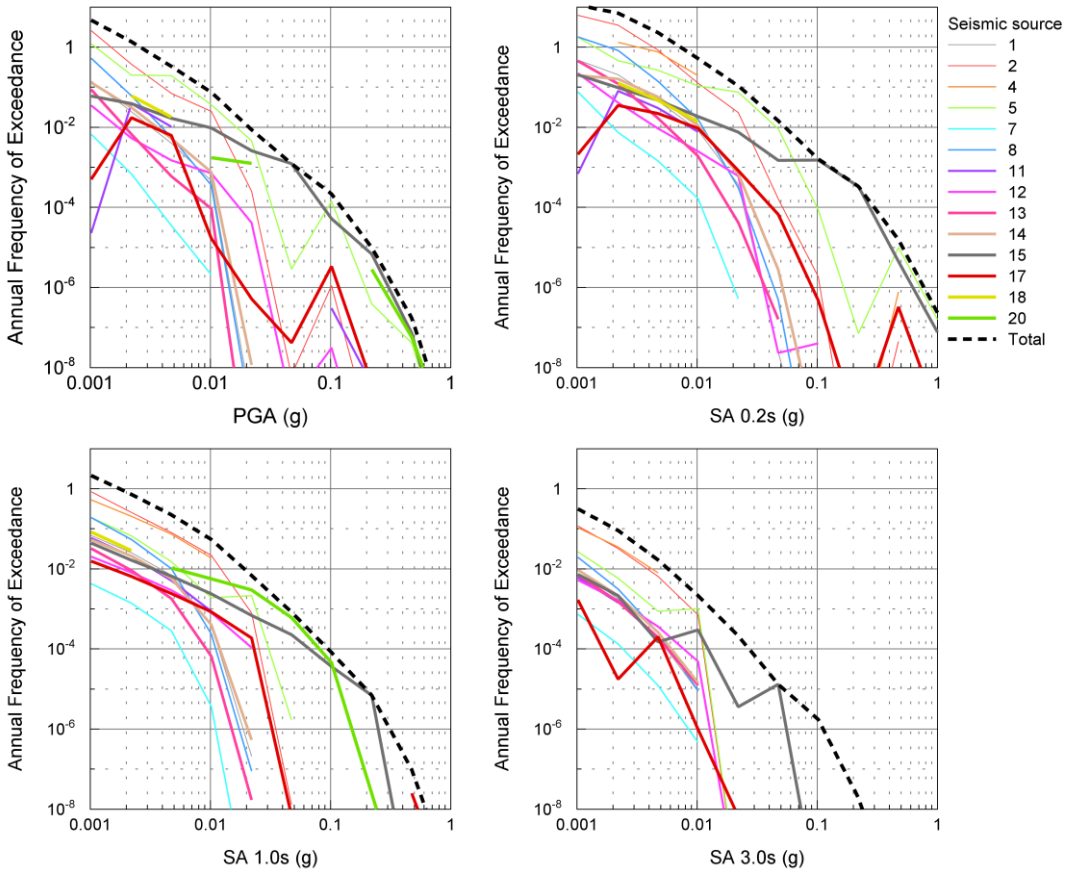

Figure 4.8. Disaggregated results of the median hazard curve presented as the contribution to the hazard from each of the seismic sources for the city of Dubai. The heavy dashed line is the median hazard curve. See Table 3.7 for source number identification.

The reason for the strange behaviour of the contributions to the hazard from each of the seismic sources for the median hazard curve is to do with how the hazard curves from the alternative branches of the logic tree are distributed. Since the hazard curves from the different branches are not parallel, but rather cross each other, the median value for two distinct ground-motion levels might correspond to different hazard curves. That is, the median value for a given ground-motion level might correspond to one hazard curve while the median value for the following ground-motion level might correspond to a different hazard curve. Given that each hazard curve

represents alternative seismic scenarios considered in the logic tree, the median values of each curve may correspond to different seismic scenarios as well. These peculiarities in the disaggregated results of the median hazard curve are logically expected at any other fractile.

In the case that the hazard curves resulting from the alternative branches of the logic tree were all parallel; the erratic behaviour of the hazard curves from each seismic source shown in Figure 4.8 would disappear. In that particular case, all the values for the median hazard curve would correspond to the same branch of the logic tree, and consequently to the same seismic scenario.

Alternatively, and in order to avoid the inconsistencies observed in Figure 4.8, a single hazard curve from the suite of curves of the logic tree could be selected as the median hazard curve. This will eliminate the possibility of having two completely different seismic scenarios for adjacent levels of ground motion. However, if only one hazard curve is selected as the "median hazard curve" the problem would then be associated with which criteria should govern the selection of the hazard curve that will be considered as "the" median hazard curve. In principle, the median curve that is identified may only represent median rates of exceedance for a very small range of ground-motion values.

As previously mentioned, one of the main purposes of plotting disaggregated results is to identify a hazard-dominating earthquake scenario at a selected return period that can be related to a specific seismic source, in order to subsequently perform time-domain structural analyses. Given this, the erratic behaviour of the contribution by seismic source shown in Figure 4.8 raises some concern regarding the use of the median hazard curve and its disaggregated results for seismic design purposes. However, fractiles have been shown to provide a good representation of the variability in the hazard curves resulting from different branches of a logic tree.

4.3. Mean hazard vs. Mean ground-motion

In current engineering practice, and for seismic design purposes, first a return period, representing the required safety level, is selected and then the value of ground motion to be used for seismic design is read from the hazard curve. Given this approach, the logical way to obtain the mean hazard curve from the suite of hazard curves resulting from a PSHA performed within a logic-tree framework would be to calculate the mean of the values of ground motion for given values of the annual rate of exceedance (Bommer & Scherbaum, 2008). However, the common practice, as mentioned in the previous section, is to calculate the mean of the probabilities of exceedance for given values of ground motion.

The difference between the two approaches is that with the latter approach (taking the mean of the probabilities of exceedance) what is obtained is the expected probability of exceedance for a given value of ground motion, whilst with the first approach (taking the mean of the ground-motion levels) what is obtained is the expected ground-motion level for a given value of exceedance probability. Once more, since in common practice the return period is fixed first and then the corresponding value of ground motion is obtained, calculating the mean of the ground-motion levels seem to be the most logical and consistent approach.

In this section a comparison of the hazard curves and their disaggregated results using both approaches is presented and discussed. The results are shown for the city of Dubai for PGA and SA at 0.2, 1.0 and 3.0 s response periods. Additionally, the hazard curves for the 15^{th}, 50^{th} and 85^{th} fractiles of the ground-motion values were calculated. This is done with the aim of evaluating the capability of the standard deviation associated with the mean of the ground-motion domain to represent the scatter in the hazard curves from the various branches of the logic tree.

In every software package that the author is aware of, the annual frequencies of exceedance in a hazard curve are obtained for fixed values of ground motion (see section 2.4.2). Therefore, in order to calculate the mean of the ground-motions at fixed return periods some interpolations are required. The interpolations of the hazard curves were performed on the logarithms of the values (i.e., exceedance probabilities and ground motions) for return periods between 5 and 100 000 years using the cubic spline interpolation method. For the disaggregated results in terms of magnitude-distance scenarios a linear interpolation of the logarithm of the contributions was performed. In order to do this, the ground motion values in the hazard curves, obtained with the cubic spline interpolation for the different return periods, are used as an indicator for performing the linear interpolation in the disaggregated results. In this way, the resultant disaggregated results correspond to the same return periods of the ground-motion levels obtained from the interpolation in the hazard curves.

A limitation of this approach is that the interpolation is constrained to a maximum return period that is dependant on the hazard results. For instance, for the case study presented in Chapter 3 the maximum value of ground motion considered for the analysis was 1 g and from all the hazard curves from each branch of the logic tree the lowest return period at 1 g was about 230 000 years. Therefore, if all of the hazard curves needs to be consider for the analysis, the longest return period at which the interpolation can be performed is 230 000 years.

The hazard curves obtained from both approaches are compared in Figure 4.9. In addition to the mean curves, the hazard curves for the mean $\pm 1\sigma$ for both approaches are also presented.

As can be seen in Figure 4.9, the curve corresponding to the mean of the ground motions always gives lower values of exceedance probability. Although the difference between both approaches seems to be not so

significant for short period ground motions, it increases with return period and with response period. At 1.0 and 3.0 s response periods the mean of the ground motions is closer to the mean -1σ rather than to the mean of the probabilities of exceedance.

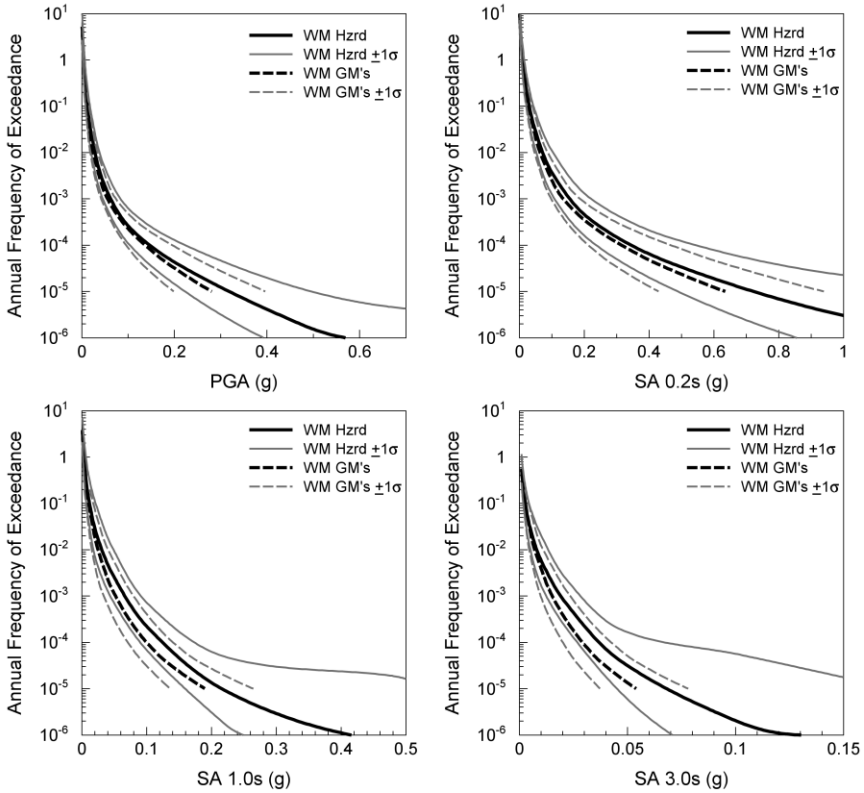

Figure 4.9. Hazard curves calculated as the weighted mean of the probabilities of exceedance (WM Hzrd), the weighted mean of the ground motion (WM GM's) and weighted mean ±1σ for both approaches. The curves are for the city of Dubai for PGA and SA at 0.2, 1.0 and 3.0 s response periods.

However, the main difference between both approaches manifests in the standard deviations associated with the estimation of each hazard curve. In a similar manner as in section 4.2, the standard deviation was calculated from the logarithm of the values for either exceedance probabilities or ground motions. The standard deviation calculated in this way represents only the epistemic uncertainty.

All of the hazard curves from the logic tree (15,552 in total) in addition to the mean and the mean ±1σ hazard curves of both approaches are

presented in Figure 4.10. As can be noticed from Figure 4.9 and Figure 4.10, the mean ±1σ hazard curves of the ground motions are considerably below their corresponding ones for the exceedance probabilities and provide a much better representation of the scatter among the suite of curves from the logic tree.

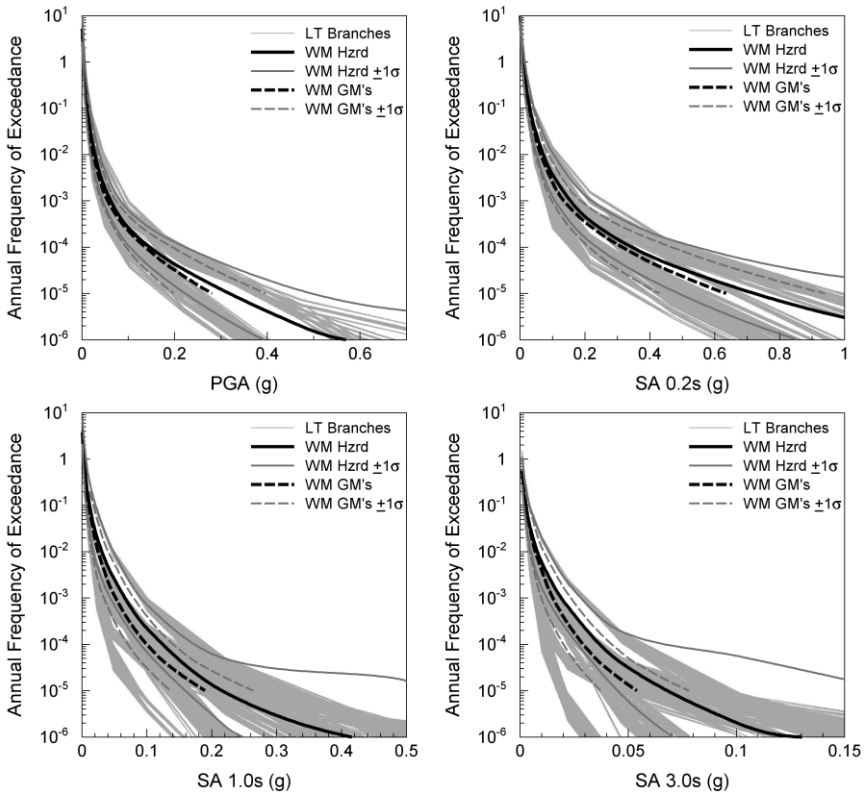

Figure 4.10. Weighted mean hazard curves for the probabilities of exceedance (WM Hzrd), ground motion values (WM GM's) and weighted mean curves ±1σ for both approaches. LT Branches are hazard curves for each of the 15,552 branches of the logic tree. The hazard curves are for the city of Dubai for PGA and SA at 0.2, 1.0 and 3.0 s return periods.

Figure 4.11 shows a comparison between the mean, mean ±1σ and the 15th, 50th (median) and 85th percentile hazard curves of the ground-motion values. In general terms, there is a good agreement between the mean and median hazard curves. However, as for the case of the mean and median curves calculated for exceedance probabilities (section 4.2), the mean hazard curve seems to be more stable across the return periods than the median, which shows a more erratic behaviour. This behaviour of the median curve

was also observed for the other two sites (i.e., Abu Dhabi and Ra's Al Khaymah).

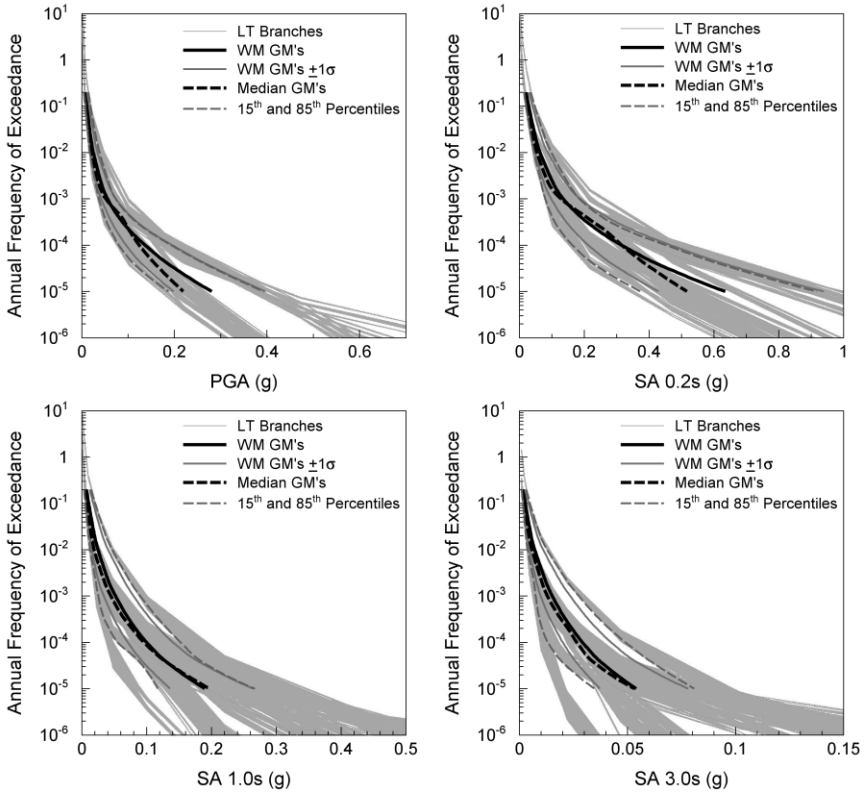

Figure 4.11. Comparison between the mean hazard curve of the ground motion (WM GM's) and its standard deviation associated (WM GM's ±1σ) and the 15th, 50th and 85th percentiles hazard curves. LT Branches are hazard curves for each of the 15552 branches of the logic tree.

The agreement between the mean ±1σ hazard curves and the 15th and 85th percentiles is better than when the hazard curves were calculated in terms of probabilities (section 4.2). This suggests that the distribution of the logarithms of the ground motions might have a distribution closer to the normal distribution than that of the probabilities of exceedance.

From Figure 4.12 to Figure 4.14 the disaggregated results by M-R for both approaches are presented. These results are for the city of Dubai for return periods of 500, 2500 and 10,000 years. The dominant scenarios for both approaches are fairly similar, with the disaggregated results of the mean of the ground motions presenting in general a small increase in the

contributions of events with slightly larger magnitudes and greater distances than those of the dominant scenario. This could lead one, in some instances, to consider slightly different earthquake scenarios for time-history selection. This situation can be observed at all return periods.

The contributions to the hazard from each seismic source for the mean hazard curve of the ground motions are presented in Figure 4.15. The results are presented for the city of Dubai for PGA and SA at 0.2, 1.0 and 3.0 s response periods. Comparing Figure 3.64 and Figure 4.15 it can be observed that the contributions from each seismic source for both approaches are not significantly different. The sources that contribute the most to the hazard are still, at the shorter return periods, the Persian Gulf for PGA and 0.2 s response period and the Simple Fold belt for 1.0 and 3.0 s response period. The Stable craton is still the dominant seismic source at the longest return periods for all intensity measures. It is worth noting that in Figure 4.15 the probabilities of exceedance are cut-off at $1x10^{-5}$.

In summary, the calculation of the hazard curves for fixed exceedance probabilities seems to be a more appropriate approach as common practice is to select first the exceedance probability (return period) and to then read the expected value of ground motion using the hazard curve. On the other hand, the calculation of the hazard curve for fixed values of ground motion should be preferred when one wishes to know the expected probability of exceedance of a given value of ground motion (Bommer & Scherbaum, 2008). It is up to the analyst to choose which hazard curve to use depending on his or her needs.

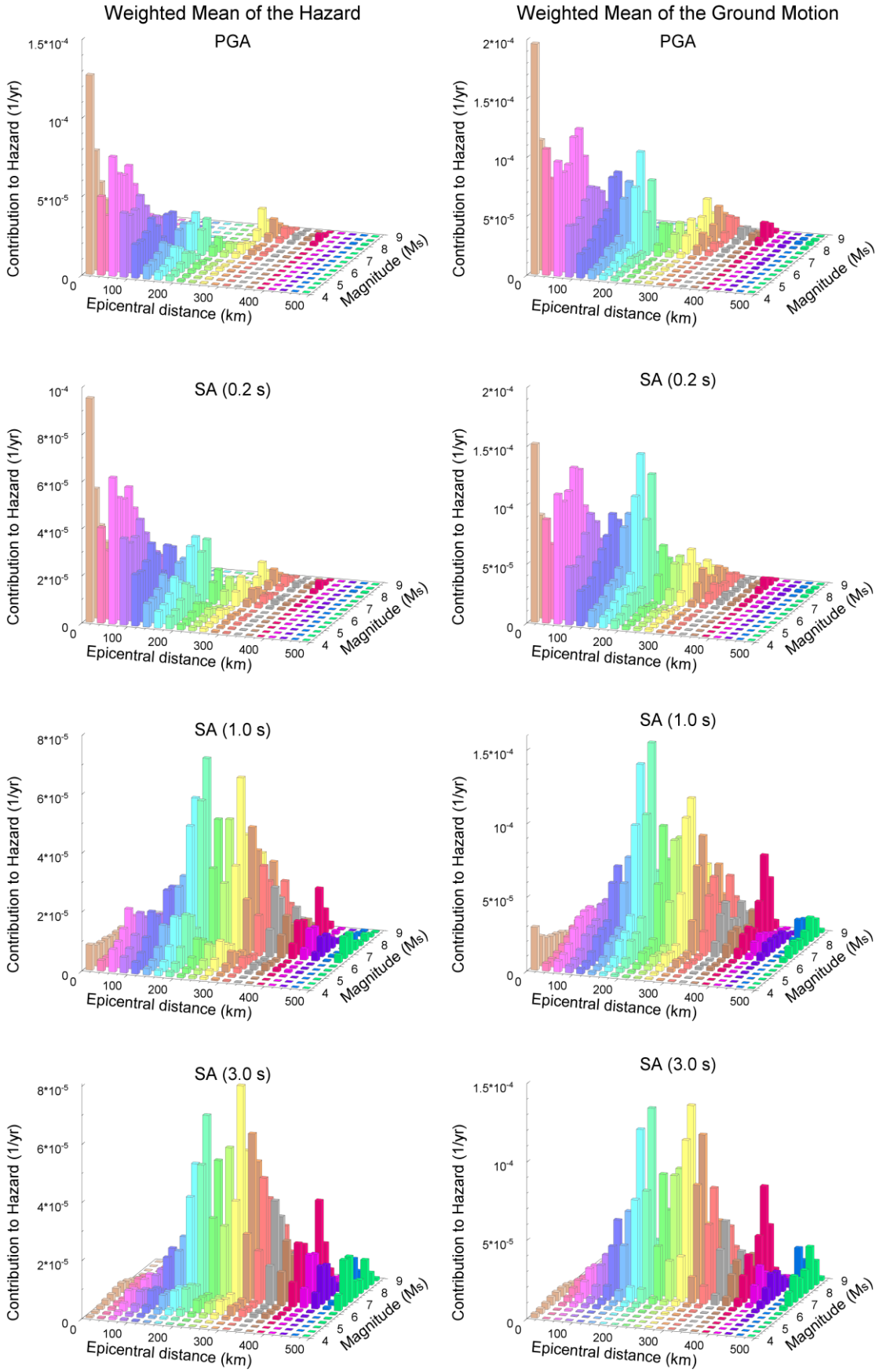

Figure 4.12. Disaggregated results for the city of Dubai at 500-yr return period for PGA and SA at 0.2, 1.0 and 3.0 s response period. On the left the results for the weighted mean of the hazard values (probabilities of exceedance) and on the right the results for the weighted mean of the ground motion values.

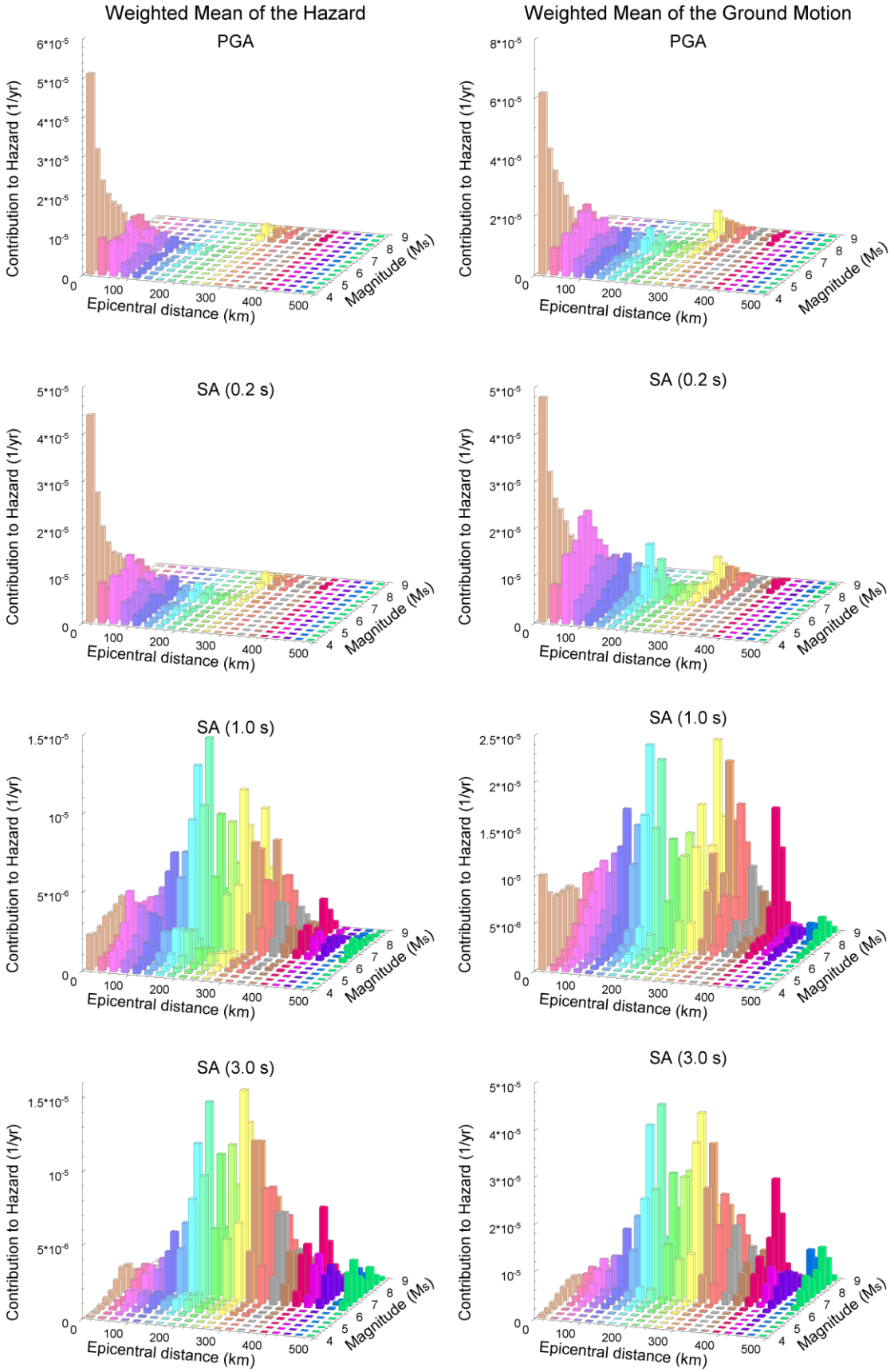

Figure 4.13. Disaggregated results for the city of Dubai at 2500-yr return period for PGA and SA at 0.2, 1.0 and 3.0 s response period. On the left the results for the weighted mean of the hazard values (probabilities of exceedance) and on the right the results for the weighted mean of the ground motion values.

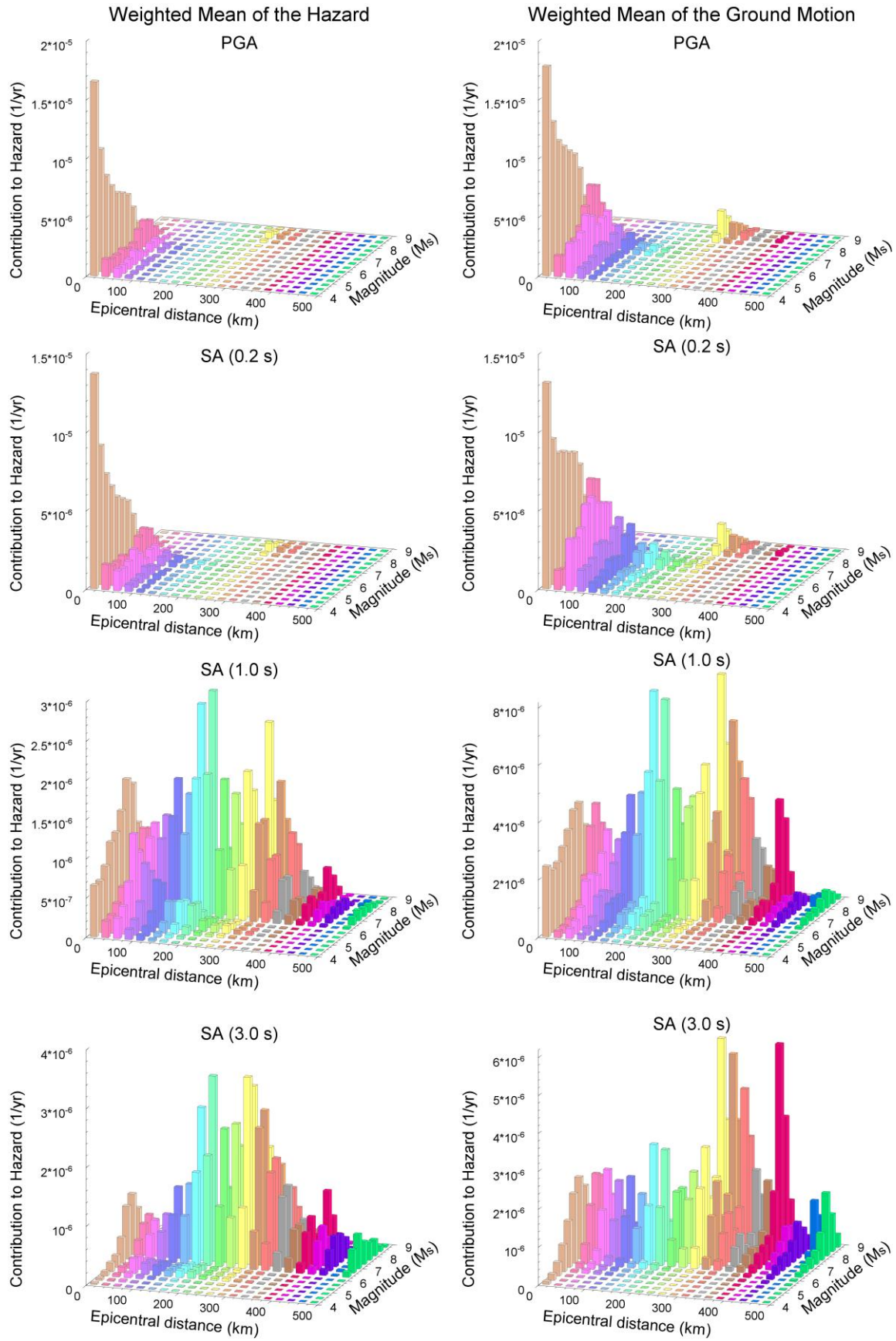

Figure 4.14. Disaggregated results for the city of Dubai at 10,000-yr return period for PGA and SA at 0.2, 1.0 and 3.0 s response period. On the left the results for the weighted mean of the hazard values (probabilities of exceedance) and on the right the results for the weighted mean of the ground motion values.

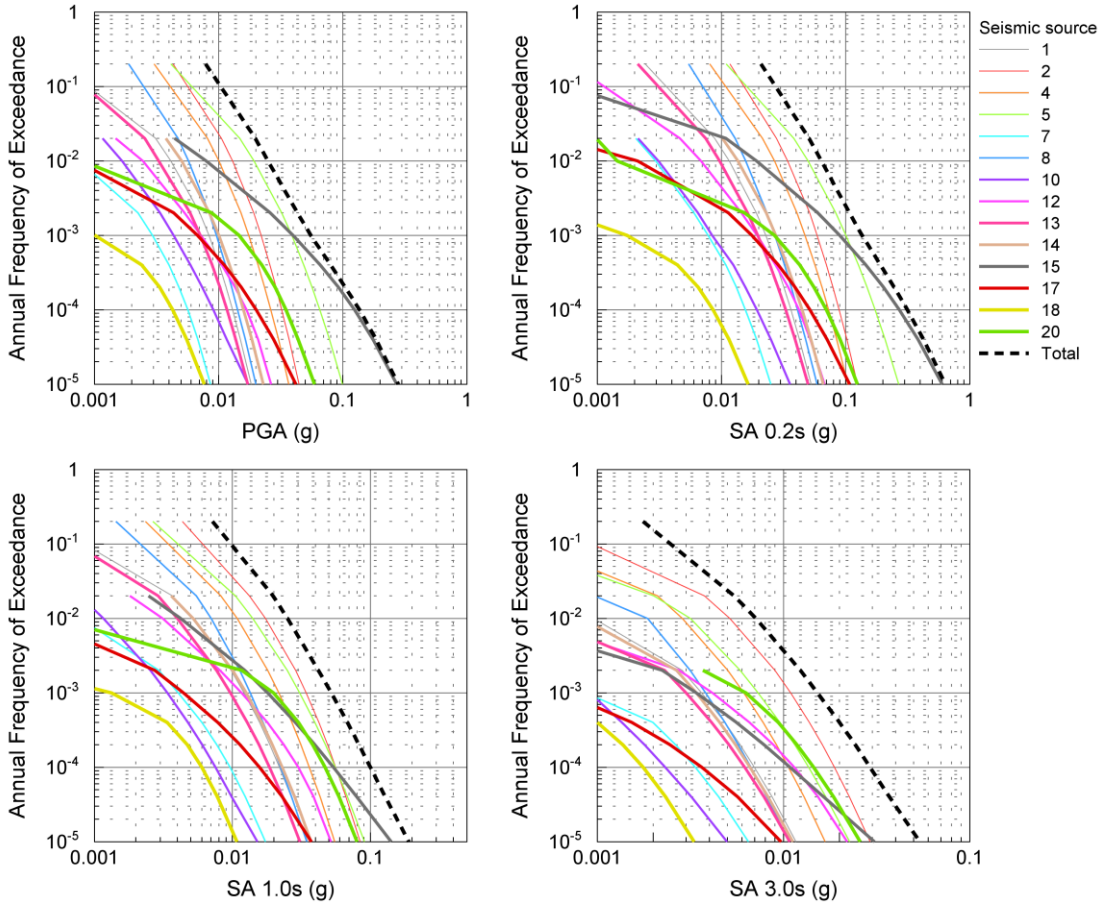

Figure 4.15. Disaggregated results of the weighted mean hazard curve using the ground-motion values presented as the contribution to the hazard from each of the seismic sources for the city of Dubai. Dashed line is the mean hazard curve of the ground motions. See Table 3.7 for source number.

The standard deviation associated with the mean hazard curve calculated from the ground motions provides a good representation of the scatter of the hazard curves from the branches of the logic tree, with a relatively good agreement with the 15th and 85th percentile hazard curves.

Some differences between the dominant scenarios that are identified must be expected between the two approaches. For the particular example presented herein, a slight shift of the dominant scenarios towards larger magnitudes and longer distances was observed for the mean of the ground motions. A similar situation was observed for the contributions to the hazard from each of the seismic sources, where although there are some differences between both approaches, the main contributors to the hazard remain unchanged.

4.4. Identification of hazard-dominating scenarios

For the purposes of seismic design a single representative earthquake scenario often needs to be identified following a PSHA. This scenario is usually characterized by a triplet of M*-R*-ε* and perhaps other information, such as the earthquake source, style-of-faulting, etc. However, there is not a single earthquake scenario that fully represents the seismic hazard for a ground-motion level corresponding to a given return period (McGuire, 1995).

Representing seismic hazard in terms of one or a few earthquake scenarios has some advantages for detailed analysis and decision making. Identifying the earthquake scenario that dominates the hazard at a given return period allows subsequent analyses to relate that earthquake scenario to a specific seismic source and to then specific additional characteristics of the seismic event such as azimuth and depth, among others.

In order to identify dominant earthquake scenarios, it becomes imperative to obtain disaggregated results not only in terms of magnitude (M) and distance (R) but also in terms of epsilon (ε). Unfortunately, the software used for the hazard analysis in the case study (Crisis2007 - Ordaz *et al.*, 2007) provide disaggregated results only as function of M and R; despite calculating the seismic hazard by directly accounting for ε. Since the disaggregated results represent the joint probability of M, R and ε of exceeding a particular ground motion level but with the contribution in terms of ε not explicitly expressed, the contribution by ε can be estimated using the ground motion equations employed for the hazard analysis.

In order to obtain the contributions by ε from disaggregated results expressed only in terms of M and R, at a specific target ground motion, the following procedure is proposed to be applied to the disaggregated results at the end tips of the logic tree regarding GMPEs:

1. Calculate the ε values required to yield the target ground motion for the central values of each bin of M and R in the

disaggregated results and for each GMPE used in the hazard analysis.

2. Calculate the relative contribution to the hazard from each seismic source for the given target ground motion. The sum of the relative contributions from all the seismic sources must be equal to one.

3. Multiply the relative contributions of each seismic source by the matrix of ε values (obtained in step 1) corresponding to the GMPE assigned to the given seismic source. Then, add up the products for each bin of M and R. This is done in order to take into account the fact that not all GMPEs contribute in the same proportion to the hazard results and hence to the contributions by epsilon. For instance, if only one GMPE were used in the hazard analysis Step 2 and Step 3 can be omitted as the same GMPE would correspond to all the sources.

4. Establish a range of values of ε within which most of the contributions to the hazard are expected to be concentrated, usually over the range ε = ±3. Subdivide this range of ε into n discrete bins of equal size ($\Delta\varepsilon$). The size of the bins may be specified by the analyst.

5. For each bin of M and R of the matrix resulting from step 3, calculate the conditional probability that ε falls in certain ranges (defined by the bins in ε) given that $\varepsilon \geq \varepsilon_{\text{target}}$. This is expressed by the equation:

$$P\left(\varepsilon_i \leq \varepsilon \leq \varepsilon_{i+1} \mid \varepsilon > \varepsilon_{target}\right) = P\left[\varepsilon_i \leq \varepsilon \leq \varepsilon_{i+1}\right] / 1 - \Phi\left(\varepsilon_{target}\right), \qquad 4.1$$

where $\varepsilon_i = \varepsilon_k - \Delta\varepsilon/2$ and $\varepsilon_{i+1} = \varepsilon_k + \Delta\varepsilon/2$ (see Figure 4.16 for further explanation). For example, if the $\varepsilon_{\text{target}}$ for a given bin of M and R is 0.25 and the bin size of ε is 0.5, calculate the

probability of a random variable lying in the interval from ε = 0.25 to ε = 0.5, then from ε = 0.5 to ε = 1.0, then from ε = 1.0 to ε = 1.5 and so on, until the maximum value of ε on the interest of the analyst. Then, divide the probability of each interval by the probability of ε = 0.25 being exceeded.

6. Multiply the contribution to the hazard of each M-R bin in the disaggregated results by the normalized probability of each ε bin obtained in step 4.

7. Merge the disaggregated results for each branch of the logic tree using the statistical estimator of interest (e.g., weighted mean or median).

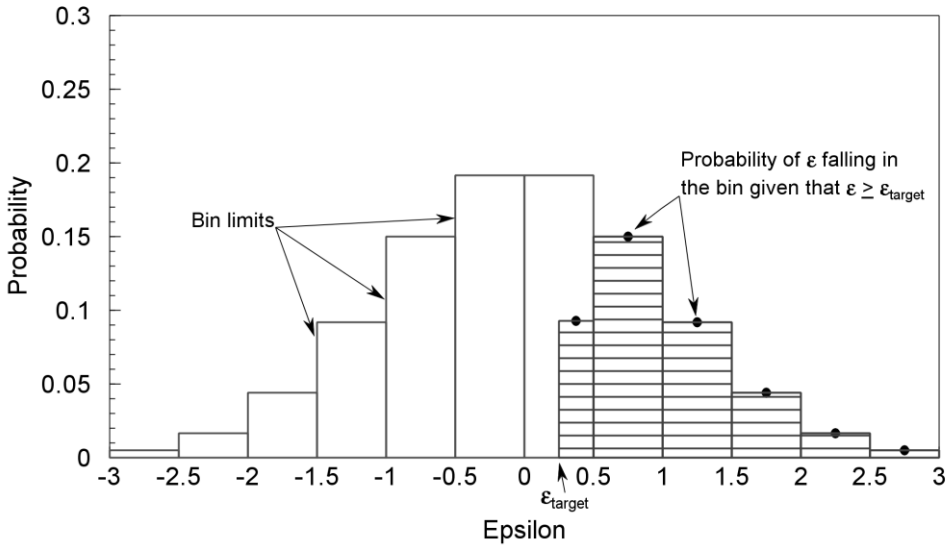

Figure 4.16. Probability mass for bins of epsilon of 0.5. Dots represent the probability of ε falling between the lower and upper limits of the bin given that $\varepsilon \geq \varepsilon_{target}$. Note that the first shadowed bin goes from the ε_{target} (0.25) to 0.5 in agreement with the example presented in the text above. Shadow area represents the probability of $\varepsilon \geq \varepsilon_{target}$ for a given M-R bin obtained in the step 3.

This procedure for estimating the contributions by ε has some associated error as not all of the GMPEs contribute to the entire range of M-R bins. For instance, the GMPEs assigned to the Makran subduction zone do not contribute at distances less than ~200 km for the city of Dubai (distance

from Dubai to the nearest point of Makran). However, this error is considered to be insignificant since the contributions by each GMPE are weighted by the contribution of the seismic source to which the given GMPE was assigned.

Using the procedure explained above, the contributions by ε were calculated for the hazard results for the city of Dubai for SA at 0.2 s and 1.0 s response periods at the 2500-year return period. This site, response periods and return period were selected only as an example in order to discuss the selection of hazard-dominating earthquake scenarios.

The disaggregated results by M, R and ε for 0.2 s response period are presented in Figure 4.17 and Figure 4.18 for the mean of the hazard and the mean of the ground motions, respectively. The contributions by ε were calculated for increments of 0.5 in ε, however, for greater clarity, the plots show the contributions for bins having increments of 1.0 in ε. It is important to mention, that the values of ε reported hereafter for the dominant scenarios correspond to the central value of the bin (for a 0.5 ε bin size) with the highest contribution to the hazard and might be not clearly seen in the disaggregated plots.

In both cases the hazard-dominating earthquake scenario is clearly defined. For the disaggregated results of the mean of the hazard (Figure 4.17) the dominant scenario is given by M* = 5.1 M_w, R* = 12.5 km (r_{epi}) and ε^* = 0.25. For the disaggregated result in terms of the mean of the ground motions (Figure 4.18) the dominant scenario is defined by M* = 5.1 M_w, R* = 12.5 km (r_{epi}) and ε^* = 0.75. The Stable craton is the dominant seismic source in both cases.

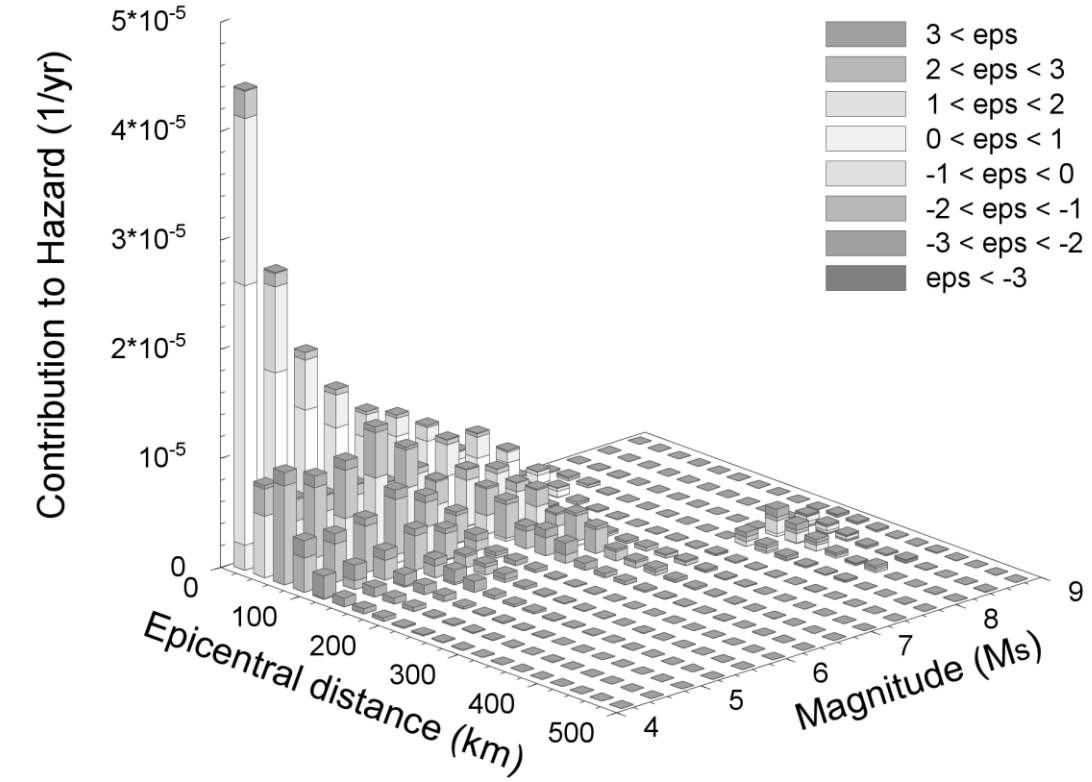

Figure 4.17. Disaggregation for the city of Dubai for SA at 0.2 s response period and at the 2500-year return period. The results are for the weighted mean of the hazard.

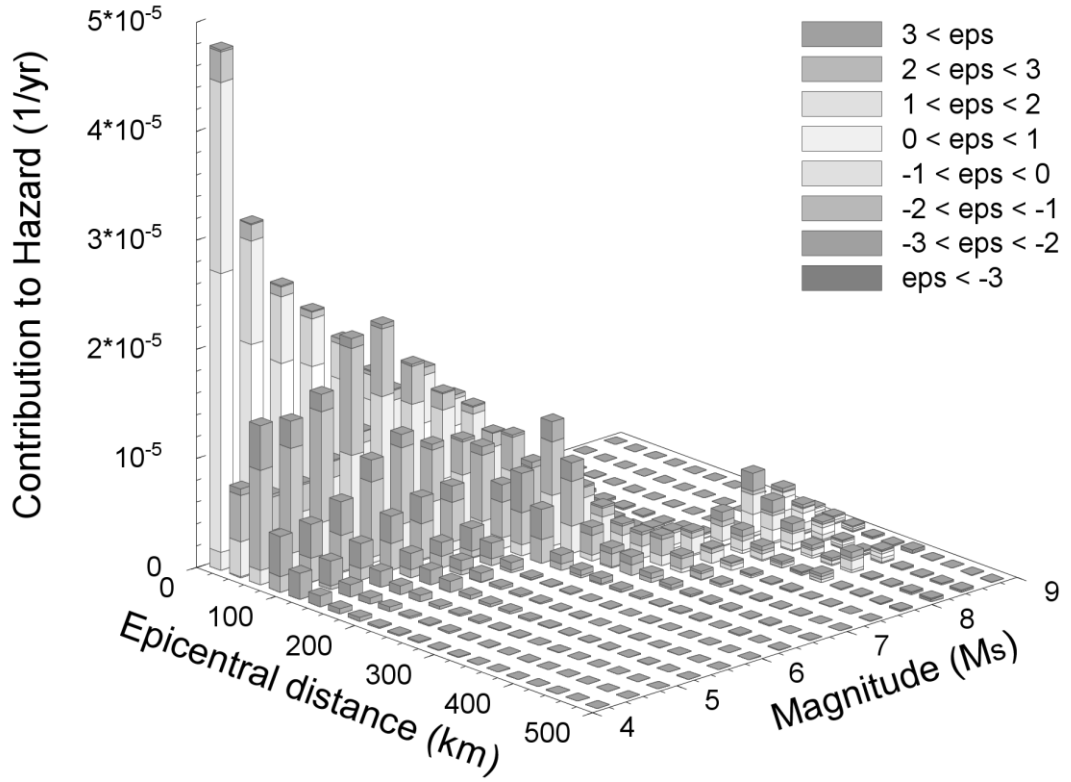

Figure 4.18. Disaggregation for the city of Dubai for SA at 0.2 s response period and at the 2500-year return period. The results are for the weighted mean of the ground motions.

The disaggregated results by M, R and ε for the city of Dubai for SA at 1.0 s response period at 2500-year return period are presented in Figure 4.19 and Figure 4.20 for the mean of the hazard and the mean of the ground motions, respectively.

The dominant earthquake scenario for the case where the results are obtained using the mean of the hazard values for SA at 1.0 s response period at 2500-year return period (Figure 4.19) is given by M* = 6.6 M_w, R* = 187.5 km (r_{epi}) and ε* = 1.75. For the alternative case using the mean of the ground motion values for SA at 1.0 s response period at 2500-year return period (Figure 4.20) the dominant earthquake scenario is given by M* = 6.6 M_w, R* = 162.5 km (r_{epi}) and ε* = 2.25.

It is worth noting in Figure 4.20 what could be referred to as a secondary dominating earthquake scenario with M' = 8.2 Mw, R' = 262.5 km (r_{epi}) and ε' = 1.75. This scenario has a contribution equal to the 96% of the contribution of the primary dominant earthquake scenario. If we were to select a scenario for design using strictly the modal values of M, R and ε, then this secondary scenario would not be considered. However, common sense suggests that if multiple scenarios are contributing in a significant and similar way to the total hazard, then these scenarios should be considered for design.

For the purposes of selecting the scenario spectra for seismic design or any other application were the M*-R*-ε* values need to be introduced in a GMPE, it is necessary to obtain the disaggregated results from the individual branches of the logic tree corresponding to alternative GMPEs. This in order to be able to associate a specific earthquake scenario with a GMPE as previously discussed in section 4.1.

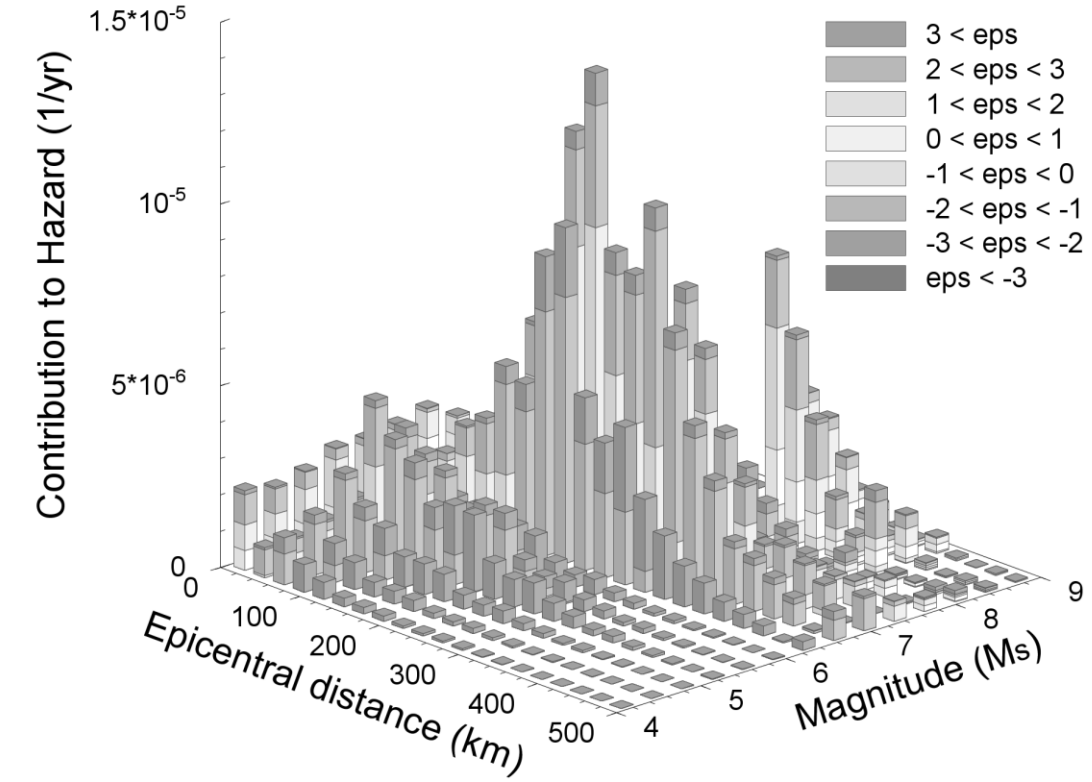

Figure 4.19. Disaggregation for the city of Dubai for SA at 1.0 s response period and at the 2500-year return period. The results are for the weighted mean of the hazard.

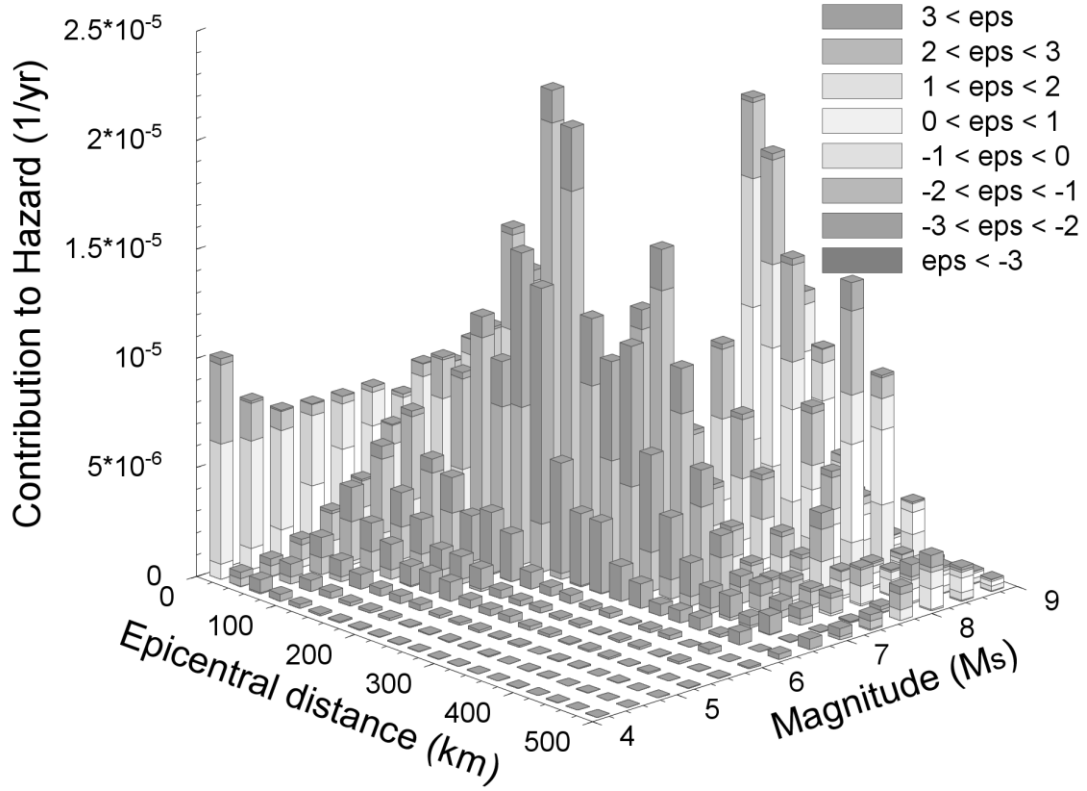

Figure 4.20. Disaggregation for the city of Dubai for SA at 1.0 s response period and at the 2500-year return period. The results are for the weighted mean of the ground motions.

Additionally, the examination of the disaggregated results from the alternative branches of the logic tree corresponding to alternative GMPEs can help one to obtain a better understanding of how sensitive the identification of the dominant earthquake scenario is to the selection of the GMPE or set of GMPEs used in each branch. Based on this information, better-informed decisions for risk analyses can be taken.

In the case study presented in Chapter 3, a total of seven GMPEs were used to model ground-motion attenuation. Two alternative GMPEs were used for the subduction zone of Makran (i.e., Atkinson & Boore, 2003; Youngs *et al.*, 1997), four for the Zagros region, Persian Gulf and Oman (i.e., Abrahamson & Silva, 1997; Akkar & Bommer, 2007b; Ambraseys *et al.*, 2005; Boore & Atkinson, 2006) and five for the Stable craton; the four just listed in addition to the ground motion equation of Atkinson & Boore (2006). Consequently, a total of sixteen sets of GMPEs were considered in the hazard analysis, one for each branch of the logic tree regarding GMPEs (see section 3.6, Figure 3.38). These sixteen sets of GMPEs are shown in Table 4.1.

Table 4.1. Sets of equations used in the PSHA for the UAE.

Stable continental region	Shallow earthquakes	Subduction zones	Set #
Akkar & Bommer (2007)	Akkar & Bommer (2007)	Atkinson & Boore (2003)	1
		Youngs *et al.* (1997)	2
Boore & Atkinson (2006)	Boore & Atkinson (2006)	Atkinson & Boore (2003)	3
		Youngs *et al.* (1997)	4
Abrahamson & Silva (1997)	Abrahamson & Silva (1997)	Atkinson & Boore (2003)	5
		Youngs *et al.* (1997)	6
Ambraseys *et al.* (2005)	Ambraseys *et al.* (2005)	Atkinson & Boore (2003)	7
		Youngs *et al.* (1997)	8
Atkinson & Boore (2006)	Akkar & Bommer (2007)	Atkinson & Boore (2003)	9
		Youngs *et al.* (1997)	10
	Boore & Atkinson (2006)	Atkinson & Boore (2003)	11
		Youngs *et al.* (1997)	12
	Abrahamson & Silva (1997)	Atkinson & Boore (2003)	13
		Youngs *et al.* (1997)	14
	Ambraseys *et al.* (2005)	Atkinson & Boore (2003)	15
		Youngs *et al.* (1997)	16

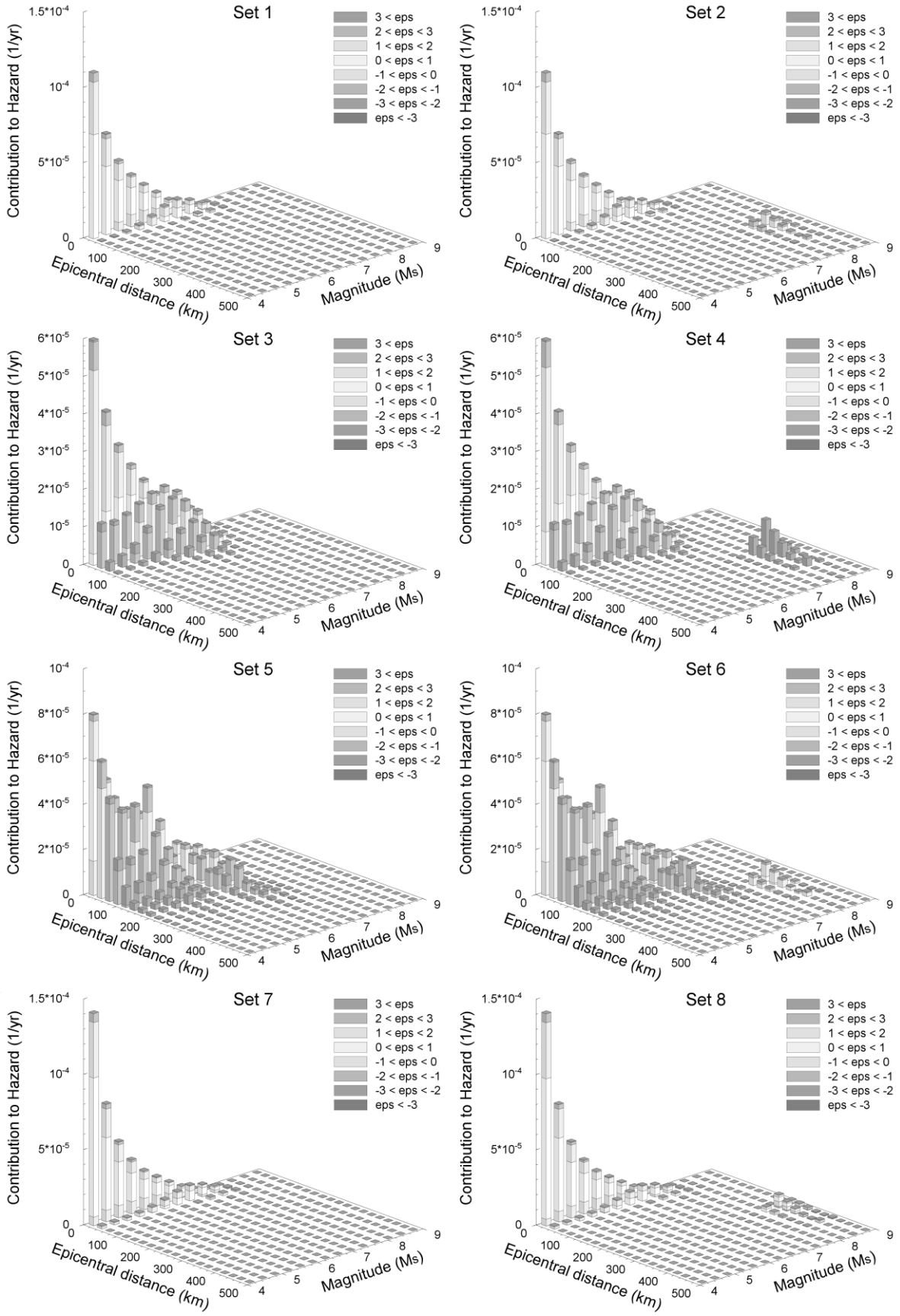

Figure 4.21. Disaggregated results for the sets of GMPEs 1 to 8 for the city of Dubai for SA at 0.2 s and for a target ground motion of 0.21 g, which corresponds to a 2500-year return period. The weighted mean hazard curve is determined on the basis of the hazard values.

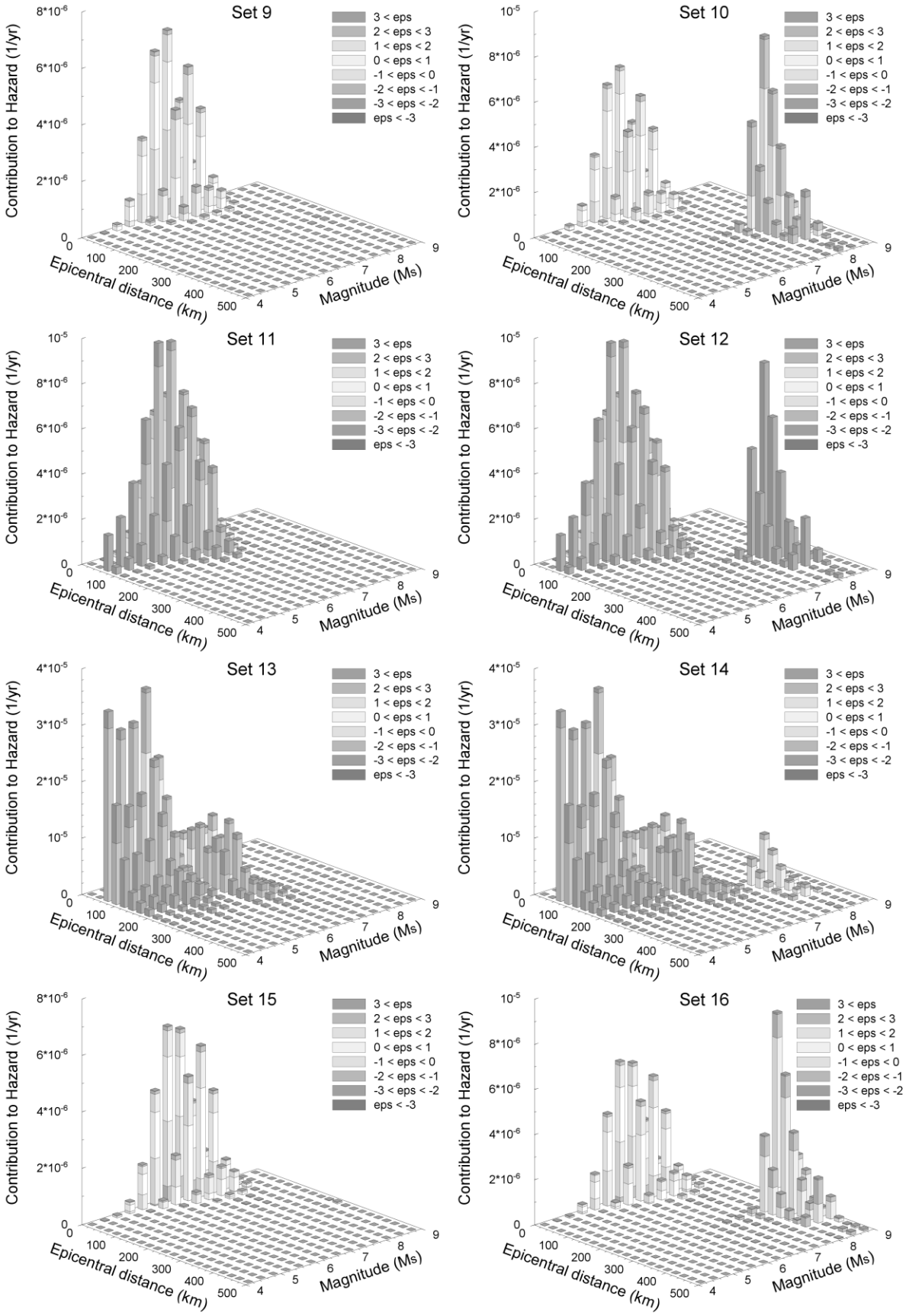

Figure 4.22. Disaggregated results for the sets of GMPEs 9 to 18 for the city of Dubai for SA at 0.2 s and for a target ground motion of 0.21 g, which corresponds to a 2500-year return period. The weighted mean hazard curve is determined on the basis of the hazard values.

The disaggregated results by M, R and ε, for each set of equations in Table 4.1 for the city of Dubai for SA at 0.2 s response period and for a target ground motion of 0.21 g are shown in Figure 4.21 (sets 1 to 8) and in Figure 4.22 (sets 9 to 18). The target ground motion of 0.21 g corresponds to a return period of 2500 years for the mean hazard curve for SA at a response period of 0.2 s (calculated based on the hazard values).

A summary of the dominant earthquake scenarios for each set of equations (one for each of the sets shown in Table 4.1) is presented in Table 4.2. The r_{epi} distance from the disaggregated results was converted to r_{jb} and r_{rup}, according to the distance definition used by the GMPE assigned to the dominant seismic source using the relationships of Scherbaum *et al.* (2004b). In addition to the dominant earthquake scenarios, Table 4.2 also shows: the return period corresponding to the target ground motion (0.21 g) for each set of equations, the dominant seismic source for each scenario, the predicted ground motion for the dominant earthquake scenario using the GMPE assigned to the dominant seismic source and the percentage error in the prediction of the target ground motion using the M*, R* and ε* from the disaggregation.

It is interesting to highlight that the dominant scenarios for most of the set of equations are similar in magnitude and distance, with greater differences in the values of ε, with the exceptions of Set 10 and Set 16 which lead to a totally different sets of M*-R*-ε* values from the rest. However, on the disaggregated plots of these two sets of equations a secondary dominating scenario with similar characteristics to the dominant scenarios of the remainder sets can be observed. The seismic source responsible for the contributions of these secondary dominant scenarios is the Stable craton (seismic source 15), which in fact is the seismic source contributing the most to the seismic hazard. In contrast, the West Makran (seismic source 20) has a contribution slightly smaller than the Stable craton; however it is clearly

responsible for the contributions of the dominant scenario as it is the only seismic source capable to produce events with magnitudes M_w above 8. These apparently contradictory results are because the contributions from the Stable craton are spread over a wider range of magnitudes and distances, while the contributions from Makran are more concentrated on the dominant scenario.

Table 4.2. Summary of the hazard-dominating earthquake scenarios for the 16 sets of equations considered in the hazard analysis for SA at 0.2 s response period and a target ground motion of 0.21 g (Figure 4.21 and Figure 4.22). r_{corr} is the corrected distance according to the distance definition used by the GMPE assigned to the dominant seismic source, (1) for r_{jb} and (2) for r_{rup}; * indicates that r_{corr} was limited to the minimum distance between the seismic source and Dubai; ε' is the value of ε required to match the target ground motion using the modal GMPE; Return period is the return period of each set of equations for the target ground motion of 0.21 g; Dom. Source is the number of the seismic source that contributes the most to the hazard at 0.2 s response period and a target ground motion of 0.21 g (for identification of the seismic sources see Table 3.10); Predicted GM is the ground motion predicted by the GMPE for the dominant scenario; Error is the percentage error to predict the target ground motion; (3) indicates that two or more seismic sources dominate the hazard for that set of equations with equal or very similar contributions.

	Set 1	Set 2	Set 3	Set 4	Set 5	Set 6	Set 7	Set 8
M_w	5.1	5.1	5.1	5.1	5.1	5.1	5.1	5.1
r_{epi} (km)	12.5	12.5	12.5	12.5	12.5	12.5	12.5	12.5
r_{corr} (km)	10.8(1)	10.8(1)	10.8(1)	10.8(1)	15.4(2)	15.4(2)	10.8(1)	10.8(1)
ε	0.75	0.75	1.25	1.25	0.25	0.25	0.25	0.25
ε'	-0.026	-0.026	0.312	0.312	-0.041	-0.041	-0.104	-0.104
Return period (yr)	2689	2422	2329	2126	933	899	2303	2103
Dom. source	15	15	15	15	15	15	15	15
Predicted GM (g)	0.38	0.38	0.29	0.29	0.27	0.27	0.34	0.34
Error (%)	81	81	38	38	29	29	62	62

	Set 9	Set 10	Set 11	Set 12	Set 13	Set 14	Set 15	Set 16
M_w	6.32	8.17	5.8	5.8	5.6	5.6	6.32	8.63
r_{epi} (km)	12.5	262.5	62.5	62.5	62.5	62.5	12.5	262.5
r_{corr} (km)	15.4(2)	205(2)	58(1)	58(1)	58(2)	58(2)	15.4(2)	200(2)*
ε	0	1.75	2.25	2.25	1.75	1.75	0	0.75
ε'	-0.445	1.364	0.826	0.826	0.508	0.508	-0.445	0.774
Return period (yr)	24155	12134	7990	6018	1809	1684	22797	11736
Dom. source	15	15-20(3)	5	5	5	5	15	15-20(3)
Predicted GM (g)	0.43	0.27	0.26	0.26	0.31	0.31	0.43	0.21
Error (%)	105	29	24	24	48	48	105	0

In order to identify the earthquake scenarios dominating the hazard at longer response periods (1.0 s and above) a summary of the hazard-dominating earthquake scenarios for the city of Dubai for the 1.0 s response period and for a target ground motion of 0.085 g is presented in Table 4.3. As in the previous case, the target ground motion of 0.085 g corresponds to a 2500-year return period from the mean hazard curve for SA at the 1.0 s response period (calculated using the hazard values).

In Table 4.3 one may observe three M*-R* dominating scenarios that are constant for all of the sets of equations. The first scenario is defined by M* = 8.17 M_w and R* = 262.5 km (r_{epi}), the second scenario is defined by M* = 6.63 M_w and R* = 187.5 km (r_{epi}) and the third scenario has M* = 8.63 M_w and R* = 262.5 km (r_{epi}). In contrast the value of ε has an important variation among sets with the same M*-R* scenario. For the first and the latter M-R scenarios the dominant seismic source is West Makran (seismic source 20) and for the second M-R scenario is the Persian Gulf (seismic source 5).

It is worth mentioning that for Set 3 and Set 4 the Stable craton (seismic source 15) has a slightly higher contribution to the hazard than West Makran, however the dominant earthquake scenario clearly corresponds to events occurring at West Makran. A comparable situation occurs for Set 11 and Set 12, where the Persian Gulf and West Makran have very similar contributions to the hazard. In some occasions supplementary information from the analyst may be required to identify which seismic source is controlling the dominant earthquake scenario. Presenting the disaggregated results in terms of longitude and latitude instead of source-to-site distance will reduce, or in the best of the cases eliminate, any ambiguity regarding which seismic source controls the dominant earthquake scenario.

It is also worth highlighting that in both cases, for SA at 0.2 s and 1.0 s, the return periods for each set of equations have a great variability, ranging from 843 to 26,156 years. A similar situation occurs with the error

on the prediction of the target ground motion, where errors of up to 501 % can be observed.

Table 4.3. Summary of the hazard-dominating earthquake scenarios for the 16 sets of equations considered in the hazard analysis of the case study for SA at 1.0 s response period and a target ground motion of 0.085 g. For definition of the different variables and notations see caption of Table 4.2.

	Set 1	Set 2	Set 3	Set 4	Set 5	Set 6	Set 7	Set 8
M_w	8.17	8.17	8.17	8.17	6.63	6.63	8.63	8.63
r_{epi} (km)	262.5	262.5	262.5	262.5	187.5	187.5	262.5	262.5
r_{corr} (km)	205(2)	205(2)	205(2)	205(2)	178(2)	178(2)	200(2)*	200(2)*
ε	0.25	1.75	2.25	2.25	1.75	1.75	-0.25	0.75
ε'	-0.043	1.115	-0.043	1.115	0.546	0.546	-0.532	0.456
Return period (yr)	12538	8633	5318	4461	869	843	13101	8841
Dom Source	20	20	15-20(3)	15-20(3)	5	5	20	20
Predicted GM (g)	0.107	0.128	0.511	0.178	0.116	0.116	0.106	0.103
Error	26%	51%	501%	109%	36%	36%	25%	21%

	Set 9	Set 10	Set 11	Set 12	Set 13	Set 14	Set 15	Set 16
M_w	8.17	8.17	8.17	8.17	6.63	6.63	8.63	8.63
r_{epi} (km)	262.5	262.5	262.5	262.5	187.5	187.5	262.5	262.5
r_{corr} (km)	205(2)	205(2)	205(2)	205(2)	178(2)	178(2)	200(2)*	200(2)*
ε	0.75	1.75	1.75	1.75	1.75	1.75	0.25	1.25
ε'	-0.043	1.115	-0.043	1.115	0.546	0.546	-0.532	0.456
Return period (yr)	26156	13456	9620	7138	1029	992	25442	13143
Dom. Source	20	20	5-20(3)	20-5(3)	5	5	20	20
Predicted GM (g)	0.158	0.128	0.346	0.128	0.116	0.116	0.157	0.142
Error	86%	51%	307%	51%	36%	36%	85%	67%

As previously discussed, the dominant earthquake scenario is defined as the modal values of M-R-ε (M*-R*-ε*) from the disaggregated results, as this set of M-R-ε is the most likely to induce a ground-motion level that will equal or exceed the target ground motion. However, when multiple GMPE are used in alternative branches of the logic tree, associating the dominant earthquake scenario to a single GMPE to estimate the expected ground-motion level seems to not have a clear justification.

Along the same lines, a most likely or modal set of equations (or most likely equation if only one equation per branch is being used) could be defined. In this way, a “modal” GMPE could be associated with the dominant

earthquake scenario as the GMPE that contributes the most to the hazard for that particular set of M*-R*-ε*.

To identify which set of GMPEs is contributing the most to the hazard-dominating earthquake scenario it is only necessary to multiply the contribution to the hazard of the dominant earthquake scenario of each set of equations by the weight assigned to that set in the logic tree. For instance, in the example presented above, for the city of Dubai for SA at a 0.2 s response period and the 2500-year return period, from all the dominant earthquake scenarios in Table 4.2, Set 7 is the one contributing the most to the final dominant earthquake scenario (shown in Figure 4.17). Figure 4.23 presents the contributions to the final hazard from each dominant earthquake scenario in Table 4.2.

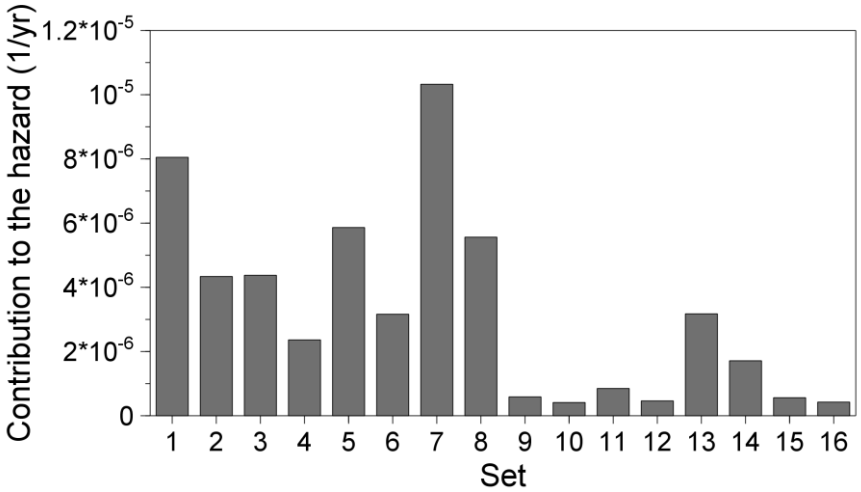

Figure 4.23. Contribution to the hazard from the dominant earthquake scenarios of each set of GMPEs.

As can be seen in Figure 4.23, Set 7 has the highest contribution to the final hazard, this contribution corresponds to 23 % of the contribution to the total hazard provided by the dominant earthquake scenario defined by M* = 5.1 M_w, R* = 12.5 km (r_{epi}) and ε* = 0.25. It is important to note that, unsurprisingly, the M-R values and the source of the dominant earthquake

scenario for Set 7 (see Table 4.2) correspond to the same values and seismic source as the final dominant earthquake scenario (see Figure 4.17).

Base on these findings, the final dominant earthquake scenario for this example (i.e., the 0.2 s response period and the 2500-year return period) can be associated with the GMPE of Ambraseys *et al.* (2005), which is the equation used to predict ground-motions for the Stable craton in Set 7 (see Table 4.1). For SA at the 1.0 s response period and the 2500-year return period, the set contributing the most to the final hazard is Set 13 and the "modal" GMPE is the equation of Abrahamson & Silva (1997).

It is important to mention that the contributions to the hazard from the different sets presented in Figure 4.23 do not all correspond to the same earthquake scenario (i.e., M-R scenarios); however the dominant M-R scenario of the set with the highest contribution to the hazard will invariably correspond, for this case or any other, to the M and R of the final dominant earthquake scenario.

The ability to associate a ground-motion equation with the final dominant earthquake scenario on the basis of the "modal" equation, has important implications for the definition of the scenario spectra to be use for seismic design. This issue will be discussed further in the following section.

As shown in Figure 4.17 to Figure 4.20, and discussed in the previous sections, the dominant earthquake scenario may change depending on the approach chosen for the calculation of the mean hazard curve (i.e., considering values in the hazard or ground-motion domains). In order to compare these differences in the dominant earthquake scenarios, the disaggregated results from each set of equations are presented in Figure 4.24 (Set 1 to Set 8) and Figure 4.25 (Set 9 to Set 18) for the city of Dubai for SA at 0.2 s and the 2500-year return period. The target ground motion for the 2500-year return period from the mean hazard curve (calculated in the ground-motion domain) is 0.19 g.

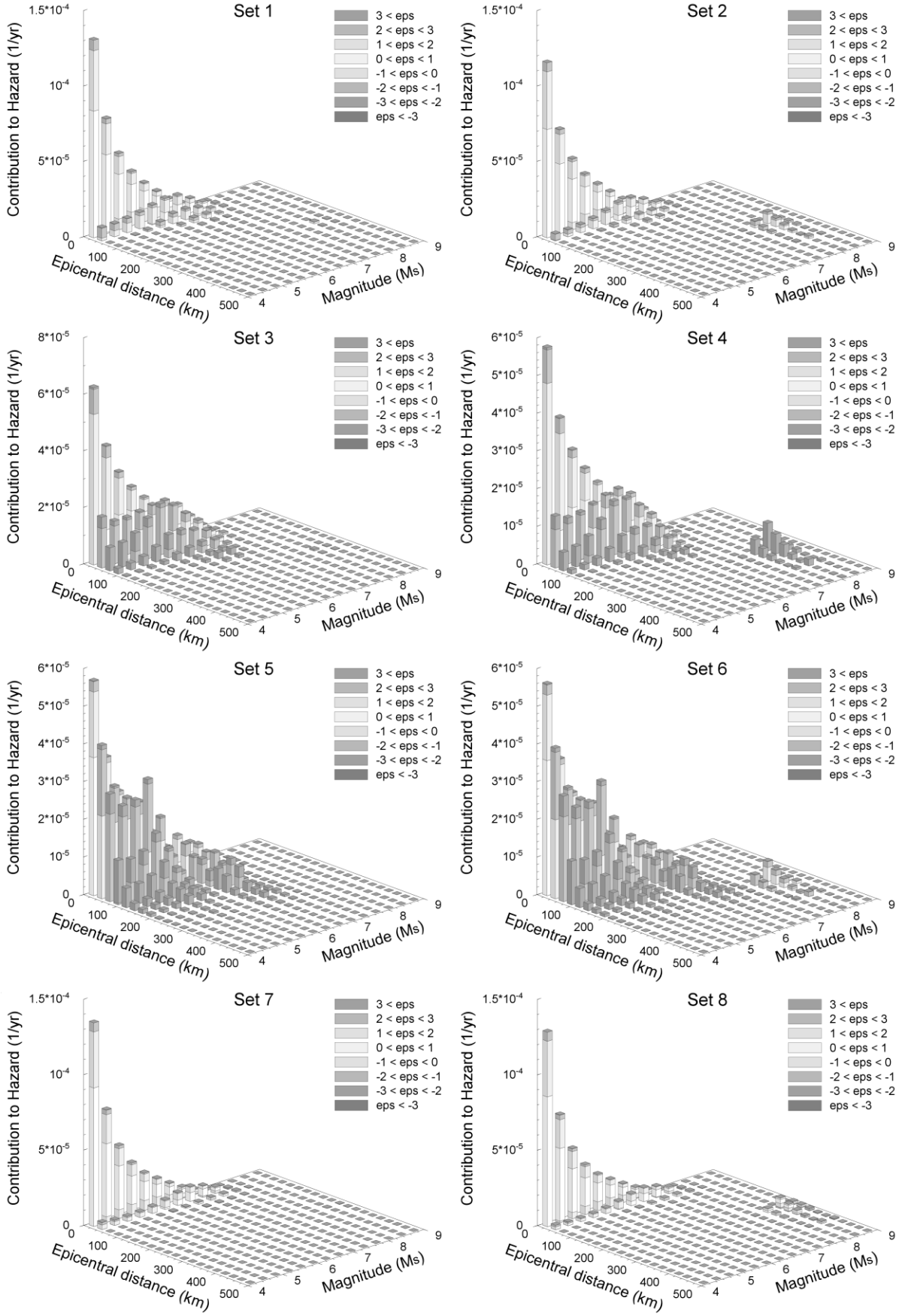

Figure 4.24. Disaggregated results for the sets of GMPEs 1 to 8 for the city of Dubai for SA at 0.2 s and a 2500-year return period.

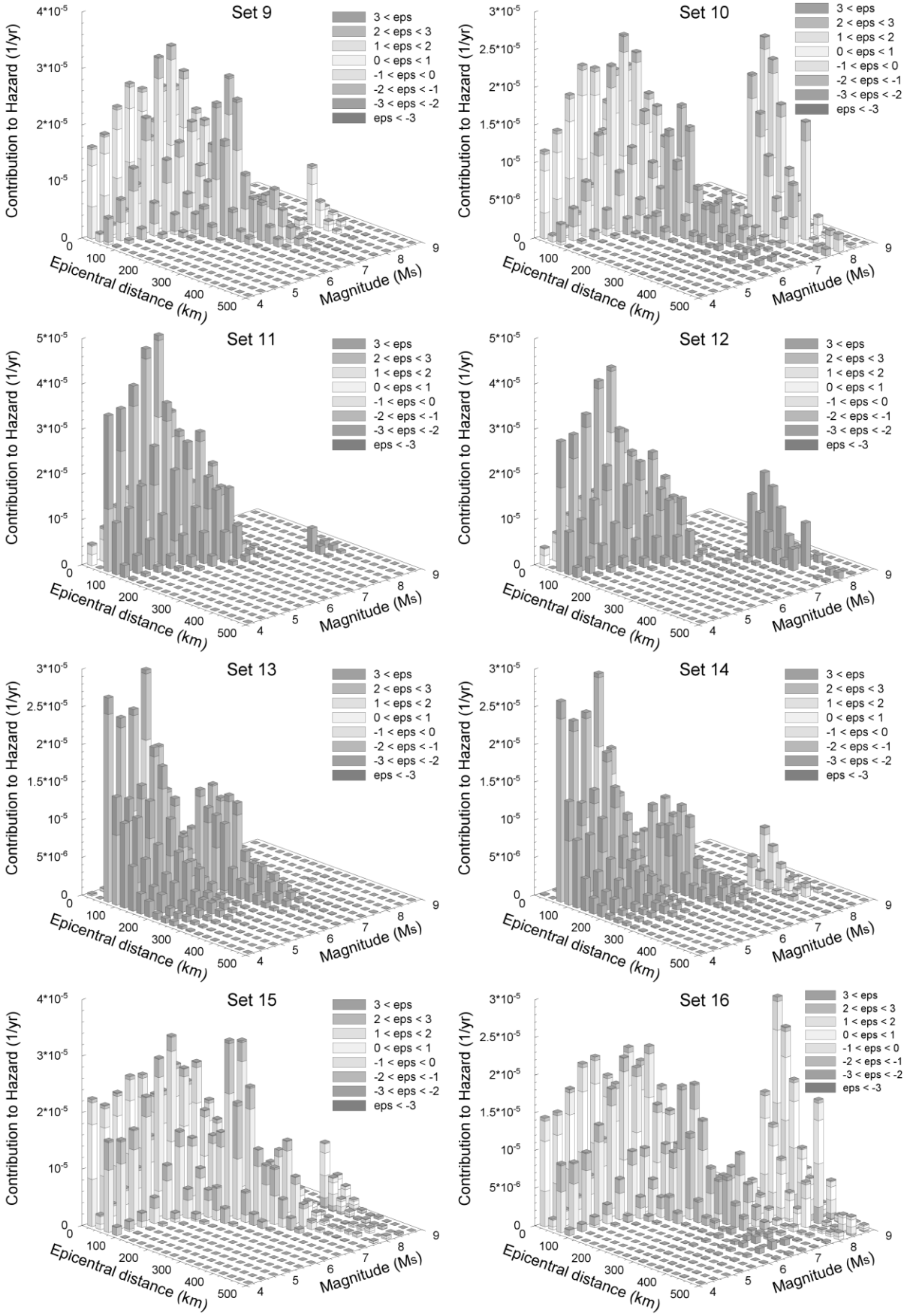

Figure 4.25. Disaggregated results for the sets of GMPEs 9 to 18 for the city of Dubai for SA at 0.2 s and a 2500-year return period.

It is worth accentuating the difference between the disaggregations presented in Figure 4.21 and Figure 4.22 and the disaggregations presented in Figure 4.24 and Figure 4.25, respectively. While in Figure 4.24 and Figure 4.25, all of the results correspond to the same target ground motion (0.21 g), in Figure 4.24 and Figure 4.25 all of the disaggregated results correspond to the same return period (2500 years).

Table 4.4 and Table 4.5 present the summary of the dominant earthquake scenarios for each set of equations for SA at 0.2 s and 1.0 s response periods, respectively. Since these scenarios correspond to the same return period (i.e., 2500 years) the individual target ground motion for each set of equations are different. For this reason two different error values are reported; "Error" which refers to the percentage error in predicting the individual target ground motion of each set and "Global Error" which refers to the percentage error in predicting the target ground motion of the mean hazard curve (0.19 g).

For SA at the 0.2 s response period (Table 4.4), in a similar manner as in Table 4.2, most of the sets of equations have similar dominant scenarios in terms of M and R, with larger variations in the values of ε. The exception in this case is Set 16 which presents a radically different dominant earthquake scenario. The set of GMPEs contributing the most at the 0.2 s response period is Set 7, hence the "modal" GMPE is the equation of Ambraseys *et al.* (2005) and the dominant seismic source is the Stable craton.

For SA at the 1.0 s response period (Table 4.5), a much wider variety of dominant earthquake scenarios can be observed among the different sets of equations. These are, in general terms, similar to the dominant scenarios presented in Table 4.3 with the exception of Set 2 and Set 8 which result in M* = 5.1 M_w and R* = 12.5 km (r_{epi}). For both sets of equations the seismic source hosting the dominant scenario is the Stable craton; however, the

West Makran has a very similar contribution to the hazard in Set 2 and, in Set 8, this contribution is even higher than the contribution from the Stable craton. The set of equations contributing the most to the final hazard for SA at 1.0 s is Set 11, since the seismic sources controlling the dominant earthquake scenario for this set are the Simple Fold belt and the Persian Gulf the "modal" GMPE is the equation of Boore & Atkinson (2007).

Table 4.4. Summary of the hazard-dominating earthquake scenarios for the 16 sets of equations considered in the hazard analysis of the case study for SA at a 0.2 s response period and the 2500-year return period (Figure 4.24 and Figure 4.25). r_{corr} is the corrected distance according the to the distance definition of GMPE assigned to the dominant seismic source, (1) for r_{jb} and (2) for r_{rup}; * indicates that r_{corr} was limited to a minimum value of 200 km which is the closest distance from Makran to Dubai; Dom. Source is the number of the seismic source that contributes the most to the hazard at the 2500-year return period (for identification of the seismic sources see Table 3.10);Target GM is the expected ground motion level at the 2500-year return period from the hazard curve for each set of equations; Predicted GM is the ground motion predicted by the GMPE for the dominant scenario; Error is the percentage error to predict the target ground motion; Global error is the percentage error to predict the target ground motion of 0.19 g, which corresponds to a 2500-year return period of the final hazard curve; (3) indicates that two or more seismic sources dominate the hazard for that set of equations.

	Set 1	Set 2	Set 3	Set 4	Set 5	Set 6	Set 7	Set 8
M_w	5.1	5.1	5.1	5.1	5.1	5.1	5.1	5.1
r_{epi} (km)	12.5	12.5	12.5	12.5	12.5	12.5	12.5	12.5
r_{corr} (km)	10.8(1)	10.8(1)	10.8(1)	10.8(1)	15.4(2)	15.4(2)	10.8(1)	10.8(1)
ε	0.75	0.75	1.25	1.25	0.75	0.75	0.25	0.25
ε'	-0.049	0.005	0.347	0.379	0.144	0.164	-0.082	-0.062
Dom Source	15	15	15	15	15	15	15	15
Target GM (g)	0.2	0.22	0.22	0.23	0.29	0.3	0.22	0.23
Predicted GM (g)	0.39	0.39	0.29	0.29	0.4	0.4	0.34	0.34
Error (%)	95	77	32	26	38	33	55	48
Global Error (%)	105	105	53	53	111	111	79	79

	Set 9	Set 10	Set 11	Set 12	Set 13	Set 14	Set 15	Set 16
M_w	6.0	6.0	5.8	5.8	5.6	5.6	6.0	8.6
r_{epi} (km)	62.5	62.5	62.5	62.5	62.5	62.5	62.5	262.5
r_{corr} (km)	57.4(2)	57.4(2)	58(1)	58(1)	60.2(2)	60.2(2)	56.2(1)	200(2)*
ε	0.75	1.25	1.75	1.75	1.75	1.75	0.75	0.25
ε'	0.493	0.548	0.583	0.63	0.591	0.591	0.414	-0.054
Dom Source	15	15	5	5	5	5	15	20
Target GM (g)	0.11	0.12	0.15	0.16	0.23	0.23	0.1	0.12
Predicted GM (g)	0.084	0.119	0.192	0.192	0.3	0.3	0.087	0.146
Error (%)	24	1	28	20	30	30	13	22
Global Error (%)	56	37	1	1	58	58	54	23

The dominant earthquake scenarios obtained from both approaches (i.e., the mean of the hazard or the mean of the ground motions), although different, are not radically dissimilar. Additionally, the seismic sources controlling the hazard are basically the same for both approaches, with the Stable craton being the dominant seismic source for PGA and the Persian Gulf and the Simple Fold belt dominating for SA at the 1.0 s response period, both for a return period of 2500 years. Although the differences between the two approaches are expected to increase with increasing return period, for return periods of interest in common practice (less than 10,000 years) a similar situation to that presented herein can be expected.

Table 4.5. Summary of the hazard-dominating earthquake scenarios for the 16 sets of equations considered in the hazard analysis of the case study for SA at a 1.0 s response period and the 2500-year return period. For the definition of the different variables and notations see Table 4.4.

	Set 1	**Set 2**	**Set 3**	**Set 4**	**Set 5**	**Set 6**	**Set 7**	**Set 8**
M_w	8.17	5.1	6.63	6.63	6.63	6.63	8.6	5.1
r_{epi} (km)	262.5	12.5	162.5	162.5	187.5	187.5	262.5	12.5
r_{corr} (km)	205(2)	10.8(1)	152.1(1)	152.1(1)	177.9(2)	177.9(2)	200(2)*	10.8(1)
ε	0	1.25	2.25	2.75	2.25	2.25	0	1.25
ε'	-0.773	0.343	0.950	0.969	0.769	0.775	-1.289	0.380
Dom Source	15-20(3)	15-20(3)	15	15	2-5-15(3)	2-5-15(3)	15-20	20-15(3)
Target GM (g)	0.048	0.050	0.071	0.073	0.118	0.119	0.047	0.048
Predicted GM (g)	0.088	0.089	0.074	0.102	0.160	0.160	0.129	0.065
Error (%)	83	78	4	40	36	34	174	35
Global Error (%)	29	31	9	50	135	135	90	4

	Set 9	**Set 10**	**Set 11**	**Set 12**	**Set 13**	**Set 14**	**Set 15**	**Set 16**
M_w	8.17	6.97	6.63	6.63	6.63	6.63	8.6	8.6
r_{epi} (km)	262.5	262.5	162.5	162.5	187.5	187.5	262.5	262.5
r_{corr} (km)	205(2)	244.2(1)	152.1(1)	152.1(2)	177.9(2)	177.9(2)	200(2)*	200(2)*
ε	0	2.25	2.25	2.25	2.75	2.25	0	0
ε'	-0.913	2.179	0.881	0.901	0.728	0.734	-1.432	-0.555
Dom Source	20	20	5-2(3)	5-20(3)	2-5(3)	2-5(3)	20	20
Target GM (g)	0.043	0.044	0.064	0.066	0.111	0.112	0.042	0.043
Predicted GM (g)	0.088	0.046	0.074	0.074	0.220	0.220	0.129	0.062
Error (%)	105	5	16	12	98	96	207	44
Global Error (%)	29	32	9	9	224	224	90	9

Regardless of the approach selected to merge the hazard results from the alternative end tips of the logic tree, obtaining the disaggregated results for the different sets of equations (or equation if only one GMPE is used in each branch) used in the hazard analysis will give valuable information to the engineer for the decision making process. Additionally, it will allow the analyst to associate a "modal" GMPE to the dominant earthquake scenario, with this having important implications for the specification of scenario spectra and consequently for the selection of ground-motion records for seismic design. These implications are discussed in the following section.

4.5. Implications for record selection and scenario spectra

When the goal of a PSHA is to provide inputs for time-domain analysis of a structure, the last stage of the PSHA must be to define a scenario spectrum and to suggest suites of ground-motion records that represent the seismic hazard for a desired return period. However, it seems that there is no single answer to the question of which scenario spectrum most appropriately represents the seismic hazard, but that rather multiple answers might be appropriate depending upon how the seismic hazard is defined.

In this section a discussion on the specification of the scenario spectra and the selection of ground–motion records for seismic design is presented. Additionally, two alternative approaches are proposed to obtain the scenario spectra based on the disaggregated results of a PSHA performed within a logic-tree framework using multiple GMPEs. These approaches take into account decisions that must be made during the PSHA and which are usually obviated, or not explicitly considered, in common practice and that may lead to alternative interpretations of the hazard results.

It is common practice, though strongly discouraged, to use the uniform hazard spectrum (UHS) as the design spectra and to match real or synthetic time-histories to the spectral amplitudes of the UHS for seismic design purposes (e.g., Hancock *et al.*, 2006). The UHS is called uniform because the probability of exceedance of the spectral amplitude at any individual response period is the same for all response periods. However, since the UHS is constructed by reading the ground motions at a given return period from the hazard curves calculated for different individual intensity measures (see section 2.4.4), the shape of the UHS does not usually represent a response spectrum of any real earthquake. If a UHS were obtained using a vector-valued approach (Bazzurro & Cornell, 2002) it would make sense to use the UHS as target response spectra for seismic design. In any other case, the use of the UHS for seismic design proposes does not have any real foundations.

To obtain a scenario spectrum from a PSHA considering alternative GMPEs that accurately represents the seismic hazard, McGuire (1995) propose an approach consisting of two steps. First, the dominant earthquake scenarios by magnitude, distance and epsilon must be obtained individually for each ground-motion equation used in the analysis. Second, the seismic hazard for two structural response periods (usually one at short periods and one at long periods) must be examined by seismic source in order to see if a single source dominates the hazard at both periods. If only one seismic source dominates the hazard at both periods it is considered reasonable to represent hazard with a single earthquake scenario, and therefore to select the most-likely combination of M, R and ε. If different sources dominate the hazard at each response period, generally more than one earthquake scenario should be used. For making this test, McGuire (1995) uses the hazard results for SA at 0.1 and 3.0 s response periods. However, what

should really be considered is the response period of the structure for design.

Once the most likely earthquake scenarios have been identified for each of the ground-motion equations, the weighted mean of the values of M, R and ε from the alternative scenarios is calculated using the weight assigned to each of the ground-motion equation in the logic tree. Finally, ε is adjusted for each equation to equal or exceed the target ground motion, if only one earthquake scenario is being used for both response periods. In the case that different earthquake scenarios are being used for each response period, ε is adjusted to predict the target ground motion for the corresponding period. The final combination of M, R and ε obtained in this way is defined by McGuire (1995) as the "beta earthquake".

An important drawback of this procedure is that the final combination of M, R and ε might not correspond to the most likely earthquake scenario to equal (or exceed if it is the case) the target ground motion and might not correspond to any possible earthquake from the seismicity model. Additionally, the most likely earthquake scenario for each GMPE obtained for the same target ground motion will correspond to different return periods and the weighted mean of these scenarios will not necessarily correspond to the desired return period in the final hazard curve.

An important issue in this approach is that McGuire (1995) derives the contributions to the seismic hazard in terms of M, R and ε to match the target ground motion. This is done instead of the traditional approach in which the contributions by M, R and ε are obtained for ground-motion values that equal or exceed the target ground motion. McGuire (1995) defines the contributions to the hazard in this way since he wishes to replicate the target ground motion for a given return period with the "design earthquake" obtained from the dominating earthquake scenario.

Here it is important to highlight that Bazzurro & Cornell (1999) present a different interpretation of the approach presented by McGuire (1995). They state that "*In order to achieve the matching, McGuire suggests disaggregating the probability of exceedance of the specified S_a level at the given frequency f by lumping the hazard contribution into the appropriate M, R and ε bin such that the target value is equaled (not exceeded) …*". However, from the examination of the original publication, it seems, as already stated, that McGuire proposes disaggregating the hazard results considering only the scenarios of M, R and ε (of course, within the precision associated with a certain M, R and ε bin size) that equal but do not exceed the target ground motion. Unfortunately, from the reading of the original publication it is not totally clear which of the two interpretations is correct. Although the two interpretations would lead to very different disaggregated results, for the purposes of the present work, the latter interpretation of the McGuire's (1995) proposal to obtain the disaggregated results is considered as the most appropriate.

Herein, two different approaches are proposed to obtain scenario spectra which are compatible with the hazard results of a PSHA performed in a logic-tree framework using alternative GMPE, or sets of GMPEs, in contiguous branches. These approaches are dependent on two decisions that the hazard analyst, together with the engineer, has to take during the PSHA process. The first decision is regarding the domain in which the mean hazard curve will be calculated (i.e., the hazard or ground-motion domain); the second decision is whether the disaggregated results will be obtained to match (McGuire, 1995) or to exceed the target ground motion. These decisions could lead to different dominant earthquake scenarios with direct implications for the selection of the scenario spectra and hence on the selection of the ground-motion records to be used for seismic design or assessment.

The two approaches proposed herein for obtaining a response spectrum from the disaggregated results are explained in what follows, along with the implications of the different decisions that must be taken during the PSHA process on the interpretation of the scenario spectrum obtained from these approaches.

Figure 4.26 presents a flowchart describing the decision-taking process to calculate scenario spectra considering the different alternatives commented on above. This flow chart has, as a starting point, the hazard results at the end tips of the logic tree. Three pieces of information are required at the starting point: the seismic hazard curves, the disaggregated results by M, R and ε and the contributions from each seismic source to the hazard from a traditional PSHA analysis.

Once these three pieces of information have been gathered, the analyst has to decide on which domain he/she is going to calculate the mean hazard curve in. As discussed in section 4.3, both approaches are completely valid. However, the analyst must keep in mind the purpose of the analysis. Calculating the mean of the hazard implies that the mean hazard curve will represent expected probabilities of exceedance for given values of ground motion, while calculating the mean of the ground motions implies that the hazard curve will represent the expected ground-motion levels for given probabilities of exceedance (see section 4.3 for a further discussion on this topic).

The following step is to define the goal of the disaggregation. As previously discussed, the disaggregated results can be obtained either to match the target ground motion, as proposed by McGuire (1995), or to equal or exceed the target ground motion, which is the common approach.

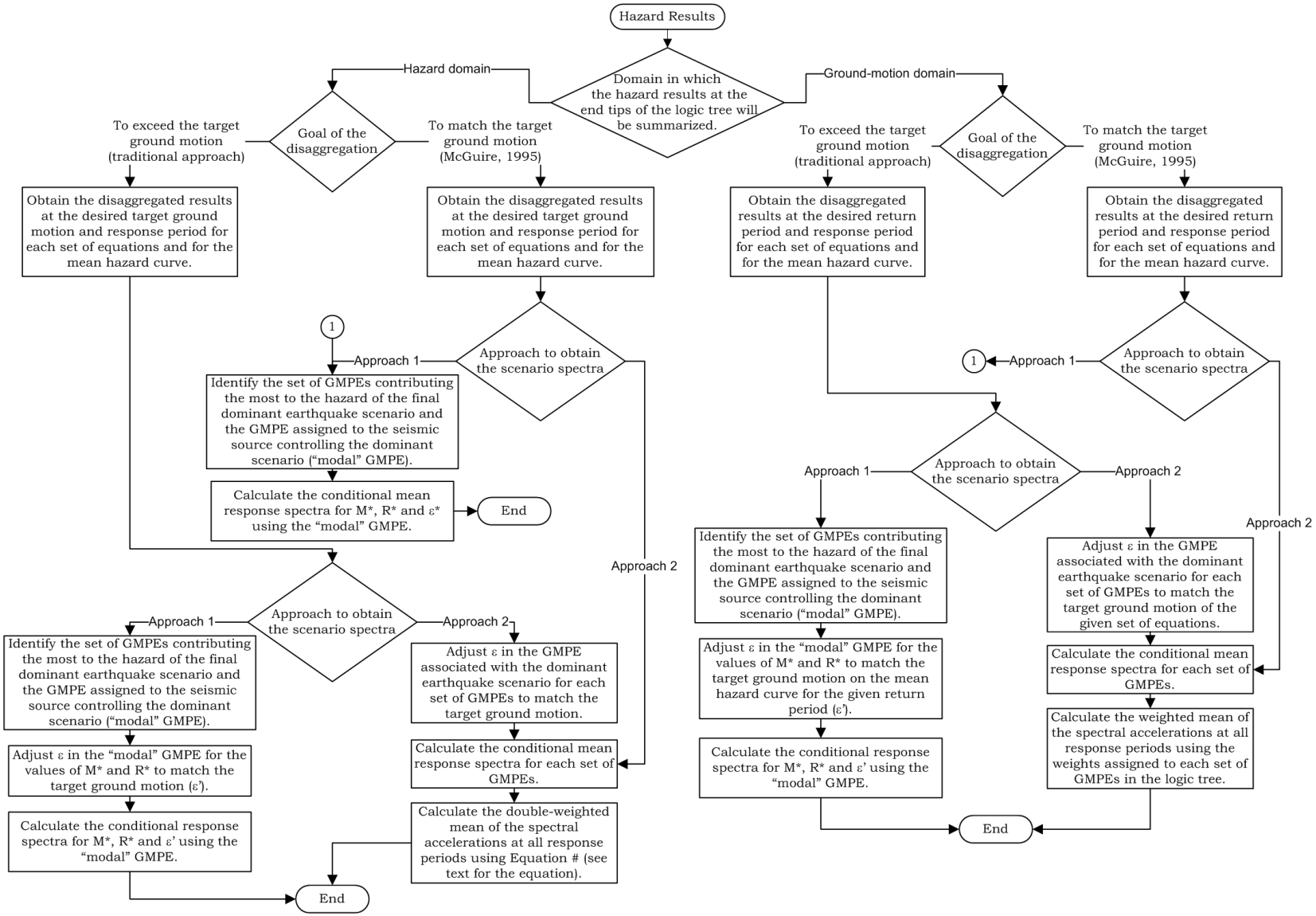

Figure 4.26. Flowchart to obtain the scenario spectra using alternative approaches.

Herein the definition of the goal of the disaggregated results is presented as a step after the running of the hazard analysis since most of the commercial software available to perform PSHA, if not all of them, report disaggregated results for the probabilities of exceeding the target ground motion. However, these results can be decomposed into rates of occurrence of spectral accelerations over small acceleration ranges for specific bins of M and R (see Equation 5.12). In this way, the decomposed disaggregated results will represent the rates of occurrence at which the target spectral acceleration is being equalled but not exceeded. This procedure to decompose the disaggregated results has been proposed by Hardy *et al.* (2006) for filtering the hazard results by removing non-damaging earthquakes using the cumulative absolute velocity (CAV), a threshold criteria (see section 5.3 and Equation 5.12 for a better understanding of this procedure). The accuracy of this procedure depends on the size of the ranges of acceleration used to decompose the disaggregated results, the smallest the range the more accurate the results.

The decision of obtaining the disaggregated results to match or to exceed the target ground motion has important implications for the interpretation of the hazard results and the identification of the dominant earthquake scenario. When the disaggregated results represent the probabilities of matching the target ground motion, the dominant earthquake scenario (M*-R*-ε*) guarantee mathematically that this specific combination of M-R-ε will reproduce the target ground motion (at least within the precision associated with the size of the bins of M, R and ε). On the other hand, when the disaggregated results present the probabilities of equal or exceed the target ground motion the triplet M*-R*-ε* will not necessarily reproduce the target the ground motion but rather it will exceed it.

Since the requirement of the engineering analyst is often to have an accelerogram whose response spectrum that matches the expected spectral amplitude (target ground motion) for a given structural period at a fixed return period, it seems logical to use the dominant scenario from the disaggregated results for matching the target ground motion to calculate the scenario spectra. However, common practice is to use the dominant scenario from the disaggregated results for exceeding the target ground motion adjusting the value of ε^* to match the expected spectral amplitude (ε'). By doing this, the final triplet of M*-R*-ε' will not represent either the most likely earthquake scenario to equal or exceed the target ground motion. If the analyst's wish is to obtain the response spectra corresponding to the most likely earthquake scenario to exceed the target ground motion he/she must invariably use the triplet M*-R*-ε^* and accept that the spectral amplitudes might exceed the target ground motion at the structural period of interest. Nevertheless, the common practice of adjusting the value of ε^* to match the target ground motion is considered herein as a valid approach despite the drawbacks mentioned above.

Before explaining the two approaches proposed herein to calculate the scenario spectra, the concept of the conditional mean spectrum needs to be introduced. Using the median spectral shape to define the response spectrum corresponding to the dominant earthquake scenario given by M*-R*-ε^*, may not be representative of the response spectrum that is expected if the M*-R*-ε^* scenario occurs and the spectral amplitude at the given structural period equals the UHS at that period (Abrahamson, 2006). Alternatively, Baker & Cornell (2006b) propose a method for developing a response spectrum with the expected spectral shape for given values of M, R and ε. For doing this Baker & Cornell (2006b) take into account the relationship between ε and the spectral shape. The latter authors propose

calculating the spectral amplitudes at the different structural periods using the following equation:

$$\mu_{\ln S_a(T_2)|\ln S_a(T_1)=\ln S_a(T_1)^*} = \mu_{\ln S_a}\left(M^*, R^*, T_2\right) + \sigma_{\ln S_a}\left(M^*, T_2\right)\rho_{\ln S_a(T_1),\ln S_a(T_2)}\varepsilon^*\left(T_1\right) \quad 4.2$$

where M*, R* and $\varepsilon^*(T_1)$ are the triplet defining the dominant earthquake scenario for the structural period T_1, $\mu_{\ln Sa}\left(M^*, R^*, T_2\right)$ and $\sigma_{\ln Sa}\left(M^*, T_2\right)$ are the marginal mean and standard deviation of $ln(S_a)$ at the structural period T_2, obtained from a ground-motion equation. Finally, $\rho_{\ln Sa(T1),\ln Sa(T2)}$ represents the correlation between response spectral accelerations at periods T_1 and T_2, and with the same orientation of the ground motion as presented by Baker & Cornell (2006a). For the present work, the up-dated correlations for response spectral accelerations presented by Baker & Jayaram (2008) were used instead of the Baker & Cornell (2006a) correlations.

Once the disaggregated results for all of the alternative set of GMPEs considered in the hazard analysis and the mean hazard curve have been obtained, for any of the alternative options previously discussed (i.e., hazard or ground-motion domain and to match or exceed the target ground motion), the scenario spectra can be calculated using any of the following two approaches (see Figure 4.26 for graphical support):

Approach 1.

1. For the structural period and at the return period of interest, identify the dominant earthquake scenario of the mean hazard curve and its corresponding "modal" GMPE, as defined in section 4.4.
2. If the disaggregated results were obtained to exceed the target ground motion, adjust the value of ε^* (ε') to match the expected spectral acceleration as read from the mean hazard curve for the given return period. Although the disaggregated results had been obtained to match the target ground motion,

some minor adjustment on the value of ε^* might be necessary due to the discrete nature of the calculations.

3. Calculate the conditional mean spectrum for the triplet M*-R*-ε' and for the modal GMPE using Equation 4.2.

Approach 2.

1. For the structural period and the return period or ground-motion level of interest, depending on which domain was used for the calculation of the mean hazard curve (i.e., hazard or ground-motion), identify the dominant earthquake scenario and its "modal" GMPE, for each set of equations and for the mean hazard curve as discussed in section 4.4.
2. If the disaggregated results were obtained to exceed the target ground motion, adjust the value of ε^* (ε') in the GMPE associated with the dominant earthquake scenario of each set of GMPEs to match the target ground motion of the given set of equations. Although the disaggregated results had been obtained to match the target ground motion, some minor adjustment on the value of ε^* might be necessary due to the discrete nature of the calculations.
3. Calculate the conditional mean spectrum for the triplet M*-R*-ε' and the GMPE associated with the dominant scenario of each set of GMPEs using Equation 4.2.
4. Calculate the weighted mean of the spectral accelerations of each set of GMPEs at all response periods using one of the following two options:
    a. If the mean hazard curve was calculated as the mean of the hazard, calculate the weighted mean of the spectral accelerations using the equation:

$$SA(T_i) = \sum_{n=1}^{N} \left(\frac{W_{1_n}}{\sum_{n=1}^{N} W_{1_n}} + \frac{W_{2_n}}{\sum_{n=1}^{N} W_{2_n}} \right) \frac{SA(T_i)_n}{2} \qquad 4.3$$

were $SA(T_i)$ is the spectral amplitude at the i^{th} structural period, N is the number of sets of GMPEs, W_{1n} is the weight assigned to the n^{th} set of equations in the logic tree and W_{2n} is the contribution to the hazard of the dominant earthquake scenario for the n^{th} set of equations.

b. If the mean hazard was calculated as the mean of the ground motions, the mean spectral accelerations can be calculated using only the weights assigned to each set of equations:

$$SA(T_i) = \sum_{n=1}^{N} \frac{W_n^1 SA(T_i)_n}{\sum_{n=1}^{N} W_n^1} \qquad 4.4$$

As it is common convention to ensure that the sum of the weights of alternative branches in the logic tree equals one, the divisor in Equation 4.4 can be skipped over.

The response spectra obtained from each of the two approaches has different conceptual interpretations. Approach 1 will give the analyst the response spectrum of the most likely earthquake scenario as dictated by the disaggregated results of the mean hazard curve. This approach has the advantage of finding the GMPE that contributes the most to the dominant earthquake scenario for a given response period at a given return period. In this way, the response spectrum obtained represents the most likely spectral shape to affect the site under study that will also equal the spectral amplitude of the UHS for a given structural period at a selected return period. This approach should be selected when one wishes to obtain the

response spectral shape of only the most likely event and not to consider the contributions from alternative hazardous earthquake scenarios.

On the other hand, the response spectrum obtained from Approach 2 represents the weighted mean spectral amplitudes of the response spectra from the dominating-hazard scenarios of each of the alternative sets of GMPEs considered in the hazard analysis. Under this approach the spectral shapes from the dominant scenario of each set of GMPE are compiled in the final scenario spectra through a double weighting. The first weighting corresponds to the weights assigned to each set of GMPEs in the logic tree, the second weighting takes into consideration the relative contribution of the dominant scenario of each set of equations to the final hazard (i.e., the hazard of the mean hazard curve).

Using the two approaches proposed herein, the conditional mean spectra were calculated for the city of Dubai for SA at 0.2 and 1.0 s response periods and for the 2500-year return period. Figure 4.27 presents the response spectra using both approaches and for the case in which the mean hazard curve is calculated in the hazard domain and the disaggregated results are obtained to equal or exceed the target ground motion.

Figure 4.28 presents the response spectra using both approaches for the same example as in Figure 4.27, but for the case in which the mean hazard curve is calculated as the mean of the ground motions and the disaggregated results are obtained to equal or exceed the target ground motion.

A significant difference can be observed between the response spectra obtained from both approaches for 0.2 s and 1.0 s response periods (left- vs. right-hand side in Figure 4.27 and Figure 4.28). It is also worth noting that the spectral shape also changes depending on the domain in which the hazard results were calculated (Figure 4.27 vs. Figure 4.28). These differences are more significant for Approach 1 since for this approach the

spectral shape is highly dependent of the modal GMPE and the values of M, R and ε of the dominant earthquake scenario. On the other hand, as Approach 2 considers the dominant scenarios from all of the sets of equations and the scenarios obtained from both domains, in general, the shapes are not expected to be radically different. Hence, important differences are not expected in the spectral shape of the final response spectrum.

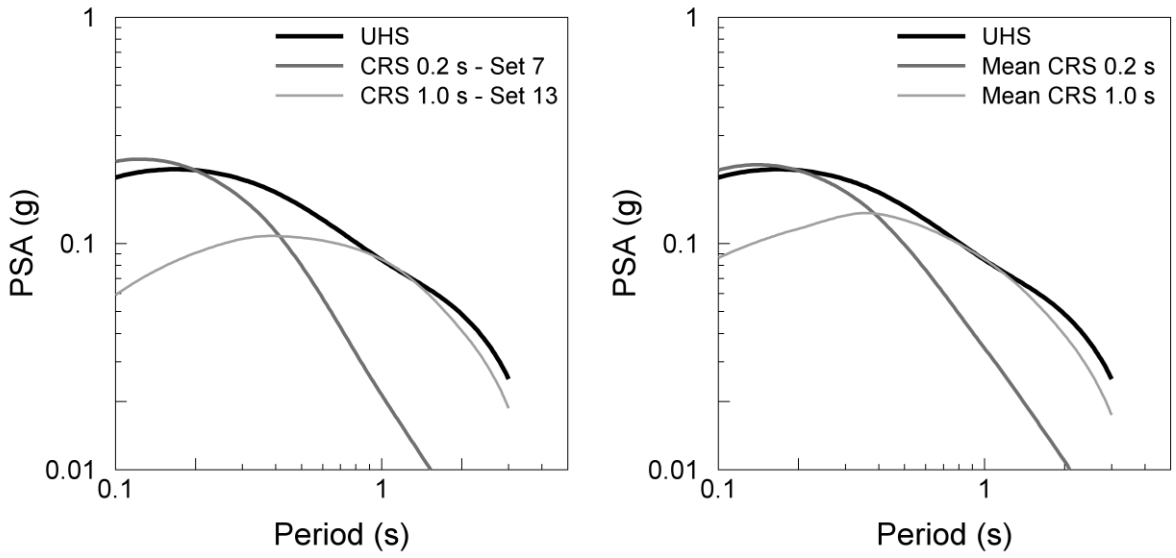

Figure 4.27. Uniform hazard spectrum (UHS) and conditional response spectra for 0.2 s (CRS 0.2 s) and 1.0 s (CRS 1.0 s) response periods at the 2500-year return period for the city of Dubai. On the left-hand-side the CRS calculated using the "modal" GMPE (Set 7 for 0.2 s and Set 13 for 1.0 s; Approach 1) are presented; on the right-hand-side the CRS as the mean spectral accelerations (Mean CRS) of the CRS of the dominant scenarios of each set of GMPEs (Approach 2) are presented. These results are for the mean hazard curve from the hazard domain and disaggregated results for probabilities of exceeding the target ground motion.

Although the differences between the response spectra obtained from the hazard results calculated on the hazard or ground-motion domain, Figure 4.27 and Figure 4.28 respectively, are not significant at this level of return period (i.e., 2500 years), these differences are likely to increase at longer return periods (see section 4.3).

It is worth mentioning that the median hazard curve (or any other fractile) was not considered here for the calculation of the scenario spectrum

as the disaggregated results for this statistical operator have shown important inconsistencies (see section 4.2). However, if a single hazard curve from the suite of hazard curves of the logic tree is selected as the median hazard curve, the general framework described herein can be applied to obtain the response spectra for seismic design.

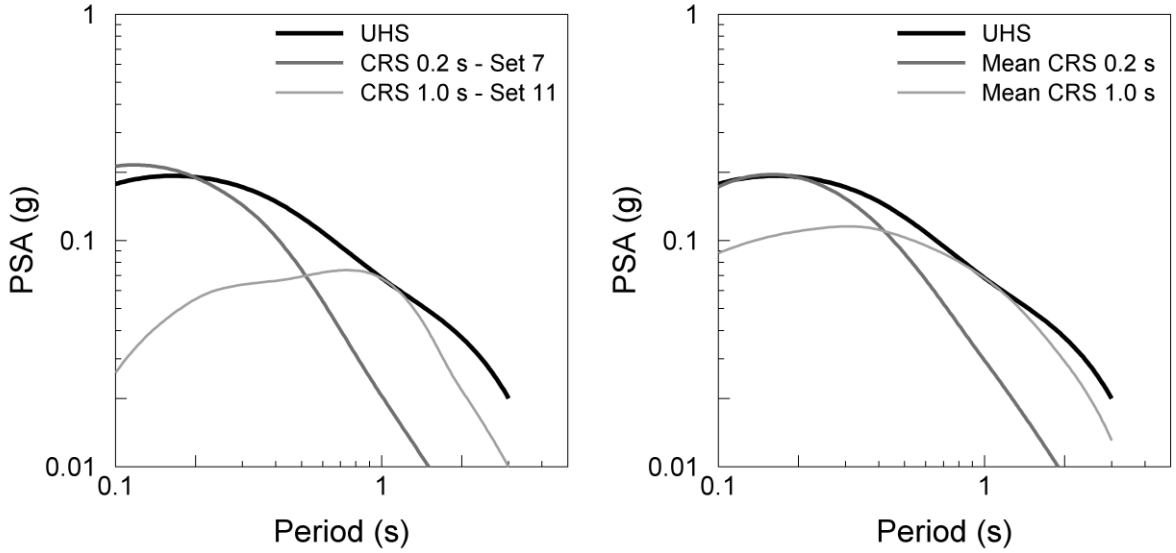

Figure 4.28. Uniform hazard spectrum (UHS) and conditional response spectra for 0.2 s (CRS 0.2 s) and 1.0 s (CRS 1.0 s) response periods at the 2500-year return period for the city of Dubai. On the left-hand-side the CRS calculated using the "modal" GMPE (Set 7 for 0.2 s and Set 13 for 1.0 s; Approach 1) are presented; on the right-hand-side the CRS as the mean spectral accelerations (Mean CRS) of the CRS of the dominant scenarios of each set of GMPEs (Approach 2) are presented. These results are for the mean hazard curve from the ground motion domain and disaggregated results for probabilities of exceeding the target ground motion.

Finally, in Figure 4.29 a comparison is presented of the response spectra calculated for the mean spectral shape (i.e., calculating the spectral accelerations for fixed values of M, R and ε in a ground motion equation) and the conditional response spectra using Equation 4.2 (expected shape). These results are for the same conditions as those presented in Figure 4.27.

As expected an important difference is observed in the spectral amplitudes between the unconditional and the conditional response spectra. Given that in this example the ground motion has a positive ε value the spectral amplitudes at structural periods apart from the structural period of

the target value are smaller than the mean spectral shape (c.f., Baker & Cornell, 2006a). The exception to this is the conditional spectra for 0.2 s – Set 7, the left-hand-side of Figure 4.29, where the ground motion for Set 7 has a negative value of ε (see Table 4.2) and hence the spectral amplitudes are lager than the mean spectral shape.

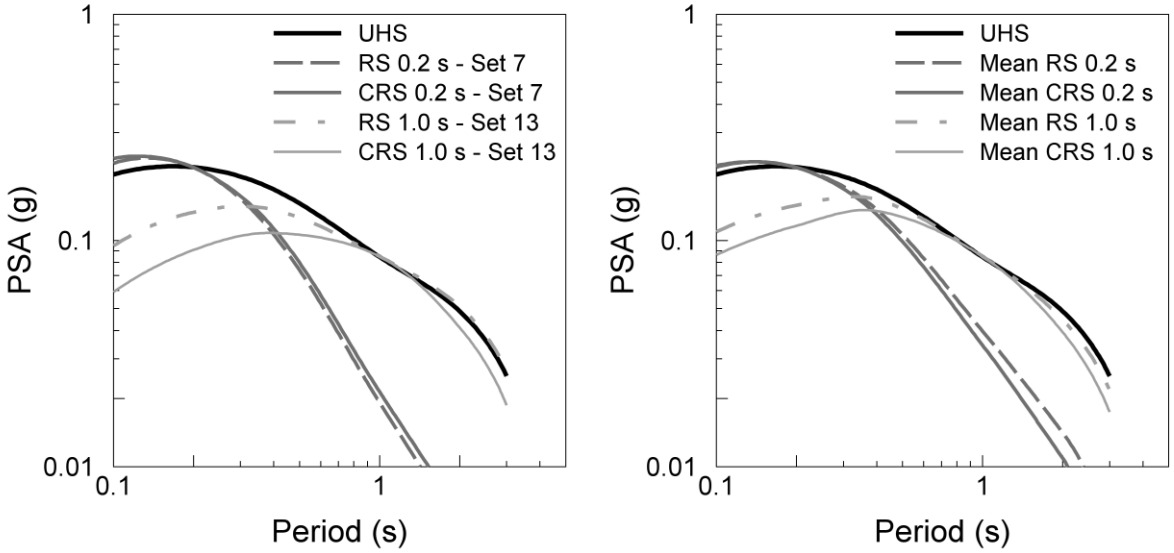

Figure 4.29. Comparison of the mean response spectra (RS) and the conditional response spectra (CRS) for response periods of 0.2 and 1.0 s at 2500-year return period. These results are for the city of Dubai and correspond to the same conditions as Figure 4.27. On the left-hand side are shown the response spectra for the Approach 1 and on the right-hand side the response spectra for the Approach 2.

As in the case of the scenario spectra, the definition of the dominant earthquake scenario has direct implications for the selection of ground-motion records for non-linear structural analysis. The selection of the ground-motion records can be based either on the spectral shape of the scenario spectra or based on the M, R and/or ε values of the dominant scenario. In addition to the M, R and ε of the dominant scenario, parameters as faulting mechanism, stress drop and soil conditions, among others parameters, related to the seismic source to which the dominant scenario belongs can be incorporated in the selection of the ground-motion record.

The most traditional approach is to select acceleration records that match the conditions of M and R of the dominant earthquake scenario.

Baker & Cornell (2006b) analyse the effects of different record-selection strategies on the resulting structural response. The latter authors conclude that the value of ε in the acceleration record at the structural period of interest is an important property to match when selecting ground-motion records for dynamic analysis. Iervolino & Cornell (2005) also found little reason to support the selection of acceleration records based purely on M and R. Additionally, Baker & Cornell (2006b) conclude that ground-motion records can be selected based on the shape of the conditional response spectral without worrying further about M or R. It worth mentioning that these findings of Baker & Cornell (2006b) are for estimating drift response and may not be valid for some other cases.

Regardless of the approach followed to select the ground-motion records it might be necessary to apply a scaling factor to the original record to match the spectral amplitudes at the structural period of interest. However, previous researchers have found that the scaling of records apparently does not induce bias in the estimation of non-linear response of structures, at least for firm soil sites and for scaling factors as high as 4 and ductility up to 6 (Iervolino & Cornell, 2005; Shome *et al.*, 1998).

Based on this, the conditional response spectra presented in Figure 4.27 and Figure 4.28 could be used as target spectra for the selection of ground-motion records for structures with fundamental periods of 0.2 s or 1.0 s and for a 2500-year return period.

In conclusion, a number of alternative approaches can lead to valid scenario spectra and hence to the selection of ground-motion records that represent the seismic hazard at a given site for a selected structural period and a given return period. Although these alternative approaches are all valid, the analyst must keep in mind and communicate to the final user the

implications of the procedure used to obtain the final scenario spectra and ground-motion acceleration records. But must importantly, the approach taken must be consistent with the purpose of the analysis. Most of the decisions that must be taken during the hazard analysis process, and that have been discussed in this chapter, may be project-specific and must be the result of a discussion between engineers, decision makers and the hazard analyst, among others.

Chapter 5.

CASE STUDY SENSITIVITY ANALYSIS

In this chapter sensitivity analyses for the case study (PSHA for the UAE) are presented in order to gain an appreciation for the influence of key parameters in the PSHA. The first of these is the impact on the seismic hazard of the inclusion of an active fault running along the west coast of the UAE, as mapped by Johnson (1998). Other variables considered are the influence of the minimum magnitude (m_{min}) deemed to be of engineering significance, the earthquake occurrence parameters (ν_{min}, β and m_{max}), the use of alternative ground-motion prediction equations (GMPEs), the sensitivity of the results due to the standard deviation associated with the GMPEs and the weighting of the branches in the logic tree.

5.1. Implications of considering a fault running along the west coast of the UAE

The possible presence of a major fault running along the west coast of the UAE, as mapped by Johnson (1998), has piqued concern among engineers practicing in the region. To the knowledge of the author, no well-defined bases exist to assert the presence of such a structure (particularly not an active structure). However, if it were shown to exist and a degree of activity were proven, the impact on seismic hazard and therefore on seismic design considerations for the region could be significant.

With this motivation an extension to the PSHA for the UAE (Chapter 3) is presented in this section by including the west coast fault (WCF) into the analysis as an active seismic source. Seismic hazard curves and uniform hazard spectra (UHS) are calculated for the cities of Abu Dhabi, Dubai and

Ra's Al Khaymah for PGA and SA at response periods of 0.1, 0.2, 0.4, 1.0, 2.0 and 3.0 s and for return periods of 500, 2500 and 10,000 years.

To this end, two magnitude-frequency distributions (an exponential and a purely characteristic distribution) were considered for modelling the activity of the WCF. A maximum credible slip rate based on the available information was estimated and considered in the analysis. Additionally, the slip rate that would be required in order to match the UBC97 response spectra for zone 1 and rock site conditions, and the slip rate needed to match the PGA values presented by Sigbjornsson & Elnashai (2006) were estimated. Among the SHA studies reviewed in section 3.3, the latter authors present the only one that considers this structure in their hazard calculations. It is important to mention that Sigbjornsson & Elnashai (2006) do not report the slip rate, exact location or recurrence parameters used in their analysis for the WCF (or any other seismic source for that matter).

5.1.1. Background.

The concern over the existence of a fault on the west coast of the UAE arose from the presence of a main geological structure in this area in Johnson's (1998) "Tectonic map of Saudi Arabia and adjacent areas". This map was developed for the Kingdom of Saudi Arabia as compilation of many independent works, but was based mainly on the "Tectonic map of the Arabian Peninsula" by Brown (1972). It is important to mention that Johnson's (1998) map presents *selected tectonic elements of Saudi Arabia and, in lesser detail, elements in adjacent parts of the Arabian Peninsula*, and it is therefore not clear how reliable the information in these maps is for the UAE.

Among all of the publications retrieved for this analysis regarding the geology of the region (e.g., Al-Hinai *et al.*, 1997; Glennie, 2001; Lippard *et al.*, 1982), only Hancock *et al.* (1984) make reference to a fault near the west

coast of the UAE. The latter authors present a figure in which a similar structure to that shown by Johnson is shown offshore, near the coast. However, this fault is marked with question marks and no further details are given in the text. Apart from these two publications, Johnson (1998) and Hancock *et al.* (1984), no further evidence of the presence of the WCF could be retrieved from the literature. If this evidence is considered sufficient to accept the existence of the WCF, the next step is to assess the seismic activity of the fault.

The first human settlements in Abu Dhabi are dated to be from as far back as the 3rd millennium BC and the earliest recorded mention of Dubai dates back to 1095. Its early history fits the nomad herding and fishing pattern typical of the region (see, for example, Musson *et al.* 2006). However, the scarce supply of timber and the extremely harsh climate defined the rudimentary design of buildings. Until the middle of the 20th century the only settlements in the region were small towns and villages and most dwellings were constructed of palm fronds with others generally being mud huts. Before 1970 the local population was very small, estimated at 86 000 in 1961. It was only after the mid 1960's that towns were transformed from mud-walled buildings into modern cities integrated in the global economy (Everyculture.com, 2008; Visitabudhabi.ae, 2008).

This history of the UAE makes it difficult, if not impossible, to identify earthquakes that have occurred in the past, including medium to large magnitude events occurring prior to the 20th century. Ambraseys *et al.* (1994) stated that this situation is similar for most of the Arabian Peninsula. Based on the earthquake catalogue compiled herein (section 3.2.1), it is possible to claim that not a single event with magnitude ≥ 4.0 M_s has occurred along the west coast of the UAE in the last 40 years; or with magnitude ≥ 5.0 M_s in the last 82 years (periods of completeness of the catalogue for magnitudes 4.0 and 5.0, as described in section 3.2.3). These

considerations allow one to speculate about the probability of there being low seismic activity on the WCF with recurrence intervals typically at least comparable with the periods of completeness of the catalogue.

5.1.2. Fault characteristics and location

The West Coast Fault (WCF), as drawn in Johnson's (1998) map, was modelled as a 322-km-long strike-slip fault running from the coordinates 23.87°N-53.59°E to 25.76°N-56.03°E (Figure 5.1). Due to the lack of additional information a dip of ~90° was assumed as it is a common characteristic on well defined strike-slip faults. A fault at this location would cross the cities of Abu Dhabi and Dubai and would pass close to the city of Ra's Al Khaymah.

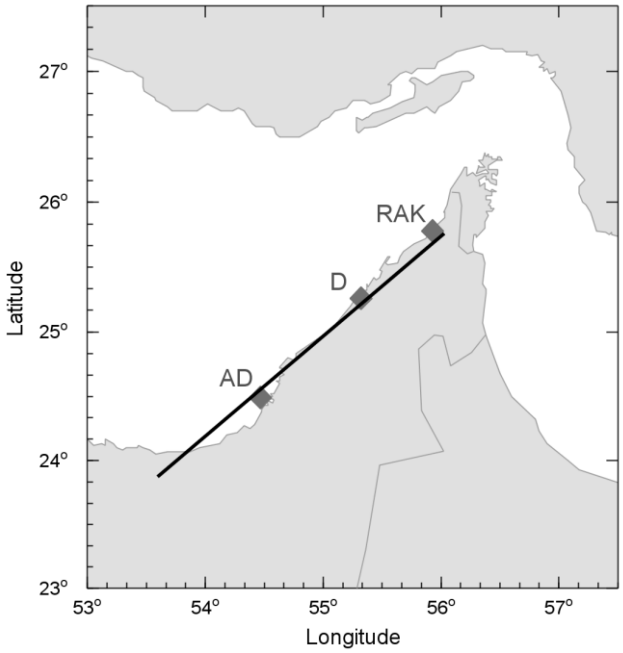

Figure 5.1. Location of the West Coast Fault (WCF) in the UAE as presented by Johnson (1998). Diamonds show the cities of Abu Dhabi (AD), Dubai (D) and Ra's Al Khaymah (RAK).

The age of the WCF was estimated based on the age of the surficial deposits and the underlying rock. The western coast of the UAE is formed of flat areas of sand, silt or clay covered by a crust of salt (halite) for at least a

part of the year; these areas are known as sabkhas. These deposits were formed during the post-glacial flooding of the Persian Gulf (~ 10-15 Ma ago) (Glennie, 2001). If we consider the WCF as a subsurface fault, located in the rock underneath the sabkhas sediments, an estimate of the age of the WCF of at least 10 Ma would be conservative. Additionally, a straight fault with these characteristics would suggest a mature structure with many hundreds or tens of million years of seismic activity. Under the latter conditions, assuming the age of the WCF on 10 Ma seems to be reasonable.

5.1.3. Recurrence parameters and maximum magnitude

Maximum magnitude.

If a scenario assuming the complete-rupture of the WCF is considered and the Wells & Coppersmith (1994) relationships are used, for a strike-slip fault with subsurface rupture and a length of the fault of 322 km, a maximum magnitude of 8.0 M_w is estimated. However, since there is no surface expression suggesting the possibility that an event of such magnitude had occurred in the past, even when considering a buried fault this magnitude seems to be very unlikely. Therefore, a maximum magnitude of 7.0 ± 0.5 M_w was assumed for the hazard calculations. Since the same moment rate would apply for both magnitudes, the latter value may be considered a conservative assumption since the recurrence interval of the characteristic event will be shorter.

Slip rate estimation.

As previously mentioned, different slip rates were considered for the hazard calculations. The first of them is the maximum credible slip rate that could be justified based on the information available. In other words, a realistic maximum slip rate that agrees with available sources of information, such as geological maps (Brown, 1972) and GPS measurements

(Vernant *et al.*, 2004) and the actual seismic data, or the lack of it, over the last 82 years. This period corresponds to that on which the earthquake catalogue is considered to be complete for events ≥5.0 M_s (table 3.6).

The second is the slip rate required to obtain a UHS that matches the UBC97 spectrum for zone 1. Finally, the third slip rate is that required to obtain PGA values similar to those reported by Sigbjornsson & Elnashai (2006) for a return period of 475 years.

To estimate the maximum credible slip rate that could be assigned to the WCF whilst still being consistent with the available data, three hypotheses were proposed:

- First, the WCF is a continuation of the Zendan-Minab and Dibba Line fault systems indicating the boundary between the Zagros fold belt and the Makran subduction zone, acting as the transition between both tectonic systems accommodating the different rates of deformation.
- Second, the WCF has a very low seismic activity with long earthquake recurrence intervals (i.e., a very small slip rate), sufficiently long so as to not to be reflected on the structural contours of the "Tectonic map of the Arabian Peninsula" of Brown (1972).
- Third, to estimate relative displacements using GPS measurements presented by Vernant *et al.* (2004) of two stations located in Oman (one in the Musandam peninsula (KHAS) and the other in Muscat (MUSC), see Vernant *et al.* (2004) for further details). This should be done in a component parallel to the strike of the WCF and assuming that all of the relative displacement is accommodated by the WCF.

Based on these hypotheses, three values of maximum slip rates were estimated. From the first hypothesis, it would be reasonable to consider that

the slip rate of the whole tectonic system decreases towards the south, since the seismic activity of the Dibba line is lower than that of the Zendan-Minad fault system. Under this assumption the slip rate of the Zendan-Minab fault system, 11 mm/yr (see section 3.1.3), should be considered as the upper bound slip rate for the WCF.

From the second hypothesis a maximum slip rate was estimated based on the tectonic map of Brown (1972), who presents structural contours for the base of the Tertiary and the approximate base of the Mesozoic rocks. Both series of contours cross the west coast of the UAE without showing any offset on them. This suggests that no important tectonic activity has occurred in this region at least during the last 65 Ma. This is valid if we consider up to the earliest stage of the Tertiary only. Considering the map scale (1:4 000 000), it could be argued that a displacement of 4 km (1 mm in the map) would not be reflected on the structural contours. This displacement, in addition to an estimated age of 10 Ma for the WCF, leads to an approximate maximum slip rate of 0.4 mm/yr.

Finally, using the GPS measurements of Vernant *et al.* (2004), a 2.06 mm/yr differential annual displacement was calculated between the stations KHAS and MUSC in a component parallel to the strike of the WCF. In this case it is important to highlight that most of the differential displacement between these stations is due to the rotational behaviour of the Arabian plate (Johnson, 1998; Vernant *et al.*, 2004; Vita-Finzi, 2001). The remaining differential displacements, if these exist, are accommodated by the Dibba Line (Lippard *et al.*, 1982). However, for the current hypothesis it is assumed that all of the relative displacement is accommodated by the WCF.

As only the smallest of the slip rates would be consistent with all three proposed hypotheses, the slip rate of 0.4 mm/yr was considered as the maximum credible slip rate that could be assigned to the WCF. This value concurs with the geologic and tectonic evidence presently available.

The estimation of the two remaining slip rates (i.e. the slip rates needed to match the UBC97 zone 1 response spectra and the PGA values reported by Sigbjornsson & Elnashai (2006)) were calculated by an iterative process, using both the exponential and characteristic magnitude-frequency distributions, until the desired results were obtained.

Estimation of recurrence parameters.

The characteristic earthquake recurrence interval (RI) and the exceedance rate for events of magnitude m_{min} or greater (υ_{min}) were calculated based on the estimated slip rates and the relationships proposed by Youngs & Coppersmith (1985). Due to the lack of seismic data β = 2.302 (b = 1) was assumed for the exponential model (Knopoff, 2000). The corresponding earthquake recurrence parameters for the different slip rates considered and for the two magnitude-frequency models are shown in Table 5.1.

Table 5.1. Summary of the earthquake occurrence parameters for the WCF. m_{max} – maximum magnitude; m_{min} – minimum magnitude; $\beta = b$ Ln(10); υ_{min} - number of earthquakes per year with magnitude equal to and greater than m_{min}; m_u – maximum magnitude of the characteristic earthquake; $m_{ch\text{-}min}$ – minimum magnitude of the characteristic earthquake; m_{ch} – expected value for the characteristic earthquake; RI – occurrence interval between characteristic earthquakes; σ() - standard deviation associated with the estimation of the parameter between brackets; S&E(06) – Sigbjornsson & Elnashai (2006).

Exponential model							
Slip rate	**m_{max}**	**m_{min}**	**σ(m_{max})**	**β**	**σ(β)**	**ν_{min}**	**Comments**
mm/yr	M_s	M_s				1/yr	
0.4	6.9	4.0	0.5	2.302	0	0.019	Maximum credible slip rate
0.5	6.9	4.0	0.5	2.302	0	0.024	Slip rate to match UBC97 Zone 1
2.4	6.9	4.0	0.5	2.302	0	0.115	Slip rate to match PGA values of S&E(06)
Characteristic model							
Slip rate	**m_u**	**m_{ch}**	**$m_{ch\text{-}min}$**	**σ(m_{ch})**	**RI(m_{ch})**	**Comments**	
mm/yr	M_s	M_s	M_s		yr		
0.4	6.9	6.3	5.7	0.5	1039	Maximum credible slip rate	
2.5	6.9	6.3	5.7	0.5	166	Slip rate to match UBC97 Zone 1	
6.0	6.9	6.3	5.7	0.5	69	Slip rate to match PGA values of S&E(06)	

The magnitude-frequency distributions for the different slip rates considered in the calculations, for both models, are presented in Figure 5.2. It is important to mention that, since the area of the fault for the estimation of v_{min} and the RI is kept constant, the seismic moment rate for both magnitude-frequency models (i.e., exponential and characteristic models) is the same when using the maximum credible slip rate (Figure 5.2-left).

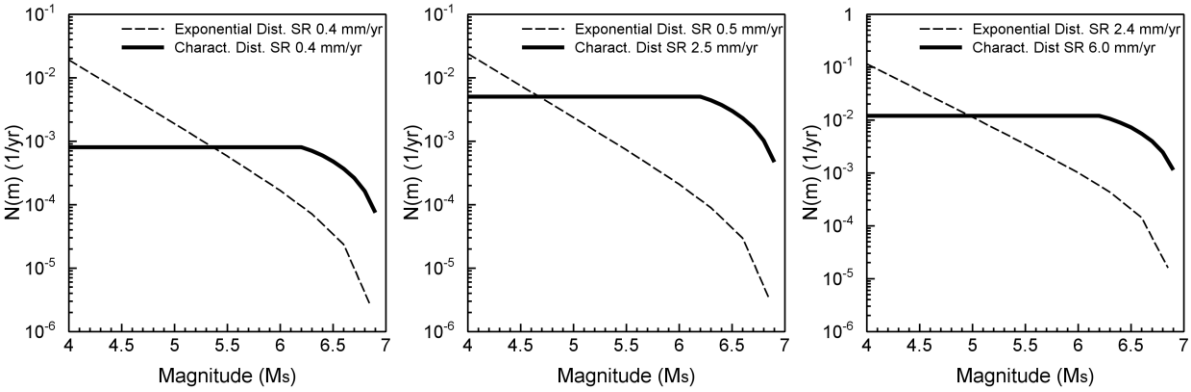

Figure 5.2. Magnitude-frequency distributions for the exponential and purely characteristic models, for the maximum credible slip rate (left); the slip rate required to match the UBC97 response spectra for zone 1 (centre); and the slip rate required to match the Sigbjornsson & Elnashai (2006) PGA values for a 475-year return period (right). SR – Slip rate.

5.1.4. Ground-motion prediction equations

The same set of GMPEs for shallow earthquakes used in the PSHA for the UAE (see section 3.5) were used to model the ground motions radiated from the WCF (i.e. Abrahamson & Silva, 1997; Akkar & Bommer, 2007b; Ambraseys *et al.*, 2005; Boore & Atkinson, 2006) through a logic-tree framework. The faulting mechanism is set to strike-slip and the site conditions as rock (V_{s30} ~760 m/s). The same conditions for compatibility between equations presented in section 3.5, in terms of horizontal component and distance definitions, were applied to this case.

As in the case study, equal weights were assigned to each GMPE in the logic tree (section 3.6).

5.1.5. Hazard analysis

The hazard analysis was carried out considering the WCF as the only seismic source. These results were then added to those obtained previously for the PSHA of the UAE.

The hazard calculations were performed using the same software (Crisis2007: Ordaz *et al.*, 2007) and following exactly the same approach as for the case study (section 3.7).

For compatibility with the former analysis (Chapter 3) the m_{min} for the integration of the hazard analysis was set to 4.0 M_s. The probability distribution of m_{max} was truncated at $m_{max} \pm 2\sigma(m_{max})$ (see section 3.7).

The WCF was modelled as a line source at a depth of 20 km. This depth was chosen as it corresponds to the average depth of the recorded earthquakes in the Arabian craton. Moreover, this depth corresponds to the upper boundary of the lower nucleating zone, as defined by Klose & Seeber (2007), for earthquakes occurring in stable continental regions. It is also worth stating that, the selection of the depth is not critical as three of the four ground-motion equations use r_{jb} as the distance definition and only one uses r_{rup} (see table 3.12). Since the fault was modelled as a line, depth is irrelevant when using r_{jb}.

As a result of the analysis, the hazard curves for PGA and SA up to 3.0 s response period were obtained for the three sites in the UAE. From these new hazard curves the uniform hazard spectra were calculated. Unfortunately, due to characteristics of the software used to perform the calculations it was not possible to add up the disaggregated results for magnitude-distance scenarios; however, disaggregated results by seismic source were obtained.

5.1.6. Results

Comparisons between the hazard curves from the original PSHA and the hazard curves considering the maximum credible slip rate (0.4 mm/yr)

for the WCF are shown from Figure 5.3 to Figure 5.5. These are for the two magnitude-frequency models. The hazard curves are for the three sites under study and for PGA and SA at 0.2, 1.0 and 3.0 s response periods.

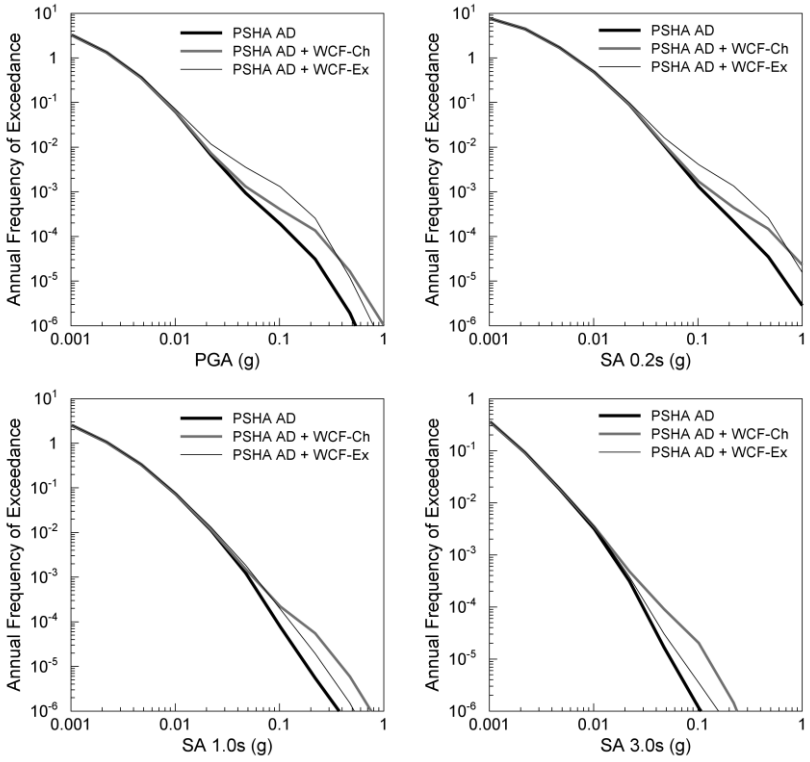

Figure 5.3. Hazard curves for the city of Abu Dhabi for PGA and SA at 0.2, 1.0 and 3.0s response periods. PSHA AD is the hazard curve from the case study for Abu Dhabi; PSHA AD + WCF-Ch is the hazard curve considering a characteristic behaviour of the WCF; and PSHA AD + WCF-Ex is the hazard curve considering an exponential behaviour of the WCF.

Figure 5.6 to Figure 5.8 present similar comparisons, but in terms of the uniform hazard spectra (UHS). The UHS are presented for the two magnitude-frequency models with a slip rate of 0.4 mm/yr and for 500-year, 2500-year and 10,000-year return periods.

Figure 5.9 to Figure 5.11 present the disaggregated results by seismic source for the three sites and the total hazard curve for PGA and SA at 0.2, 1.0 and 3.0 s. These results include the contribution to the hazard from the WCF from the purely characteristic model. Similar plots, but considering the exponential model for the WCF, are shown from Figure 5.12 to Figure 5.14.

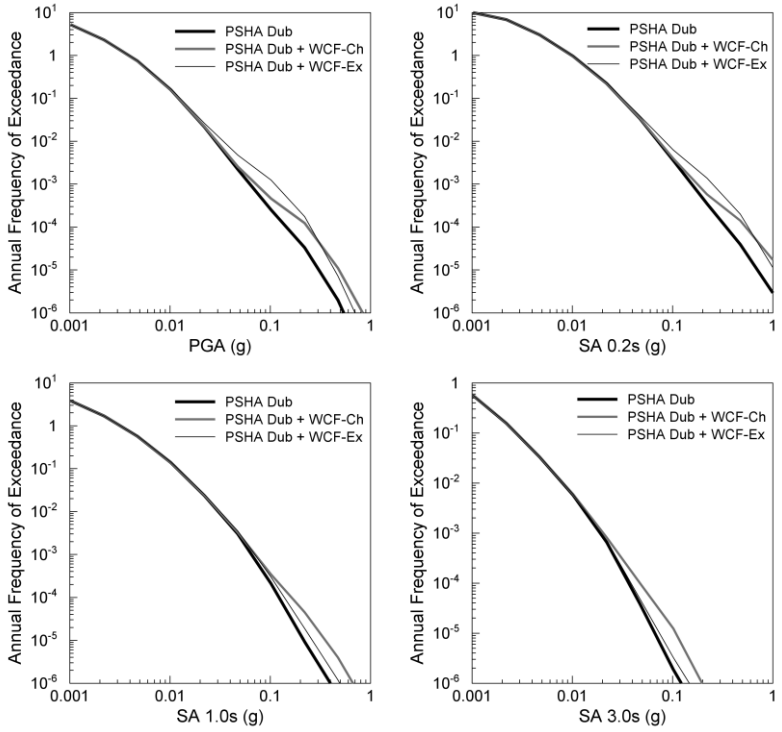

Figure 5.4. Hazard curves for the city of Dubai for PGA and SA at 0.2, 1.0 and 3.0 s response periods. PSHA Dub is the hazard curve from the case study for Dubai; PSHA Dub + WCF-Ch is the hazard curve considering a characteristic behaviour of the WCF; and PSHA Dub + WCF-Ex is the hazard curve considering an exponential behaviour of the WCF.

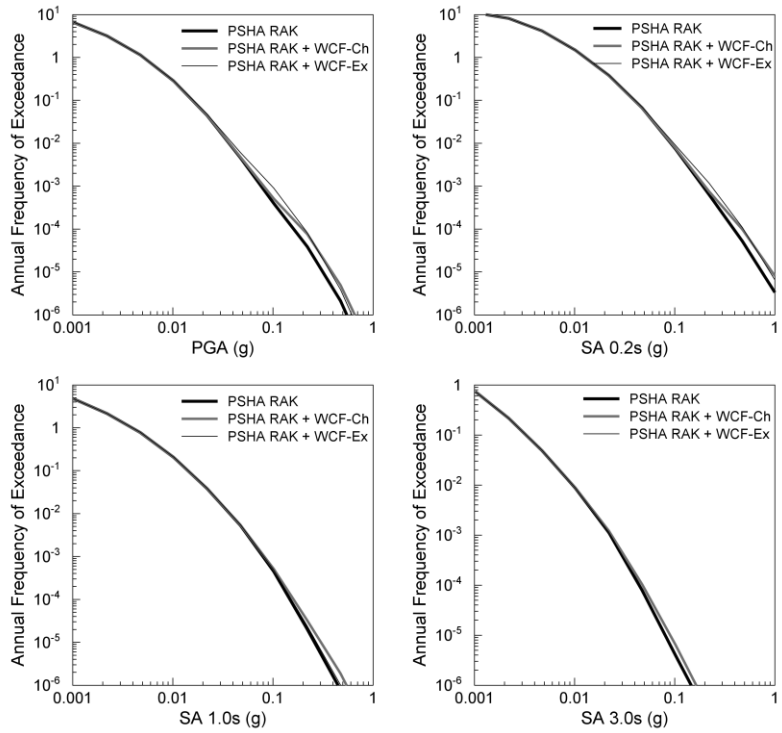

Figure 5.5. Hazard curves for the city of Ra's Al Khaymah for PGA and SA at 0.2, 1.0 and 3.0 s response periods. PSHA RAK is the hazard curve from the case study for Ra's Al Khaymah; PSHA RAK + WCF-Ch is the hazard curve considering a characteristic behaviour of the WCF; and PSHA RAK + WCF-Ex is the hazard curve considering an exponential behaviour of the WCF.

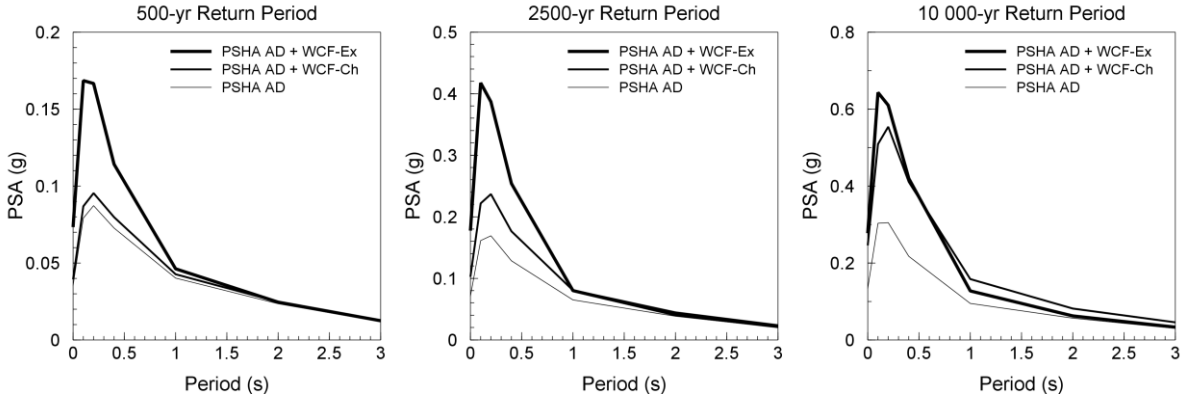

Figure 5.6. Uniform hazard spectra for the city of Abu Dhabi for the PSHA of the UAE (PSHA AD), PSHA of the city of Abu Dhabi plus the WCF using the purely characteristic model (PSHA AD + WCF-Ch) and exponential model (PSHA AD + WCF-Ex) at different return periods.

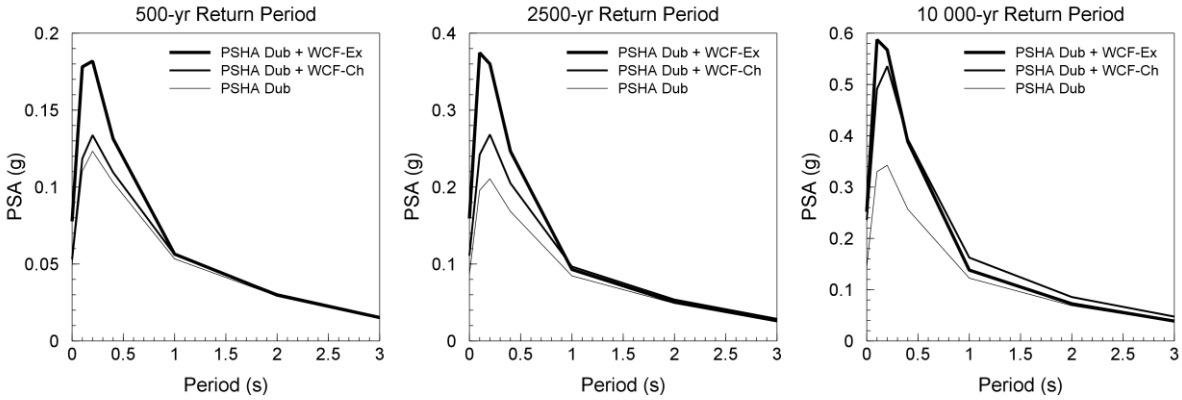

Figure 5.7. Uniform hazard spectra for the city of Dubai for the PSHA of the UAE (PSHA Dub), PSHA of the city of Dubai plus the WCF using the purely characteristic model (PSHA Dub + WCF-Ch) and exponential model (PSHA Dub + WCF-Ex) at different return periods.

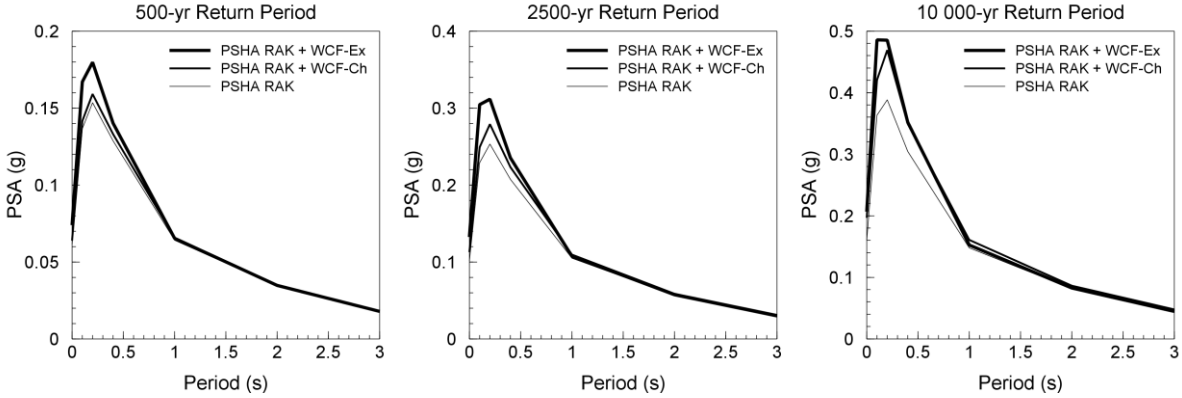

Figure 5.8. Uniform hazard spectra for the city of Ra's Al Khaymah for the PSHA of the UAE (PSHA RAK), PSHA of the city of Ra's Al Khaymah plus the WCF using the purely characteristic model (PSHA RAK + WCF-Ch) and exponential model (PSHA RAK + WCF-Ex) at different return periods.

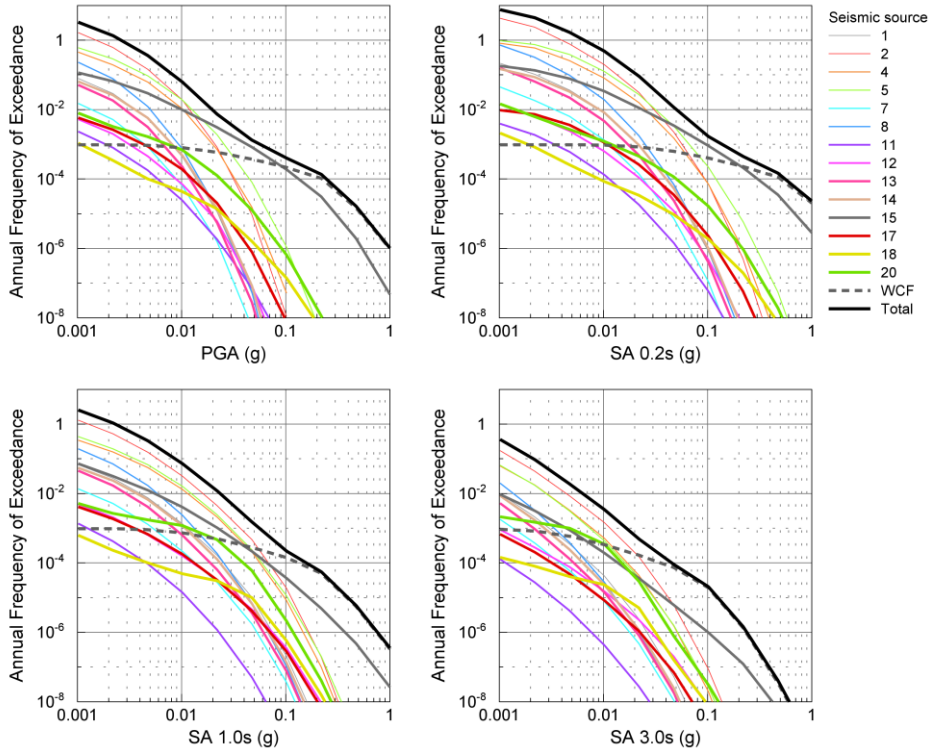

Figure 5.9. Disaggregated results by seismic source for the city of Abu Dhabi, using the purely characteristic model and the maximum credible slip rate (0.4 mm/yr). The dashed line is the contribution from the WCF and the black solid line is the total hazard curve. See table 3.7 for identification of the other sources.

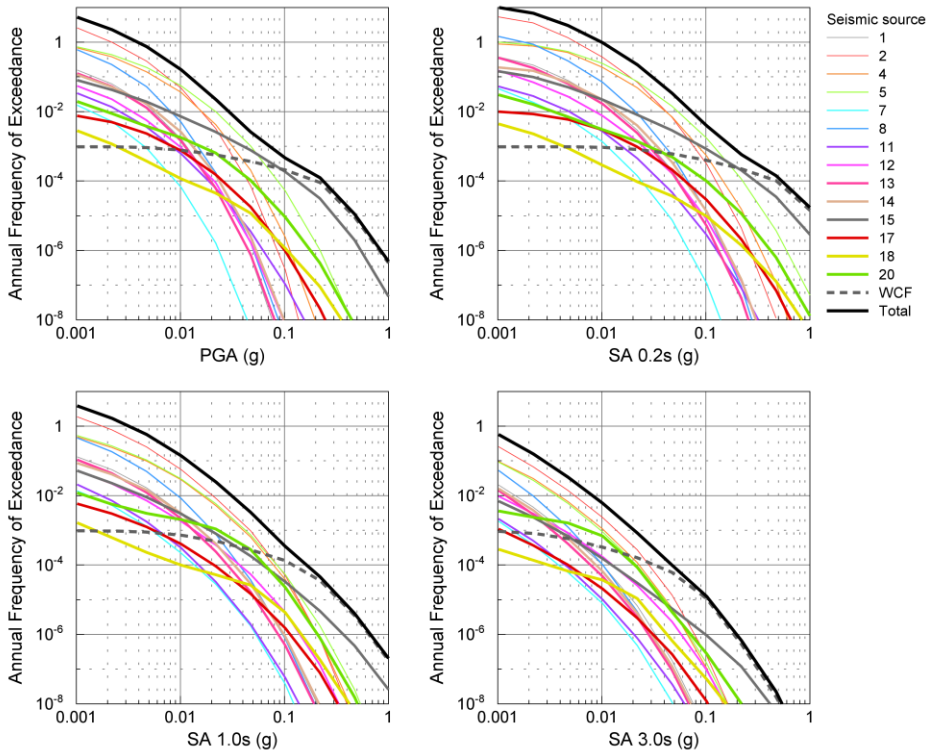

Figure 5.10. Disaggregated results by seismic source for the city of Dubai, using the purely characteristic model and the maximum credible slip rate (0.4 mm/yr). The dashed line is the contribution from the WCF and the black solid line is the total hazard curve. See table 3.7 for identification of the other sources.

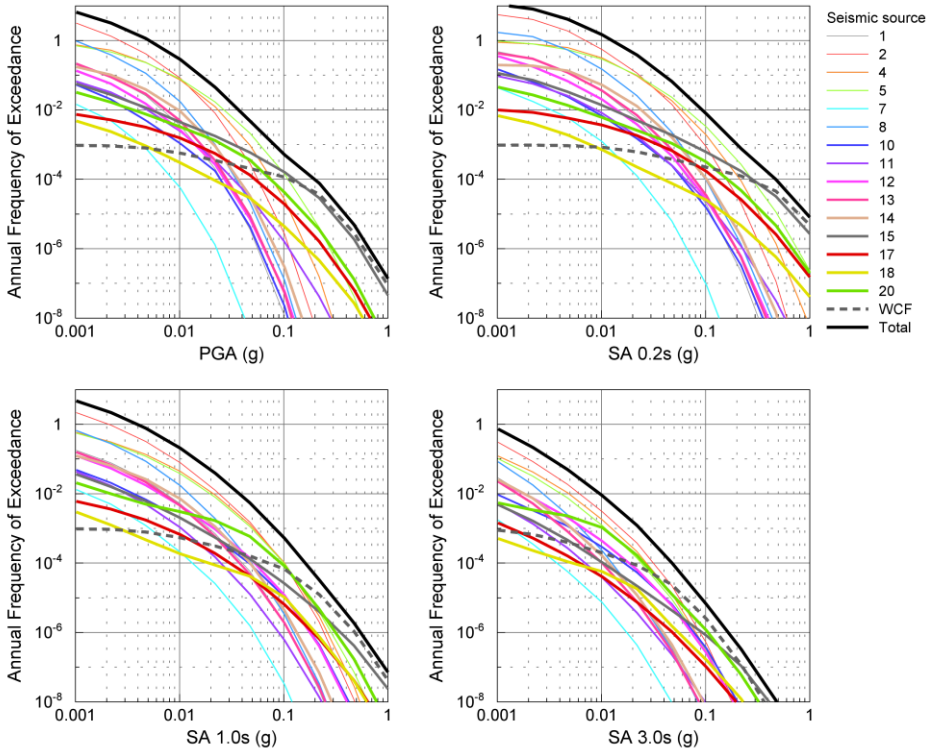

Figure 5.11. Disaggregated results by seismic source for the city of Ra's Al Khaymah, using the purely characteristic model and the maximum credible slip rate (0.4 mm/yr). The dashed line is the contribution from the WCF and the black solid line is the total hazard curve. See table 3.7 for identification of the other sources.

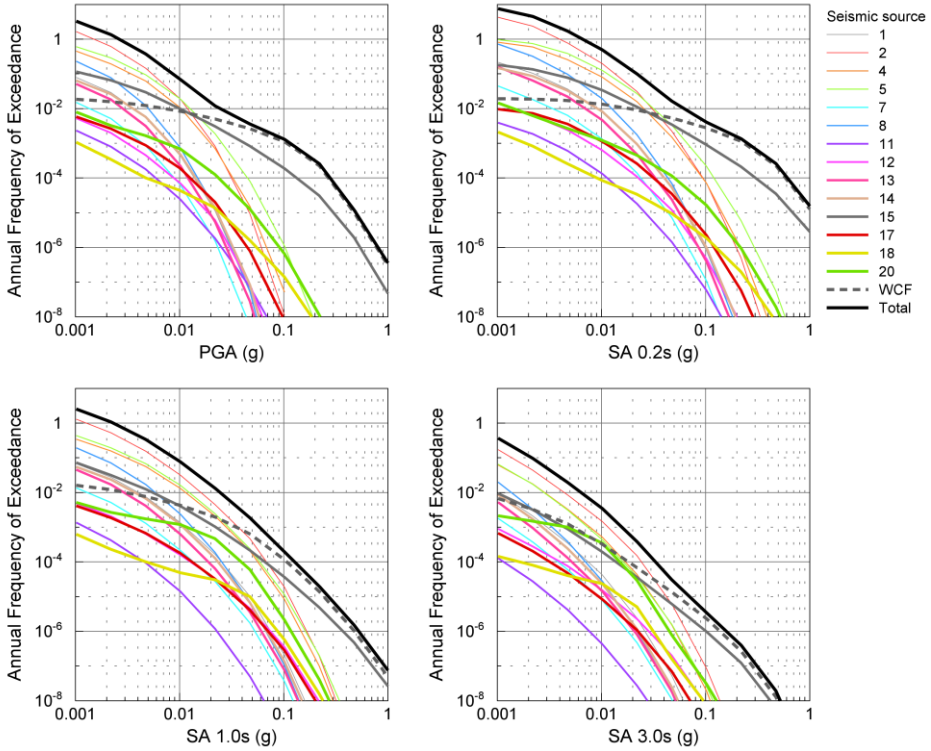

Figure 5.12. Disaggregated results by seismic source for the city of Abu Dhabi, using the exponential model and the maximum credible slip rate (0.4 mm/yr). The dashed line is the contribution from the WCF and the black solid line is the total hazard curve. See table 3.7 for identification of the other sources.

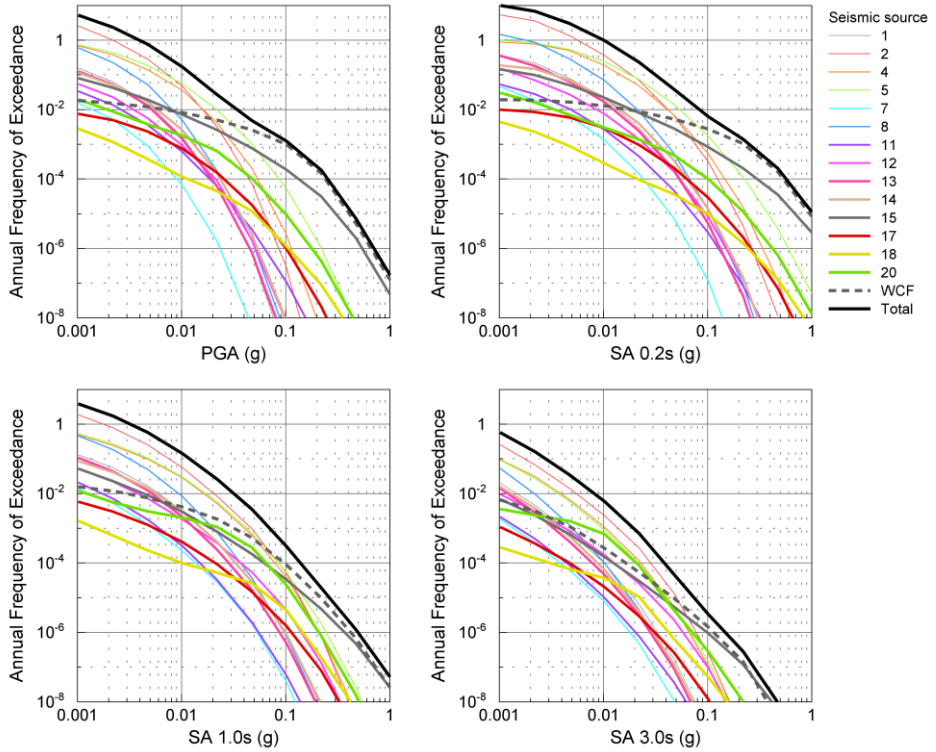

Figure 5.13. Disaggregated results by seismic source for the city of Dubai, using the exponential model and the maximum credible slip rate (0.4 mm/yr). The dashed line is the contribution from the WCF and the black solid line is the total hazard curve. See table 3.7 for identification of the other sources.

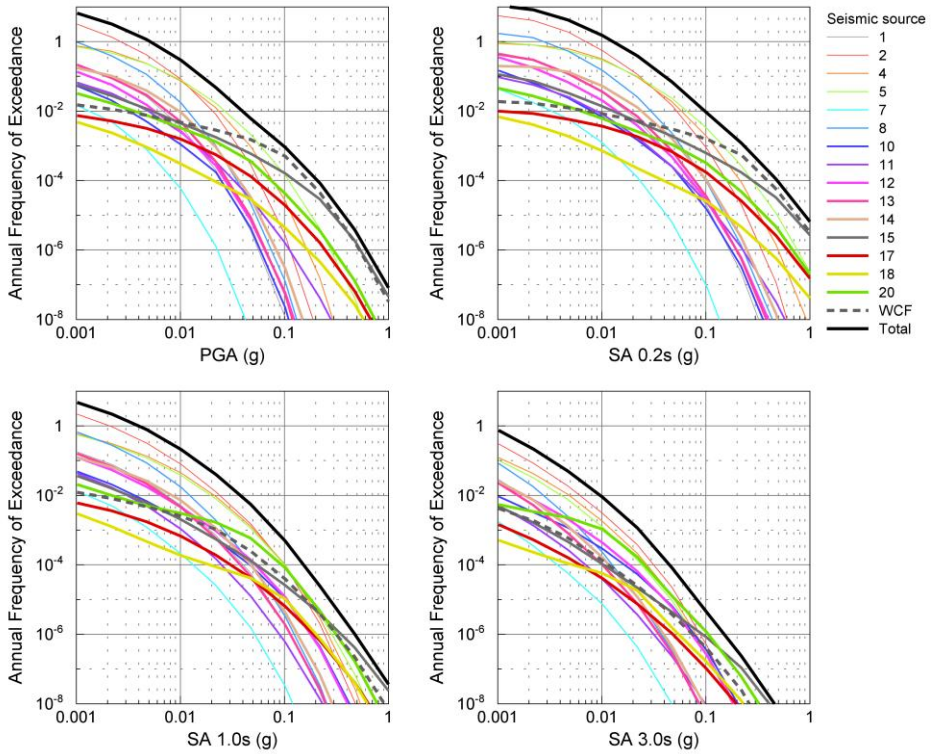

Figure 5.14. Disaggregated results by seismic source for the city of Ra's Al Khaymah, using the exponential model and the maximum credible slip rate (0.4 mm/yr). The dashed line is the contribution from the WCF and the black solid line is the total hazard curve. See table 3.7 for identification of the other sources.

To obtain UHS that match the UBC97 response spectra for zone 1, slip rates of 0.5 mm/yr and 2.5 mm/yr were required for the exponential and purely characteristic models, respectively. The UBC97 response spectra for zone 1 and the UHS for both magnitude-frequency models are shown in Figure 5.15.

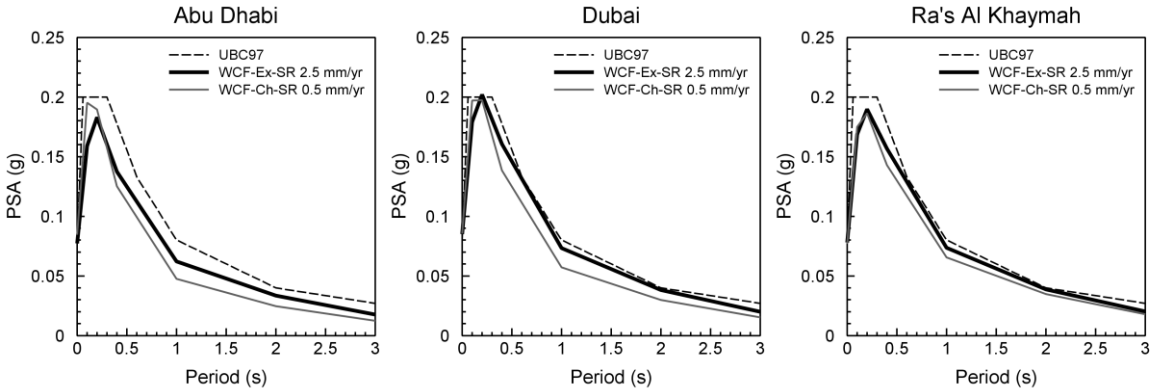

Figure 5.15. Comparison of the UBC97 response spectra for zone 1 (rock site conditions) and the uniform hazard spectra of the three sites for slip rates (SR) of 0.5 mm/yr and 2.5 mm/yr for the exponential (Ex) and purely characteristic models (Ch), respectively.

The slip rates required to match the PGA values reported by Sigbjornsson & Elnashai (2006) for the city of Dubai, for a return period of 475 years, are 2.4 mm/yr and 6.0 mm/yr for the exponential and the purely characteristic models, respectively. Table 5.2 summarises the PGA values presented by Sigbjornsson & Elnashai (2006) at different return periods and those obtained in this study for both magnitude-frequency models.

Table 5.2. Summary of PGA values for the city of Dubai at different return periods. S&E06 – Sigbjornsson & Elnashai (2006); Exp. Mod. – Exponential model for a slip rate of 2.4 mm/yr; Char. Mod. – Purely characteristic model for a slip rate of 6.0 mm/yr.

Return period	PGA (g)		
	S&E06	Exp. Mod.	Char. Mod.
475 yr	0.16	0.16	0.16
975 yr	0.18	0.21	0.25
2475 yr	0.22	0.26	0.33

Figure 5.16 presents the UHS of Sigbjornsson & Elnashai (2006) and the UHS obtained in this study for both magnitude-frequency models at return periods of 1000 years and 2500 years.

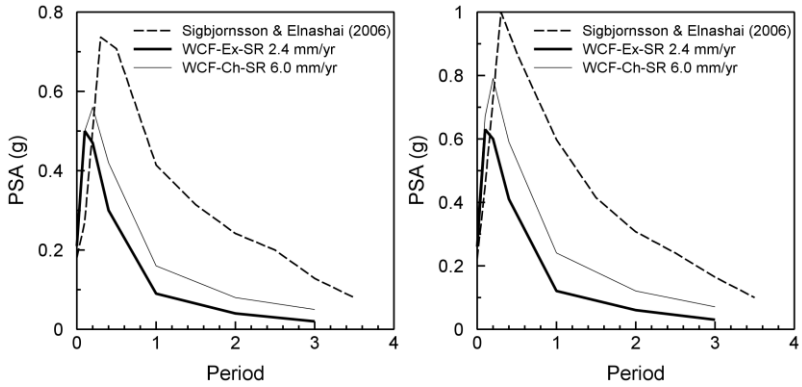

Figure 5.16. Comparison of the Sigbjornsson & Elnashai (2006) UHS for 975-year and 2475-year and the UHS for the slip rates of 2.4 mm/yr for the exponential model and 6.0 mm/yr for the purely characteristic model at 1000-year (left) and 2500-year (right) return periods.

5.1.7. Discussion and conclusions

From Figure 5.3 to Figure 5.5 it may be appreciated that the WCF has its largest influence on the city of Abu Dhabi and that the influence decreases as one moves north towards the city of Ra's Al Khaymah, where at long response periods (1.0 and 3.0 s), the influence is almost negligible.

The main difference between using the exponential model or the purely characteristic model is the annual frequencies of exceedance at which the WCF has influence on the hazard curve. For example, for PGA at the city of Dubai (Figure 5.4), the exponential model increases the hazard at annual frequencies of exceedance below 10^{-2}, while the characteristic model does it at annual frequencies of exceedance below 10^{-3}.

The increment to the seismic hazard for PGA and SA at 0.2 s, due to the activity of the WCF, is higher at the shortest return periods when an exponential behaviour of the fault is considered. For return periods above ~10,000 years the increment to the hazard for PGA and SA at 0.2 s is very

similar for both models (i.e., exponential and characteristic). On the other hand, the purely characteristic model has higher influence at longer response periods (i.e., 1.0 and 3.0 s) (see Figure 5.3 to Figure 5.5). This behaviour is better appreciated for the cities of Abu Dhabi and Dubai, while at the city of Ra's Al Khaymah the contribution to seismic hazard of the WCF is essentially negligible.

These differences in the hazard curves of the two magnitude-frequency models are clearly reflected in the UHS. In Figure 5.6 to Figure 5.8 it is clear that at 500-year and 2500-year return periods, the purely characteristic model has less influence on the UHS than the exponential model for response periods below 1 second at all sites. For the 10,000-year return period, the UHS for both models have similar values of SA, except at response periods above 1 second where the pure characteristic model gives slightly larger values of SA.

From Figure 5.9 to Figure 5.14 one may observe the hazard curve for the WCF and how it contributes to the total seismic hazard. The contribution of the WCF is certainly more important at the city of Abu Dhabi where the seismicity level is very low and where a close seismic source, albeit with low seismic activity, would have an important impact on the calculated seismic hazard. On the other hand, at Ra's Al Khaymah, which is located nearer to seismic sources with high seismic activity (i.e. Zagros and Makran), the presence of a seismic source of low seismic activity near to the site will not have such a significant impact upon the hazard.

The validity of the results is always dependent on the assumptions made in order to arrive at these results. As can be observed from the results presented herein, modelling the seismic activity of the WCF as having either an exponential or a purely characteristic distribution leads to significantly different results.

The assumption of a purely characteristic distribution in the seismic activity of the WCF, with a slip rate of 0.4 mm/yr, requires the acceptance that earthquakes with magnitude < 5.7 M_s do not take place on the WCF. Events above this level, with characteristic magnitude ~6.3 M_s, would have recurrence intervals of about 1040 years (see Figure 5.2). This situation agrees with the data currently available, assuming that earthquakes of medium to large magnitude have occurred in the past, prior to the period of complete observation of the earthquake catalogue, and will continue to occur in the future.

On the other hand, the assumption of an exponential distribution for the seismic activity of the WCF, with the same slip rate of 0.4 mm/yr, implies that earthquakes of magnitude ≥ 4.0 M_s occur, on average, every 52 years (Figure 5.2). Although, in theory, it is possible that the last 40 years (the period of completeness of the earthquake catalogue for events ≥ 4.0 M_s) has coincided with a period of quiescence for events on the WCF, this seems highly unlikely.

It is necessary to consider that the truncation of the exponential model at M_s = 4.0 is just a matter of convenience for engineering purposes; whence, events below this magnitude must be expected to occur. By extrapolating the recurrence rate to lower magnitudes, events with magnitude ~ 3.0 M_s should occur on average every 5.8 years (for a non-cumulative magnitude-frequency distribution). Although events of such magnitude would probably be missed by the international seismic networks, it is probable that they would be felt by the increasing population in the region due to their proximity to the source.

Additionally, the recently installed seismic networks in the region have not reported any seismic activity along the west coast of the UAE. They commenced operation in June 2006 (Al Khatibi *et al.*, 2007). Given the above considerations, it is difficult to justify the use of the exponential distribution

to model the seismicity on the WCF, even for a slip rate as small as 0.4 mm/yr.

To obtain a UHS that matches the UBC97 spectrum for zone 1 and rock site conditions, it was necessary to adopt slip rates of 0.5 and 2.5 mm/yr for the exponential and the purely characteristic models, respectively (Figure 5.15).

A 0.5 mm/yr slip rate for the exponential model implies that earthquakes with $M_s \geq 4.0$ have a recurrence interval of 46.5 years and that the characteristic earthquake (M_s 6.3) of the purely characteristic model has a recurrence interval of 166 years. For the same reasons discussed earlier, modelling the WCF seismicity with an exponential distribution is probably inappropriate. However, given our lack of data it is still possible. Modelling the WCF seismicity as purely characteristic seems to be more realistic given the absence of small events near this source. It is worth noting the good agreement between the shape of the UBC97 response spectra and the UHS obtained in this work. It is also important to highlight, that these slip-rate levels in a 10 Ma-age fault would imply a cumulative displacement over this period of 5 km and 25 km for the exponential and purely characteristic models, respectively.

Finally, the slip rates required in order to obtain PGA values for a return period of 500 years similar to those presented by Sigbjornsson & Elnashai (2006) were 2.4 mm/yr for the exponential model and 6.0 mm/yr for the purely characteristic model. These slip rates imply recurrence intervals of 8.7 years for events ≥ 4.0 M_s for the exponential model and 69 years for the characteristic earthquake (M_s 6.3) when the purely characteristic distribution is considered. Based on the periods of completeness of the earthquake catalogue for events ≥ 4.0 M_s (40 years) and events ≥ 5.0 M_s (82 years) it is difficult to justify these slip rates as being credible levels for either of the magnitude-frequency distributions.

Additionally, the cumulative displacements for the WCF at these slip rates would be 25 km and 60 km for the exponential and purely characteristic models respectively. These levels of displacement would surely be reflected on Brown's (1972) tectonic map.

It is also worth noting the appreciable difference in shape between the UHS obtained in this study and those presented by Sigbjornsson & Elnashai (2006). Despite the PGA values being very similar, the SA values of Sigbjornsson & Elnashai's (2006) UHS are much larger. These differences could be due to differences between the site conditions considered by Sigbjornsson & Elnashai (2006) and those considered in the present work. However, as the information presented in the Sigbjornsson & Elnashai's (2006) paper is limited, any reason to justify the differences between both UHS are merely speculations.

In conclusion, from two magnitude-frequency distributions considered to model the seismicity of the WCF, the purely characteristic model seems to have a better agreement with the information currently available. The use of the exponential model is difficult to support given the lack of small events in the recent years that would be required to validate the model, even for slip rates as small as 0.4 mm/yr.

Considering a fault running along the west coast of the UAE (WCF) using a characteristic earthquake model with long recurrence intervals that concurs with data available at date, do not induce any significant increment in the seismic hazard at short return periods. However, its influence increases with the return period, mainly at response periods below 1.0 s. This effect becomes of significance at return periods above 10,000 years. This could be of high importance as structures that require these levels of seismic safety such as nuclear power plants, which are being planned to be built in the UAE (BBC-News, 2008).

At the light of the results presented herein, the UBC97 seismic zone classification for the cities of Abu Dhabi and Ra's Al Khaymah remain zone 0 and zone 1, respectively, as in the original PSHA for the UAE (Chapter 3). Only the city of Dubai will pass from zone 0 to zone 1 if the boundary between these zones is set at 0.05 g. The UBC97 does not define the boundary between different seismic zones, but it is common practice to take the middle point between the PGA values assigned to each seismic zone and 0.05 g as the limit between zone 0 and zone 1.

The slip rates required to match the UBC97 spectrum for zone 1 corresponds to a level of accumulated displacements along the fault of about 25 km for the purely characteristic model. This level of displacement would be reflected on the structural curves of the Tertiary rocks on Brown's (1972) map. In the case of the slip rates required to match the PGA values for a 475-year return period reported by Sigbjornsson & Elnashai (2006), the accumulated displacement along the WCF would reach values up to 60 km and the seismic activity required, even when using the purely characteristic model, would imply that at least some seismic activity should have been observed during recent times.

Despite the fact that the contribution to the hazard of a low-activity fault running along the west coast of the UAE is relatively low, studies to prove the existence of such structure and to estimate its seismicity level are recommended.

This study has not considered site or directivity effects, which could amplify the ground motions significantly.

5.2. Minimum magnitude (m_{min})

The choice of the minimum magnitude (m_{min}) that should be considered for the hazard analysis is a decision that an analyst must take

when performing PSHA. Events of magnitude below m_{min} are considered so small that they should not produce damage to engineered structures. In the case study presented in this thesis (Chapter 3) a minimum magnitude of 4.0 M_s (~4.9 M_w) was chosen.

In order to evaluate how the, in some ways arbitrary or subjective, selection of m_{min} used for the hazard analysis affects the resulting hazard curves and the disaggregated results, a sensitivity analysis using different values of m_{min} was carried out. The results of this analysis are shown and discussed in this section.

Since the aim of the sensitivity analysis is to assess the influence on the resulting hazard curves due to the consideration of different levels of m_{min} on the integration process, only one branch of the logic tree from the case study was analysed. The selected branch is that with the highest weights (best-estimate branch, see Figure 3.38 or alternatively Figure 5.55 for a clearer presentation of the best estimate branch). For the epistemic uncertainty in the Makran Interplate source, where the west and east segmented ruptures have the same weight, the west option was preferred as the east halve does not contribute to the hazard at the studied sites. Atkinson & Boore's (2006) equation was selected to model ground motion from earthquakes in the Stable craton, Boore & Atkinson's (2006) equation for shallow earthquakes in active regions and Atkinson & Boore's (2003) equation for earthquakes in subduction zones.

Two approaches were considered to perform the sensitivity analysis. In the first approach, m_{min} was set at values of 3.5, 4.0 (value used for the case study), 4.5 and 5.0 M_s for all the seismic sources. In the second approach, different m_{min} were assigned to each seismic source, giving lower values of m_{min} to those closer to the sites and increasing it as the sources become more distant. For the second approach two different sets of m_{min} were studied (Table 5.3). In both approaches and for all the seismic sources the

values of β and m_{max} remained the same as in the case study and are assumed independent of the m_{min} selected for the integration of the hazard.

The first approach represents the common practice of considering the same m_{min} for all the seismic sources, independent of the distance between the seismic source and the site. The second approach represents a more logical approach, where small earthquakes occurring at distant seismic sources are expected not to produce ground-motion levels of engineering significance. Usually these scenarios, of small earthquakes at very long distances, can only contribute to the seismic hazard if the scenario is associated with very high epsilon values. For these small events, while the amplitudes can be high, the energy is low.

Table 5.3 presents both sets of values of m_{min} considered for each seismic source. A map of the seismic sources with the values of m_{min} for Set 1 is presented in Figure 5.17 showing the spatial distribution of m_{min}. The spatial distribution for the Set 2 is the same as Set 1 with exception of seismic sources 3 and 16, for which a m_{min} of 5.5 M_s was kept as their maximum magnitudes are 5.8 and 6.0 M_s, respectively.

The hazard curves for the different levels of m_{min} of the first approach are shown in Figure 5.18. The hazard curves are shown for the city of Dubai in terms of PGA and SA for periods of 0.2, 1.0 and 3.0 s.

In Figure 5.19 a comparison is shown of the results from the first and second approaches. From the first approach only the hazard curves corresponding to the values of m_{min} 4.0 and 4.5 M_s are presented; these correspond to the values of m_{min} for the stable craton in Set 1 and Set 2 of the second approach, respectively.

Table 5.3. Values of m_{min} for each seismic zone considered for the two sets of values in the second approach. Magnitudes are in M_s scale.

Source number	Source name	Set 1				Set 2			
		4.0	4.5	5.0	5.5	4.5	5.0	5.5	6.0
1	High Zagros thrust belt				x				x
2	Simple Fold belt			x				x	
3	Dezful Embayment				x			x	
4	Zagros Foredeep		x				x		
5	Persian Gulf I		x				x		
6	Kazerum fault				x				x
7	Borazjan Fault				x				x
8	Aliabad zone				x				x
9	Nek south fault				x				x
10	Gow fault zone				x				x
11	Makran Intraplate				x				x
12	Makran Background				x				x
13	Jorift-Sabzevaran fault				x				x
14	Minab-Zendan fault			x				x	
15	Stable craton I	x				x			
16	Owen fracture zone				x			x	
17	Oman mountains		x				x		
18	Makran Interplate				x				x
19	Makran Interplate East				x				x
20	Makran Interplate West				x				x

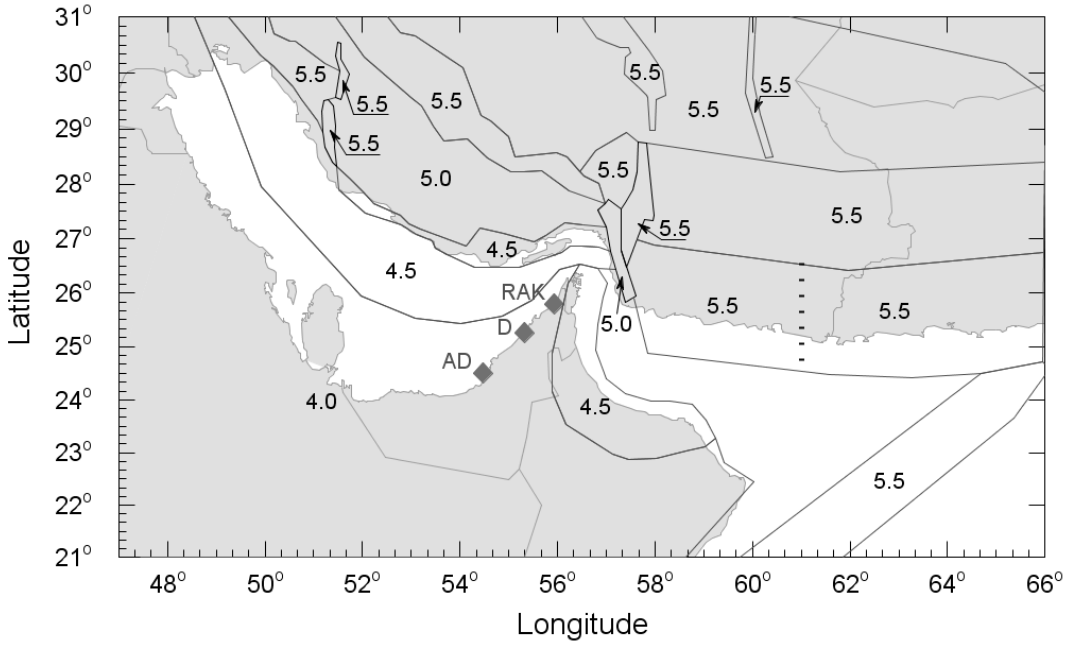

Figure 5.17. Map of the seismic sources with the values of m_{min} considered for Set 1 of the second approach. Diamonds represent the cities of Abu Dhabi (AD), Dubai (D) and Ra's Al Khaymah (RAK).

As can be seen from Figure 5.18 and Figure 5.19, regardless of the approach used, the selection of different values of m_{min} has the highest influence for the lower levels of ground motion. This influence is larger at response periods of about 0.2 s and decreases as the response period increases, becoming negligible at a response period of 3.0 s.

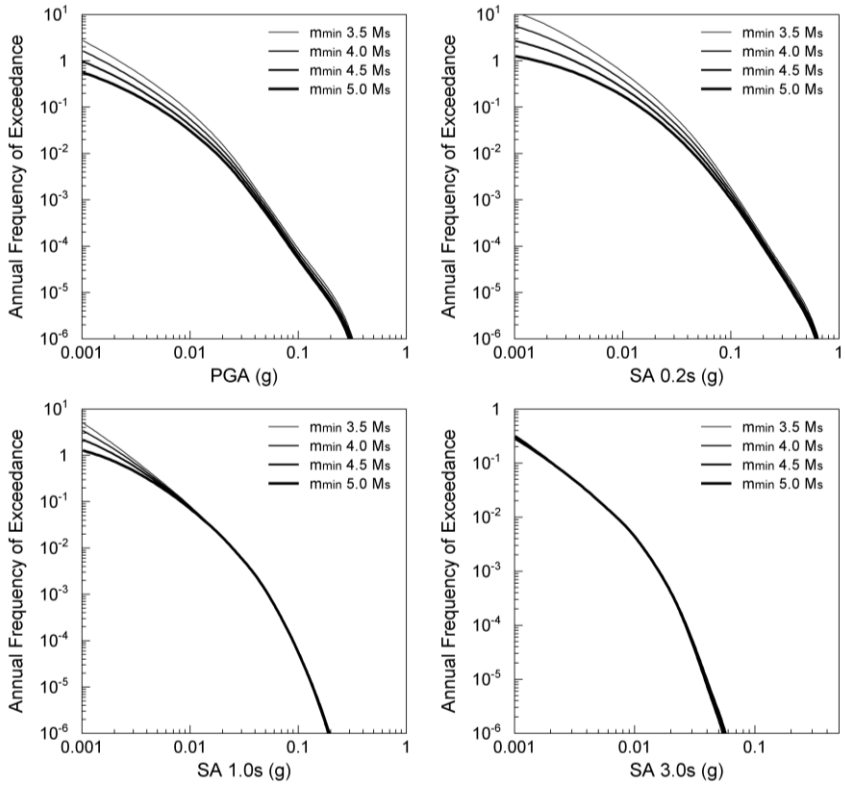

Figure 5.18. Hazard curves for the city of Dubai for different levels of m_{min}. m_{min} is the same at all the seismic sources. m_{min} 4.0 M_s corresponds to the minimum magnitude considered for the case study.

These differences are confirmed in Figure 5.20, which compares the uniform hazard spectra for a 500-year return period for the different m_{min} values of the two approaches. The UHS confirms that the main differences in the spectral amplitudes are at 0.2 s and 0.4 s response periods, and above 1 s response period the selection of m_{min} has no influence.

It is worth noting that exceedance frequencies increase as m_{min} decreases. This implies that a conservative assumption on the selected value of m_{min} would lead to an increase in the calculated seismic hazard,

particularly at the shorter response periods. On the other hand, a large value of m_{min} would lead to non-conservative exceedance frequencies.

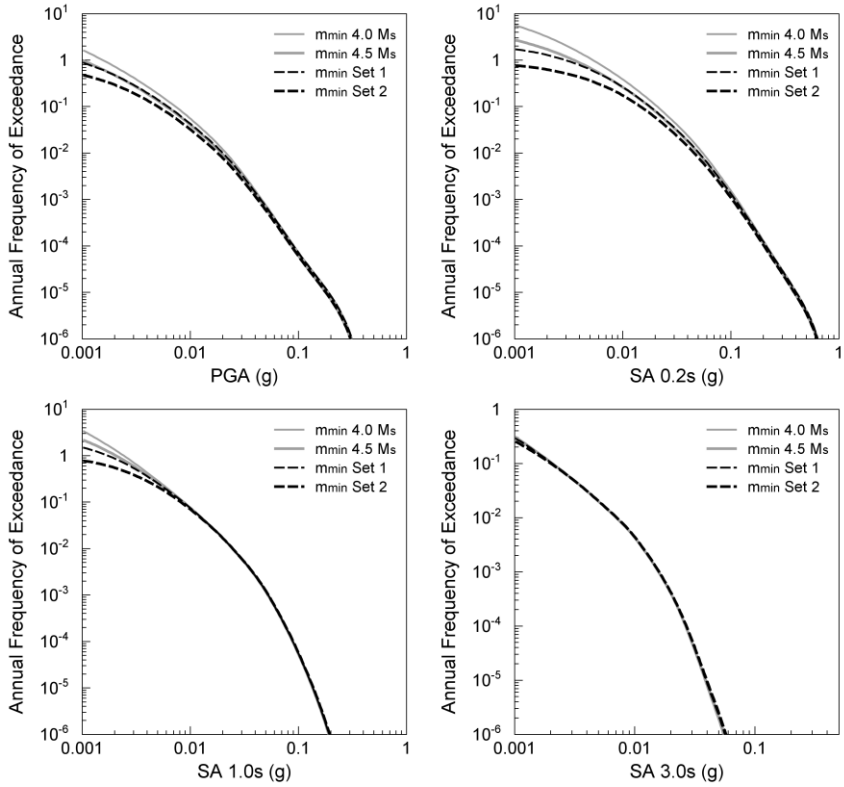

Figure 5.19. Comparison for the city of Dubai of the resulting hazard curves from the first approach for m_{min} of 4.0 and 4.5 M_S and both sets of values of m_{min} of the second approach.

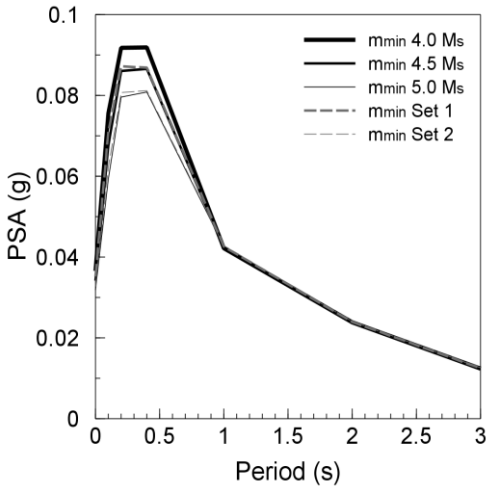

Figure 5.20. Comparison of the uniform hazard spectra for the city of Dubai for PGA at 500-year response period.

The difference between the hazard curves from both approaches can be better understood if we consider that, for the city of Dubai, the seismic sources that contribute the most to the hazard at short and medium response periods are the Persian Gulf and the Simple fold belt, respectively, while the Stable craton is the dominant seismic source at longer return periods (see Figure 3.64). This situation is similar for the other two sites of the case study. Given this situation, the differences, for example, between m_{min} 4.0 M_s and m_{min} Set 1 are mainly due to the increment in the values of m_{min} for the Persian Gulf and the Simple fold belt from 4.0 to 4.5 M_s.

It is common practice to use a 475-year return period for seismic design of structures of normal occupancy. At this return period some difference in the spectral amplitudes should be expected as result of the selection of different values of m_{min} for natural frequencies below 1 s. However, for longer return periods the influence on the hazard of different levels on m_{min} is negligible.

These results cannot be taken as typical of analyses using different levels of m_{min} in the integration process. The seismic hazard in the UAE is a particular case, where ground-motion levels at short and medium return periods are dominated by seismic sources relatively far from the UAE, while local seismicity (i.e. the Stable craton) only dominates the hazard at very long return periods.

The disaggregated results by magnitude-distance scenarios for the city of Dubai for PGA and a 500-yr return period are shown in Figure 5.21. These results correspond to minimum magnitudes of 4.0 and 4.5 M_s using the first approach and both sets of m_{min} from the second approach. In all cases, although some differences can be noticed, the dominant magnitude-distance scenario remains essentially the same.

In conclusion, the selection of the minimum magnitude at which the integration of the hazard commences, for the particular case of the UAE, has

a small, almost negligible, influence on the ground-motion levels at the return periods that normally govern seismic design (475-yr return period and above). However, as was previously mentioned, a conservative value of m_{min} could lead to an unrealistic increase in the exceedance frequencies, particularly at lower response periods.

The two approaches presented here were selected according to the characteristics and limitations of the software used to estimate the hazard (Crisis2007 - Ordaz *et al.*, 2007). Alternative approaches to the truncation of the integration of the hazard process at a fixed value of m_{min} will be discussed in the following sections.

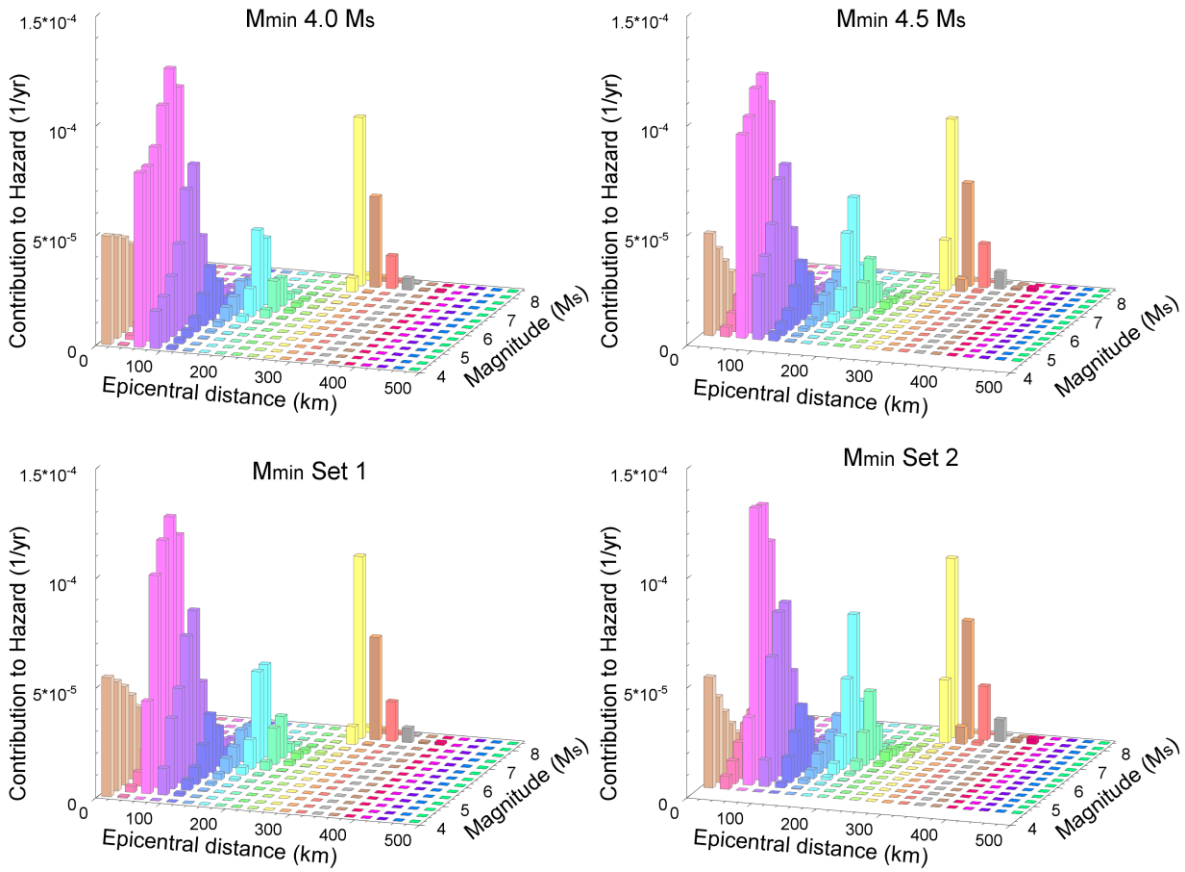

Figure 5.21. Disaggregated results for the city of Dubai for PGA and a 500yr return period. Minimum magnitudes of 4.0 M_s, 4.5 M_s, and for Set 1 and Set 2 are shown.

5.3. Alternatives to m_{min}: CAV

The use of earthquake magnitude as the lower bound in the hazard integration process is not necessarily the most effective way to distinguish between damaging and non-damaging earthquake scenarios.

As mentioned in the previous section, in traditional PSHA, a minimum magnitude (m_{min}) is set as the lower bound for the hazard integration process. All events with magnitude below m_{min} are considered as not capable of producing ground-motion levels that are potentially damaging to engineered structures, regardless of the proximity of the event to the site or of any other characteristic of the event.

A conservative low value of m_{min} will lead to an unrealistic estimate of the seismic hazard (not as far as the ground motions are concerned, but as far as the basic assumptions of the method are concerned). This is due to the incorporation of small-magnitude events at long source-to-site distances in the hazard calculations that are not likely to produce damage to engineered structures. Nevertheless, these events will still contribute to the hazard due to the mechanics of PSHA.

Many other parameters rather than earthquake magnitude have been recognised as good predictors of damage (e.g. Cabañas *et al.*, 1997; Hancock & Bommer, 2006; Reed *et al.*, 1988). In a recent study, sponsored by the Electric Power Research Institute (EPRI), the use of the cumulative absolute velocity (CAV), as defined by O'Hara & Jacobson (1991) (see section 2.3.1), is proposed as an alternative for distinguishing which scenarios should be included in the integration process (Hardy *et al.*, 2006).

Based on the findings of O'Hara & Jacobson (1991), Hardy *et al.* (2006) proposed to use a CAV value of 0.16 g-s as the lower bound to define potentially damaging earthquake scenarios (i.e., damaging scenarios which must generate ground motions that exceed CAV = 0.16 g-s). Re-writing the

hazard integral to include CAV as lower bound, the authors present the equation:

$$\gamma\left(SA > z, CAV > CAV_{\min}\right) = \sum_{i=1}^{N_{source}} \nu_i \int_{m_{\min}}^{m_{\max}} \int_{r=0}^{\infty} \int_{\varepsilon=-\infty}^{\infty} f_{mi}(M) f_{ri}(r) f_{\varepsilon}(\varepsilon) P\left(SA > z, CAV > CAV_{\min} \mid M, r, \varepsilon\right) dr dM d\varepsilon \quad 5.1$$

Here SA is the spectral acceleration, z is the target ground-motion level (in terms of spectral acceleration), ν_i is the rate of earthquakes with magnitude ≥ m_{min} for the i^{th} source, and $f_{mi}(M)$ and $f_{ri}(r)$ are the probability density functions for magnitude and distance, respectively.

The difference with respect to the original hazard integral (Equation 2.13) is that instead of the probability of SA > z for a given M and r, now it is the joint probability of SA > z and CAV > CAV_{min} for a given M and r.

Since some correlation is expected between the CAV and the SA, the authors decompose the joint probability by accounting for this dependence. Thus the joint probability can be expressed as:

$$P\left(SA > z, CAV > CAV_{\min} \mid M, r, \varepsilon\right) = P\left(SA > z \mid M, r, \varepsilon\right) P\left(CAV > CAV_{\min} \mid SA > z, M, r\right) \quad 5.2$$

Finally, incorporating Equation 5.2 into Equation 5.1 and explicitly integrating over the ground motion variability, Hardy *et al.* (2006) re-write the hazard integral as:

$$\gamma\left(SA > z, CAV > CAV_{\min}\right) = \sum_{i=1}^{N_{source}} \nu_i \int_{m_{\min}}^{m_{\max}} \int_{r=0}^{\infty} \int_{\varepsilon=-\infty}^{\infty} f_{mi}(M) f_{ri}(r) f_{\varepsilon}(\varepsilon) P\left(SA > z \mid M, r, \varepsilon\right) P\left(CAV > CAV_{\min} \mid SA\left(M, r, \varepsilon\right), M, r\right) dM dr d\varepsilon \quad 5.3$$

In Equation 5.3 the probability of CAV > CAV_{min} is dependent upon the values of SA, M and r. Therefore, Hardy *et al.* (2006) developed two empirical models for estimating CAV based on these parameters.

The first model is called the 2-step approach. In this model the authors first develop a model for CAV as function of the uniform duration (Dur_{uni}), PGA, moment magnitude and V_{s30} (step 1). Then, they model the dependence of the uniform duration on PGA, moment magnitude and V_{s30} (step 2). For the application of the overall approach, the uniform duration needs to be estimated first and then this is used to calculate CAV conditional upon the other parameters (including duration).

Hardy *et al.* (2006) estimate the uniform duration using the following equation:

$$Ln\left(Dur_{uni}\right) = a_1 + a_2 \ln\left(PGA\right) + \frac{a_3}{\ln\left(PGA\right) + a_4} + a_5\left(M_w - 6.5\right) + a_6\left(M_w - 6.5\right)^2 + a_7\left(\ln\left(V_{s30}\right) - 6\right) \quad 5.4$$

where Dur_{uni} is in units of seconds, a_1 to a_7 are the coefficients listed in Table 5.4, PGA is the peak ground acceleration in units of g, M_w is the moment magnitude and V_{s30} is the shear-wave velocity on the uppermost 30 m of the soil deposit given in units of m/s.

Table 5.4. Coefficients and standard deviation for the uniform duration model (Equation 5.4).

Coefficient	Estimate (standard error)
a_1	3.50 (0.05)
a_2	0.0714 (0.0421)
a_3	-4.19 (0.30)
a_4	4.28 (0.03)
a_5	0.733 (0.010)
a_6	-0.0871 (0.0105)
a_7	-0.355 (0.020)
σ_{lnDUR}	0.509

Subsequently, ln(CAV) can be calculated using the expression:

$$\ln(CAV) = \begin{cases} c_0 + c_1(M_w - 6.5) + c_2(M_w - 6.5)^2 + c_3 \ln(PGA) \\ +c_4(\ln(PGA))^2 + c_5(\ln(PGA))^3 + c_6(\ln(PGA))^4 \\ +c_7(\ln(V_{s30}) - 6) + c_8 \ln(Dur_{uni}) + c_9(\ln(Dur_{uni}))^2 \quad for \quad PGA \le 1g \\ \\ c_0 + c_1(M_w - 6.5) + c_2(M_w - 6.5)^2 + c_3 \ln(PGA) \\ +c_7(\ln(V_{s30}) - 6) + c_8 \ln(Dur_{uni}) + c_9(\ln(Dur_{uni}))^2 \quad for \quad PGA > 1g \end{cases} \quad 5.5$$

where CAV is in g-s units, Dur_{uni} is the uniform duration in seconds for PGA values above 0.025 g estimated from Equation 5.4, and c_0 to c_9 are the coefficients listed in Table 5.5.

Table 5.5. Coefficients for CAV model (Equation 5.5).

Coefficient	Estimate (standard error)
c_0	-1.75 (0.04)
c_1	0.0567 (0.0062)
c_2	-0.0417 (0.0043)
c_3	0.0737 (0.10)
c_4	-0.481 (0.096)
c_5	-0.242 (0.036)
c_6	-0.0316 (0.0046)
c_7	-0.00936 (0.00833)
c_8	0.782 (0.006)
c_9	0.0343 (0.0013)

The standard deviation of the ln(CAV) model (Equation 5.5) is given by:

$$\sigma_{\ln CAV_1} = \begin{cases} 0.37 & for \quad Dur_{uni} < 0.2 \\ 0.37 - 0.090(\ln(Dur_{uni}) - \ln(0.2)) & for \quad 0.2 \le Dur_{uni} \le 4 \\ 0.10 & for \quad Dur_{uni} > 4 \end{cases} \quad 5.6$$

To apply the CAV model in a standard PSHA, the variability in the prediction of uniform duration ($\sigma_{\ln Dur}$) needs to be propagated into the variability of CAV. Hence, the total standard deviation of the ln(CAV) is given by:

$$\sigma_{\ln CAV} = \sqrt{\left(c_8 + 2c_9 \ln\left(\overline{Dur}_{uni}\right)\right)^2 \sigma^2_{\ln Dur} + \sigma^2_{\ln CAV_1}} \qquad 5.7$$

where c_8 and c_9 are given in Table 5.5, $\ln\left(\overline{Dur}_{uni}\right)$ is the median duration obtained from Equation 5.4, and $\sigma_{\ln Dur}$ and $\sigma_{\ln CAV_1}$ are the standard deviations associated with the estimation of $\ln(Dur_{uni})$ and $\ln(CAV)$, respectively.

The second model is called the 1-step approach. This is a simplified version of the 2-step approach where Hardy *et al.* (2006) derive a model for CAV without going through the ground-motion duration. This model is given by:

$$\ln(CAV) = d_1 + d_2\left(\ln(PGA) + 2.5\right) + \frac{d_3}{\ln(PGA) + d_4} + d_5\left(M_w - 6.5\right) + d_6\left(M_w - 6.5\right)^2 + d_7\left(\ln(V_{s30}) - 6\right) \qquad 5.8$$

The coefficients d_1 to d_7 are given in Table 5.6, and the standard deviation is 0.46 in natural log units.

Table 5.6. Coefficients for the 1-step CAV model (Equation 5.8).

Coefficient	Estimate (standard error)
d_1	-0.405 (0.11)
d_2	0.509 (0.036)
d_3	-2.11 (0.24)
d_4	4.25 (0.05)
d_5	0.667 (0.009)
d_6	-0.0947 (0.009)
d_7	-0.266 (0.023)

Irrespective of which of the two methods is used to calculate CAV, the probability of exceeding a CAV value of 0.16 g-s is given by:

$$P\left(CAV > 0.16 \mid PGA, M_w, V_{s30}\right) = \begin{cases} 1 - \Phi\left(\varepsilon^*_{CAV}\right) & for \quad PGA \geq 0.025g \\ 0 & for \quad PGA < 0.025g \end{cases} \quad 5.9$$

where Φ is the cumulative normal distribution and ε^*_{CAV} is the number of standard deviations in the CAV model that will produce 0.16 g-s. That is:

$$\varepsilon^*_{CAV} = \frac{\ln(0.16) - \ln CAV\left(PGA, M_w, V_{s30}, Dur\left(PGA, M_w, V_{s30}\right)\right)}{\sigma_{\ln CAV}} \quad 5.10$$

In the two models developed by Hardy *et al.* (2006) CAV is function of PGA but not of SA. In order to be able to calculate exceedance probabilities of CAV(0.16) as function of spectral acceleration values, Hardy *et al.* (2006) propose to use a linear correlation between the normalized residuals of PGA and SA from ground-motion prediction equations, expressed as:

$$\varepsilon_{SA}(f) = b_1(f)\,\varepsilon_{PGA} \quad 5.11$$

where b_1 is a coefficient depending on the frequency of the spectral acceleration and the tectonic regime (Table 5.7), ε_{PGA} is the epsilon value of PGA and $\varepsilon_{SA}(f)$ is the epsilon value of spectral acceleration at frequency *f*.

The coefficients presented in Table 5.7 take into account the differences on the spectral shape between earthquakes in the eastern (EUS) and western (WUS) United States.

Table 5.7. Coefficients for the correlation between $\varepsilon_{SA}(f)$ and ε_{PGA}.

	WUS	**EUS**
Frequency (Hz)	**b_1**	**b_1**
0.5	0.590	0.50
1.0	0.590	0.55
2.5	0.600	0.60
5.0	0.633	0.75
10	0.787	0.88
20	0.931	0.90
25	0.956	0.91
35	0.976	0.93

If one wishes to filter the results from a standard PSHA by removing non-damaging earthquakes according to the CAV filter (events producing values of CAV ≤ 0.16 g-s), Hardy *et al.* (2006) propose the following methodology.

First, the disaggregated results need to be broken down into rates of occurrence of spectral acceleration over small acceleration ranges for specific ranges of magnitude and distance:

$$\begin{aligned}&\gamma\left(z_k < SA(T)_{Rock} < z_{k+1}, M_i < M < M_{i+1}, R_j < R < R_{j+1}\right) = \\ &\gamma\left(SA(T)_{Rock} > z_k\right) Disagg\left(M_i < M < M_{i+1}, R_j < R < R_{j+1}, z_k\right) \\ &-\gamma\left(SA(T)_{Rock} > z_{k+1}\right) Disagg\left(M_i < M < M_{i+1}, R_j < R < R_{j+1}, z_{k+1}\right)\end{aligned} \qquad 5.12$$

Then, the epsilon for the given SA(T) is calculated for each magnitude and distance scenario. With this information and Equation 5.9 the probability that CAV(0.16) will be exceeded is estimated for each scenario. This probability is then multiplied by the rate of occurrence of spectral acceleration of the scenario. Finally, the filtered rates of all scenarios are summed up to obtain the CAV-filtered hazard curve.

Defining the CAV-filtered hazard curve as ν', it can be expressed as:

$$\begin{aligned}\gamma'\left(SA(T)_{Rock} > z_n\right) = \sum_{i=1}^{N_m}\sum_{j=1}^{N_r}\sum_{k=n}^{N_a} &\nu_{occur}\left(z_k, M_i, R_j\right) \\ &P\left(CAV > 0.16 \mid z_k, M_i, R_j\right)\end{aligned} \qquad 5.13$$

where $\gamma_{occur}\left(z_k, M_i, R_j\right)$ is the rate of occurrence obtained from Equation 5.12 and N_a is the number of considered discrete SA values.

The seismic hazard results from the case study (Chapter 3) were filtered using this procedure for a CAV value of 0.16 g-s. However, some considerations were required before implementing the filtering process.

The filtering of the hazard results, as proposed by Hardy *et al.* (2006), requires the estimation of the number of standard deviations (ε_{SA}) for a given

ground-motion model that will yield the target ground motion for each magnitude and distance combination considered in the disaggregation process. This value of ε_{SA} will vary depending on the ground-motion prediction equation used for the estimation, because the median and standard deviation of ln[SA(T)] vary among models. When the hazard analysis is carried out using a single ground-motion model, the filtering process is straightforward as a single equation can be used to estimate the value of ε_{SA}. However, when multiple GMPEs are used in the hazard analysis, the estimation of ε_{SA} from only one GMPE will not be appropriated for the other GMPEs in general.

As it is not possible to know how much of the total exceedance rate is contributed by each GMPE for the hazard results of the case study, there is no option other than to use a single GMPE to estimate ε_{SA}. This will introduce some error in the analysis as non-damaging earthquakes will be removed based only on the prediction equation selected for the calculation of ε_{SA}. However, these errors are likely to be relatively small in comparison to the overall effect of applying the CAV filter.

As mentioned in section 3.5, a total of 7 GMPEs were used in the case study hazard analysis, and at least two of these are used in any branch of the logic tree. With the aim of minimizing the error due to the estimation of ε_{SA}, the filtering was applied to the results at the end tips of the logic tree in the section of ground-motion prediction equations (see bottom section in Figure 3.38). In this way, and given that most of the small-magnitude earthquake scenarios (i.e., non-damaging events) that are expected to be removed by the CAV filter may occur at relatively near to the site, the GMPE used for the estimation of ε_{SA} was that assigned to the stable craton at each particular branch. After the filtering was applied to the hazard results at the end tips of the logic tree corresponding to the section of ground-motion prediction equations, the new total hazard results were calculated as the

weighted mean of the set of filtered results. For this, the same weights assigned to the logic-tree branches of the case study were considered (Figure 3.38).

The seismic hazard curves, before and after applying the filter to remove events with expected CAV values ≤ 0.16 g-s (CAV16), are presented in Figure 5.22 to Figure 5.24. These results are for the three sites for PGA and SA with response periods of 0.2, 1.0 and 3.0 s.

A comparison of the uniform hazard spectra for the three sites at 2500- and 10,000-year return periods is shown in Figure 5.25. It is worth noting that the spectral amplitudes of the UHS at 2500-year return period for the cities of Abu Dhabi and Dubai are equal to zero for all periods.

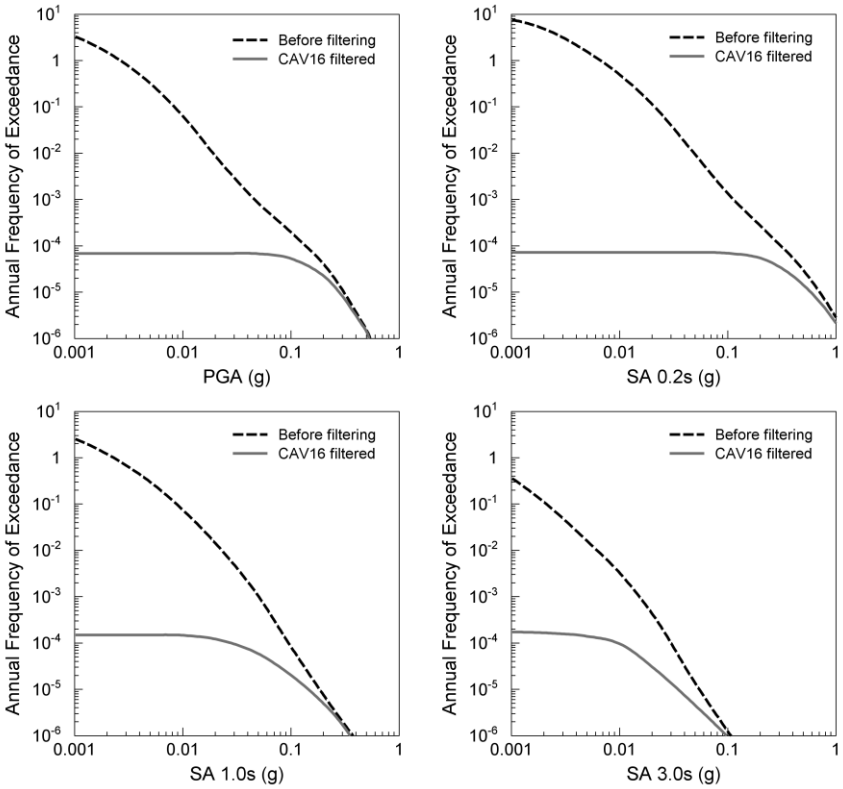

Figure 5.22. Comparison of the seismic hazard curves for the city of Abu Dhabi before and after the CAV16 filtering. The hazard curves are for PGA and SA at 0.2, 1.0 and 3.0 s response periods.

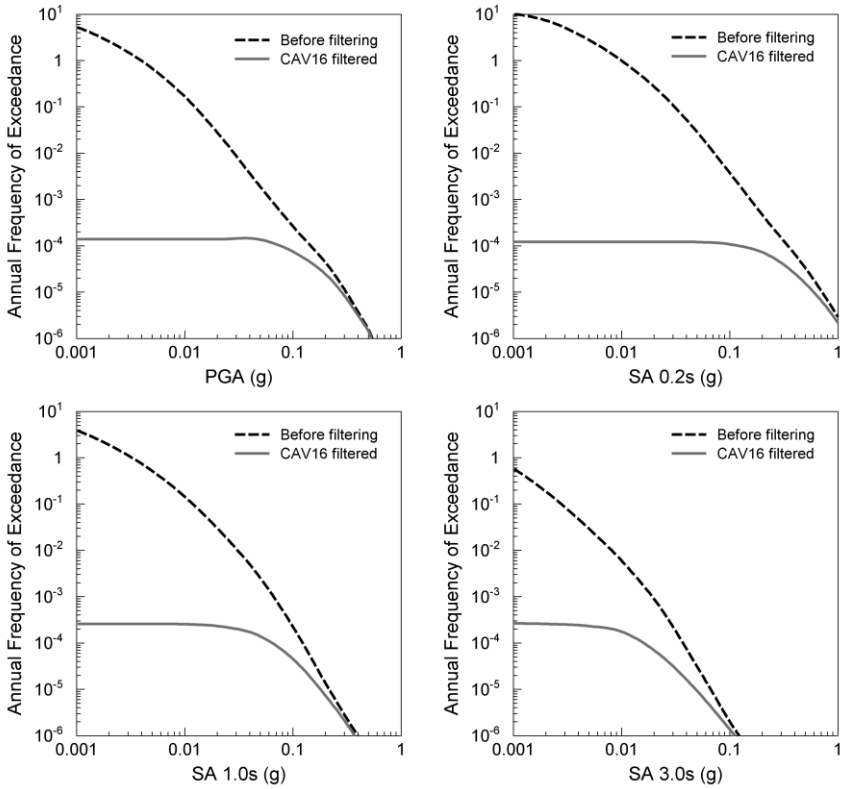

Figure 5.23. Seismic hazard curves for the city of Dubai before and after the CAV16 filtering. The hazard curves are for PGA and SA at 0.2, 1.0 and 3.0 s response periods.

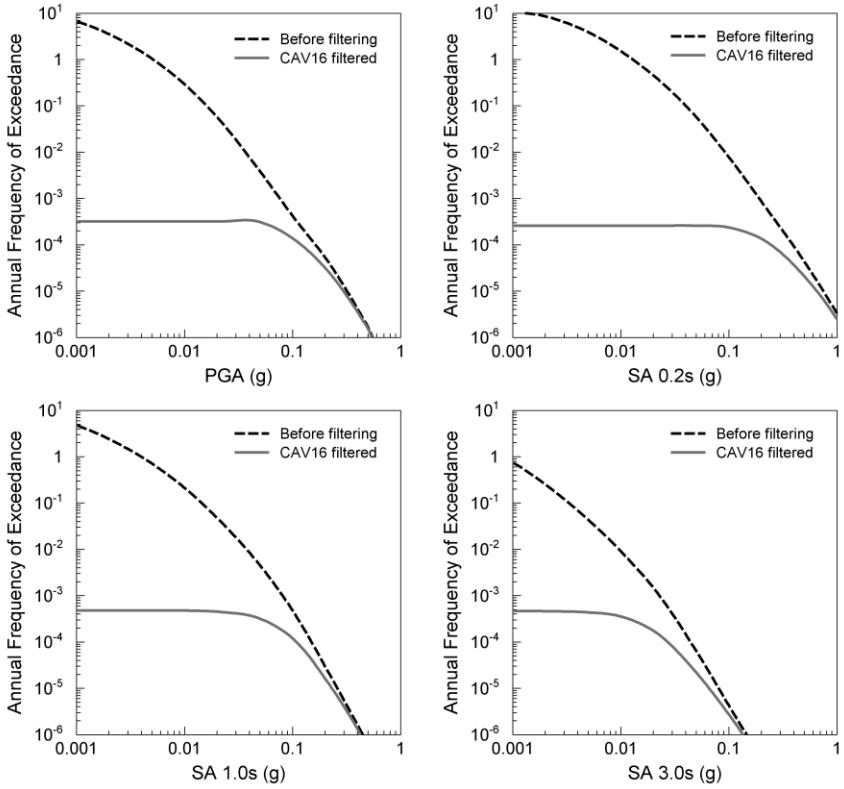

Figure 5.24. Seismic hazard curves for the city of Ra's Al Khaymah before and after the CAV16 filtering. The hazard curves are for PGA and SA at 0.2, 1.0 and 3.0 s response periods.

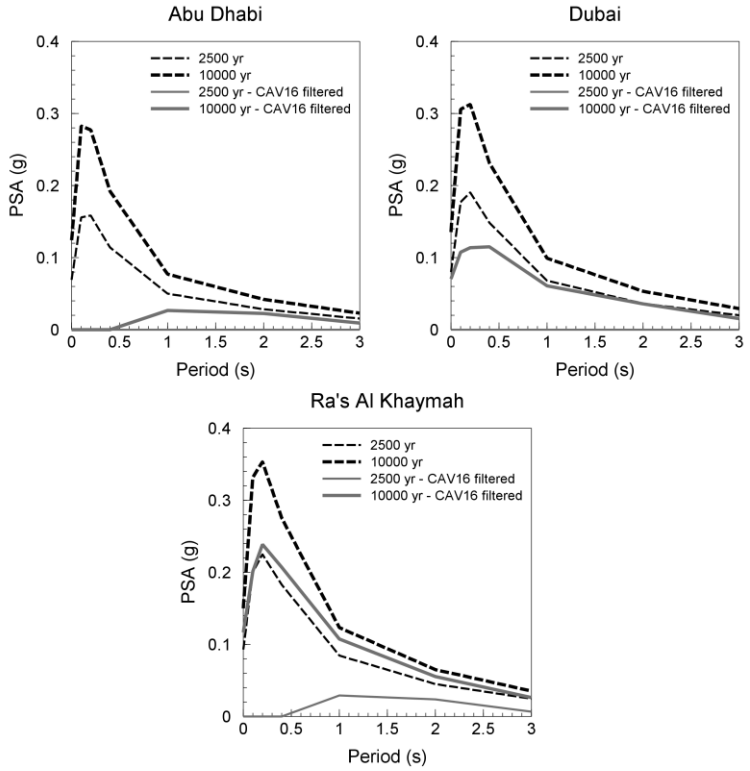

Figure 5.25. Comparison of the response spectra of the three sites before and after the CAV16 filtering for 2500- and 10,000-year return periods.

The disaggregated results for the three sites for PGA and SA at 0.2, 1.0 and 3.0 s response periods at 10,000-year return period are presented from Figure 5.26 to Figure 5.28. On the left-hand-side of these figures the disaggregated results are shown before applying the filtering and on the right-hand-side the disaggregated results after applying the CAV16 filter are shown.

It is important to highlight that the annual frequencies of exceedance of the CAV16 filtered results represent the annual probability of exceeding both the target ground motion (e.g., a PGA value of 0.1 g) and a CAV value of 0.16 g-s. On the other hand, the annual frequencies of exceedance of the non-filtered results represent only the probability that a given target SA (or PGA) will be exceeded.

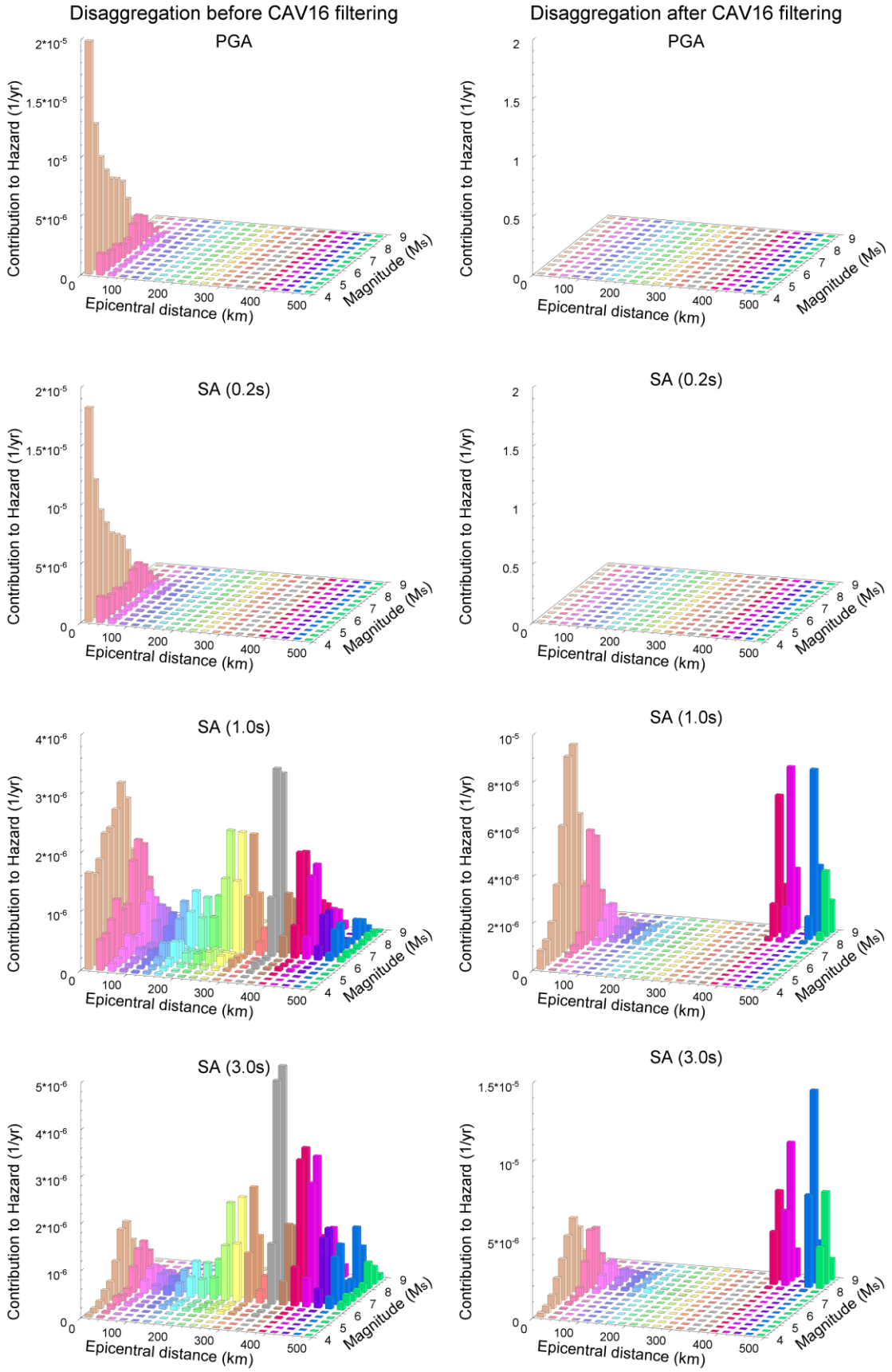

Figure 5.26. Disaggregated results for the city of Abu Dhabi before (left column) and after (right column) the CAV16 filtering for PGA and SA at 0.2, 1.0 and 3.0 s response periods at 10,000-year return period.

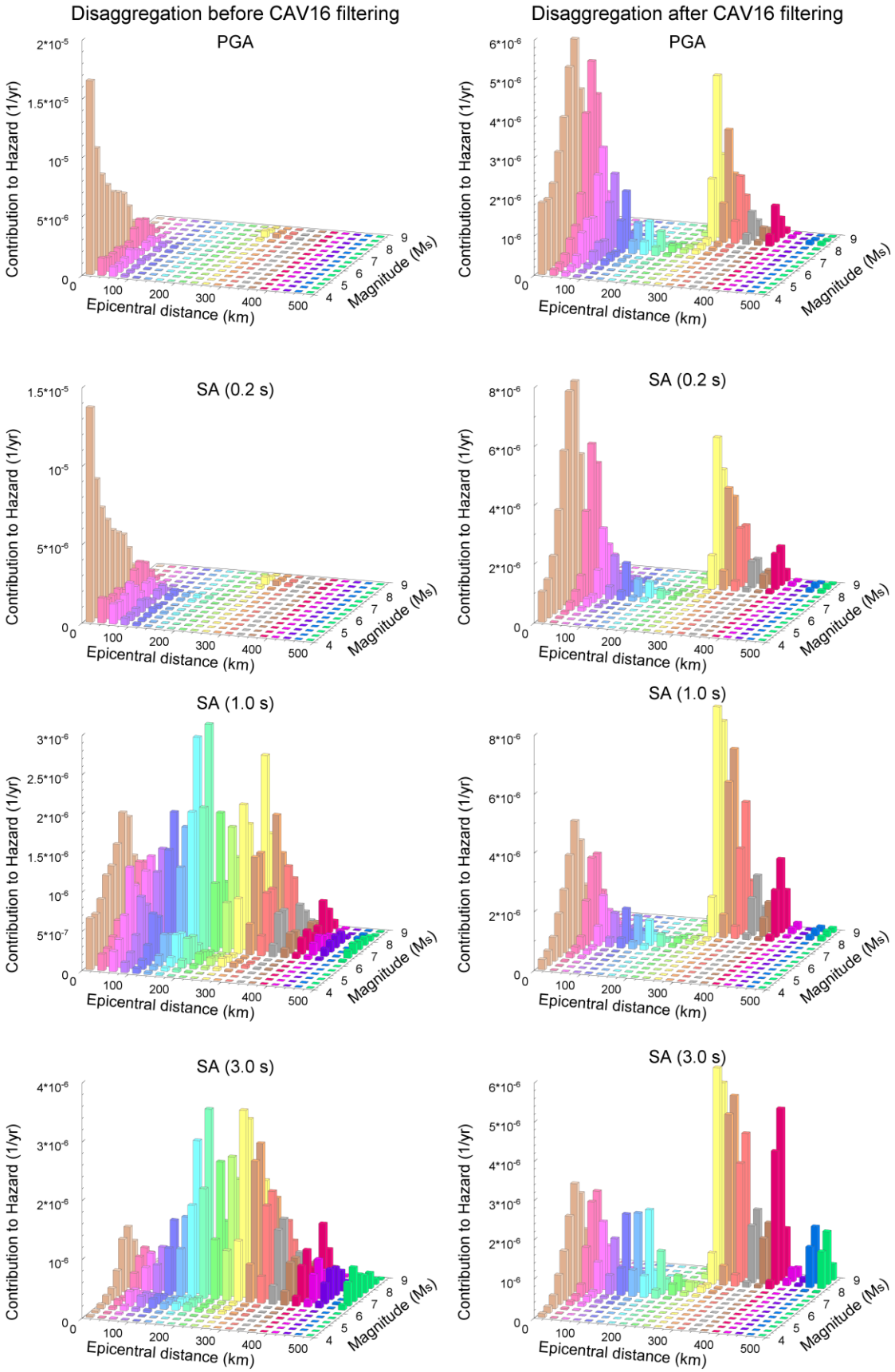

Figure 5.27. Disaggregated results for the city of Dubai before (left column) and after (right column) the CAV16 filtering for PGA and SA at 0.2, 1.0 and 3.0 s response periods at 10,000-year return period.

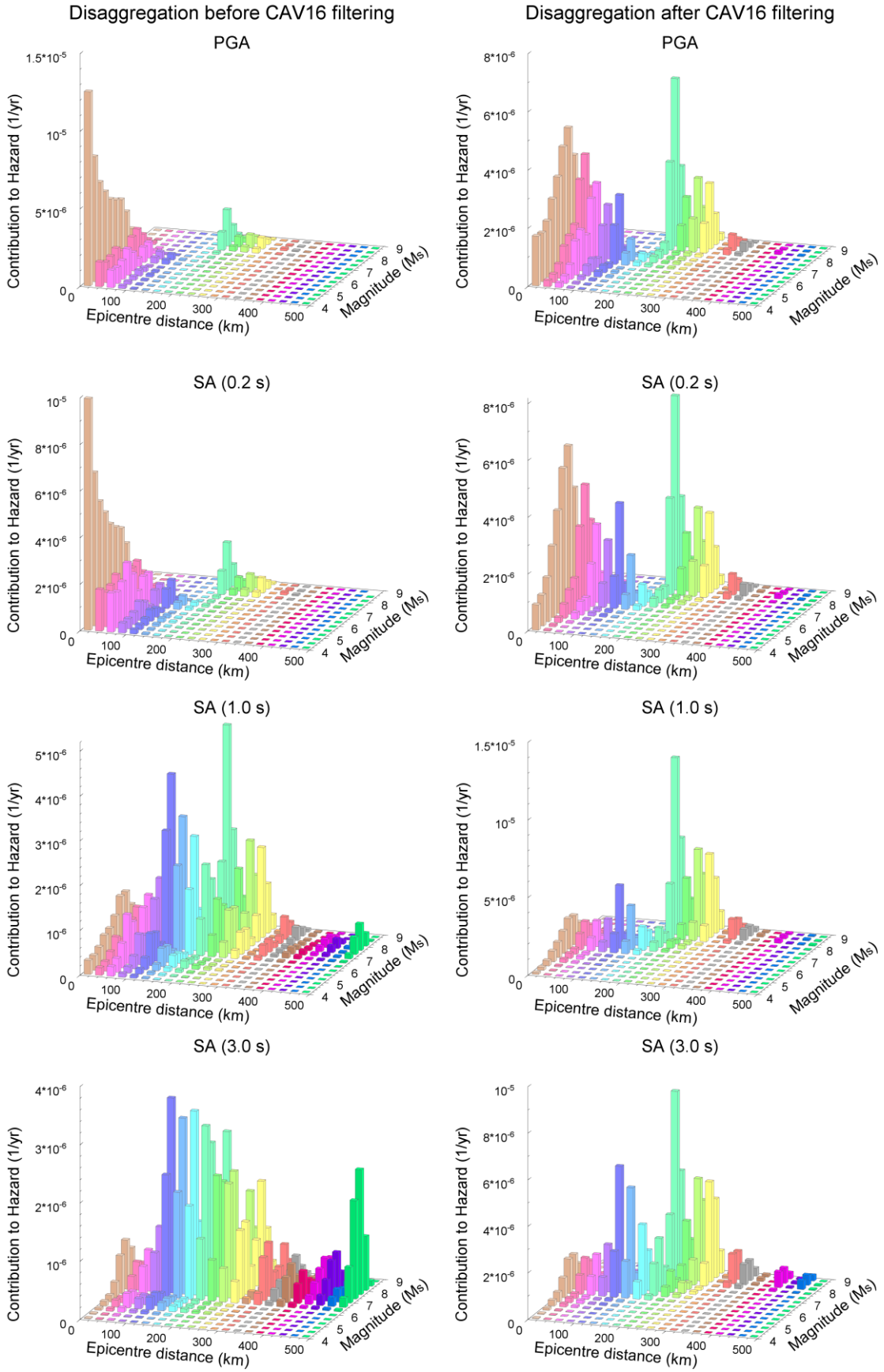

Figure 5.28. Disaggregated results for the city of Ra's Al Khaymah before (left column) and after (right column) the CAV16 filtering for PGA and SA at 0.2, 1.0 and 3.0 s response periods at 10,000-year return period.

An important reduction in the hazard at the three sites is observed due to the removal of earthquakes that are not expected to produce CAV values larger than 0.16 g-s. Based on these results, for return periods less than ~ 5000 years and short response periods (i.e. PGA and 0.2 s) potentially damaging ground-motion levels will not be expected at any of the three sites. For longer response periods (i.e. 1.0 and 3.0 s) the threshold return period is about 2500 years.

The reduction in the hazard is clearly observed from the decrease of the spectral amplitudes of the UHS. In fact, the spectral amplitudes at a 2500-year return period for the cities of Abu Dhabi and Dubai are zero for all response periods. At the 10,000-year return period the differences in the spectral amplitudes reach many orders of magnitude. These differences are larger at response periods less than 1.0 s and tend to decrease at higher response periods.

The removal of non-damaging earthquakes not only reduces the hazard levels as is shown directly by the hazard curves, but it leads also to a change in the hazard-dominating seismic scenarios as can be observed in the plots of the disaggregated results. This has important implications for the selection of acceleration time-histories and the specification of scenario spectra for seismic design.

Despite the fact that the CAV16 filtering is proposed as an alternative to m_{min} for removing non-damaging small earthquakes, it is worth noting, in the filtered disaggregated results, that not only small events were removed, but also medium-to-large events at longer distances (> 200 km). These scenarios are not expected to produce values of CAV larger than 0.16 g-s.

It is important to emphasise that CAV, as ground motion parameter, is not an absolute filter. The filter is the probability of exceeding a threshold value of CAV. Although Hardy *et al.* (2006) propose to use a threshold value

of CAV equal to 0.16 g-s, the filtering process can be performed for any other value depending on the requirements of the project.

5.4. Alternatives to m_{min}: other parameters

Alternatively to CAV, there are parameters such as Arias intensity (I_a) that have also been shown to have a good correlation with damage to engineered and natural structures. I_a has been shown to be a good estimator particularly for the prediction of liquefaction potential and landslides (e.g., Cabañas *et al.*, 1997; Kayen & Mitchell, 1997).

In this section, a model for predicting I_a as function of PGA, moment magnitude (M_w) and V_{s30} is developed. This model is then incorporated into the framework proposed by Hardy *et al.* (2006) instead of the CAV model, to remove non-damaging earthquakes from the hazard results of the case study (Chapter 3).

In order to be able to compare the hazard results using the CAV16 filter and those reported in this section, an I_a threshold of 0.06 m/s was selected. This value was obtained from the inspection of the relation between the inter-storey drifts of the various floors of a six-storey building and CAV and the relation between these drifts for the same structure and I_a (Figure 5.29).

For this, the results of a structural response analysis of a six-storey building carried out by Nicola Buratti during a period spend at Imperial College were used (Buratti *et al.*, 2008). Figure 5.29 shows the correlation between CAV and I_a and the relative drift of the upper storey of the six-storey building. Similar correlations were observed for the remaining storeys.

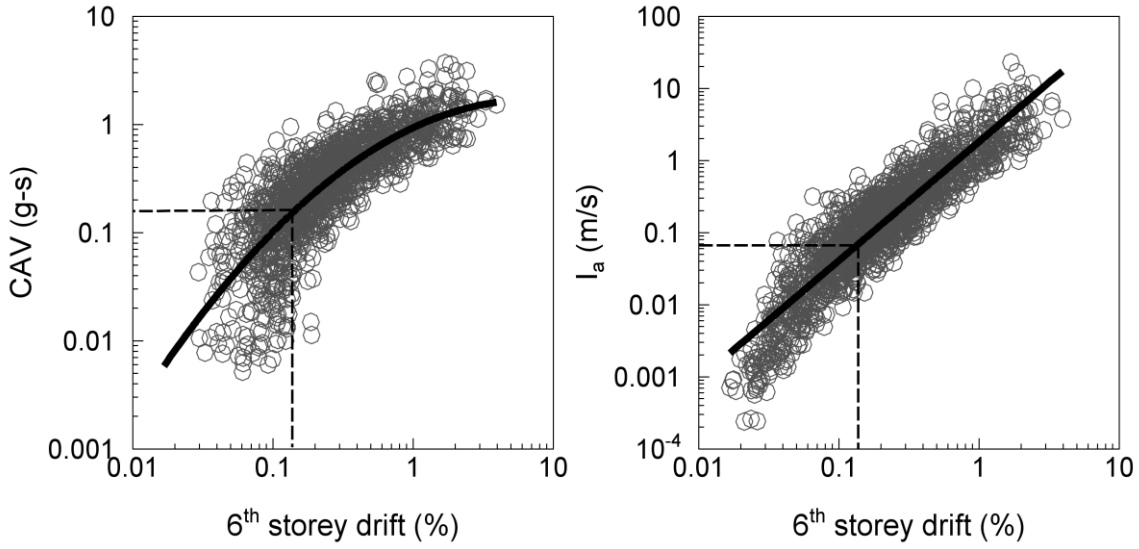

Figure 5.29. Correlations between CAV (left) and I_a (right) and the relative drifts for the 6th storey of the studied building. Black solid lines are the best-fit curve to the data; dashed black lines show the drift level for a CAV value of 0.16 g-s and the I_a value corresponding to the same drift level.

Based on the correlations observed between CAV and the inter-storey drifts of the six-storey building, a CAV value of 0.16 g-s can be regarded as being an appropriate damage threshold for the structure used in this analysis, as it is essentially at this point that a break in linearity of the inter-storey drifts can be observed with increasing CAV (indicating the onset of non-linear behaviour of the structure). Additionally, some researches have suggested that damage to non-structural elements initiate at drift ratios between 0.1 and 0.3 % (Crowley *et al.*, 2004), consistent with the drift ratio identified for this case of around 0.13 % for CAV values of 0.16 g-s.

Buratti *et al.*, (2008) use a sub set of ground motion records from the Next Generation Attenuation (NGA) project database (Power *et al.*, 2008) consisting of 1666 observations (833 recordings with two horizontal components) from 53 earthquakes. To define this sub set, all records from the Chi-Chi sequence were excluded, as well as records with only one horizontal component and records for which M_w, r_{jb} or V_{s30} were not available.

The model for predicting I_a as function of PGA, M_w and V_{s30} presented herein was derived using the same strong motion data set used for the structural response analysis. The distribution of M_w and r_{jb} from the data set used to develop the I_a model is shown in Figure 5.30. The data set consists primarily of earthquakes with magnitudes, M_w, between 5.5 and 7.5 and r_{jb} distances between 4 and 200 km.

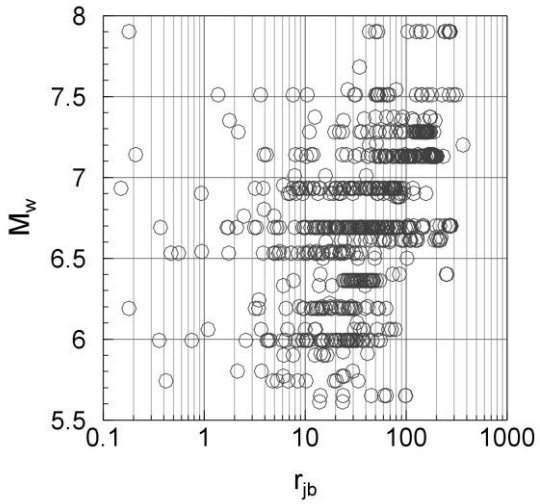

Figure 5.30. Distribution of the magnitudes (M_w) and distances (r_{jb}) of the earthquake data set used to derive the I_a model.

The I_a values from the data set are shown in Figure 5.31 as function of PGA, M_w, r_{jb} and V_{s30}. A good linear correlation and small variability can be observed between I_a and PGA. A clear correlation can be observed as well between I_a and r_{jb}. However, the correlation between I_a and M_w, and I_a and V_{s30} is less evident.

Note however, that the trends are hidden by the fact that I_a vs. M_w is for all distances and it is not easy to visually separate out the magnitude – distance correlation of the underlying data set.

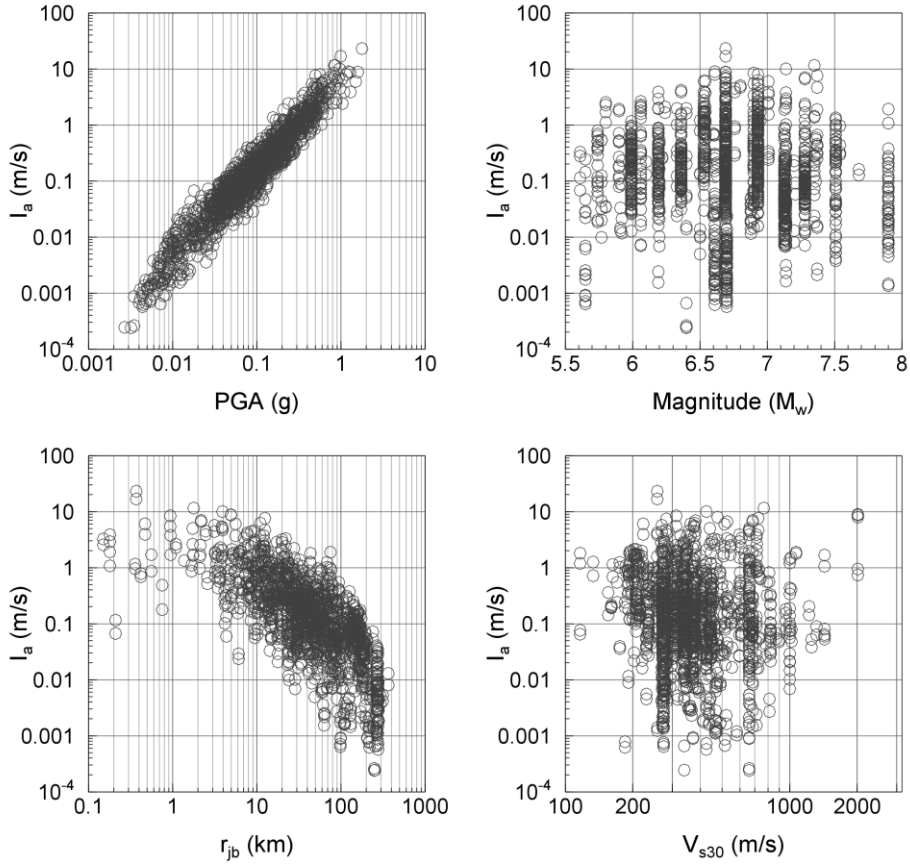

Figure 5.31. Dependence of Arias intensity (I_a) on PGA, moment magnitude (M_w), Joyner-Boore distance (r_{jb}) and shear-wave velocity (V_{s30})

Since PGA has a direct correlation with the source-to-site distance, considering I_a as function of PGA will incorporate in some way the dependence of I_a on r_{jb}. Based on this, a first I_a model is proposed herein as a function of only PGA and M_w:

$$\log_{10}\left(I_a\right) = c_0 + c_1 \log_{10}\left(PGA\right) + c_2 M_w \qquad 5.14$$

where I_a is in units of m/s, PGA is in units of g, c_0 = -0.843, c_1 = 1.643 and c_2 = 0.251. The standard deviation of the I_a model in Equation 5.14 is 0.193 in $\log_{10}$ units.

The residuals for I_a of the first model (Equation 5.14) are shown as function of PGA, M_w, r_{jb} and V_{s30} in Figure 5.32. The only trend that can be observed is in the residuals with respect to $\log(V_{s30})$ showing a linear dependence with a negative slope.

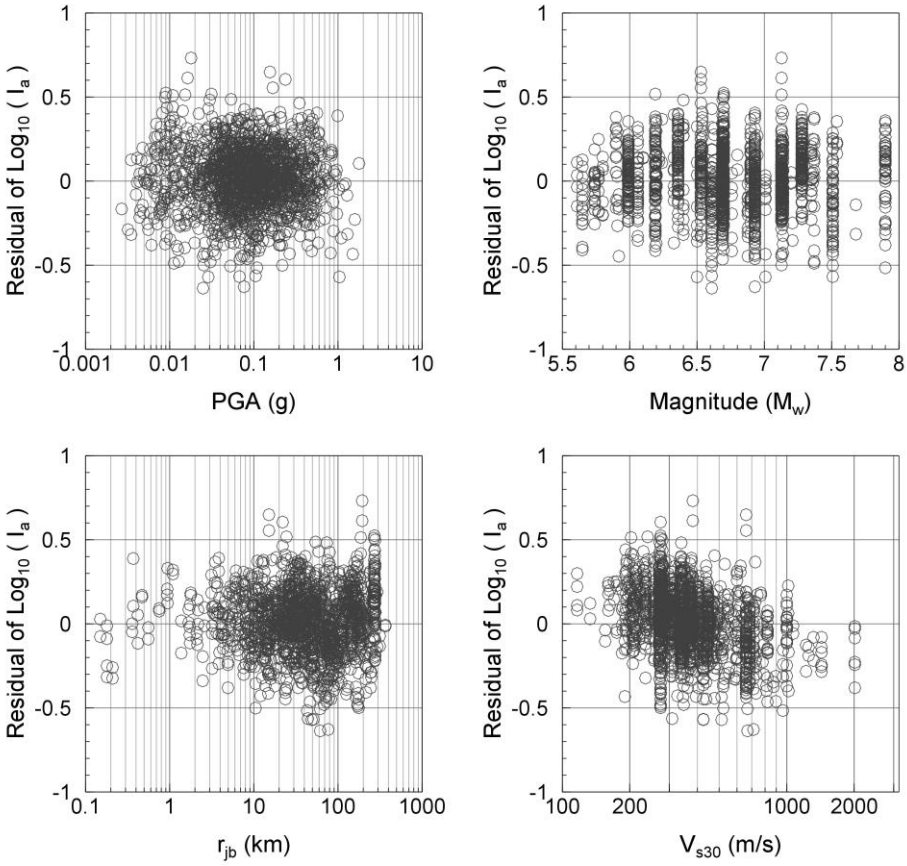

Figure 5.32. Dependence of the residuals of the first I_a model (Equation 5.14) on PGA, M_w, r_{jb} and V_{s30}.

Based on the evaluation of the residuals, the $\log_{10}$ of V_{s30} was incorporated in the model. Thus the final I_a model is given by:

$$\log_{10}(I_a) = b_0 + b_1 \log_{10}(PGA) + b_2 M_w + b_3 \log_{10}(V_{s30}) \qquad 5.15$$

where the coefficients b_0 to b_3 are given in Table 5.8. The standard deviation for the final I_a model is 0.179 in $\log_{10}$ units (Equation 5.15).

Table 5.8. Coefficients for the final I_a model (Equation 5.15).

Coefficient	Estimate
b_0	0.0459
b_1	1.6500
b_2	0.2591
b_3	-0.3615

The residuals for the final I_a model derived in this study as function of PGA, M_w, r_{jb} and V_{s30} are shown in Figure 5.33. These residuals do not

shown any significant trend. Therefore, the I_a model in Equation 5.15 was used to filter the hazard results of the case study.

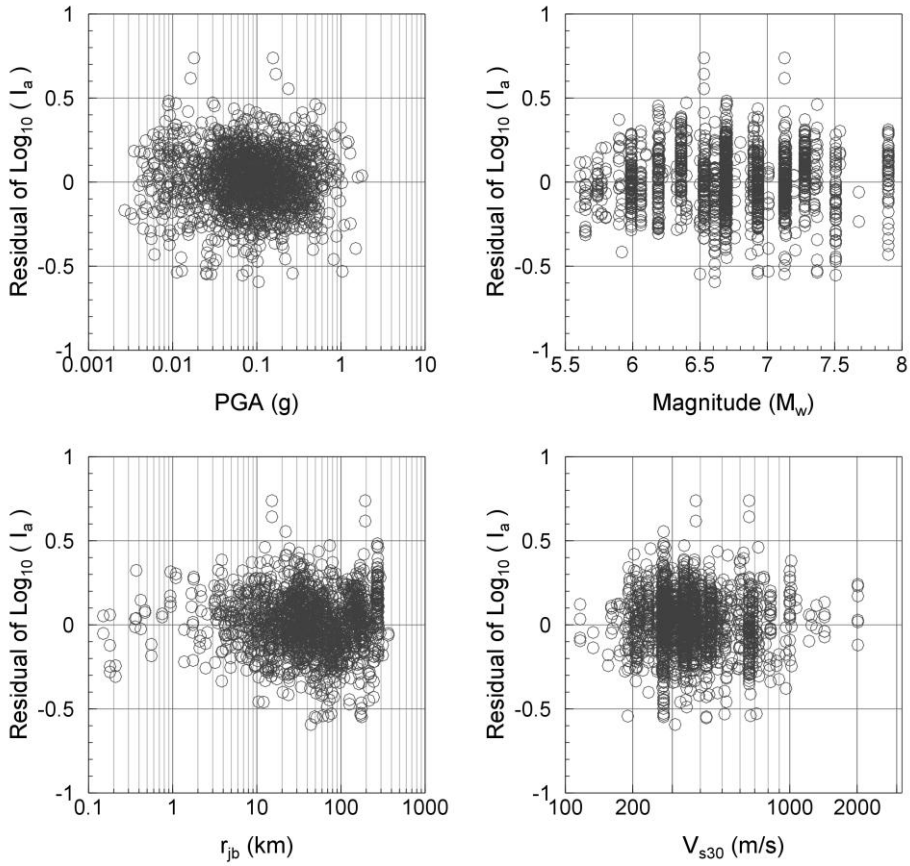

Figure 5.33. Dependence of the residuals of the final I_a model (Equation 5.15) on PGA, M_w, r_{jb} and V_{s30}.

The coefficients for the I_a model were obtained using a non-linear model fit by maximum likelihood. Random effects were not considered in the regression analysis.

In a similar way to the CAV16 filtering process presented in the previous section, the hazard results from the case study were filtered for an I_a value of 0.06 m/s (I_a06 filtering). This filtering was applied to the hazard results at the end tips of the logic tree corresponding to the section of ground-motion prediction equations. Then, the new total hazard curve was obtained as the weighted mean of the set of filtered results using the weights originally assigned to the logic-tree branches in the case study.

A comparison of the seismic hazard curves before and after using the I_a06 and the CAV16 filtering is presented for the three cities from Figure 5.34 to Figure 5.36. The hazard curves are shown for PGA and SA at 0.2, 1.0 and 3.0 s response periods.

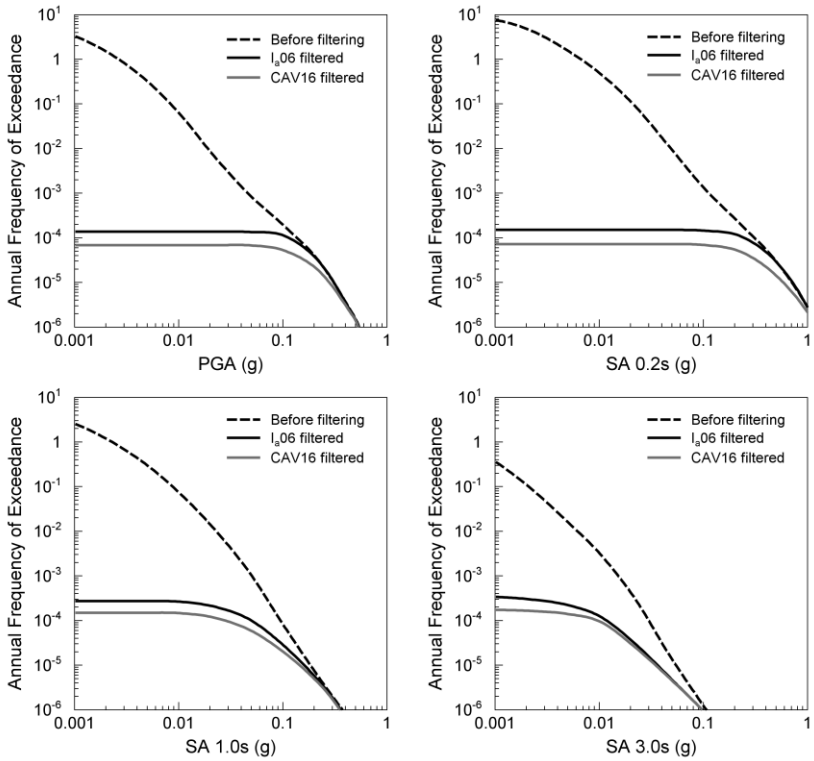

Figure 5.34. Seismic hazard curves for the city of Abu Dhabi before filtering (dashed line) and after the I_a06 (black-solid line) and the CAV16 (grey-solid line) filtering. The hazard curves are presented for PGA and SA at response periods of 0.2, 1.0 and 3.0 s.

The response spectra for the three sites at return periods of 2500 and 10,000 years are presented in Figure 5.37. It is important to note that, again, spectral amplitudes at the 2500-year return period are zero for the city of Abu Dhabi for all response periods and for periods less than 1 second for the city of Dubai.

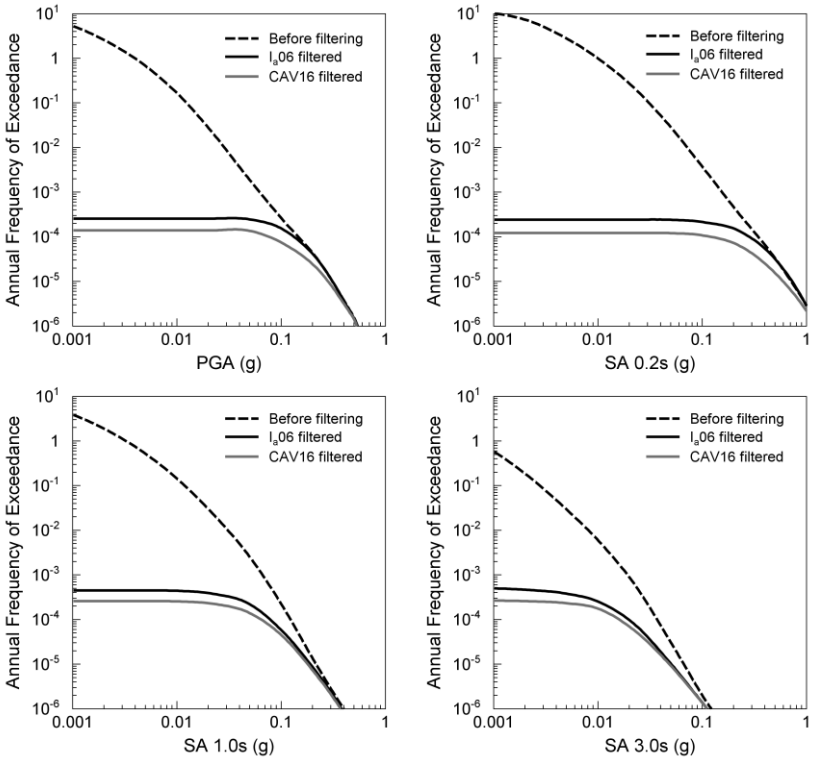

Figure 5.35. Seismic hazard curves for the city of Dubai before filtering (dashed line) and after the I_a06 (black-solid line) and the CAV16 (grey-solid line) filtering. The hazard curves are presented for PGA and SA at response periods of 0.2, 1.0 and 3.0 s.

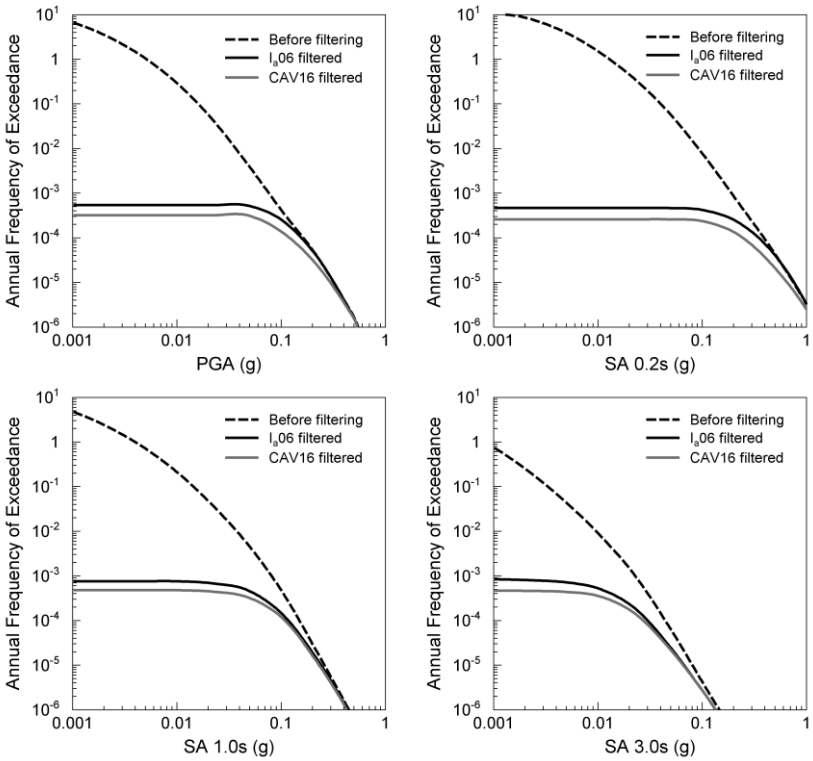

Figure 5.36. Seismic hazard curves for the city of Ra's Al Khaymah before filtering (dashed line) and after the I_a06 (black-solid line) and the CAV16 (grey-solid line) filtering. The hazard curves are presented for PGA and SA at response periods of 0.2, 1.0 and 3.0 s.

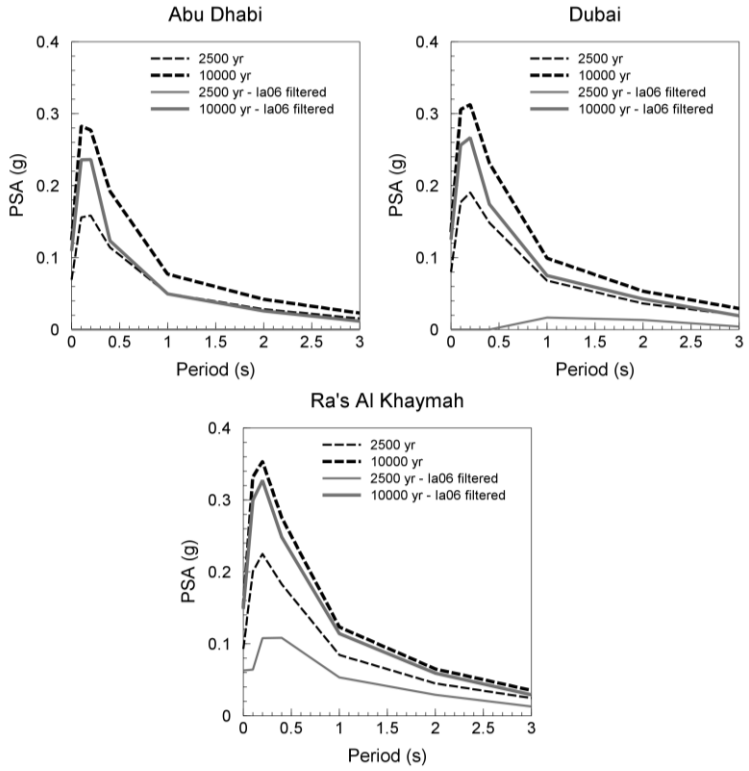

Figure 5.37. Response spectra for the cities of Abu Dhabi, Dubai and Ra's Al Khaymah at 2500- and 10,000-year return periods, before filtering and after the I_a06 filtering.

The disaggregated results, in terms of magnitude and distance scenarios, are presented in Figure 5.38, Figure 5.39 and Figure 5.40 for the cities of Abu Dhabi, Dubai and Ra's Al Khaymah, respectively. On the left-hand-side of the figures the disaggregated results before the filtering are shown, while on the right-hand-side the results after applying the I_a06 filtering are presented.

It is worth highlighting that as in the case of the CAV16 filtering, the annual frequencies of exceedance on the hazard results, represent the annual probability of exceeding both the target ground motion (e.g., a SA(2.0 s) value of 0.1 g) and a value of I_a of 0.06 m/s.

Similarly to the CAV16 filtering a significant reduction in the hazard results of the case study is observed after the I_a06 filtering. In both cases, for the CAV16 and the I_a06 filtering, the exceedance frequencies of the filtered hazard results are very similar, but with those corresponding to the I_a06 filtering consistently being higher.

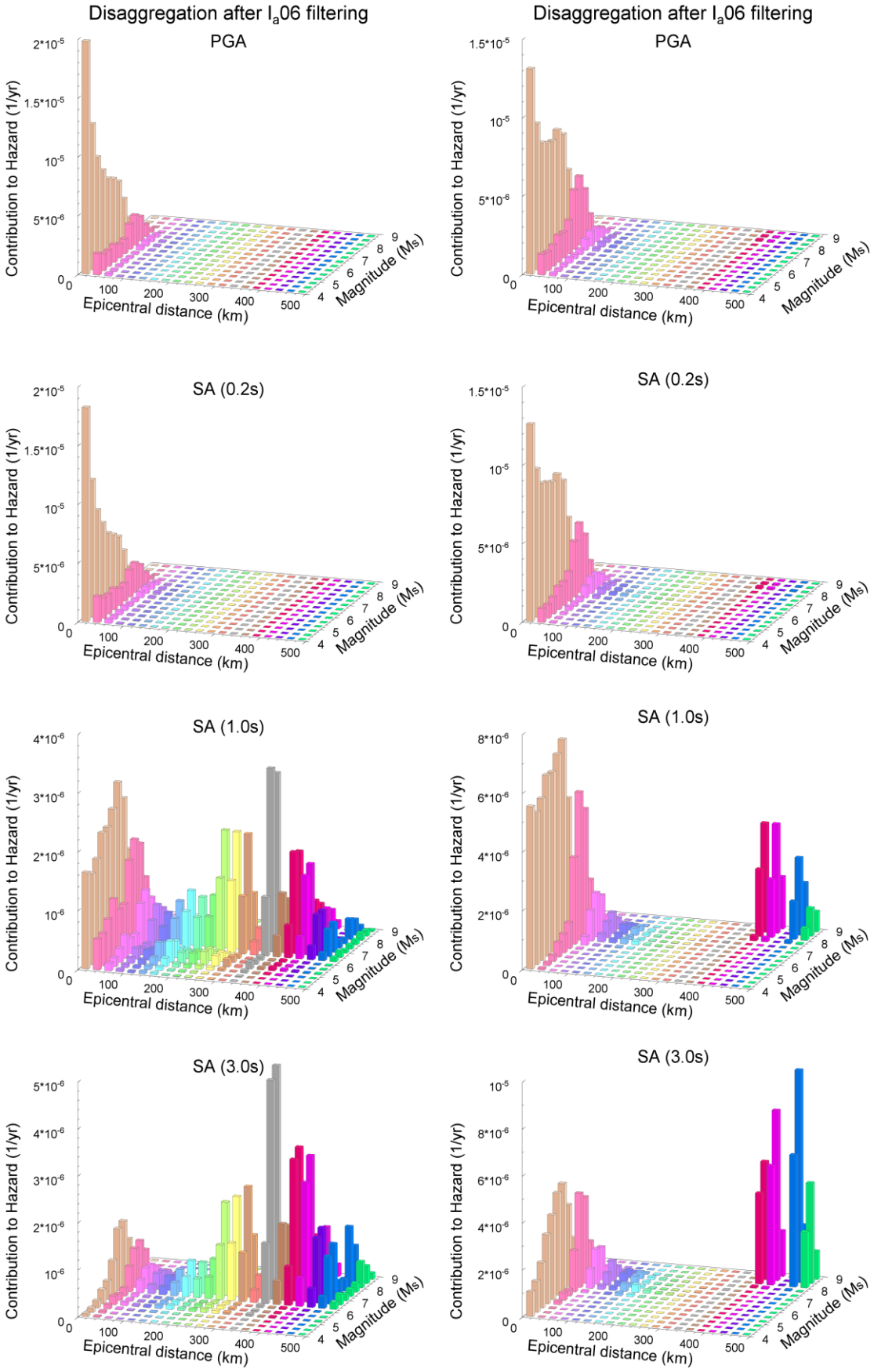

Figure 5.38. Disaggregated results for the city of Abu Dhabi for PGA and SA at 0.2, 1.0 and 3.0 s response periods. On the left-hand-side the results before filtering are presented while on the right-hand-side the results after the I_a06 filtering are shown.

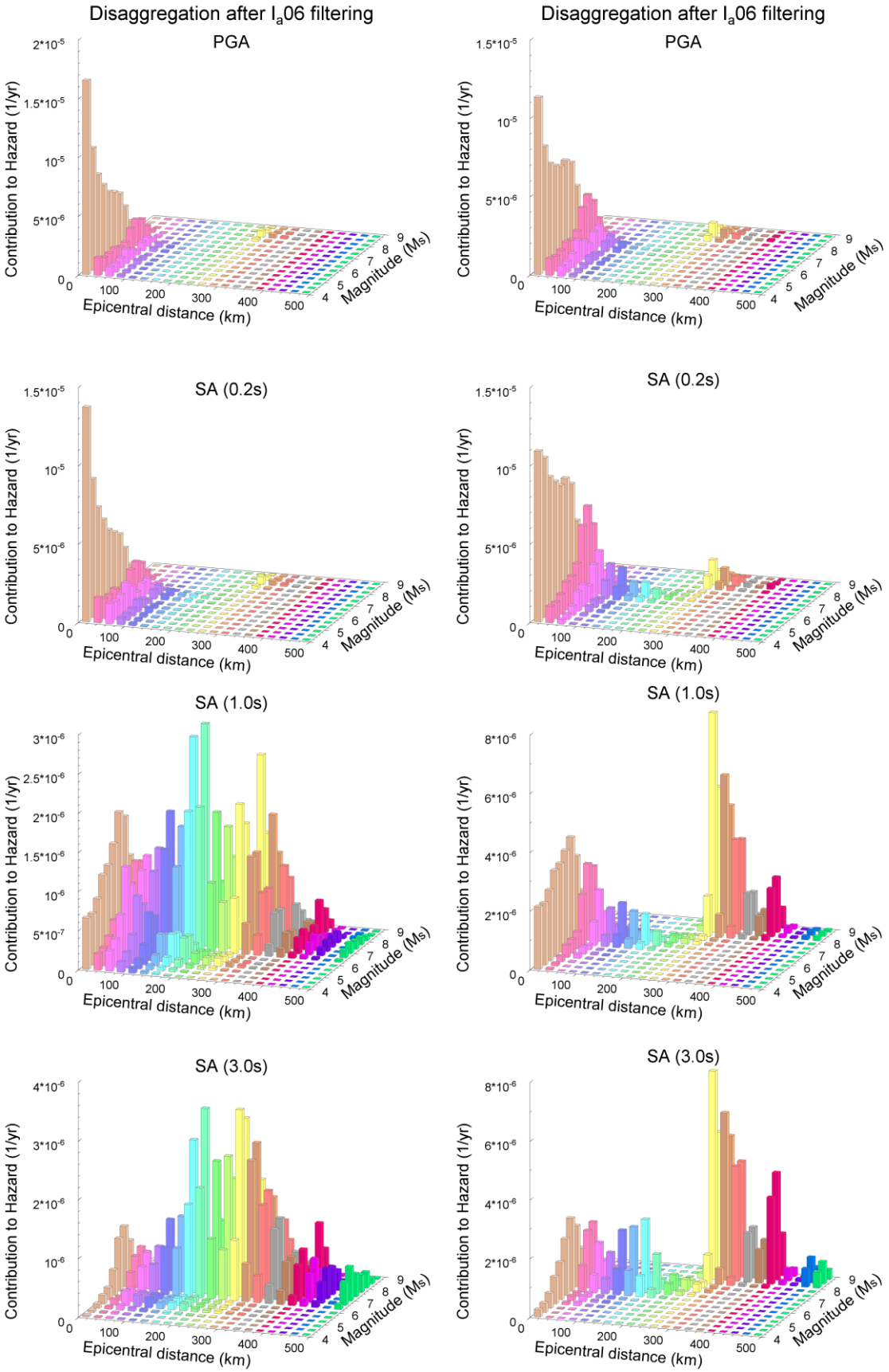

Figure 5.39. Disaggregated results for the city of Dubai for PGA and SA at 0.2, 1.0 and 3.0 s response periods. On the left-hand-side the results before filtering are presented while on the right-hand-side the results after the I_a06 filtering are shown.

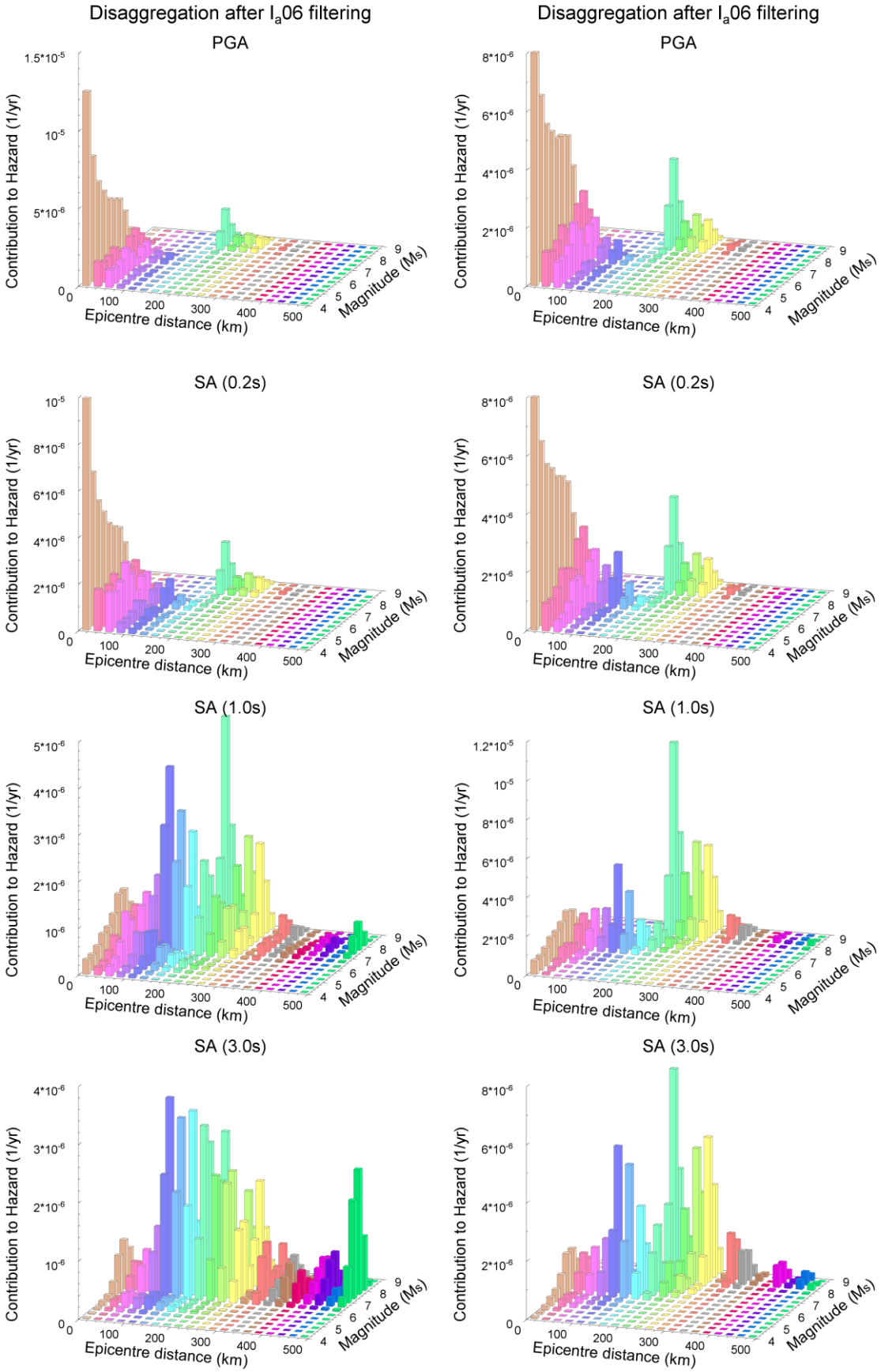

Figure 5.40. Disaggregated results for the city of Ra's Al Khaymah for PGA and SA at 0.2, 1.0 and 3.0 s response periods. On the left-hand-side the results before filtering are presented while on the right-hand-side the results after the I_a06 filtering are shown.

Although the differences in the hazard curves from the CAV16 and I_a06 do not appear to be significant, the differences in the spectral amplitudes at 2500- and 10,000-year return periods are noteworthy. For the I_a06 filtering, at a return period of 2500 years the spectral amplitudes for the city of Abu Dhabi are equal to zero and those for the city of Dubai are so small that they may be ignored for practical purposes. However, at the 10,000-year return period, in contrast to the CAV16 filtering, the reduction in the spectral amplitudes for the three sites is small. At the city of Ra's al Khaymah the UHS at the 10,000-year return period, before and after the I_a06 filtering process, are not significantly different.

Regarding the disaggregated results, in a similar manner as when the CAV16 filtering was used, not only contributions from small-magnitude events were removed but also those from medium-to-large events at long distances (> 200 km). However, the CAV16 filtering is apparently more restrictive for events at shorter distances than the I_a06 filtering. Comparing the disaggregated results from both approaches it can be seen that the main difference is in the contribution to the hazard of events at distances less than 50 km.

A slight advantage of the I_a model over the CAV model is the better correlation of I_a with PGA, M_w and V_{s30}. This leads to slightly smaller values of the standard deviation. While the smallest $\sigma_{\ln CAV}$ for the 2-step CAV model is about 0.45 in natural log units for a duration value of 2.3 s, for the I_a model the $\sigma_{\ln I_a}$ is 0.41 in natural log units. For the 1-step CAV model the $\sigma_{\ln CAV}$ is 0.46 in natural log units.

The procedure proposed by Hardy *et al.* (2006) has shown to be efficient in removing earthquake scenarios that potentially lead to an inflation of the seismic hazard. This applies to the two the ground-motion parameters used in this work as criteria to filter the results of a standard PSHA (i.e., CAV16 and I_a06).

However, the filtered results must be interpreted with caution as these could easily be misunderstood. For instance, the hazard results presented in this and the previous section indicate zero seismic hazard for return periods less than ~2000 years for the three sites. This does not mean that the probability of feeling an earthquake in the next 2000 years is zero, but that seismic resistant design is not required for structures with seismic-safety levels below ~2000-year return period.

These results must be understood as the joint probability of two events, in other words, the probability that two threshold values will be exceeded.

It is important to mention that the comparison of the CAV16 and I_a06 filters presented herein are just for one six-storey building and may not hold in other cases. The threshold values for both CAV and I_a, or for any other parameter of interest can be set to any value. For example, Harp & Wilson (1995) found a minimum threshold of I_a = 0.08 m/s to observe rock falls and landslides in Tertiary and younger deposits. Thus, the filtering of the PGA curve for this I_a threshold value could be useful to assess the hazard of a landslide in this type of geological structures.

5.5. υ_{min}, β and m_{max} values for the sources with the highest contributions

The estimation of the earthquake occurrence parameters (β and υ_{min}) and the maximum magnitude (m_{max}), which together describe the seismic activity of a specific seismic source, are always associated with some degree of uncertainty.

Generally, this uncertainty is mostly due to the random variability of the data and is represented by the standard deviation, which is obtained from the regression analysis used to estimate the recurrence parameters (e.g. Kijko & Sellevoll, 1989, 1990; Weichert, 1980a) or the use of empirical

relationships (e.g. Wells & Coppersmith, 1994) or statistical approaches (e.g. Kijko, 2004) to estimate m_{max}.

When insufficient data exist to allow a robust estimation of the occurrence parameters or m_{max}, assumptions must be made by the analyst to come up with values to be used in the hazard analysis. In this case, at least part of the overall uncertainty associated with the allocated values must be treated as epistemic uncertainty.

In this section, the influence of the epistemic uncertainty of the β value used for the Stable craton in the case study seismic hazard analysis (Chapter 3) will be discussed. Additionally, a sensitivity analysis for different values of β and m_{max}, keeping the seismic moment rate constant, is carried out. The results presented herein are for the city of Dubai; however, the same behaviour was observed for the other two sites.

In the case study presented in Chapter 3, the epistemic uncertainty regarding the β value for the Stable craton was considered in the logic-tree framework. Since there are not enough data available to estimate the recurrence parameters for this seismic source using statistical approaches, β values suggested by Fenton *et al.* (2006) and Johnson *et al.* (1994) as worldwide average values for stable continental regions were considered for the analysis. υ_{min} was calculated by fitting the earthquake occurrence curves to the available data from the Arabian Stable craton by fixing the value of β within Weichert's (1980a) procedure (see section 3.4.1). For the case of m_{max}, the common (but far from robust) practice of adding 0.5 units to the maximum observed magnitude was applied.

As two different geometries for the Arabian stable craton were proposed (see section 3.4) a total of four sets of parameters for the Stable craton were used in the analysis; that is two for each value of β. Table 5.9 presents the four sets of parameters: for the two β values (i.e., Fenton *et al.*, 2006; Johnson *et al.*, 1994), and for both geometries (i.e., Stable craton I &

III and Stable craton II). Each set of parameters implies a different seismic moment rate being used for the Stable craton.

Table 5.9. Earthquake occurrence parameters and maximum magnitude used in the case study for the Stable craton. SC – Stable craton; I, II and III correspond to the different seismic source zonations considered in the hazard analysis (see section 3.4 and Figure 3.33 to Figure 3.35). Magnitudes are on M_s scale.

	Fenton *et al.* (2006)		Johnson *et al.* (1994)	
	SC I & III	SC II	SC I & III	SC II
m_{min}	4.0	4.0	4.0	4.0
m_{max}	7.0	7.0	7.0	7.0
σ (m_{max})	0.50	0.50	0.50	0.50
β	1.840	1.840	2.245	2.245
σ (β)	0.449	0.371	0.523	0.433
ν_{min}	0.267	0.390	0.284	0.415
σ (ν_{min})	0.021	0.021	0.022	0.022

Figure 5.41 shows the hazard curves from each branch of the logic tree for the city of Dubai for PGA and SA at 3.0 s response period. The hazard curves are divided in two groups: one for those with β = 1.84 (solid line) (Fenton *et al.*, 2006) and other with those with β = 2.24 (dash-dotted line) (Johnson *et al.*, 1994). An appreciation of the influence of β may be gained by analysing the results of a single set of GMPEs and hence only one equation was considered for each type of source Atkinson & Boore (2006) for predicting ground-motions in the stable craton, Boore & Atkinson (2006) for shallow earthquakes in active continental regions, and Atkinson & Boore (2003) for subduction zones.

As can be seen in Figure 5.41, the epistemic uncertainty of using either the β values of Fenton *et al.* (2006) or Johnson *et al.* (1994) has very little, almost zero, influence on the seismic hazard at both PGA and 3.0 s response period.

To this point, only the epistemic uncertainty in the β value used for the Stable craton has been addressed. However, both earthquake occurrence parameters (i.e., ν_{min} and β) as well as m_{max} have some associated aleatory

variability. This variability is expressed in terms of standard deviation. Since integrating the hazard along the aleatory variability of υ_{min}, β and m_{max} would imply that these are independent aleatory variables, which is not the case as they are all correlated and are dependent on the seismic moment, only the expected values of these parameters should be used for the hazard calculations. Otherwise, the integration of the hazard must account for the correlation among these variables.

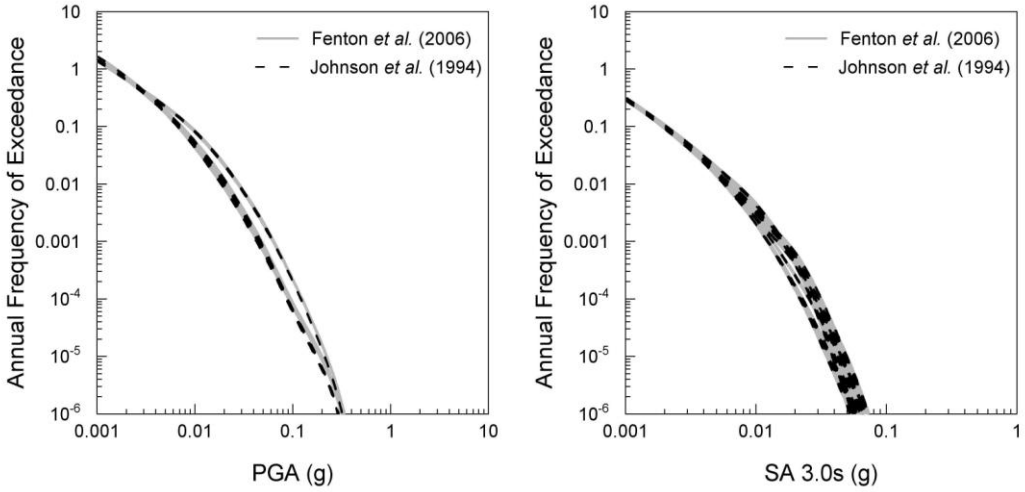

Figure 5.41. Comparison of the hazard curves for the two values of β considered in the hazard analysis for the Stable craton. The hazard curves are for the city of Dubai for PGA and SA at 3.0 s response period, and for the set of attenuation equations: Atkinson & Boore (2006), Boore & Atkinson (2006) and Atkinson & Boore (2003).

In order to assess the influence of different values of β and m_{max} in the seismic hazard results, a sensitivity analysis varying these parameters at the seismic sources with higher contribution to the hazard was carried out. For this analysis only one branch of the logic tree was used. The selected branch was that with the highest weighting (the same as that used for the sensitivity analysis in section 5.2). The set of attenuation equations used for the analysis was again: Atkinson & Boore (2006), Boore & Atkinson (2006), and Atkinson & Boore (2003).

To obtain the sets of parameters to be use in the analysis, the rate of earthquake occurrence for M ≥ m_{min} (υ_{min}) and the seismic moment rate

corresponding to the mean parameters were kept constant, while either β or m_{max} were modified by ±1σ. The remaining parameter, either β or m_{max} depending on which parameter was modified, was estimated using Equation 11 of Youngs & Coppersmith (1985).

Table 5.10 shows the earthquake occurrence parameters used in the sensitivity analysis for the Simple Fold belt, Persian Gulf I, Zagros Foredeep and Stable craton I (see Figure 3.27). The values shown as Mean correspond to the values used for the case study.

Table 5.10. Earthquake occurrence parameters and m_{max} for the sources with the highest contribution to the hazard in the UAE. The Mean column represents the parameter values used in the case study. The values in italics within brackets are the standard deviations. Magnitudes are on M_s scale.

Simple Fold belt

	Mean	**m_{max} - 1σ**	**m_{max} + 1σ**	**β - 1σ**	**β + 1σ**
m_{min}	4.0	4.0	4.0	4.0	4.0
m_{max}	7.3 *(0.17)*	7.1	7.4	7.2	7.4
β	1.91 *(0.075)*	1.76	2.05	1.84	1.99
v_{min}	9.66 *(0.021)*	9.66	9.66	9.66	9.66

Zagros Foredeep

	Mean	**m_{max} - 1σ**	**m_{max} + 1σ**	**β - 1σ**	**β + 1σ**
m_{min}	4.0	4.0	4.0	4.0	4.0
m_{max}	6.9 *(0.14)*	6.8	7.0	6.8	7.1
β	1.40 *(0.157)*	1.18	1.53	1.24	1.55
v_{min}	1.56 *(0.019)*	1.56	1.56	1.56	1.56

Persian Gulf I

	Mean	**m_{max} - 1σ**	**m_{max} + 1σ**	**β - 1σ**	**β + 1σ**
m_{min}	4.0	4.0	4.0	4.0	4.0
m_{max}	6.1 *(0.23)*	5.9	6.3	6.0	6.4
β	1.78 *(0.261)*	1.34	1.95	1.52	2.04
v_{min}	1.08 *(0.021)*	1.08	1.08	1.08	1.08

Stable craton I

	Mean	**m_{max} - 1σ**	**m_{max} + 1σ**	**β - 1σ**	**β + 1σ**
m_{min}	4.0	4.0	4.0	4.0	4.0
m_{max}	7.0 *(0.50)*	6.5	7.5	6.6	7.6
β	1.84 *(0.449)*	1.28	2.22	1.39	2.29
v_{min}	0.27 *(0.021)*	0.27	0.27	0.27	0.27

Figure 5.42 presents the hazard curves from the analyses carried out. As can be seen, the influence of considering different values of β and m_{max} is very weak. Only for annual rates of exceedance below $1x10^{-5}$ (100 000-year return period) can some influence be noticed. This influence is more significant for PGA and the 0.2 s response period and decreases for longer response periods. The hazard curves in Figure 5.42 are for the city of Dubai; however, the analysis was performed for the three sites of the case study. The same behaviour of the hazard curves was observed for the other two sites.

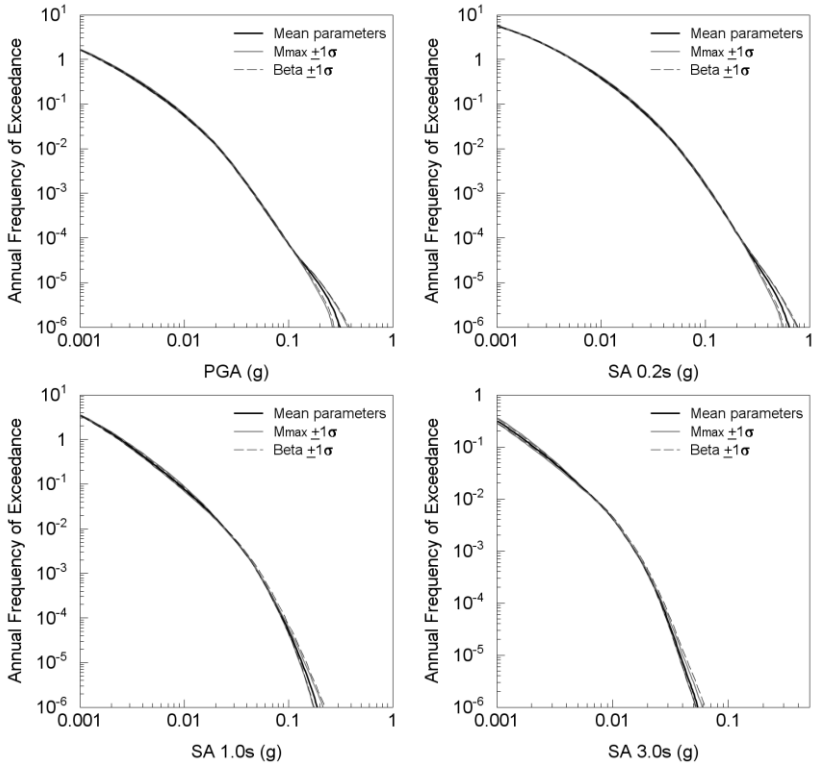

Figure 5.42. Hazard curves corresponding to the same seismic moment and different values of β and m_{max}. The hazard curves are for the city of Dubai for PGA and SA at 0.2, 1.0 and 3.0 s response spectra, and for the set of attenuation equations Atkinson & Boore (2006), Boore & Atkinson (2006) and Atkinson & Boore(2003).

Overall, it is very reasonable to assert that the epistemic and aleatory uncertainties regarding earthquake occurrence parameters and maximum magnitudes, assigned to the seismic sources with higher contribution to the

seismic hazard in the UAE, have a very low impact on the total seismic hazard for the region.

A reason for this might be the low coefficients of variation, ranging from 0.04 to 0.15 for β and from 0.02 to 0.04 for m_{max}, for the Simple Fold belt, Persian Gulf and Zagros Foredeep. For the Stable craton the coefficients of variation are slightly larger, 0.24 for β and 0.07 for m_{max}; however, as can be seen in Figure 5.41, changes made to the recurrence parameters for this source have a very small effect on the hazard curves at low annual rates of occurrence.

5.6. Ground Motion Prediction Equations (GMPEs)

The selection of the ground motion prediction equation (GMPE) to use in a seismic hazard analysis has been recognized as one of the main contributors to the total uncertainty in PSHA (Sabetta *et al.*, 2005; Toro, 2006). Since the uncertainty about which GMPE would model better the ground-motion attenuation in a particular region is due to the lack of knowledge, this uncertainty must be regarded as epistemic and is normally addressed through a logic-tree framework.

As described in sections 3.5 and 4.4, a total of seven GMPEs were used in the hazard analysis for the case study presented in Chapter 3; one for modelling ground-motion attenuation in stable continental regions (i.e., Atkinson & Boore, 2006), four for shallow earthquakes in active continental regions (i.e., Abrahamson & Silva, 1997; Akkar & Bommer, 2007b; Ambraseys *et al.*, 2005; Boore & Atkinson, 2006) and two for subduction zones (i.e., Atkinson & Boore, 2003; Youngs *et al.*, 1997). As an alternative to the model of Atkinson & Boore (2006), the equations for shallow earthquakes were also used to model ground-motion attenuation for the Arabian stable craton. As a result of this, a logic tree with sixteen branches for the GMPEs

(one for each combination of GMPEs) and three node levels was set up (see section 3.6, Figure 3.38).

A combined total of 15 552 branches were considered in the logic tree (Figure 3.38), 972 for each set of GMPEs. The sixteen sets of equations used for the PSHA of the UAE are shown in Table 4.1. This table is reproduced herein for ease of reference. Each set of equations in Table 4.1 corresponds to each of the alternative branches on the logic tree regarding GMPEs.

Table 4.1. Sets of equations used in the PSHA for the UAE.

Stable continental region	Shallow earthquakes in active regions	Subduction zones	Set #
Akkar & Bommer (2007)	Akkar & Bommer (2007)	Atkinson & Boore (2003)	1
		Youngs *et al.* (1997)	2
Boore & Atkinson (2006)	Boore & Atkinson (2006)	Atkinson & Boore (2003)	3
		Youngs *et al.* (1997)	4
Abrahamson & Silva (1997)	Abrahamson & Silva (1997)	Atkinson & Boore (2003)	5
		Youngs *et al.* (1997)	6
Ambraseys *et al.* (2005)	Ambraseys *et al.* (2005)	Atkinson & Boore (2003)	7
		Youngs *et al.* (1997)	8
Atkinson & Boore (2006)	Akkar & Bommer (2007)	Atkinson & Boore (2003)	9
		Youngs *et al.* (1997)	10
	Boore & Atkinson (2006)	Atkinson & Boore (2003)	11
		Youngs *et al.* (1997)	12
	Abrahamson & Silva (1997)	Atkinson & Boore (2003)	13
		Youngs *et al.* (1997)	14
	Ambraseys *et al.* (2005)	Atkinson & Boore (2003)	15
		Youngs *et al.* (1997)	16

The hazard curves from each branch of the logic tree for the city of Dubai for PGA and SA at response periods of 0.2, 1.0 and 3.0 s are shown in Figure 5.43. Different colours distinguish hazard curves corresponding to different sets of GMPEs. As the purpose of this section is to show the uncertainty due to the selection of different GMPEs, only the hazard curves for the city of Dubai are presented in Figure 5.43. It is worth stating that, the

same behaviour was observed for the other two sites showing a similar level of scatter among the hazard curves.

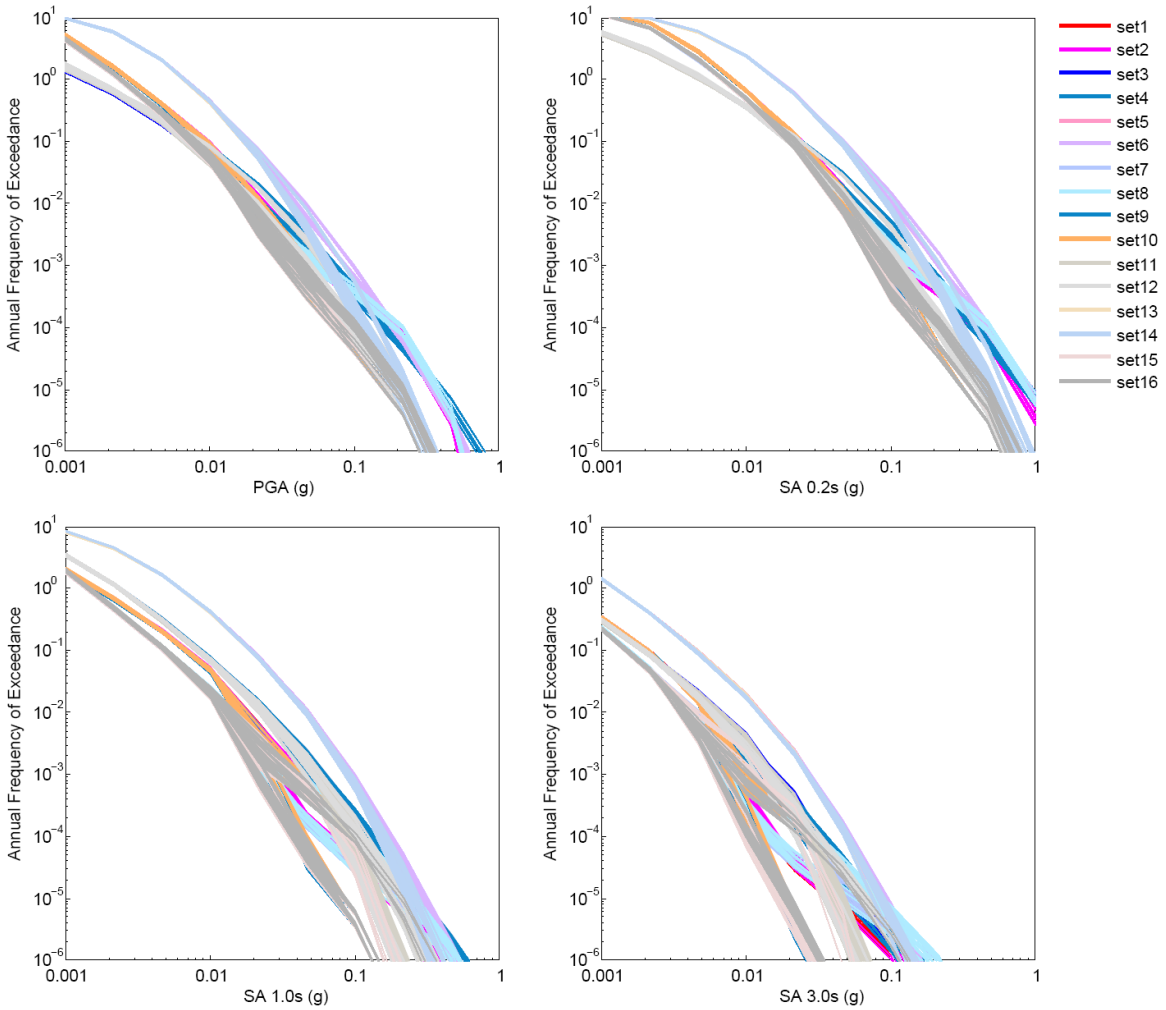

Figure 5.43. Hazard curves from all the branches of the logic tree. The hazard curves are for the city of Dubai for PGA and SA at 0.2, 1.0 and 3.0 s response period.

Figure 5.43 shows significant scatter in the hazard curves, which increases as the response period increases. However, it is rather difficult to appreciate to what extent this scatter is due to the selection of a given combination of ground-motion equations or to what extent it is due to other sources of epistemic uncertainty.

In Figure 5.44 only the mean hazard curves for each set of GMPEs are shown. Here it is easier to appreciate that most of the scatter on the hazard curves is mainly owing to the use of different GMPEs. However, a better way

to appreciate this is to quantify the variability through the standard deviation.

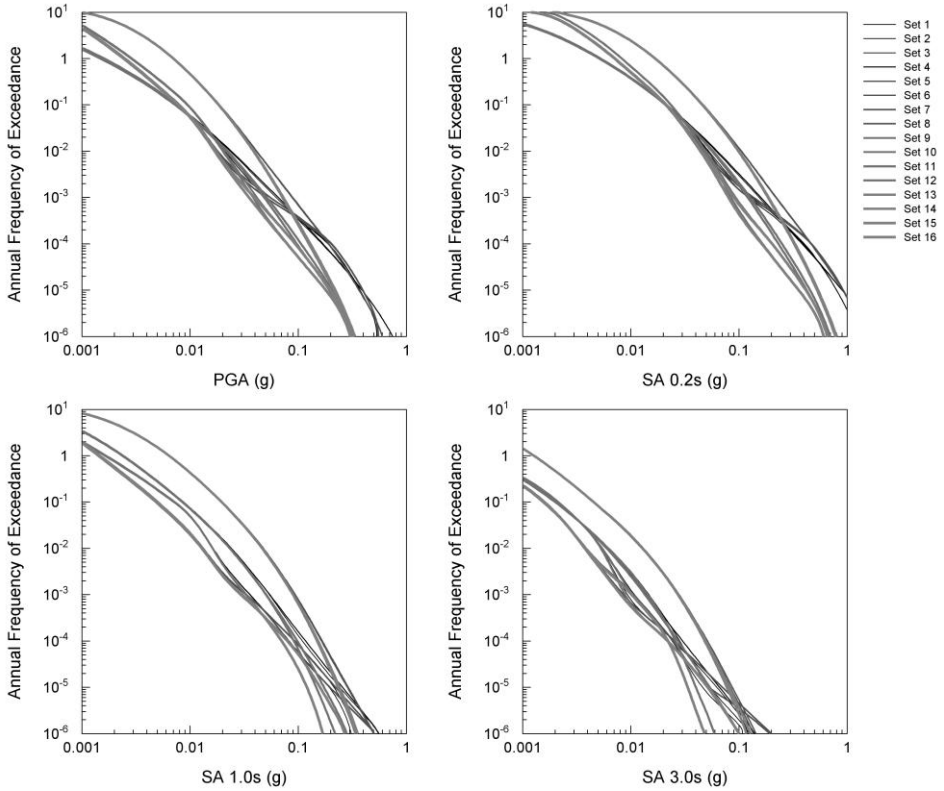

Figure 5.44. Mean hazard curves for each set of attenuation equations considered in the logic tree, for the city of Dubai for PGA and SA at 0.2, 1.0 and 3.0 s response period.

Figure 5.45 presents the variation of the standard deviation with respect to the ground motion amplitudes for the hazard curves shown in Figure 5.43. These values of standard deviation correspond to the scatter in the logarithms of the exceedance probabilities and represent only epistemic uncertainties. The dashed black line is the standard deviation of all the hazard curves of each branch on the logic tree; in other words, it is the total standard deviation of the mean hazard curve of the PSHA. The solid black line is the standard deviation resulting from the scatter of the mean hazard curves corresponding to each of the 16 sets of equations; this is the epistemic uncertainty due to the use of different GMPEs. Finally, the thin grey lines are the standard deviations corresponding to the epistemic

uncertainty on the modelling of the seismic sources (the remaining uncertainties in the logic tree apart from the selection of the GMPEs) for any given set of attenuation equations.

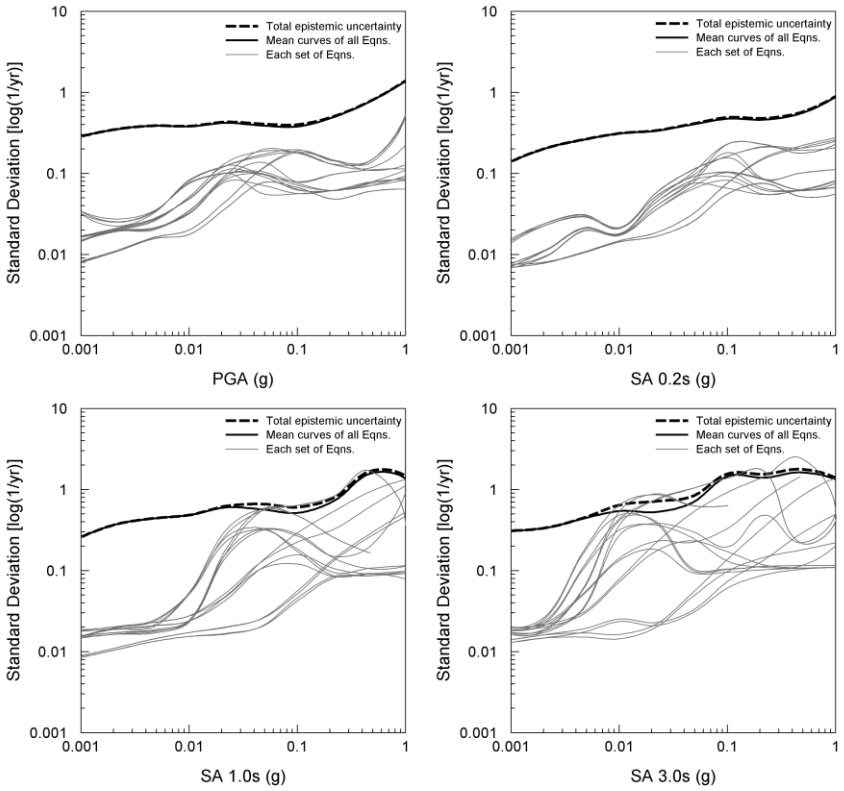

Figure 5.45. Variation of the standard deviation with ground-motion level for the city of Dubai for PGA and SA at 0.2, 1.0 and 3.0 s response periods. The dashed line is the standard deviation due to all the branches in the logic tree (total epistemic uncertainty); the bold line is the standard deviation of the mean hazard curves of each set of attenuation equations; the thin grey lines are the standard deviations for the 972 hazard curves corresponding to each set of GMPEs shown in Table 4.1.

The total standard deviation in this case is calculated using the following equation:

$$\sigma_T^{\,2} = \sigma_{me}^{\,2} + \sum \frac{\sigma_i^{\,2} * W_i}{\sum W_i} \qquad 5.16$$

Where σ_{me} is the standard deviation of the mean values of the 16 sets of equations, σ_i is the standard deviation corresponding to the variability about any given set of equations and W_i is the weight assigned to each branch. Following the common practice, where the sum of the weights for

alternative branches in the logic tree is equal to one, the term ΣW_i can be simply neglected.

Two main observations can be made from the results shown in Figure 5.45. Firstly, the greatest contributor to the total uncertainty is the selection of the GMPE set and that all of the remaining sources of epistemic uncertainty only contribute in a very minor way. This latter contribution simply being the difference between the dashed and the solid black lines. Secondly, the standard deviation resulting from different combinations of attenuation equations, in order to make a set, can be significantly different. For PGA, the standard deviation from each set of equations follows roughly the same pattern, while at 3.0 s response period the differences are of many orders of magnitude.

If, instead of a group of equations, only one attenuation equation were used for modelling ground motions at all of the seismic sources the standard deviation of the hazard curves, due to epistemic uncertainties, for each alternative equation should be expected to be the same or at least very similar. However, when different equations are used for modelling ground-motion attenuation at different seismic sources the differences in the estimation of the hazard can become very important.

As an example, in Figure 5.46 the hazard curves of each of the branches of the logic tree corresponding to the sets of equations 9 and 11 (see Table 4.1) are presented. These hazard curves are for the city of Dubai and 3.0 s response period. Between these two groups, only the equation used to model ground-motion attenuation of shallow earthquakes occurring in active regions changes. In Set 9 the equation of Akkar & Bommer (2007b) is used, while in Set 11 the equation of Boore & Atkinson (2006) is used.

A clear bifurcation of the hazard curves for Set 9 can be observed at spectral amplitudes above 0.007 g. Thereafter, the standard deviation of the spectral amplitudes increases significantly. As a comparison, the standard

deviation at 0.02 seconds for Set 9 is 0.88 while for Set 11 it is only 0.23. In this case, due to the bifurcation of the hazard curves for Set 9, one could argue that the standard deviation is not the best way to measure the scatter and the comparison with values of standard deviation of other sets of equations may not to be appropriate. That is, the overall distribution is clearly bi-modal and the interpretation of the standard deviation may be misleading. However, in this particular case the statistic still reflects a higher level of uncertainty in the results of Set 9 over those of Set 11.

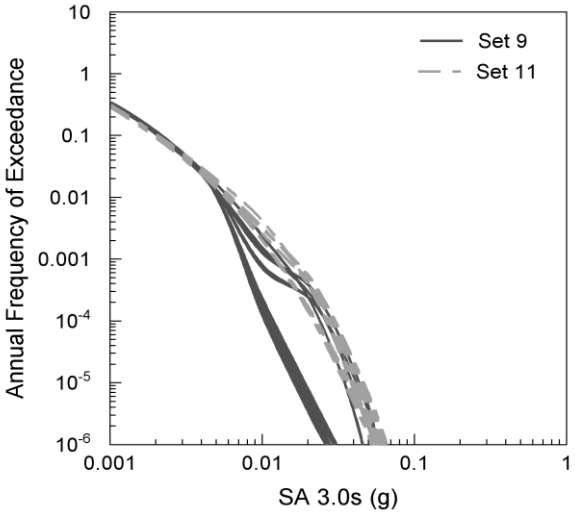

Figure 5.46. Hazard curves for the branches in the logic tree corresponding to the sets of attenuation equations 9 and 11 (see Table 4.1). The hazard curves are for the city of Dubai and SA at 3.0 s response period.

In order to appreciate the differences between different branches of the logic tree relating to different sets of GMPEs, for the three levels of uncertainty (i.e., Stable craton regions, shallow earthquakes in active regions and earthquakes in subduction zones), from Figure 5.47 to Figure 5.49 the mean hazard curves for the city of Dubai, grouped according to the different branches of each node, are shown.

Figure 5.47 shows the mean hazard curves for the city of Dubai for the two options regarding the GMPE used to model ground-motion attenuation for earthquakes in the Arabian stable craton. As can be seen, at the longest

return periods, the hazard curves for which the attenuation equation of Atkinson & Boore (2006) was used present lower probabilities of exceedance for given ground-motion levels than those where attenuation equations for active regions were used. This difference is larger at PGA and 0.2 s response period and decreases for longer response periods. The differences are clearly correlated with the contribution to the hazard of the Arabian stable craton, which is higher at long return periods (see section 3.8).

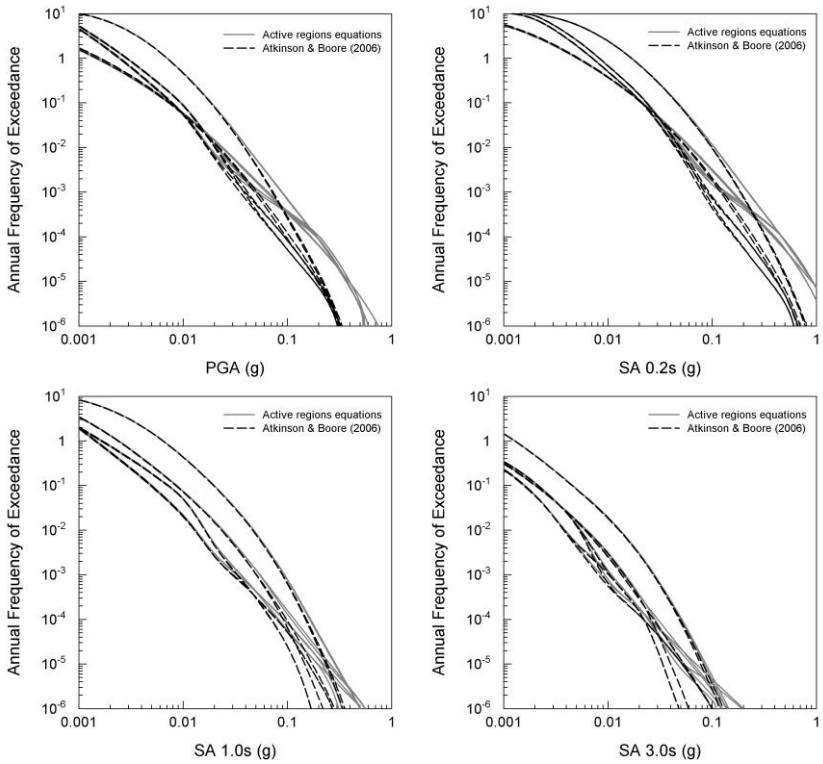

Figure 5.47. Mean hazard curves for the two options of GMPEs for modelling attenuation on the Arabian stable craton. The hazard curves are for the city of Dubai for PGA and SA at 0.2, 1.0 and 3.0 s response periods.

Figure 5.48 shows the mean hazard curves, for the city of Dubai, for the four alternatives at the node of the logic tree regarding the GMPE used to model ground-motion attenuation for shallow earthquakes in active regions. Most of the equations present similar behaviours with the exception of Abrahamson & Silva (1997) which constantly presents higher probabilities of exceedance.

The biggest differences are at the shorter return periods and for PGA and SA at 0.2 s and extend to longer return periods for SA at 1.0 and 3.0 s response periods. As in the case for the Stable craton, these differences match the contribution to the hazard of the seismic sources from the active crustal regions (Persian Gulf, Simple Fold belt and Zagros Foredeep).

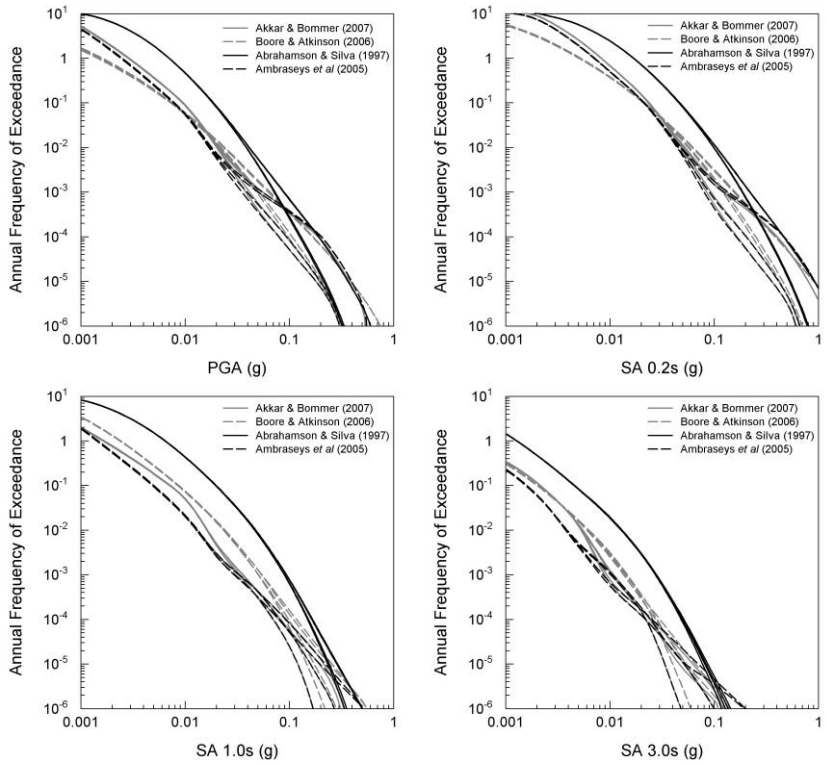

Figure 5.48. Mean hazard curves for the GMPEs modelling attenuation for shallow earthquakes in active regions. The hazard curves are for the city of Dubai for PGA and SA at 0.2, 1.0 and 3.0 s response periods.

The differences between the two equations used to model ground-motion attenuation for earthquakes from the Makran subduction zone are shown in Figure 5.49. For the city of Dubai, the implication of using either of these models only has some relevance at 1.0 and 3.0 s response periods and at very low probabilities of exceedance (<~$1x10^{-5}$). However, at Ra's Al Khaymah the difference between the curves associated with each of the models is more important, mainly at PGA and 0.2 s response period (Figure 5.50) and at return periods as short as 10,000 years.

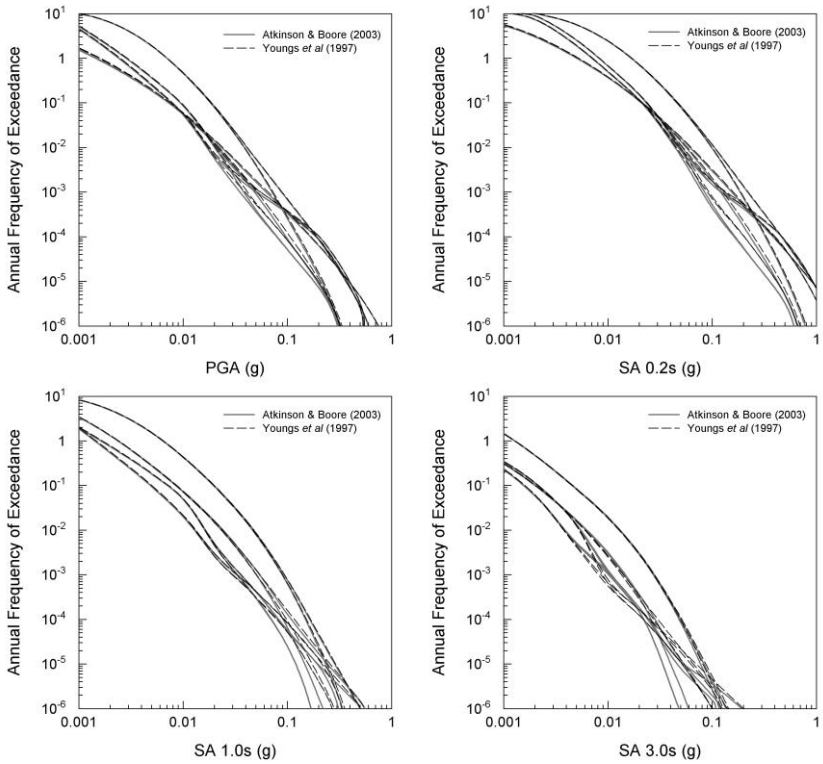

Figure 5.49. Mean hazard curves for the two GMPEs for modelling attenuation for earthquakes in the Makran subduction zone. The hazard curves are for the city of Dubai for PGA and SA at 0.2, 1.0 and 3.0 s response periods.

These results highlight, once more, that the seismicity in the Makran subduction zone, mainly on its west half, provides some important contribution to the seismic hazard on the north-eastern part of the UAE. These results are of high relevance for the seismic resistant design of facilities requiring consideration of very long return periods such as nuclear power plants.

It is clear that once a reasonable number of ground-motion prediction equations (three or more), or combinations of them, have been included in the logic tree, the epistemic uncertainty is mainly dominated by these equations. For this reason, special care must be taken to select the most suitable attenuation equations for the region under study. A detailed discussion of the criteria for selecting ground motion models for a particular area is presented by Cotton *et al.* (2006).

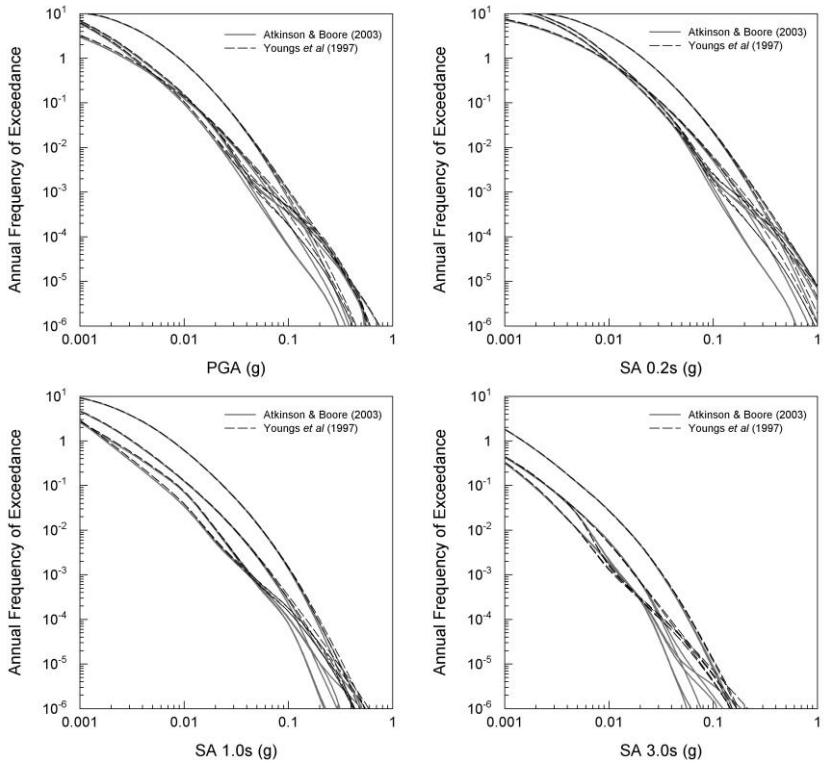

Figure 5.50. Mean hazard curves for the two GMPEs for modelling attenuation for earthquakes in the Makran subduction zone. The hazard curves are for the city of Ra's al Khaymah for PGA and SA at 0.2, 1.0 and 3.0 s response periods.

In some cases the use of different GMPEs could lead to hazard results that are more or less sensitive to the other sources of uncertainty. This is the case shown in Figure 5.46, where the effect of the epistemic uncertainty regarding the rupture model for the Makran has a differing degree of influence on the scatter of the hazard curves depending on the attenuation equation assigned to shallow earthquakes in active crustal regions.

There is still an ongoing discussion regarding whether or not the weights assigned to the branches of a logic tree should be treated as approximate probabilities or as subjective weights, since the basic axioms of probability theory, mutual exclusivity and collective exhaustiveness, are difficult satisfy. This being particularly true for ground-motion models (Bommer & Scherbaum, 2008). However, so far the most broadly accepted way to capture the epistemic uncertainty in ground-motion modelling is through a logic-tree framework.

5.7. Sigma

Ground-motion prediction equations predict the median value of ground-motion given a set of independent variables such as magnitude, distance, site condition and faulting mechanism, among potentially others. Each equation always has an associated standard deviation (sigma, σ) representing the aleatory variability of the ground-motions for any given set of independent variables.

In addition to the previously mentioned variables, attenuation equations predict ground motions also as function of ε (see Equation 2.7), where ε represents the number of standard deviations that a level of ground-motion is from the median prediction for a given earthquake scenario (consisting of magnitude, distance and other variables). Therefore, the probability of exceeding a target ground motion is directly related to the σ value of the ground-motion equation.

As an example, Figure 5.51 shows the probability distribution and the cumulative distribution functions for the logarithm of PGA using the equation of Boore & Atkinson (2006) for an earthquake of magnitude 6.5 M_w at a distance of 10 km and for values of 0.5σ, 1.0σ and 1.5σ, where σ is the original standard deviation of the equation. Based on this, the probability of exceeding a target ground motion of 0.4 g [Ln(0.4) = -0.9] for the stated magnitude and distance is 0.5, 10.0 and 19.7 % for values of sigma of 0.5σ, 1.0σ and 1.5σ respectively.

In this section, a sensitivity analysis on the influence on the resulting hazard curves due to modifying the value of sigma corresponding to each GMPE is presented. As in previous sections, only one branch of the logic tree of the case study was used to perform the analysis. The branch was selected following the highest weights for the different options at each node of the logic tree. For the epistemic uncertainty in Makran, where the east and west segments have the same weight, the west-segment branch was preferred.

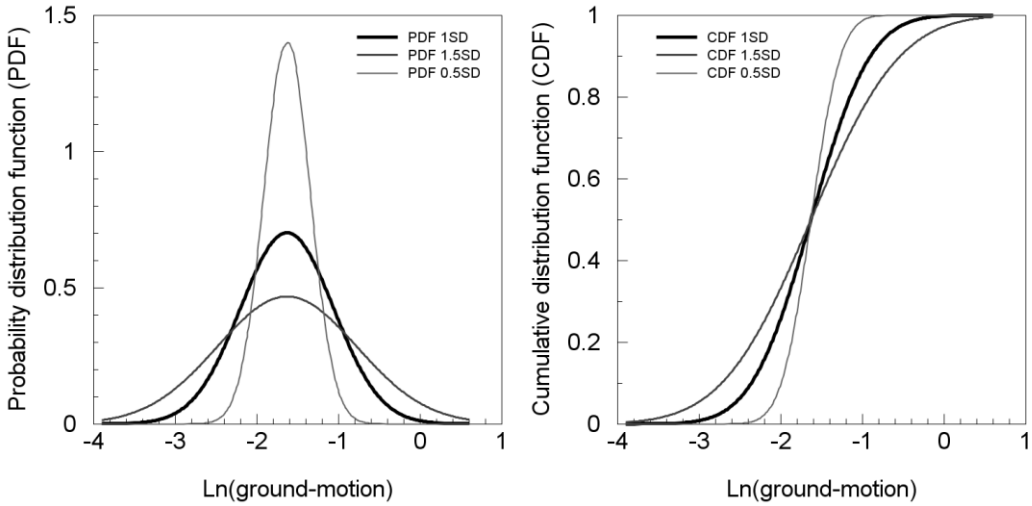

Figure 5.51. Probability distribution function (left) and cumulative distribution function (right) of the logarithm of PGA for an earthquake 6.5 M_w at a distance of 10 km (r_{jb}) for the GMPE of Boore & Atkinson (2006). PDF 1SD is the probability distribution corresponding to the original value of σ; PDF 1.5SD is the probability distribution for a 50% increase on the original value of σ; and PDF 0.5SD is the probability distribution of a 50% decrease on the original value of σ.

The ground-motion equations selected for this analysis were: Atkinson & Boore for predicting ground-motions in the stable craton, Boore & Atkinson (2006) for shallow earthquakes in active continental regions and Atkinson & Boore (2003) for subduction zones. The value of sigma for these equations is not magnitude dependent but it is response-period dependent, with the exception of Atkinson & Boore (2006) where the same value of sigma is applied to all response periods. In the latter two equations sigma tends to increase with the response period. To perform the sensitivity analysis the value of sigma for these three equations was varied by ±10 and 20% of the original value.

In Figure 5.52 the hazard curves resulting from the use of the adjusted σ values are shown for the city of Dubai. The influence of sigma is clearly greatest at longer response periods and increases as the exceedance probability decreases. Only at PGA and SA at a period of 0.2 s and at exceedance probabilities smaller than $1x10^{-5}$ can a decrease in the influence of sigma be noticed for the curves of σ-10% and σ-20%. This behaviour can be associated with the change of the seismic source dominating the hazard;

this change in the dominating seismic source translated to a change in the GMPE that most influences the hazard results.

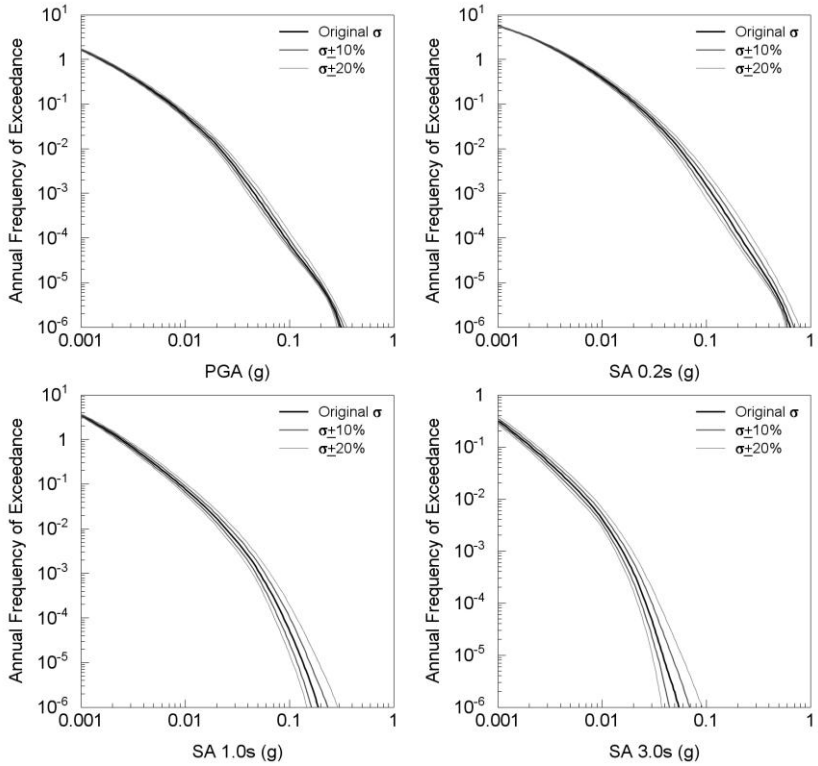

Figure 5.52. Hazard curves for the city of Dubai for PGA and SA at 0.2, 1.0 and 3.0 s response period, using different values of standard deviation for the GMPEs.

At the range of exceedance rates below $1x10^{-5}$ the dominating seismic source is the Stable craton, in which ground-motion attenuation is modelled by the equation of Atkinson & Boore (2006). At any other level of exceedance rate the ground-motion attenuation for the dominating sources is modelled by the equation of Boore & Atkinson (2006).

The variation of sigma does not only influence the expected annual frequency of exceedance of a given value of ground-motion but also the distribution of the contributions to the hazard from different bins of magnitude and distance in the disaggregated results.

Figure 5.53 and Figure 5.54 show the disaggregated results by magnitude, distance and epsilon (M-R-ε) for values of sigma of 0.8σ, 1.0σ and 1.2σ; these results are for the city of Dubai for PGA and SA at 3.0 s

response period respectively. To obtain the disaggregated results in terms of ε the procedure described in section 4.4 was applied.

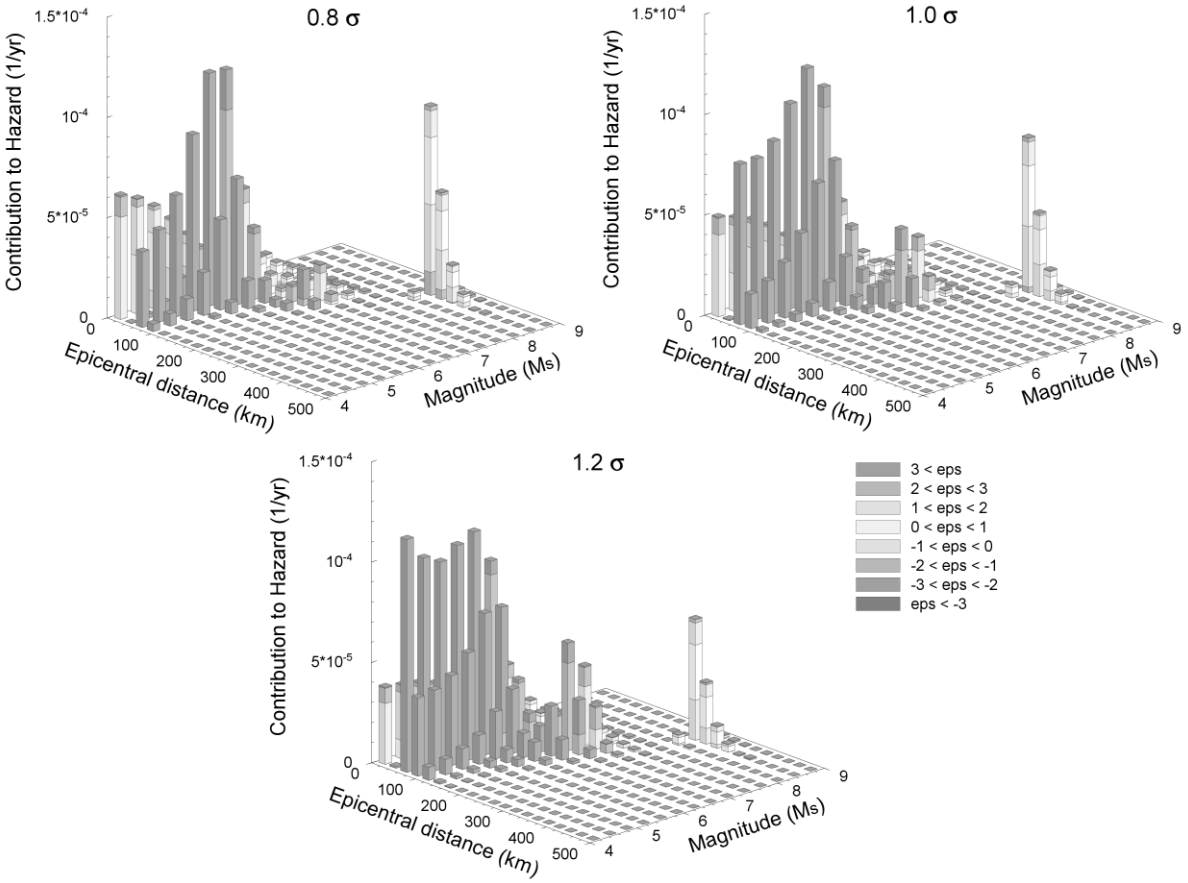

Figure 5.53. Disaggregated results for different values of sigma (σ) for the city of Dubai, for a return period of 500 year and PGA.

Although when viewing the hazard curves, the differences in the expected value of ground motion at the 500-year return period does not appear significant, the disaggregated results present quite different perspectives, which in some cases can lead an analyst to consider different dominant earthquake scenarios.

For example, for PGA at the 500-year return period (Figure 5.53) for 0.8σ the dominant earthquake scenario corresponds to an M* = 5.9 M_s, R* = 62.5 km (r_{epi}) and ε^* > 3, while at 1.2σ the dominant earthquake scenario corresponds to an M* = 4.2 M_s, R* = 62.5 km (r_{epi}) and ε^* > 3. At 3.0 s response period (Figure 5.54), a smooth transition of the contributions can

be observed from a concentration at events >7.5 M_s at distances between 275 to 400 km at 0.8 σ, towards events of magnitude 6.0-7.0 M_s at distances between 175 to 300 km at 1.2σ. Although this transition is not enough to modify the dominant earthquake scenario, the changes in the overall distribution of the disaggregated contributions might lead to different decisions being made regarding subsequent analyses.

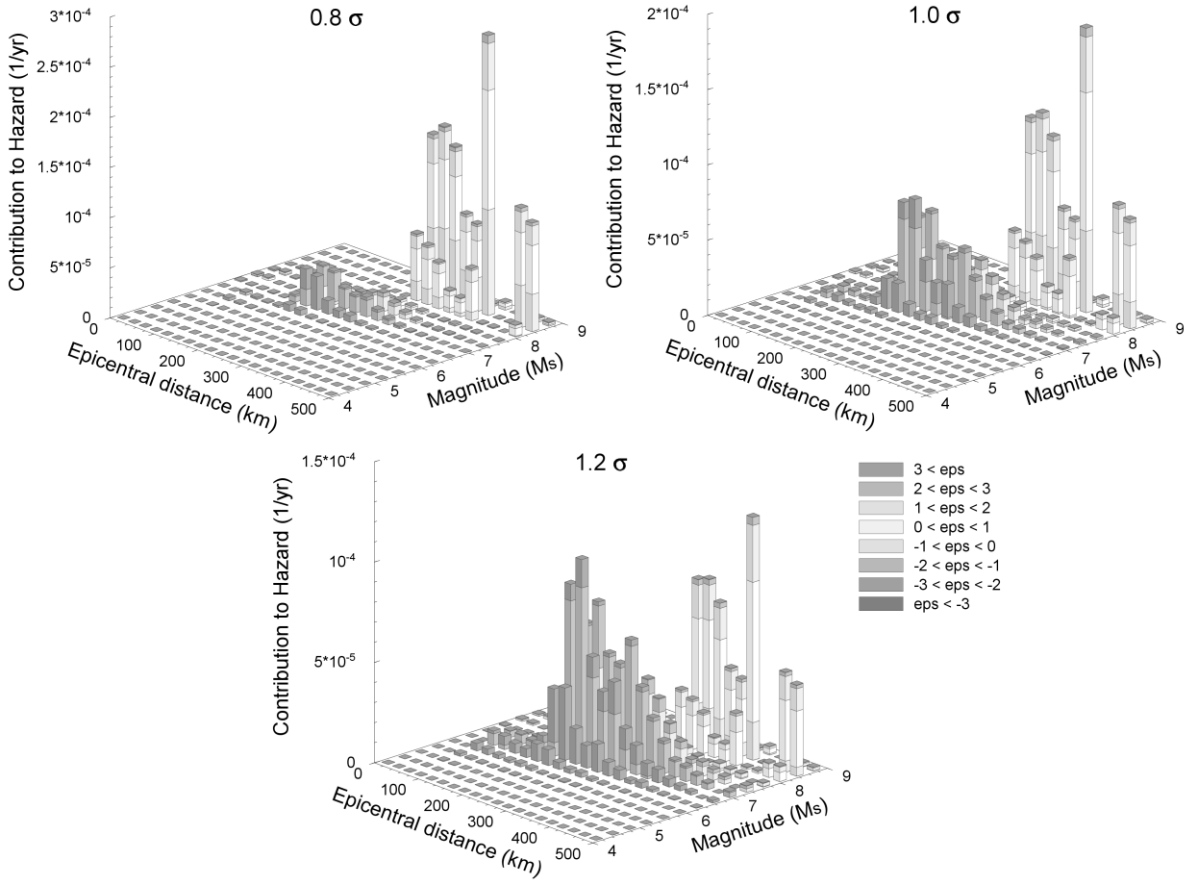

Figure 5.54. Disaggregates results for different values of (σ) for the city of Dubai, for a return period of 500 years and SA of 3.0 seconds.

In more general terms, an increase in the σ value of the ground-motion equation leads to a higher increase in the contributions to the hazard from small but more frequently occurring events than in the contributions from larger but less frequent events. In this way, a shift in the relative contributions by magnitude-distance scenarios can be observed from large-

magnitude scenarios towards small-magnitude scenarios as the value of σ increases.

It is important to note that in both cases, the contributions by ε for the same bins of magnitude and distance have roughly the same distributions. In other words, although the contribution to the hazard of each M-R bin changes for the different values of sigma (i.e., 0.8σ, 1.0σ and 1.2σ) the percentage of this contribution corresponding for each bin of ε does not have a significant change.

In conclusion, the standard deviation associated with the GMPE has an important impact on the resulting hazard curve, particularly at low annual rates of exceedance. Higher values of sigma lead to higher exceedance probabilities for a given value of ground-motion. In terms of changes in the disaggregated results, a shift in the contributions from large-magnitude to small-magnitude scenarios is observed as sigma increases. This shift in the contributions is expected to be more significant when using ground-motion models where sigma is dependent of magnitude [σ(M)] since in these models sigma usually decreases with increasing magnitude. This situation could lead to different dominant scenarios for different values of sigma.

An important point to highlight is that when multiple GMPEs are used the shape of the hazard curves would vary depending on the GMPE assigned to the dominating seismic source. This is the case of the hazard curves for PGA and 0.2 s response period shown in Figure 5.52.

5.8. Weights in the logic tree

The process of assigning weights to each branch of the logic tree is a controversial issue in PSHA due to the significant degree of subjectivity that is involved. Different experts would assign different weights to each of the

branches (as well as selecting branches to begin with). Due to this, some concern has arisen about the influence of the weighting process on the hazard results. This has additional relevance when branches with alternative ground-motion models are weighted, as it is here that most of the epistemic uncertainty is located (as was seen earlier).

The objective of this section is to explore the sensitivity of the hazard results to different weightings of the branches in the logic tree. To this end, the weights assigned to each branch of the logic tree in the case study (see section 3.6) were modified using four alternative weighting criteria in addition to the initial set of weights used in the case study.

The criteria for setting the first two alternative sets of weights was to increase or decrease by about 0.1 the initial weight assigned to the branch considered to be the “best estimate” or the “most likely scenario”. The “best estimate” or “most likely scenario”, for this particular case, is defined as that with the highest weight (in the initial set of weights) among the alternative branches at a single node, in Figure 5.55 the branches with the best estimates are marked with an asterisk (*). The weights of the alternative options to the “best estimate” are reduce in proportion to their original values in order to keep the sum of all the alternative branches on each node equal one.

In Figure 5.55 the set of weights marked as (2) corresponds to the case when the weight of the best estimation was increased, while for those marked as (3) the weight of the best estimation was decreased. The weight of the branch with the best estimate was never decreased to have values lower than the adjacent branches. These two cases would reflect the hypothetical case in which, once the logic tree has been set up, a group of analysts agree on which of the alternatives on each node is the most likely scenario but their level of confidence on it varies. It is worth noting that the difference in the weights for the best estimate varies by up to 20% of the total weight of

each node (0.2 difference between the lowest and the highest weight). On those branches where equal weights were assigned to all alternative options, these were kept the same for the different set of weights.

A third option was to assign equal weights to each branch on each node, thus representing equal levels of confidence in each alternative option. It is important to keep in mind that this does not imply that each alternative scenario at the ending tips of the logic tree will necessarily have the same weight (as it depends on how many nodes exist along each branch). Even though this option, in many cases, results in weights to the case when the weights of the best estimate are decreased, it was considered for the analysis due to the presence of highly skewed weights on some nodes of the logic tree. For these nodes, assigning equal weights may have an impact on the resulting hazard. This is the case, for example, for the rupture model in Makran where for the complete-rupture option was originally assigned a weight of 0.05 while for the segmented-rupture option a weight of 0.95 was set. In Figure 5.55 the weights for this option are marked as (4).

Finally, a last alternative was considered taking into account only the scenario corresponding to the best estimate. This is equivalent to assign a weight equal to one to the branch with the best estimate and zero to all the others. Although all GMPEs for shallow earthquakes in active continental regions were originally assigned equal weights, the equation of Boore & Atkinson (2006) was selected as the best estimate for this analysis as it is the most recent of the equations and was derived using the most comprehensive earthquake catalogue.

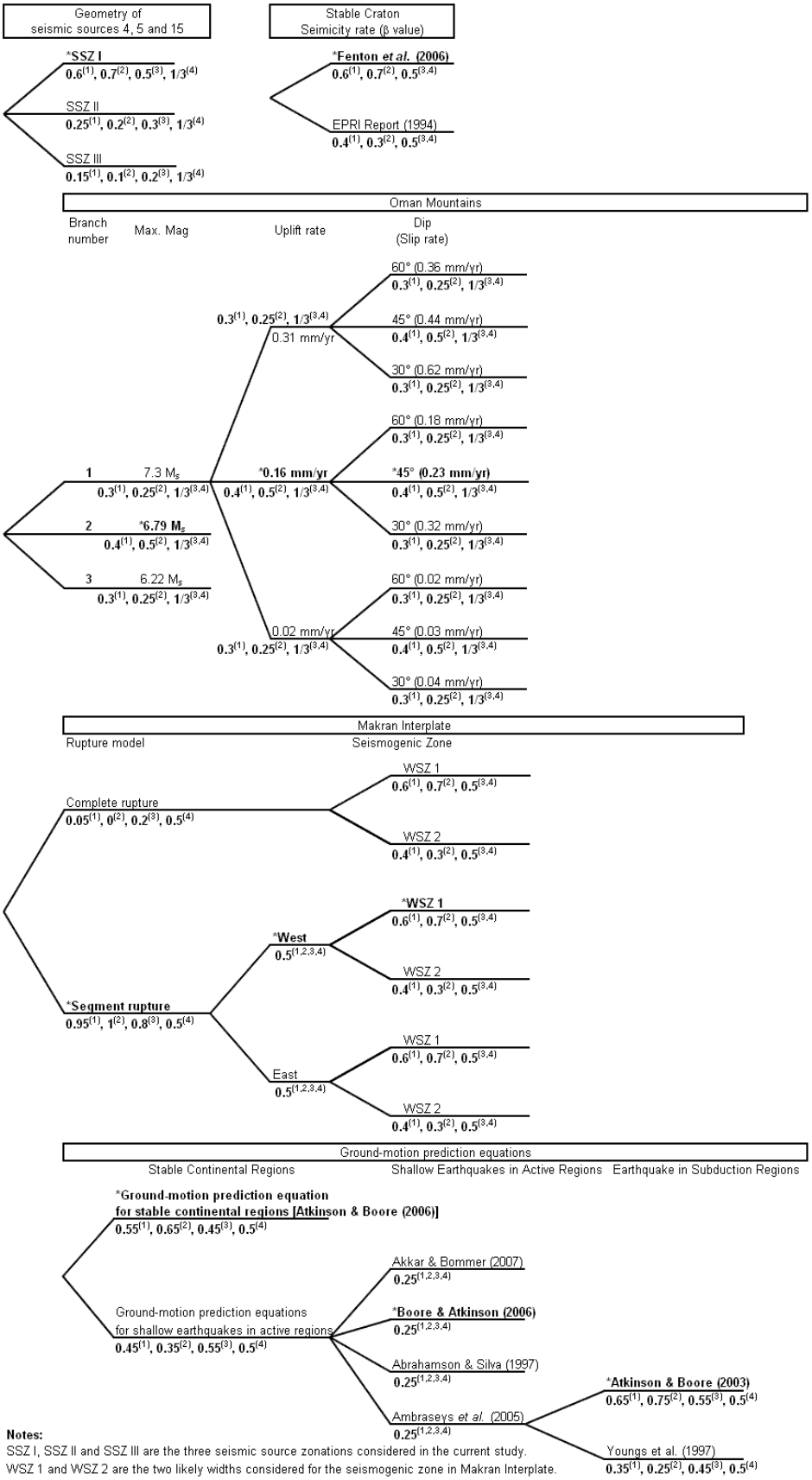

Figure 5.55. Weights on the logic tree used for the sensitivity analysis. (1) Weights used on the original analysis in the case study; (2) Increasing the weight of the "best estimate" option; (3) Decreasing the weight of the "best estimate" option; (4) Equal weights for each alternative option. Branches on bold marked with asterisk (*) are the "best estimate" option.

In Figure 5.56 the resulting hazard curves for the five sets of weights (i.e., the initial weights plus the four weighting sets proposed herein for the sensitivity analysis) are shown. These results are for the city of Dubai for PGA and SA at 0.2, 1.0 and 3.0 s. A similar influence on the resulting hazard curves from considering the different weighting schemes was observed at the cities of Abu Dhabi and Ra's Al Khaymah.

The discrepancy between the hazard curves from all the different sets of weights is negligible with the exception of the "best-estimate" option, which results in lower values of exceedance probabilities for given values of ground motion.

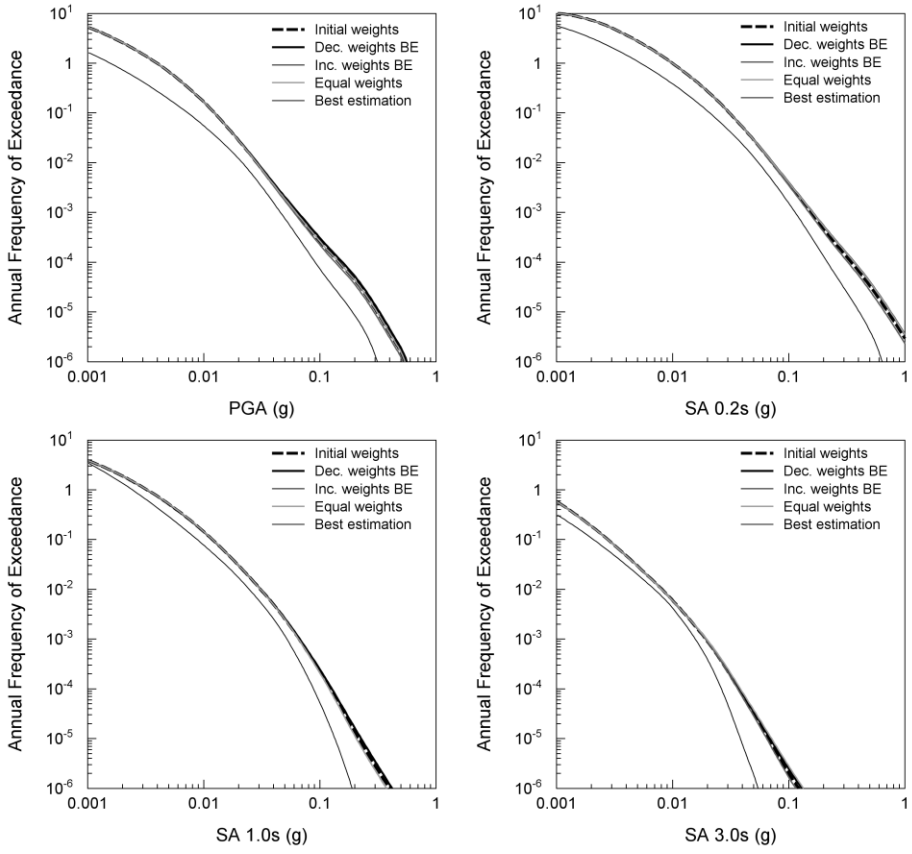

Figure 5.56. Hazard curves for the city of Dubai for different sets of weights of the logic tree. The hazard curves are for PGA and SA at 0.2, 1.0 and 3.0 s response periods. Initial weights – weights used in the case study; Dec. weights BE – decreasing the weight of the best estimation; Inc. weights BE – increasing the weight of the best estimation; Equal weights – equal weights for each alternative branch of each node; Best estimation – the analyst's best-estimation scenario.

From Figure 5.57 to Figure 5.60 the disaggregated results for the five sets of weights for PGA and SA at 3.0 s, and for return periods of 500 and 10,000 years, are shown. As in the case of the hazard curves, the disaggregated results for the different sets of weights present very similar views, with exception of the "best-estimate" option, which presents a slightly different view for PGA at 500 and 10,000-year return periods and notably different panoramas for 3.0 s response period at both return periods.

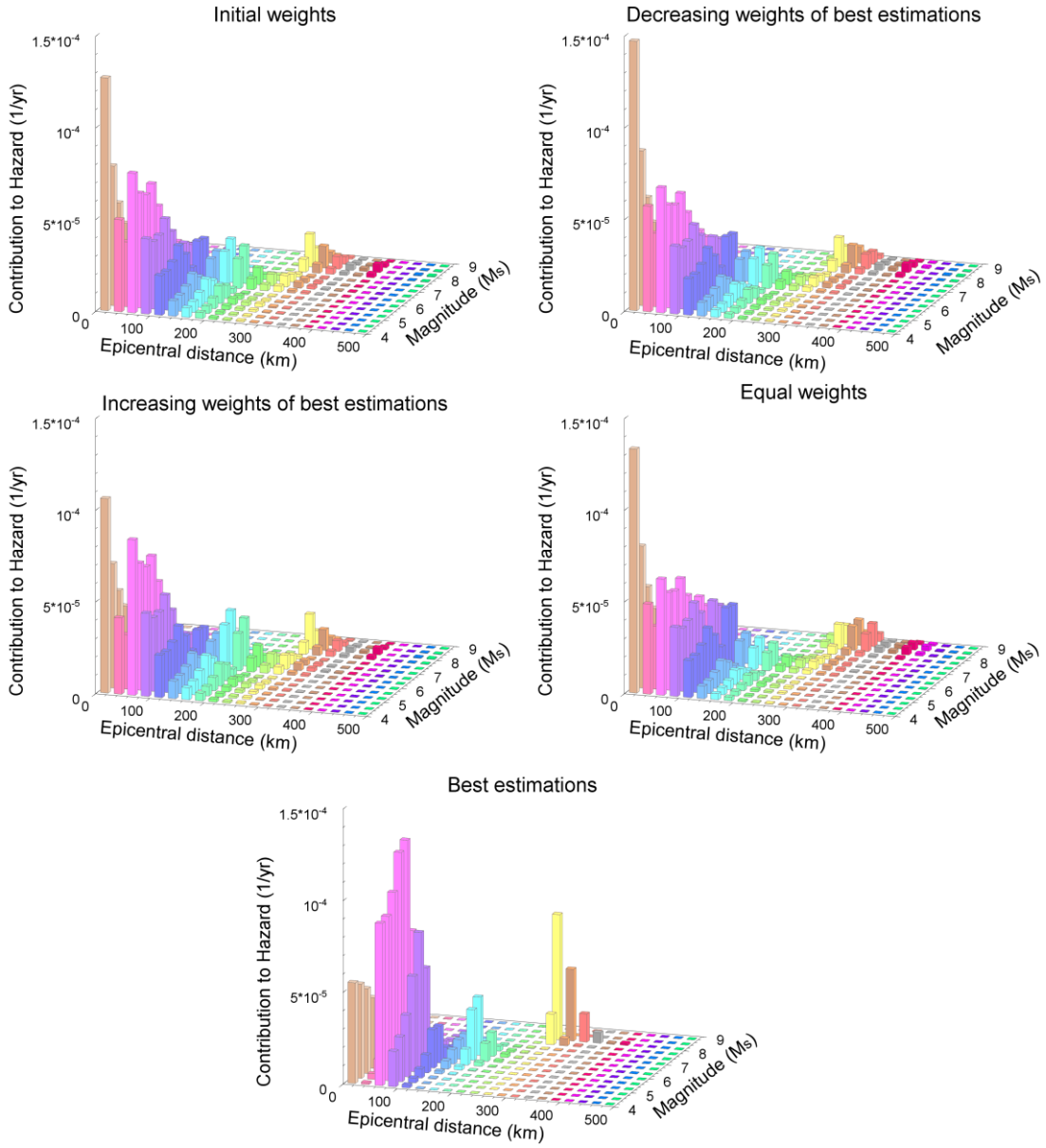

Figure 5.57. Disaggregated results for different weightings of the logic tree for the city of Dubai for PGA at 500-year return period.

In conclusion, once the logic tree has been set up and a general consensus on which of the alternative options of each node represents the most likely scenario or the best estimates have been reached, the process of assigning weights to the alternative branches on the logic tree has only a small, and essentially negligible, impact upon the final hazard in this case. Similar results are presented by Sabetta *et al.* (2005).

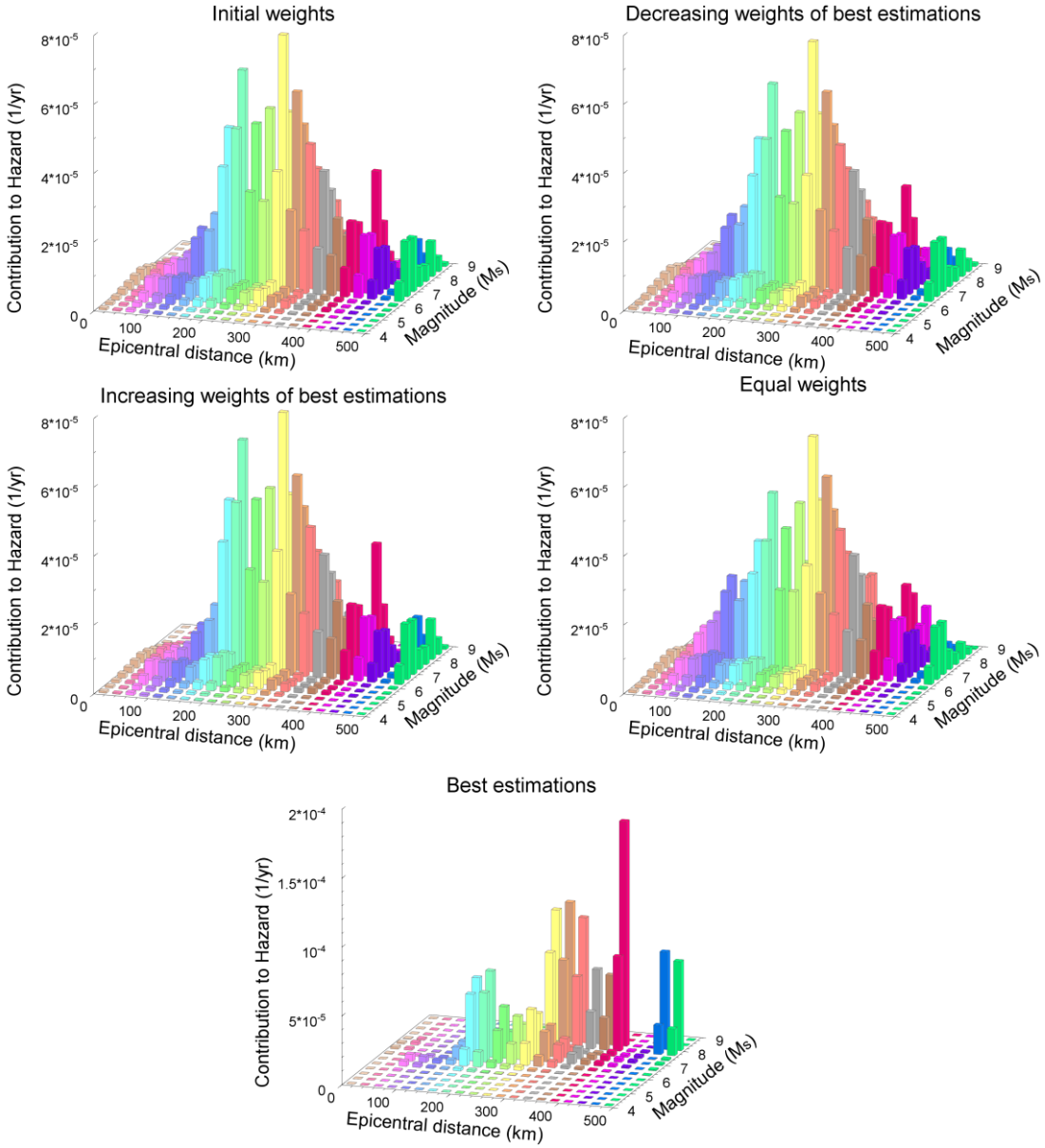

Figure 5.58. Disaggregated results for different weightings of the logic tree for the city of Dubai for SA at 3.0 s respond period and a 500-year return period.

Only for the case where very skewed weights are assigned towards one of the options will significant differences in the hazard results be obtained. This is the case of the best-estimate option considered in the analysis, where a weight equal to one was assigned to the preferred option.

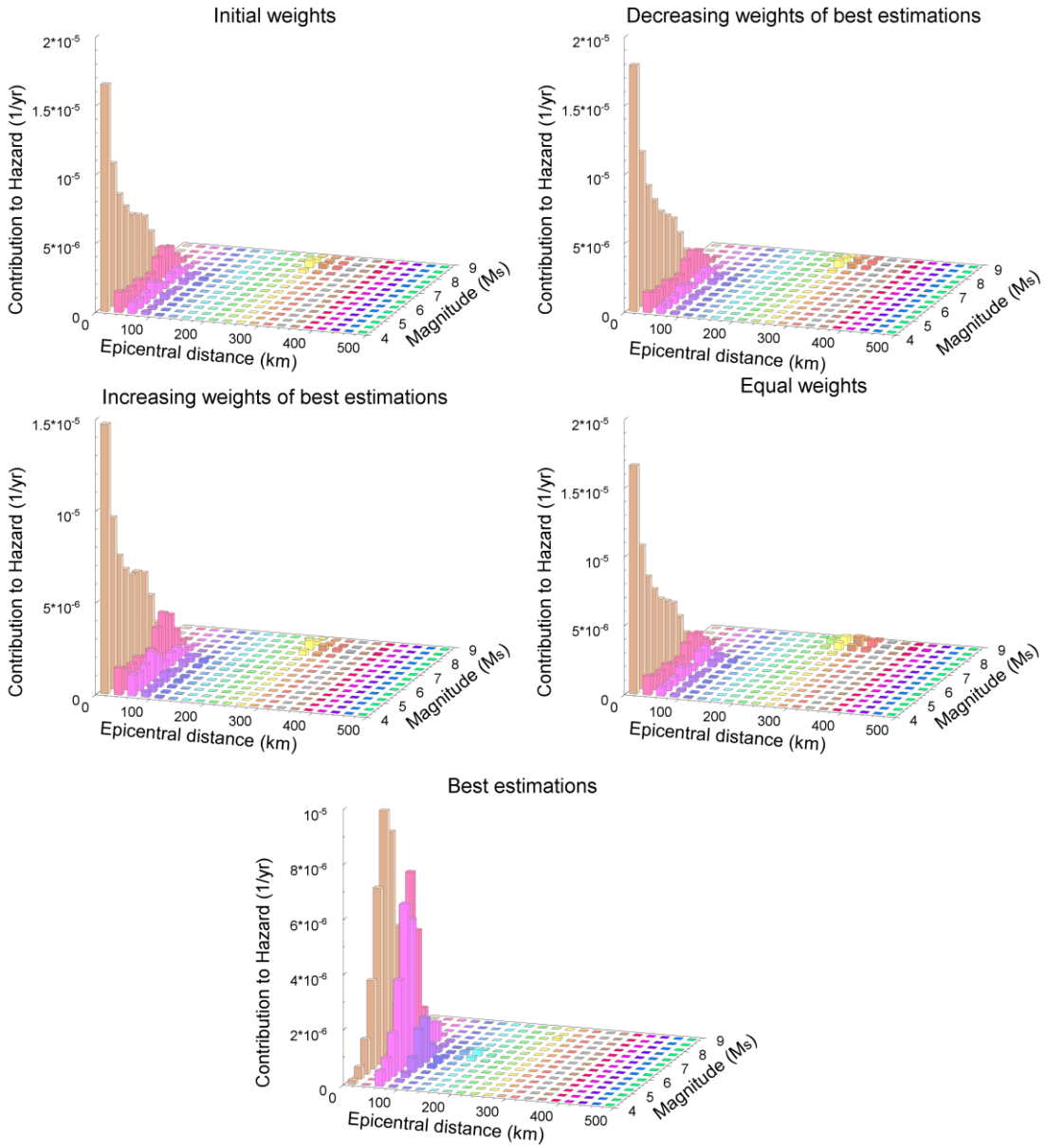

Figure 5.59. Disaggregated results for different weightings of the logic tree for the city of Dubai for PGA at the 10,000-year return period.

Since most of the epistemic uncertainty is due to the consideration of alternative GMPEs, the weights assigned to them will have higher influence on the hazard results than any other source of epistemic uncertainty. As can

be seen in Figure 5.48, for the case presented herein, the decision of which GMPE would be considered for the best-estimation option completely dominates the hazard results.

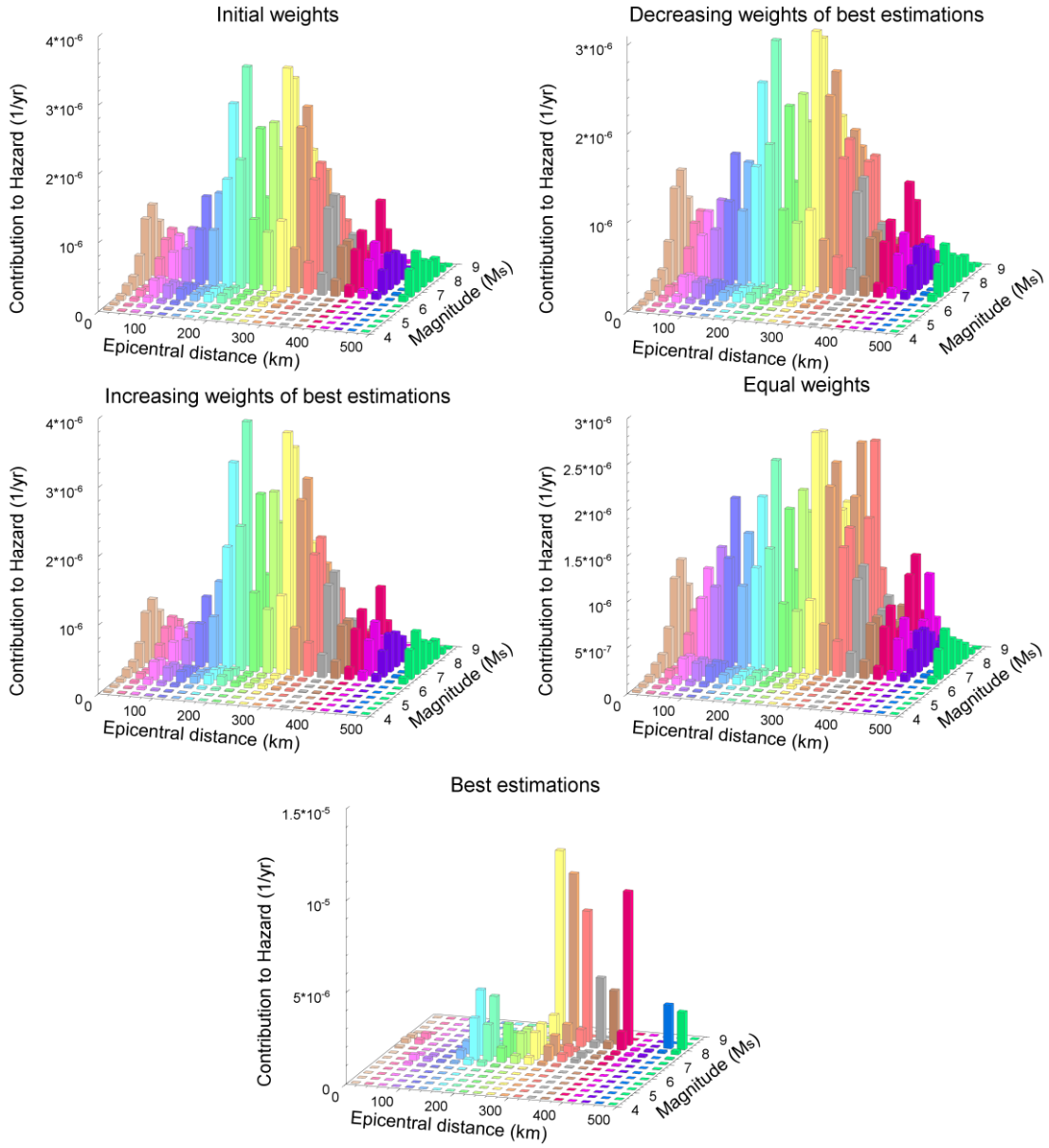

Figure 5.60. Disaggregated results for different weightings of the logic tree for the city of Dubai for SA at 3.0 s respond period and a 10,000-year return period.

Chapter 6.

HAZARD IN TERMS OF OTHER PARAMETERS

Nowadays seismic hazard analyses conducted in terms of peak ground acceleration (PGA) and spectral acceleration at particular response periods [SA(T)] are still the standard despite the proven utility of a number of parameters such as peak ground velocity (PGV), Arias intensity (I_a), and spectral intensity (SI), among others.

To some degree, one of the reasons for this is the relatively small number of predictive equations for parameters such as PGV or the complete lack of these equations as is the case for SI. Additionally, PGA and SA(T) have traditionally received more attention since these parameters govern seismic design in building codes. This has led to the use of correlation factors for converting, for instance, spectral ordinates to PGV, instead of performing a rigorous PSHA study directly in terms of the ground-motion parameter of interest. However, it has been shown that this type of practice does often not have well founded basis and could lead to significantly biased results (Bommer & Alarcón, 2006).

In this chapter, the relationships between the hazard results for SA(T) and the expected values of PGV and SI, obtained from PSHA performed in terms of each of these parameters, are explored. In order to do this, a new ground motion prediction equation (GMPE) for spectral intensities was developed using the same functional form and database as the predictive equation for spectral displacements (SD) of Akkar & Bommer (2007b).

Using the same framework of the case study presented in Chapter 3, the seismic hazard was calculated in terms of SI using the predictive equation derived herein, PGV using the predictive equation of Akkar &

Bommer (2007a) and SA(T, ξ) using the predictive equations of Akkar & Bommer (2007b). These prediction equations were chosen since they were developed using the same functional form, same earthquake database, same explanatory variables and same definition of horizontal component; they are therefore fully compatible.

Since the aim of this study is to explore the relationship between the ground-motion values obtained from PSHA directly in terms of SI and PGV and the values inferred from SA(T), only one branch of the logic tree presented in Figure 3.38 was considered for the analysis and the same predictive equation was assigned to all seismic sources regardless of its tectonic regime. State that it is acknowledged that this is not correct, but provides a direct comparison. The selected branch is the "best-estimation" branch defined as the branch with the highest weights (see Figure 3.38 or alternatively Figure 5.55 for greater clarity on the identification of the "best-estimation" branch). For the epistemic uncertainty associated to the Makran Interplate source, where the west and east segmented ruptures have the same weight, the west option was preferred as the east halve does not contribute to the hazard at the sites under study.

The results of the PSHA for SI, PGV and SA(T, ξ) are presented in the following sections. In the last section of this chapter, together with the hazard results for SA(T, ξ), values of SI and PGV are inferred from SA(T, ξ) and compared with the values obtained from PSHA directly.

6.1. Spectral Intensity

Housner (1952) defined the "response spectrum intensity" as:

$$SI(\xi) = \int_{0.1}^{2.5} PSV(\xi, T)\, dT, \qquad 6.1$$

where ξ is the damping ratio of the linear elastic single-degree-of-freedom system and T is the response period. The spectral ordinates in the range between 0.1 and 2.5 were considered by Housner (1952) as providing a good indication of the potential of a ground motion to excite response of most structures (as these generally have fundamental periods within this range). Therefore, SI may be considered as a measure that captures structural response of typical structures during their initial and damaged states.

SI have been shown to have a good correlation with displacement ductility demand (Martínez-Rueda, 1998) and with damage to long-period structures (Milana *et al.*, 2008). Alternatively, SI has been proposed as a reference parameter for scaling ground-motion records for the assessment of the dynamic response of structures (e.g., Fintel & Ghosh, 1982; Kappos, 1991).

To begin this section, a new empirical ground-motion prediction equation for SI as function of moment magnitude (M_w), Joyner-Boore distance (r_{jb}), site conditions, and for damping ratios equal to 2, 5, 10, 20 and 30 % is presented. To the knowledge of the author, the only other prediction equation that has been derived directly for SI as function of magnitude and distance is that presented by Danciu & Tselentis (2007), who derived an equation using a ground-motion dataset consisting of recordings from Greek earthquakes. Indirect models have also been developed. For example, Martínez-Rueda (2006) presents a model for spectral intensity based on the prediction equation for spectral accelerations of Ambraseys *et al.* (2005). However, the model presented by Martínez-Rueda (2006) contains several drawbacks that restricts its application, the most important of which being the failure of the model to account for ground-motion variability.

A total of 512 records from 130 events contained in the strong-motion databank for Europe and the Middle East were used in the regression analysis. The dataset is the same as that used by Akkar & Bommer (2007b)

but considering only records with usable periods spanning the range from 0.1 to 2.5 s. The distribution of the dataset in terms of magnitude and distance values of the records is presented in Figure 6.1.

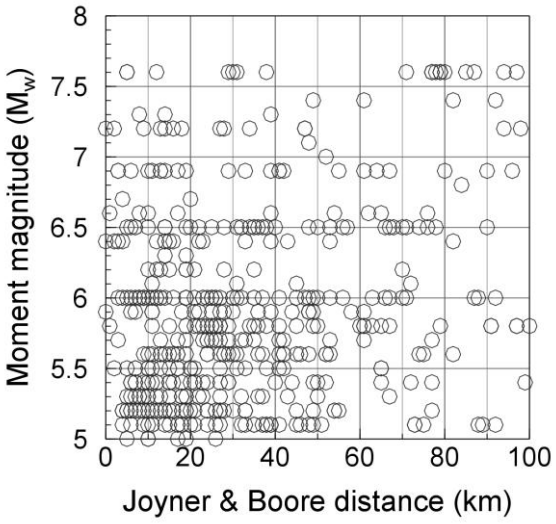

Figure 6.1. Distribution of the dataset respect to magnitude and distance.

The functional form is the same as that used by Akkar & Bommer (2007b) for the prediction of spectral displacements (SD) with the exception that, in the equation presented herein, faulting mechanism is not included as an explanatory variable. The faulting mechanism was removed from the original functional form on the basis that a regression analysis conducted using the original functional form proved that no statistical dependence upon faulting mechanism could be found. The ranges of predictor variables for which the model is applicable correspond to moment magnitudes between 5.0 and 7.6 and r_{jb} distances between 0 and 100 km. SI is calculated using the geometric means of the horizontal components of the spectral amplitudes at each period, i.e., using the geometric mean of the individual spectra.

The equation for predicting spectral intensities has the following form:

$$\log\left[SI\left(T,\xi\right)\right] = b_1 + b_2 M + b_3 M^2 + \left(b_4 + b_5 M\right)\log\sqrt{r_{jb}^2 + b_6^2} + b_7 S_S + b_8 S_A, \qquad 6.2$$

where SI is the spectral intensity in units of cm/s/s, M_w is the moment magnitude, r_{jb} is the Joyner-Boore distance in km, S_S and S_A are binary variables taking values of 1 for soft and stiff soil conditions respectively, and zero otherwise. Sites with an average shear-wave velocity over the uppermost 30 m greater than 750 m/s are regarded as rock, those below 360 m/s are regarded as soft soil, and intermediate values correspond to stiff soil sites.

The coefficients b_1 to b_8 were estimated using the one-stage maximum likelihood approach of Boore & Joyner (1993). The regression approach explicitly distinguishes between inter- and intra-event variability. A pure-error analysis was employed in order to determine the magnitude dependence of these variabilities (Ambraseys *et al.*, 2005). In order to perform the pure-error analysis, the dataset was divided into magnitude increments of 0.2 units and distance intervals of 2 km and only bins with three or more records were considered in the analysis. Figure 6.2 shows the results for the pure-error analysis for SI with a damping ratio of 2%. For further details on the characteristics of the earthquake dataset and the regression method used, the reader is referred to Akkar & Bommer (2007a) and for more details on the pure-error analysis to Ambraseys *et al.* (2005) and Douglas & Smit (2001).

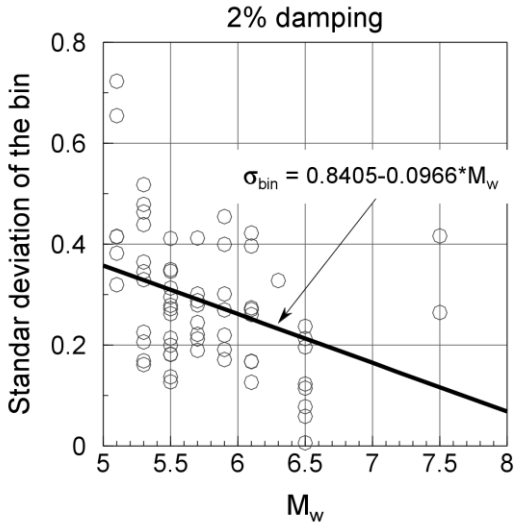

Figure 6.2. Results of the pure-error analysis for SI with a damping ratio of 2%.

It is important to note the strong dependence of the sigma of the bins on magnitude shown in Figure 6.2. The strong magnitude-dependence of this scatter will have an important influence on the hazard results of a PSHA.

The regression coefficients for Equation 6.2 and the magnitude-dependent intrer- (σ_1) and intra-event (σ_2) standard deviation for the five damping levels are presented in Table 6.1. The total standard deviation for Equation 6.2 can be calculated as $\sigma = \sqrt{\sigma_1^2 + \sigma_2^2}$.

Table 6.1. Coefficients of the prediction equation for SI (Equation 6.2) for different damping levels. σ_1 and σ_2 denote the magnitude-dependent inter- and intra-event standard deviations, respectively.

Damping (%)	b_1	b_2	b_3	b_4	b_5	b_6	b_7	B_8
2	-5.011	2.184	-0.153	-2.110	0.188	5.657	0.339	0.129
5	-4.867	2.138	-0.151	-2.222	0.201	5.544	0.330	0.125
10	-4.777	2.104	-0.150	-2.309	0.211	5.460	0.321	0.121
20	-4.574	2.034	-0.146	-2.421	0.227	5.424	0.313	0.116
30	-4.386	1.969	-0.142	-2.495	0.238	5.412	0.306	0.113

Damping (%)	σ_1	σ_2
2	$0.079-0.014M_w$	$0.180-0.031M_w$
5	$0.078-0.014M_w$	$0.177-0.031M_w$
10	$0.076-0.013M_w$	$0.173-0.030M_w$
20	$0.075-0.013M_w$	$0.172-0.030M_w$
30	$0.074-0.013M_w$	$0.171-0.030M_w$

In Figure 6.3 the total residuals of the prediction equation for SI for a damping ratio of 2% are shown with respect to M_w and r_{jb}. These residuals do not show any significant trend which suggests that the model is able to capture the general scaling with magnitude and distance well. Similar performance was observed for the remaining damping ratios, but the plots are not shown here.

Figure 6.4 presents the variation of SI with distance, as predicted by the model derived herein, for different damping ratios and magnitudes. The curves shown are the median predictions and for rock site conditions. As

expected, SI decreases with increasing distance and increases with decreasing damping ratios.

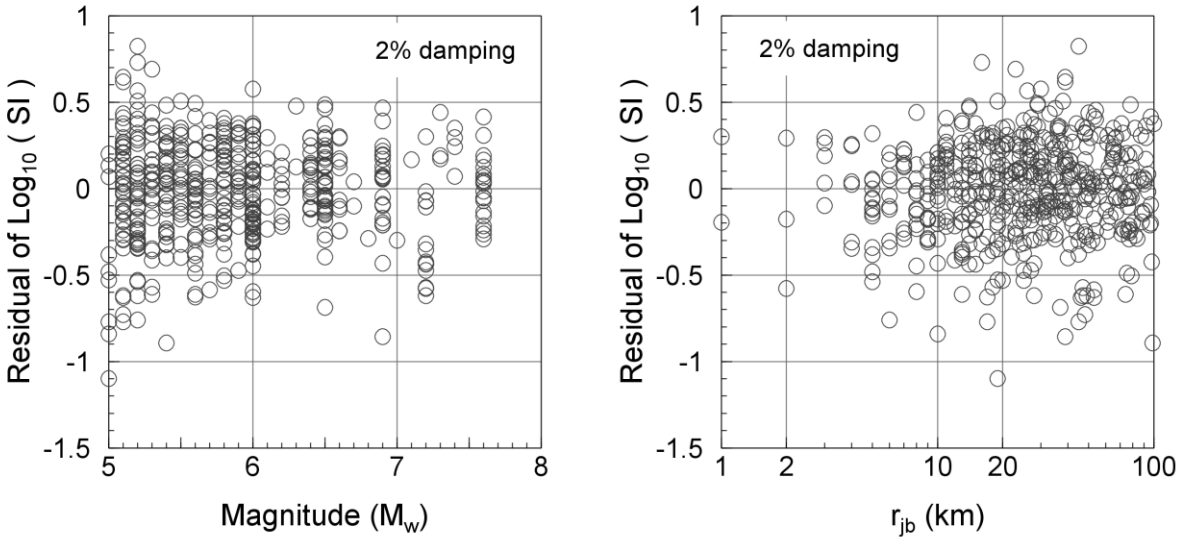

Figure 6.3. Distribution of the total residuals as function of magnitude and distance for SI for a damping ratio of 2% of critical.

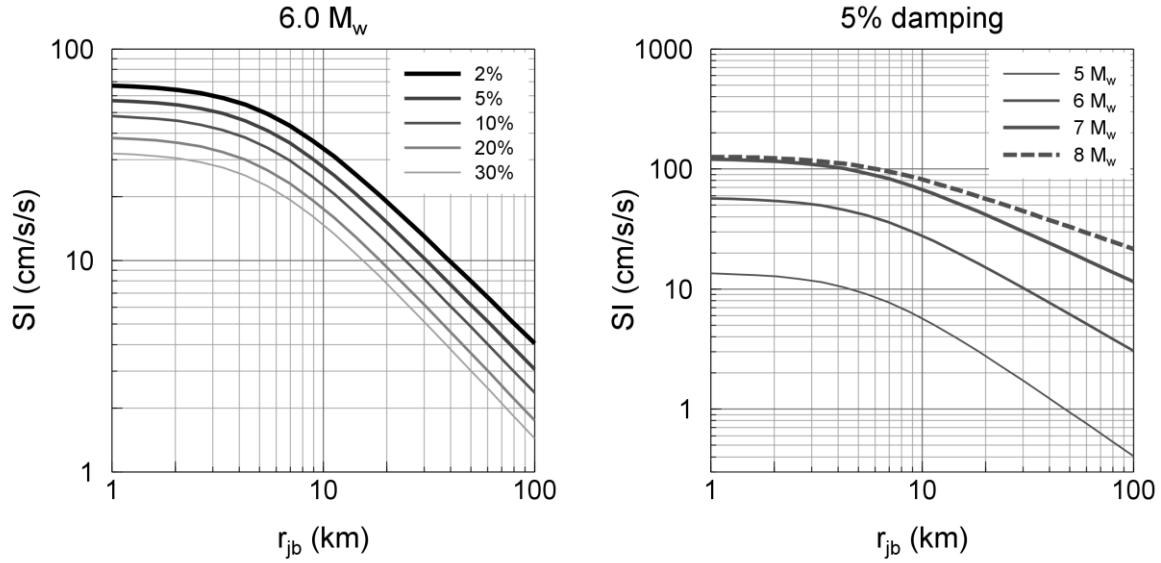

Figure 6.4. Variation of the median predictions with distance for different damping levels (left) and magnitudes (right). The dashed line indicates that this level of magnitude is outside the range of applicability of the equation.

In Figure 6.5 the predicted median SI values for rock from the prediction equation proposed herein for a damping ratio of 5% are compared

with those from the prediction equation of Danciu & Tselentis (2007). Since the dataset used in the present work is dominated by events with normal faulting, this mechanism was considered in the equation of Danciu & Tselentis (2007) for the prediction of the median SI values.

Given that Danciu & Tselentis (2007) use the r_{epi} distance definition and in order to make the graphical comparisons, the empirical relationships of Scherbaum *et al.* (2004b) were used to convert from r_{epi} to r_{jb}. A reasonably good agreement between both equations can be observed in Figure 6.5, with the larger differences at the smaller magnitudes. Note that the relationships of Scherbaum *et al.* (2004b) have a huge uncertainty associated and some of the observed differences in Figure 6.5 may be due to this use of these relationships.

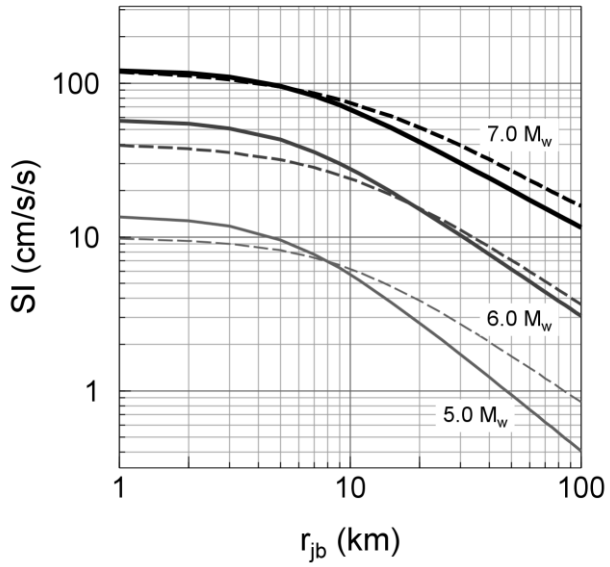

Figure 6.5. Comparison of the SI predictions from the present work (solid lines) with those of Danciu & Tselentis (2007) (dashed lines). A normal faulting mechanism was considered in the equation of Danciu & Tselentis (2007). The comparison is made for rock and a damping ratio of 5%.

Using Equation 6.2, a PSHA for SI was performed for the cities of Abu Dhabi, Dubai and Ra's Al Khaymah for rock site conditions. In Figure 6.6, the seismic hazard curves for spectral intensity for damping ratios of 2, 5, 10, 20 and 30 % are shown for the three sites.

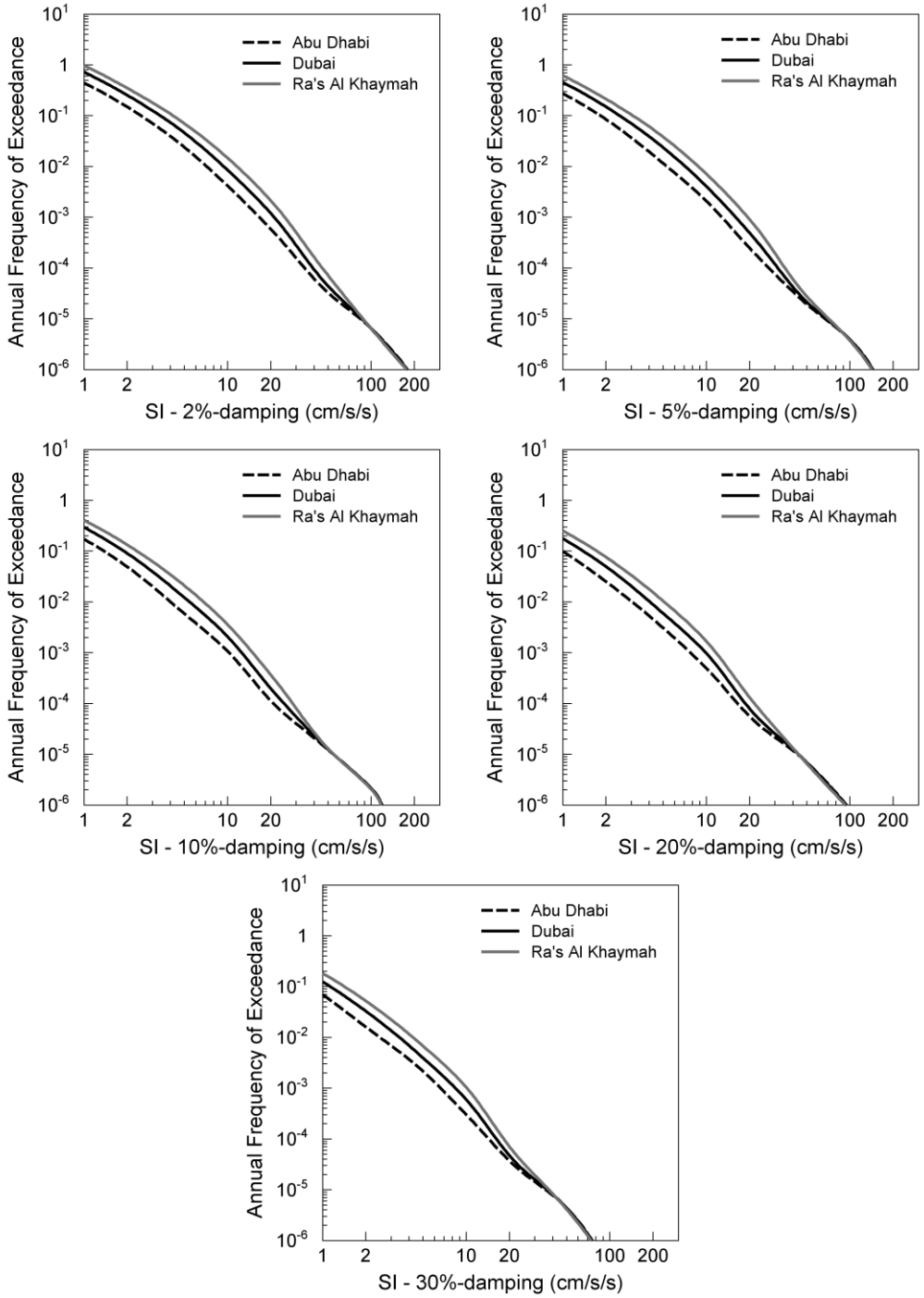

Figure 6.6. Spectral intensity hazard curves for different damping levels for the cities of Abu Dhabi, Dubai and Ra's Al Khaymah.

As expected, the seismic hazard in terms of SI is lower at Abu Dhabi and increases as one moves north towards Ra's Al Khaymah. In a similar manner to the hazard results for spectral accelerations presented in the case study (Chapter 3), the hazard curves of the three sites converge at the longest return periods (above ~100,000 years). This is because at these

return periods the local seismicity becomes the main contributor to the hazard; in other words, the stable craton becomes the dominant seismic source. As all the sites are within this source the hazard becomes the same.

Figure 6.7 presents a comparison of the hazard curves for the city of Dubai only and for different damping levels. It is clear that the expected values of SI for fixed return periods decrease as the damping ratio increases. This is, of course, precisely what one would expect.

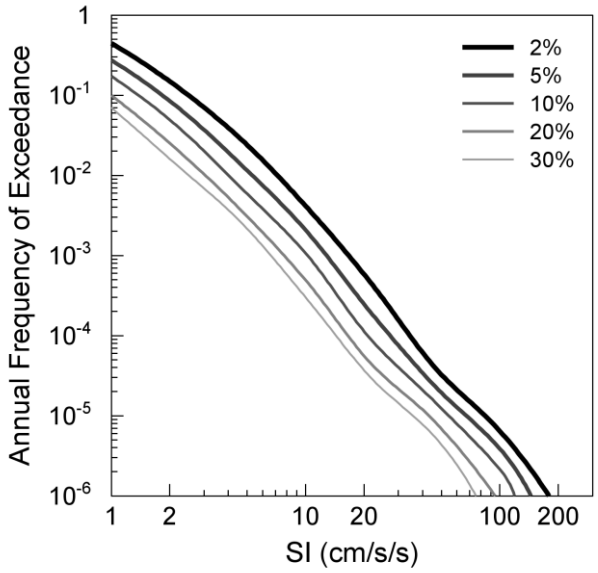

Figure 6.7. Comparison of spectral intensity hazard curves for different damping ratios for the city of Dubai.

The disaggregated results in terms of magnitude (M) and distance (R) for the three sites at return periods of 500, 2500 and 10,000 years and for damping ratios of 5 and 30% are presented in Figure 6.8 to Figure 6.13.

From the disaggregated results it may be observed that the seismic hazard for the three sites at short return periods (~500 years) is dominated by large events at long distances originating in the Zagros and the Makran. However, for the longer return periods (≥ 10,000 years) the dominant scenarios are located at distances shorter than 25 km and have magnitudes around 6.1 M_w, with the exception of Ra's Al Khaymah, where Zagros and

Makran still dominate the hazard even at 10,000-year return period. However, at much longer return periods it is expected that the Stable craton dominates the hazard also at Ra's Al Khaymah.

It is worth noting that the contributions from the different M and R scenarios remain basically the same, as would be expected, for the different damping ratios. This view was observed in the disaggregated results for the remaining damping levels (i.e., 2, 10 and 20%), but these results are not shown here. Note that the magnitude units in the disaggregated plots are in M_s scale, the relationship of Ambraseys & Free (1997) was used to transform from M_s to M_w.

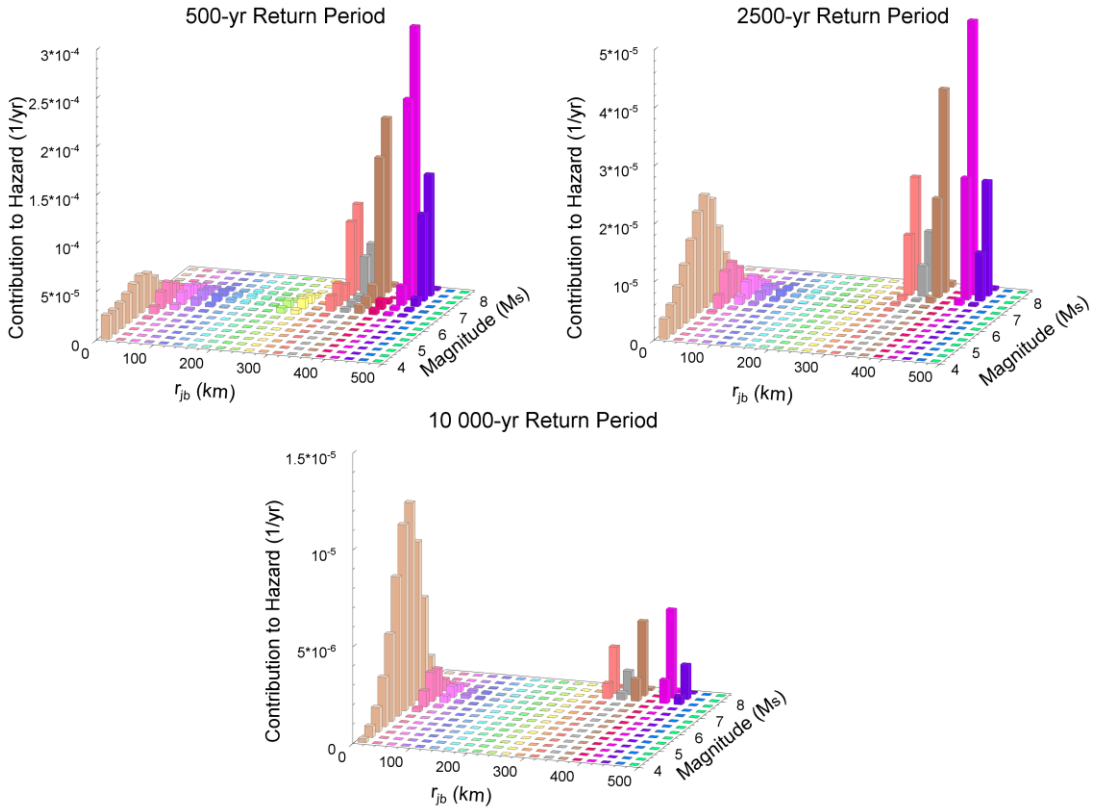

Figure 6.8. Disaggregated results for the city of Abu Dhabi in terms of spectral intensity for 5% damping at different return periods.

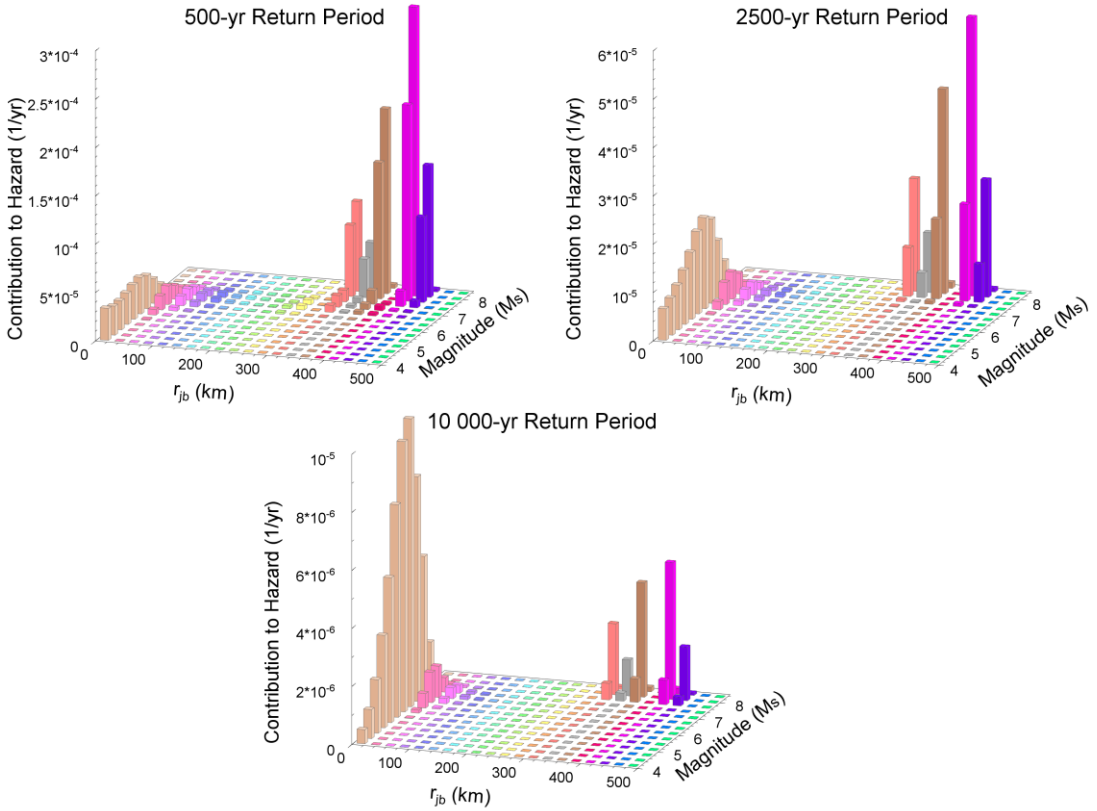

Figure 6.9. Disaggregated results for the city of Abu Dhabi in terms of spectral intensity for 30% damping at different return periods.

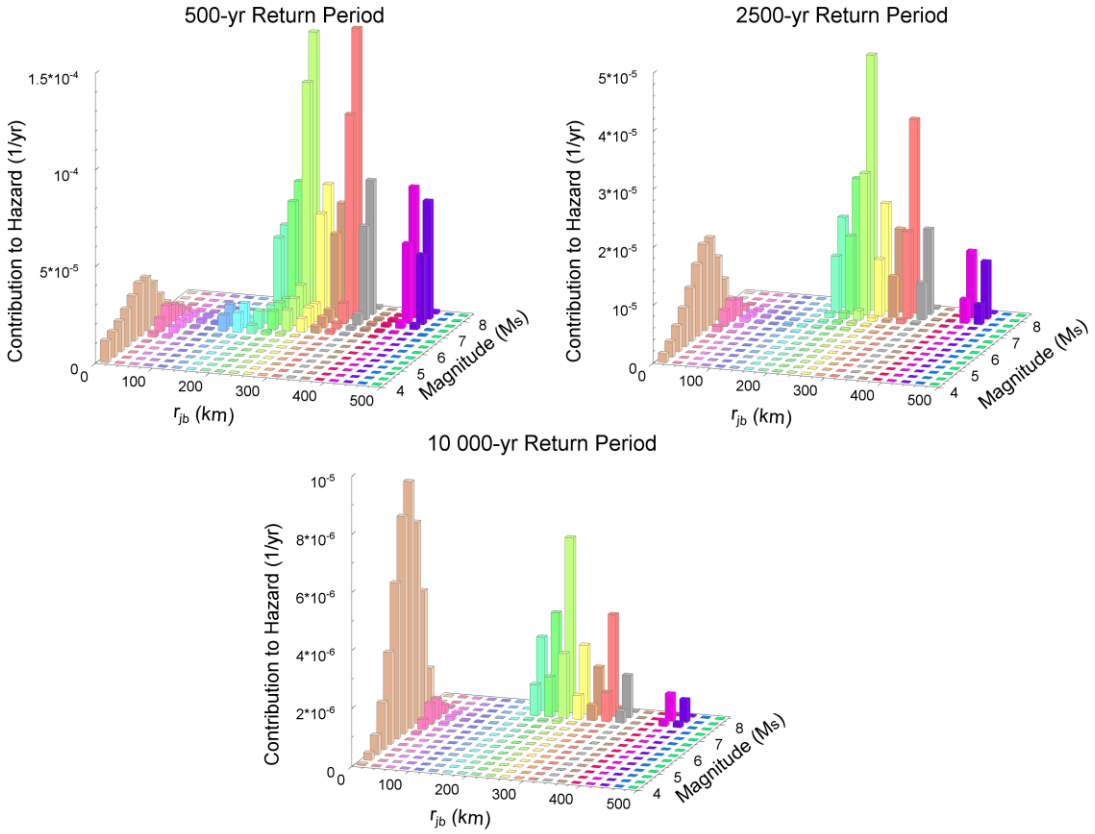

Figure 6.10. Disaggregated results for the city of Dubai in terms of spectral intensity for 5% damping at different return periods.

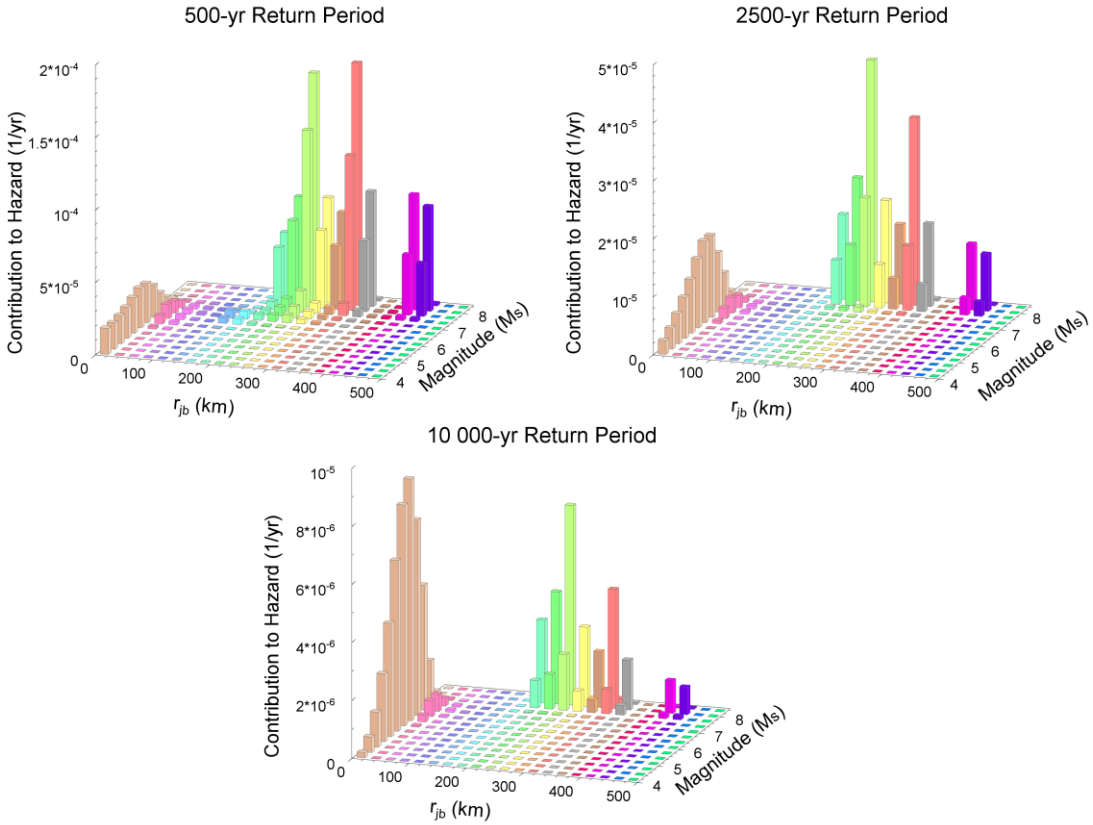

Figure 6.11. Disaggregated results for the city of Dubai in terms of spectral intensity for 30% damping at different return periods.

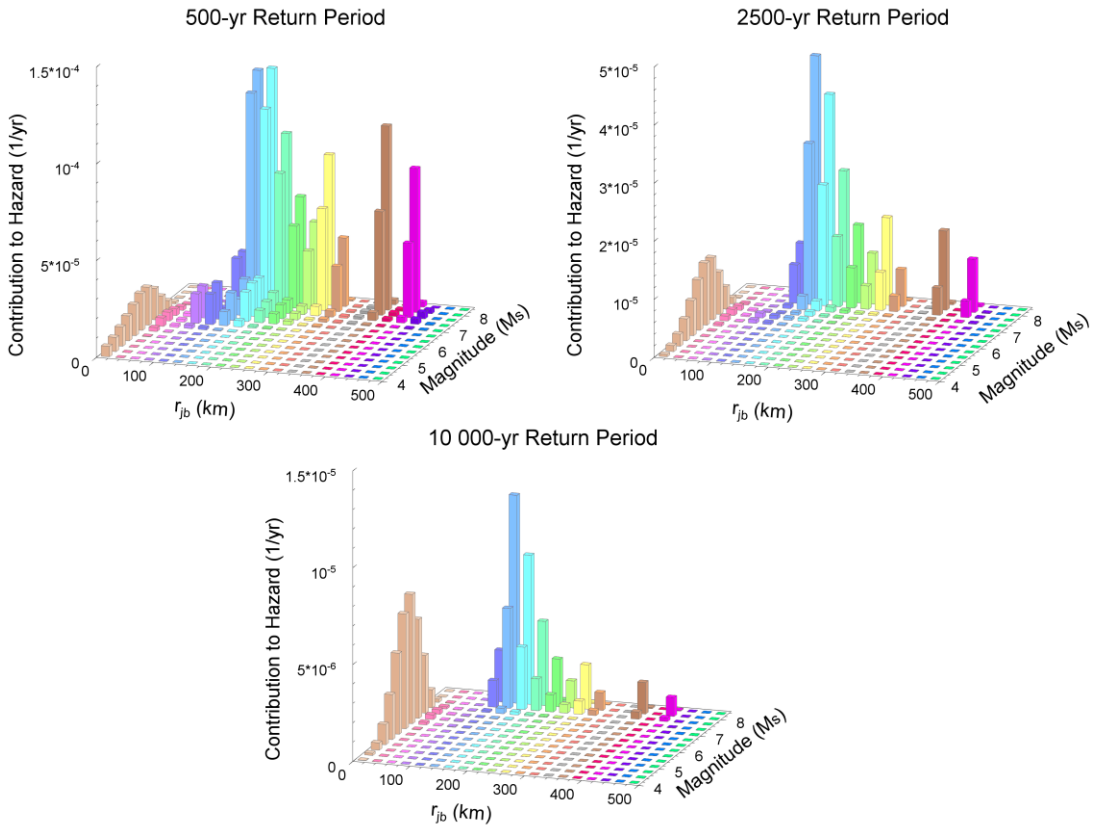

Figure 6.12. Disaggregated results for the city of Ra's Al Khaymah in terms of spectral intensity for 5% damping at different return periods.

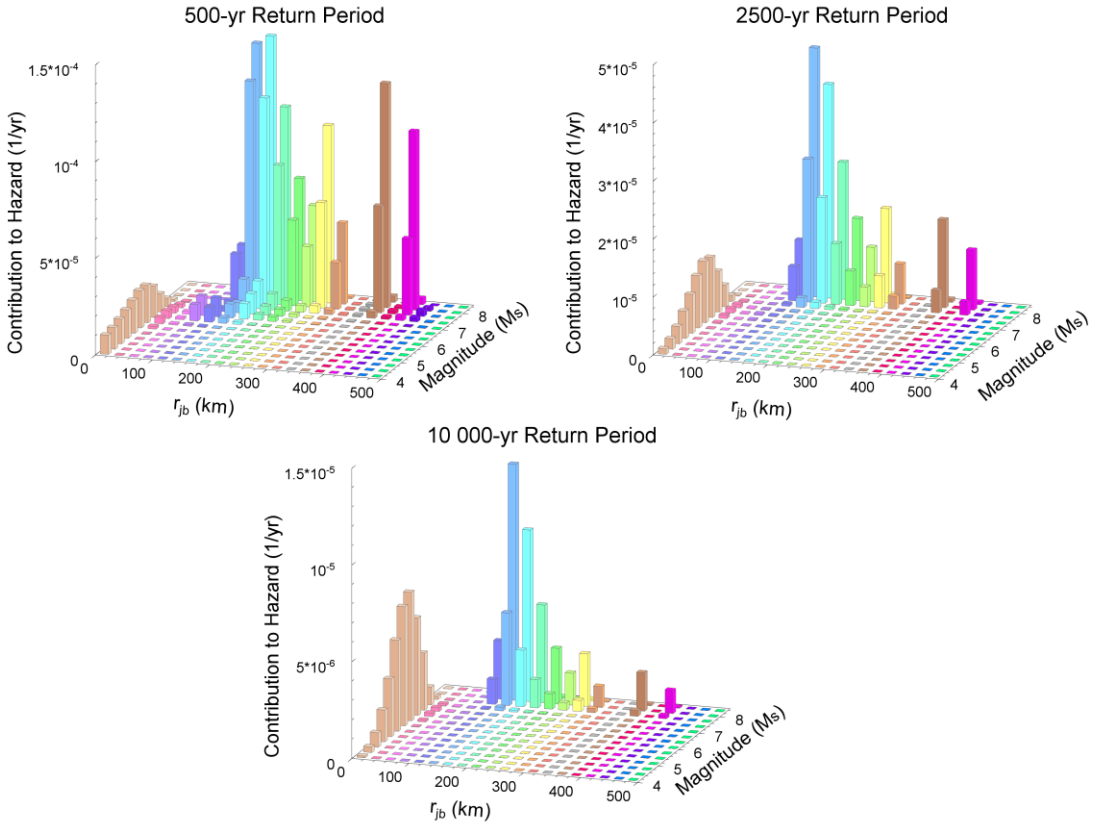

Figure 6.13. Disaggregated results for the city of Ra's Al Khaymah in terms of spectral intensity for 30% damping at different return periods.

6.2. Peak ground velocity (PGV)

PGV has been found to be a useful parameter in many engineering applications; examples of which include the evaluation of the damage potential of a ground motion and the assessment of liquefaction potential among others (Bommer & Alarcón, 2006). Despite this, there are relatively few prediction equations for this parameter in comparison with the large number of equations that have been derived for PGA and SA(T). The relative scarcity of predictive equations for PGV has been largely remedied through the recent development of a predictive equation for PGV for Europe and the Middle East by Akkar & Bommer (2007a) as well as those developed as part of the Next Generation Attenuation (NGA) project (e.g., Boore & Atkinson, 2007; Campbell & Bozorgnia, 2007).

A PSHA for PGV was carried out using the prediction equation of Akkar & Bommer (2007a) for the cities of Abu Dhabi, Dubai and Ra's Al Khamah for rock site conditions. As previously mentioned, only the "best-estimate" branch of the logic tree of the case study is considered for the hazard analyses in this chapter. The same ground-motion equation was assumed appropriate for all the seismic sources regardless of their tectonic regime.

Figure 6.14 presents the hazard curves in terms of PGV for the three sites under study. Once again the seismic hazard is lower at Abu Dhabi and increases as one moves north towards Ra's Al Khaymah. In a similar manner to the hazard results for SI, the hazard curves for the three sites converge for return periods longer than about 100,000-year. For such return periods, the Stable Craton becomes the dominant seismic source and as all sites are internal to this source, the hazard is driven by the same mechanism at all sites.

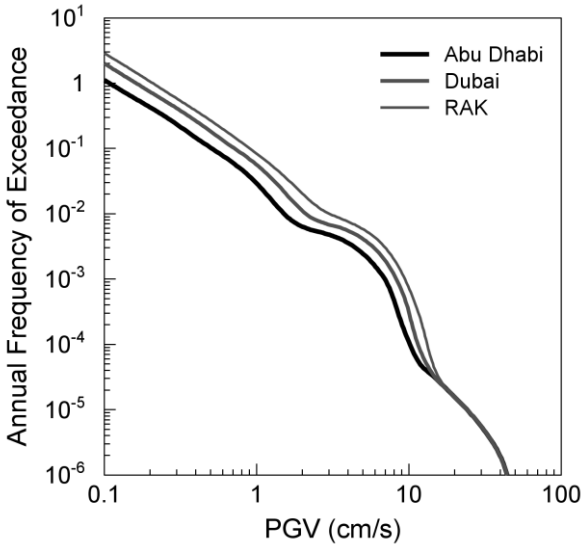

Figure 6.14. Seismic hazard curves for PGV for the cities of Abu Dhabi, Dubai and Ra's Al Khaymah.

It is important to note the convex nature of the hazard curves within the range of 10^{-2} to 10^{-4} on the exceedance probabilities. This convex portion

is due to the influence of the Makran subduction zone which is the dominant seismic source for this range of exceedance probabilities. Despite using the same seismicity model as in the previous section for the estimation of the seismic hazard for SI, the influence of the large-magnitude earthquakes generated in the Makran is more significant for PGV than for SI. Another reason for this may be that the equation of Akkar & Bommer (2007a) is being used well beyond the upper magnitude of applicability (7.6 M_w) and this may be influencing the shape of the hazard curve.

These results must be taken with caution as the prediction equation of Akkar & Bommer (2007a) for PGV and the prediction equation for SI presented in the previous section were derived for the purpose of being used for shallow earthquakes in active regions and should not be applied to subduction regions (particularly given the use of the r_{jb} metric). However, since the aim of the work presented in this chapter is to study the relationships between the expected SA(T) and the expected values of SI and PGV obtained from a PSHA, the use of these predictive equations for modelling ground-motion attenuation in the Makran subduction zone is permissible. Provide that the hazard for SA(T) is done in the same way.

From Figure 6.15 to Figure 6.17 the disaggregated results are presented for the three sites and for return periods of 500, 2500 and 10,000 years. It can be observed that the hazard- dominating scenarios at all return periods have an earthquake magnitude of 8.1 M_w, which can be associated with events generated in the Makran. The distances of these scenarios vary according to the relevant distance between the individual sites and Makran (for obvious reasons). The exception is the disaggregation for Abu Dhabi at the 10,000-year return period, where the governing seismic source is the Stable Craton, with a dominant earthquake scenario defined by 6.4 M_w and 12.5 km (r_{jb}).

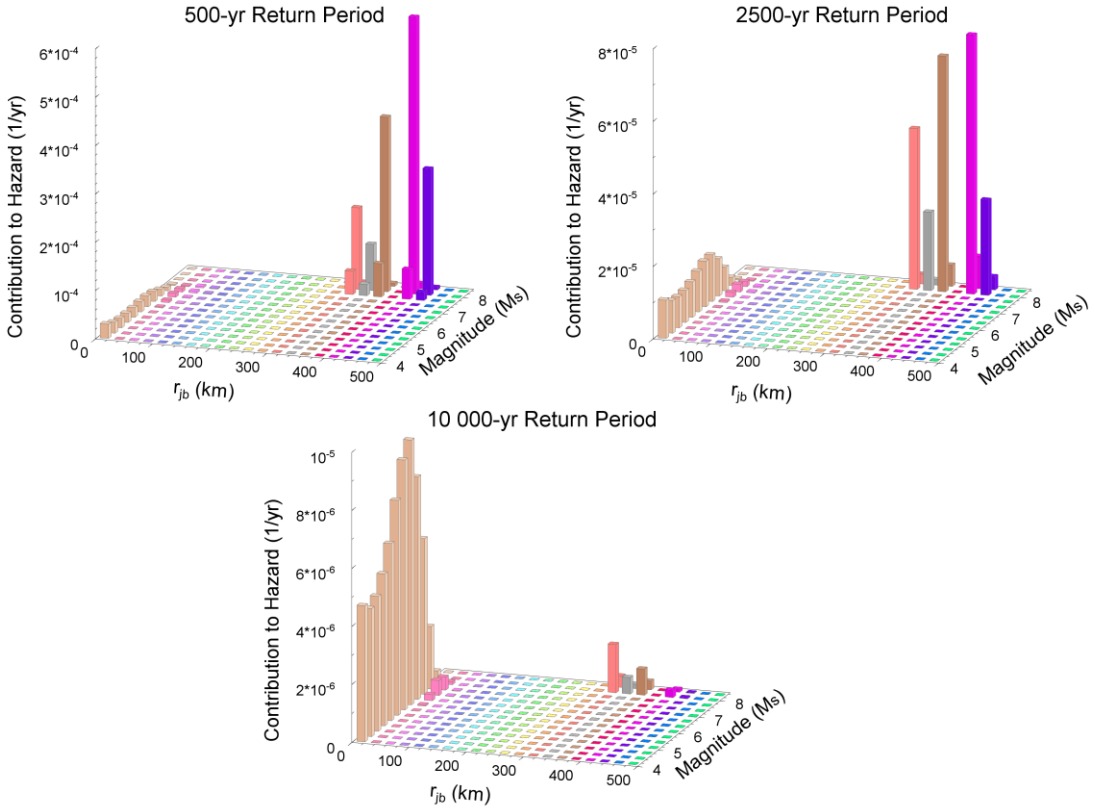

Figure 6.15. Disaggregated results for the city of Abu Dhabi for PGV at the 500, 2500 and 10,000-year return periods.

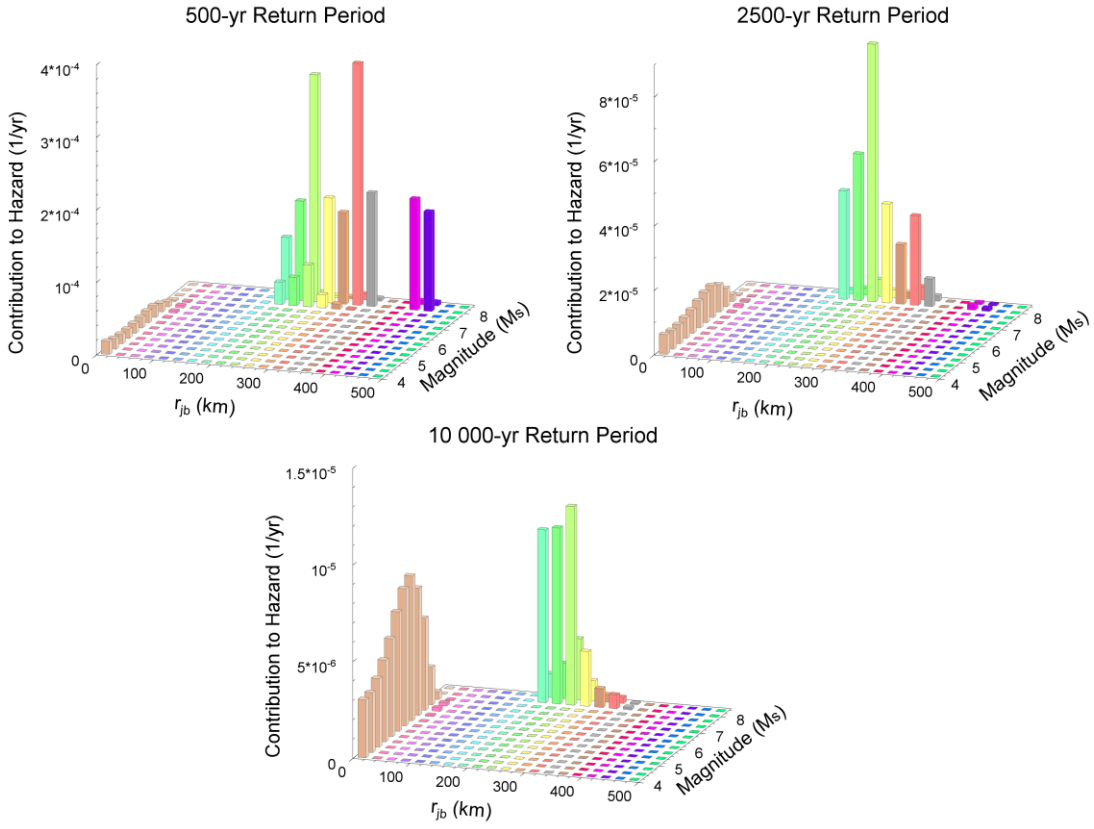

Figure 6.16. Disaggregated results for the city of Dubai for PGV at the 500, 2500 and 10,000-year return periods.

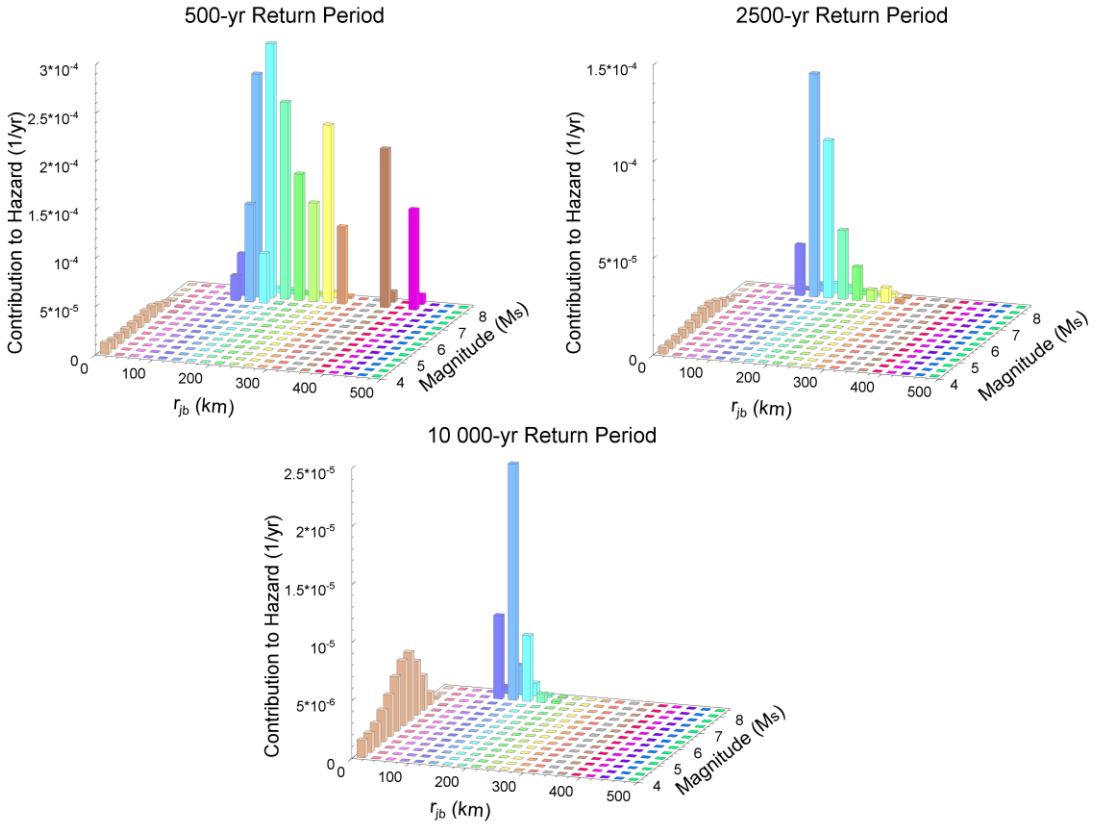

Figure 6.17. Disaggregated results for the city of Ra's Al Khaymah for PGV at the 500, 2500 and 10,000-year return periods.

6.3. Spectral accelerations for other damping levels

Almost all empirical ground-motion models have been derived to predict ground motions in terms of PGA and SA(T) for a damping ratio of 5% (Douglas, 2006). There are very few prediction equations that have been derived for other damping levels (e.g., Berge-Thierry *et al.*, 2003; Boore *et al.*, 1993). Despite its limited explanatory ability in earthquake engineering, PGA remains one of the most commonly used ground motion parameters. One of the main reasons for this is the common practice in seismic codes of anchoring a predefined spectral shape to the expected PGA value in order to obtain the uniform hazard spectrum to be used for seismic design. On the other hand, predictions of SA(T) have been shown to be a useful ground-

motion parameter for the seismic design of structures, since these can be modelled approximately as an equivalent linear oscillator.

The predictions of SA(T) at different structural periods are widely used, being one of its most important applications the construction of the response spectrum for seismic design of structures. On the other hand, PGA has little geophysical significance and a very limited applicability in earthquake engineering. However, PGA remains as the most used ground-motion parameter since it corresponds to SA at zero response period and as it is of common practice in seismic codes to anchor a predefined spectral shape to the expected PGA value in order to obtain the response spectrum to be used for seismic design.

For the reasons mentioned above in addition to the scarcity of prediction equations for other ground-motion parameters (e.g., SI and PGV), the majority of PSHA are performed in terms of PGA and SA(T). In the past, people have attempted to use hazard results in terms of SA(T) to infer hazard corresponding to other ground-motion parameters such as SI and PGV instead of performing a PSHA directly in terms of these parameters. An example of this is the practice of inferring PGV from the pseudo-spectral velocity (PSV) corresponding to a period of 1.0 s, as is embodied in the HAZUS programme of the Federal Emergency Management Agency of the United States (FEMA, 2003). A practice that has no technical basis (Bommer & Alarcón, 2006).

In this section a PSHA is presented for the cities of Abu Dhabi, Dubai and Ra's Al Khaymah for PGA and SA at 0.1, 0.2,..., 2.5 and 3.0 s response periods and for damping ratios of 2, 5, 10, 20 and 30%. As in the previous sections, the seismicity model for the hazard analysis is the "best-estimate" branch of the logic tree of the case study. The prediction equation of Akkar & Bommer (2007b) was used to predict SA(T) for all of the damping levels. Furthermore, a discussion is presented on the relationships between the

hazard results for SA(T) obtained in this section and the expected values of SI and PGV obtained in section 6.1 and section 6.2, respectively.

Figure 6.18 presents the hazard curves for PGA for the three sites under study. It is worth noting that spectral accelerations at zero response period (i.e., PGA) are independent of the damping ratio.

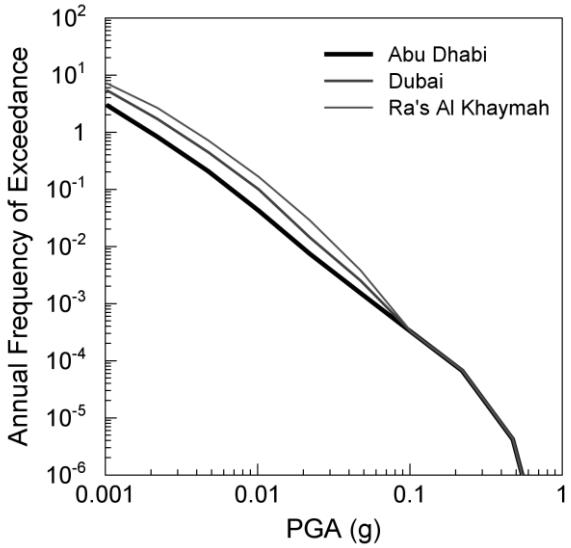

Figure 6.18. Seismic hazard curves for PGA for the cities of Abu Dhabi, Dubai and Ra's Al Khaymah.

Figure 6.19, Figure 6.20 and Figure 6.21 show the hazard curves for the cities of Abu Dhabi, Dubai and Ra's Al Khaymah, respectively. These results are for SA at response periods of 0.2, 0.6, 1.0 and 2.5 s and for damping ratios of 2, 5, 10, 20 and 30%.

As expected, spectral amplitudes decrease as the damping ratio increases. Although, in general, the hazard curves for the different damping ratios are essentially parallel, some irregularities can be observed, particularly at the longer response periods. These irregularities are a combination of the changes in the dominant seismic sources that occur across the frequencies of exceedance and the nature of the predictions of the ground motion model used for the analysis.

The uniform hazard spectra (UHS) for the three sites for a return period of 500-year and for the five damping ratios are presented in Figure 6.22. Once again, the spectral amplitudes increase as the damping ratio decreases. The largest differences occur for response periods between 0.1 and 1.0 s. At response periods above 2 seconds the differences in the spectral amplitudes for the different damping ratios are insignificant.

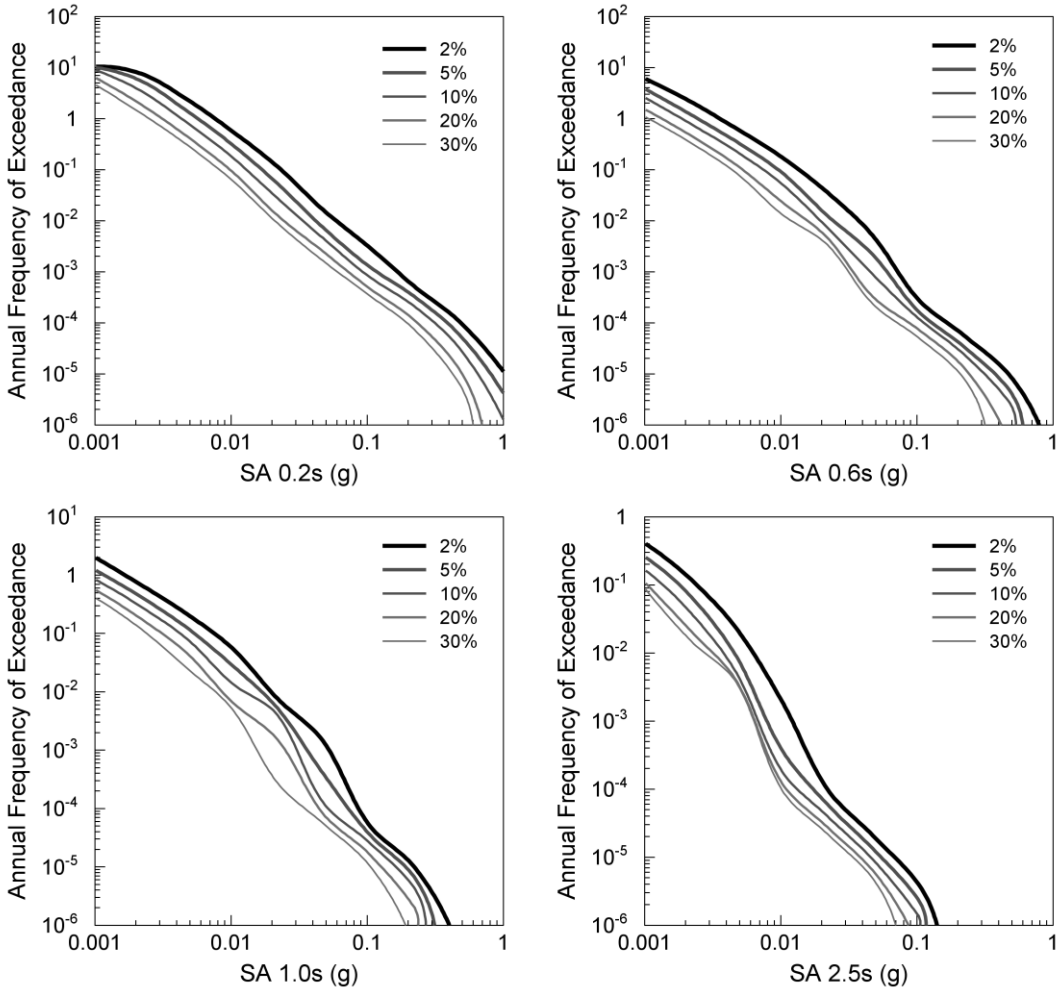

Figure 6.19. Seismic hazard curves for SA at periods of 0.2, 0.6, 1.0 and 2.5 s for different damping ratios for the city of Abu Dhabi.

Figure 6.23 shows the disaggregated results in terms of magnitude (M_s) and distance (r_{jb}) for the city of Dubai for PGA and for return periods of 500, 2500 and 10,000 years. In good agreement with the hazard results of the far more comprehensive case study, the seismic hazard for PGA is

dominated at all return periods by the local seismicity, although in this case a higher contribution from earthquake scenarios of large magnitude at long distances is observed for the 500-year return period.

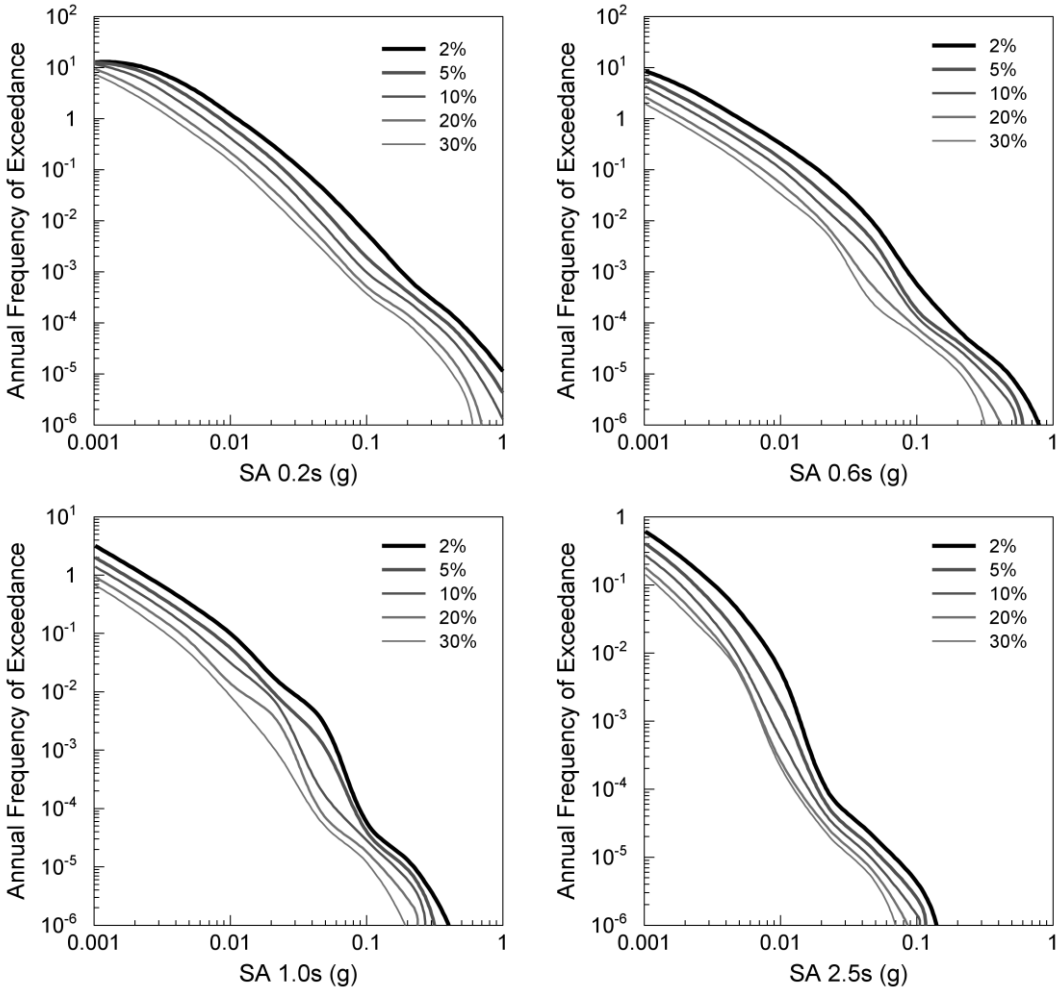

Figure 6.20. Seismic hazard curves for SA at periods of 0.2, 0.6, 1.0 and 2.5 s for different damping ratios for the city of Dubai.

Figure 6.24 to Figure 6.29 show the disaggregated results for the city of Dubai for SA at periods of 0.2, 1.0 and 3.0 s, return periods of 500, 2500 and 10,000 years, and for damping ratios of 5 and 30%. Only the disaggregated results for the city of Dubai are presented. However, the disaggregated results for the cities of Abu Dhabi and Ra's Al Khaymah show similar patterns in general, with the seismicity of Zagros and Makran having a higher influence at Ra's Al Khaymah and a lower influence at Abu Dhabi.

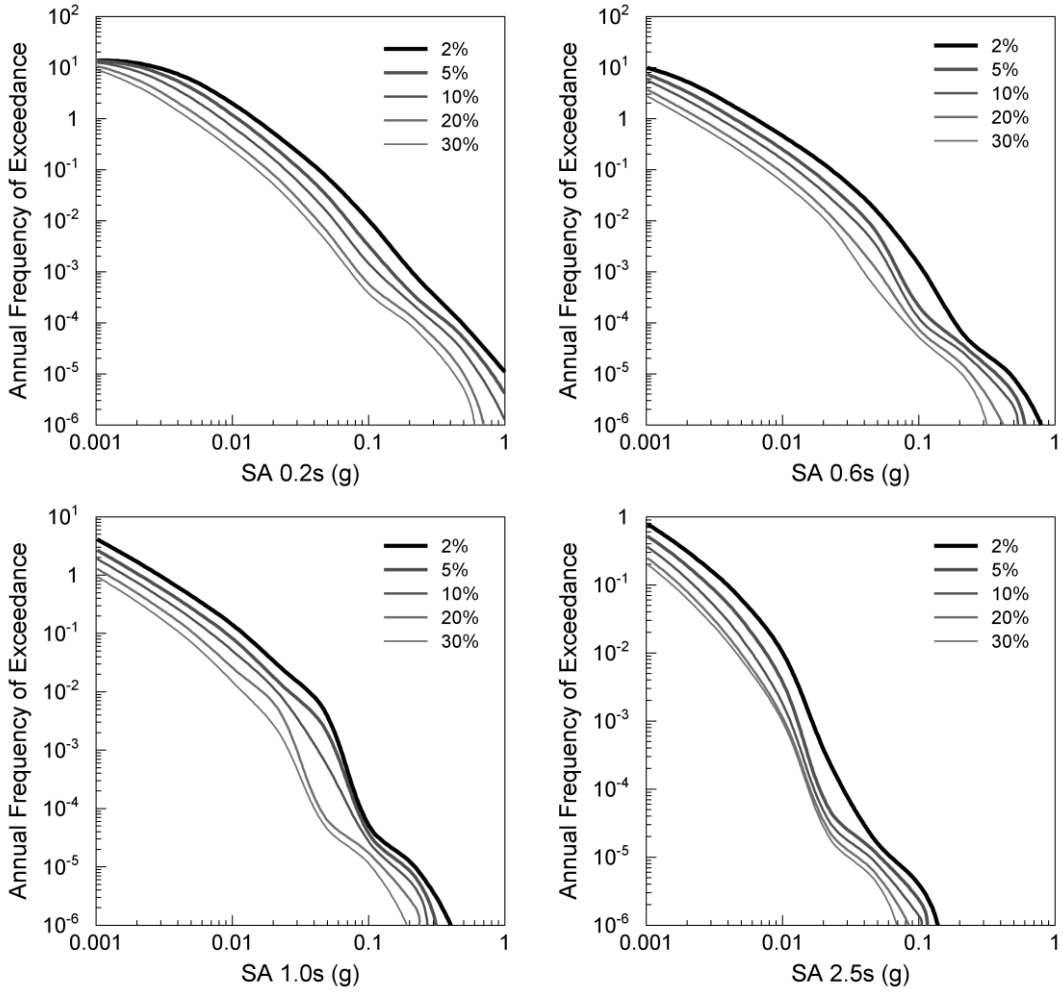

Figure 6.21. Seismic hazard curves for SA at periods of 0.2, 0.6, 1.0 and 2.5 s for different damping ratios for the city of Ra's Al Khaymah.

It is important to note that, as for SI(ξ), the contributions from the different magnitude and distance scenarios remain essentially unchanged for the different damping ratios. As previously commented with respect to SI(ξ), this is to be expected. The same situation is observed for the disaggregated results for the cities of Abu Dhabi and Ra's Al Khaymah and for all damping ratios.

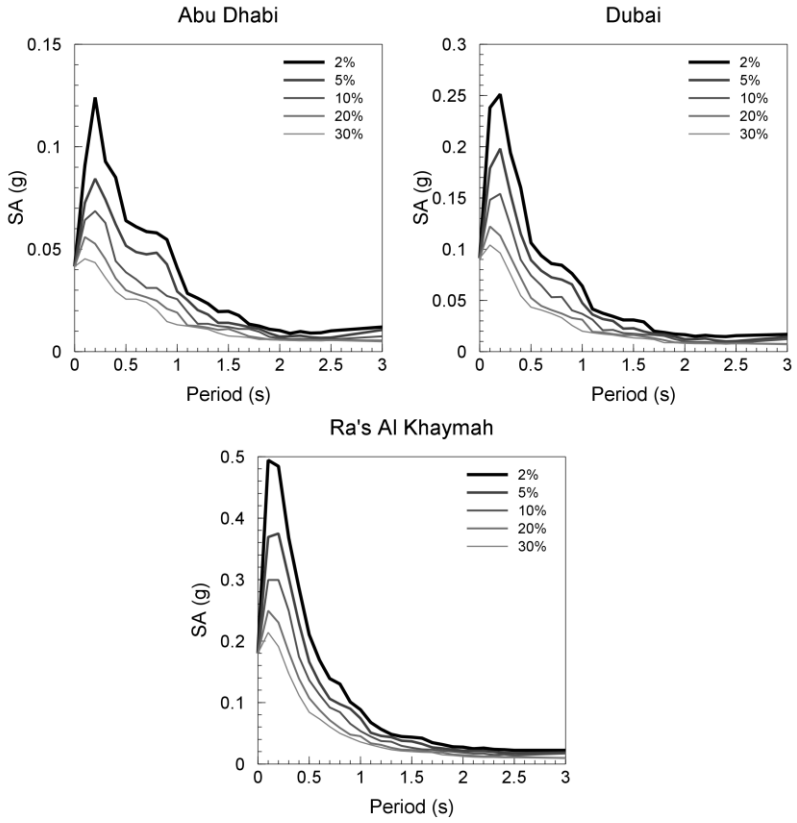

Figure 6.22. Uniform hazard spectra for the cities of Abu Dhabi, Dubai and Ra's Al Khaymah for different damping levels at the 500-year return period.

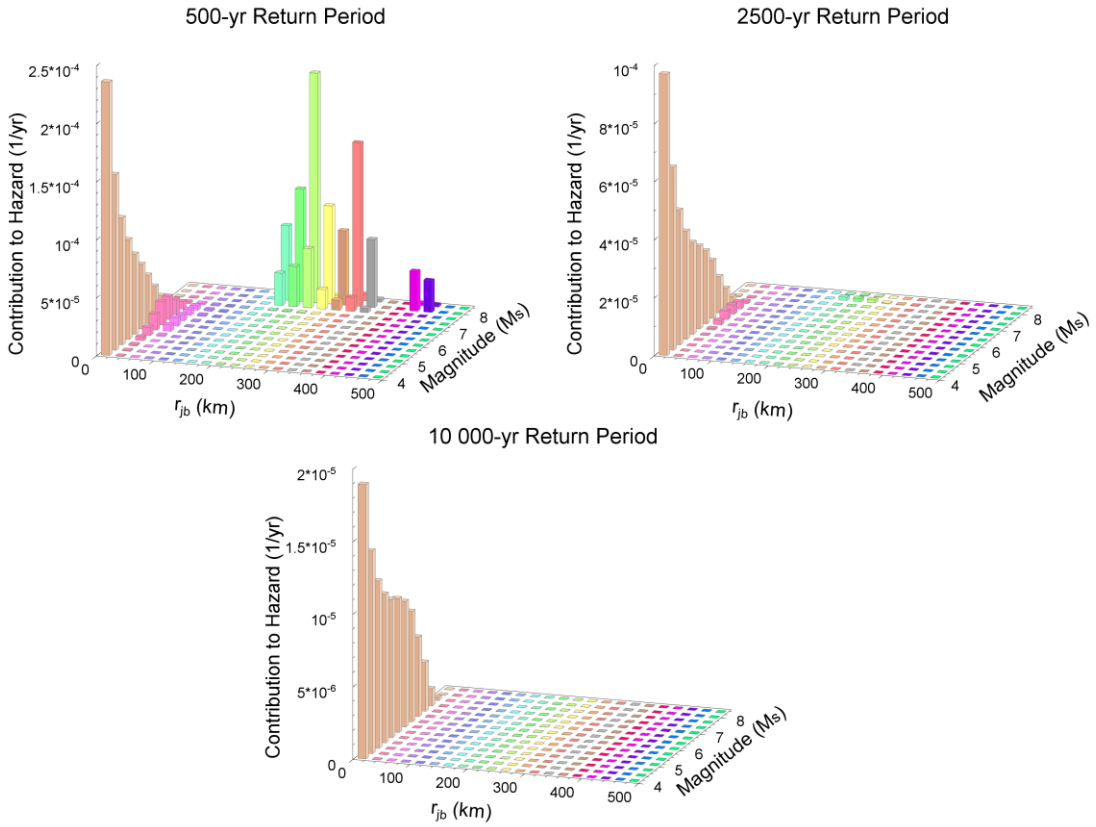

Figure 6.23. Disaggregated results for the city of Dubai for PGA at 500, 2500 and 10,000-year return periods. Note that PGA is independent of the damping ratio.

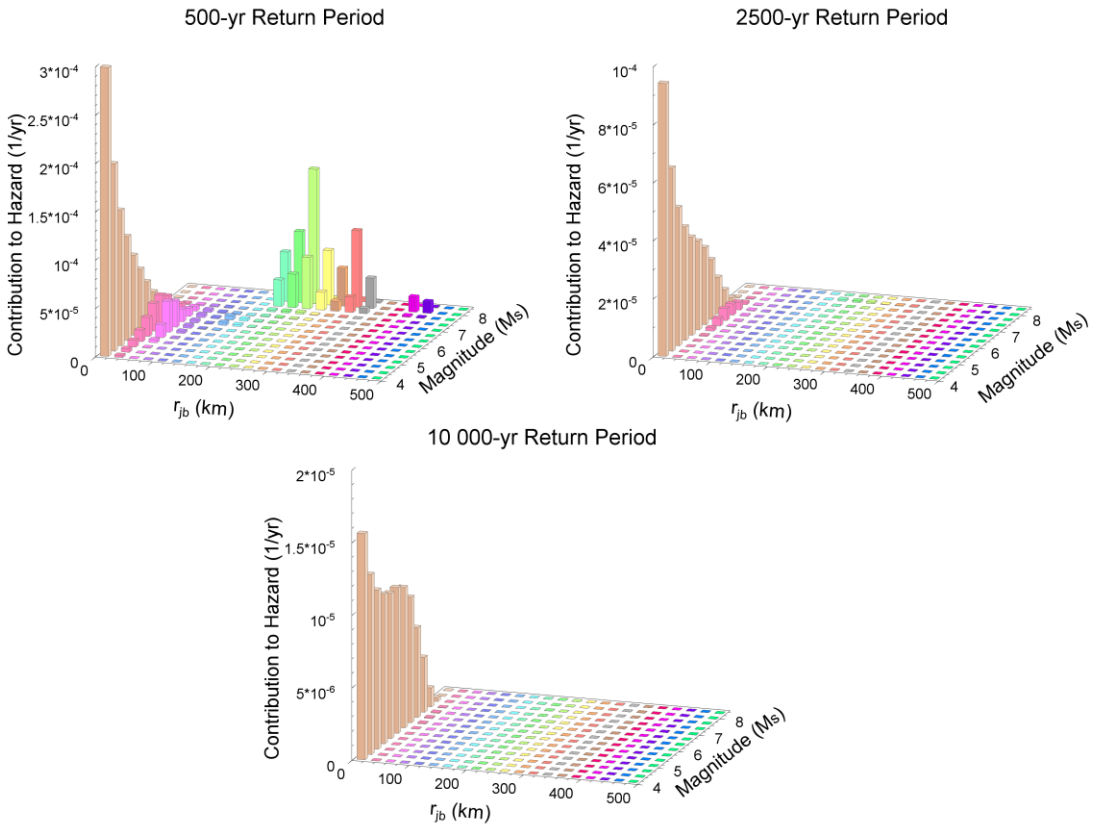

Figure 6.24. Disaggregated results for the city of Dubai for SA at 0.2 s and for 5% damping for 500, 2500 and 10,000-year return periods.

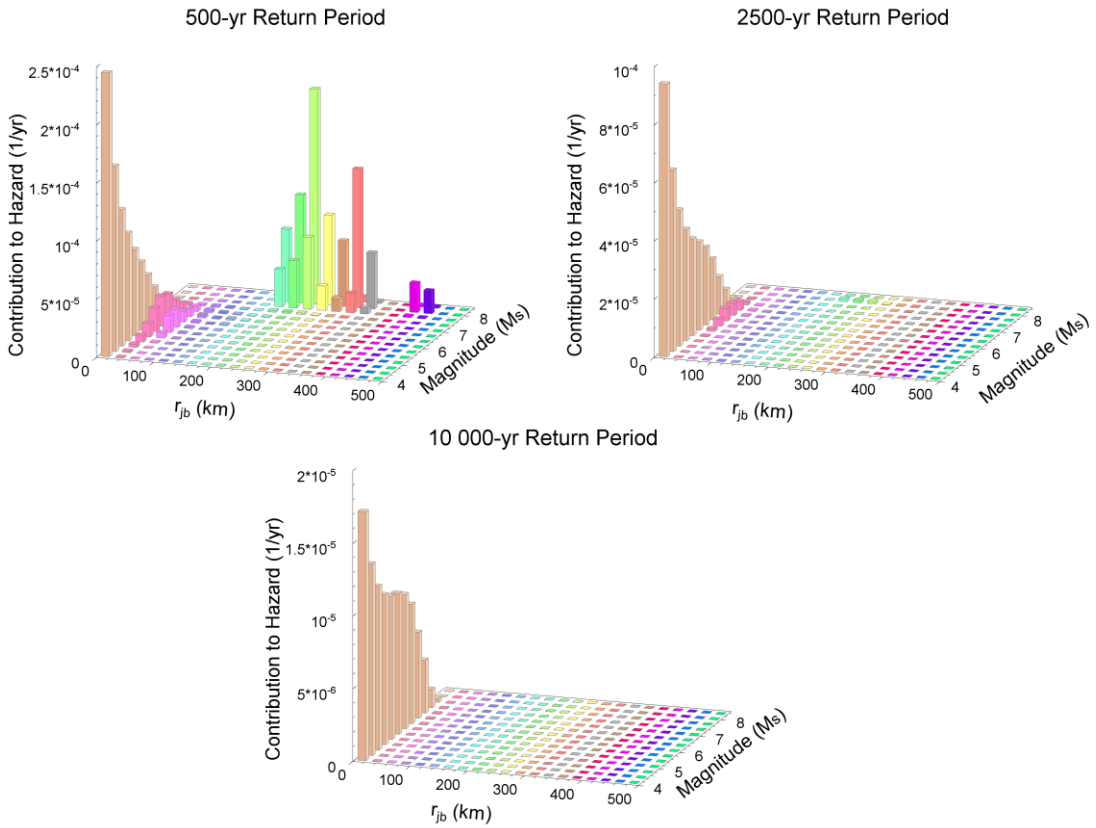

Figure 6.25. Disaggregated results for the city of Dubai for SA at 0.2 s and for 30% damping for 500, 2500 and 10,000-year return periods.

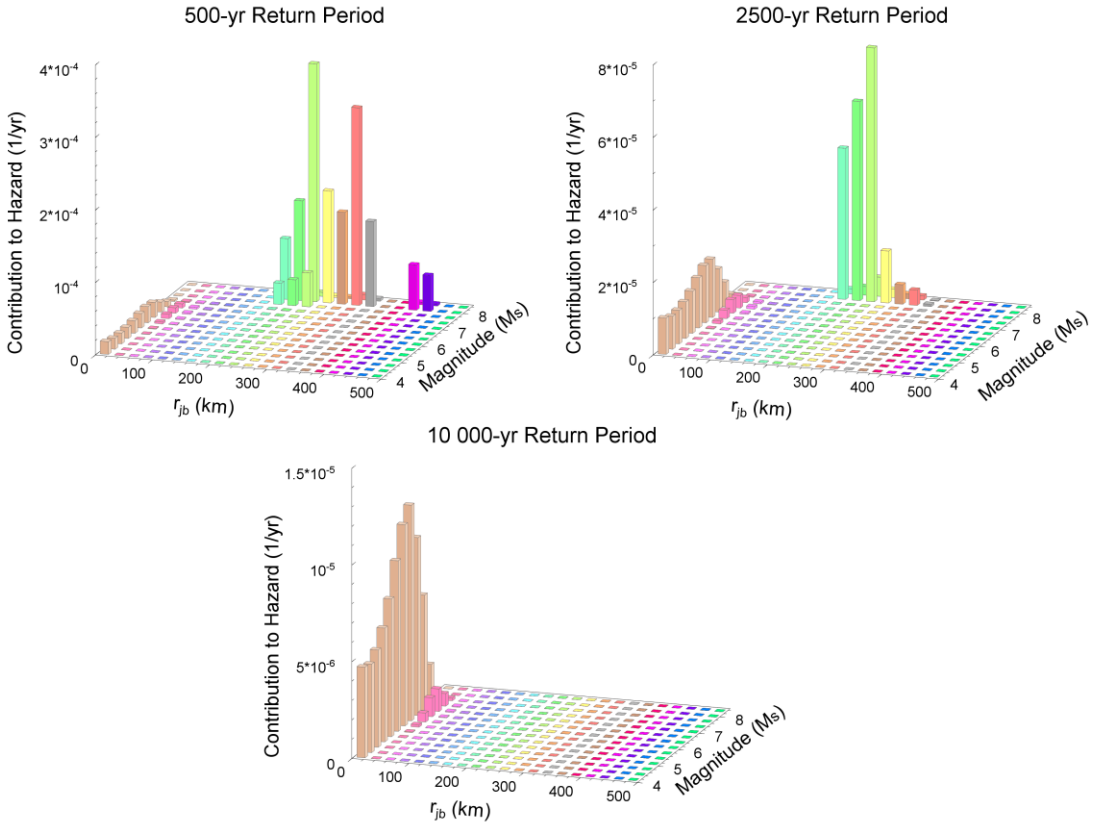

Figure 6.26. Disaggregated results for the city of Dubai for SA at 1.0 s and for 5% damping for 500, 2500 and 10,000-year return periods.

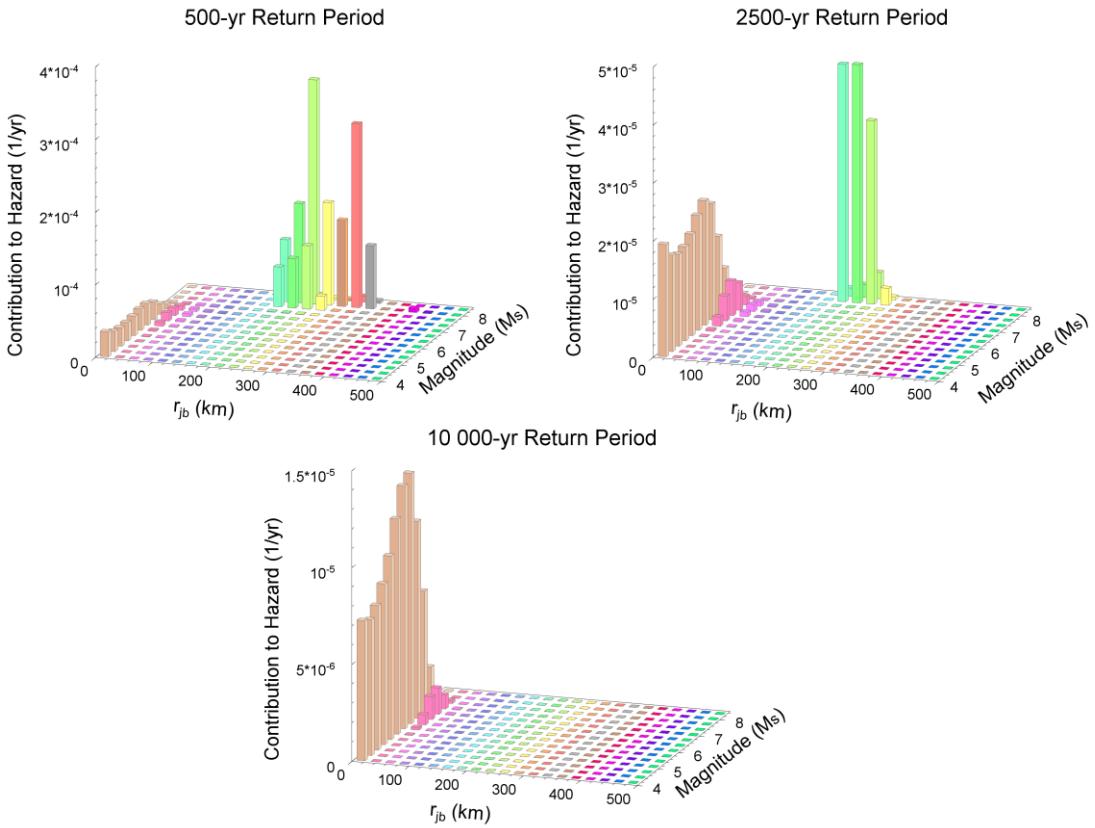

Figure 6.27. Disaggregated results for the city of Dubai for SA at 1.0 s and for 30% damping for 500, 2500 and 10,000-year return periods.

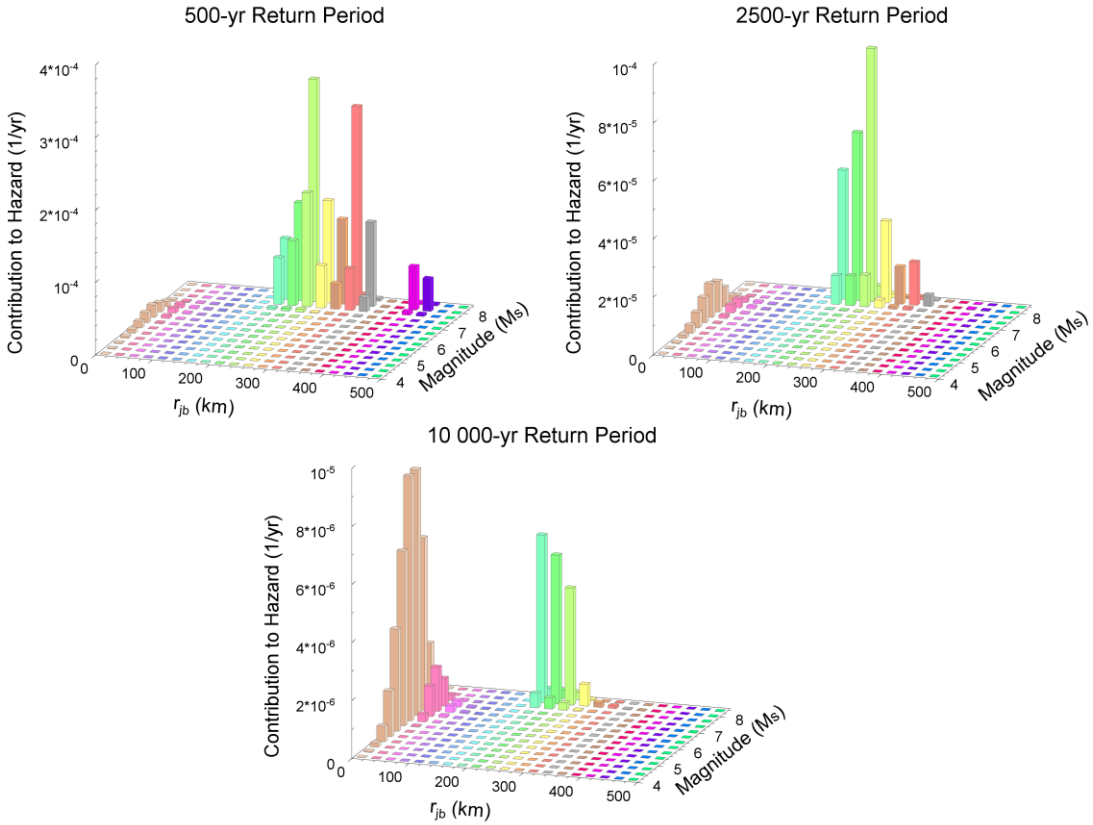

Figure 6.28. Disaggregated results for the city of Dubai for SA at 3.0 s and for 5% damping for 500, 2500 and 10,000-year return periods.

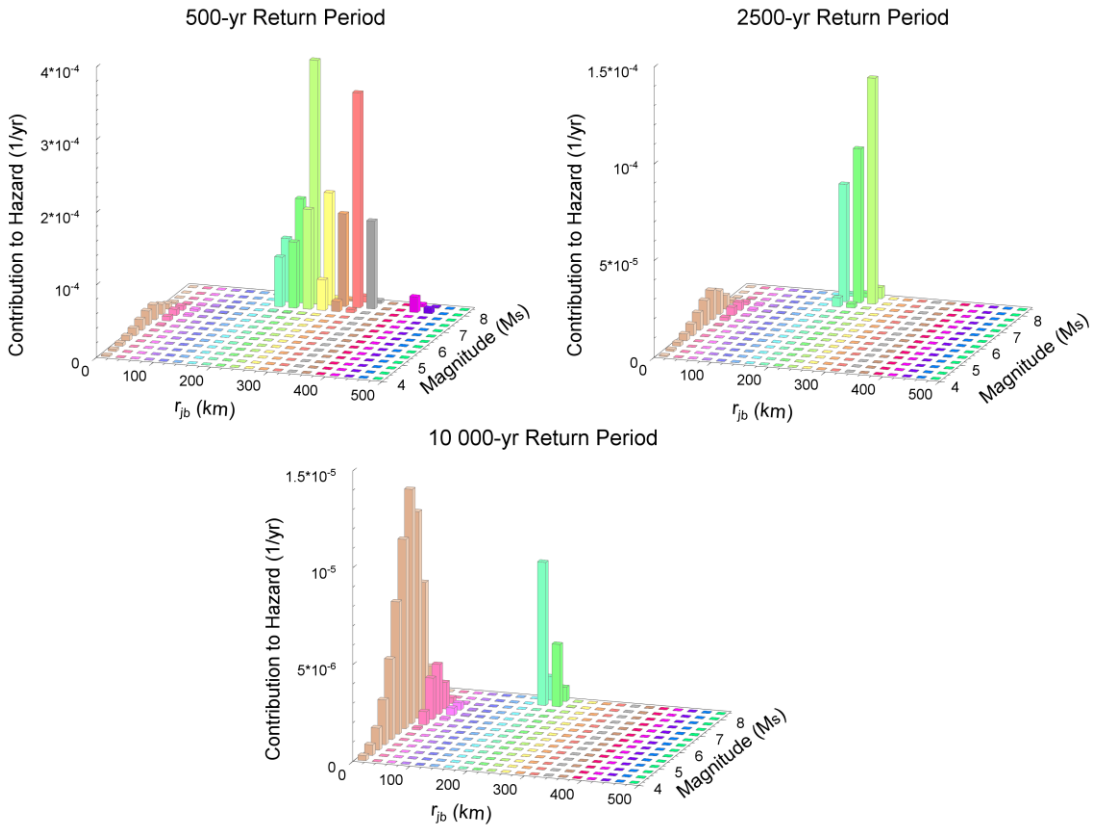

Figure 6.29. Disaggregated results for the city of Dubai for SA at 3.0 s and for 30% damping for 500, 2500 and 10,000-year return periods.

On the basis of these hazard results, values of SI and PGV were inferred for different return periods and, in the case of SI, for different damping ratios. These inferred values were compared with the expected values of SI and PGV obtained directly from the hazard analyses presented in section 6.1 and section 6.2, respectively.

For inferring SI from the hazard results for SA(T) two approaches were considered: (1) calculating the SI from the UHS corresponding to a given return period; and (2) calculating the SI of the scenario spectrum of the dominant seismic scenario defined in terms of M*, R* and ε', for a given return period and for the hazard curve corresponding to a specific response period. Here, ε' is the number of standard deviations required by a given ground-motion model to match the target ground motion for the particular combination of M* and R*.

Using the first approach, a seismic hazard curve for SI can be constructed by calculating the SI corresponding to the UHS at different response periods. Here, SI is calculated using the original definition of Housner (1952) (Equation 6.1) and treating the UHS as though it is a response spectrum. A clear drawback of this procedure is that the UHS is not a response spectrum and does not relate to any particular earthquake. However, this approach is considered herein as it is common practice to regard the UHS as a response spectrum for seismic design and often the UHS is the only "spectrum" that is available. Figure 6.30 shows a comparison between the hazard curves for SI as predicted by the PSHA in section 6.1 and the hazard curves for SI inferred using the approach described above.

For the second approach, one first needs to identify a scenario spectrum and this must correspond to a particular response and return period. In practice, it makes sense to use the scenario spectrum corresponding to a response period related to the structure in question. SI

values were calculated for the scenario spectra corresponding to the dominant scenarios (M*, R*, ε') for 500, 2500, 5000 and 10,000-year return period and for the hazard curves for SA at 0.1 to 2.5 s response periods. The scenario spectra were calculated as the conditional mean response spectra (c.f., Baker & Cornell, 2006b; Baker & Jayaram, 2008) corresponding to M*, R* and ε'. The values of SI obtained in this way were compared to the predicted SI values from the PSHA in section 6.1.

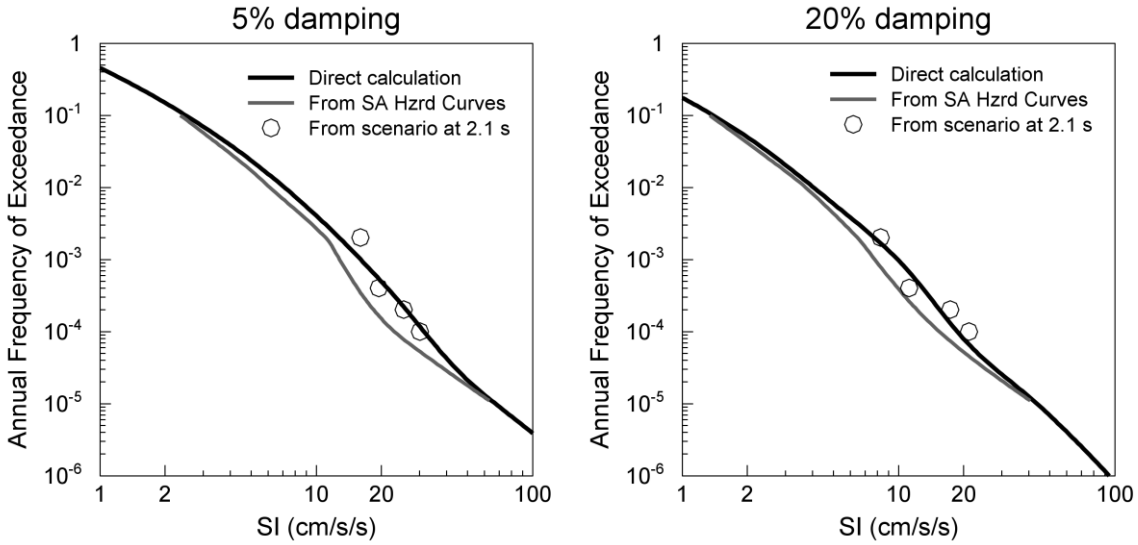

Figure 6.30. Comparison of the hazard curves for SI obtained from a PSHA using the prediction equation for SI presented in section 6.1 (black solid line), the hazard curves for SI inferred from the PSHA in terms of spectral accelerations presented in this section (grey solid line) and SI values obtained from the expected response spectra corresponding to the hazard-dominating scenario at the 2.1 s response period (circles). These results are for the city of Dubai and for SI of 5% (left) and 20% (right) damping of critical.

Figure 6.31 shows the relationship between the ratio $\log_{10}(SI)/\log_{10}(SI[SA(T)])$ and period for 5% damping at different return periods and for the three sites under study. $\log_{10}(SI)$ is the base 10 logarithm of the expected SI obtained from the PSHA in section 6.1, and $\log_{10}(SI[SA(T)])$ is the base 10 logarithm of the SI obtained from the conditional mean spectrum of the dominant scenario for SA at a response period T.

It is important to mention that the standard deviation of the equation of Akkar & Bommer (2007b) is magnitude dependent [$\sigma(M)$] and for

magnitudes larger than 7.6 σ was fixed at the value corresponding to σ(7.6) in order to avoid having unrealistic low values of sigma, or even negative values, for magnitudes above the range of applicability. This restriction was also considered for the calculation of the conditional mean spectra from which values SI were inferred.

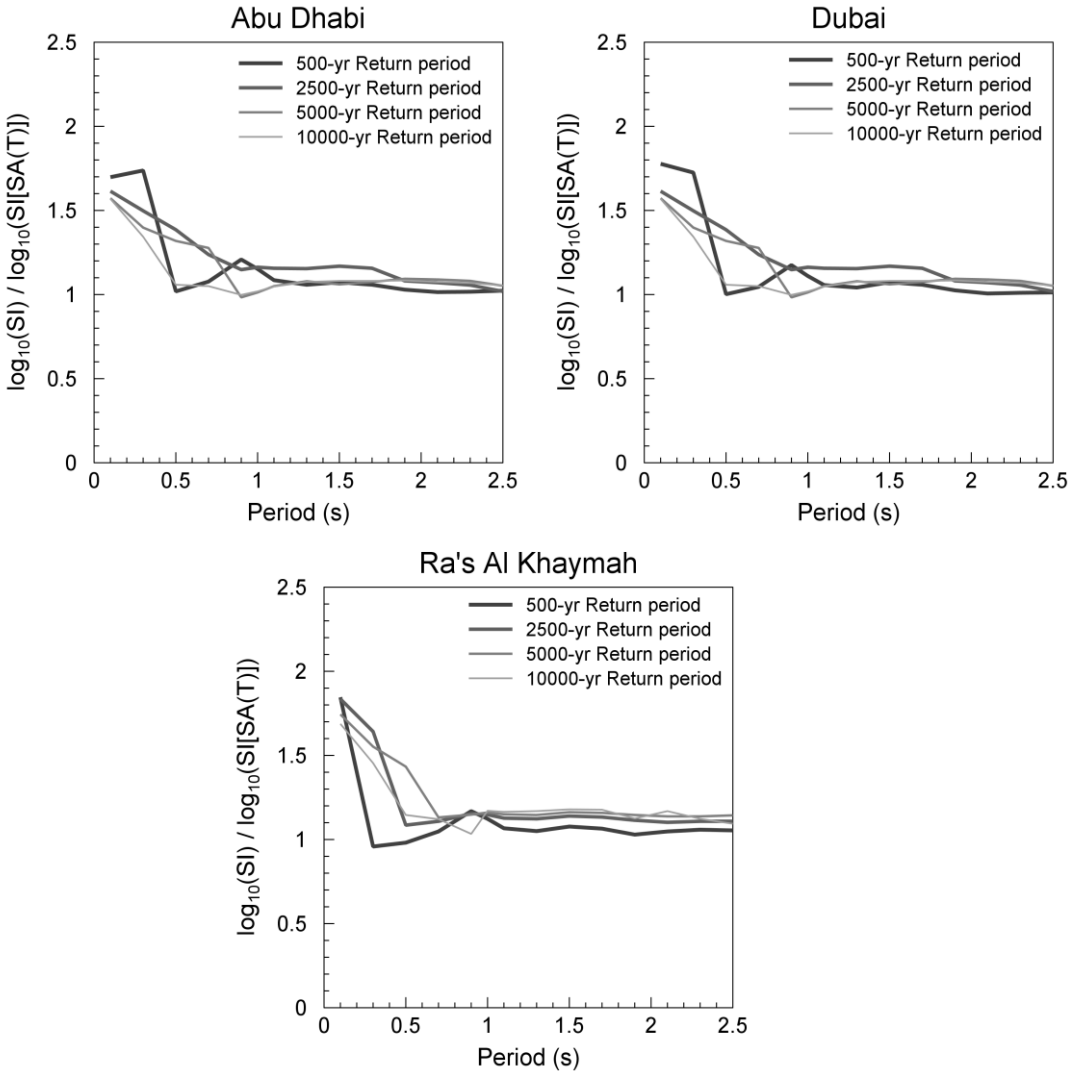

Figure 6.31. Relationship between $\log_{10}$(SI) / $\log_{10}$(SI[SA(T)]) and period at different return periods and for 5% damping of critical. SI is the expected spectral intensity from the PSHA in section 6.1, and SI[SA(T)]) is the spectral intensity obtained from the expected response spectrum corresponding to the hazard-dominating scenario for SA at T response period.

As can be observed in Figure 6.31, the ratio $\log_{10}$(SI)/$\log_{10}$(SI[SA(T)]) flattens to an average value of approximately 1.1 for response periods above

1.2 s. The reason for the behaviour of the ratios shown in Figure 6.31 is that the conditional mean spectra corresponding to the dominant scenarios of structural periods larger than 1.0 s provides a better match to the UHS over the period range from 0.1 to 2.5 s (see Figure 6.32) than the conditional spectra for shorter periods. This is because the longest structural periods are generally dominated by large magnitude scenarios (at long distances), whose response spectra have richer frequency content than small magnitude earthquakes (at short distances), which normally control the hazard at shorter periods and PGA. The same behaviour was observed for all damping levels (i.e., 2, 10, 20 and 30%).

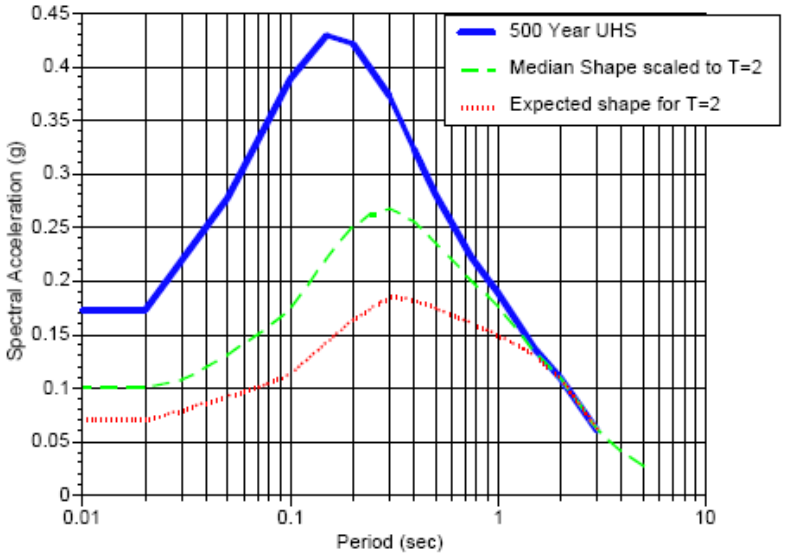

Figure 6.32. Comparison of the UHS, and the median response spectrum (median shape) and the conditional mean spectrum (expected shape) scaled to match the UHS at 2.0 s (Abrahamson, 2006).

Based on these findings, an estimation of the SI for a given return period can be made using the following equation:

$$\log_{10}(SI) = 1.1\log_{10}\left(SI\left[SA(T)\right]\right) \qquad 6.3$$

where SI[SA(T)] is the spectral intensity of the expected response spectrum corresponding to the dominant scenario (M*, R*, ε*) for SA at T response period.

Using Equation 6.3, SI values were estimated for 500, 2500, 5000 and 10,000-year return periods and for 5 and 20% damping, using the expected response spectrum of the dominant scenario for SA at a response period of 2.1 s. These estimates of SI are presented in Figure 6.30 as open circles. 2.1 s was arbitrarily selected in order to provide an example. However, based on the results of Figure 6.31, similar results can be obtained from the use of the dominant scenario for SA at any period above 1.0 s.

In order to compare the influence of the magnitude-dependence of sigma in the equations of Akkar & Bommer (2007b) for SA(T) and the one derived herein for SI (Equation 6.2), in Figure 6.33 a comparison is shown between the attenuation curves of SI versus distance (r_{jb}), for the median predictions and the median ±1σ, obtained from these two equations. The SI values for the equation of Akkar & Bommer (2007b) were obtained by first calculating spectra for given values of magnitude, distance and epsilon (assuming ε being equal for all periods), where ε takes the value of 0 for the median, 1 for median +1σ and -1 for median -1σ prediction, and using this spectrum to calculate the SI values.

From inspection of Figure 6.33 a good agreement can be observed for the median predictions of both equations, for all the magnitudes considered. However, as one moves to the median +1σ, a higher dispersion in the attenuation curves for the different magnitudes can be observed for the predictions of the equation derived herein for SI in comparison with the predictions of SI inferred from Akkar & Bommer (2007b). This higher dispersion on the direct predictions of SI reflects the strong magnitude-dependence of sigma of Equation 6.2. The opposite effect is observed in the results of the median -1σ.

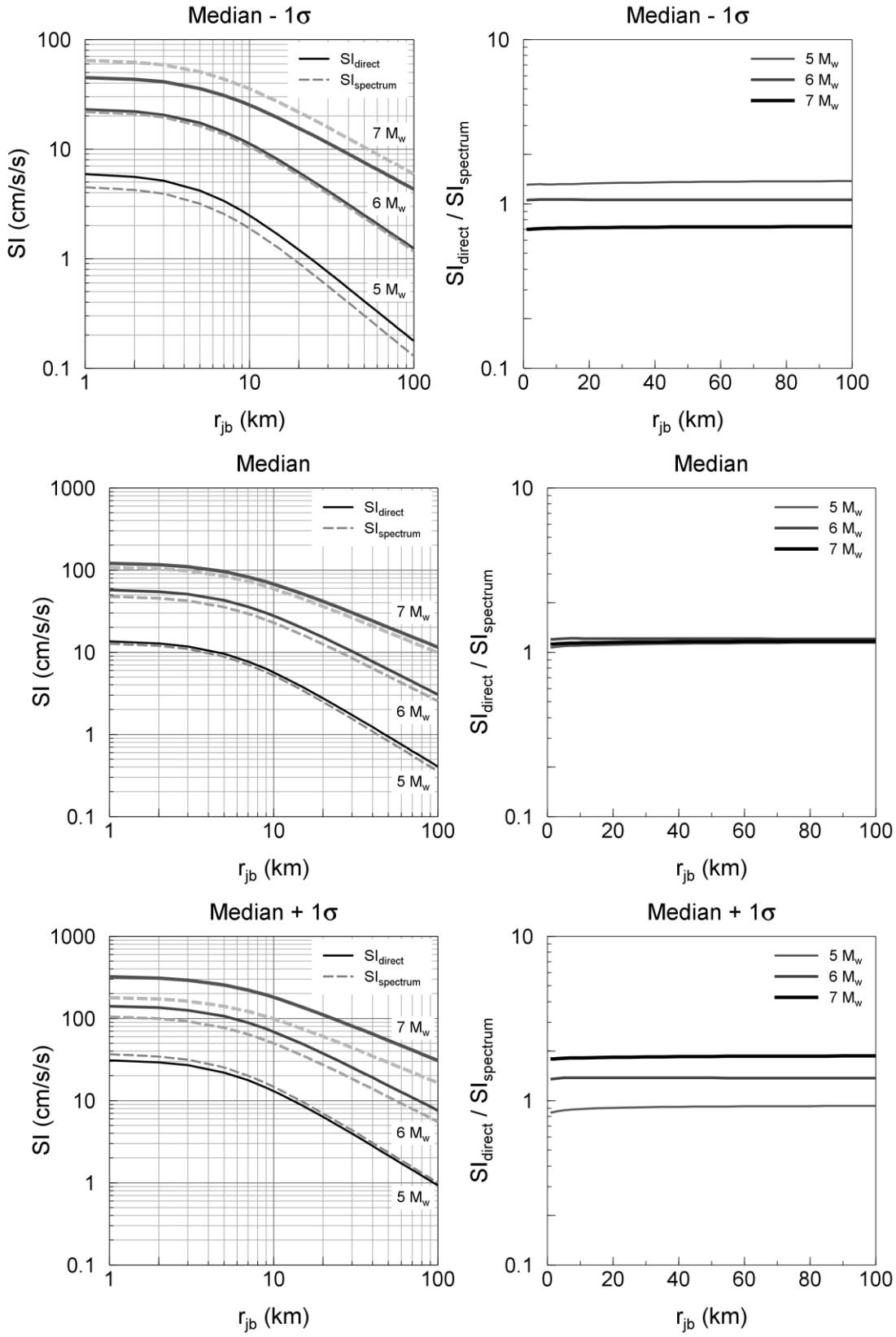

Figure 6.33. Attenuation of SI with distance (left), for the median prediction and the median ±1σ, for SI predictions of Equation 6.2 (SI_{direct}) and for SI inferred from response spectra obtained from the equation of Akkar & Bommer (2007b) ($SI_{spectrum}$), and the relation between the ratio of this predictions ($SI_{direct}/SI_{spectrum}$) and distance (right).

As expected, the $SI_{direct}/SI_{spectrum}$ relationship does not change with distance as sigma for both equations is independent of this variable. However, it worth noting that the ratio $SI_{direct}/SI_{spectrum}$ for magnitude 6 is basically the same for the median and the median $\pm1\sigma$, but significantly changes for the other magnitudes at the median $\pm1\sigma$. Once again, this variation is due to the influence in the predicted SI of the magnitude-dependence of sigma in Equation 6.2.

It is also interesting to note that the ratio $SI_{direct}/SI_{spectrum}$ for the median values in Figure 6.33 is very similar to those presented in Figure 6.31 and recommended in Equation 6.3 (i.e., ~1.1). The reason for this is that the values of ε' of the dominant scenarios of the hazard analysis presented herein in terms of SA(T) were always close to zero. This confirms that the relationship in Equation 6.3 is valid, at least when the value of ε' corresponding to the dominant scenario (M*-R*) is close to zero.

As can be seen in Figure 6.30, the first approach, while underestimating the seismic hazard for SI, is still a relatively good approximation to the predictions of the PSHA made directly in terms of SI. On the other hand, since the conditional mean spectrum represents the most likely response spectrum to affect a structure at a given response period, the second approach is not only a more rational way to estimate the SI value but has also been shown to have a much better correlation with the expected values from the PSHA performed directly in terms of this parameter.

In order to explore the correlation between the SA(T) and PGV, a similar exercise to the estimation of SI using the second approach was carried out. Figure 6.34 shows the relationship between the ratio PGV/SA'(T) and period, where SA'(T) represents the amplitude of the expected response spectrum of the dominant scenario for SA at a given response period. In other words, each curve in Figure 6.34 shows the variation of the ratio

PGV/SA'(T) across the response periods of the conditional mean spectrum corresponding to the dominant scenario for a given SA(T) and return period. It is worth re-emphasising that, here, SA'(T) refers to the spectral amplitudes of the expected response spectrum, while SA(T) refers to the spectral acceleration at a given return period obtained from PSHA.

In Figure 6.34 it can be observed that the scatter in the ratio PGV/SA'(T) for response periods below 0.5 s is considerable smaller than for periods above 0.5 s. The same behaviour was observed for each of the three sites under study. On average, the ratio PGV/SA'(T) is equal to approximately 0.07 for the response periods of 0.1 and 0.3 s and equal to approximately 0.11 for 0.5 s response period. At response periods above 0.5 s the ratio PGV/SA'(T) varies considerably and is clearly dependent on the dominant earthquake scenario. Although the variation of the ratio PGV/SA'(T) for response periods below 0.5 s is still important, it is less dependent of the magnitude, distance and epsilon of the dominant scenario than for response periods above this value.

Table 6.2 presents a comparison between the PGV values obtained from the PSHA performed in terms of PGV (section 6.2), PGV values estimated by multiplying the 5%-damped SA' at 0.5 s by a factor of 0.11 (from this study) and the PGV values estimated using the previously commented practice of dividing the 5%-damped PSV at a response period of 1.0 s by a factor of 1.65. From the observation of the results in Table 6.2 can be observed that, although the estimate of PGV from SA' at 0.5 s are more robust than the estimates from PSV at 1.0 s (c.f., Bommer & Alarcón, 2006) the variability on the results is still very important, with errors up to 76 %. PSV was calculated from SA using the equation:

$$PSV(T) = SA(T)T/2\pi\,, \qquad 6.4$$

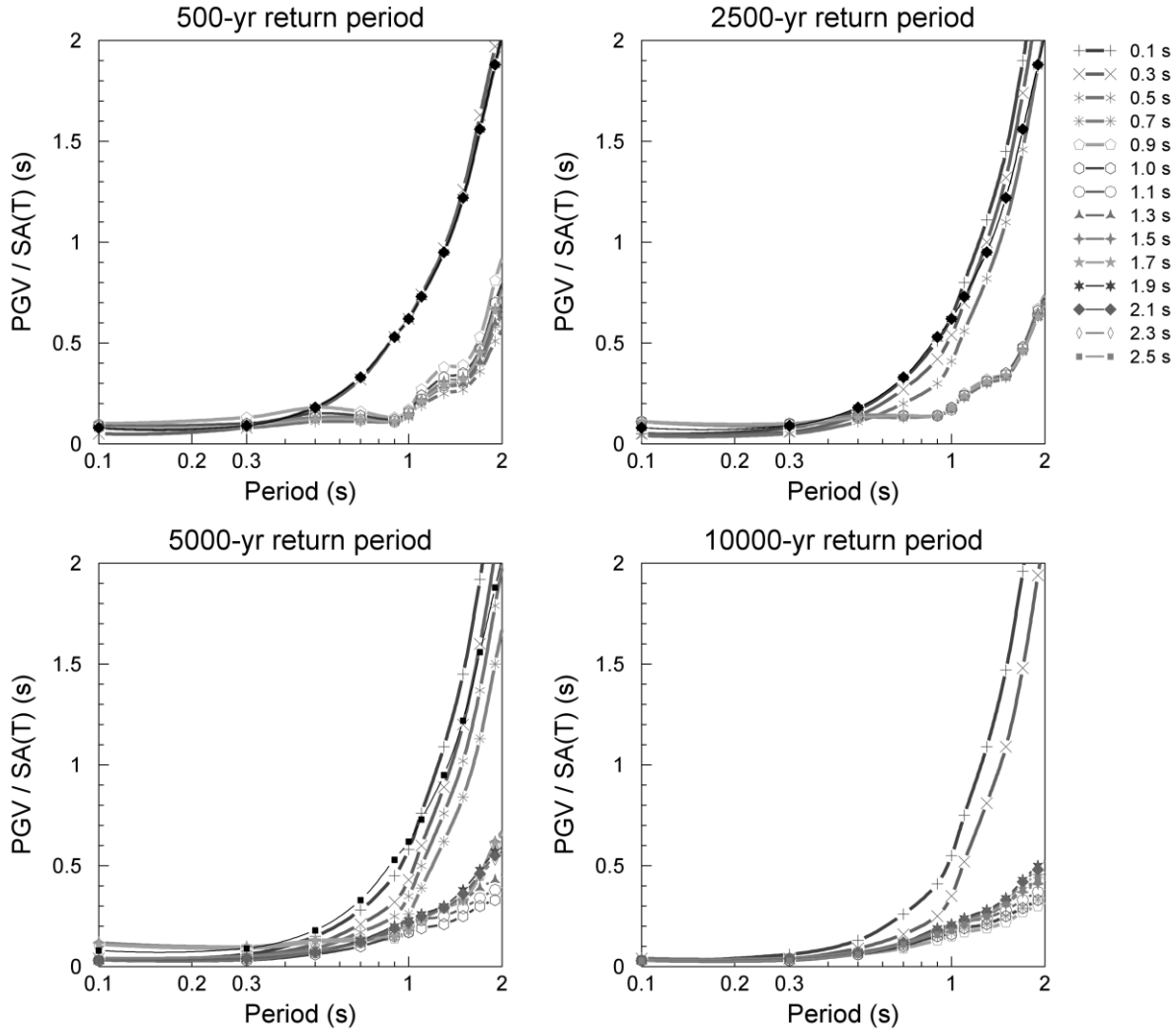

Figure 6.34. Relationships between PGV / SA(T) and the period of the expected response spectra corresponding to the hazard-dominating scenario for SA(T) with 5% damping. These results are for the city of Dubai.

In general, the results obtained herein are in reasonable agreement with those obtained by Bommer & Alarcón (2006). The latter authors presented relationships between PGV/SA(T) and period for different predictive equations and for multiple sets of magnitude, distance and site conditions. Bommer & Alarcón (2006) concluded that the practice of estimating PGV from PSV at 1.0 s should be discontinued, and that, if it is necessary to infer PGV values from SA(T), a better practice is to estimate PGV by dividing the SA at 0.5 s response period by a factor of 20.

Table 6.2. Comparison of PGV values obtained from a PSHA for PGV (section 6.2) and PGV values estimated from correlations to spectral accelerations at 0.5 and 1.0 s response periods for 5% damping of critical. PGV values are in units of cm/s.

	Obtained from the PSHA for PGV				
Return period (yr)	**500**	**1000**	**2500**	**5000**	**10,000**
Abu Dhabi	5.44	6.85	8.13	9.05	10.31
Dubai	6.84	8.17	9.66	10.56	11.54
Ra's Al Khaymah	7.90	9.41	11.03	12.22	13.3
	Calculated from SA'(0.5) for 5% damping multiplied by a factor of 0.11				
Return period (yr)	**500**	**1000**	**2500**	**5000**	**10,000**
Abu Dhabi	5.42	6.65	9.13	12.88	18.14
Dubai	6.60	7.79	9.99	13.02	18.22
Ra's Al Khaymah	7.77	9.13	11.19	13.56	17.73
	Calculated from PSV(1.0) for 5% damping divided by a factor of 1.65				
Return period (yr)	**500**	**1000**	**2500**	**5000**	**10,000**
Abu Dhabi	3.36	3.98	4.58	5.06	6.02
Dubai	4.12	4.54	5.15	5.79	6.69
Ra's Al Khaymah	4.57	5.26	5.92	6.42	6.96

Two key differences must be noted between the results of Bommer & Alarcón (2006) and the results presented herein: (1) the variability of the PGV/SA'(T) ratios for response periods less than 0.5 s is smaller in the present work. Bommer & Alarcón (2006) found that the variability in the PGV/SA(T) ratios was smallest at response periods between 0.3 and 0.5 s, and usually increased at 0.1 s; and, (2) the ratio between PGV and SA' at 0.5 s for the present work is higher than reported by Bommer & Alarcón (2006) by about a factor of two.

The main reasons for these differences could be that Bommer & Alarcón (2006) calculate the mean response spectra rather than the conditional mean response spectra. The reader is referred to section 4.5 for further details on the definitions of the "mean" and the "conditional mean" response spectra. Additionally, the latter authors do not explicitly consider epsilon (ε) for the construction of their response spectra, which is omitted and hence considered as equal to zero.

As common practice is to infer PGV from the SA of the UHS and not from the response spectrum of the dominant scenario, in Figure 6.35 the

relationship of PGV/SA(T) with return period for response periods of 0.5 and 1.0 s. SA(T) are shown (all for 5% damping).

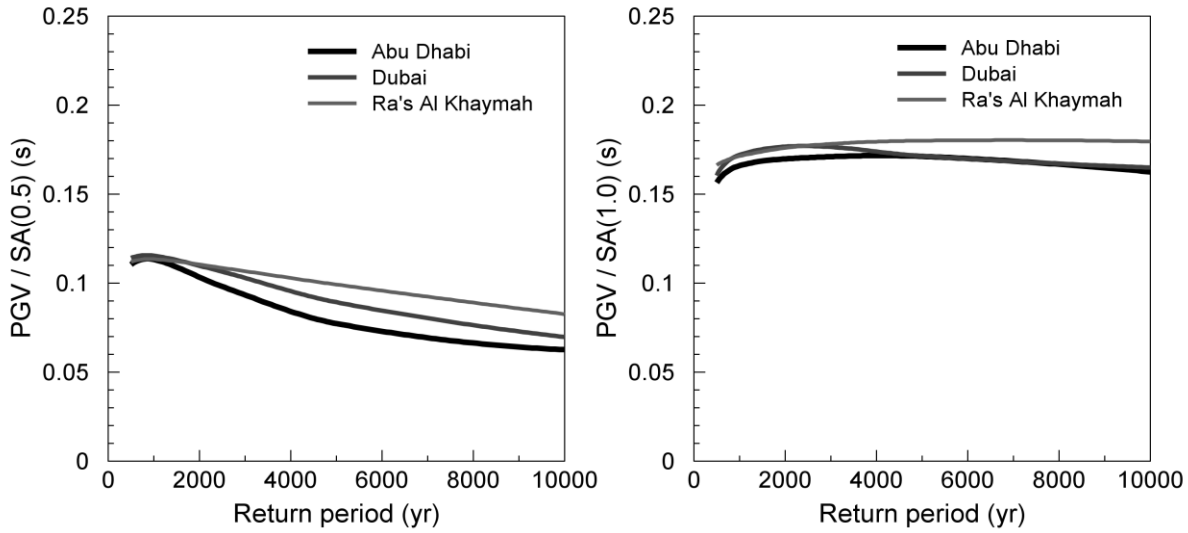

Figure 6.35. Relationship between PGV/SA(T) and return period for response periods of 0.5 s (left) and 1.0 s (right). These results are for the three sites under study.

As can be observed in Figure 6.35 (left) the ratio PGV/SA(0.5) over the considered return periods is higher than the relationship proposed by Bommer & Alarcón (2006) of 0.05, but is in better agreement to the relationship of 0.11 proposed in the present work. The latter proposal being good at short return periods but becoming progressively worse as the return period increases. On the other hand, the ratio PGV/SA(1.0) shown on the right-hand-side is much higher than the traditionally assumed ratio of 0.09 [note that the correlation factor between PGV and PSV(1.0) of 1/1.65 corresponds to a factor of 0.09 for the correlation between PGV and SA(1.0)].

In conclusion, a good correlation was observed between the expected values from a PSHA performed in terms of SI and the values of SI inferred from the hazard results in terms of SA(T) when SI was calculated from the scenario spectrum of the dominant seismic scenario for a given return period and for a specific response period. The calculation of SI from the UHS should be avoided as it apparently underestimates the hazard and more important

because the use of the UHS for estimating the expected SI has no technical basis.

The findings of the present work reinforce the conclusion of Bommer & Alarcón (2006) that the practice of inferring PGV from the 5%-damped PSV at 1.0 s should be discontinued as it has been shown here that this relationship has a large variability and that it is highly dependent on the earthquake scenario used to construct the PSV. If it is necessary to infer PGV values from spectral ordinates, spectral accelerations at response periods below 0.5 s should be used instead. However, based on the results of the present work, a new value for the ratio PGV/SA(0.5) of 0.11 is suggested when scaling off the SA(0.5) value. For SA(T) at response periods below 0.3 s a PGV/SA(T) ratio of 0.07 should be used. Nevertheless, the analyst must keep in mind the very large uncertainty associated with the PGV values obtained from these relationships.

In any case, carrying out a formal PSHA directly in terms of either SI or PGV must be always preferred over the relationships presented herein.

Chapter 7.

DISCUSSION & CONCLUSIONS

To begin this thesis a comprehensive PSHA for three cities in the United Arab Emirates (UAE) has been presented. The UAE is undergoing very rapid development with one of the highest construction rates in the world. Previous published studies regarding the seismic hazard in the region present diverse interpretations of the seismic threat in this country, creating confusion regarding the appropriate seismic design levels.

The results of this PSHA study support the conclusion of some previous studies that the hazard levels in the UAE are low and that, for structures of normal occupancy, seismic design should not be necessary. The exception to this is the most northerly region of the UAE, including the city of Ra's Al Khaymah, which could be classified as zone 1 according to the UBC97 classification scheme. For a return period of 500 years, PGA values of 0.031, 0.043 and 0.054 g were obtained for the cities of Abu Dhabi, Dubai and Ra's Al Khaymah respectively.

In general, the seismic hazard in the region for PGA and SA for short response periods is dominated by events of medium to low magnitude (M_s < 6) located at short distances from sites (r_{epi} < 75 km), both for short and long return periods. These scenarios are mainly contributed by the Stable craton and the Persian Gulf seismic sources. Some contribution also comes from the Simple Fold belt and the Zagros Foredeep sources, with this contribution increasing as one moves north towards the city of Ra's Al Khaymah. For the longest response periods (greater than 1.0 s), seismic hazard is primarily dominated by events with magnitudes between M_s 6.0 and M_s 7.5 and distances between 200 and 350 km from the sites. The seismic sources that

contribute the most at these periods are the Simple Fold belt, the Zagros Foredeep and the Persian Gulf for all three sites, and the Makran West source for the city of Ra's Al Khaymah.

Using the hazard results of the case-study PSHA as a reference, the mechanics and implications for disaggregation of using multiple GMPEs in a PSHA conducted within a logic-tree framework were studied. Alternative ways of representing the results from a logic-tree implementation of PSHA were also studied. Although the representations studied herein are all valid in their own right, the hazard analyst must be aware of the different context for which certain representations are more appropriate than others. For the results of the case study, the mean hazard curve showed a more stable behaviour across exceedance probabilities than the median hazard curve, which tends to have abrupt changes in slope when different groups of hazard curves cross each other. On the other hand, the median curve and the 15th and 85th percentiles provide a better depiction of the dispersion in the suite of hazard curves corresponding to the end points of the logic tree. The most important finding on this topic is the erratic behaviour of the hazard curves of the different seismic sources when calculating the median hazard curve, a behaviour that in some instances leads to an apparent increase of the probabilities of exceedance as the ground-motion increases, which is impossible by definition. This finding in the results of the median hazard curve has raised some concern regarding whether the median hazard curve and its disaggregated results are appropriate for use in seismic design. The erratic behaviour of the contributions by seismic source can be avoided if a single hazard curve from the complete set of curves of the logic tree is selected as "the" median hazard curve. However, the problem would then be associated with which criteria should govern the selection of the median hazard curve. Regarding the calculation of the mean hazard curve, whether one computes the mean in the hazard or the ground-motion domain, at least

for the case study, does not seem to make a significant difference to the hazard results, although some minor differences are expected in terms of identifying the dominant scenarios from each approach.

Following the same criteria used in this work to identify hazard-dominating scenarios, the concept of a "modal" GMPE has been introduced in order to identify a GMPE that is most suitable for generating a scenario spectrum associated with a particular scenario. Making use of the concept of a modal GMPE, two approaches have been proposed to obtain scenario spectra from hazard disaggregation when multiple GMPEs have been used. Different representations of the hazard results, together with alternative procedures to obtain the disaggregated results are considered within these two approaches. There are many alternative paths that the hazard analyst can follow for the purpose of obtaining a scenario spectrum and selecting ground-motion records for seismic design. Each of these paths leads to alternative scenario spectra which are valid within a certain context. The selection of the path to follow may be project-specific and must result from a discussion between engineers, decision makers and the hazard analyst, among others. However, the analyst must bear in mind, and communicate to the others involved in the decision-making process, the conceptual interpretations and implications of the alternative procedures to obtain the final scenario spectra and ground-motion records.

A series of sensitivity analyses for the case study were carried out in order to gain an appreciation for the influence of key parameters in the PSHA. The first of these analyses is an extension of the PSHA to account for the hypothetical case where an active fault running along the west coast of the UAE, as mapped by Johnson (1998), is included as an active source. In the light of the corresponding analyses, it can be stated that the presence of such a fault, considering levels of slip rate compatible with the instrumental and historical seismicity and the available geological data, does not lead to

any significant increment in the seismic hazard at the sites under study and at return periods that would normally govern the design of non-critical structures. Additionally, to include this fault as an active seismic source in PSHA calculations on the basis of existing evidence is excessively conservative, since the existence of such a structure has not been proven. However, if it were shown to exist, its seismic potential should be quantified by means of geomorphic or bathymetric indicators or paleoseismological investigations (if it is possible given the hypothesised location).

The sensitivity of the hazard results to the value of m_{min} that is chosen for the hazard calculations was also studied. It was observed that the selection of different values of m_{min} has the greatest influence at the lowest levels of ground motion (short return periods), with the effect being most significant for PGA and for SA at short response periods and becoming essentially negligible at response periods around, and above, 3.0 s. In general, the selection of m_{min} only has a small influence on the ground-motion levels at the return periods that normally govern seismic design (475 years and above). However, a conservative value of m_{min} could lead to an unrealistic increase in the exceedance frequency of a given ground-motion level, particularly for SA at short response periods.

As an alternative to m_{min}, the use of the cumulative absolute velocity (CAV) for identifying potentially damaging earthquake scenarios, as proposed by Hardy *et al.* (2006), was investigated. This new method was applied to the hazard results of the case study using the recommended threshold value of CAV = 0.16 g-s (CAV16). A significant reduction in the seismic hazard was observed for the three sites under study as a result of the application of this procedure. An important impact on the disaggregated results in terms of magnitude (M) and distance (R) could also be observed. It was observed that not only the contributions from small events at short distances were removed from the hazard results, but also medium-to-large events at long

distances (> 200 km) were removed. Hence, the approach is able to deal with a major short-coming of the current m_{min} prescription.

Alternatively to CAV, there are other ground-motion parameters that have been shown to be good estimators of damage potential, such as Arias Intensity (I_a), and that could also be used to define potentially damaging earthquake scenarios. Based on this, the same methodology proposed by Hardy *et al.* (2006) was applied to the hazard results of the case study but using an I_a threshold value of 0.06 m/s (I_a06). This threshold value corresponds to the I_a value required to produce the same level of interstorey drifts in the storeys of a six-storey building as a CAV value of 0.16 g-s. In a similar manner as when using a threshold value of CAV = 0.16 g-s, a significant reduction in the seismic hazard for the case study was observed. In both cases, the resultant exceedance frequencies were very similar. However, the differences in the disaggregated results were more significant, with I_a06 removing more medium-to-large events at shorter distances than CAV16.

In conclusion, the procedure proposed by Hardy *et al.* (2006) has been shown to be efficient at removing earthquake scenarios from the hazard calculations that potentially lead to an inflation of the seismic hazard. However, the results from this procedure must be interpreted with caution as they could easily be misunderstood. These results must be interpreted as being related to the joint probability of two events, that is, the probability that two threshold values will be exceeded.

Regarding the earthquake activity parameters (β and ν_{min}) and the m_{max}, which together describe the seismic activity of a specific seismic source, a sensitivity analysis was conducted to assess the degree to which epistemic uncertainty in these parameters influences the hazard results. It is shown that the epistemic uncertainty associated with these parameters exerts almost zero influence on the total seismic hazard for typically

considered return periods. This epistemic uncertainty only has some influence at very long return periods (above 100 000 years).

The selection of the GMPE to use in a seismic hazard assessment has been recognized as one of the main contributors to the total uncertainty in PSHA (Sabetta *et al.*, 2005; Toro, 2006). In order to assess the influence on the results of the different sets of equations used in the case-study hazard analysis, the values at the end tips of the branches of the logic tree were compared and discussed. As expected, the greatest contributor to the total uncertainty is the selection of the GMPEs and all of the remaining sources of epistemic uncertainty only contribute in a very minor way. For instance, in the hazard results of the case study, epistemic uncertainty associated with the selection of the GMPEs represents around 95% of the total epistemic uncertainty for PGA. It is clear that once a reasonable number of GMPEs have been included in the logic tree, the epistemic uncertainty is totally dominated by the selection of these equations. For this reason, special care must be taken to select the most suitable ground-motion models for the region under study.

Another point of interest in PSHA is the standard deviation (sigma, σ) corresponding to each GMPE. This sigma value represents the aleatory variability of ground-motion values for any given set of independent variables. A sensitivity analysis on the influence on the resulting hazard curves due to modifying the value of sigma corresponding to each GMPE used in the hazard analysis of the case study was carried out. This sensitivity analysis was performed only with academic purposes as in principle the value of sigma corresponding to a given GMPE must not be modified. It was observed that the influence of sigma is clearly most significant at the longest return periods. The variation of sigma does not only influence the expected annual frequency of exceedance of a given value of ground-motion but also the contributions observed in the disaggregated

results. In general, an increase in the sigma value of the GMPEs leads to an increase in the contributions in terms of M and R; the increase being higher for small but more frequently occurring events than for larger but less frequently occurring events. In this way, a shift in the relative contributions in terms of M and R is observed from larger-magnitude scenarios towards small-magnitude scenarios as the value of sigma increases.

The last of the sensitivity analyses carried out in this work addresses the process of assigning weights to each branch of the logic tree. In order to do this, the weights assigned to each branch of the logic tree in the case study were modified using multiple alternative weighting criteria in addition to the original weightings. The main conclusion of this analysis is that once the logic tree has been set up and a general view has been formulated as to which of the alternative options at each node represents the most likely scenario, the specific numerical weights allocated to the alternative branches has a fairly small (essentially negligible) impact upon the final hazard estimate. In the results of this sensitivity analysis, differences of up to 20% in the weight of the most like scenario showed a negligible impact on the hazard results. However, when very skewed weights were assigned towards one of the options significant changes in the hazard results were observed.

Finally, the relationships between the hazard results for spectral amplitudes [SA(T)] and the expected values of peak ground velocity (PGV) and spectral intensity (SI) obtained from hazard assessments performed in terms of each of these parameters were explored. For inferring SI from hazard results in terms of SA(T) two approaches were proposed. Both approaches showed a relatively good correlation between the inferred values of SI and the values of SI obtained directly from a PSHA performed in terms of this variable.

Regarding the relationships between the hazard results for SA(T) and PGV, the findings of the present work reinforce the conclusion of Bommer &

Alarcón (2006) that the practice of inferring PGV from the 5%-damped PSV at 1.0 second should be discontinued as it has been proven that this relationship has a very large variability associated with it. If it were necessary to infer PGV values from spectral ordinates it is better to use spectral accelerations at response periods less than 0.5 s, which have been shown to have a much better correlation with PGV. However, a new value for the ratio PGV/SA(0.5) of 0.11 is proposed herein to be used by those continuing this ill-conceived practice. In any case, the performance of a formal PSHA in terms of either SI or PGV must be always preferred over the relationships presented in this work.

In light of these conclusions the following recommendations for future research are made:

- A re-evaluation of the PSHA presented in the case study is recommended, once new geologic and tectonic information, along with more instrumental seismicity, becomes available for the Arabian Peninsula and in particular for the UAE territory and the Hajar Mountains. Given the rate at which this information becomes available, it is unlikely that any reassessment of the hazard will yield markedly different results for some time to come. The notable exception would, of course, be the discovery of new faults, or evidence of the occurrence of major events in the vicinity of the considered sites.
- Particularly in the Dibba zone, where seismic activity has been observed in recent years, additional research needs to be done in order to assess the seismic potential of the geological structures in this region such as paleoseismological studies and measurements of slip rates. These types of studies may provide valuable information, in the short to the medium term, that would enable an improved assessment of the seismic hazard in

the region. However, as with most regions of the world, paleoseismological investigations often do not result in amounts of data that allow activity rates to be constrained with much certainty. Therefore, while the situation would undoubtedly be inmproved, a significant degree of epistemic uncertainty regarding the activity of these sources would remain.

- The recently established seismological network in the UAE needs to be extended to increase the network's capabilities, particularly in the northern part of the UAE. Such an expansion is perfectly feasiable given the amount of investment that is pouring into the region. Estimates of the long term rates of activity would not change over the short term if this network was expanded, but it would enable event locations to be resolved with greater accuracy and the recorded motions would be extremely valuable for the purposes of ground-motion modelling within the region.
- Once enough recordings become available for the UAE, native ground-motion prediction models for the UAE need to be developed in order to reduce the epistemic uncertainty regarding the selection of ground-motion models that heavily dominate the current uncertainty in the hazard results.
- Research needs to be conducted in order to prove the existence or otherwise of an active geological structure running along the west coast of the UAE. If such a fault were proved to exist, research oriented to assess the seismic activity of the fault, such as paleoseismological investigations, if possible, should be carried out.
- Further analysis needs be performed in order to incorporate the effects of surface soil deposits on the modification of the ground

shaking, mainly at long response periods, generated by medium-to-large earthquakes in the Zagros and Makran regions. This could have direct effects on the high-rise structures of the region. The work required to complete such a task depends upon the precision that is desired. It is a relatively straightforward exercise to repeat the analyses presented herein for generic soil sites that would allow users to select hazard levels that they deemed to be appropriate. However, if site-specific analyses are required for major structures then the results presented here provide a solid platform from which such analyses may be completed. Detailed models of the near surface soil deposits would obviously be required as well as the identification of accelerograms that are suitable for use in site-specific site-response studies for the region.

- More research needs to be done in order to have a better understanding of the implications of using multiple GMPEs in a PSHA carried out within a logic tree framework and how the decision of selecting one equation over another influences the hazard results. Such research is primarly theoretical in nature and the optimal approach is likely to be identified within the next few years.
- Alternatives to the use of the logic tree to incorporate epistemic uncertainties into the hazard analysis should be explored in order to overcome some of the disadvantages of using this tool.
- Better methods for representing the variability of the hazard results from a logic tree should be explored. Like the previous two points, such methods require theoretical development and are likely to be topics of research over the coming few years.

Whether or not researchers will be able to develop preferable methods is an open question.

- The different representations of the hazard results studied herein (i.e., mean vs. median and hazard vs. ground-motion domain) should be applied for other areas, this is in order to corroborate whether the findings of this work apply to other regions or not.
- The implications of using GMPEs for values of magnitude and distance outside their strict ranges of applicability should be explored. Alternatively, GMPEs should be derived to consider larger ranges of magnitudes and longer distances. The models that have recently been derived as part of the NGA project make an effort along the lines of this latter alternative.
- The CAV and I_a threshold values should be calibrated for different building classes and different levels of damages. Additionally, more research should be done to correlate these threshold values with ground failure due to liquefaction and landslides. Such extensions should be structure-specific, or at least specific to particular classes or structures. It may be that CAV proves to be effective for broad classes of structures. However, only time will tell if this is the case.

REFERENCES

Abdalla, J. A., and Al-Homoud, A. S. (2004). "Seismic hazard assessment of United Arab Emirates and its surroundings." *Journal of Earthquake Engineering*, **8**(6), pp. 817-837.

Abrahamson, N. A. (2000a). "Effects of rupture directivity on probabilistic seismic hazard analysis." *Proceedings of the 6th international conference on seismic zonation*, Palm Springs, CA, Nov 12-15, 2000.

Abrahamson, N. A. (2000b). "State of the practice of seismic hazard assessment." *Proceedings of GeoEng 2000*, Melbourne, Australia. **1**, pp. 659-685

Abrahamson, N. A. (2006). "Seismic hazard assessment: Problems with current practice and future developments." *First European conference on earthquake engineering and seismology*, Geneva, Switzerland,

Abrahamson, N. A., and Bommer, J. J. (2005). "Probability and uncertainty in seismic hazard analysis." *Earthquake Spectra*, **21**(2), pp. 603-607.

Abrahamson, N. A., and Shedlock, K. M. (1997). "Overview." *Seismological Research Letters*, **68**(1), pp. 9-23.

Abrahamson, N. A., and Silva, W. J. (1997). "Empirical response spectra attenuation relations for shallow crustal earthquakes." *Seismological Research Letters*, **68**(1), pp. 94-127.

Abrahamson, N. A., and Somerville, P. G. (1996). "Effects of the hanging wall and footwall on ground motions recorded during the Northridge earthquake." *Bulletin of the Seismological Society of America*, **86**(1), S93-S99.

Akkar, S., and Bommer, J. J. (2006). "Influence of long-period filter cut-off on elastic spectral displacements." *Earthquake Engineering & Structural Dynamics*, **35**, pp. 1145-1165.

Akkar, S., and Bommer, J. J. (2007a). "Empirical Prediction Equations for Peak Ground Velocity Derived from Strong-Motion Records from Europe and the Middle East." *Bulletin of the Seismological Society of America*, **97**(2), pp. 511-530.

Akkar, S., and Bommer, J. J. (2007b). "Prediction of elastic displacement response spectra in Europe and the Middle East." *Earthquake Engineering & Structural Dynamics*, **36**(10), pp. 1275-1301.

Akkar, S., and Özen, Ö. (2005). "Effect of peak ground velocity on deformation demands for SDOF systems." *Earthquake Engineering & Structural Dynamics*, **34**(13), pp. 1551-1571.

Al-Haddad, M., Siddiqi, G. H., Al-Zaid, R., Arafah, A., Necioglu, A., and Turkelli, N. (1994). "A basis for evaluation of seismic hazard and design criteria for Saudi Arabia." *Earthquake Spectra*, **10**(2), pp. 231-258.

Al-Hinai, K. G., Dabbagh, A. E., Gardner, W. C., Khan, M. A., and Saner, S. (1997). "Shuttle imaging radar views of some geological features in the Arabian Peninsula." *GeoArabia*, **2**(2), pp. 165-178.

Al-Homoud, A. S. (2003). "The Fujairah "United Arab Emirates (UAE) (M_L = 5.1) earthquake of March 11, 2002" A reminder for the immediate need to develop and implement a national hazard mitigation strategy." *Geophysical Research Abstracts*, **5**(01700).

Al Khatibi, E., Al Marzooqi, Y., Megahed, A. S., Mathias, F., and Mallalah, A. (2007). "Preliminary seismicity of the United Arab Emirates deduced from Dubai seismic network." The fourth Gulf seismic forum, Kuwait.

Albini, P., (2004). "A survey of the past earthquakes in the Eastern Adriatic (14th to early 19th century)." *Annali di Geofisica*, **47**(2-3), pp. 675-703.

Allen, M., Jackson, J. A., and Walker, R. (2004). "Late Cenozoic reorganization of the Arabia-Eurasia collision and the comparison of short-term and long-term deformation rates." *Tectonics*, **23**(TC2008, doi:10.1029/2003TC001530).

Ambraseys, N. N. (1995). "The prediction of earthquake peak ground acceleration in Europe." *Earthquake Engineering & Structural Dynamics*, **24**, pp. 467-490.

Ambraseys, N. N. (2001). "Reassessment of earthquakes, 1900-1999, in the Eastern Mediterranean and the Middle East." *Geophysical Journal International*, **145**(2), pp. 471-485.

Ambraseys, N. N., and Adams, R. D. (2001). "The seismicity of Central America: A descriptive catalogue 1898-1995." Imperial College Press.

Ambraseys, N. N., and Bilham, R. (2003a). "Earthquakes and associated deformation in northern Baluchistan 1892-2001." *Bulletin of the Seismological Society of America*, **93**(4), pp. 1573-1605.

Ambraseys, N. N., and Bilham, R. (2003b). "Earthquakes in Afghanistan." *Seismological Research Letters*, **74**, pp. 107-123.

Ambraseys, N. N., and Bommer, J. J. (1990). "Uniform magnitude re-evaluation for strong motion database of Europe." *European Earthquake Engineering*, **4**(2), pp. 3-16.

Ambraseys, N. N., Douglas, J., Sarma, S. K., and Smit, P. M. (2005). "Equations for the estimation of strong ground motions from shallow crustal earthquakes using data from Europe and the Middle East: Horizontal peak ground acceleration and spectral acceleration." *Bulletin of Earthquake Engineering*, **3**(1), pp. 1-53.

Ambraseys, N. N., and Free, M. W. (1997). "Surface-wave magnitude calibration for European region earthquakes." *Journal of Earthquake Engineering*, **1**(1), pp. 1-22.

Ambraseys, N. N., and Melville, C. P. (1982). "A history of Persian earthquakes." Cambridge University Press, Cambridge. 212 pp.

Ambraseys, N. N., Melville, C. P., and Adams, R. D. (1994). "The seismicity of Egypt, Arabia and the Red Sea: a historical review." Cambridge University Press, Cambridge. 181 pp.

Ambraseys, N. N., Simpson, K. A., and Bommer, J. J. (1996). "Prediction of horizontal response spectra in Europe." *Earthquake Engineering & Structural Dynamics*, **25**(4), pp. 371-400.

Ambraseys, N. N., and Srbulov, M. (1994). "Attenuation of earthquake-induced ground displacements." *Earthquake Engineering & Structural Dynamics*, **23**(5), pp. 467-487.

Arias, A. (1970). "Seismic design for nuclear power plants", A measure of earthquake intensity. R. J. Hansen, ed., MIT Press, Cambridge, Massachusetts, pp. 438-483.

Atkinson, G. M., and Boore, D. M. (1997). "Some comparisons between recent ground-motion relations." *Seismological Research Letters*, **68**(1), pp. 24-40.

Atkinson, G. M., and Boore, D. M. (2003). "Empirical ground-motion relations for subduction-zone earthquakes and their application to Cascadia and other regions." *Bulletin of the Seismological Society of America*, **93**(4), pp. 1703-1729.

Atkinson, G. M., and Boore, D. M. (2006). "Earthquake ground-motion prediction equations for Eastern North America." *Bulletin of the Seismological Society of America*, **96**(6), pp. 2181-2205.

Baker, C., Jackson, J., and Priestley, K. (1993). "Earthquakes on the Kazerun line in the Zagros Mountains of Iran: strike-slip faulting within a fold-and-thrust belt." *Geophysical Journal International*, **115**, pp. 41-61.

Baker, J. W., and Cornell, C. A. (2006a). "Correlation of response spectra values for multicomponent ground motions." *Bulletin of the Seismological Society of America*, **96**(1), pp. 215-227.
Baker, J. W., and Cornell, C. A. (2006b). "Spectral shape, epsilon and record selection." *Earthquake Engineering & Structural Dynamics*, **35**, pp. 1077-1095.
Baker, J. W., and Jayaram, N. (2008). "Correlation of spectral acceleration values from NGA ground motion models." *Earthquake Spectra*, **24**(1), pp. 299-341.
Bayer, R., Chery, J., Tatar, M., Vernant, P., Abbassi, M., Masson, F., Nilforoushan, F., Doerflinger, E., Regard, V., and Bellier, O. (2006). "Active deformation in Zagros-Makran transition zone inferred from GPS measurements." *Geophysical Journal International*, **165**, pp. 373-381.
Bazzurro, P., and Cornell, C. A. (1999). "Disaggregation of seismic hazard." *Bulletin of the Seismological Society of America*, **89**(2), pp. 501-520.
Bazzurro, P., and Cornell, C. A. (2002). "Vector-valued probabilistic seismic hazard analysis (VPSHA)." *7th U.S. National conference on earthquake engineering*, Boston, MA., Earthquake Engineering Research Institute, 10 pp.
Bazzurro, P., and Cornell, C. A. (2004). "Nonlinear soil-site effects in probabilistic seismic-hazard analysis." *Bulletin of the Seismological Society of America*, **94**(6), pp. 2110-2123.
BBC-News. (2008) "Sarkozy to sign a UAE nuclear deal." http://news.bbc.co.uk/1/hi/world/europe/7185660.stm, 13 January 2008.
Bender, B., and Perkins, D. M. (1987). "SEISRISK III, A computer program for seismic hazard estimations." *U.S. Geology Survey Bulletin*, **1772**, pp. 1-20.
Berberian, M. (1973). "The seismicity of Iran, preliminary map of epicentres and focal depths." scale 1:2,500,000, Geological survey of Iran - Seismotectonic group
Berberian, M. (1979). "Evaluation of the instrumental and relocated epicentres or Iranian earthquakes." *Geophysical Journal of the Royal Astrological Society*, **58**, pp. 62-630.
Berberian, M. (1994). "Natural hazards and the first earthquake catalogue of Iran, Volume 1: Historical hazards in Iran Prior to 1900." 2, United Nations Educational Scientific and Cultural Organization (UNESCO) / International Institute of Earthquake Engineering and Seismology (IIEES), Tehran. 631 pp.
Berberian, M. (1995). "Master 'blind' thrust faults hidden under the Zagros folds: active basement tectonics and surface morphotectonics." *Tectonophysics*, **241**(3-4), pp. 193-195.
Berberian, M., Jackson, J. A., Fielding, E., Parsons, B. E., Priestley, K., Qorashi, M., Talebian, M., Walker, R., Wright, T. J., and Baker, C. (2001). "The 1998 March 14 Fandoqa earthquake (Mw 6.6) in Kerman province, southeast Iran: re rupture of the 1981 Sirch earthquake fault, triggering of slip on adjacent thrusts and the active tectonics of the Gowk fault zone." *Geophysical Journal International*, **146**(2), pp. 371-398.
Berberian, M., and Yeats, R. S. (1999). "Patterns of historical earthquake rupture in the Iranian Plateau." *Bulletin of the Seismological Society of America*, **89**(1), pp. 120-139.
Berge-Thierry, C., Cotton , F., Scotti, O., Griot-Pommera, D.-A., and Fukushima, Y. (2003). "New empirical response spectra attenuation laws for moderate European earthquakes." *Journal of Earthquake Engineering*, **7**(2), pp. 193 - 222.

Bernard, P., and Herrero, A. (1994). "Slip heterogeneity, body-wave spectra, and directivity of earthquake ruptures." *Annali di geofisica*, **37**(6), pp. 1679-1690.
Beyer, K., and Bommer, J. J. (2006). "Relationships between median values and between aleatory variabilities for different definitions of the horizontal component of motion." *Bulletin of the Seismological Society of America*, **96**(4A), pp. 1512-1522.
Bommer, J. J. (2005). "Lecture notes of the Soil Mechanics and Earthquake Engineering MSc course: Engineering seismology." Department of civil and environmental engineering, Imperial College London, 237 pp.
Bommer, J. J., and Abrahamson, N. A. (2006). "Why Do Modern Probabilistic Seismic-Hazard Analyses Often Lead to Increased Hazard Estimates?" *Bulletin of the Seismological Society of America*, **96**(6), pp. 1967-1977.
Bommer, J. J., Abrahamson, N. A., Strasser, F. O., Pecker, A., Bard, P.-Y., Bungum, H., Cotton, F., Fäh, D., Sabetta, F., Scherbaum, F., and Studer, J. (2004). "The challenge of defining upper bounds on earthquake ground motions." *Seismological Research Letters*, **75**(1).
Bommer, J. J., and Alarcón, J. E. (2006). "The prediction and use of peak ground velocity." *Journal of Earthquake Engineering*, **10**(1), pp. 1 - 31.
Bommer, J. J., Douglas, J., and Strasser, F. O. (2003). "Style-of-faulting in ground-motion prediction equations." *Bulletin of Earthquake Engineering*, **1**(2), pp. 171-203.
Bommer, J. J., and Martínez-Pereira, A. (1999). "The effective duration of earthquake strong motion." *Journal of Earthquake Engineering*, **3**(2), pp. 127 - 172.
Bommer, J. J., and Scherbaum, F. (2008). "The use and misuse of logic trees in probabilistic seismic hazard analysis." *Earthquake Spectra*, **24**(4), pp. 997-1009.
Bommer, J. J., Scherbaum, F., Bungum, H., Cotton, F., Sabetta, F., and Abrahamson, N. A. (2005). "On the use of logic trees for ground-motion prediction equations in seismic-hazard analysis." *Bulletin of the Seismological Society of America*, **95**(2), pp. 377-389.
Boore, D. M., and Atkinson, G. M. (2006). "Boore-Atkinson NGA empirical ground motion model for the average horizontal component of PGA, PGV and SA at spectral periods of 0.1, 0.2, 1, 2, and 3 seconds." report to the PEER-Lifelines Next Generation Project [Revised 27 October 2006] [http://peer.berkeley.edu/lifelines/nga docs/nov 13 06/Boore-Atkinson-NGA 11-13-06.html]. 63 pp.
Boore, D. M., and Atkinson, G. M. (2007). "Boore-Atkinson NGA ground motion relations for the geometric mean horizontal component of peak and spectral ground motion parameters." PEER 2007/01, Pacific Earthquake Engineering Research Center, Berkeley, California.
Boore, D. M., and Joyner, W. B. (1993). "Empirical prediction of strong ground motion." *Proceedings structures '93 congress*, Irvine, California,
Boore, D. M., Joyner, W. B., and Fumal, T. E. (1993). "Estimation of response spectra and peak accelerations from western North America earthquakes: An interim report." U.S. Geological Survey. *Open-file report 93-509*. 70 pp.
Bray, J. D., and Rodriguez-Marek, A. (2004). "Characterization of forward-directivity ground motions in the near-fault region." *Soil Dynamics and Earthquake Engineering*, **24**(11), pp. 815-828.
Brown, G. F. (1972). "Tectonic map of the Arabian Peninsula: Saudi Arabian directorate general of mineral resources Arabian Peninsula Map AP-2." scale 1:4,000,000., Saudi Arabian directorate general of mineral resources
BSSC - Building Seismic Safety Council. (1994). "NEHRP recommended provisions for seismic regulations for new buildings." 1994 edition, Part 1: Provisions: FEMA 222A / May 1995. 290 pp.

Buratti, N., Stafford, P., and Bommer, J. J. (2008). "Earthquake accelerogram selection and scaling procedures for estimating the distribution of structural response." *Journal of Structural Engineering*, **Submitted**.

Byrne, D. E., and Sykes, L. R. (1992). "Great thrust earthquakes and aseismic slip along the plate boundary of the Makran subduction zone." *Journal of Geophysical Research*, **97**(B1), pp. 449-478.

Cabañas, L., Benito, B., and Herráiz, M. (1997). "An approach to the measurement of the potential structural damage of earthquake ground motions." *Earthquake Engineering & Structural Dynamics*, **26**(1), pp. 79-92.

Campbell, K. W., and Bozorgnia, Y. (2007). "Campbell-Bozognia NGA ground motion relations for the geometric mean horizontal component of peak and spectral ground motion parameters." UCB/PEER 2007/2, Pacific Earthquake Engineering Research Center, Berkeley, California. 240 pp.

Campbell, W. K. (1985). "Strong motion attenuation relations: A ten-year perspective." *Earthquake Spectra*, **1**(4), pp. 759-804.

Choi, Y., Stewart, J. P., and Graves, R. W. (2005). "Empirical Model for Basin Effects Accounts for Basin Depth and Source Location." *Bulletin of the Seismological Society of America*, **95**(4), pp. 1412-1427.

Cornell, C. A. (1968). "Engineering seismic risk analysis." *Bulletin of the Seismological Society of America*, **58**(5), pp. 1583-1606.

Cornell, C. A. (1971). "Probabilistic analysis of damage to structures under seismic loads", in Dynamic Waves in Civil Engineering. D. A. Howells, I. P. Haigh, and C. Taylor, eds., John Wiley & Sons, New York, pp. 473-488.

Cornell, C. A., and Vanmarcke, E. H. (1969). "The major influences on seismic risk." *Proceedings of the fourth world conference on earthquake engineering*, Chile. **A-1**, pp. 69-93

Cornell, C. A., and Winterstein, S. R. (1988). "Temporal and magnitude dependence in earthquake recurrence models." *Bulletin of the Seismological Society of America*, **78**(4), pp. 1522-1537.

Cosentino, P., Ficarra, V., and Luzio, D. (1977). "Truncated exponential frequency-magnitude relationship in earthquake statistics." *Bulletin of the Seismological Society of America*, **67**(6), pp. 1615-1623.

Cotton, F., Scherbaum, F., Bommer, J. J., and Bungum, H. (2006). "Criteria for selecting and adjusting ground-motion models for specific target regions: Application to central Europe and rock sites." *Journal of Seismology*, **10**(2), pp. 137-156.

Cramer, C. H., Petersen, M. D., Cao, T., Toppozada, T. R., and Reichle, M. (2000). "A Time-Dependent Probabilistic Seismic-Hazard Model for California." *Bulletin of the Seismological Society of America*, **90**(1), pp. 1-21.

Crowley, H., Pinho, R., and Bommer, J. J. (2004). "A probabilistic displacement-based vulnerability assessment procedure for earthquake loss estimation." *Bulletin of Earthquake Engineering*, **2**, pp. 173-219.

Dahle, A., Bungum, H., and Kvamme, L. B. (1990). "Attenuation models inferred from intraplate earthquake recordings." *Earthquake Engineering & Structural Dynamics*, **19**, pp. 1125-1141.

Danciu, L., and Tselentis, G.-A. (2007). "Engineering ground-motion parameters attenuation relationships for Greece." *Bulletin of the Seismological Society of America*, **97**(1B), pp. 162-183.

Dong, W. M., Bao, A. B., and Shah, H. C. (1984). "Use of maximum entropy principle in earthquake recurrence relationships." *Bulletin of the Seismological Society of America*, **74**(2), pp. 725-737.

Douglas, J. (2003a). "Earthquake ground motion estimation using strong-motion records: a review of equations for the estimation of peak ground acceleration and response spectral ordinates." *Earth-Science Reviews*, **61**(1-2), pp. 43-104.
Douglas, J. (2003b). "Earthquake ground motion estimation using strong-motion records: a review of equations for the estimation of peak ground acceleration and response spectral ordinates." *Earth-Science Reviews*, **61**(1-2), 43-104.
Douglas, J. (2004). "Ground motion estimation equations 1964-2003. Reissue of ESEE Report No. 01-1: 'A comprehensive worldwide summary of strong-motion attenuation relationships for peak ground acceleration and spectral ordinates (1969 to 2000)' with corrections and additions." Research report, Imperial College London *04-001-SM*, London.
Douglas, J. (2006). "Errata of and additions to 'Ground motion estimation equations 1964-2003'." Intermediary report, BRGM *BRGM/RP-54603-FR*. 103 pp., 2 tables
Douglas, J., and Smit, P. M. (2001). "How Accurate Can Strong Ground Motion Attenuation Relations Be?" *Bulletin of the Seismological Society of America*, **91**(6), 1917-1923.
Easton, V. J., and McColl, J. H. (2008) "Statistics Glossary." <http://www.stats.gla.ac.uk/steps/glossary/index.html>, June 2008
Ellison, R. A., and Styles, M. T. (2006). "The geology and geophysics of the United Arab Emirates", **Vol. 1:** Executive summary. British Geological Survey, Keyworth, England, 27 pp.
EMSC. (2006) "Earthquake on-line database." <http://www.emsc-csem.org/>, European-Mediterranean Seismological Centre, Bruyères-le-Châtel, France,
Engdahl, E. R., Van der Hilst, R. D., and Buland, R. P. (1998). "Global teleseismic earthquake relocation with improved travel times and procedures for depth determination." *Bulletin of the Seismological Society of America*, **88**(3), pp. 722-743.
Esteva, L. (1967). "Criteria for the construction of spectra for seismic design." *Third Panamerican symposium on structures*, Caracas, Venezuela,
Esteva, L., and Rosenblueth, E. (1964). "Espectros de temblores a distancias moderadas y grandes." *Boletin de la sociedad mexicana de ingeneria sísmica*, **2**, pp. 1-18.
Everyculture.com. (2008) "Culture of United Arab Emirates." <http://www.everyculture.com/To-Z/United-Arab-Emirates.html>, 28th January 2008.
Falcon, N. L. (1961). "Major earth-flexing in the Zagros Mountains of southwest Iran." *Quarterly Journal of the Geological Society of London*, **117**(4), pp. 367-376.
Farhoudi, G., and Karig, D. E. (1977). "Makran of Iran and Pakistan as an active arc system." *Geology*, **5**(11), pp. 664-668.
FEMA. (2003). "Hazus-MH, FEMA's software program for estimating potential losses from disasters." http://www.fema.gov/hazus.
Fenton, C. H., Adams, J., and Halchuk, S. (2006). "Seismic hazards assessment for radioactive waste disposal sites in regions of low seismic activity." *Geotechnical and Geological Engineering*, **24**, pp. 579-592.
Fintel, M., and Ghosh, S. K. (1982). "Explicit inelastic dynamic design procedure for aseismic structures." *ACI Journal*, **79**(2), pp. 110-118.
Gardner, J. K., and Knopoff, L. (1974). "Is the sequence of earthquakes in southern California, with aftershocks removed, poissonian?" *Bulletin of the Seismological Society of America*, **64**(5), pp. 1363-1367.

Gaull, B. A., Michael-Leiba, M. O., and Rynn, J. M. W. (1990). "Probabilistic earthquake risk maps of Australia." *Australian Journal of Earth Sciences*, **37**(2), pp. 169-187.
Giardini, D. (1999). "The global seismic hazard assessment program (GSHAP)-1992/1999." *Annali di geofisica*, **42**(6), pp. 957-974.
Giardini, D., Grünthal, G., Shedlock, K. M., and Zhang, P. (1999). "The GSHAP global seismic hazard map." *Annali di geofisica*, **42**(6), pp. 1225-1230.
Glennie, K. W. (2001). "United Arab Emirates, a new perspective", Evolution of The Emirates' land surface: an introduction. I. Al-Abed and P. Hellyer, eds., Trident Press Ltd, London, 316 pp.
Griscom, M., and Arabasz, W. J. (1979). "Earthquake Studies in Utah 1850 to 1978", A local magnitude (M_L) in the Wasatch Front and Utah Region: Wood-Anderson calibration, coda-duration estimates of M_L, and M_L versus m_b. W. J. Arabasz, R. B. Smith, and W. D. Richins, eds., University of Utah, Salt Lake City, Utah.
Grünthal, G., Bosse, C., Sellami, S., Mayer-Rosa, D., and Giardini, D. (1999). "Compilation of the GSHAP regional seismic hazard for Europe, Africa and the Middle East." *Annali di geofisica*, **42**(6), pp. 1215-1223.
GSHAP. (1999) "Global seismic hazard assessment program." <http://www.seismo.ethz.ch/GSHAP/index.html>,
Gutenberg, B., and Richter, C. F. (1944). "Frequency of earthquakes in California." *Bulletin of the Seismological Society of America*, **34**(4), pp. 185-188.
Hancock, J., and Bommer, J. J. (2006). "A state-of-knowledge review of the influence of strong-motion duration on structural damage." *Earthquake Spectra*, **22**(3), pp. 827-845.
Hancock, J., Watson-Lamprey, J., Abrahamson, N. A., Bommer, J. J., Markatis, A., McCoy, E., and Mendis, R. (2006). "An improved method of matching response spectra of recorded earthquake ground motion using wavelets." *Journal of Earthquake Engineering*, **10**, pp. 67-89.
Hancock, P. L., Al-Kadhi, A., and Sha'at, N. A. (1984). "Regional joint sets in the Arabian Platform as indicators of intraplate processes." *Tectonics*, **3**(1), pp. 27-43.
Hanks, T. C., and Kanamori, H. (1979). "A moment magnitude scale." *Journal of Geophysical Research*, **84**, pp. 2348-2350.
Hardy, G., Merz, K., Abrahamson, N. A., and Watson-Lamprey, J. (2006). "Program on technology innovation: Use of cumulative absolute velocity (CAV) in determining effects of small magnitude earthquakes on seismic hazard analyses." EPRI, Palo Alto, CA, and the U.S. Department of Energy, Germantown. *EPRI report MD: 2006 1014099*.
Harp, E. L., and Wilson, R. C. (1995). "Shaking intensity thresholds for rock falls and slides: Evidence from 1987 Whittier Narrows and superstition hills earthquake strong-motion records." *Bulletin of the Seismological Society of America*, **85**(6), pp. 1739-1757.
Helton, J. C., and Oberkampf, W. L. (2004). "Alternative representations of epistemic uncertainty." *Reliability Engineering & System Safety*, **85**(1-3), pp. 1-10.
Hessami, K., Jamali, F., and Tabassi, H. (2003). "Major active faults of Iran." scale 1:2,500,000, Ministry of Science, Research and Technology (IIEES)
Hollingsworth, J., Jackson, J., Alarcon, J. E., Bommer, J. J., and Bolourchi, M. J. (2007). "The 4th February 1997 Bojnurd (Garmkhan) Earthquake in NE Iran: Field, Teleseismic, and Strong-Motion Evidence for Rupture Directivity Effects on a Strike-Slip Fault." *Journal of Earthquake Engineering*, **11**(2), pp. 193-214.
Housner, G. W. (1952). "Intensity of ground motion during strong earthquakes." California Institute of Technology *Report on research*

conducted under contract with the Office of Naval Research, Project NR-081-095, Pasadena, California.
Hubert, H. (1977). "Geological map of Iran." scale 1:1,000,000, National Iran Oil Co. Explor. Prod. Affairs
Iervolino, I., and Cornell, C. A. (2005). "Record selection for nonlinear seismic analysis of structures." *Earthquake Spectra*, **21**(3), pp. 685-713.
IIEES. (2003) "Earthquake data bank." <http://www.iiees.ac.ir/English/bank/eng_databank.html>, International institute of earthquake engineering and seismology, Teheran, Iran,
IIEES. (2006) "Earhtquake data bank." http://www.iiees.ac.ir/English/bank/eng_databank.html, International institute of earthquake engineering and seismology, Teheran, Iran,
ISC. (2003) "On-line bulletin." < http://www.isc.ac.uk >, International Seismological Centre, Thatcham, United Kingdom,
ISC. (2006) "On-line bulletin." http://www.isc.ac.uk, Intenational Seismological Centre, Thatcham, United Kingdom,
Ishimoto, M., and Iida, K. (1939). "Observations of earthquakes registered with the microseismograph constructed recently (I)." *Bulletin of the Earthquake Research Institute, University of Tokyo*, **17**, pp. 443-478 (in Japanese).
Jackson, J. A., and Fitch, T. (1981a). "Basement faulting and the focal depths of the larger earthquakes in the Zagros mountains (Iran)." *Geophysical Journal of the Royal Astrological Society*, **64**, pp. 561-586.
Jackson, J. A., and Fitch, T. (1981b). "Basement faulting and the focal depths of the larger earthquakes in the Zagros mountains (Iran)." *Geophysical Journal of the Royal Astrological Society*, **64**, 561-586.
Jackson, J. A., and McKenzie, D. (1984). "Active tectonics of the Alpine-Himalayan belt between Turkey and Pakistan." *Geophysical Journal of the Royal Astrological Society*, **77**, pp. 185-264.
Jacob, K. H., and Quittmeyer, R. C. (1979). "Geodynamics of Pakistan", The Makran region of Pakistan and Iran: Trench-arc system with active plate subduction. A. Farah and K. DeJong, eds., Spec. Publ. Geological Survey Pakistan, Quetta, pp. 305-317.
Johnson, A. C., Coppersmith, K. J., Kanter, L. R., and Cornell, C. A. (1994). "The earthquakes of stable continental regions", **Vol. 1:** Assessment of large earthquake potential. J. F. Schneider, ed., Electric Power Research Institute, Palo Alto, California.
Johnson, P. R. (1998). "Tectonic map of Saudi Arabia and adjacent areas." USGS *Technical report USGS-TR-98-3 (IR 948)*. 2 pp.
Joyner, W. B., and Boore, D. M. (1988). "Measurement, characterization, and prediction of strong ground motion." *Earthquake engineering and soil dynamics II - Recent advances in ground-motion evaluation*, Utah, ASCE publications, pp. 43-102
Kappos, A. J. (1991). "Analytical prediction of the collapse earthquake for R/C buildings: suggested methodology." *Earthquake Engineering & Structural Dynamics*, **20**(2), pp. 167-176.
Karnik, V. (1973). "Magnitude differences." *Pure and Applied Geophysics*, **103**(II), pp. 362-369.
Kassler, P. (1973). "The Persian Gulf", The structural and geomorphic evolution of the Persian Gulf. B. H. Purser, ed., Springer, Berlin Heidelberg New York, pp. 11-32.
Kayen, R. E., and Mitchell, J. K. (1997). "Assessment of liquefaction potential during earthquakes by Arias intensity." *Journal of Geotechnical and Geoenvironmental Engineering*, **123**(12), pp. 1162-1174.

Kazmi, A. (2002). "Second tremor in three years." gulfnews.com, Dubai. Latest access date March 2007.
Kennet, B. N. L., Engdahl, E. R., and Buland, R. P. (1995). "Constrains on seismic velocities in the earth from travel times." *Geophysical Journal International*, **122**(1), pp. 108-124.
Kijko, A. (2004). "Estimation of the maximum earthquake magnitude, Mmax." *Pure and Applied Geophysics*, **161**, pp. 1655-1681.
Kijko, A., and Graham, G. (1998). "Parametric-historic procedure for probabilistic seismic hazard analysis. Part I: Estimation of maximum regional magnitude Mmax." *Pure and Applied Geophysics*, **152**, pp. 413-442.
Kijko, A., and Graham, G. (1999). "Parametric-historic procedure for probabilistic seismic hazard analysis. Part II: Assessment of seismic hazard at specified site." *Pure and Applied Geophysics*, **154**, pp. 1-22.
Kijko, A., and Sellevoll, M. A. (1989). "Estimation of earthquake hazard parameters from incomplete data files, part I. Utilization of extreme and complete catalogs with different threshold magnitudes." *Bulletin of the Seismological Society of America*, **79**(3), pp. 645-654.
Kijko, A., and Sellevoll, M. A. (1990). "Estimation of earthquake hazard parameters for incomplete and uncertain data files." *Natural Hazards*, **3**, pp. 1-13.
Klose, C. D., and Seeber, L. (2007). "Shallow seismicity in stable continental regions." *Seismological Research Letters*, **78**(5), pp. 554-562.
Knopoff, L. (1964). "The statistics of earthquake in southern California." *Bulletin of the Seismological Society of America*, **54**(6), pp. 1871-1873.
Knopoff, L. (2000). "The magnitude distribution of declustered earthquakes in Southern California." *PNAS*, **97**(22), pp. 11880-11884.
Kramer, S. L. (1996). "Geotechnical earthquake engineering." Prentice Hall, Upper saddle river, N.J.
Kramer, S. L., and Mitchell, R. A. (2006). "Ground motion intensity measures for liquefaction hazard evaluation." *Earthquake Spectra*, **22**(2), pp. 413-438.
Kulkarni, R. B., Youngs, R. R., and Coppersmith, K. J. (1984). "Assessment of confidence intervals for results of seismic hazard analysis." *Eighth world conference on earthquake engineering*, San Francisco, USA. **1**, pp. 263-270
Kusky, T., Robinson, C., and El-Baz, F. (2005). "Tertiary-Quaternary faulting and uplift in the northern Oman Hajar Mountains." *Journal of the Geological Society*, **162**(5), pp. 871-888.
Lees, G. M., and Falcon, N. L. (1952). "The geographical history of the Mesopotamian plains." *Geographical Journal*, **118**, pp. 24-39.
Lippard, S. J., Smewing, J. D., Rothery, D. A., and Browning, P. (1982). "The geology of the Dibba Zone, northern Oman Mountains; a preliminary study." *Journal of the Geological Society*, **139**(1), pp. 59-66.
Maggi, A., Jackson, J. A., Priestley, K., and Baker, C. (2000). "A re-assessment of focal depth distributions in southern Iran, the Tien Shan and northern India: do earthquakes really occur in the continental mantle?" *Geophysical Journal International*, **143**(3), pp. 629-661.
Maggi, A., Priestley, K., and Jackson, J. (2002). "Focal depths of moderate and large size earthquakes in Iran." *Journal of Seismology and Earthquake Engineering*, **4**(2 & 3 - Summer & Fall 2002).
Malkawi, A. I. H., Barakat, S. A., Shanableh, A., Omar, M., and Altoubat, S. (2007). "Seismic hazard assessment and mitigation of earthquake risk in United Arab Emirates." College of graduate studies and research, University of Sharjah. 88 pp.

Martínez-Rueda, J. E. (1998). "Scaling procedure for natural accelerograms based on a system of spectrum intensity scales." *Earthquake Spectra*, **14**(1), pp. 135-152.
Martínez-Rueda, J. E. (2006). "Proposal of an attenuation relationship of Housner spectrum intensity in Europe." *First European conference on earthquake engineering and seismology*, Geneva, Switzerland, paper number: 1193
McCalpin, J. P. (1996). "Paleoseismology." Academic Press, San Diego, California. 588 pp.
McCann, M. W., and Reed, J. W. (1989). "Proceedings: Engineering characterization of small-magnitude earthquakes." EPRI *Report NP-6389*.
McGuire, R. K. (1977). "Seismic design spectra and mapping procedures using hazard analysis based directly on oscillator response." *Earthquake Engineering & Structural Dynamics*, **5**(3), pp. 211-234.
McGuire, R. K. (1993). "The practice of earthquake hazard assessment." International Association of Seismology and Physics of the Earth's Interior / European Seismological Commission, Denver. 284 pp.
McGuire, R. K. (1995). "Probabilistic seismic hazard analysis and design earthquakes: Closing the loop." *Bulletin of the Seismological Society of America*, **85**(5), pp. 1275-1284.
McGuire, R. K. (1997). "EZ-FRISK: software for earthquake ground motion estimation." Risk Engineering Inc.
McGuire, R. K. (2004). "Seismic hazard and risk analysis." Earthquake Engineering Research Institute, Oakland, CA. 221 pp.
McGuire, R. K. (2008). "Probabilistic seismic hazard analysis: Early history." *Earthquake Engineering & Structural Dynamics*, **37**, pp. 329-338.
McGuire, R. K., Cornell, C. A., and Toro, G. R. (2005). "The case for using mean seismic hazard." *Earthquake Spectra*, **21**(3), pp. 879-886.
McGuire, R. K., Silva, W. J., and Costantino, C. J. (2002). "Technical basis for revision of regulatory guidance on design ground motions: development of hazard- and risk-consistent seismic spectra for two sites." U.S. Nuclear Regulatory Commission *Report NUREG/CR-6769*, Washington, DC.
Melville, C. P. (1978). "Arabic and Persian source material on the historical seismicity of Iran from 7th to the 17th centuries." University of Cambridge, Cambridge, UK.
Milana, G., Rovelli, A., De Sortis, A., Calderoni, G., Coco, G., Corrao, M., and Marsan, P. (2008). "The Role of Long-Period Ground Motions on Magnitude and Damage of Volcanic Earthquakes on Mt. Etna, Italy." *Bulletin of the Seismological Society of America*, **98**(6), 2724-2738.
Miller, I., and Freund, J. E. (1977). "Probability and statistics for engineers." Prentice-Hall, Inc., Englewood Cliffs, New Jersey.
Musson, R. M. W. (2000). "Generalised seismic hazard maps for the Pannonian Basin using probabilistic methods." *Pure and Applied Geophysics*, **157**, pp. 147-169.
Musson, R. M. W. (2001). "Wizmap II." British Geological Survey.
Musson, R. M. W. (2004). "A critical history of British earthquakes." *Annali di Geofisica*, **47**(2-3), pp. 597-609.
Musson, R. M. W. (2005). "Against fractiles." *Earthquake Spectra*, **21**(3), pp. 887-891.
Musson, R. M. W., Northmore, K. J., Sargeant, S. L., Phillips, E. R., Boon, D., Long, D., McCue, K., and Ambraseys, N. N. (2006). "The geology and geophysics of the United Arab Emirates", **Vol. 4:** Geological Hazards. British Geological Survey, Keyworth, 237 pp.
NEIC. (2006) "National earthquake information center." <http://earthquake.usgs.gov/regional/neic/>,

O'Hara, T. F., and Jacobson, J. P. (1991). "Standardization of the cumulative absolute velocity." EPRI, Palo Alto, CA. *EPRI Report TR-100082*.

Oliveira, C. S., Roca, A., and Goula, X. (2006). "Assessing and managing earthquake risk: geo-scientific and engineering knowledge for earthquake risk mitigation; developments, tools, techniques." Springer. 543 pp.

Ordaz, M., Aguilar, A., and Arboleda, J. (2007). "CRISIS2007." Institute of Engineering, UNAM, Mexico city.

Othman, A. (2002). "Study of the effects of the Fujairah earthquake, March 2002." Technical report (in Arabic), United Arab Emirates University, Al-Ain, UAE. 58 pp.

Page, W. D., Anttonen, G., and Savage, W. U. (1978). "The Makran coast of Iran, a possible seismic gap." Proc. of conference VI: Methodology for identifying seismic gaps and soon-to-break gaps, USGS Open file report 78-943. pp. 611-634

Peiris, N., Free, M. W., Lubkowski, Z., and Hussein, A. T. (2006). "Seismic hazard and seismic design requirements for the Arabian Gulf region." *First European conference on earthquake engineering and seismology*, Geneva, Switzerland,

Petersen, M. D., Cao, T., Campbell, W. K., and Frankel, A. D. (2007). "Time-independent and Time-dependent seismic hazard assessment for the state of California: Uniform California earthquake rupture forecast model 1.0." *Seismological Research Letters*, **78**(1), pp. 99-109.

Pisarenko, V. F., Lyubushin, A. A., Lysenko, V. B., and Golubeva, T. V. (1996). "Statistical estimation of seismic hazard parameters: Maximum possible magnitude and related parameters." *Bulletin of the Seismological Society of America*, **86**(3), pp. 691-700.

Pitarka, A., Irikura, K., Iwata, T., and Sekiguchi, H. (1998). "Three-dimensional simulation of the near-fault ground motion for the 1995 Hyogo-Ken Nanbu (Kobe), Japan, earthquake." *Bulletin of the Seismological Society of America*, **88**(2), pp. 428-440.

Power, M., Chiou, B., Abrahamson, N., Bozorgnia, Y., Shantz, T., and Roblee, C. (2008). "An Overview of the NGA Project." *Earthquake Spectra*, **24**(1), 3-21.

Quittmeyer, R. C. (1979). "Seismicity variations in the Makran region of Pakistan and Iran: Relation to great earthquakes." *Pure and Applied Geophysics*, **V117**(6), pp. 1212-1228.

Quittmeyer, R. C., and Jacob, K. H. (1979). "Historical and modern seismicity of Pakistan, Afghanistan, northwestern India, and southeastern Iran." *Bulletin of the Seismological Society of America*, **69**(3), pp. 773-823.

Reasenberg, P. A. (1985). "Second-Order moment of central California seismicity, 1969-1982." *Journal of Geophysical Research*, **90**(B7), pp. 5479-5495.

Reed, J. W., Anderson, N., Chokshi, N. C., Kennedy, R. P., Metevia, W. J., Ostrom, D. K., and Stevenson, J. D. (1988). "A criterion for determining exceedance of the operating basis earthquake." EPRI, Palo Alto, CA. *EPRI report NP-5930*.

Regard, V., Bellier, O., Thomas, J. C., Abbassi, M., Mercier, J., Shabanian, E., Feghhi, K., and Soleymani, S. (2004). "Accommodation of Arabia-Eurasia convergence in the Zagros-Makran transfer zone, SE Iran: A transition between collision and subduction through a young deforming system." *Tectonics*, **23**(TC2004, doi:10.1029/2003TC001599).

Regard, V., Bellier, O., Thomas, J. C., Bourles, D., Bonnet, S., Abbassi, M. R., Braucher, R., Mercier, J., Shabanian, E., Soleymani, S., and Feghhi, K. (2005). "Cumulative right-lateral fault slip rate across the

Zagros-Makran transfer zone: role of the Minab-Zendan fault system in accommodating Arabia-Eurasia convergence in southeast Iran." *Geophysical Journal International*, **162**(1), pp. 177-203.
Reid, H. F. (1910). "The California earthquake of April 18, 1906. Report of the state earthquake investigation commission." Carnegie Institute, Washington DC.
Richter, C. F. (1958). "Elementary seismology." W.H. Freeman, San Francisco, CA.
Rodgers, A., Fowler, A.-R., Al-Amri, A. M. S., and Al-Enezi, A. (2006). "The March 11, 2002 Masafi, United Arab Emirates earthquake: Insights into the seismotectonics of the northern Oman Mountains." *Tectonophysics*, **415**(1-4), pp. 57-64.
Ross, D. A., Uchupi, E., and White, R. S. (1986). "The geology of Iran-Gulf of Oman region: A synthesis." *Reviews of Geophysics*, **24**(3), pp. 537-556.
Rotondi, R., and Garavaglia, E. (2002). "Statistical analysis of the completeness of a seismic catalogue." *Natural Hazards*, **25**, pp. 245-258.
Rowshandel, B. (2006). "Incorporating source rupture characteristics into ground-motion hazard analysis models." *Seismological Research Letters*, **77**, pp. 708-722.
Sabetta, F., Lucantoni, A., Bungum, H., and Bommer, J. J. (2005). "Sensitivity of PSHA results to ground motion prediction relations and logic-tree weights." *Soil Dynamics and Earthquake Engineering*, **25**, pp. 317-329.
Sadigh, K., Chang, C.-Y., Egan, J. A., Makdisi, F., and Youngs, R. R. (1997). "Attenuation relationships for shallow crustal earthquakes based on California strong motion data." *Seismological Research Letters*, **68**(1), pp. 180-189.
Scherbaum, F., Bommer, J. J., Bungum, H., Cotton, F., and Abrahamson, N. A. (2005). "Composite Ground-Motion Models and Logic Trees: Methodology, Sensitivities, and Uncertainties." *Bulletin of the Seismological Society of America*, **95**(5), pp. 1575-1593.
Scherbaum, F., Bommer, J. J., Cotton, F., Bungum, H., and Sabetta, F. (2006). "Ground-Motion prediction in PSHA: A Post-Pegasos perspective." First European conference on earthquake engineering and seismology, Geneva, Switzerland.
Scherbaum, F., Cotton, F., and Smit, P. (2004a). "On the Use of Response Spectral-Reference Data for the Selection and Ranking of Ground-Motion Models for Seismic-Hazard Analysis in Regions of Moderate Seismicity: The Case of Rock Motion." *Bulletin of the Seismological Society of America*, **94**(6), pp. 2164-2185.
Scherbaum, F., Schmedes, J., and Cotton, F. (2004b). "On the Conversion of Source-to-Site Distance Measures for Extended Earthquake Source Models." *Bulletin of the Seismological Society of America*, **94**(3), pp. 1053-1069.
Schwartz, D. P., and Coppersmith, K. J. (1984). "Fault behaviour and characteristic earthquakes: Examples from the Wasatch and San Andreas fault zones." *Journal of Geophysical Research*, **89**(B7), pp. 5681-5698.
Scordilis, E. M. (2006). "Empirical Global Relations Converting MS and mb to Moment Magnitude." *Journal of Seismology*, **V10**(2), pp. 225-236.
Shaghouri, T. (2002). "East Coast residents are still wary." gulfnews.com, Dubai. Latest access date March 2007.
Shimazaki, K., and Nakata, T. (1980). "Time-predictable recurrence model for large earthquakes." *Geophysical Research Letters*, **7**, pp. 279-282.
Shome, N., Cornell, C. A., Bazzurro, P., and Carballo, J. E. (1998). "Earthquakes, Records, and Nonlinear Responses." *Earthquake Spectra*, **14**(3), 469-500.

Sigbjornsson, R., and Elnashai, A. S. (2006). "Hazard assessment of Dubai, United Arab Emirates, for close and distant earthquakes." *Journal of Earthquake Engineering*, **10**(5), pp. 749-773.
Simpson, K. A. (1996). "Attenuation of strong ground-motion incorporating near-surface foundation conditions." PhD Thesis, Imperial College, University of London, London.
Somerville, P. G. (2000). "New developments in seismic hazard estimation." *Proceedings sixth international conference on seismic zonation*, Palm Spring, California,
Somerville, P. G., Smith, N. F., Graves, R. W., and Abrahamson, N. A. (1997). "Modification of empirical strong ground motion attenuation relations to include the amplitude and duration effects of rupture directivity." *Seismological Research Letters*, **68**(1), pp. 199-222.
Spudich, P., and Chiou, B. (2008). "Directivity in NGA earthquakes ground motions: Analysis using isochrone theroy." *Earthquake Spectra*, **24**(1), pp. 279-298.
Spudich, P., Joyner, W. B., Lindh, A. G., Boore, D. M., Margaris, B. M., and Fletcher, J. B. (1999). "SEA99: A revised ground motion prediction relation for use in extensional tectonic regimes." *Bulletin of the Seismological Society of America*, **89**(5), pp. 1156-1170.
Stepp, J. C. (1972). "Analysis of the completeness of the earthquake sample in the Puget Sound area and its effect on statistical estimates of earthquake hazard." *Proceedings of the international conference on microzonation for safer construction: research and application*, Seattle, USA. **2**, pp. 897-909
Stoneley, R. (1970). "The History of the International Seismological Summary." *Geophysical Journal International*, **20**(4), pp. 343-349.
Strasser, F. O., Bommer, J. J., and Abrahamson, N. A. (2008). "Truncation of the distribution of ground-motion residuals." *Journal of Seismology*, **12**(1), pp. 79-105.
Styles, M. T., Ellison, R. A., Arkley, S., Crowley, Q. G., Farrant, A. R., Goodenough, K. M., McKervey, J. A., Pharoah, T. C., Phillips, E. R., Schofield, D. I., and Thomas, R. J. (2006). "The geology and geophysics of the United Arab Emirates", **Vol. 2:** Geology. British Geological Survey, Keyworth, England.
Suleiman, A. S., Albini, P., Migliavacca, P., (2004). "A short introduction to historical earthquakes in Lybia.", *Annali de Geofisica*, **47**(2-3), pp. 545-554.
Talebian, M., and Jackson, J. (2004). "A reappraisal of earthquake focal mechanisms and active shortening in the Zagros mountains of Iran." *Geophysical Journal International*, **156**(3), pp. 506-526.
Tavakoli, F., and Ghafory-Ashtiany, M. (1999). "Seismic hazard assessment of Iran." *Annali di geofisica*, **42**(6), pp. 1013-1021.
Thenhaus, P. C., Algermissen, S. T., Perkins, D. M., Hanson, S. L., and Diment, W. H. (1987). "Probabilistic estimates of the seismic ground motion hazard in western Saudi Arabia, Kingdom of Saudi Arabia." Open-File Report, USGS *87-173*. 64 pp.
Tichelaar, B. W., and Ruff, L. J. (1993). "Depth of seismic coupling along subduction zones." *Journal of Geophysical Research*, **98**(B2), pp. 2017-2037.
Toro, G. R. (2006). "The effects of ground-motion uncertainty on seismic hazard results: examples and approximate results." *Abstracts of the centennial meeting of the seismological society of America*, San Francisco, USA,
Toshinawa, T., Hisada, Y., Konno, K., Shibayama, A., Honkawa, Y., and Ono, H. (2004). "Topographic site response at a quaternary terrace in Hachioji, Japan, observed in strong motions and microtremors " *13th*

world conference on earthquake engineering, Vancouver, B. C., Canada, Paper No. 3453
UAEInteract.com. (2005) "UAE signs contract for installation of an advanced earthquake monitoring station." <http://www.uaeinteract.com/news/archive.asp>, UAEInteract.com, Dubai, UAE, April 2007.
UBC. (1997). "Uniform building code." International conference of building officials, Whittier, California.
USGS. (2003) "On-line bulletin." <http://neic.usgs.gov/neis/epic/>, Unites States Geological Survey - National Earthquake Information Centre, USA,
USGS. (2006) "On-line bulletin." http://neic.usgs.gov/neis/epic/, Unites States Geological Survey - National Earthquake Information Centre, USA,
Utsu, T. (1999). "Representation and analysis of the earthquake size distribution: A historical review and some new approaches." *Pure and Applied Geophysics*, **155**(2), pp. 509-535.
Vernant, P., Nilforoushan, F., Hatzfeld, D., Abbassi, M. R., Vigny, C., Masson, F., Nankali, H., Martinod, J., Ashtiani, A., Bayer, R., Tavakoli, F., and Chery, J. (2004). "Present-day crustal deformation and plate kinematics in the Middle East constrained by GPS measurements in Iran and northern Oman." *Geophysical Journal International*, **157**(1), pp. 381-398.
Vick, S. G. (2002). "Degrees of belief: Subjective probability and engineering." ASCE Publications. 455 pp.
Visitabudhabi.ae. (2008) "Architecture-Abu Dhabi." <http://www.visitabudhabi.ae/en/what.to.do/art.and.culture/architecture.aspx>, 28th January 2008
Vita-Finzi, C. (2001). "Neotectonics at the Arabian plate margins." *Journal of Structural Geology*, **23**(2-3), pp. 521-530.
Walker, R., and Jackson, J. (2002). "Offset and evolution of the Gowk fault, S.E. Iran: a major intra-continental strike-slip system." *Journal of Structural Geology*, **24**(11), pp. 1677-1698.
Walker, R., Jackson, J., and Baker, C. (2004). "Active faulting and seismicity of the Dasht-e-Bayaz region, eastern Iran." *Geophysical Journal International*, **157**(1), pp. 265-282.
Walker, R., and Jackson, J. A. (2004). "Active tectonics and late Cenozoic strain distribution in central and eastern Iran." *Tectonics*, **23**(TC5010, doi:10.1029/2003TC001529).
Walker, R. T., Andalibi, M. J., Gheitanchi, M. R., Jackson, J. A., Karegar, S., and Priestley, K. (2005). "Seismological and field observations from the 1990 November 6 Furg (Hormozgan) earthquake: a rare case of surface rupture in the Zagros mountains of Iran." *Geophysical Journal International*, **163**(2), pp. 567-579.
Weichert, D. H. (1980). "Estimation of the earthquake recurrence parameters for unequal observation periods for different magnitudes." *Bulletin of the Seismological Society of America*, **70**(4), 1337-1346.
Wells, D. L., and Coppersmith, K. J. (1994). "New empirical relationships among magnitude, rupture length, rupture width, rupture area, and surface displacement." *Bulletin of the Seismological Society of America*, **84**(4), pp. 974-1002.
Wesnousky, S. G., Scholz, C. H., Shimazaki, K., and Matsuda, T. (1984). "Integration of geological and seismological data for the analysis of seismic hazard: A case study of Japan." *Bulletin of the Seismological Society of America*, **74**(2), pp. 687-708.
Woessner, J., and Wiemer, S. (2005). "Assessing the quality of earthquake catalogues: estimating the magnitude of completeness and its

uncertainty." *Bulletin of the Seismological Society of America*, **95**(2), pp. 684-698.
Wu, S.-C., Cornell, C. A., and Winterstein, S. R. (1995). "A hybrid recurrence model and its implication on seismic hazard results." *Bulletin of the Seismological Society of America*, **85**(1), pp. 1-16.
Wyss, M., and Al-Homoud, A. S. (2004). "Scenarios of Seismic Risk in the United Arab Emirates, an Approximate Estimate." *Natural Hazards*, **32**(3), pp. 375-393.
Youngs, R. R., Chiou, S.-J., Silva, W. J., and Humphrey, J. R. (1997). "Strong ground motion attenuation relationships for subduction zone earthquakes." *Seismological Research Letters*, **68**, pp. 58-73.
Youngs, R. R., and Coppersmith, K. J. (1985). "Implications of fault slip rates and earthquake recurrence models to probabilistic seismic hazard estimates." *Bulletin of Earthquake Engineering*, **75**(4), pp. 939-964.
Zaré, M. (2002). "Attenuation relation and coefficients of movement in Iran." *International Institute of Earthquake Engineering*.
Zaré, M., Ghafory-Ashtiany, M., and Bard, P.-Y. (1999). "Attenuation law for the strong motions in Iran." *Proceedings of the third international conference on seismology and earthquake engineering*, Teheran, Iran. **1**, pp. 245-354

APPENDICES

APPENDIX A

PRELIMINARY EARTHQUAKE DATA SET, SHOWING EVENTS WITH MAGNITUDE EQUAL TO OR BIGGER THAN 6.5 IN ANY MAGNITUDE SCALE REPORTED.

ID	Year	Month	Day	Hour	Minute	Seconds	Latitude	Longitude	Depth	Magnitude			Reference	Comments
										M_s	m_b	M_w		
1	658						30.5	47.8		6.50			A2M	
	658						?	?					MB94	(0)
	658						**30.5**	**47.8**		**6.5**				*
2	734						31	60.5		6.50			A2M	
	729-738						31	60.5		6.5-7.4			M78	Data from MB94
	734												MB94	(0), (1)
	734						**31**	**60.5**		**6.5**				*
3	805	12	2				29.5	60.5		7.00			A2M	
	805	12	2				29.5	60.5		6.5-7.4			M78	Data from MB94
	905	12	2				?	?					MB94	(0), (1), (3)
	805	**12**	**2**				**29.5**	**60.5**		**7.0**				*
4	815						29.5	60.5		7.00			A2M	
	815						28.5	61.5		5.5-6.4			M78	Data from MB94
	815						?	?					MB94	(0), (1)
	815						**29.5**	**60.5**		**7.0**				*
5	1008						27.7	52.3		6.5			A2M	
	1008						27.7	52.5		5.5-6.4			M78	Data from MB94
	1008	spring					27.68	52.37		6.5		6.4	MB94	(0), MB95
	1008						**27.7**	**52.3**		**6.5**		**6.4**		*
6	1440						28.4	53.1		7.1			A2M	

	1440						28.3	53.1		6.5			NOAA	
	1440						28.3	53.1		6.5-7.4			M78	Data from MB94
	1440						28.42	53.08		6.9		6.8	MB94	(0)
	1440									7.1			MB95	
	1440						**28.4**	**53.1**		**7.1**		**6.8**		*
7	1483	2	18				24.9	57.9		7.7			A2M	
	1483	2	18				24.9	57.9		7.7			NOAA	
	1483	2	18				26	56.9		6.5-7.4			M78	Data from MB94
	1483	2	18				25.7	57.3		7.7			MB94	(0), (1)
	1483	**2**	**18**				**24.9**	**57.9**		**7.7**				*
8	1497						27.2	56.3		6.5			A2M	
	1497	4					27.1	56.6		5.5-6.4			M78	Data from MB94
	1497						27.18	56.18		6.5		6.4	MB94	(0), MB95
	1497	**4**					**27.2**	**56.3**		**6.5**		**6.4**		*
9	1593	9					27.7	54.3		6.5			A2M	
	1593	9					27.6	54.5		6.5-7.4			M78	Data from MB94
	1593	9					27.7	54.3		6.5		6.4	MB94	(0), MB95
	1593	**9**					**27.7**	**54.3**		**6.5**		**6.4**		*
10	1703	5	17				26.6	56.2					NOAA	(2)
10a	1703						26.6	54.9		6.8			A2M	
	1703						26.4	55.5					NOAA	
	1703						?	?					MB94	(0), (1)
	1703						**26.6**	**54.9**		**6.8**				*

11	1838						29.6	59.9		7.0			A2M	
	1838						29.5	59.96		7.0		6.9	MB94	
	1838						29.5	60		7.0			BY99	Data from a map
	1838						**29.6**	**59.9**		**7.0**		**6.9**		*
12	1853	5	4				29.6	52.5		6.5			NOAA	(2)
	1853	5	5	12			29.6	52.5		6.2			A2M	
	1853	5	5	12			29.6	52.5		6.2		6.1	MB94	(0), MB95
	1853	**5**	**5**	**12**			**29.6**	**52.5**		**6.2**		**6.1**		*
13	1905	6	19	1	27	0	29.89	59.98		6.0	6.8		A2I	AB03
	1905	**6**	**19**	**1**	**27**		**29.89**	**59.98**		**6.0**	**6.8**			*
14	1914	2	6	11	42	18	29.5	65	100	7.0			ISC	
	1914	2	6	11	42	0	28.67	64.75			5.9		A2I	
	1914	**2**	**6**	**11**	**42**	**18**	**28.67**	**64.75**	**100**	**7.0**	**5.9**			*
15	1923	9	22	20	47	38	29	56.5	35	6.9			ISC	
	1923	9	22	20	47	33	29.5	56			6.7		IIEES(ISS)	
	1923	9	22	20	48		29	56.5		6.9			NOAA	
	1923	9	22	20	47	0	29.51	56.63		6.7	6.9		A2I	
	1923	**9**	**22**	**20**	**47**	**38**	**29.51**	**56.63**	**35**	**6.7**	**6.9**			*
16	1927	7	7	20	6	30	27	62	100	6.5			ISC	
	1927	7	7	20	6	22.6	26.98	62.15	80	6.5			QR79	(5)
	1927	7	7	0	0	0	27	62.26		5.7	6.4		A2I	
	1927	7	7	20	6	21	28	62			6.2		IIEES(ISS)	
							27	61.81		?			MB73	(4)

	1927	**7**	**7**	**20**	**6**	**30**	**27**	**62.26**	**100**	**5.7**	**6.4**			*
17	1929	9	3	12	7	39	26.5	62.25	110	6.5			ISC	
	1929	9	3	12	7	36.2	26.61	61.94	80	6.5			QR79	(5)
	1929	9	3	0	0	0	26.59	62.07		5.6	5.9		A2I	
	1929	9	3	12	7	32	26.4	62.3	110		6.5		IIEES(ISS)	
							26.5	62.25		5<6			MB73	(4)
	1929	**9**	**3**	**12**	**7**	**39**	**26.59**	**62.07**	**110**	**5.6**	**5.9**			*
18	1934	6	13	22	10	28	27.5	62.5	80	7.0			ISC	
	1934	6	13	22	10	23.6	27.71	62.7	80	7.0			QR79	(5)
	1934	6	13	0	0	0	27.63	62.64		6.6	6.9		A2I	
	1934	6	13	22	10	24	27.5	62.5			7.0		IIEES(ISS)	
							27.5	62.5	60-100	7<8			MB73	(4)
	1934	**6**	**13**	**22**	**10**	**28**	**27.63**	**62.64**	**80**	**6.6**	**6.9**			*
19	1945	11	27	21	56		24.5	63	25	8.3			NOAA	
	1945	11	27	21	56	50	24.5	63	35	8.2			ISC	
	1945	11	27	21	56	55.2	25.15	63.48	33	8.0			QR79	(5)
	1945	11	27	0	0	0	25.02	63.47		8.0	7.6		A2I	
	1945	11	27	21	56	49	24.9	63.5			8.2		IIEES(ISS)	
	1945	**11**	**27**	**21**	**56**	**50**	**25.02**	**63.47**	**35**	**8.0**	**7.6**			*
20	1947	8	5	14	24		25.1	63.4		7.6			NOAA	

	1947	8	5	14	24	10	25.5	63	35	7.3			ISC	
	1947	8	5	14	24	0	25.25	63.2		7.0	7.6		A2I	
	1947	8	5	14	24	14	25.04	63.49	33	7.3			QR79	(5)
	1947	8	5	14	24	7	24.9	63.5			7.2		IIEES(ISS)	
	1947	**8**	**5**	**14**	**24**	**10**	**25.25**	**63.2**	**35**	**7.0**	**7.6**			*
21	1949	4	24	4	22		22.2	56.4	100	6.5			NOAA	
	1949	4	24	4	22	16	27.28	56.46		6.3	6.5		A2I	
	1949	4	24	4	22	8	27.2	56.2		6.5			IIEES(ISS)	(6)
							27.2	56.17	100-150	6<7			MB73	(4)
	1949	**4**	**24**	**4**	**22**	**16**	**27.28**	**56.46**	**100**	**6.3**	**6.5**			*
22	1956	10	31	14	3		27	54.5		6.8			NOAA	
	1956	10	31	14	3	0	27.27	54.55		6.3	5.9		A2I	
							27.25	54.5	34-60	6<7			MB73	(4)
	1956	10	31	14	3	43	27.2	54.4		6.0			IIEES(ISS)	(6)
	1956	**10**	**31**	**14**	**3**	**43**	**27.27**	**54.55**	**43**	**6.3**	**5.9**			*
23	1961	6	11	5	10		27.9	54.5	37	7.2			NOAA	
	1961	6	11	5	10		27.78	54.51		6.5	6.4		A2I	
	1961	6	11	5	10	23	27.93	54.1		6.5			IIEES(ISS)	(6)
							27.94	54.68	34-60	6<7			MB73	(4)
	1961	**6**	**11**	**5**	**10**	**23**	**27.78**	**54.51**	**37**	**6.5**	**6.3**			*
24	1972	4	10	2	7		28.4	52.8	33	7.1			NOAA	
	1972	4	10	2	6	0	28.38	52.98		6.9	6.3		A2I	
	1972	4	10	2	6	50	28.395	52.7846	10.6		6.0		ISC	
	1972	4	10							6.9			MB95	

	1972	4	10				28.39	53.74	6			6.7	MJ00	(7)
	1972	4	10	2	6	53.2	28.43	52.82	9±3		6.1	6.6	BJP93	(8)
	1972	4	10				28.43	52.79	12±4		6.0		JT81	(8)
	1972	4	10	2	6	51.21	28.406	52.787	6.7		6.0	6.7	EHB98	
	1972	**4**	**10**	**2**	**6**	**51.21**	**28.38**	**52.98**	**6.7**	**6.9**	**6.0**	**6.7**		*
25	1977	3	21	21	18	54.2	27.61	56.39	29	7.0			PDE	
	1977	3	21	21	18	0	27.59	56.45		6.9	6.2		A2I	
	1977	3	21	21	18	54	27.5884	56.3786	23.8		6.2		ISC	
	1977	3	21							7.1			MB95	
	1977	3	21				27.59	56.38	12±4		6.2		JT81	(8)
	1977	3	21	21	18	53.37	27.583	56.363	12		6.2	6.7	EHB98	
	1977	**3**	**21**	**21**	**18**	**53.37**	**27.59**	**56.45**	**12**	**6.90**	**6.2**	**6.7**		*
26	1981	7	28	17	22	24.62	30.01	57.79	33	7.3			PDE	
	1981	7	28	17	22	23	29.9875	57.77	11.1	7.0	5.9		ISC	
	1981	7	28	17	22	24	29.99	57.79	18	7.1	5.7	7.0	BJ01	(9)
	1981	7	28	17	22	24	30.17	57.84	33	7.1	5.8		JD84	
	1981	7	28	17	22	24.05	29.976	57.767	13.6	7.0	5.9	7.3	EHB98	
	1981	**7**	**28**	**17**	**22**	**24.05**	**29.98**	**57.77**	**13.6**	**7.0**	**5.9**	**7.3**		*
27	1981	6	11	7	24	25.23	29.91	57.72	33	6.9			PDE	
	1981	6	11	7	24	25	29.8952	57.7184	30.9	6.6	6.0		ISC	
	1981	6	11	7	24	24	29.86	57.68	20	6.7	6.1	6.6	BJ01	(9)
	1981	6	11	7	24	25	29.91	57.72	33	6.7	6.1		JD84	
	1981	6	11	7	24	24.75	29.858	57.686	17.3	6.6	6.0	6.6	EHB98	
	1981	**6**	**11**	**7**	**24**	**24.75**	**29.86**	**57.69**	**17.3**	**6.6**	**6.0**	**6.6**		*

28	1983	4	18	10	58	49	27.7824	62.0698	44.5	6.3	6.4		ISC	
	1983	4	18	10	58	51.26	27.79	62.05	64		6.5		PDE	
	1983	4	18				27.77	62.06	63			6.6	MJ00	(7)
	1983	4	18	10	58	52.8	27.766	62.055	63.7	6.3	6.4	6.7	EHB98	
	1983	**4**	**18**	**10**	**58**	**52.8**	**27.77**	**62.05**	**63.7**	**6.3**	**6.4**	**6.7**		*
29	1990	11	6	18	45	52.23	28.25	55.46	10	6.7			PDE	
	1990	11	6	18	45	53	28.2299	55.4695	15.7	6.6	6.1		ISC	
	1990	11	6	18	46		28.24	55.461	5			6.5	RW05	
	1990	11	6	18	45		28.32	55.46	10			6.5	MJ00	(7)
	1990	11	6	18	45	53.98	28.242	55.457	11.1	6.6	6.1	6.6	EHB98	
	1990	**11**	**6**	**18**	**45**	**53.98**	**28.24**	**55.46**	**11.1**	**6.6**	**6.1**	**6.6**		*
30	1998	3	14	19	40	27.05	30.15	57.6	9	6.9			PDE	
	1998	3	14	19	40	32	30.1606	57.6123	43.5	6.7	5.8		ISC	
	1998	3	14	19	40	28	30.08	57.58	5	6.9	5.9	6.6	BJ01	(9)
	1998	3	14	19	40	29.61	30.126	57.585	13.8	6.9	5.8	6.6	EHB98	
	1998	**3**	**14**	**19**	**40**	**29.61**	**30.13**	**57.59**	**13.8**	**6.9**	**5.8**	**6.6**		*
31	1999	3	4	5	38	27	28.277	57.203		6.4	6.1		ISC	
	1999	3	4	5	38	26.52	28.34	57.19	33			6.6	PDE	
	1999	3	4	5	38		28.34	57.19	28			6.2	TJ04	
	1999	3	4	5	38	27.26	28.271	57.207	27.7	6.4	6.0	6.6	EHB98	
	1999	**3**	**4**	**5**	**38**	**27.26**	**28.27**	**57.21**	**27.7**	**6.4**	**6.0**	**6.6**		*

*	Data included in the final catalogue.
(0)	Information presented by MB94 as "*the most probable and acceptable seismic parameters (revised or accepted)*".
(1)	Considered by the reference as not enough reliable macroseismic data to be presented with some confidence and it is excluded from the final catalogue.
(2)	Probably duplicate event.
(3)	Likely typographic error on the year data.
(4)	Data obtained from a map, not date specified.
(5)	Author stated that the magnitude was taken from ISS.
(6)	The ISS is stated as source of the information.
(7)	Depth from EHB catalogue
(8)	Only depth was review in this publication, date and location from ISC.
(9)	Epicentres are from Engdahl *et al.* (1998). Magnitudes (m_b and M_s) are from the USGS.
AB03	Ambraseys & Bilham (2003b).
A1M/A1I	Ambraseys *et al.* (1994).
A2M/A2I	Ambraseys & Melville (1982).
BJP93	Baker *et al.* (1993).
MB73	Berberian (1973).
MB94	Berberian (1994).
MB95	Berberian (1995).
BY99	Berberian & Yeats (1999).
BJ01	Berberian *et al.* (2001).
EHB98	Engdahl *et al.* (1998).
ISC	ISC (2003).
JT81	Jackson & Fitch (1981).
JD84	Jackson & McKenzie (1984).
MJ00	Maggi *et al.* (2000).
M78	Melville (1978).
NOAA	National Oceanic and Atmospheric Administration (USGS, 2005).
PDE	Preliminary Determination of Epicenters, National Earthquake Information Center (USGS, 2005).
QR79	Quittmeyer (1979).
TJ04	Talebian & Jackson (2004).
RW05	Walker *et al.* (2005).

APPENDIX B

FINAL EARTHQUAKE CATALOGUE FOR THE REGION OF THE UAE CONTAINING EVENTS WITH $M_S \geq 4.0$, INCLUDING FORE- AND AFTERSHOCKS.

ID	Year	Month	Day	Hour	Minute	Second	Latitude	Longitude	Depth	Magnitude		
										M_s	m_b	M_w
1	658						30.50	47.80		6.5		
2	734						31.00	60.50		6.5		
3	805	12	2				29.50	60.50		7.0		
4	815						29.50	60.50		7.0		
5	978	6	17				27.70	52.30		5.3		5.3
6	1008						27.70	52.30		6.5		6.4
7	1085	5					30.70	50.30		5.8		
8	1361						26.90	56.20		5.3		5.3
9	1400						27.70	54.30		5.3		5.3
10	1440						28.40	53.10		7.1		6.8
11	1483	2	18				24.90	57.90		7.7		
12	1497	4					27.20	56.30		6.5		6.4
13	1591						29.80	52.40		5.9		
14	1593	9					27.70	54.30		6.5		6.4
15	1622	10	4				27.22	56.35		5.5		
16	1623						29.85	52.85		5.5		
17	1677						27.90	54.20		6.4		6.3
18	1703						26.60	54.90		6.8		
19	1824	6	2				29.70	51.50		6.0		
20	1824	6	25	5			29.80	52.40		6.4		6.3
21	1838						29.60	59.90		7.0		6.9
22	1853	5	5	12			29.60	52.50		6.2		6.1
23	1854	11					30.50	57.30		5.8		
24	1858	6	13	5			29.60	50.50		5.9		
25	1862	12	21	10			29.50	52.50		6.2		6.1
26	1864	1	17				30.60	57.00		6.0		
27	1865	6					29.60	53.10		6.0		5.9
28	1865						27.20	53.10		5.6		5.5
29	1875	3	21	15			30.50	50.50		5.7		
30	1877						30.10	57.60		5.6		
31	1880	8	12				27.02	54.20		5.3		
32	1883	10	13	15			22.90	57.50		5.1		
33	1883	10	16				27.70	52.30		5.8		5.7
34	1884	5	19	18			26.90	56.00		5.4		
35	1890	3	25				28.80	53.50		6.4		6.3
36	1891	12	14				29.90	51.58		5.3		
37	1892	8	15				29.10	52.70		5.3		
38	1894	2	26				29.50	53.30		5.9		5.8
39	1897	1	10	21			26.90	56.00		6.4		6.3
40	1902	7	9	3	38		27.08	56.34		6.4		
41	1903	1	14	2	46	0	24.00	64.00		5.8	5.5	
42	1904	4	25	14	1		27.00	56.00		5.8		

43	1905	4	25	14	1		27.67	56.03		5.8		
44	1905	6	19	1	27		29.89	59.98		6.0	6.8	
45	1907	3	31	14	12		30.00	50.00		5.8	5.5	
46	1907	7	4	9	12		27.18	56.28		5.7	6.0	
47	1909	10	57	18	45		30.09	57.58		5.5		
48	1911	1	20	4	5		29.30	51.20		5.2		
49	1911	4	29	5	33		30.36	57.58		5.6	6.4	
50	1911	9	13	3	22		27.67	54.44		5.5		
51	1913	3	24	10	34	11	26.80	53.70		5.8		
52	1914	2	6	11	42	18	28.67	64.75	100	7.0	5.9	
53	1919	10	24	20	32	15	26.11	62.05	33	5.6		
54	1923	9	14	8	10	30	28.97	59.33		5.6		
55	1923	9	22	20	47	38	29.51	56.63	35	6.7	6.9	
56	1923	9	23	3	18	58	29.50	56.00		5.8	5.5	
57	1924	1	18	14	56	20	29.50	56.00		5.8	5.5	
58	1924	6	30	3	41	12	27.50	53.80		5.8		
59	1924	12	11	23	1	0	25.20	56.30		5.1		
60	1925	7	11	21	52	22	29.50	59.50		4.0	4.5	
61	1925	7	30	18	43	16	28.50	51.80		5.1		
62	1925	9	24	4	28	39	25.60	55.50		5.5	6.1	
63	1925	12	18	5	53	38	28.80	51.30		5.4		
64	1926	4	23	1	31	31	26.90	56.40		5.3		
65	1926	5	19	21	14	5	26.20	58.50	35	5.1		
66	1927	5	9	10	31	47	27.68	56.70	35	5.8	6.4	
67	1927	7	7	20	6	30	27.00	62.26	100	5.7	6.4	
68	1927	7	24	13	25	12	28.50	56.00		4.4	4.7	
69	1927	7	30	4	4	40	28.70	51.90		4.0	4.5	
70	1927	11	16	1	27		27.50	53.80		4.0	4.5	
71	1927	12	14	7	50	18	24.70	63.00		4.0	4.5	
72	1928	4	15	10	9	28	27.50	52.10		5.0		
73	1928	4	30	11	19	48	27.60	57.80		4.0	4.5	
74	1928	8	14	0	9	9	27.60	57.80		4.0	4.5	
75	1928	8	26	23	16	21	28.70	51.90		4.0	4.5	
76	1928	8	27	3	37	54	28.70	51.90		4.0	4.5	
77	1928	8	27	4	19	57	28.70	51.90		4.0	4.5	
78	1928	9	20	14	59	0	25.20	56.80		4.6		
79	1929	1	21	15	48	5	30.50	54.50		4.4	4.7	
80	1929	3	26	14	0	10	28.00	62.00		4.9	5.0	
81	1929	7	16	19	43	15	28.70	51.90		5.1		
82	1929	8	11	10	8	2	30.50	54.50	130	4.0	4.5	
83	1929	9	3	12	7	39	26.59	62.07	110	5.6	5.9	
84	1929	10	2	11	51	54	28.70	51.90		4.0	4.5	
85	1929	10	29	5	53	39	27.50	54.50	35	5.6		
86	1929	10	29	8	57	35	25.00	51.50		4.4	4.7	
87	1929	10	29	10	32	36	25.00	51.50		4.4	4.7	
88	1929	10	29	11	48	20	25.00	51.50		4.4	4.7	
89	1929	11	20	19	56	58	27.50	55.50		4.4	4.7	

90	1930	2	15	9	7	5	28.70	51.80		5.2		
91	1930	4	15	9	56	27	29.00	54.00	35	5.6		
92	1930	5	11	22	35	46	27.70	55.27	35	5.8	5.8	
93	1930	5	12	0	21	15	27.50	55.00		6.1	5.7	
94	1930	5	13	20	14	14	27.50	55.00		4.4	4.7	
95	1930	7	8	17	15	42	28.70	51.90		4.4	4.7	
96	1930	8	17	12	29	32	27.50	55.00		5.8	5.5	
97	1930	8	23	10	53	18	27.88	55.02		6.1	6.2	
98	1930	9	2	18	58	48	30.00	51.50	35	5.6		
99	1930	9	5	16	20	38	27.50	55.00		5.2	5.2	
100	1930	10	9	21	30	30	21.00	60.00		5.2		
101	1930	10	18	1	2	20	29.40	51.40		4.0	4.5	
102	1931	5	3	19	22	30	30.50	54.50		4.4	4.7	
103	1931	5	5	6	42	21	26.50	54.30	35	5.1		
104	1931	5	5	11	40	7	26.00	54.80		4.0	4.5	
105	1931	5	5	14	10	45	26.00	54.80		4.4	4.7	
106	1931	5	7	0	45	40	26.00	54.80		5.2	5.2	
107	1931	7	28	17	36	25	29.50	52.00	35	5.6		
108	1931	9	2	3	28	23	30.50	54.50		4.0	4.5	
109	1931	11	16	8	25	5	27.50	55.00		4.4	4.7	
110	1932	2	4	21	18	9	26.50	62.25	35	5.6		
111	1932	4	18	11	23	21	25.00	64.00	35	6.0		
112	1932	9	8	7	25	32	31.00	58.50	35	5.6		
113	1933	2	21	19	2	59	27.50	57.50	35	5.6		
114	1933	2	26	5	9	42	27.50	57.50		4.0	4.5	
115	1933	7	7	7	30	51	24.00	65.00	35	5.6		
116	1934	1	2	20	55	38	29.97	57.42	35	5.6		
117	1934	2	4	13	27	14	30.65	51.64	35	6.3		
118	1934	2	16	7	59	50	25.90	55.40		4.9		
119	1934	2	26	14	47	19	27.50	57.50		4.4	4.7	
120	1934	3	10	2	3	18	26.50	52.50		4.4	4.7	
121	1934	3	13	23	23	38	30.50	51.70		4.4	4.7	
122	1934	3	18	22	19	33	26.50	52.50		4.0	4.5	
123	1934	3	18	22	44	31	26.10	53.60		5.0		
124	1934	3	19	3	28	28	27.30	52.70		5.2		
125	1934	4	19	23	27	0	24.00	65.00	35	5.6		
126	1934	6	13	22	10	28	27.63	62.64	80	6.6	6.9	
127	1934	8	31	0	40	2	27.50	53.30		4.4	4.7	
128	1935	7	2	15	24	59	26.50	55.00		5.1		
129	1935	9	22	1	40	23	29.00	61.00		4.0	4.5	
130	1935	10	15	17	2	45	28.90	51.30		5.2		
131	1935	10	27	6	43	9	27.60	54.60		4.4	4.7	
132	1936	1	8	12	34	38	26.90	52.90		4.9		
133	1936	4	17	22	15	21	28.00	55.70		4.9	5.0	
134	1936	4	21	2	14	38	26.30	55.30		5.5	6.2	
135	1936	6	10	3	29	9.2	26.50	64.00		5.7		
136	1936	7	17	8	40	53	25.90	54.70		4.6		

137	1936	8	16	21	37	1	26.00	54.40		5.1		
138	1936	8	20	2	8	47	30.40	51.50		5.3		
139	1936	9	7	8	52	30	29.00	61.00		4.4	4.7	
140	1936	11	6	20	27	12	28.50	56.80		4.4	4.7	
141	1937	5	11	16	2	17	29.50	57.50		4.0	4.5	
142	1937	5	12	9	10	33	29.50	57.50		4.0	4.5	
143	1937	5	21	21	56	24	29.00	54.00		4.0	4.5	
144	1938	4	23	6	4	3	27.22	53.28		5.5		
145	1938	4	23	9	26	1	27.30	53.20		5.2	5.2	
146	1939	1	25	11	2	25	29.30	51.00	35	5.4		
147	1939	2	25	5	5	8	21.00	60.00		5.3		
148	1939	8	18	22	52	35	26.80	54.50		5.0		
149	1940	6	1	15	10	0	27.00	54.00		4.0	4.5	
150	1941	2	4	19	9	7	27.30	53.20		4.0	4.5	
151	1941	3	28	21	13	19	28.30	54.20		5.2	5.2	
152	1941	3	29	0	37	36	28.30	54.20		4.0	4.5	
153	1941	6	15	12	38	55	26.40	53.50		5.2		
154	1942	6	7	10	47	43	27.00	54.50		4.4	4.7	
155	1942	7	29	20	22	4	29.50	57.50		4.9	5.0	
156	1943	2	6	2	35	58	24.89	63.25	35	5.9	6.2	
157	1943	12	31	9	35	35	28.00	61.00		4.0	4.5	
158	1944	7	23	12			29.86	56.82		5.5		
159	1945	1	11	2	3	2	26.30	55.40		4.9	5.0	
160	1945	1	15	17	21	33	27.00	54.80		5.6		
161	1945	11	27	21	56	50	25.02	63.47	35	8.0	7.6	
162	1946	3	12	2	21	54	29.80	51.45		5.7	5.7	
163	1946	3	17	21	6	0.1	24.99	63.59	33	4.9	5.0	
164	1946	5	29	23	14	31	30.50	54.50		4.0	4.5	
165	1946	6	20				29.50	66.00		5.8		
166	1946	8	7	22	46	54	25.00	63.00		5.2	5.2	
167	1946	9	19	0	11	20	29.50	57.50		4.4	4.7	
168	1946	10	23	8	2	5	30.00	47.50		4.9		
169	1947	1	2	14	11	8	28.50	51.90		5.0		
170	1947	5	4	0	49	55	26.30	55.40		4.4	4.7	
171	1947	5	4	22	34	8	26.50	55.30		5.1		
172	1947	8	5	14	24	10	25.25	63.20	35	7.0	7.6	
173	1947	10	3	6	13	50	25.90	57.40	35	5.8	5.8	
174	1947	10	29	22	5	38	28.00	61.00		4.0	4.5	
175	1947	12	9	16	32	23.5	24.84	63.55	33	4.9	5.0	
176	1948	1	30	8	43	55	25.16	63.78	39	6.8	6.5	
177	1948	2	1	23	38	28	26.90	57.80	33	5.3		
178	1948	7	5	13	53	14	29.88	57.73		6.0	5.9	
179	1948	7	30	3	30	7	31.00	49.00		5.2	5.2	
180	1948	8	5	22	35	14	31.00	49.00		4.4	4.7	
181	1949	1	2	12	50	27.2	25.06	64.19	33	5.8	5.5	
182	1949	3	6	16	36	40	29.80	51.80		5.2	5.2	
183	1949	4	24	4	22	16	27.28	56.46	100	6.3	6.5	

184	1949	5	13	5	3	12	27.50	56.20		4.0	4.5	
185	1949	7	4	3	40	38	27.20	56.20		6.1	5.7	
186	1949	7	4	4	22	37	27.20	56.20		4.4	4.7	
187	1949	7	5	2	30	0	27.20	56.20		5.8	5.5	
188	1949	7	21	21	26	0.7	26.29	59.06	33	4.9	5.0	
189	1949	8	5	7	14	39	27.20	56.20		4.9	5.0	
190	1949	11	22	15	21	15.4	28.08	57.05	33	5.8	5.5	
191	1949	12	16	23	24	0	28.00	54.50		4.4	4.7	
192	1950	1	19	17	27	16	27.31	52.83		5.5	5.8	
193	1950	1	19	23	10	53	27.30	53.20		4.9	5.0	
194	1950	1	22	4	7	13	27.30	53.20		5.8	5.5	
195	1950	2	2	15	46		29.00	49.00		4.7		
196	1950	2	2	22	45	13	25.50	54.00		4.7		
197	1950	2	27	3	55	12	26.00	52.00		4.5		
198	1950	7	9	0	28	39.3	25.62	63.31	124	5.8		
199	1950	11	14	22	4	48.8	24.91	63.67	64	5.6		
200	1951	7	19	22	27	21	27.10	51.70		4.0	4.5	
201	1951	8	16	23	52	9.9	27.49	57.25	29	5.7		
202	1951	10	28	1	53	34	27.30	53.20		4.9	5.0	
203	1951	12	30	18	21	8.5	27.14	57.08	33	5.5	5.9	
204	1952	1	20	14	43	4	29.30	60.50		5.8	5.5	
205	1952	8	1	10	30	35	29.80	51.80		4.4	4.7	
206	1952	9	20	18	41	21	26.59	62.00	67	4.5	4.5	
207	1952	12	4	15	0	57	27.30	53.20		4.4	4.7	
208	1952	12	23	22	30	24.5	30.90	49.40	33	5.1		
209	1953	1	15	13	15	12	27.90	54.80		5.2	5.2	
210	1954	2	28	21	23	43	27.00	56.00		4.7		
211	1954	4	6	14	35	8	28.30	54.20		5.2	5.2	
212	1954	8	20	15	30	30	27.80	52.10		5.0	5.6	
213	1954	9	19	4	16	37	25.00	53.00		4.4		
214	1954	11	11	5	14	22	27.20	53.20		5.8	5.5	
215	1955	3	13	16	58	5	28.00	56.70		4.9	5.0	
216	1955	4	18	19	16	10	27.70	52.30		5.0	5.4	
217	1956	2	15	15	49	25	27.80	53.10		5.3	5.4	
218	1956	3	1	12	47	56	27.80	53.00		5.2	5.2	
219	1956	3	6	8	55	28	27.80	52.80		5.8	5.5	
220	1956	3	9	16	44	50	26.00	53.20		5.8	5.5	
221	1956	5	8	20	50	1	27.80	53.00		5.2	5.2	
222	1956	5	19	14	14	25	27.50	52.50		4.9	5.0	
223	1956	6	29	2	18	31.7	28.46	57.22	33	5.9		
224	1956	10	31	14	3	43	27.27	54.55	43	6.3	5.9	
225	1956	10	31	14	22	23	27.30	54.60		5.8	5.5	
226	1956	11	1	5	52	34	27.50	54.00		4.9	5.0	
227	1956	11	10	8	18	55	25.90	54.70		5.0		
228	1957	9	5	11	36	5	28.51	53.61		5.8	5.5	
229	1957	10	2	13	9	8	26.70	54.80		5.2	5.5	
230	1957	10	11	19	44	30	31.00	55.00		4.4	4.7	

231	1958	3	1	9	26	48	27.70	54.91		5.8	5.5	
232	1958	4	9	4	36	34	29.10	52.00		5.0	5.8	
233	1958	5	2	21	20	13	28.50	55.00		4.9	5.0	
234	1958	6	10	7	4	2	30.27	51.11		5.8	5.5	
235	1958	8	14	23	26	58	29.18	63.45	103	5.0	5.0	
236	1958	12	25	18	33	28	26.90	54.10		5.0		
237	1959	1	7	5	13	9	27.00	54.20	32	5.2	5.3	
238	1959	4	29	0	23	45	27.00	54.80		5.0	5.4	
239	1959	7	24	7	19	30	28.00	50.00		4.0	4.5	
240	1959	10	9	3	29	40	28.00	57.00		4.0	4.5	
241	1959	12	8	12	50	47	31.00	57.03		5.2	5.2	
242	1960	4	24	12	14	27	27.70	54.29		5.8	6.0	
243	1960	5	3	6	58	55	27.63	54.39		5.2	5.2	
244	1960	5	10	21	51	55	27.00	47.50		4.0	4.5	
245	1960	5	18	8	41	1	27.12	53.13		5.8	5.5	
246	1960	5	20	4	14	30	27.45	53.13	53	5.2	5.2	
247	1960	5	25	12	50	0	27.20	54.20		4.0	4.5	
248	1960	6	10	13	49	21	26.50	53.00		4.5	5.0	
249	1960	7	4	3	43	35	30.00	52.00		4.0	4.5	
250	1960	7	10	22	56	10	26.50	53.00		4.5	5.0	
251	1960	7	31	22	26	53	28.07	54.42		5.2	5.2	
252	1960	8	1	2	20	50	28.12	54.38	62	6.6	6.0	
253	1960	8	23	8	58	12	29.33	60.01	51	5.5	5.5	
254	1960	9	25	8	36	28	28.40	53.20	53	4.0	4.5	
255	1960	11	4	16	52		27.00	54.00		6.3	5.8	
256	1961	4	6	18	12	39	28.10	56.80	29	5.3	5.7	
257	1961	5	21	19	44	14	30.10	57.20	32	4.0	4.5	
258	1961	6	5	3	31	0	27.88	54.79	57	4.9	5.0	
259	1961	6	11	5	10	23	27.78	54.51	37	6.5	6.3	
260	1961	6	11	5	30	15	27.92	54.90	68	6.3	5.8	
261	1961	6	11	6	46	48	27.69	54.98	39	4.9	5.0	
262	1961	6	11	6	51	30	27.80	54.90	49	5.1	5.1	
263	1961	6	11	11	24	9	28.10	54.70	33	4.5	4.8	
264	1961	6	11	12	31	26	27.89	54.49	12	5.8	5.5	
265	1961	6	11	13	58	1	27.89	54.74	54	5.2	5.2	
266	1961	6	11	15	6	17	27.80	54.50	39	4.4	4.7	
267	1961	6	12	21	2	38	27.50	54.30	33	4.4	4.7	
268	1961	6	12	23	17	12	28.00	55.00	0	4.2	4.6	
269	1961	6	14	0	24	27	27.90	55.00	36	4.4	4.7	
270	1961	6	14	9	3	37	28.00	55.00	34	4.0	4.5	
271	1961	6	15	6	21	35	27.70	54.80	37	4.9	5.0	
272	1961	6	17	8	5	53	27.90	55.00	38	4.9	5.0	
273	1961	6	18	10	10	9	27.80	55.20	33	4.4	4.7	
274	1961	6	21	6	39	24	27.88	54.71	39	5.1	5.1	
275	1961	6	21	19	14	38	27.80	54.84	47	4.9	5.0	
276	1961	6	23	16	36	34	27.78	55.03	121	5.2	5.2	
277	1961	6	25	12	40	24	27.90	53.70	54	4.0	4.5	

278	1961	7	17	5	13	34	27.55	55.28	140	4.7	4.9	
279	1961	9	28	22	36	25.2	27.29	57.03	37	5.6		
280	1961	10	22	22	56	32	27.50	54.60	33	4.4	4.7	
281	1961	10	23	4	40	22	27.90	54.50	33	4.4	4.7	
282	1962	1	20	20	45	47	27.90	54.90	34	4.0	4.5	
283	1962	2	3	3	0	0	30.20	52.00		4.0	4.5	
284	1962	2	8	20	10	15	31.00	49.00		4.4		
285	1962	3	7	21	8	3	26.90	57.20	33	4.0	4.5	
286	1962	6	23	5	5	1	29.70	49.30		5.4	5.6	
287	1962	6	30	9	45	50	27.60	57.70	25	4.0	4.5	
288	1962	7	14	6	44	26	27.30	56.70	30	4.0	4.5	
289	1962	8	14	7	27	45	28.00	55.60	43	4.9	5.0	
290	1962	9	19	7	28	43	30.10	50.40	62	4.9	5.0	
291	1962	9	29	6	53	59.9	28.29	57.48	83	5.5		
292	1962	10	1	12	13		27.76	54.00		5.5	5.8	
293	1962	10	16	11	58	46	30.60	57.30		4.0	4.5	
294	1962	11	6	0	9	48	28.17	55.79	30	5.4	5.6	
295	1963	2	4	7	18	10	27.60	54.30	66	4.0	4.5	
296	1963	5	2	1	58	25	28.50	54.90	46	6.3	5.8	
297	1963	5	3	10	44	30	30.70	51.80	35	5.4	5.3	
298	1963	5	20	10	19	20	25.70	56.50		4.8		
299	1963	5	29	0	47	49	28.16	52.50	44	4.0	4.5	
300	1963	5	29	8	35	6.6	27.17	59.46	71	5.7		
301	1963	7	8	8	58	5	26.70	55.70	33	4.5	4.8	
302	1963	7	13	8	24	25	29.63	50.88	43	4.9	5.0	
303	1963	7	29	6	10	27	28.18	55.72	51	5.2	5.2	
304	1963	8	10	4	27	34	28.10	53.30	46	4.5	4.8	
305	1963	8	12	7	19	55	27.70	53.20	33	4.9	5.0	
306	1963	8	12	18	29	39.7	25.32	62.74	33	5.4		
307	1963	9	22	10	40	56	29.30	55.30	33	4.4	4.7	
308	1963	9	23	18	33	47	29.60	50.90	39	4.4	4.7	
309	1963	10	16	19	2	28	28.21	57.85	96	4.8		
310	1963	10	31	9	57	1	27.40	55.60	35	5.4	5.3	
311	1964	1	19	9	13	53	26.80	54.90	12.9	5.3	5.6	
312	1964	1	19	9	13	54	26.79	54.00	38	5.8	5.5	
313	1964	2	16	0	17	14.52	29.97	51.11	15	5.4	5.3	
314	1964	2	26	9	16	53	27.26	54.44	14	4.5	4.8	
315	1964	3	11	23	34	23	27.90	57.61	40	4.4	4.7	
316	1964	3	17	12	5	10	26.91	53.96	33	4.7	4.9	
317	1964	3	20	3	15	47	27.93	55.21	64	4.4	4.7	
318	1964	3	21	10	25	31	26.96	54.02	22	4.7	4.9	
319	1964	5	9	7	47	1	29.50	52.40	36	4.5	4.8	
320	1964	5	11	6	7	41	28.13	57.38	68	5.3	5.3	
321	1964	7	9	3	38	8	28.86	52.76	59	4.7	4.9	
322	1964	7	14	1	57	39	27.56	54.83	54	4.2	4.6	
323	1964	7	21	11	46	55	27.60	56.46	46	4.4	4.7	
324	1964	7	22	4	41	57	27.85	55.01	59	4.2	4.6	

325	1964	8	10	18	18	41	30.10	57.67	52	4.7	4.7	
326	1964	8	12	2	34	24	26.90	56.40	53	4.5	4.8	
327	1964	8	12	19	26	27	30.90	49.70	15	5.4	5.2	
328	1964	8	16	15	52	45	28.10	52.48	52	5.2	5.2	
329	1964	8	19	9	33	7.04	28.21	52.63	15	5.5	5.5	
330	1964	8	19	15	20	11.11	28.10	52.60	15	5.8	5.5	
331	1964	8	19	22	40	16	28.21	52.52	46	5.1	5.1	
332	1964	8	20	5	8	47.84	28.05	52.58	15	5.6	5.4	
333	1964	8	20	5	39	44.37	28.10	52.56	15	5.9	5.6	
334	1964	8	21	7	59	12.95	28.10	52.51	15	5.1	5.1	
335	1964	8	27	11	58	36.13	28.11	55.80	15	5.1	5.1	
336	1964	8	27	12	56	49.48	28.07	55.83	15	5.4	5.3	
337	1964	9	1	10	40	4	30.94	50.07	64	4.4	4.7	
338	1964	9	14	15	21	12	28.18	55.86	49	5.1	5.1	
339	1964	10	18	13	20	21	29.64	50.91	49	4.9	5.0	
340	1964	10	18	21	25	25.76	27.85	54.84	15	4.7	4.9	
341	1964	10	18	22	35	45	29.71	50.97	26	4.9	5.0	
342	1964	10	19	17	38	44	29.82	51.08	48	5.1	5.1	
343	1964	10	29	20	47	24	28.20	55.79	33	5.4	5.3	
344	1964	10	30	3	43	18	27.90	55.80	87	4.4	4.7	
345	1964	10	31	14	59	38	27.87	55.81	59	4.7	4.9	
346	1964	11	3	2	25	48.94	29.51	51.02	15	4.9	5.0	
347	1964	11	8	10	33	25.93	29.59	50.94	15	5.4	5.3	
348	1964	11	15	9	33	48	30.00	50.90	37	5.0	5.1	
349	1964	12	11	5	25	56	28.05	52.87	45	4.5	4.8	
350	1964	12	11	12	48	5	28.50	52.98	59	4.9	5.0	
351	1964	12	12	7	3	42	29.70	51.10	55	5.2	5.2	
352	1964	12	18	0	35	22	28.20	52.80	46	4.7	4.9	
353	1964	12	19	23	31	56	27.50	56.88	54	5.4	5.3	
354	1964	12	22	4	36	34.3	28.12	56.80	18	6.1	5.7	5.5
355	1964	12	23	10	52	24	28.23	56.74	70	4.9	5.0	
356	1965	2	28	8	5	37	27.79	55.00	33	4.2	4.6	
357	1965	3	17	7	18	54	27.71	56.64	55	4.7	4.9	
358	1965	4	11	1	55	48	30.70	51.90	76	4.4	4.7	
359	1965	4	19	1	20	5	28.24	56.58	36	4.2	4.6	
360	1965	4	25	16	39	46	30.39	50.64	47	4.0	4.5	
361	1965	4	26	22	4	38	27.43	52.35	33	4.5	4.8	
362	1965	6	18	13	49	37	29.72	51.37	65	4.9	5.0	
363	1965	6	21	0	21	13.4	28.17	56.01	8	5.4	5.8	6.0
364	1965	6	21	1	30	39	28.26	55.89	64	4.7	4.9	
365	1965	6	24	10	54	3	29.30	53.00	105	4.2	4.6	
366	1965	7	23	21	29	30	25.70	65.33	19	4.2	4.6	
367	1965	7	30	19	7	7	27.90	57.12	74	4.9	4.9	
368	1965	9	20	23	23	25	30.59	50.14	54	4.7	4.9	
369	1965	9	21	15	46	2	27.30	55.32	41	4.0	4.5	
370	1965	11	8	1	57	25.93	27.96	56.89	26.2	5.1	5.1	
371	1965	11	10	10	3	34	27.00	54.60	40	5.0	4.3	

372	1965	11	13	6	14	26.19	26.22	65.22	15	4.9	5.0	
373	1965	12	23	11	10	1	27.63	54.51	37	4.5	4.8	
374	1966	2	26	20	50	33.41	30.43	50.75	10	4.4	4.7	
375	1966	3	30	4	18	39.4	21.86	62.16	18.8	5.4	5.3	
376	1966	6	9	22	24	41.64	27.61	52.58	10	4.9	5.0	
377	1966	7	9	17	1	52	28.20	57.00	47	4.0	4.5	
378	1966	7	29	8	20	47	28.34	51.62	38	4.4	4.7	
379	1966	8	22	21	28	31	25.10	61.80	33	4.4	4.7	
380	1966	9	2	11	13	0	27.68	52.41	31	4.7	4.9	
381	1966	9	18	20	43	54.41	27.81	54.21	12	5.4	5.9	5.9
382	1966	9	24	10	0	47.14	27.38	54.47	23.4	5.4	5.3	
383	1966	9	29	17	44	37	27.76	54.38	46	4.2	4.6	
384	1966	10	29	8	59	40.58	27.63	65.58	46	4.8	4.8	
385	1966	12	2	3	7	51.97	28.08	53.57	18.1	4.9	5.0	
386	1967	1	2	13	50	6.47	30.65	50.43	22.2	5.1	5.1	
387	1967	1	8	1	43	47	27.70	55.68	39	4.0	4.5	
388	1967	1	9	1	55	14.68	27.60	54.45	14.8	5.2	5.2	
389	1967	1	12	18	14	19.55	27.88	54.47	15	4.5	4.8	
390	1967	1	15	0	3	21	29.96	51.55	90	4.9	5.0	
391	1967	1	29	3	53	56.93	26.45	55.22	5.6	4.7	4.9	
392	1967	1	29	7	5	58	26.48	55.35	38	4.4	4.7	
393	1967	1	29	7	12	3.79	26.51	55.25	10	4.5	4.8	
394	1967	1	29	7	13	10	26.47	55.28	33	4.5	4.8	
395	1967	1	29	7	13	38	26.50	55.30	0	5.4	5.3	
396	1967	1	29	7	56	38.68	26.56	54.89	14.1	5.5	5.1	
397	1967	1	29	13	20	27	26.50	55.34	4	4.0	4.5	
398	1967	1	31	19	0	24.16	26.42	55.24	6.9	5.1	5.1	
399	1967	1	31	20	6	38	26.46	55.31	26	4.5	4.8	
400	1967	1	31	20	52	49	26.68	55.35	32	4.2	4.6	
401	1967	2	1	1	7	19.22	26.52	55.24	7.8	4.9	5.0	
402	1967	2	11	15	18	7	30.58	50.70	44	5.1	5.1	
403	1967	2	12	16	46	11	30.16	50.50	102	4.2	4.6	
404	1967	3	1	10	12	48.85	28.08	56.86	23.6	5.1	5.1	
405	1967	3	3	7	36	34	30.20	50.70	74	5.4	5.3	
406	1967	3	15	16	26	1	30.50	50.50	75	4.4	4.7	
407	1967	3	25	22	26	27	28.57	60.36	36	4.7	4.9	
408	1967	4	6	12	57	14.38	29.87	51.02	10	5.2	5.2	
409	1967	4	28	19	38	27.1	27.68	57.27	25	4.2	4.6	
410	1967	5	20	21	48	54	29.63	52.18	32	4.0	4.5	
411	1967	7	25	13	0	37.8	28.80	54.66	15	4.2	4.6	
412	1967	8	2	13	55	15	30.70	53.54	57	4.0	4.5	
413	1967	9	14	14	49	45.06	28.40	57.04	40	4.4	4.7	
414	1967	11	15	19	35	48.6	30.81	51.43	10	4.2	4.6	
415	1967	11	21	15	5	3	30.50	50.50	121	4.2	4.6	
416	1968	1	2	11	59	31.75	29.45	52.56	10	4.5	4.8	
417	1968	3	26	4	42	20.4	29.79	51.36	14.3	4.9	5.0	
418	1968	4	23	12	38	59	27.65	56.67	36	4.7	4.9	

419	1968	4	23	12	39	45.79	27.74	56.73	22.4	5.2	5.2	
420	1968	5	30	1	10	29.72	27.82	53.95	13.7	5.2	5.2	
421	1968	5	30	19	53	4.59	29.68	51.24	8.8	5.2	5.2	
422	1968	6	13	23	4	2.76	29.84	51.36	25	4.7	4.9	
423	1968	6	15	0	8	30	29.80	51.93	88	4.0	4.5	
424	1968	6	20	8	24	58	29.91	51.23	81	4.4	4.7	
425	1968	6	22	15	56	46.32	29.64	51.24	10	4.4	4.7	
426	1968	6	23	9	16	16.2	29.74	51.25	8.2	5.1	5.3	5.5
427	1968	6	26	1	54	13	29.74	51.12	17	4.9	5.0	
428	1968	7	1	23	42	23	29.56	51.20	50	4.2	4.6	
429	1968	7	8	11	27	24.64	27.98	56.90	25	4.4	4.7	
430	1968	7	8	17	15	28.19	29.70	51.10	26.8	4.5	4.8	
431	1968	7	12	10	34	3.07	29.75	50.67	10	4.4	4.7	
432	1968	8	2	13	30	25.36	27.55	60.89	64.8	5.4	5.7	5.7
433	1968	8	3	14	1	41	25.19	62.87	29	4.4	4.7	
434	1968	9	14	13	48	28.6	28.34	53.23	7	5.9	5.8	5.8
435	1968	9	14	19	20	20.07	28.34	53.22	10	4.9	5.0	
436	1968	9	15	6	15	1	28.39	53.25	50	4.0	4.5	
437	1968	9	19	22	12	38.37	28.37	53.20	20	5.1	5.1	
438	1968	9	19	23	35	56	28.31	53.23	37	4.4	4.7	
439	1968	11	9	13	43	37.27	23.72	64.61	12.5	5.1	5.1	
440	1969	2	8	23	23	34	29.80	50.90	27.4	5.0	5.2	
441	1969	2	13	11	11	27.29	24.98	62.71	27.4	5.1	5.1	
442	1969	3	4	17	35	49	30.14	57.61	53	4.3	4.3	
443	1969	3	12	17	43	38	28.30	53.26	48	4.4	4.7	
444	1969	4	14	13	13	20.14	27.75	54.62	13	4.7	4.9	
445	1969	4	29	4	37	40.52	29.56	51.53	22	5.8	5.5	
446	1969	5	12	19	9	7.73	27.92	56.55	20	4.4	4.7	
447	1969	6	1	12	36	30	26.66	60.52	50	4.6	4.6	
448	1969	6	4	16	21	32	25.50	61.13	19	4.4	4.7	
449	1969	6	21	16	35	8.79	27.41	57.51	52.5	5.2	5.2	
450	1969	7	1	6	0	54	28.23	55.36	81	4.2	4.6	
451	1969	7	8	16	27	22	23.57	64.44	30	4.0	4.5	
452	1969	7	20	22	37	32	28.26	57.55	71	4.6	4.6	
453	1969	9	1	23	16	11.56	30.85	49.64	20	4.7	4.9	
454	1969	9	2	13	30	4.74	30.19	57.71	15	4.7	4.9	
455	1969	11	3	21	53	16	26.74	53.67	8	4.5	4.8	
456	1969	11	5	19	2	20	26.60	53.71	50	4.7	4.9	
457	1969	11	6	4	36	8	26.60	53.80	89	4.5	4.8	
458	1969	11	7	13	18	42	26.60	53.61	19	4.2	4.6	
459	1969	11	7	15	16	5	26.60	53.72	35	4.5	4.8	
460	1969	11	7	16	30	27	26.55	53.59	23	4.9	5.0	
461	1969	11	7	18	34	6.66	27.42	60.40	80	6.1	6.1	6.1
462	1969	11	15	23	58	50	26.70	53.61	29	4.4	4.9	
463	1969	12	1	13	4	34	26.54	53.55	39	4.5	4.8	
464	1969	12	3	2	31	51.89	24.81	65.57	45	4.7	4.7	
465	1970	1	20	11	0	18	30.43	51.36	73	4.5	4.8	

466	1970	2	23	11	22	26.3	27.83	54.64	9	5.6	5.4	5.6
467	1970	2	28	19	58	46.66	27.82	56.31	11.9	5.1	5.5	5.5
468	1970	3	6	19	40	7	28.25	57.43	71	4.6	4.6	
469	1970	3	10	22	6	25	28.20	57.38	75	4.4	4.4	
470	1970	3	21	13	23	16	27.89	54.55	52	4.4	4.7	
471	1970	4	1	23	54	3.68	27.94	56.69	27.8	4.7	4.9	
472	1970	5	11	3	12	20.7	28.58	52.30	14.6	4.9	5.0	
473	1970	5	12	23	59	12	27.27	57.21	44	4.4	4.7	
474	1970	5	18	6	55	26	27.66	52.87	42	4.4	4.7	
475	1970	5	31	10	17	40	27.39	52.73	0	4.4	4.7	
476	1970	6	16	17	25	1.63	29.65	51.36	15	4.2	4.6	
477	1970	7	4	23	38	13	26.70	54.78	38	4.0	4.5	
478	1970	7	21	10	39	24	29.46	52.02	97	4.2	4.6	
479	1970	8	20	15	29	53	29.39	51.59	28	4.5	4.8	
480	1970	8	30	12	31	36	30.95	57.12	62	4.6	4.6	
481	1970	9	8	12	45	8.42	28.55	58.79	15	4.4	4.7	
482	1970	10	7	2	20	37.17	27.85	56.56	27.9	4.4	4.7	
483	1970	10	18	6	10	39.21	27.35	54.94	21.2	4.5	4.8	
484	1970	10	20	10	34	17.71	27.56	56.67	15	4.5	4.8	
485	1970	10	27	20	11	8	26.54	55.24	45	4.2	4.6	
486	1970	11	9	17	41	43.22	29.50	56.78	98.7	5.1	5.4	5.5
487	1970	12	26	19	51	58.79	27.70	57.85	15	4.5	4.8	
488	1971	1	28	6	9	31	28.27	57.29	77.5	4.7	4.7	
489	1971	3	3	2	15	58	22.10	59.41	21.1	4.7	5.0	
490	1971	4	6	6	49	54.07	29.78	51.88	5.7	4.6	5.2	5.2
491	1971	4	12	19	3	22.79	28.37	55.75	10	5.8	6.0	5.9
492	1971	4	13	20	42	58.12	28.23	55.50	10	4.4	4.7	
493	1971	5	7	23	18	42.86	28.25	55.46	10	4.2	4.6	
494	1971	5	25	4	32	37.15	27.70	55.35	10	4.5	4.8	
495	1971	5	25	6	52	51.77	27.37	53.51	15	4.4	4.7	
496	1971	5	27	6	20	18	28.12	51.77	51.4	4.4	4.7	
497	1971	6	2	10	5	8.22	29.30	51.72	15	4.4	4.7	
498	1971	7	24	0	49	18.23	30.37	59.76	15	4.7	4.9	
499	1971	8	22	17	54	14.9	30.01	50.71	20	4.7	4.9	
500	1971	8	26	6	55	6.91	30.01	50.77	15	4.4	4.7	
501	1971	8	27	5	20	12.21	30.12	50.72	15	4.5	4.8	
502	1971	9	2	12	24	26	30.54	50.47	60.7	4.5	4.8	
503	1971	9	2	18	24	44	30.30	50.70	7.4	5.0	5.1	
504	1971	9	2	22	21	42	30.02	50.87	66.9	4.2	4.6	
505	1971	9	4	13	42	21	30.01	50.85	46.9	4.4	4.7	
506	1971	9	8	12	53	37.1	29.03	60.19	20	5.6	5.3	
507	1971	10	5	18	31	19	27.24	55.88	43.7	5.1	5.1	
508	1971	10	23	11	49	20.18	29.64	51.45	15	4.4	4.7	
509	1971	11	5	14	55	50.3	24.69	63.06	25	4.7	4.9	
510	1971	11	5	14	55	51	24.74	63.16	50	4.9	4.9	
511	1971	11	8	3	6	34.69	27.01	54.46	9	5.7	5.6	5.9
512	1971	11	8	3	24	30	26.94	54.66	67.3	4.7	4.9	

513	1971	11	8				27.07	54.46		5.9	5.6	
514	1971	11	9	0	16	56	26.90	54.51	10	4.7	4.7	
515	1971	12	9	1	42	31.93	27.29	56.38	9.5	5.7	5.3	5.8
516	1971	12	9	2	36	12	27.38	56.36	36.9	4.2	4.6	
517	1971	12	9	2	54	0	27.32	56.37	36.4	4.2	4.6	
518	1971	12	15	15	24	55.65	30.22	50.54	15	5.1	5.1	
519	1971	12	20	23	27	44	28.32	57.19	84.5	5.0	5.0	
520	1971	12	29	21	12	39.01	29.55	52.73	15	4.7	4.9	
521	1972	1	6	9	41	31.69	30.33	50.54	15	5.1	5.1	
522	1972	2	8	19	54	52.88	29.61	50.84	10	4.0	4.5	
523	1972	2	10	6	49	17.28	29.50	50.96	15	4.2	4.6	
524	1972	2	28	18	44	54	29.80	50.60	84.7	5.1	4.7	
525	1972	3	8	21	49	13	27.62	56.77	66.7	4.2	4.6	
526	1972	4	3	8	6	9	28.54	52.72	56.6	4.0	4.5	
527	1972	4	3	9	7	14.46	28.12	57.16	20	4.9	5.0	
528	1972	4	10	2	6	51.21	28.38	52.98	6.7	6.9	6.0	6.7
529	1972	4	10	2	34	37	28.42	52.90	79.7	4.4	4.7	
530	1972	4	10	3	54	44.97	28.52	52.67	10	4.4	4.7	
531	1972	4	10	4	36	16	28.29	52.99	33	4.0	4.5	
532	1972	4	10	8	33	54	28.35	53.16	48.3	4.0	4.5	
533	1972	4	10	20	27	6.48	28.34	52.88	10	4.5	4.8	
534	1972	4	12	18	37	39.58	28.32	53.04	10	4.7	4.9	
535	1972	4	12	18	37	44	28.35	53.12	58.1	4.7	4.9	
536	1972	4	12	23	7	48.2	28.40	53.06	10	4.9	5.0	
537	1972	4	12	23	7	57	28.48	53.05	96	4.9	5.0	
538	1972	4	24	14	41	7.99	28.48	52.96	10	4.0	4.5	
539	1972	4	24	14	41	9	28.53	53.02	29.9	4.0	4.5	
540	1972	4	25	13	21	12.19	28.35	53.10	10	4.9	5.0	
541	1972	4	29	16	4	19.39	28.26	53.00	8	4.7	4.9	
542	1972	5	2	16	58	20	28.50	52.64	59	4.0	4.5	
543	1972	5	16	10	59	50.55	28.34	52.61	10	4.5	4.8	
544	1972	5	18	2	42	58	27.96	55.78	49.4	4.4	4.7	
545	1972	5	20	6	44	31	28.38	52.87	79.3	4.5	4.8	
546	1972	6	6	17	54	41.49	26.87	53.36	20	4.9	5.0	
547	1972	7	2	12	56	6	30.00	50.90	9	5.3	5.4	5.3
548	1972	7	2	14	5	4.82	30.02	50.81	10	4.2	4.6	
549	1972	7	3	2	9	58.87	30.06	50.84	15	4.7	4.9	
550	1972	7	3	21	38	19.59	30.03	50.89	10	4.7	4.9	
551	1972	8	2	21	33	5.42	27.94	56.81	21.3	4.2	4.6	
552	1972	8	2	23	3	29.48	28.12	56.80	20	4.9	5.0	
553	1972	8	2	23	12	20	27.99	56.89	90.9	4.4	4.7	
554	1972	8	3	22	47	46	28.08	56.86	74	4.5	4.8	
555	1972	8	6	1	12	50.35	24.99	61.14	20	5.6	5.4	
556	1972	8	6	1	32	13	25.23	60.98	33	4.5	4.8	
557	1972	8	8	19	9	33.65	25.02	61.14	30	5.6	5.4	
558	1972	8	18	10	3	5	24.83	63.14	33	4.2	4.6	
559	1972	9	9	1	42	27.96	28.48	52.64	23.4	4.7	4.9	

560	1972	10	9	1	58	12	30.06	57.72	83	4.8	4.8	
561	1972	10	9	7	18	23.42	28.18	55.96	15.8	5.2	5.2	
562	1972	11	4	9	32	26	28.14	57.00	93.8	4.9	5.0	
563	1972	11	10	4	45	10.83	30.21	57.69	15	4.2	4.6	
564	1972	11	17	9	9	1.89	27.37	59.12	65	4.9	5.2	5.4
565	1972	11	25	22	43	30.21	28.33	53.11	15	4.0	4.5	
566	1972	12	1	7	31	53	28.43	52.91	52.1	4.2	4.6	
567	1972	12	26	18	35	31	28.43	52.78	109.2	4.4	4.7	
568	1973	1	13	14	14	40.94	25.52	63.82	29.9	4.4	4.7	
569	1973	2	24	0	2	40	28.54	52.62	14.3	4.9	5.0	
570	1973	3	3	2	46	29	29.79	51.19	56.9	4.9	5.0	
571	1973	3	14	1	16	44	29.20	49.01		4.2	4.6	
572	1973	3	28	2	36	37.82	28.56	52.68	20	4.9	5.0	
573	1973	4	2	1	27	14	27.57	61.67	57.6	4.7	4.7	
574	1973	4	22	21	29	54.66	30.69	49.80	20	4.9	5.0	
575	1973	4	25	8	35	38	26.93	55.48	44.7	4.2	4.6	
576	1973	4	26	14	30	9.11	27.17	60.80	57.3	5.0	5.0	
577	1973	5	3	7	44	24	28.10	52.00	15	4.6	4.7	
578	1973	5	6	3	59	19.93	27.26	55.45	15	4.5	4.8	
579	1973	5	31	19	50	41	28.17	56.17	69.6	4.4	4.7	
580	1973	6	8	17	57	0	26.54	61.12	33	4.2	4.6	
581	1973	6	9	20	36	11.6	27.79	52.18	15	4.5	4.8	
582	1973	6	9	20	38	43	28.17	52.06	35.4	4.5	4.8	
583	1973	6	25	10	29	0.16	29.91	50.42	15	4.7	4.9	
584	1973	8	6	5	31	43	30.96	49.99	34.7	4.2	4.6	
585	1973	8	14	18	24	21.69	25.45	65.55	24.2	4.7	4.9	
586	1973	8	24	2	5	3	27.90	52.81	6.5	5.0	5.1	
587	1973	8	24	9	34	9.24	27.88	52.66	10	4.5	4.8	
588	1973	8	25	14	58	8.17	28.11	56.76	17.5	5.4	5.3	
589	1973	9	2	7	23	18.69	24.80	63.15	26.6	5.2	5.2	
590	1973	9	22	9	21	11	30.44	59.85	33	4.2	4.6	
591	1973	10	27	9	50	38	24.58	62.17	33	4.4	4.7	
592	1973	11	11	7	14	51.57	30.57	53.04	2	5.5	5.4	5.5
593	1973	12	10	21	6	50	27.63	57.04	30.3	4.0	4.5	
594	1973	12	16	8	24	59.41	28.43	52.71	14.5	4.5	4.8	
595	1974	1	9	21	10	42	29.64	57.67	65.1	4.1	4.1	
596	1974	3	11	20	21	32.9	28.45	52.81	16.8	4.4	4.7	
597	1974	4	23	19	27	35	26.85	54.61	46.8	4.0	4.5	
598	1974	8	2	8	23	42.4	30.37	50.70	18.5	4.5	4.8	
599	1974	8	5	13	19	42.77	28.02	53.59	20	5.2	5.2	
600	1974	9	4	6	43	31	27.38	62.00	0	4.4	4.7	
601	1974	10	17	4	10	15.03	30.85	49.61	15	4.4	4.7	
602	1974	11	15	17	37	47	27.74	62.50	75.3	4.5	4.5	
603	1974	12	2	9	5	43.29	28.04	55.87	14.6	4.6	5.4	5.2
604	1974	12	10	19	50	16	27.91	65.25	54.2	4.5	4.5	
605	1974	12	20	3	28	53	26.61	61.17	50.2	4.9	4.9	
606	1974	12	24	9	42	9	25.55	64.84	33	4.2	4.6	

607	1974	12	26	18	36	20.88	29.47	52.85	15	4.5	4.8	
608	1975	1	10	14	19	21	29.41	51.54	56.1	4.4	4.7	
609	1975	1	11	12	8	8.44	29.08	51.77	22.1	4.9	5.0	
610	1975	1	12	4	12	45	29.05	51.97	47.5	4.4	4.7	
611	1975	3	7	7	4	42.16	27.47	56.44	11	6.1	5.8	6.1
612	1975	3	7	14	26	57.05	27.49	56.23	17.4	5.1	5.1	
613	1975	3	7	14	26	58	27.48	56.27	39.2	5.1	5.1	
614	1975	3	7	15	36	43	27.63	56.31	50.2	4.4	4.7	
615	1975	3	7	17	42	30	27.27	56.45	33	4.0	4.5	
616	1975	3	9	6	39	42.98	27.32	56.23	16.2	4.4	4.7	
617	1975	4	12	4	13	6	27.36	56.44	40.1	4.2	4.6	
618	1975	5	5	19	47	42	28.17	55.74	54.4	4.0	4.5	
619	1975	5	9	18	1	41.22	30.15	52.04	7.6	4.5	4.8	
620	1975	5	17	16	19	15.18	27.57	57.79	35	4.7	4.9	
621	1975	5	18	14	44	31.66	27.46	57.80	30	4.2	4.6	
622	1975	5	19	7	59	56	21.06	61.75	1.9	4.7	4.9	
623	1975	5	19	8	0	0.78	21.03	61.76	23.8	4.7	4.9	
624	1975	6	13	10	12	49	26.92	54.95	57	4.7	4.9	
625	1975	6	20	9	16	44	26.18	54.38	41.6	4.2	4.6	
626	1975	6	20	14	10	51	27.77	58.75	96.7	4.8	4.8	
627	1975	7	29	13	25	22.41	25.09	62.97	23.8	4.9	5.0	
628	1975	8	27	16	59	30.78	27.55	56.11	18.5	4.9	5.0	
629	1975	9	22	23	0	5.7	27.79	53.83	10	4.0	4.5	
630	1975	10	8	8	15	49.16	28.18	55.61	25	5.1	5.1	
631	1975	10	8	9	53	43	28.40	55.66	69.7	4.2	4.6	
632	1975	10	9	21	14	41	27.08	65.97	40	4.5	4.8	
633	1975	11	1	18	1	55	26.97	56.31	56.6	4.0	4.5	
634	1975	11	6	10	15	43	27.43	56.07	42.6	4.5	4.8	
635	1975	12	17	13	35	1	28.40	57.14	82	4.7	4.7	
636	1975	12	19	8	2	15	28.99	56.91	99	4.2	4.6	
637	1975	12	19	12	46	33.3	28.40	57.06	25	4.2	4.6	
638	1975	12	24	11	35	9	26.91	55.48	42.7	4.0	4.5	
639	1975	12	24	11	48	57	26.98	55.67	8	5.5	5.5	5.5
640	1975	12	24	18	40	31.76	27.00	55.50	9.3	4.4	4.7	
641	1975	12	24	19	55	9.29	26.98	55.50	9.4	4.7	4.9	
642	1975	12	24	21	4	12	27.01	55.55	10	4.4	4.7	
643	1975	12	26	5	46	44	26.99	55.46	34.7	4.2	4.6	
644	1975	12	30	1	9	39	27.07	55.49	51.6	4.4	4.7	
645	1976	1	2	4	30	35	28.50	49.01		4.7	4.5	
646	1976	1	7	7	10	17	29.92	59.27	44.3	4.0	4.5	
647	1976	1	16	5	36	18.29	30.12	50.92	15	4.4	4.7	
648	1976	2	3	14	54	18	25.23	63.49	33	4.4	4.7	
649	1976	2	20	13	37	52.39	30.65	50.35	15	4.4	4.7	
650	1976	3	7	0	42	37	28.25	57.30	66.8	4.6	4.6	
651	1976	3	10	4	39	20	28.45	57.44	83.2	4.7	4.7	
652	1976	3	16	7	28	55.78	27.31	54.98	9	4.6	5.4	5.2
653	1976	3	16	9	9	46	27.43	55.04	38.8	4.0	4.5	

654	1976	3	20	9	24	2	27.23	55.00	43	4.2	4.6	
655	1976	3	31	2	34	18.87	28.04	56.73	25.9	4.5	4.8	
656	1976	4	22	17	3	6.94	28.80	52.11	5.4	5.7	5.9	5.7
657	1976	4	24	10	19	52	28.26	56.79	75.2	4.0	4.5	
658	1976	4	26	4	57	24.52	28.67	52.02	10	5.2	5.2	
659	1976	5	2	16	57	3.46	28.14	53.24	15	4.2	4.6	
660	1976	6	2	18	4	45	28.34	53.48	70.1	4.5	4.8	
661	1976	6	13	21	33	20.01	28.03	55.55	15	4.4	4.7	
662	1976	6	27	9	26	35.08	29.46	52.13	15	4.0	4.5	
663	1976	7	17	8	37	0	29.75	51.50	41	4.2	4.6	
664	1976	8	10	21	12	9.7	30.75	50.59	66	4.0	4.5	
665	1976	9	14	23	41	27.53	28.02	53.49	15	4.5	4.8	
666	1976	9	22	19	39	47	23.63	64.20	38.2	4.4	4.7	
667	1976	10	15	23	3	27.66	30.10	52.00	5.2	5.1	5.1	
668	1976	10	18	10	20	11.6	30.09	52.02	2.9	4.9	5.0	
669	1976	10	24	16	20	56.01	27.55	56.68	6.9	4.9	5.0	
670	1976	10	26	1	0	24	27.24	58.12	71	4.5	4.5	
671	1976	11	6	23	18	51	28.15	56.96	33	4.2	4.6	
672	1976	11	13	10	12	34.36	28.21	57.33	30	4.9	5.0	
673	1976	12	1	11	59	35	26.92	55.04	54.3	4.0	4.5	
674	1977	1	5	5	44	40.47	27.44	56.22	20	4.4	5.5	5.1
675	1977	1	27	0	20	40.6	24.82	62.49	15	4.5	4.8	
676	1977	1	29	23	39	57.47	28.31	53.28	15	4.2	4.6	
677	1977	2	19	17	37	30	27.37	53.15	38.6	4.2	4.6	
678	1977	3	21	21	18	53.37	27.59	56.45	12	6.9	6.2	6.7
679	1977	3	21	21	33	16.91	27.55	56.36	10	5.2	5.2	
680	1977	3	21	21	41	24	27.29	56.77	33	4.5	4.8	
681	1977	3	21	21	50	47	27.60	56.54	33	4.4	4.7	
682	1977	3	21	21	51	40	27.71	56.51	33	4.9	5.0	
683	1977	3	21	22	17	30	26.66	56.66	0	4.4	4.7	
684	1977	3	21	22	42	5.56	27.60	56.47	15	6.0	5.7	6.1
685	1977	3	21	23	56	56.68	27.41	56.47	15	4.4	4.7	
686	1977	3	22	1	28	21	27.43	56.26	52.5	4.4	4.7	
687	1977	3	22	1	37	9	27.52	56.26	51.8	4.4	4.7	
688	1977	3	22	2	25	56.69	27.43	56.27	15	4.9	5.0	
689	1977	3	22	2	42	6.38	27.66	56.49	15	4.7	4.9	
690	1977	3	22	4	47	56	27.40	56.44	53.5	4.0	4.5	
691	1977	3	22	5	7	13	26.72	56.41		4.0	4.5	
692	1977	3	22	5	32	2.65	29.42	51.38	15	4.7	4.9	
693	1977	3	22	7	29	40	27.48	56.14	61.3	4.0	4.5	
694	1977	3	22	9	14	39.28	27.65	56.58	15	4.9	5.0	
695	1977	3	22	11	57	29.41	27.60	56.42	12.5	5.7	5.7	5.9
696	1977	3	22	12	32	57	27.62	56.61	59.2	4.5	4.8	
697	1977	3	22	16	37	4	27.55	56.48	67.2	4.0	4.5	
698	1977	3	22	21	28	9.18	27.57	56.63	15	4.0	4.5	
699	1977	3	22	21	31	2.06	27.68	56.35	15.8	4.5	4.8	
700	1977	3	23	0	17	50.03	27.50	56.37	15.5	4.7	4.9	

701	1977	3	23	2	24	56	27.36	56.73	0	4.0	4.5	
702	1977	3	23	2	31	36.16	27.57	56.56	15	4.7	4.9	
703	1977	3	23	7	46	56.41	27.64	56.46	15	4.9	5.0	
704	1977	3	23	10	11	11	27.99	56.18	53.3	4.2	4.6	
705	1977	3	23	13	45	8.99	27.40	56.37	15	4.4	4.7	
706	1977	3	23	20	40	56.95	27.49	56.44	20	4.9	5.0	
707	1977	3	23	23	51	13.82	27.59	56.56	9	5.1	5.7	5.5
708	1977	3	24	0	4	51	27.89	56.60	33.3	4.5	4.8	
709	1977	3	24	0	13	50.51	27.60	56.48	14.9	5.2	5.2	
710	1977	3	24	0	19	54	27.69	56.77	0	4.4	4.7	
711	1977	3	24	4	42	23.92	27.63	56.59	15.4	4.7	5.2	5.3
712	1977	3	24	13	57	55	27.11	56.54	45.8	4.2	4.6	
713	1977	3	24	14	10	42	27.37	56.60	47	4.4	4.7	
714	1977	3	25	22	55	20.34	27.67	56.59	15	4.7	4.9	
715	1977	3	26	0	32	38	27.52	56.54	47.5	4.5	4.8	
716	1977	3	26	14	28	2	28.17	56.04	32.2	4.4	4.7	
717	1977	3	27	7	19	50	28.02	56.19	70.5	4.0	4.5	
718	1977	3	28	4	9	49	27.64	56.52	57.9	4.7	4.9	
719	1977	3	28	4	54	4.63	27.46	56.52	15	4.7	4.9	
720	1977	3	29	22	29	15.4	27.58	56.37	10.9	5.1	5.1	
721	1977	3	31	10	5	59.29	27.58	56.52	15	4.4	4.7	
722	1977	3	31	13	36	25.42	27.54	56.54	15	4.4	4.7	
723	1977	3	31	19	11	19.14	27.54	56.26	15	4.5	4.8	
724	1977	3	31	19	53	18	28.14	52.15	40.7	5.1	5.1	
725	1977	4	1	6	59	4	27.31	56.30	12	4.2	4.6	
726	1977	4	1	13	36	24.2	27.55	56.28	12	5.8	5.9	6.0
727	1977	4	1	16	0	23.84	27.47	56.24	15	4.5	4.8	
728	1977	4	2	6	53	35	27.72	56.13	33	4.7	4.9	
729	1977	4	7	3	34	39.94	28.11	57.03	20	4.7	4.9	
730	1977	4	8	16	49	43.86	27.41	56.30	15	4.2	4.6	
731	1977	4	9	17	34	21	27.90	52.07	40.9	4.7	4.9	
732	1977	4	10	5	2	29	27.82	56.07	63.2	4.0	4.5	
733	1977	4	11	3	10	9	27.61	56.19	51.3	4.4	4.7	
734	1977	4	16	4	6	30	23.44	64.59	33	4.0	4.5	
735	1977	4	17	3	47	32	27.59	56.46	55.3	4.0	4.5	
736	1977	4	17	13	4	45	27.22	56.44	26.9	4.2	4.6	
737	1977	4	17	17	15	15	27.61	56.42	62.1	4.0	4.5	
738	1977	4	20	4	22	22.83	26.95	55.44	8.2	5.1	5.1	
739	1977	4	30	14	35	35.63	27.56	56.50	13.2	5.1	5.1	
740	1977	5	19	0	8	14.57	29.77	51.14	15	4.5	4.8	
741	1977	5	19	22	58	29.94	27.10	55.27	10	5.2	5.2	
742	1977	5	19	23	4	51.8	27.09	55.28	10	5.2	5.2	
743	1977	5	20	12	25	20	27.05	55.28	45.2	4.2	4.6	
744	1977	5	20	17	37	45	27.68	56.55	62.3	4.5	4.8	
745	1977	5	24	12	43	26.9	27.00	55.42	17.1	4.4	4.7	
746	1977	5	24	12	59	9.57	27.05	55.45	15	4.4	4.7	
747	1977	5	25	21	6	39.3	29.23	53.40	19.3	4.5	4.8	

748	1977	5	26	16	43	37.73	29.71	51.11	15	4.4	4.7	
749	1977	5	26	22	39	29.01	27.58	56.55	22.9	4.4	4.7	
750	1977	5	29	2	22	2.82	23.43	64.56	11.1	4.6	4.9	5.2
751	1977	5	29	3	20	35	23.51	64.75	33	4.2	4.6	
752	1977	6	2	3	57	4	29.45	53.27	46	4.4	4.7	
753	1977	6	6	18	39	47.85	29.73	51.09	15	4.7	4.9	
754	1977	6	6	18	39	48	29.77	51.13	30.8	4.7	4.9	
755	1977	6	10	5	28	2	28.60	52.23	0	4.5	4.8	
756	1977	6	25	17	43	31	27.70	56.14	29.1	4.0	4.5	
757	1977	6	26	2	25	26.48	27.46	56.13	6.7	4.5	4.8	
758	1977	6	28	3	44	51.48	27.52	56.16	7	4.7	4.9	
759	1977	7	3	6	38	41	25.17	60.92	27.8	4.4	4.7	
760	1977	7	14	15	23	55.43	26.83	53.56	15	4.5	4.8	
761	1977	7	26	1	17	58.25	27.43	56.47	15	4.4	4.7	
762	1977	8	6	21	44	4	30.62	57.61	96.2	4.2	4.2	
763	1977	8	28	23	50	29.2	27.87	54.97	12.1	4.5	4.8	
764	1977	9	13	0	16	4.68	27.63	56.43	13.7	4.2	4.6	
765	1977	9	13	11	48	46.62	27.66	59.89	15	4.4	4.7	
766	1977	9	16	7	5	6.97	30.04	51.46	15	4.2	4.6	
767	1977	9	19	0	23	5.56	29.62	51.31	15	4.5	4.8	
768	1977	10	19	6	35	12.61	27.81	54.89	31.6	5.1	5.5	5.5
769	1977	10	27	0	22	21.23	29.65	50.65	15	4.7	4.9	
770	1977	12	1	21	11	17.73	27.72	56.49	15	5.1	5.1	
771	1977	12	1	23	28	21	27.76	56.59	61.5	4.4	4.7	
772	1977	12	10	5	46	20.68	27.69	56.58	13.9	5.2	5.1	5.6
773	1977	12	11	8	11	32	27.79	56.96	95.6	4.0	4.5	
774	1977	12	19	23	34	33.04	30.90	56.61	11.6	5.7	5.3	5.9
775	1978	1	5	19	30	17.94	27.48	53.80	15	4.4	4.6	
776	1978	1	8	2	55	51	30.39	50.78	44.2	4.4	4.7	
777	1978	1	15	7	3	20	30.19	50.75	57.8	4.2	4.6	
778	1978	2	10	20	50	48.59	25.30	62.40	24.1	5.1	5.1	
779	1978	2	11	21	40	11.41	28.17	55.38	20	4.9	5.2	4.6
780	1978	2	22	20	17	59.84	28.11	56.88	20.8	4.7	5.0	
781	1978	2	23	23	24	49.7	28.14	56.85	20	4.7	5.1	
782	1978	3	1	9	53	51	27.60	56.48	61.4	4.0	4.5	
783	1978	3	23	11	14	30	27.30	53.28	33	4.0	4.5	
784	1978	4	11	22	49	22.55	27.22	56.20	14.3	4.2	4.6	
785	1978	5	4	16	18	37	27.90	54.90	12.3	4.0	4.5	
786	1978	5	24	1	56	11.51	23.75	65.30	21.8	5.0	5.1	5.3
787	1978	5	26	12	22	23	27.65	56.55	48.9	4.0	4.5	
788	1978	6	28	16	0	56	25.69	62.24	33	4.2	4.6	
789	1978	8	2	6	54	31	27.33	55.89	46.5	4.0	4.5	
790	1978	8	26	16	23	40	29.82	51.77	55.4	4.2	4.6	
791	1978	8	29	14	11	3.33	29.56	51.53	12.2	4.5	4.9	
792	1978	8	31	20	24	5	29.41	51.53	34.3	4.0	4.5	
793	1978	9	6	13	0	57	28.54	56.98	33	4.2	4.6	
794	1978	10	12	6	54	32.89	27.77	54.84	15	4.2	4.7	

795	1979	1	5	20	0	17.45	27.82	55.63	15	4.0	4.5	
796	1979	1	10	1	26	6.9	26.52	61.01	6.8	6.0	5.5	6.0
797	1979	1	10	15	5	45.89	26.49	60.99	5	6.1	5.5	6.1
798	1979	1	11	3	33	13.95	26.32	61.01	5	4.5	4.9	
799	1979	1	12	8	15	19.71	26.28	61.09	10	4.5	4.8	
800	1979	1	15	12	27	5	27.67	56.57	58.2	4.2	4.6	
801	1979	1	18	1	21	46.14	26.44	60.93	13.5	4.9	4.8	
802	1979	1	19	10	5	52.11	26.36	60.96	10	4.7	4.7	
803	1979	1	21	4	32	8	26.19	61.26	10	4.1	4.3	
804	1979	1	31	13	59	14	26.37	61.18	33	4.7	4.9	
805	1979	2	11	22	25	21	27.89	54.82	56.3	4.5	4.8	
806	1979	2	26	13	41	25	26.31	60.86	33	4.2	4.6	
807	1979	3	4	5	43	44.24	28.26	56.24	31.9	4.8	5.0	
808	1979	3	11	2	9	8	27.64	57.55	48.9	4.5	4.5	
809	1979	3	17	12	36	32.75	26.49	60.95	15.5	5.0	4.8	
810	1979	3	28	1	33	28.22	30.90	49.94	28	4.9	5.0	5.2
811	1979	4	5	4	5	14.51	26.43	60.90	6.9	5.0	4.7	
812	1979	4	8	18	30	17	30.12	51.70	33	4.0	4.5	
813	1979	5	13	20	12	55	26.19	60.95	10	4.0	4.5	
814	1979	5	21	8	6	48	26.36	61.06	33	4.3	4.5	
815	1979	5	28	15	12	43	26.88	55.95	42.5	4.4	4.7	
816	1979	6	14	20	53	57	26.66	54.92	33	4.0	4.5	
817	1979	6	26	16	14	28	30.69	49.88	33	4.0	4.5	
818	1979	7	21	15	8	34	28.01	57.21	33	4.0	4.5	
819	1979	8	12	1	25	18	23.71	65.16	31.2	4.2	4.6	
820	1979	8	13	15	40	12	26.38	61.12	33	4.0	4.4	
821	1979	8	14	23	24	18.7	28.12	56.91	17.9	4.1	4.5	
822	1979	8	19	12	23	15.49	30.39	50.88	17.4	4.0	4.8	
823	1979	8	27	12	41	9	30.74	50.13	70.1	4.2	4.6	
824	1979	9	29	18	5	59	26.87	55.36	46.2	4.0	4.5	
825	1979	9	30	20	42	37.41	27.79	54.66	25	4.4	4.7	
826	1979	10	25	17	37	5	25.66	62.19	44.7	4.5	4.8	
827	1979	11	28	13	15	28	26.23	58.99	10	4.2	4.6	
828	1979	12	3	9	47	25	26.37	61.25	33	4.0	4.5	
829	1979	12	11	21	41	9	30.76	50.40	33	4.2	4.6	
830	1979	12	24	19	54	49.45	29.15	52.13	15	4.4	4.7	
831	1980	1	1	2	45	56.05	27.33	60.33	31	5.1	5.3	5.5
832	1980	1	11	16	52	53.89	26.26	54.21	15	4.0	4.4	
833	1980	2	1	18	4	15.07	26.39	61.09	15	4.7	4.8	
834	1980	2	6	12	56	2.84	26.69	53.87	12.8	4.7	5.0	
835	1980	2	7	21	18	38.39	27.98	53.34	15	4.2	4.8	
836	1980	2	13	17	32	26	28.19	57.42	59.7	4.6	4.6	
837	1980	2	26	15	53	5.46	27.43	53.49	15	4.0	4.5	
838	1980	2	26	17	37	12.21	27.33	53.51	15	4.4	4.7	
839	1980	3	30	4	42	14	29.23	60.14	33	4.5	4.8	
840	1980	4	28	7	4	46.1	27.55	64.49	54	4.8	5.3	5.5
841	1980	6	11	23	41	50	27.99	57.73	78.2	4.5	4.5	

842	1980	7	16	8	53	53	29.55	51.83	70	4.0	4.5	
843	1980	7	20	10	3	27.36	27.45	56.24	15	4.4	4.7	
844	1980	8	11	17	17	41	26.53	60.99	33	4.2	4.7	
845	1980	8	15	20	48	12	26.60	60.96	39	4.4	4.8	
846	1980	9	6	21	29	0.65	28.50	65.96	10.8	4.8	4.7	
847	1980	9	10	14	38	16	28.10	57.83	58.7	4.5	4.5	
848	1980	10	1	12	5	38	29.16	57.02	118.3	4.2	4.2	
849	1980	10	15	13	27	18.17	29.34	51.63	12.4	4.3	4.9	
850	1980	11	17	18	26	30.16	27.40	56.06	15	4.7	5.1	5.3
851	1980	11	22	22	16	21	28.01	52.14	35.4	4.0	4.5	
852	1980	11	28	21	15	28.2	27.61	56.53	7.6	5.1	5.5	5.4
853	1980	12	14	12	39	29.05	29.11	50.84	15	4.2	4.6	
854	1981	1	2	4	1	21	28.67	56.27	0	4.2	4.6	
855	1981	1	6	7	23	40.65	28.13	56.56	25	4.0	5.0	
856	1981	3	9	5	26	52.57	27.76	55.20	15	4.0	4.5	
857	1981	3	21	6	18	29.97	28.07	53.15	15	4.3	5.1	
858	1981	4	1	10	16	58.63	29.82	51.48	16	4.4	5.5	5.2
859	1981	4	16	10	27	17.96	27.72	56.35	28.9	4.3	5.3	5.1
860	1981	4	24	4	48	37	29.04	56.98	33	4.0	4.5	
861	1981	5	18	19	36	17	27.21	55.37	71	4.1	4.9	
862	1981	5	20	23	38	23	28.23	51.78	39.9	4.2	4.6	
863	1981	6	11	7	24	24.75	29.86	57.69	17.3	6.6	6.0	6.6
864	1981	6	11	14	32	41.44	29.81	57.77	15	4.4	4.7	
865	1981	6	12	1	11	46	26.57	61.16	33	4.0	4.7	
866	1981	6	12	1	43	19.39	29.87	57.77	15	4.0	4.5	
867	1981	6	12	2	5	25	29.83	57.79	24.9	4.0	4.5	
868	1981	6	12	6	43	59.05	29.75	57.76	15	4.2	4.6	
869	1981	6	12	10	32	32	30.57	57.85	73.8	4.4	4.4	
870	1981	6	12	10	45	15	29.95	57.95	33	4.0	4.5	
871	1981	6	12	11	45	2	29.74	58.31	44.6	4.4	4.7	
872	1981	6	13	7	52	32.26	29.91	57.88	15	4.4	4.7	
873	1981	6	21	13	8	46.09	29.81	57.79	17.7	4.3	4.9	
874	1981	7	3	3	51	59.27	27.10	55.83	10.6	4.4	5.3	
875	1981	7	15	23	51	28	27.62	58.23	70.9	4.3	4.3	
876	1981	7	28	17	22	24.05	29.98	57.77	13.6	7.0	5.9	7.3
877	1981	7	28	18	4	27.07	29.93	57.70	15	4.2	4.6	
878	1981	7	28	18	30	26.94	30.26	57.52	15	4.4	4.7	
879	1981	7	28	18	48	33.89	30.26	57.56	15	4.2	4.6	
880	1981	7	28	19	5	52.7	30.10	57.59	9.4	4.7	4.9	
881	1981	7	28	20	33	0	30.13	57.83	70	4.3	4.3	
882	1981	7	28	21	54	21.54	29.97	57.69	12.3	4.7	4.9	
883	1981	7	28	22	35	11	29.88	57.74	16.9	4.2	4.6	
884	1981	7	28	22	56	52	30.24	57.71	76	4.4	4.4	
885	1981	7	29	1	50	27	30.26	57.78	47.2	4.1	4.1	
886	1981	7	29	4	33	20	30.29	57.86	59.1	4.6	4.6	
887	1981	7	29	5	4	44.16	30.07	57.51	13.6	4.5	4.8	
888	1981	7	29	5	11	42	30.56	57.55	24.9	4.2	4.6	

889	1981	7	29	6	59	26	30.58	57.79	72.8	4.3	4.3	
890	1981	7	31	0	37	49	30.00	57.55	68.5	4.5	4.5	
891	1981	8	2	14	50	43	30.48	57.95	69.6	4.0	4.0	
892	1981	8	4	0	6	17	30.79	57.75	64.8	4.3	4.3	
893	1981	8	4	17	14	51.85	30.04	57.56	15	4.2	4.6	
894	1981	8	6	9	6	26	30.49	58.34	50.7	4.2	4.2	
895	1981	8	8	4	17	47	30.03	57.71	44.8	4.0	4.8	
896	1981	8	10	21	29	25	30.38	57.77	64.2	4.1	4.1	
897	1981	8	20	19	2	9.36	30.12	57.54	18.8	4.2	4.6	
898	1981	8	25	9	20	24	30.69	57.34	62	4.3	4.3	
899	1981	9	1	12	24	40	27.17	55.45	0	4.4	4.7	
900	1981	9	3	17	5	6.22	27.60	55.28	15.2	4.4	4.9	
901	1981	9	8	17	3	13.73	28.47	56.94	20	4.2	4.6	
902	1981	9	12	2	29	18	27.82	56.98	32.5	4.5	4.8	
903	1981	9	13	1	43	32	27.47	53.86	70.5	4.2	4.6	
904	1981	9	17	13	44	10	30.64	57.90	74	4.1	4.1	
905	1981	9	26	7	33	24.64	30.25	57.60	15	4.2	4.6	
906	1981	10	14	9	12	37.05	29.81	57.69	10.2	4.6	5.2	
907	1981	10	27	16	17	52	30.83	48.42	33	4.2	4.6	
908	1981	11	22	17	22	53	27.68	55.17	33	4.0	4.5	
909	1981	11	28	6	42	37.84	30.71	50.58	15	4.7	4.9	
910	1982	1	2	19	0	48.62	30.61	57.49	15	4.1	4.9	
911	1982	1	13	1	46	32	29.88	52.07	33	4.0	4.5	
912	1982	2	5	16	28	58	30.61	57.51	32	4.0	4.5	
913	1982	2	20	21	24	40	30.33	50.55	91.6	4.5	4.8	
914	1982	2	25	23	30	24.24	29.86	57.77	24.5	4.4	4.7	
915	1982	2	25	23	52	2	30.10	57.92	63.2	4.4	4.4	
916	1982	2	28	13	42	9	28.61	57.22	81.1	4.3	4.3	
917	1982	3	20	4	9	28	27.59	52.80	56.5	4.2	4.6	
918	1982	3	23	9	58	39	27.47	57.25	36.6	4.2	4.6	
919	1982	4	17	2	42	3	28.55	51.74	15	4.2	4.6	
920	1982	6	14	15	33	51	30.15	57.73	47.5	4.6	4.6	
921	1982	7	11	13	19	48.48	27.83	56.28	13.6	4.8	5.3	
922	1982	7	17	8	8	10	30.30	57.60	70.8	4.1	4.1	
923	1982	7	31	16	5	15	27.61	57.44	33	4.2	4.6	
924	1982	10	15	2	53	52.38	28.19	57.33	35	4.9	5.0	
925	1982	11	10	11	28	27.45	26.59	54.94	15	4.4	4.7	
926	1982	12	8	19	34	20.67	30.51	57.58	15	4.2	4.6	
927	1982	12	19	19	40	51.4	30.50	57.51	15	6.2	5.1	
928	1982	12	23	2	48	19	27.48	56.39	33	4.2	4.6	
929	1983	1	1	21	54	30.29	30.25	50.77	19.8	4.7	4.9	
930	1983	1	7	22	28	38.62	30.34	50.80	15	4.7	4.9	
931	1983	1	16	11	24	30.29	30.17	50.82	15	4.0	4.5	
932	1983	1	17	20	57	9.98	27.63	56.70	15	4.9	5.0	
933	1983	1	31	18	56	42.57	28.71	57.24	25	4.9	5.0	
934	1983	2	7	15	6	27.89	26.87	57.57	21.8	5.7	5.5	6.0
935	1983	2	18	7	40	21.57	27.90	53.82	6	4.3	5.2	5.2

936	1983	2	18	14	32	10.07	27.91	53.79	10	4.5	4.8	
937	1983	2	20	10	9	48	27.35	56.50	33	4.2	4.6	
938	1983	2	28	1	37	35	29.99	57.81	36.3	4.0	4.5	
939	1983	3	25	10	40	22	27.55	61.91	33	4.4	4.7	
940	1983	4	15	6	18	44.39	30.53	50.24	15	4.4	4.7	
941	1983	4	18	10	58	52.8	27.77	62.06	63.7	6.3	6.4	6.7
942	1983	4	18	17	39	15	27.76	62.13	57.8	4.6	4.6	
943	1983	4	19	14	1	15	27.52	62.34	50	4.4	4.4	
944	1983	4	19	20	36	29	27.63	62.17	33	4.0	4.5	
945	1983	5	1	23	6	31	30.44	57.62	47.6	4.6	4.6	
946	1983	5	3	0	55	27	30.15	57.76	49.6	4.2	4.2	
947	1983	5	20	20	38	5	28.41	57.00	76.9	4.1	4.1	
948	1983	5	21	16	9	31	28.21	57.03	33	4.2	4.6	
949	1983	7	11	20	34	9.77	29.05	51.89	15	4.2	4.6	
950	1983	7	12	11	34	18.19	27.60	56.40	17.5	5.8	5.7	6.0
951	1983	7	12	11	41	28	27.63	56.47	33	5.2	5.2	
952	1983	7	12	11	54	1	27.65	56.45	38.1	4.5	4.8	
953	1983	7	15	1	57	36	28.29	56.96	73.7	4.7	4.9	
954	1983	7	15	2	1	21	28.49	57.04	10	4.7	4.9	
955	1983	7	16	1	35	26	27.61	56.21	64.3	4.0	4.5	
956	1983	7	16	17	25	51	27.78	56.42	33	4.2	4.6	
957	1983	8	13	17	18	35.86	28.26	53.30	15	4.1	4.8	
958	1983	9	9	15	6	58	28.84	57.37	78.1	4.2	4.2	
959	1983	9	23	11	23	21	30.75	50.33	41.6	4.0	4.5	
960	1983	10	9	15	25	36.3	28.91	61.32	15	4.4	4.7	
961	1983	10	29	2	37	2.4	28.44	57.00	20	4.5	4.8	
962	1983	12	2	10	45	9	27.75	56.56	42.1	4.5	4.8	
963	1984	1	15	3	47	5	27.08	63.29	10.4	4.4	4.7	
964	1984	1	18	14	8	20.66	28.01	65.75	9.7	5.4	5.5	5.7
965	1984	2	14	4	43	8	27.32	55.96	0	4.0	4.5	
966	1984	2	29	10	1	7.24	26.85	55.60	25	4.7	5.0	
967	1984	3	1	21	24	52.74	27.25	53.84	10.7	4.6	5.2	
968	1984	3	2	1	51	33.43	27.26	53.72	15	4.1	4.7	
969	1984	3	17	12	26	55.32	23.90	64.70	18.4	4.7	4.9	
970	1984	3	20	12	25	56	26.78	54.26	35.5	4.5	4.8	
971	1984	3	21	17	51	50	26.97	54.41	88.8	4.5	4.8	
972	1984	3	21	18	11	52	26.90	54.33	60.3	4.7	4.9	
973	1984	3	21	18	26	14	26.86	54.24	33.3	4.2	4.6	
974	1984	3	22	0	22	4.27	26.73	54.25	15	4.7	4.9	
975	1984	3	30	3	15	13	26.79	54.28	60.3	4.5	4.8	
976	1984	4	22	13	39	32.53	27.63	56.64	21.9	4.6	4.9	
977	1984	4	25	18	34	57	28.42	57.58	82.5	4.0	4.0	
978	1984	7	23	7	13	50.04	29.46	53.41	15	4.7	4.9	
979	1984	7	23	8	21	6	30.71	57.38	33	4.0	4.5	
980	1984	8	2	22	49	47.32	28.03	51.29	15	4.7	4.9	
981	1984	8	6	11	14	35.14	30.80	57.17	4.9	5.3	5.6	5.4
982	1984	8	14	1	30	53.09	30.75	57.14	15	4.2	4.6	

983	1984	8	15	2	0	56.12	30.78	57.06	7.7	5.1	5.1	
984	1984	8	19	17	34	21	27.40	64.94	50	4.4	4.4	
985	1984	8	28	3	26	9.23	30.92	51.28	15	4.7	4.9	
986	1984	9	6	22	21	4.25	26.11	54.38	15	4.8	4.9	
987	1984	9	7	11	10	20	28.18	55.14	46.5	4.2	4.6	
988	1984	9	10	21	16	13	29.16	57.02	111	4.5	4.5	
989	1984	9	12	18	0	46.84	27.35	60.81	65	5.1	5.1	
990	1984	9	19	16	57	12.81	29.83	50.36	15	4.0	4.5	
991	1984	9	21	0	47	25.08	29.92	50.26	15	4.5	4.8	
992	1984	10	11	5	9	24.51	29.48	57.96	13.6	5.1	5.1	
993	1984	10	23	7	8	15	30.66	57.35	33	4.2	4.6	
994	1984	10	28	12	3	50	22.33	59.86	33	4.4	4.7	
995	1984	11	15	6	19	22	28.39	57.14	86.6	4.8	4.8	
996	1984	12	6	11	31	21	27.51	55.72	65.6	4.0	4.5	
997	1984	12	22	16	5	12.45	27.82	54.44	25	4.5	5.1	5.1
998	1985	1	10	13	15	28	28.01	56.60	12	4.4	4.7	
999	1985	2	2	20	52	32.91	28.35	52.97	13.8	5.3	5.1	5.5
1000	1985	2	2	22	40	8.41	28.37	52.92	14.5	4.2	4.6	
1001	1985	4	7	21	27	40.17	21.19	61.87	17.8	4.8	5.3	5.3
1002	1985	4	25	4	58	46.28	29.36	52.76	25.1	4.5	4.8	
1003	1985	5	17	17	1	25	26.70	57.46	38.6	4.2	4.6	
1004	1985	5	19	0	55	11.75	29.64	51.12	26.9	4.4	4.7	
1005	1985	6	22	12	41	2.02	29.45	61.15	12.6	4.8	5.0	
1006	1985	6	28	13	35	31.38	30.54	57.52	15	4.4	4.7	
1007	1985	7	4	6	4	47	29.47	52.65	24.6	4.4	4.7	
1008	1985	7	23	23	51	41.69	30.35	50.61	15	4.7	4.9	
1009	1985	7	31	18	9	42.48	28.91	52.26	15	4.5	4.8	
1010	1985	8	7	15	43	24.55	27.86	53.04	13.4	5.4	5.4	5.6
1011	1985	8	7	15	47	0	27.61	52.32	0	4.5	4.8	
1012	1985	8	10	13	29	53	27.97	53.41	33	4.1	4.6	
1013	1985	10	10	10	19	54	26.80	54.91	22.7	5.1	5.0	
1014	1985	11	1	22	36	25	27.81	56.56	50.1	4.4	4.7	
1015	1985	11	2	15	49	28	27.66	56.38	33	4.0	4.5	
1016	1985	11	15	6	12	8	28.06	51.25	22.4	4.4	4.8	
1017	1985	11	16	1	56	26	27.71	56.44	49.6	4.0	4.5	
1018	1985	12	5	21	50	10	29.60	51.61	33	4.0	4.5	
1019	1985	12	5	23	30	16	29.61	51.51	42.5	4.0	4.5	
1020	1985	12	13	1	54	8	30.50	57.65	33	4.2	4.6	
1021	1985	12	31	11	51	4	27.70	54.45	15	4.4	4.7	
1022	1986	1	27	3	2	4.57	28.44	51.42	15	4.6	4.5	
1023	1986	3	8	5	55	2	30.97	50.29	64.3	4.0	4.5	
1024	1986	3	25	1	32	33	26.80	54.81	30	5.4	4.9	
1025	1986	3	27	11	41	56	30.10	57.90	33	4.0	4.5	
1026	1986	4	3	2	49	30.33	26.93	56.15	15	4.2	4.6	
1027	1986	4	29	14	37	59	30.26	51.68	33	4.3	3.7	
1028	1986	4	30	18	19	37	27.80	53.25	33	4.8	4.2	
1029	1986	5	2	3	18	36.8	28.00	53.31	15	5.1	5.5	5.6

1030	1986	5	3	10	37	41.68	27.98	53.34	15	4.7	5.4	5.2
1031	1986	5	7	17	54	34.44	26.77	57.68	15	4.0	4.5	
1032	1986	5	26	21	7	1.36	28.99	51.84	15	4.0	4.5	
1033	1986	7	12	7	54	27.71	29.91	51.56	5.4	5.5	5.7	5.7
1034	1986	7	12	17	31	41	29.87	51.61	33	4.4	4.7	
1035	1986	7	13	0	48	48.06	29.94	51.48	15	4.5	5.0	
1036	1986	7	19	9	12	19.19	28.26	56.77	15	4.5	4.8	
1037	1986	7	20	15	56	25.88	29.95	51.70	15	4.4	4.7	
1038	1986	7	25	10	8	7.18	27.99	57.28	32.7	5.2	5.2	
1039	1986	8	8	8	31	24.59	27.44	57.91	15	4.9	5.0	
1040	1986	8	9	6	37	24.68	26.74	54.98	25	4.4	5.2	
1041	1986	8	24	4	0	39	28.45	56.17	67.2	4.0	4.5	
1042	1986	9	18	0	12	3.21	26.58	54.60	15	4.6	4.6	
1043	1986	10	1	3	57	56.49	28.92	51.41	15	4.2	4.4	
1044	1986	10	6	2	21	42.37	26.52	54.55	15	4.7	4.9	
1045	1986	10	10	11	50	55.29	29.91	51.60	15	4.2	4.6	
1046	1986	10	16	19	1	47.3	28.95	52.75	15	4.4	4.7	
1047	1986	11	20	20	8	0.74	29.92	51.58	13.4	4.1	5.2	
1048	1986	12	14	9	9	16.98	27.37	54.34	15	4.5	4.8	
1049	1986	12	20	23	47	8.34	29.90	51.58	10.7	4.9	5.4	5.4
1050	1986	12	21	0	11	51.8	29.92	51.60	15	4.7	4.9	
1051	1986	12	31	16	56	49.94	25.26	63.25	24	4.3	5.0	
1052	1987	1	1	4	31	44	24.44	63.32	33	4.0	4.5	
1053	1987	1	9	22	5	20	29.95	51.82	10	4.0	4.1	
1054	1987	1	10	13	6	53	26.43	61.00	10	4.2	4.6	
1055	1987	1	11	12	31	28.59	29.93	51.80	15	4.1	4.8	
1056	1987	2	18	20	46	56.7	26.05	57.39	15	4.7	4.5	
1057	1987	3	2	21	51	6	25.56	63.24	10	4.4	4.7	
1058	1987	3	19	14	32	19.07	23.68	64.71	18.4	4.0	5.2	5.0
1059	1987	3	20	11	15	16	26.48	56.86	33	4.0	4.5	
1060	1987	4	29	1	45	24.39	27.42	56.11	9.6	5.4	5.8	5.7
1061	1987	5	12	7	15	11.58	28.14	55.57	14.9	4.9	5.2	5.5
1062	1987	5	12	18	18	5	28.23	55.60	55.4	4.2	4.6	
1063	1987	5	14	10	11	18	27.46	56.05	45.1	4.2	4.6	
1064	1987	6	1	16	45	12	30.86	50.01	48.9	4.0	4.5	
1065	1987	6	16	17	27	52	28.41	57.28	45.6	4.8	4.8	
1066	1987	6	18	17	22	39	28.54	54.30	44.3	4.0	4.5	
1067	1987	7	16	11	29	46.93	29.70	50.66	15	4.4	4.6	
1068	1987	8	1	13	43	21.09	30.01	57.71	12.6	4.2	4.6	
1069	1987	8	1	13	55	18.17	30.00	57.75	10	4.2	4.6	
1070	1987	8	10	10	52	21.34	29.87	63.88	162	6.0	5.5	6.1
1071	1987	9	22	14	24	25.45	27.67	55.27	15	4.2	4.6	
1072	1987	9	29	18	36	12.8	28.50	52.78	15	5.1	5.1	
1073	1987	10	28	21	47	25	27.63	56.40	46.8	4.5	4.8	
1074	1987	11	25	22	53	32	28.11	56.70	55.5	4.4	4.7	
1075	1987	12	18	16	24	4.42	28.15	56.66	17.8	5.5	5.7	5.9
1076	1987	12	18	20	54	34	28.19	56.65	37.6	4.4	4.7	

1077	1988	1	14	19	5	1	27.26	56.04	10	4.2	4.6	
1078	1988	1	28	21	8	55.62	28.00	53.84	20	4.5	4.9	
1079	1988	1	29	15	29	30.4	28.02	53.82	20	4.4	4.7	
1080	1988	2	16	12	44	44.74	28.06	53.70	20	4.4	5.0	
1081	1988	2	17	10	9	22.75	27.71	54.27	20	4.4	4.5	
1082	1988	2	22	14	51	51.03	27.22	53.23	20	4.3	4.8	
1083	1988	2	23	6	41	6.96	27.18	53.29	20	4.3	4.7	
1084	1988	3	14	2	26	40.27	24.97	62.92	22.9	4.4	4.7	
1085	1988	3	28	15	40	51	30.73	50.12	46.1	4.4	4.7	
1086	1988	3	30	2	12	43.45	30.85	50.18	25	5.7	5.4	5.9
1087	1988	3	30	3	14	56.17	30.72	50.22	20	4.2	4.6	
1088	1988	4	13	3	40	3	30.16	57.55	46	4.4	4.4	
1089	1988	4	20	13	30	15	30.56	50.10	33	4.4	4.7	
1090	1988	4	22	1	54	8.85	30.73	50.37	19.3	4.5	5.1	
1091	1988	5	19	8	1	7	30.73	50.06	51.4	4.0	4.5	
1092	1988	6	6	8	42	0.7	29.74	51.11	15	4.2	4.9	
1093	1988	6	9	0	9	50.77	28.28	56.88	26	4.6	5.0	5.2
1094	1988	6	13	21	31	49	28.24	56.86	63.9	4.4	4.7	
1095	1988	7	6	2	10	58.81	29.31	52.46	15	4.4	4.5	
1096	1988	7	23	19	10	1.68	30.83	50.15	15	4.5	4.6	
1097	1988	7	26	23	59	23	28.09	57.32	17.7	4.2	4.6	
1098	1988	8	7	15	15	47.65	30.87	50.17	15	4.5	4.8	
1099	1988	8	11	16	0	5.69	29.94	51.59	7.8	5.6	5.4	5.8
1100	1988	8	11	16	4	44.14	29.89	51.66	11	5.9	5.6	6.1
1101	1988	8	11	16	39	55	29.97	51.55	4.6	4.7	4.9	
1102	1988	8	11	21	52	17.8	29.97	51.55	15	4.5	4.8	
1103	1988	8	13	16	46	25.41	29.93	51.66	15	4.5	4.8	
1104	1988	8	28	19	51	14	26.80	55.94	27.1	4.3	4.9	
1105	1988	8	30	17	30	23.82	29.96	51.72	16	4.7	4.9	5.2
1106	1988	9	8	23	45	46.52	24.55	65.96	15	4.2	4.9	
1107	1988	9	21	16	42	54.01	30.19	51.72	15	4.5	5.0	
1108	1988	9	23	1	2	58	27.36	57.22	36.9	4.2	4.6	
1109	1988	9	27	14	31	42	30.01	51.66	9.8	4.2	4.6	
1110	1988	11	15	5	4	6	27.24	61.24	70.7	4.0	4.0	
1111	1988	11	20	23	8	20.46	30.78	50.36	15	4.7	4.9	
1112	1988	11	21	17	27	4.3	29.66	51.35	15	4.2	4.6	
1113	1988	11	28	5	19	5.37	28.65	63.96	15	4.7	4.9	
1114	1988	12	3	1	23	33	30.27	57.54	25	4.7	4.9	
1115	1988	12	6	13	20	43.11	29.90	51.63	11.3	5.6	5.5	5.9
1116	1988	12	20	14	53	36	29.74	51.70	44.9	4.0	4.5	
1117	1988	12	21	6	27	43	30.12	50.50	33	4.0	4.5	
1118	1989	1	1	15	55	59.05	27.09	54.20	10	4.2	4.6	
1119	1989	1	13	14	26	22.94	27.71	54.24	15	4.4	4.7	
1120	1989	2	6	8	5	53.12	30.71	50.16	15	4.0	4.5	
1121	1989	3	19	1	36	23	30.73	50.11	43.1	4.0	4.5	
1122	1989	3	23	18	57	47	27.74	56.93	33	4.0	4.5	
1123	1989	4	2	6	42	4.55	28.17	57.28	30.5	4.8	5.2	5.4

1124	1989	4	11	5	23	5	29.44	64.10	99.6	4.6	4.6	
1125	1989	5	3	9	12	44.5	29.90	51.81	15	4.9	5.0	5.2
1126	1989	5	3	9	13	24	29.96	51.69	33	4.6	5.0	
1127	1989	5	3	12	16	43.55	29.94	51.86	15	4.0	4.5	
1128	1989	5	27	17	52	31	30.07	51.01	48	4.4	4.7	
1129	1989	5	27	20	8	36.95	30.15	50.89	15	5.7	5.6	6.0
1130	1989	5	27	20	36	5.5	30.17	50.91	15	4.0	4.5	
1131	1989	5	27	20	39	58.24	30.37	50.94	15	4.3	4.5	
1132	1989	5	27	21	31	57.16	30.02	50.78	15	4.6	4.4	
1133	1989	5	28	16	28	41.1	30.19	50.89	15	4.2	4.6	
1134	1989	5	29	5	46	40.63	30.06	50.94	15	4.5	4.7	
1135	1989	6	17	16	52	51	29.87	59.81	6.9	4.6	4.9	
1136	1989	7	18	21	24	1	30.91	49.70	36	4.0	4.4	
1137	1989	10	1	2	59	6.98	30.95	51.40	30	4.4	5.2	
1138	1989	11	4	20	47	20.38	30.56	57.63	15	5.6	5.0	
1139	1989	11	20	4	19	5.96	29.90	57.72	14.9	5.7	5.5	5.9
1140	1989	11	20	12	19	31	30.53	60.04	33	4.0	4.5	
1141	1989	12	7	12	59	34.43	25.92	58.97	10.3	5.8	5.7	6.0
1142	1990	1	6	6	1	35	27.91	52.09	57.8	4.0	4.5	
1143	1990	2	4	20	34	44	28.20	57.68	56.3	4.5	4.8	
1144	1990	3	22	17	53	23	28.26	57.42	10	4.5	4.8	
1145	1990	3	23	5	37	37.03	29.69	51.33	15	4.2	4.6	
1146	1990	5	7	14	48	3	30.97	51.69	21.5	4.7	4.4	
1147	1990	5	28	19	12	26	30.32	50.81	33	4.2	4.6	
1148	1990	6	17	4	51	47.34	27.39	65.67	13.7	6.2	5.9	6.1
1149	1990	6	17	17	17	45.27	27.38	65.60	14.4	5.3	5.3	5.6
1150	1990	6	26	4	59	0.17	28.44	59.09	12.3	4.8	4.9	
1151	1990	7	11	0	39	22.1	28.27	57.07	25	4.4	4.7	
1152	1990	7	26	6	53	58.02	27.34	65.55	16.1	5.8	5.8	5.9
1153	1990	8	1	14	54	5	27.93	53.36	33	4.3	4.3	
1154	1990	8	16	23	52	18	27.78	56.85	62	4.4	4.7	
1155	1990	8	24	11	14	22.86	29.79	60.64	15	4.1	4.9	
1156	1990	8	31	14	26	11	26.85	53.99	33	4.2	4.6	
1157	1990	8	31	15	42	58.06	27.21	53.89	15	4.2	4.5	
1158	1990	9	24	19	51	53	28.16	56.91	59.3	4.2	4.6	
1159	1990	9	26	15	32	37.83	29.05	60.89	6.1	5.4	5.4	5.6
1160	1990	9	26	20	16	24	26.90	57.48	33	4.0	4.5	
1161	1990	9	27	12	34	53	29.05	60.91	34.1	4.3	4.8	
1162	1990	9	29	17	53	8	28.99	60.86	19.5	4.2	4.8	
1163	1990	9	30	6	24	3	29.06	60.89	21.3	4.8	4.8	
1164	1990	10	1	20	42	42	29.99	50.45	33	4.9	5.0	
1165	1990	10	2	15	0	54	24.53	64.69	10	4.0	4.5	
1166	1990	10	12	1	49	19.94	29.03	60.96	20	4.3	4.7	
1167	1990	10	18	23	25	51	27.28	53.01	33	4.0	4.2	
1168	1990	10	19	23	39	21.17	30.24	57.48	15	4.4	4.8	
1169	1990	10	25	14	15	27.45	28.28	54.20	15	4.0	4.7	
1170	1990	10	26	21	40	55	29.73	50.83	43.7	4.0	4.5	

1171	1990	10	26	22	18	9.57	28.35	52.48	15	4.0	4.4	
1172	1990	11	6	18	45	53.98	28.24	55.46	11.1	6.6	6.1	6.6
1173	1990	11	6	19	30	21.29	28.23	55.37	15	5.7	5.3	
1174	1990	11	21	3	42	39	28.34	55.54	56.8	4.1	4.6	
1175	1990	11	30	11	39	10	27.78	64.04	33	4.0	4.5	
1176	1990	12	5	18	36	26	27.78	56.64	44.8	4.0	4.5	
1177	1990	12	8	21	22	48	28.18	55.31	54.5	4.0	4.5	
1178	1990	12	10	1	27	30	28.16	57.06	53.4	5.0	5.0	
1179	1990	12	16	22	18	51.7	29.02	51.31	16.3	5.5	5.3	5.7
1180	1990	12	17	2	18	38.29	29.08	51.31	20	4.3	4.8	
1181	1990	12	17	2	45	34.01	29.16	51.33	15	4.2	4.6	
1182	1990	12	22	23	25	27.69	28.95	51.40	15	4.4	4.7	
1183	1990	12	23	0	1	5	29.17	51.27	0	4.4	4.7	
1184	1990	12	26	16	18	1	27.58	56.45	33	4.0	4.5	
1185	1990	12	29	7	36	30.56	28.33	55.38	15	4.2	4.6	
1186	1991	1	19	10	8	21	26.14	60.83	0.8	4.5	4.8	
1187	1991	1	30	5	9	9.06	29.06	51.40	15	4.0	4.5	
1188	1991	1	30	23	42	14	27.46	55.86	33	4.0	4.5	
1189	1991	2	14	8	25	56.72	30.26	50.82	21.6	4.6	5.3	
1190	1991	2	21	21	59	2	29.76	51.89	26.7	4.2	4.6	
1191	1991	4	5	5	38	17.75	29.10	51.40	15	4.7	4.9	
1192	1991	4	5	9	15	27.66	29.05	51.44	15	4.8	5.0	
1193	1991	4	11	16	2	18	27.62	56.52	61.1	4.5	4.8	
1194	1991	5	6	18	33	46	30.98	49.75	38.4	4.2	4.6	
1195	1991	5	20	20	54	5	27.71	56.36	44.4	4.2	4.6	
1196	1991	5	22	3	31	25.53	28.04	54.20	19.2	4.7	4.6	
1197	1991	5	22	16	29	3.06	27.38	55.77	17.6	5.1	5.7	5.4
1198	1991	5	29	23	9	29.39	27.03	53.50	15	4.3	4.7	
1199	1991	6	24	6	10	9	27.70	56.60	51.7	4.5	4.8	
1200	1991	7	4	10	17	49	28.15	57.30	44.9	4.0	4.8	
1201	1991	8	8	11	12	39.26	26.89	65.91	44	4.4	5.4	
1202	1991	8	12	22	55	26	27.69	54.48	52.5	4.2	4.3	
1203	1991	8	28	0	51	53	24.68	62.82	33	4.0	4.5	
1204	1991	9	16	13	23	39.85	28.97	51.31	25	4.9	4.9	
1205	1991	10	13	15	38	28	27.95	53.15	55.7	4.2	4.6	
1206	1991	10	31	14	35	10.36	30.62	50.21	25	4.8	4.9	
1207	1991	11	1	6	28	15	30.73	49.96	48.8	4.5	4.8	
1208	1991	11	2	22	3	34	30.59	50.01	55.5	5.0	4.4	
1209	1991	11	4	1	50	30.99	30.69	50.25	18.3	5.5	5.3	5.6
1210	1991	11	4	3	4	7	30.78	50.16	55.7	4.0	4.5	
1211	1991	11	4	4	9	42.99	30.62	50.15	25	4.5	4.7	
1212	1991	11	5	7	49	49.61	30.65	50.18	25	4.9	4.9	
1213	1991	11	10	15	19	13.95	30.59	50.27	25	4.5	5.0	
1214	1991	11	11	7	17	1	30.58	50.24	50.5	4.0	4.5	
1215	1991	11	13	21	4	29.88	30.75	50.10	25	4.6	5.1	
1216	1991	11	18	22	18	0.72	28.09	55.31	15	4.0	4.5	
1217	1991	11	29	21	24	57.55	30.16	50.88	15.4	4.5	4.8	

1218	1991	12	7	14	22	33.94	25.15	62.97	28.9	5.1	5.2	5.6
1219	1991	12	14	10	30	13	27.60	56.33	33	4.0	4.5	
1220	1991	12	19	18	55	18.16	28.04	57.27	20	4.8	5.3	5.4
1221	1992	1	30	5	22	3.19	24.95	63.16	27.1	5.6	5.4	5.9
1222	1992	2	6	2	18	14.15	28.29	52.59	15	4.8	4.6	
1223	1992	2	10	16	38	38	30.15	57.46	43.5	4.2	4.6	
1224	1992	3	3	18	35	5	28.25	57.14	61.6	4.7	4.7	
1225	1992	3	27	11	18	7.18	28.20	55.55	25	4.4	4.7	
1226	1992	4	10	8	45	2.91	29.12	52.56	15	4.0	4.5	
1227	1992	4	29	10	42	13.12	27.95	51.30	15	4.5	4.4	
1228	1992	5	5	10	13	24	29.54	50.84	37.9	4.2	4.6	
1229	1992	5	5	11	16	0	29.78	50.76	42.4	4.2	4.6	
1230	1992	5	5	13	57	50.19	29.72	50.85	15	4.5	4.5	
1231	1992	5	5	15	57	41	30.09	50.83	10	4.2	4.3	
1232	1992	5	17	3	55	42	24.92	63.25	30.4	4.7	4.7	
1233	1992	5	19	12	24	56.37	28.28	55.60	15	5.1	5.6	5.6
1234	1992	5	20	2	2	9	25.28	57.77	33	4.0	4.5	
1235	1992	7	19	3	58	3.54	23.29	63.97	23.7	4.4	4.7	
1236	1992	8	15	14	15	16.51	28.61	51.20	15	4.4	4.4	
1237	1992	8	15	23	26	9.8	28.60	51.04	15	4.2	4.4	
1238	1992	9	8	0	38	18.59	29.13	52.15	26.8	4.8	5.2	
1239	1992	9	9	21	41	48.28	29.88	51.04	20	4.5	5.1	
1240	1992	9	9	21	44	49	30.06	50.87	33	4.4	4.7	
1241	1992	9	10	21	28	42.88	29.91	51.04	22.5	4.4	4.7	
1242	1992	9	11	12	6	3	29.92	51.13	20	5.0	5.1	5.4
1243	1992	9	11	17	4	2	30.00	60.71	15.4	4.4	4.9	
1244	1992	9	11	18	24	14.41	30.01	60.74	19.2	4.8	5.2	5.3
1245	1992	9	11	20	20	8	29.63	51.09	50.2	4.5	4.4	
1246	1992	9	12	2	34	51.22	30.03	60.70	10.5	4.6	5.0	
1247	1992	9	23	21	59	19.21	29.84	51.10	24.6	4.5	5.1	
1248	1992	12	11	4	44	14	28.55	53.89	37.4	4.0	4.5	
1249	1992	12	17	10	39	31.48	25.91	61.45	39	5.3	5.7	5.7
1250	1993	1	2	8	39	0.37	30.12	50.86	21.6	4.5	4.7	
1251	1993	1	6	22	51	46.84	29.05	52.13	25	5.4	5.4	5.4
1252	1993	1	11	19	54	22	30.57	49.86	30.1	4.0	4.5	
1253	1993	1	14	6	8	1.91	30.58	50.28	15	4.4	4.7	
1254	1993	2	4	19	41	33.98	24.85	62.85	26.4	4.8	5.1	
1255	1993	2	11	19	37	52.24	27.61	59.82	15	4.2	4.6	
1256	1993	2	21	20	56	44.1	29.08	52.19	15	4.2	4.5	
1257	1993	3	14	21	23	17	26.71	57.96	33	4.0	4.5	
1258	1993	3	26	22	52	47.72	30.70	50.89	21.7	4.9	5.0	5.1
1259	1993	3	29	15	20	40.46	28.00	52.74	25	4.8	4.9	5.2
1260	1993	4	11	23	25	36.97	29.93	50.93	15	4.6	4.5	
1261	1993	4	12	14	0	41.83	28.26	57.13	28.3	4.4	5.2	5.0
1262	1993	4	24	20	30	10	27.10	57.88	29.2	4.2	4.7	
1263	1993	5	2	16	12	4	27.01	57.85	4.7	4.0	4.5	
1264	1993	5	19	4	3	37	27.00	54.60	33	4.0	4.5	

1265	1993	5	20	19	58	53.02	27.20	54.57	15	4.3	4.6	
1266	1993	6	2	22	1	50	28.91	47.57	21	4.1	4.6	
1267	1993	6	22	16	32	42.7	30.18	50.83	12.6	4.9	5.4	5.4
1268	1993	6	22	16	37	22	30.23	50.59	33	4.5	4.8	
1269	1993	7	6	13	41	24.77	28.89	51.28	15	4.6	4.7	
1270	1993	7	9	10	29	22.84	28.39	55.36	19.6	4.6	5.2	5.2
1271	1993	7	9	10	36	7	28.10	55.88	33	4.5	4.8	
1272	1993	8	2	16	0	58.81	30.97	51.88	17.3	4.5	4.8	
1273	1993	8	4	7	59	45	30.22	51.24	32	4.0	4.5	
1274	1993	9	8	11	38	37.93	30.09	52.05	19.1	4.5	4.9	
1275	1993	10	11	9	13	4	25.27	63.34	24	4.5	4.5	
1276	1993	10	18	13	57	16.71	22.05	62.83	13.1	4.8	5.2	
1277	1993	10	21	21	52	21.91	30.20	51.24	12.2	4.3	5.1	5.0
1278	1993	10	29	23	47	34	29.67	64.00	185.9	4.7	4.7	
1279	1993	11	1	6	42	3	27.93	57.40	53.4	4.3	4.3	
1280	1993	11	1	6	46	35	28.16	57.55	33	4.2	4.6	
1281	1993	12	7	13	17	24.36	30.77	51.29	25	4.1	4.7	
1282	1993	12	19	11	45	32.98	25.24	62.57	25.2	4.9	5.1	
1283	1994	1	1	5	10	48.26	28.18	55.57	11	4.4	4.7	
1284	1994	1	4	9	29	40.29	29.30	51.46	25	4.5	4.8	
1285	1994	2	23	8	2	6.83	30.79	60.53	7	6.1	6.0	6.1
1286	1994	2	23	11	54	34.84	30.81	60.54	9	5.0	5.3	5.5
1287	1994	2	23	22	45	19.9	30.90	60.55	9	4.7	5.3	
1288	1994	2	24	0	11	14.04	30.79	60.51	9	6.0	6.0	6.3
1289	1994	2	26	2	31	12.2	30.80	60.54	9	5.9	5.7	6.1
1290	1994	2	28	10	14	1	30.80	60.59	61.1	4.0	4.0	
1291	1994	2	28	11	13	56.52	30.91	60.62	7	5.5	5.5	5.6
1292	1994	3	1	3	49	2.82	29.14	52.64	12.9	6.1	5.8	6.1
1293	1994	3	1	5	42	55	29.05	52.61	14.8	4.0	4.5	
1294	1994	3	2	14	57	20.67	30.75	60.42	9	4.0	4.5	
1295	1994	3	3	14	56	52	27.50	57.47	33	4.4	4.7	
1296	1994	3	3	23	53	59.05	29.05	52.58	4.2	4.2	4.8	
1297	1994	3	17	8	6	16.33	29.04	52.63	15	4.4	4.7	
1298	1994	3	23	17	14	44.45	29.05	52.69	10	4.4	4.7	
1299	1994	3	29	7	56	52.1	29.20	51.36	7	4.6	5.3	5.1
1300	1994	3	30	19	55	42.13	28.97	52.81	10	5.2	5.3	5.4
1301	1994	4	1	14	24	57	28.91	52.68	10	4.3	4.5	
1302	1994	4	3	6	51	59.04	28.95	52.77	16.4	4.9	5.0	5.2
1303	1994	4	3	7	19	36.05	28.90	52.77	17.6	4.5	4.7	
1304	1994	4	14	11	3	42.52	28.40	55.43	23.5	4.4	5.2	
1305	1994	4	14	11	26	37	28.23	55.34	19.9	4.0	4.5	
1306	1994	4	20	0	5	10.93	28.39	55.30	22.8	4.2	4.7	
1307	1994	4	21	11	50	34	27.38	54.39	45.8	4.2	4.6	
1308	1994	4	26	6	25	55	30.69	50.74	3.2	4.0	4.5	
1309	1994	5	7	14	24	42.27	30.41	50.62	14.8	4.2	4.6	
1310	1994	6	5	16	54	10	29.47	52.24	53.5	4.0	4.5	
1311	1994	6	11	9	37	57.25	29.06	52.58	9	4.3	4.8	

1312	1994	6	14	8	51	3	23.13	64.40	33	4.0	4.5	
1313	1994	6	14	13	46	26	23.29	64.46	33	4.2	4.6	
1314	1994	6	18	12	42	2.57	29.10	52.70	11.8	4.4	5.1	
1315	1994	6	20	9	9	5.17	29.05	52.67	10.8	5.8	5.8	5.9
1316	1994	6	21	3	17	54	29.14	52.53	26.1	4.5	4.4	
1317	1994	6	21	4	15	50.14	29.00	52.65	10	4.4	4.7	
1318	1994	7	1	13	5	55.02	27.69	56.53	25	4.5	4.9	
1319	1994	7	14	20	13	52	28.07	55.48	37.6	4.2	4.6	
1320	1994	8	6	21	2	17.57	27.07	54.44	22.7	4.2	5.2	
1321	1994	8	10	2	11	15	26.97	54.40	39.4	4.4	4.8	
1322	1994	8	11	6	46	34.1	27.01	54.49	25	4.4	5.1	
1323	1994	9	5	5	26	15	29.41	51.28	33	4.5	4.8	
1324	1994	9	8	13	33	37.09	28.05	61.81	60	5.0	5.0	
1325	1994	9	17	8	57	55.87	26.52	55.59	35	4.0	4.7	
1326	1994	10	1	8	25	13.82	27.36	57.54	15	4.9	5.0	
1327	1994	11	3	11	43	33.53	28.23	52.21	20.9	4.2	4.8	
1328	1994	12	2	10	14	8	30.59	50.28	10	4.4	4.7	
1329	1994	12	8	12	54	38.66	29.08	52.53	15.9	4.6	4.8	
1330	1994	12	10	12	16	2.8	27.89	64.94	55.1	4.2	5.1	5.2
1331	1994	12	15	23	24	48.73	29.01	52.61	15	4.2	4.6	
1332	1995	1	1	8	51	9.06	30.68	50.44	22.7	4.9	4.7	
1333	1995	1	4	2	22	12.15	27.55	56.57	15	4.0	4.5	
1334	1995	1	21	3	2	32.61	29.15	52.03	15	4.2	4.6	
1335	1995	1	25	19	36	31.66	28.85	51.38	15	4.2	4.6	
1336	1995	1	25	19	38	16	28.78	51.40	0	4.0	4.5	
1337	1995	1	27	21	7	57	28.05	56.80	51.2	4.0	4.5	
1338	1995	1	29	18	8	9	27.94	57.45	56.2	4.4	4.4	
1339	1995	2	1	13	6	3.87	28.09	56.56	15	4.0	4.5	
1340	1995	2	6	17	25	6	28.43	57.06	23.2	4.0	4.5	
1341	1995	2	15	13	5	19.98	29.10	51.26	15	4.2	4.6	
1342	1995	4	22	0	21	49.6	30.97	49.93	17.6	5.0	5.1	5.3
1343	1995	5	3	2	49	53.29	28.45	52.78	22.5	4.5	4.7	
1344	1995	5	31	20	44	11.42	28.23	53.32	20	4.1	5.0	
1345	1995	6	23	15	54	42	29.88	57.33	54.8	4.1	4.1	
1346	1995	8	25	10	53	2	28.43	57.12	82.8	4.8	4.8	
1347	1995	9	4	17	47	8.55	29.85	57.43	15	4.2	4.4	
1348	1995	10	8	1	38	31	27.41	58.64	82.8	4.0	4.0	
1349	1995	10	14	16	21	49.52	26.96	54.83	15.5	4.4	4.8	
1350	1995	10	14	16	32	18.13	27.06	54.63	15	4.5	4.3	
1351	1995	11	6	3	53	24.32	27.76	57.49	29.7	4.5	5.0	
1352	1995	11	6	11	53	10.23	29.02	64.27	25	4.4	4.7	
1353	1995	11	21	2	20	23.03	29.69	51.55	25	4.4	4.8	
1354	1995	12	18	3	45	11.11	30.63	50.64	15	4.0	4.5	
1355	1995	12	21	7	39	2	27.71	57.25	57.4	4.1	4.1	
1356	1995	12	28	18	23	32.77	27.90	56.53	15	4.2	4.6	
1357	1995	12	31	11	56	39.12	29.33	52.36	15	4.2	4.6	
1358	1996	1	13	9	57	23	28.35	57.35	82	4.3	4.3	

1359	1996	1	24	5	28	7	29.49	51.00	42.3	4.2	4.4	
1360	1996	1	24	6	5	28.02	29.56	51.09	25	4.5	4.4	
1361	1996	1	24	7	7	3.09	29.40	51.03	25	4.5	4.6	
1362	1996	1	25	18	5	21.24	29.37	50.99	25	4.6	4.2	
1363	1996	1	26	13	11	14.99	29.33	51.05	25.4	4.3	4.5	
1364	1996	2	26	8	8	20.67	28.27	57.03	30	5.1	5.2	5.5
1365	1996	2	26	8	9	25.82	28.31	57.10	27.7	4.9	5.4	
1366	1996	3	16	20	18	33.09	29.37	50.98	15	4.3	4.5	
1367	1996	3	20	22	24	5.36	29.43	50.99	25	4.4	4.5	
1368	1996	3	31	21	13	27.27	29.75	50.50	15	4.7	4.1	
1369	1996	4	1	14	20	51.93	29.38	51.01	15	4.6	4.4	
1370	1996	4	10	21	50	43.03	28.11	56.78	20.5	4.3	4.7	
1371	1996	4	20	18	30	27.63	28.01	51.88	15	4.2	4.2	
1372	1996	5	24	6	35	58.61	27.82	53.56	18.3	4.7	4.8	5.2
1373	1996	5	24	7	16	47	21.69	61.93	47.3	4.0	4.0	
1374	1996	5	25	17	0	58.62	27.87	53.52	29	4.4	4.7	
1375	1996	6	2	12	42	14.15	30.73	50.77	12.1	4.4	4.8	
1376	1996	6	12	15	42	11.63	21.87	62.09	26.9	4.7	5.0	
1377	1996	8	6	20	27	20.33	27.63	53.01	26	4.4	4.8	
1378	1996	9	18	14	36	43.34	25.99	60.97	15	4.1	4.4	
1379	1996	9	25	16	22	19.07	28.05	51.28	15	4.2	4.3	
1380	1996	9	28	13	53	56.46	28.41	57.53	25	4.4	4.7	
1381	1996	10	8	1	29	4	29.75	61.12	63.7	4.1	4.1	
1382	1996	10	18	9	26	6.68	27.66	57.54	46.5	4.9	5.2	5.4
1383	1996	10	18	13	31	30	27.92	57.57	67.4	4.1	4.1	
1384	1996	11	18	11	52	15.17	29.92	51.58	20	4.9	5.3	5.3
1385	1996	12	4	2	39	36.26	27.46	52.50	25	4.6	4.3	
1386	1996	12	14	19	49	54.69	28.61	49.71	15	4.3	4.3	
1387	1996	12	20	0	18	12.97	29.39	51.40	17.4	4.5	4.7	
1388	1997	2	8	3	28	23.75	30.98	56.77	30	4.1	4.2	
1389	1997	2	12	14	42	52.07	28.32	55.46	15	4.1	4.3	
1390	1997	2	17	4	31	26.23	27.38	56.14	17.5	4.4	4.9	
1391	1997	3	23	7	15	38	26.24	64.42	33	4.0	3.8	
1392	1997	4	19	5	53	15.24	27.95	56.86	23.2	5.4	5.3	5.6
1393	1997	4	19	22	31	38.81	27.86	56.80	21	4.0	4.4	
1394	1997	4	22	17	39	36.73	28.32	52.81	10	4.5	4.8	
1395	1997	5	3	17	1	50	27.30	53.50	33	4.0	4.5	
1396	1997	5	5	15	11	54.88	27.09	53.88	25	4.5	4.8	5.1
1397	1997	5	26	5	1	24.67	28.65	51.53	24.3	4.0	4.5	
1398	1997	6	23	19	31	35.15	28.04	51.88	25	4.5	4.4	
1399	1997	7	21	4	58	45.1	28.23	57.32	29.3	4.0	4.5	
1400	1997	7	27	1	59	31.92	29.13	52.37	28.6	4.1	4.5	
1401	1997	7	27	23	33	25.7	27.42	56.62	19.4	4.7	4.8	5.1
1402	1997	8	14	19	38	27.33	29.00	51.51	25	4.0	4.7	
1403	1997	8	24	21	11	22.88	28.83	52.69	8.2	4.1	5.0	
1404	1997	8	29	14	43	54.66	27.24	53.81	10	4.2	4.5	
1405	1997	8	29	15	55	58	27.06	53.87	17.4	4.2	4.3	

1406	1997	9	18	14	52	51.33	27.06	53.88	3.5	4.1	4.7	
1407	1997	10	3	11	28	40.03	27.76	54.70	16.5	4.8	5.1	5.3
1408	1997	10	3	17	1	1.62	27.67	54.68	25	4.1	4.7	
1409	1997	10	6	16	9	37.92	28.43	57.21	29	4.2	4.6	
1410	1997	10	20	6	9	5.77	28.45	57.28	32	5.0	5.5	5.4
1411	1997	10	23	14	35	35.14	28.11	53.87	34.5	4.1	4.7	
1412	1997	10	31	5	50	16.15	28.12	53.72	30	4.0	4.2	
1413	1997	11	1	4	7	44.85	28.11	53.79	30	4.0	4.2	
1414	1997	11	1	13	36	34	28.45	57.16	64.4	4.4	4.4	
1415	1997	12	4	10	17	1.87	29.02	64.16	23.2	4.5	4.9	5.1
1416	1997	12	26	1	5	35.4	28.06	53.38	13.1	4.0	4.2	
1417	1997	12	26	5	8	3.29	28.04	53.33	12.1	4.2	4.1	
1418	1998	1	5	16	58	36.6	28.95	64.37	16.4	4.9	4.8	5.2
1419	1998	1	11	8	8	5.8	30.40	50.63	20	4.2	4.6	
1420	1998	1	18	3	13	1.38	30.44	50.57	30.5	4.2	4.7	
1421	1998	2	8	20	22	36	29.52	50.59	55.1	4.1	3.9	
1422	1998	3	14	19	40	29.61	30.13	57.59	13.8	6.9	5.8	6.6
1423	1998	3	15	0	8	6	30.06	57.69	130.4	4.1	4.1	
1424	1998	3	19	8	33	30.72	29.96	55.99	25	4.3	4.6	
1425	1998	3	20	0	12	15	27.64	58.75	51.7	4.1	4.1	
1426	1998	3	27	4	29	48.71	29.90	57.60	17.7	4.2	4.7	
1427	1998	4	19	19	57	23.85	25.01	63.28	25.1	4.1	4.5	
1428	1998	5	28	20	32	47.31	26.54	62.16	35.6	4.2	4.6	
1429	1998	5	30	6	54	56.68	28.43	63.71	0	4.4	4.7	
1430	1998	6	10	8	30	15.37	28.15	58.48	90	4.9	5.0	5.4
1431	1998	7	1	21	36	32	27.75	53.57	28.5	4.5	3.9	
1432	1998	8	1	23	38	31.06	27.69	56.53	12.2	4.8	5.0	5.2
1433	1998	11	13	13	1	9.2	27.79	53.64	12.5	5.1	5.3	5.4
1434	1998	11	14	15	55	43.64	27.83	53.57	15	4.3	4.3	
1435	1998	11	18	7	39	23.15	30.33	57.58	20	4.9	4.8	5.4
1436	1998	12	10	14	21	50.03	27.84	53.56	15.6	4.0	4.7	
1437	1998	12	27	4	10	40.59	27.81	53.63	18.9	4.0	4.7	
1438	1999	1	10	9	9	39.34	21.04	61.87	13.8	4.3	4.6	
1439	1999	1	14	22	12	49.47	28.96	56.28	24.6	4.2	5.0	5.0
1440	1999	1	29	5	22	32.48	30.43	50.68	27.6	4.5	4.7	
1441	1999	3	4	5	38	27.26	28.27	57.21	27.7	6.4	6.0	6.6
1442	1999	3	4	5	47	51.49	28.33	57.15	31.1	5.8	5.5	
1443	1999	3	4	5	50	28	28.45	57.12	30.2	4.7	4.9	
1444	1999	3	4	6	21	54	28.39	57.12	58	4.3	4.3	
1445	1999	3	4	7	16	37.54	28.37	57.04	30	4.5	4.8	
1446	1999	3	4	7	19	19.46	28.04	57.10	31	4.5	5.0	
1447	1999	3	4	7	26	5.49	28.37	56.95	30	4.9	5.0	
1448	1999	3	4	9	52	3.99	28.38	57.19	30	5.1	5.1	
1449	1999	3	4	11	13	0.37	28.28	57.08	32	4.2	4.6	
1450	1999	3	4	19	25	54.95	28.27	57.04	25	4.0	4.5	
1451	1999	3	4	23	50	45	28.49	57.26	33	4.0	3.9	
1452	1999	3	10	7	45	39.71	28.62	56.57	40	4.2	4.6	

1453	1999	3	29	4	0	38.29	29.61	51.55	13.4	4.0	4.7	
1454	1999	4	28	18	11	43.2	27.83	53.54	15	4.0	4.5	
1455	1999	4	30	4	19	59.46	27.77	53.54	4.1	4.8	4.9	5.2
1456	1999	5	6	23	0	52.7	29.52	51.91	16.3	6.3	5.7	6.2
1457	1999	5	6	23	13	23.32	29.43	51.93	10	5.7	5.2	
1458	1999	5	7	0	27	50.75	29.49	51.91	15	4.9	4.4	
1459	1999	5	30	0	15	39.39	29.46	51.95	30	4.2	4.5	
1460	1999	7	5	12	23	12.84	30.51	50.19	26.5	4.3	4.6	
1461	1999	8	18	17	30	54	26.56	59.66	10	4.2	4.6	
1462	1999	9	24	19	17	13.43	28.65	51.35	13.2	4.7	5.2	5.3
1463	1999	9	25	9	56	23.32	29.35	51.83	15	4.0	4.3	
1464	1999	9	25	9	56	24.18	29.41	51.76	33	4.0	4.5	
1465	1999	9	25	19	19	29.19	28.68	51.26	16.5	4.6	4.7	
1466	1999	9	27	2	31	23.14	28.67	51.32	10.7	4.2	4.6	
1467	1999	10	19	13	2	27.26	30.01	57.64	15	4.2	4.4	
1468	1999	10	31	15	9	38.98	29.37	51.85	15	4.9	4.9	5.2
1469	1999	12	5	0	6	43.07	29.52	51.77	15	4.4	4.6	
1470	1999	12	17	1	51	21.9	27.05	54.36	15	4.0	4.5	
1471	1999	12	22	21	52	20	27.85	54.13	40.3	4.6	4.1	
1472	1999	12	23	3	7	29.85	29.46	51.80	25	4.4	4.7	
1473	2000	2	10	1	26	20.67	28.78	54.86	25	4.4	4.7	
1474	2000	3	1	20	6	27.99	28.34	52.84	21.9	4.6	5.0	5.0
1475	2000	3	5	9	40	6.61	27.93	56.45	23.4	5.2	5.4	5.4
1476	2000	3	11	7	8	33.56	28.62	51.30	25	4.6	3.9	
1477	2000	3	13	23	16	19.6	29.26	51.40	20	4.0	4.7	
1478	2000	3	14	21	13	53.46	28.92	51.91	25	4.3	4.2	
1479	2000	3	20	22	40	1.55	28.43	52.30	15	4.2	3.4	
1480	2000	5	3	9	1	14.99	29.59	50.83	12.7	4.6	4.9	5.1
1481	2000	5	3	9	6	10	29.55	50.84	54.8	4.0	4.5	
1482	2000	5	3	10	26	57	29.55	50.79	19.9	4.0	4.5	
1483	2000	6	4	17	52	15	28.72	65.27	11.5	6.6	6.0	
1484	2000	6	23	6	15	12.54	30.09	51.63	20.9	4.5	4.8	5.2
1485	2000	7	29	18	26	59	28.45	57.17	78.4	4.0	4.0	
1486	2000	8	20	22	20	29	28.02	57.26	125.2	4.2	4.2	
1487	2000	9	13	3	55	11.84	27.78	51.72	25	4.2	4.4	
1488	2000	9	13	4	17	2.57	27.83	51.74	10	4.1	4.6	
1489	2000	9	13	13	9	45.55	27.80	51.69	15	4.3	4.9	
1490	2000	10	13	21	12	5.62	30.65	49.70	15	4.3	4.5	
1491	2000	11	11	15	37	28.11	27.48	52.91	20	4.1	4.4	
1492	2000	12	21	10	39	47.82	26.61	55.79	15	4.0	4.5	
1493	2001	1	1	5	14	3	27.30	52.96	18	4.0	4.6	
1494	2001	2	13	3	42	38.95	28.17	56.33	15	4.5	3.2	
1495	2001	2	22	3	19	57.44	29.38	52.00	16.3	4.8	4.1	
1496	2001	3	23	20	31	12.59	27.12	53.84	12.7	4.4	3.6	
1497	2001	3	28	16	34	22.41	29.93	51.28	14.8	5.1	4.7	5.3
1498	2001	4	12	23	8	51.46	28.22	54.93	15	4.3	3.6	
1499	2001	4	13	1	4	27.36	28.22	54.86	25.9	4.9	4.5	5.1

1500	2001	4	13	2	8	39.49	28.24	54.82	25	4.3	3.8	
1501	2001	4	13	4	57	16.58	28.22	54.88	21.2	4.5	3.6	
1502	2001	4	13	11	30	43	27.56	60.96	60.1	4.2	4.2	
1503	2001	4	14	21	39	55.21	28.21	54.90	25	4.1	2.9	
1504	2001	4	18	1	35	37.17	28.20	54.83	25	4.2	3.7	
1505	2001	4	24	20	13	9.76	29.52	51.96	17.5	4.4	3.5	
1506	2001	5	6	17	39	27.32	29.13	51.33	15	4.3	3.7	
1507	2001	5	9	23	48	18	27.91	58.17	59	4.1	4.1	
1508	2001	5	23	14	31	13.48	29.89	51.28	23.1	4.6	4.1	
1509	2001	5	24	21	56	28.83	26.77	53.43	15	4.5	3.8	
1510	2001	6	9	4	45	32.4	29.39	52.23	15	4.4	3.5	
1511	2001	8	4	14	7	48.52	24.99	61.46	28.2	4.3	3.6	
1512	2001	8	6	10	51	59.44	28.89	52.30	15	4.3	3.6	
1513	2001	8	12	11	3	28.62	27.52	57.69	19.3	4.6	3.7	
1514	2001	8	14	21	19	30.62	29.96	65.16	28.7	4.7	4.4	
1515	2001	8	16	13	31	59.85	23.80	65.31	20.1	4.3	3.2	
1516	2001	8	25	23	29	21.66	30.49	57.42	15	4.3	3.7	
1517	2001	9	24	22	3	22.21	30.19	51.81	15	4.0	3.2	
1518	2001	9	26	18	4	37.09	30.00	50.97	15	4.5	3.6	
1519	2001	10	10	17	50	42	28.33	58.06	50.6	4.2	4.2	
1520	2001	10	16	11	44	25.49	29.98	50.47	15	4.1	3.6	
1521	2001	10	16	13	1	5.08	29.90	50.48	25	4.5	4.0	
1522	2001	11	1	19	54	36.63	28.10	57.45	20	4.6	3.0	
1523	2001	11	2	22	5	29.66	27.08	54.59	15	5.2	4.1	
1524	2001	11	4	16	38	8.72	27.07	54.57	15	4.8	4.0	
1525	2001	11	16	1	9	28.26	30.44	50.46	29.7	4.5	3.6	
1526	2001	11	17	12	14	47.96	30.44	50.52	25	4.0	4.5	
1527	2001	11	22	17	0	3.2	27.74	57.47	24.4	4.4	3.5	
1528	2001	11	25	21	30	55.14	28.22	57.28	35	5.0	4.4	5.1
1529	2001	12	15	14	18	39.14	27.96	56.37	28.8	4.7	4.3	
1530	2001	12	15	23	41	19.27	28.19	52.66	12.4	4.6	3.3	
1531	2002	1	18	18	26	16.08	27.38	60.79	15	4.3	3.6	
1532	2002	1	30	18	39	1.71	27.36	60.78	32.5	4.6	4.2	
1533	2002	2	17	13	3	52.12	28.09	51.79	16.4	5.5	5.0	5.3
1534	2002	2	17	16	49	26.25	28.28	51.64	15	4.3	3.4	
1535	2002	2	23	17	9	36.25	26.87	54.75	17.3	4.5	3.9	
1536	2002	2	27	15	49	13.06	27.19	53.09	15	4.4	3.2	
1537	2002	3	9	15	43	22.56	28.09	51.66	15	4.0	4.5	
1538	2002	3	10	4	55	14.48	25.03	58.07	15	4.1	3.3	
1539	2002	3	10	19	43	33.32	27.66	54.43	15	4.3	4.3	
1540	2002	3	11	20	6	41.48	25.19	56.09	25.4	5.1	4.1	5.0
1541	2002	3	13	11	45	51.25	30.53	50.79	15	4.3	3.6	
1542	2002	3	26	10	52	11	29.14	50.97	41.9	4.0	3.6	
1543	2002	3	29	13	40	6.07	30.52	50.50	15	4.5	3.3	
1544	2002	4	4	15	44	34.11	27.07	55.25	16.7	4.8	4.0	
1545	2002	4	6	19	10	50.48	28.10	51.81	29.7	4.4	3.5	
1546	2002	4	8	16	34	2.76	27.05	55.21	13.3	4.9	3.4	

1547	2002	4	11	6	5	47.68	27.64	56.69	15	4.8	3.7	
1548	2002	4	13	6	58	22.46	29.00	51.23	15	4.6	3.0	
1549	2002	4	17	8	47	21.47	27.64	56.74	11	5.3	4.9	5.3
1550	2002	4	20	9	35	13.83	27.37	56.56	15	4.6	4.0	
1551	2002	4	25	6	1	4.58	28.59	52.16	15	4.1	3.2	
1552	2002	5	8	1	7	3.64	27.29	53.74	16	4.5	3.8	
1553	2002	5	16	11	0	13.64	29.66	51.57	25	4.7	3.7	
1554	2002	5	17	15	52	21.29	29.48	51.96	25	4.8	4.2	
1555	2002	5	28	19	5	29.28	27.62	56.71	15	4.2	4.6	
1556	2002	6	1	16	12	35.98	29.57	51.27	13.6	4.9	4.2	5.0
1557	2002	6	2	20	8	23.49	27.82	57.68	25	4.6	4.2	
1558	2002	6	2	20	17	28.31	27.95	57.73	39.5	4.3	4.3	
1559	2002	6	3	13	35	26.97	29.44	52.00	15	4.4	3.5	
1560	2002	6	3	20	17	31.09	25.50	63.50	28.7	4.6	4.1	
1561	2002	6	16	22	30	19.08	29.91	50.86	15	4.4	3.9	
1562	2002	6	18	21	7	3.25	27.66	54.14	25	4.5	4.1	
1563	2002	6	18	22	51	59.93	27.61	54.08	25	4.2	3.7	
1564	2002	6	19	1	0	1.87	27.68	54.12	25	4.3	3.5	
1565	2002	6	19	2	23	20.6	27.58	54.33	25	4.1	3.3	
1566	2002	6	19	15	48	26.24	27.36	54.02	25	4.6	4.1	
1567	2002	6	23	2	43	23.19	29.20	51.29	15	4.4	3.7	
1568	2002	7	1	8	20	52.6	27.36	53.90	23.8	4.5	3.9	
1569	2002	8	22	6	7	23.85	28.76	51.38	15	4.5	3.6	
1570	2002	8	28	23	58	17.67	30.61	50.45	15	4.6	3.9	
1571	2002	8	29	9	53	49.61	30.13	51.58	20	4.7	3.6	
1572	2002	9	9	7	56	52	29.32	51.35	25	4.6	3.4	
1573	2002	9	18	11	27	39.45	25.08	65.67	38.2	4.8	3.8	
1574	2002	10	6	9	51	45.02	28.23	52.91	15	4.4	3.4	
1575	2002	10	9	19	36	3.88	28.22	56.64	15	4.0	3.4	
1576	2002	10	13	23	19	30.11	30.64	56.95	15	4.0	4.5	
1577	2002	11	8	19	39	38.13	27.67	52.25	15	4.0	3.3	
1578	2003	1	11	17	45	30.02	29.62	51.53	15	5.0	5.2	5.2
1579	2003	1	14	14	13	58.59	27.97	62.34	55.4	4.8	5.5	5.4
1580	2003	1	16	2	7	40.93	27.91	55.31	15	4.7	4.6	
1581	2003	1	16	8	45	4.91	30.42	50.41	15	4.0	4.8	
1582	2003	2	14	10	29	0.68	28.00	56.80	38.8	5.4	5.3	5.6
1583	2003	3	1	18	45	55	28.26	57.46	66.3	4.3	4.3	
1584	2003	3	16	5	42	10	28.54	53.04	74.7	4.0	4.5	
1585	2003	4	16	11	6	3.85	30.18	57.47	15	4.0	4.5	
1586	2003	5	8	22	23	9.55	27.44	54.43	15	4.6	4.8	
1587	2003	5	27	10	30	50.64	29.49	51.26	12	4.2	5.0	5.3
1588	2003	6	24	6	52	53.2	27.29	60.96	61	5.1	5.3	5.5
1589	2003	7	6	16	4	20.37	27.98	57.72	21.9	4.3	4.9	5.0
1590	2003	7	10	17	6	39.08	28.31	54.17	10	5.5	5.9	5.8
1591	2003	7	10	17	40	18	28.26	54.11	13.9	5.5	5.7	5.7
1592	2003	7	11	23	55	46.65	28.39	53.99	15	4.0	4.9	
1593	2003	8	4	3	28	20.93	29.04	59.73	30	5.3	5.3	5.6

1594	2003	8	21	4	2	10.85	29.02	59.74	20.2	5.8	5.5	5.9
1595	2003	8	28	18	31	56.22	28.33	54.07	15	4.0	4.8	
1596	2003	8	29	6	55	50.81	28.37	51.52	15	4.2	4.9	